THE UNIVERSITY OF
SYDNEY

Modulation of oxidative damage by selenium compounds

Luke Carroll

A thesis submitted in fulfilment of the requirements for the award of the degree of Doctor of Philosophy.

June 2015

The University of Sydney

Declaration

The work contained in this thesis is original work conducted by the author at the Heart Research Institute, Sydney. It has not been submitted to any other institution for a higher degree and does not contain any materials previously published or written by another person except where due reference is made in the text.

Luke Carroll BSc (For. Sci. in App. Chem.) (Hons)

Randall Munroe, xkcd.com

Table of Contents

Abstract

Myeloperoxidase (MPO) is the enzyme that is responsible for the formation of hypochlorous acid (HOCl), which is utilised by neutrophils and other cell types of the immune system to destroy invading pathogens. HOCl reacts with amine groups to form the secondary oxidants *N*-chloramines. HOCl and *N*-chloramines are potent bactericidal agents, however, under chronic inflammatory conditions, excessive oxidant production can lead to damage of host tissue, and is implicated in the initiation and progression of disease.

Antioxidants react with oxidant species such as HOCl and *N*-chloramines, removing them from biological systems thereby limiting damage. Thiol compounds, including the endogenous antioxidant glutathione (GSH), have demonstrated efficacy as oxidant scavengers, due to their rapid rates of reaction with MPO-derived oxidants. Recently, selenium containing compounds have gained interest due to their elevated rate constants for the reaction with oxidants compared to thiol compounds, and the potential for them to be recycled by thiols. This thesis assesses the potential for selenomethionine (SeMet) and 1,4-anhydro-5-selenotalitol (SeTal), a novel seleno-sugar, to act as catalytic scavengers of MPO-derived oxidants.

Previous studies have demonstrated that oxidation of SeMet by hydrogen peroxide (H_2O_2) and peroxynitrous acid (ONOOH) yields a selenoxide as the major product. The studies in Chapter 3 characterise the reactions of SeMet and SeTal with HOCl and various model *N*-chloramines. It is shown that SeMet and SeTal react with MPO-derived oxidants to form the respective selenoxides, SeMetO and SeTalO. These compounds are characterised using mass spectrometry and NMR spectroscopy, and quantification of their conversion is assessed by HPLC. In each case these reactions are near stoichiometric with low oxidant doses. The second-order rate constants for the reaction with *N*-chloramines have been determined using stopped flow techniques, and are in the range $k = 10^2 – 10^3$ M^{-1} s^{-1}. These represent some of the fastest biologically relevant rate constants for *N*-chloramines, suggesting that SeMet and SeTal could provide a competitive target for *N*-chloramines *in vivo*.

Previous studies have demonstrated that GSH is capable of reducing SeMetO to reform SeMet. The studies in Chapter 4 confirm and extend this observation, and assess the potential for the reduction of SeTalO by GSH. The rate constants for the reaction of SeMetO and SeTalO with thiols have been determined, and found to be in the range of $k = 10^3 – 10^4\ M^{-1}\ s^{-1}$. This rapid reduction of selenoxides demonstrates the potential for a catalytic oxidant scavenging cycle, where small amounts SeMet and SeTal may be capable of efficiently consuming oxidants.

Antioxidant enzymes have also been demonstrated to reduce SeMetO to SeMet. The initial studies reported in Chapter 5 assess the potential for a number of enzymes to reduce SeMetO and SeTalO. The thioredoxin reductase enzyme system (NADPH/TrxR) is capable of reducing SeMetO, but not SeTalO. The glutathione reductase enzyme system (NADPH/GSR/GSH) is capable of reducing both SeMetO and SeTalO, facilitated by the reaction between GSH and the selenoxides. Further studies assess the ability of SeMet and SeTal to remove *N*-chloramines in the presence of these enzymatic systems. The presence of SeMet and SeTal reduces the rate at which NADPH is consumed when *N*-chloramines are added to the TrxR system (and in the presence of other enzymes). In contrast, NADPH consumption is increased in the presence of SeMet when the GSR system is exposed to TauCl.

The ability of SeMet and SeTal to rapidly react with MPO-derived oxidants, and subsequently be reduced by GSH and enzymes systems suggests that SeMet and SeTal may be able to prevent oxidative damage to cellular systems. The studies in Chapter 6 assess the ability of SeMet and SeTal to modulate the oxidative damage to J774A.1 murine macrophage-like cells resulting from exposure to HOCl and TauCl. However, limited protection is observed, with the presence of SeMet and SeTal unable to ameliorate the loss of thiols, oxidation of Met residues, or inhibit necrosis when the cells are exposed to either HOCl or TauCl. This lack of protection may arise from insufficient concentration of SeMet and SeTal, and suggest that additional functional cellular assays to assess cellular damage may be more informative.

Overall, the studies presented in this Thesis demonstrate the potential for SeMet and SeTal to act as catalytic MPO-derived oxidant scavengers. They are capable of rapidly reacting with HOCl and N-chloramines to form products that are reduced by endogenous antioxidant systems, including GSH and TrxR. This work

provides a detailed analysis of the potential efficacy of SeMet and SeTal as catalytic MPO-derived oxidant scavengers, and provides the basis for further studies to assess the potential of SeMet and SeTal to modulate damage in cellular and biological systems.

Acknowledgements

Firstly, I would like to thank my primary supervisor A/Prof Clare Hawkins. Your support and guidance through the last three years has been truly invaluable, and I believe I am a better scientist and person for it. Thank you to my associate supervisors as well, Dr David Pattison, Dr Shanlin Fu and Prof Michael Davies. All of you have been a great help over my candidature and always happy to answer questions or help out with problems. I have thoroughly enjoyed my PhD project, and this is in no small part because of supervisory team.

I would also like to thank the people who assisted with my project, by either supplying reagents or allowing me to use their instruments. Thank you to Dr Lara Malins and Dr Richard Payne for synthesising *N*-acetylselenomethionine; Prof Carl Scheisser for the provision of 1,4-anhydro-5-selenotalitol; Dr Aviva Levina and Prof Peter Lay for the use of the stopped-flow apparatus; and especially, Dr Ronald Shimmon for the assistance you provided and the use of the NMR machine.

Thank you to all the members of the Inflammation and Free Radical groups, both past and present, at the Heart Research Institute, who were all helpful through my project, particularly when I had issues trouble shooting various experiments. In particular, Dr Jihan Talib and Dr Phil Morgan, who were the first to show me around the lab and teach me techniques at the beginning of my time at the HRI. Thank you to Dr Ben Rayner, Dom Love and Jess Macer-Wright, who taught me the ways of cell culture and flow cytometry. Thank you to Pat Pinsansarakit for all the work you do in tissue culture at HRI. A special thank you goes to Pam Vanichkitrungruang for all the lunch times and tea breaks spent solving cryptic crosswords.

Finally, I would like to thank my family and friends; without your support and encouragement I would not be where I am today. Your friendship through this period of my life has been fantastic – particularly through these final stages, reminding me that I'm so close to achieving my goals, and encouraging me all the way to the end. I am truly grateful for all of you in my life.

List of abbreviations

Abbreviation for all amino acids in this Thesis employs the "three-letter system" as described by the IUPAC-IUB Joint Commission on Biochemical Nomenclature.

ACN	Acetonitrile
apoA-I	Apolipoprotein AI
BCA	Bicinchoninic acid
BPG	Bisphosphate glycerate
3-Br-Tyr	3-bromotyrosine
CK	Creatine kinase
3-Cl-Tyr	3-chlorotyrosine
COX-2	Cylcooxygenase 2
CVD	Cardiovascular disease
DMEM	Dulbecco's modified Eagle's medium
DTNB	Disulfide 5,5'-thiobis(2-nitrobenzoic acid)
DTT	Dithiothreitol
EDTA	Ethylenediaminetetraacetic aid
eNOS	Endothelial nitric oxide synthase
EPO	Eosinophil peroxidase
ERK	Extracellular signal-regulated kinase
EtBr	Ethidium bromide
FCS	Fetal calf serum
GAP	Glyceraldehyde phosphate
GAPDH	Glyceraldehyde phosphate dehydrogenase
GlyCl	Glycine *N*-chloramine
GPx	Glutathione peroxidase

GSH	Glutathione
GSR	Glutathione reductase
GSSG	Diglutathione
HBSS	Hanks buffered saline solution
HCAEC	Human coronary artery endothelial cells
HisCl	Histidine *N*-chloramine
HMDM	Human monocyte-derived macrophages
HOBr	Hypobromous acid
HOCl	Hypochlorous acid
HOI	Hypoiodous acid
HOP-1	Hypochlorite oxidised protein 1
HOSCN	Hypothiocyanous acid
HUVEC	Human vein endothelial cells
IAF	5-iodoacetamide fluroscein
ImdCl	Imidazole *N*-chloramine
iNOS	Inducible nitric oxide synthase
IκB	Inhibitor κB
LDH	Lactate dehydrogenase
LDL	Low-density lipoprotein
LPO	Lactoperoxidase
LysCl	Lysine *N*-chloramine
MeSeCys	Methylselenocysteine
MetSO	Methionine sulfoxide
MPO	Myeloperoxidase
MSA	Methane sulfonic acid
MSCO	Methylselenocysteine selenoxide

Msr	Methionine sulfoxide reductase
NADH	Nicotinamide adenine dinucleotide
NADPH	Nicotinamide adenine dinucleotide phosphate
NASMO	*N*-acetylselenomethionine
NASMO	*N*-acetylselenomethionine selenoxide
NEM	*N*-ethylmalemide
NF-κB	Nuclear factor κB
NMR	Nuclear magnetic resonance
$NO^{\bullet}$	Nitric oxide
NQO-1	NADPH : quinone oxidase 1
Nrf2	Nuclear response factor 2
$O_2^{\bullet-}$	Superoxide
OPA	Orthophthaldehyde
PDA	Photodiode array
PI	Propidium iodide
PMA	Phorbol 12-myristrate 13-acetate
Prx	Peroxiredoxin
PTP	Protein tyrosine phosphotase
ROS	Reactive oxygen species
RS-Cl	Sulfenyl chloride
RS-SCN	Sulfenyl thiocyanate
RSOH	Sulfenic acid
SDS	Sodium dodecyl sulfate
SeGul	1,5-Anhydro-5-seleno-L-gulitol
SeMet	Selenomethionine
SeMetO	Selenomethionine selenoxide

SeTal	1,4-anhydro-4-seleno-D-talitol
SOD	Superoxide dismutase
SPO	Seleno-*bis*-propionic acid selenoxide
TauCl	Taurine *N*-chloramine
TCA	Trichloroacetic acid
TFA	Tetrafluoroacetic acid
THF	Tetrahydrofuran
TMB	3,3',5,5'-tetramethylbenzidine
TNB	5-thio-2-nitrobenozic acid
TNF-α	Tissue necrosis factor α
Trx	Thioredoxin
TrxR	Thioredoxin reductase
VPO	Vascular peroxidase

List of figures

List of tables

Publication arising from this Thesis

Research Articles

Carroll, L., Pattison, D. I., Fu, S., Schiesser, C. H., Davies, M. J., & Hawkins, C. L., (2015), Reactivity of selenium-containing compounds with myeloperoxidase-derived chlorinating oxidants: Second-order rate constants and implications for biological damage. *Free Radical Biology and Medicine*, Volume 84, Page 279-288

Review Articles

Carroll, L., Davies, M. J., & Pattison, D. I., (2015), Reaction of low-molecular-mass organoselenium compounds (and their sulphur analogues) with inflammation-associated oxidants. *Free Radical Research*, Volume 49, Issue 6, Page 750-767

Conference Abstracts

Luke Carroll, Clare L. Hawkins, Shanlin Fu, Corin Storkey, Carl H. Schiesser, Michael J. Davies, (2014), Seleno compounds are effective catalytic scavengers of myeloperoxidase-derived oxidants, *Journal of Clinical Biochemistry and Nutrition*, Volume 54, Supplement, Page 95

Luke Carroll, Clare L. Hawkins, Shanlin Fu, Corin Storkey, Carl H. Schiesser, Michael J. Davies, (2014), Enzymatic reduction of selenoxides by Trx and GSR, *Journal of Clinical Biochemistry and Nutrition,* Volume 54, Supplement, March 2014, Page 95

Luke Carroll, David I. Pattison, Shanlin Fu, Corin Storkey, Carl H. Schiesser, Michael J. Davies, Clare L. Hawkins, (2013), Selenium containing compounds react with MPO-derived oxidants with high second order rate constants, *Free Radical Biology and Medicine*, Volume 65, Supplement 2, Page S122

Luke Carroll, Clare L. Hawkins, David I. Pattison, Shanlin Fu, Corin Storkey, Carl H. Schiesser, Michael J. Davies, (2012), Seleno compounds are effective scavengers of myeloperoxidase-derived oxidants, *Free Radical Biology and Medicine*, Volume 53, Supplement 2, Page S107

Luke Carroll, Clare L. Hawkins, Shanlin Fu, Corin Storkey, Carl H. Schiesser, Michael J. Davies, (2012), Seleno compounds are effective catalytic scavengers of

myeloperoxidase-derived oxidants, *Free Radical Biology and Medicine,* Volume 53, Supplement 1, Page S97

Conference Presentations

(Presenter in bold)

Luke Carroll, David I. Pattison, Shanlin Fu, Corin Storkey, Carl H. Schiesser, Michael J. Davies, Clare L. Hawkins, (2014), Selenium-containing compounds as catalytic oxidant scavengers: Determination of selenoxide reduction rates by thiols, Oral presentation, *22nd Annual Meeting of The Society of Free Radical Research Australasia, Melbourne, 3-6 Dec 2014*

Luke Carroll, David I. Pattison, Clare L. Hawkins, Shanlin Fu, Corin Storkey, Carl H. Schiesser, Michael J. Davies, (2014), Seleno compounds are catalytic scavengers of myeloperoxidase-derived oxidants, Poster presentation, *Australian Society for Medical Research 22nd NSW Scientific Meeting, Sydney, 23 Mar – 26 Mar 2014*

Luke Carroll, David I. Pattison, Clare L. Hawkins, Shanlin Fu, Corin Storkey, Carl H. Schiesser, Michael J. Davies, (2014), Seleno compounds are effective catalytic scavengers of myeloperoxidase-derived oxidants, Poster presentation, *Society for Free Radical Research International, Kyoto, 23 Mar – 26 Mar 2014*

Luke Carroll, David I. Pattison, Clare L. Hawkins, Shanlin Fu, Corin Storkey, Carl H. Schiesser, Michael J. Davies, (2013), Enzymatic reduction of selenoxides by Trx and GSR, Poster presentation, *Society for Free Radical Biology and Medicine, San Antonio, 20 Nov – 24 Nov 2013*

Luke Carroll, David I. Pattison, Shanlin Fu, Corin Storkey, Carl H. Schiesser, Michael J. Davies, Clare L. Hawkins, (2013), Selenium containing compounds react with MPO-derived oxidants with high second order rate constants, Poster presentation, *Society for Free Radical Biology and Medicine, San Antonio, 20 Nov – 24 Nov 2013*

Luke Carroll, David I. Pattison, Shanlin Fu, Corin Storkey, Carl H. Schiesser, Michael J. Davies, Clare L. Hawkins, (2013), Selenium compounds react with chloramines with high second order rate constants and are potent scavengers of inflammatory oxidants, Oral presentation, *Combined International Human Peroxidase and Society for Free Radical Research Australasia and Japan, Sydney, 9 Sept – 14 Sept 2013*

Luke Carroll, **Clare L. Hawkins**, David I. Pattison, Shanlin Fu, Corin Storkey, Carl H. Schiesser, Michael J. Davies, (2012), Seleno compounds are effective scavengers of myeloperoxidase-derived oxidants, Poster presentation, *Society for Free Radical Biology and Medicine, San Diego, 14 Nov – 18 Nov 2012*

Luke Carroll, Clare L. Hawkins, David I. Pattison, Shanlin Fu, Corin Storkey, Carl H. Schiesser, Michael J. Davies, (2012), Seleno compounds are effective scavengers of myeloperoxidase-derived oxidants, Oral presentation, *Free Radical and Metal Biology, Brisbane, 28 Nov – 1 Dec 2012*

Luke Carroll, Clare L. Hawkins, Shanlin Fu, Corin Storkey, Carl H. Schiesser, Michael J. Davies, (2012), Seleno compounds are effective catalytic scavengers of myeloperoxidase-derived oxidants, Poster presentation, *Society for Free Radical Research International, London 6 Sep – 9 Sep 2012*

1 Introduction

1.1 Immune response and inflammation

When bacteria and other pathogens enter the body, the innate immune system responds, initiating inflammation [1]. Pathogens are detected by cell-surface receptors on cell types such as macrophages, dendritic cells, Kupffer cells and mastocytes [1]. These cells then release inflammatory mediators and chemokines, which perform a variety of functions such as vasodilation and increased permeability of vessels [1]. The released chemokines attract circulating immune cells to the site of inflammation along a chemotactic gradient [1].

Neutrophils, a key effector cell of the immune response, engulf pathogens, and during this process of phagocytosis, a nicotinamide adenine dinucleotide phosphate-oxidase (NADPH) complex is activated [1]. The purpose of this oxidase is to produce superoxide ($O_2^{\bullet-}$), a strong oxidant. $O_2^{\bullet-}$ can dismutate either spontaneously or by action of superoxide dismutases (SOD), to give hydrogen peroxide (H_2O_2) [1]. Alternatively, $O_2^{\bullet-}$ can combine with other species, including nitric oxide ($NO^{\bullet}$), to form other oxidants such as peroxynitrite and radical species. Immune cells contain specialised enzymes, such as myeloperoxidase, whose major function is to catalyse the reaction of H_2O_2 and halide ions to form hypohalous acids [2]. These strongly oxidising species are then involved in the destruction of the invading pathogen by chemically attacking its cellular components [1].

1.2 Myeloperoxidase and related peroxidases

Neutrophils are generally considered to be the major effector cells of the innate immune system. Their role is to seek out and destroy invading pathogens. They achieve this by phagocytosis, engulfing the pathogen followed by bombardment with strong oxidants designed to destroy the foreign body. One of the major oxidant producing enzymes found in neutrophils is myeloperoxidase (MPO), which makes up about 5% the dry cell mass [2]. MPO is stored in the azurophilic granules of neutrophils [3], and is released into the phagolysomal compartment after neutrophil activation. Eosinophils play similar roles to neutrophils, with eosinophil peroxidase (EPO) producing strong oxidants.

1.2.1 Structure of peroxidases

MPO is a dimeric protein consisting of two 73 kDa monomers linked by a disulfide bond at Cys153 [4]. The monomers are identical and functionally independent, and dimerisation appears to have no effect on the function of MPO [5]. The monomer has 2 major components, a large glycosylated (heavy) chain of 58.5 kDa (red) and a shorter (light) chain of 14.5 kDa (blue) (Figure 1.1) [4]. The modified iron protoporphyrin IX active site [6] (green) is located in the heavy chain, and is surrounded by α-helices from both chains (H2, H6, H7, H9, H10 and H14), which hinders access to the heme for most materials except H_2O_2 and small anions [4, 7]. The heme is bound to the protein by two ether linkages and a sulfonium ion link [8]. Helices H2, H6 and H7 form a hydrophobic pocket at the distal heme entrance which allows substrates to bind and be oxidised by MPO [9]. The calcium ion (yellow) plays a role in the distal His orientation and interactions between monomers [9].

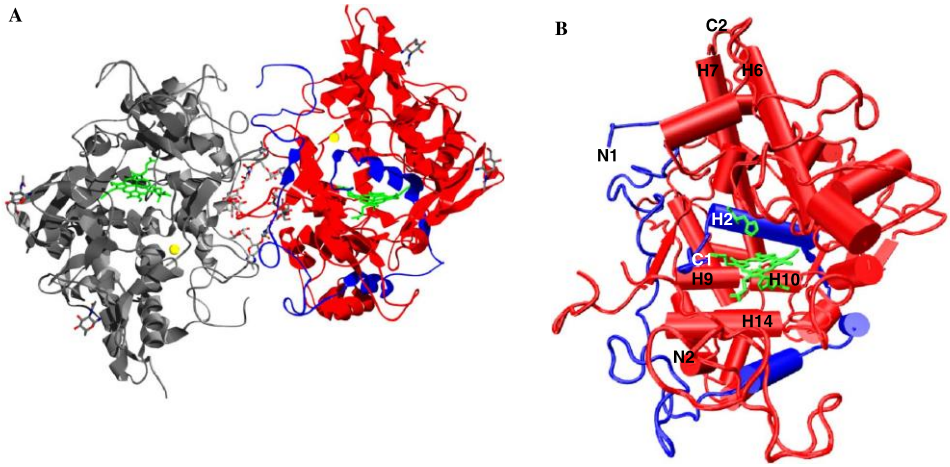

Figure 1.1 - (A) Overall structure of mature homodimeric human myeloperoxidase. (B) Monomer structure of myeloperoxidase showing assignment of structural elements – Taken from [9]

EPO is found in the granular compartments of eosinophils [10] whose function is to eliminate parasites as part of the immune system. EPO is similar in size and structure to MPO, being a highly cationic protein consisting of a heavy 57.9 kDa chain and a light 11.9 kDa chain surrounding a modified iron protoporphyrin IX group [9]. Lactoperoxidase (LPO) is a *ca.* 80 kDa single chain glycoprotein secreted in human tears, milk, saliva and vaginal fluid [9]. The primary role of LPO, like MPO and EPO, is as a first line of defense of the immune system in destroying invading bacteria and other pathogens. Vascular peroxidase (VPO) is a peroxidase expressed

in vascular cells and heart tissues, with a 42 % sequence identity with MPO [11]. LPO and MPO have similar heme group and binding sites [12] with an overall 51% sequence identity [13]. EPO and LPO have the ether linkages to the heme conserved, but do not contain the sulfonium ion link to the heme group characteristic of MPO, resulting in a more planar structure [8].

1.2.2 Function of peroxidases

Peroxidases use H_2O_2 produced by enzymes such as SOD in order to produce strong oxidants [14]. SOD produces H_2O_2 from $O_2^{\bullet-}$ generated by NADPH during the respiratory burst of neutrophils, which is caused by activation in response to invading pathogens [1]. The heme active site of peroxidases is oxidised by H_2O_2 forming an oxy-ferryl heme centre and porphyrin radical known as Compound I [9]. Compound I can be reduced back to the native ferric enzyme by a 2-electron reaction with halides and pseudohalides forming hypohalous acids (Figure 1.2 - Halogenation cycle) [9]. Alternatively, Compound I can undergo 2 one-electron reductions to reform the native enzyme, via Compound II, a ferryl-oxy heme centred intermediate (Figure 1.2 - Peroxidase cycle) [15, 16]. Human peroxidases are capable of oxidising a wide variety of substances due to their high reduction potentials (See Table 1.1).

H_2O_2 and $O_2^{\bullet-}$ can interact with each step of the MPO catalytic cycles. Reaction with Compound I oxidises H_2O_2 to $O_2^{\bullet-}$ and forms Compound II [9, 14, 17]. Compound II can also react with H_2O_2 to form Compound III, a ferrous enzyme with molecular oxygen bound to the heme centre [17]. However this reaction is relatively slow compared to the reaction of Compound II with $O_2^{\bullet-}$ and other substrates, that reduce MPO back to the native compound [17]. Compound III can also be formed by reaction of $O_2^{\bullet-}$ with the native enzyme. Compound III is then recycled to the native enzyme by a second reaction with $O_2^{\bullet-}$, producing H_2O_2 [17, 18]. In this way, MPO displays SOD activity. Compound III is capable of reacting very slowly with substrates, including acetaminophen and ascorbate to form radicals, and regenerate the native form of the enzyme [19, 20].

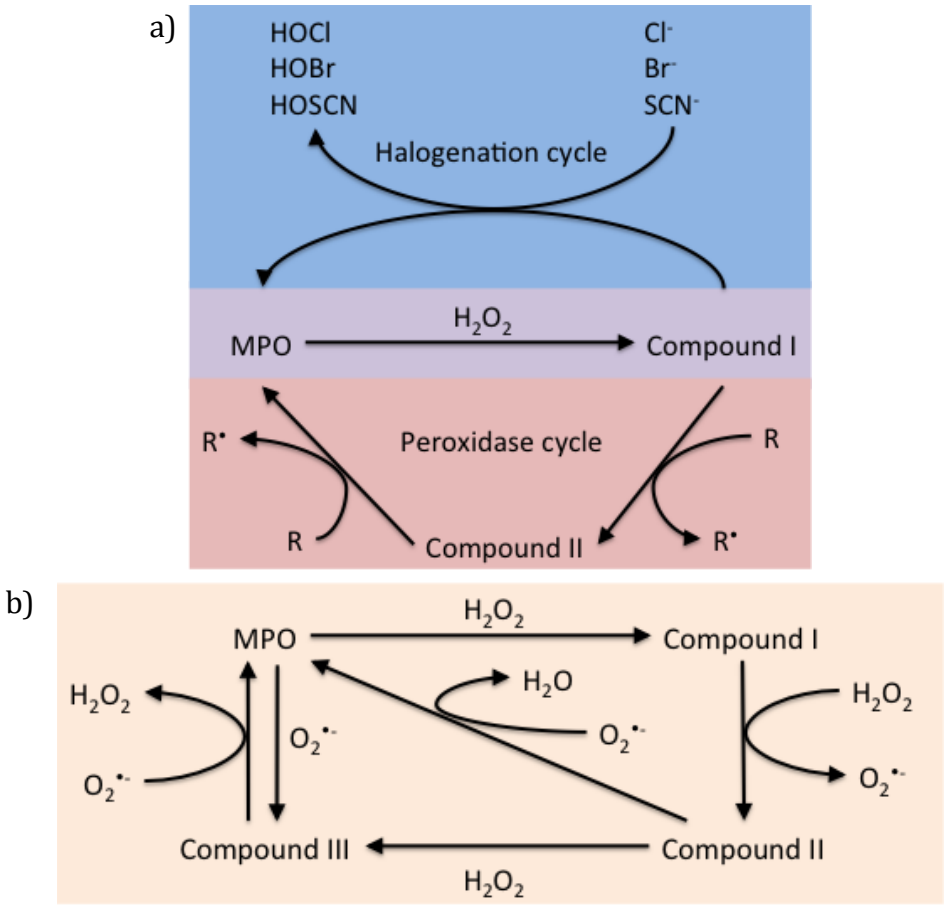

Figure 1.2 – Catalytic cycles of myeloperoxidase a) Halogenation and peroxidase cycles of MPO b) Interaction of MPO with superoxide and hydrogen peroxide

MPO has the highest reduction potential of the human peroxidases (Table 1.1). This is thought to be due to the sulfonium ion linkage between the heme and Met 243 [8]. This linkage, combined with the ester bond from Glu242, has the effect of puckering the heme surface distorting the planar symmetry, and acts as an electron-withdrawing moiety due to its positive charge. EPO, LPO and VPO do not contain this Met 243 linkage, but all three contain 2 ester links to the heme group from Asp94 and Glu 242 [8, 11].

Table 1.1 - Standard reduction potentials of species in the catalytic cycles of human peroxidases at pH 7

	Standard reduction potentials (V)		
	MPO	EPO	LPO
Compound I/native enzyme	1.16 [a]	1.10 [a]	1.09 [b]
Compound I/Compound II	1.35 [c]		1.14 [b]
Compound II/native enzyme	0.97 [c]		1.04 [b]

[a][21]; [b] [22]; [c] [23]

1.2.3 Halogenation cycle

The major function of MPO is to oxidise halide ions Cl^-, Br^- and the pseudohalide SCN^- to hypohalous acids, hypochlorous acid (HOCl), hypobromous acid (HOBr) and hypothiocyanous acid (HOSCN) respectively. Human peroxidases preferentially oxidise SCN^- when compared to Cl^- and Br^-, with MPO recognised as the primary peroxidase capable of oxidising Cl^- at reasonable rates (See Table 1.2). MPO produces primarily HOCl and HOSCN under physiological conditions, with about 45 % and 50 % of the H_2O_2 consumed producing these respectively (HOBr production represents the final 5 %) [24]. Kinetic analysis would suggest that HOCl production would be preferred over HOSCN production, as Cl^- is at a much higher concentration *in vivo* compared to SCN^-. However, the high levels of HOSCN produced by MPO reflects the specificity of MPO for SCN^- over Cl^-, with the relative specificity for SCN^- being 730-fold greater than Cl^- [24]. EPO produces HOSCN and HOBr [25] and LPO almost exclusively produces HOSCN [26]. VPO produces primarily HOBr and HOSCN, though 18 % of the H_2O_2 consumed is used to produce HOCl [27]. The preference for SCN^- oxidation is reflected in the apparent second order rate constants for these processes (see Table 1.2). The reduction potentials for the different peroxidases do not necessarily correlate with the rate constants (see Table 1.1 and Table 1.2), as halide and pseudohalide specificity is strongly affected by differences in the active and binding sites [9]. Hence, an increase of ca. 10 fold in the rate of Br^- and SCN^- oxidation for EPO over MPO is observed, even though MPO has a greater reduction potential compared to EPO.

Table 1.2 – Apparent second order kinetics and reduction potentials for hypohalous acids produced by human peroxidases

Reaction	Second order rate constant ($M^{-1}s^{-1}$)				Reduction potential of halide (HOX/X^-) (V)
	MPO	EPO	LPO	VPO	
Compound I + Cl^- ➔ Native enzyme + HOCl	2.5×10^4 [a]	3.1×10^3 [b]	-	2.0×10^2 [c]	1.28 [d]
Compound I + Br^- ➔ Native enzyme + HOBr	1.1×10^6 [e]	1.9×10^7 [f]	4.1×10^4 [a]	7.3×10^4 [c]	1.13 [d]
Compound I + SCN^- ➔ Native enzyme + HOSCN	9.6×10^6 [e]	1.0×10^8 [g]	2.0×10^8 [g]	1.4×10^5 [c]	0.56 [d]

[a] [28]; [b] [29]; [c] [27]; [d] [30]; [e] [31]; [f] [32]; [g] [33]

The relative concentrations of oxidants produced by human peroxidases are also drastically affected by pH [9, 30, 34]. At acidic pH, the rates of oxidation of halides and pseudohalides are dramatically increased [30], particularly Cl^- oxidation. The increased affinity for Cl^- at low pH is proposed to be due to the protonated distal His allowing direct access of the heme centre to Cl^- but not the larger Br^- and SCN^- ions [35]. At pH > 7, the proportion of HOBr produced by MPO is significantly enhanced [34], possibly due to a lower reduction potential of MPO at high pH, inhibiting the oxidation of Cl^- due to its higher reduction potential [36].

1.2.4 Peroxidase cycle

MPO is also capable of oxidising substrates, to form radicals, in 2 one-electron reduction steps in a process known as the peroxidase cycle. The porphyrin radical of compound I oxidises the substrate to give a substrate radical and forms Compound II, which retains the oxy-ferryl heme [15, 30]. Compound II then accepts a second electron from another substrate and is reduced back to the native enzyme [15]. Due to the lower oxidation potential of Compound II, some substrates can be oxidised by Compound I but not Compound II. These substrates, termed "poor" substrates, act as inhibitors of MPO activity as Compound II accumulates, inhibiting further oxidation of substrates in either the peroxidase or halogenation cycle [37]. However, $O_2^{\bullet-}$ and ascorbate radicals are capable of recycling Compound II, reforming the native enzyme [38].

Due to the high reduction potential of human peroxidases, a wide variety of substrates can be oxidised by their peroxidase cycles. MPO has the widest range of possible substrates due to its higher reduction potential compared to EPO and LPO

(Table 1.1). Major targets for the peroxidase cycle include phenolic and aromatic compounds such as Tyr, Trp, ascorbate and urate, the oxidation of which produces radical species, as well as nitrogen species such as nitrate and nitrite forming reactive nitrogen species. Second order rate constants for these reactions are summarised in Table 1.3.

Table 1.3 - Second order rate constants for reactions between Compounds I and II of human peroxidases in the peroxidase cycle

Substrate	Second order rate constant ($M^{-1}s^{-1}$)	
	MPO	
	Compound I	Compound II
Tyr	7.7×10^5 [a]	1.6×10^4 [a]
Dityrosine	1.12×10^5 [b]	7.5×10^2 [b]
Trp	4.5×10^5 [a]	6.9 [a]
Nitrite	2.0×10^6 [c]	5.5×10^2 [c]
Substrate	Second order rate constant ($M^{-1}s^{-1}$)	
	LPO	
	Compound I	Compound II
Tyr	1.1×10^5 [a]	1.0×10^4 [a]
Dityrosine	ND	ND
Trp	2.4×10^4 [a]	8.4×10^1 [a]
Nitrite	2.2×10^7 [c]	3.5×10^5 [c]

[a] [15]; [b][37]; [c][39]; ND – not determined

Compounds I and II of MPO and LPO are capable of oxidising the amino acids Tyr and Trp to form radicals [15, 40-43]. The tyrosyl radicals formed can undergo radical-radical termination with a major product being dityrosine [44]. Radicals formed on Tyr residues on proteins can also react with nitrogen dioxide radicals ($NO_2^{\bullet}$) forming nitrotyrosine [45, 46]. Dityrosine is also capable of reaction with Compounds I and II [37], though the second order rate constant with Compound II is 2 orders of magnitude slower than for Tyr. Tyr radicals can promote the cross linking of proteins via the formation of dityrosine [40]. The oxidation of Trp residues is considerably faster for Compound I than Compound II for MPO and LPO [15]. Other phenolic and aromatic compounds are oxidised by Compound I of peroxidases, but not by Compound II, leading to accumulation of Compound II when no species capable of recycling Compound II are present [38].

MPO can oxidise $NO^{\bullet}$ to form nitrite ions (NO_2^-) at low levels of $NO^{\bullet}$ [29, 47, 48] though at higher levels of $NO^{\bullet}$ a Fe-nitrosyl complex is formed, inhibiting the action of MPO [49]. However, at physiological levels of SCN^- and ascorbate, the consumption of $NO^{\bullet}$ by MPO is inhibited [50]. MPO can also oxidise NO_2^- to form

$NO_2^{\bullet}$ [39, 51]. Nitrite shows an increased binding capacity at lower pH, proposed to be due to the protonation of the distal His, and consequently the rate of reaction increases by two orders of magnitude for oxidation by Compound I [39]. The nitrating and chlorinating ability of neutrophils is enhanced in the presence of nitrite, and this is likely to be by NO_2Cl, which is produced by the interaction of the MPO-derived oxidants HOCl and $NO_2^{\bullet}$ [52].

1.2.5 Production of secondary oxidants

HOCl and HOBr are capable of reacting with nucleophilic nitrogens to form *N*-chloramines and *N*-bromamines respectively [53-58]. Under physiological conditions, the major target for the formation of *N*-halamines are free amino acids, the *N*-termini of proteins, or amino acids with a nitrogen centre in the side chain, i.e. Lys, His and Arg. Taurine chloramine (TauCl) is a major product of neutrophils as approximately 20 mM Tau is released locally upon stimulation, which then reacts with the HOCl produced by MPO [59]. Rate constants for the reaction with HOCl are approximately 10^4 – 10^5 $M^{-1}s^{-1}$ for the α-amino groups of amino acids [60, 61]. Secondary amines react less rapidly, with second order rate constants for the reaction of HOCl with endocyclic DNA bases residues are around 10^3 - 10^4 M^{-1} s^{-1} [62, 63], though the imidazole ring in His reacts with a rate constants of 1 x 10^5 M^{-1} s^{-1} [60]. Other primary amines (i.e. not the α-amine groups of amino acids), including those on the Lys side chain, have rate constants of typically 5 x 10^3 M^{-1} s^{-1} [60, 61]. HOBr reacts with Lys and His residues much faster than HOCl, with rate constants of 2.9 x 10^5 and 3.0 x 10^6 M^{-1} s^{-1} respectively, yielding *N*-bromamines [61].

At low pH, MPO may be capable of producing Cl_2, Br_2 and the transhalogen BrCl [36, 64]. These species would be capable of halogenation reactions with biological substrates. The transhalogen species BrCl is produced by oxidation of Br^- by HOCl [64]. *In vitro* studies have demonstrated that the MPO-H_2O_2-Cl^-/Br^- system is capable of bromination at acidic pH values using deoxycytidine as a bromination target through an interaction between HOCl and Br^- [65]. However, at pH > 7 with physiological Br^- concentrations, the MPO system showed no bromination of deoxycytidine [65] or Tyr residues [66], suggesting that bromination by MPO is unlikely to be significant pathway *in vivo*.

In addition, the formation of singlet oxygen [67-74] and ozone [75-81] by MPO, LPO and EPO systems has been suggested, through a reaction between HOCl or HOBr and H_2O_2 [68, 69, 74]. However, this is unlikely to be physiologically relevant due to the slow kinetics [17, 74], making it unable to compete with the faster reactions.

1.3 Reactions of MPO-derived oxidants

1.3.1 Hypohalous acids

At physiological pH, HOCl, HOBr and HOSCN exist in equilibrium with their conjugate bases, OCl^-, OBr^- and $OSCN^-$ respectively. As the pK_a of HOCl is 7.59, it exists as an approximately 1:1 ratio of HOCl : OCl^- at pH 7.4 [82, 83]. The pK_a of HOBr is 8.7, and so it primarily exists as the neutral HOBr species at pH 7.4 [83]. In contrast, the pK_a of HOSCN is 5.3, and therefore exists mainly as the anion $OSCN^-$ at pH 7.4 [83]. In acidic conditions, with an excess of halide ions, HOCl and HOBr are also in equilibrium with Cl_2 and Br_2 [36]. In addition to HOSCN production by MPO, HOCl and HOBr are capable of directly oxidising SCN^- to form HOSCN [84, 85].

HOCl is capable of reacting with a wide variety of substrates [86]. Due to the high reactivity of HOCl, it will react with most biomolecules, and therefore proteins are major substrates, owing to their abundance in biological systems [87]. HOCl reacts most rapidly with sulfur residues, followed by amine and Trp residues, followed by other targets [60]. HOSCN, on the other hand, is a much more selective oxidant and reacts preferentially with thiols [88]. HOBr is less reactive with thiols compared to HOCl, however with other amino acid targets, such as amines, and aromatic residues such as Tyr, HOBr is more reactive [61]. The reaction of these oxidants with biological components can have a wide range of detrimental effects, including protein fragmentation or aggregation, and inactivation or modification of enzymatic function [2, 89].

1.3.2 Sulfur containing amino acids

The reactions with thiols (e.g. Cys, glutathione (GSH)) and thioethers (e.g. Met) are some of the fastest biologically relevant reactions known for HOCl, HOBr and HOSCN. The reaction of HOCl and HOBr with Cys is extremely rapid with rate constants of 3.6×10^8 and 1.2×10^7 M^{-1} s^{-1} (at pH 7.4) respectively [61, 90]. However,

these rates can dramatically change with pH, and are dependent on the pK_a of the thiol with lowered pH resulting in a lower rate of reaction observed [61, 90]. This is because the thiolate ion is more reactive towards the hypohalous acids than the protonated thiol [61, 90]. The reaction with Met is slower, but still extremely rapid with second order rate constants of 3.4×10^7 and 3.6×10^6 $M^{-1} s^{-1}$ for HOCl and HOBr respectively [61, 90]. Rate constants for HOSCN are significantly less with Cys and GSH at a rate of 7.8×10^4 and 2.5×10^4 $M^{-1} s^{-1}$ respectively [91, 92]. HOSCN reacts with Met slowly, with an upper limit of ~1000 $M^{-1} s^{-1}$ [92].

The initial reaction product between HOCl and thiols is the sulfenyl chloride species (RS-Cl) [93-96] (Figure 1.3). The sulfenyl chloride species are short lived and can react either with H_2O to yield a sulfenic acid (RSOH), or with excess thiols to yield a disulfide [95]. Sulfenic acids can be further oxidised to give sulfinic and sulfonic acids, by HOCl or other 2-electron oxidants [95]. Alternatively, RS-Cl can decompose via radical pathways to form thiyl radicals [97]. For HOSCN, the reaction with a thiol initially produces the corresponding RS-SCN species [91, 98]. RS-SCN groups can also react to yield sulfenic acids, but are more stable than their RS-Cl counterparts, and have lifetimes of a few minutes to hours depending on their environment [99, 100]. The formation of sulfenic acids is a key mechanism of antioxidants enzymes such as peroxiredoxin [101], as they can react with nearby cysteine residues to form disulfides that can be reduced through the action of other enzymes such as thioredoxin (Trx) [102]. However, over-oxidation of these residues can inactivate proteins, with sulfinic acid formation being reversible only through the action of sulfiredoxin, though this process is slow [103]. Sulfonic acid formation is irreversible, leading to permanent inactivation of enzymes [103-105].

Sulfenamides are produced when RS-Cl react with a nucleophilic nitrogen [95, 106] (Figure 1.3). Subsequent oxidation of a sulfenamide produces sulfinamides and sulfonamides [95]. HOCl induces the formation of glutathione sulfonamide at sub-stoichiometric amounts of HOCl, where *N*-chloramines needed to be in excess of GSH in order to produce detectable levels of the sulfonamide [107]. The formation of sulfonamides can induce crosslinking in peptides, including GSH, and proteins when the nucleophile is a Lys or Arg side chain [95, 108].

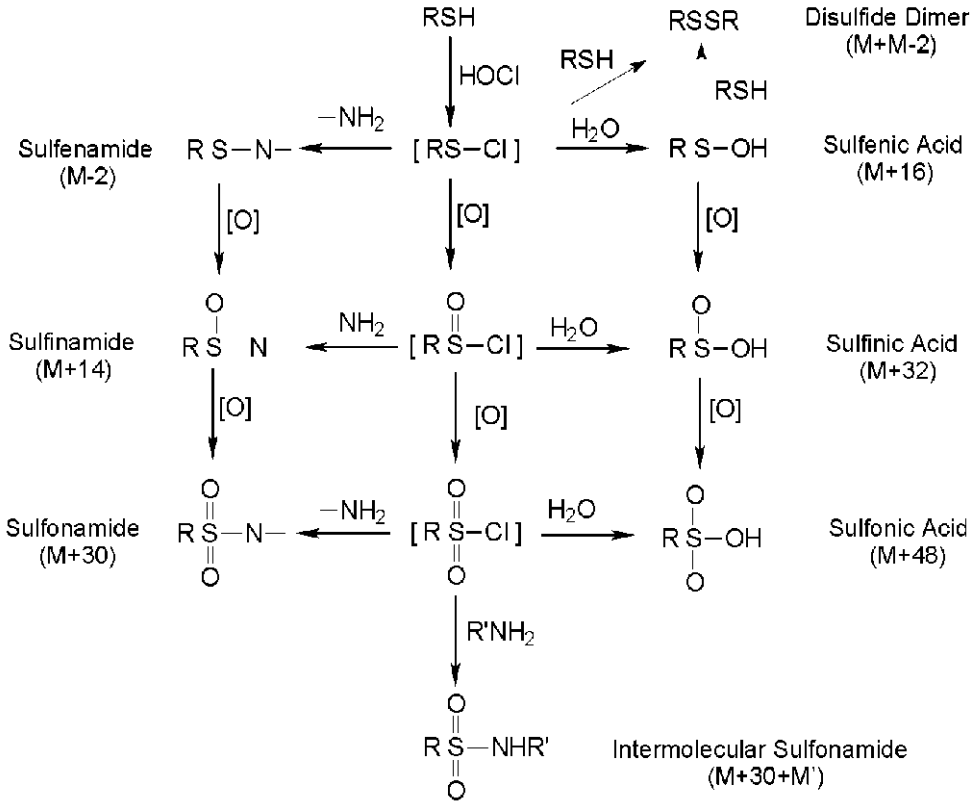

Figure 1.3 - Reaction schemes for production of sulfenic, sulfinic and sulfonic acid and sulfenamides, sulfinamides and sulfonamides produced from reactions of HOCl with thiol groups. Taken from [95]

Oxidation of Met residues by HOCl primarily gives rise to methionine sulfoxide (MetSO) [106]. MetSO is a stable product, which is only reduced *in vivo* by methionine sulfoxide reductases [109, 110]. Formation of MetSO at the active site of proteins can lead to inactivation. A classic example of this is the inactivation of α_1-proteinase by HOCl [111, 112], which can be prevented by the presence of antioxidants [112-114]. Further oxidation of MetSO residues results in the formation of methionine sulfone, an irreversible oxidation product [88].

Oxidation of Met by HOCl and *N*-chloramines can form dehydromethionine as a lower yield product [115]. The formation of this product can occur at N-terminal Met residues [116]. Thiols are capable of reducing dehydromethionine, with the half-life of this product in cytosol where GSH concentration is higher is predicted to be only a few hours [117]. Exposure of peptides containing Met and Lys residues to HOCl can also result in the formation of inter and intra-molecular sulfilimine crosslinks, though HOBr was more effective in forming these products [118]. The mechanism is proposed to be via a halamine intermediate reaction [118].

1.3.3 Aromatic amino acids

HOCl can react with the aromatic side chains of amino acids. Tyr residues are particularly important due to the formation of the stable 3-Cl-Tyr, which has been used a biomarker for HOCl, and hence MPO damage [119]. HOCl chlorinates Tyr to form 3-Cl-Tyr [64, 120-122] and can further chlorinate Tyr to form 3,5-dichloro-Tyr [122, 123]. This can occur by direct chlorination by HOCl or chlorine transfer from *N*-chloramines formed near Tyr residues [121, 124]. The reaction of HOCl with Tyr is much slower than other reactions mediated by HOCl, with second order rate constants of 71 M^{-1} s^{-1}, and 238 M^{-1} s^{-1} for the reaction of 3-Cl-Tyr with HOCl [125].

HOBr is also capable of reacting with Tyr residues to form the 3-brominated product, and this reaction is significantly faster than the reaction with HOCl, with a second order rate constant of 2.3 x 10^5 M^{-1} s^{-1} [61]. 3-Br-Tyr has been used a biomarker for MPO and EPO damage, and increased relative levels of 3-Br-Tyr to 3-Cl-Tyr have been interpreted as HOBr being the primary oxidant present [33, 126]. However, based on the relative rate constants of the oxidants with Tyr, and relative to other targets, 3-Br-Tyr would be a more favourable product than 3-Cl-Tyr, which may make interpretation of relative oxidant levels based off relative halogenated Tyr residues more difficult [60, 61]. Tyr does not react directly with HOSCN, though the LPO/H_2O_2/SCN^- system can oxidise Tyr residues, it is thought to be mediated by the formation of thiocyanogen, $(SCN)_2$ or require the presence of LPO [127]. It should be noted the formation of these chlorinated and brominated products may also be mediated by the formation of Cl_2 and Br_2 [36, 64], though these halogen species are only formed at low pH, and are unfavourable under physiological conditions [66].

HOCl reacts with Trp with a second order rate constant of 7.8 x 10^3 [60] and can form a number of different products [128, 129]. Reaction of Trp with excess HOCl gives rise to products with chlorinated aromatic groups [128]. In the presence of TEMPO, a stable nitroxide capable of rapidly scavenging free radical species, a different chlorinated epoxide product formed at the amino acid, suggesting that radical interactions are important in the oxidation of Trp by HOCl [128]. Oxidation of Trp residues in peptides by HOCl gives rise to hydroxytryptophan and oxyindolyalanine products [94, 130]. Alternatively, the reaction can produce

kynurenine and *N*-formylkynurenine *via* reaction of nitrogen-centred radicals produced by *N*-chloramine formation and subsequent decomposition [131]. These reactions are protein structure dependent and Trp residues adjacent to Gly residues can be oxidised to a cyclic Trp-Gly species [130]. HOSCN is also capable of oxidising Trp to yield oxyindolamine products [132], though these reactions are favoured at low pH and therefore may have limited biological relevance [133].

HOCl also reacts with His residues, with the major product being the formation of *N*-chloramines on the imidazole ring [60]. These *N*-chloramines are more reactive than those formed at the α-amino acid group, and capable of mediating transchlorination reactions [134-136]. It has also been suggested that the formation of 2-oxohistidine may occur with HOCl treatment [137].

1.3.4 Amides

Similar to the reaction with amines (Sections 1.2.5 and 1.3.2), HOCl can react with amides to form *N*-chloramides, though these reactions are much slower with rate constants in the range of < 10^2 [60, 138]. HOBr can also react with amides to form *N*-bromamides and this reaction is faster than that reported for HOCl at 1 x 10^3 M^{-1} s^{-1} for the reaction with protein backbone amide groups [61]. *N*-Chloramides are capable of transferring chlorine and oxidising other substrates such as nicotinamide adenine dinucelotide (NADH), though this reaction is slow with rate constants <10^2 M^{-1} s^{-1} and dependent on *N*-chloramide structure [138, 139]. In the presence of water, *N*-chloramides can undergo hydrolysis, which results in the cleavage of the amide bond [56]. One potential mechanism involves formation of a nitrogen-centred radical followed by hydrogen abstraction [140-144]. Protein backbone fragmentation can be prevented by the presence of radical scavenging antioxidants such as Trolox, ascorbate and GSH, indicating radical processes are occurring [145].

1.3.5 Lipids

In addition to protein targets, HOCl can react with the unsaturated fatty acid side chains of lipids, forming halohydrins [9, 119, 146]. The second order rate constants for these reactions are in the range of 5 – 50 M^{-1} s^{-1} in aqueous solutions [63, 147]. However, kinetic studies have shown that the rate constant for lipids contained in liposome cores *in vivo* to be considerably (up to 10-fold) slower [148]. This is

attributed to the limited ability of HOCl to diffuse into the lipid environments. HOCl has been shown to react with cholesterol, forming halohydrin isomers, which can then undergo dehydrohalogenation reactions to form epoxides [119, 149, 150].

Plasmalogens are glycerophosphospholipids characterised by a vinyl ether group at the sn-1 position, and represent up to 15 – 20% of total phospholipid in the body. HOCl and HOBr react with plasmalogens, with the primary target of the reaction being the vinyl-ether bond [151-153]. HOCl reacts more slowly compared to HOBr, with rate constants for the HOCl and HOBr reaction with a model vinyl-ether being 1.6 x 10^3 and 3.5 x 10^6 M^{-1} s^{-1} [151]. The reaction with HOCl cleaves the vinyl ether bond, and the products of the reaction depend on the fatty acid bound to the plasmalogen. Low levels of HOCl react with oleic fatty acids to yield chloro fatty aldehydes [152, 154, 155], with higher concentrations yielding chlorohydrin products [152]. Glycerophosphocholine products are formed upon reaction of HOCl with fatty acids with higher levels of unsaturation, [152, 153].

Reaction of HOCl with amine-containing phospholipid head groups results in the formation of *N*-chloramines [147]. Phosphatidyl-ethanolamine and phosphatidyl-serine react with HOCl with second-order rate constants of 1.8 x 10^4 $M^{-1}s^{-1}$ and 3.3 x 10^4 $M^{-1}s^{-1}$ [147]. In contrast, *N*-chloramine formation on the quarternary ammonium group of phosphatidyl-choline head groups is significantly slower at 0.018 $M^{-1}s^{-1}$ [147]. HOBr also reacts with phospholipids, though faster than HOCl with rate constants of ca. 10^6 M^{-1} s^{-1} [156]. HOSCN has limited reactivity with lipids, though it has been shown that HOSCN and the MPO/H_2O_2/SCN^- system can promote the formation of lipid peroxides upon exposure to low-density lipoproteins [157, 158].

1.3.6 RNA and DNA

HOCl can react with DNA and RNA bases and form *N*-chloramines through reaction with amine groups, or react with the aromatic ring to form chlorinated products. The predominant reaction is believed to be the formation of *N*-chloramines [55, 159-161]. The second order rates for monomeric endocyclic amines (thymidine, uridine and guanosine monophosphates) range from 10^3 – 10^4 $M^{-1}s^{-1}$ [62, 63] and between 10^1 and 10^2 $M^{-1}s^{-1}$ [62, 63] for monomeric exocylic amines (adenosine and cytidine monophosphates). The *N*-chloramines formed are capable of oxidising GSH, NADH, free amino acids and peptide bonds [63], with rates

10-100 times slower than HOCl itself. The reaction of HOCl with polymeric bases, such as in DNA, is considerably slower ($\sim$10 $M^{-1}s^{-1}$), and is attributed to base pairing protecting amine sites from HOCl oxidation, with heat denatured DNA reacts $\sim$10 times faster than native DNA [63].

Alternatively, HOCl and *N*-chloramines are capable of chlorinating DNA and RNA components with adenine, guanine and cytosine being major targets [162]. 5-chloro-2'-deoxycytidine, 8-chloro-2'-deoxyadenosine and 8-chloro-2'-deoxyguanosine are formed as *in vitro* products of these reactions, and 5-chloro-2'-deoxycytidine has also been detected when cells are exposed to HOCl [162]. These products can also be formed by the degradation of *N*-chloramines formed on DNA bases [55, 163, 164]. HOCl is also capable of oxidising nucleosides to form other products including 5-hydroxy-cytosine, 5-hydroxy-uracil, and hypoxanthine [165, 166]. HOBr is also capable of similar reaction, with exposure of guanine forming various oxy-guanine products as well as 8-bromoguanine [167]. In contrast, HOSCN has no reported reactivity with DNA [168].

1.3.7 Carbohydrates

HOCl reacts with the carbohydrates hyaluronan and glucosamine sugars at the amine site forming *N*-chloramines [169]. Amines are the primary target of HOCl, with substitution of the N decreasing reactivity [169]. HOCl reacts with amine and amide moieties of heparan sulfate, forming products including *N*-monochloramines, *N*-dichloramines, *N*-chlorosulfonamides, and *N*-chloramides [170-172], though the rate constants for these reaction are significantly slower (< 1 M^{-1} s^{-1}) than those other chlorination reactions [173]. *N*-Monochloramines can decompose with no significant modifications to structure, but *N*-dichloramines and *N*-chlorosulfonamides can cause strand breakage via radical mechanisms [172]. *N*-Chloramides formed on hyaluronan and chondrotin sulfate chains cause fragmentation when exposed to radicals [170, 174, 175]. These reactions may be of particular relevance in arthritis, where oxidation of proteoglycans leads to degradation of cartilage [176, 177], and in atherosclerosis, where degradation of the matrix proteins in the arterial wall may contribute to the development of the disease [178].

1.3.8 *N*-Chloramines

N-Chloramines undergo transchlorination reactions [134, 179, 180], demonstrated by the equilibrium between Tau, Gly and His *N*-chloramines [135]. As *N*-chloramines, particularly β-*N*-chloramines such as TauCl, are less reactive than HOCl, it has been hypothesised that *N*-chloramines may be able to propagate oxidative damage away from the source of HOCl, by travelling further before decomposition or further reaction [181]. Transfer of chlorine to imidazole or N-acetylhistidine from monochloroamine allowed for chlorination of Tyr to occur via the more reactive imidazole chloramine (ImdCl) [182]. Alternatively, *N*-chloramines can undergo chlorine transfer or decomposition to radicals, transferring the damage to different sites [141].

Degradation of *N*-chloramines can occur in two ways, forming aldehydes or nitrogen-centred radicals (Figure 1.4) [86]. Aldehyde formation occurs when the *N*-chloramine bond forms an imine intermediate (Figure 1.4), which is then hydrolysed to yield an aldehyde [183, 184]. These aldehyde products can form by degradation of *N*-chloramines formed on either free amino acids, such as Tau [183, 184], peptides such as GSH [185], or on protein residues, as in low-density lipoprotein (LDL) [186, 187]. The resulting aldehydes can form advanced glycation end products, typically associated with diabetes and cardiovascular disease, via Schiff base imine intermediates [188].

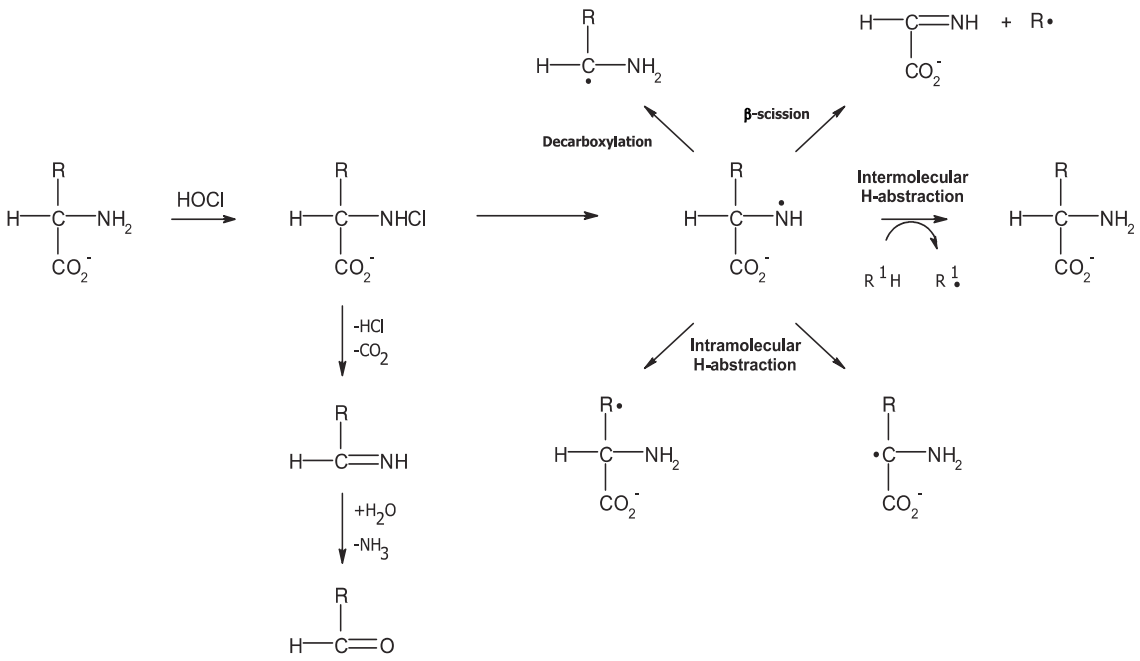

Figure 1.4 - Reaction scheme of degradation of *N*-chloramines to form aldehyde and Schiff bases and nitrogen centred radicals and subsequent products – taken from [137]

Alternatively, one-electron reduction of the *N*-chloramine can occur, resulting in the formation of nitrogen-centred radicals (Figure 1.4) [145, 189, 190]. The radicals form in a time dependent manner through thermal decomposition, though can be accelerated in the presence of one-electron reductants, such as metal ions Cu^{+} and Fe^{2+} [190]. These radicals can then undergo a range of intra and intermolecular reactions [145, 189]. In the case of proteins, hydrogen abstraction from the backbone carbon yields carbon-centred radicals, which can then cause protein cleavage [145, 189]. This cleavage can be inhibited by the presence of radical scavengers such as Trolox, GSH and ascorbate [145], which rapidly react with the nitrogen-centred radical [191].

N-chloramines retain the oxidising power of HOCl, though the rates of reaction are significantly decreased [136, 192]. *N*-chloramines have been shown to be capable of oxidising thiols and thioether groups, including Cys and Met residues and GSH [86, 136, 192]. Analogous to HOCl reactions, oxidation of thiols such as GSH primarily yields disulfides [136, 192]. Oxidation of Met by *N*-chloramines results in the formation of MetSO [192]. The rate constants for these reactions depend on the amino acid on which the *N*-chloramine is formed, particularly with side chain N-

chloramines. *N*-chloramine formed on the imidazole ring of His (HisCl) react with sulfur residues with rate constants of 721 and 91 M^{-1} s^{-1} for GSH and Met respectively [136]. *N*-chloramines formed on the amine groups of Gly (GlyCl) and Tau, and those formed on the side chain amine of Lys (LysCl), are significantly less reactive than HisCl, with rate constants for the reaction with the thiol species Cys and GSH in the range of 1 – 2 x 10^2 M^{-1} s^{-1} [192]. Similarly, the reaction of these *N*-chloramines with Met is also decreased in comparison to HOCl and HisCl with rate constants in the range of 0.4 – 2 x 10^2 M^{-1} s^{-1} [192].

Table 1.4 – Second order rate constants for the reaction of hypohalous acids and *N*-chloramines with Cys, GSH and Met.

	Second order rate constants / M^{-1} s^{-1}						
Compound	HOCl[a]	HOBr	HOSCN[b]	HisCl[c]	GlyCl[d]	LysCl[d]	TauCl[d]
Cys	3.6 x 10^8	1.2 x 10^7 [e]	7.8 x 10^4	9.1 x 10^2	3.5 x 10^2	4.8 x 10^2	2.1 x 10^2
GSH	1.2 x 10^8		2.5 x 10^4	7.2 x 10^2	2.3 x 10^2	2.6 x 10^2	1.2 x 10^2
Met	3.4 x 10^7	3.6 x 10^6 [f]	Slow	91	2.1 x 10^2	53	39

[a][90]; [b][92]; [d][136]; [e][192]; [e][61]; [f][61] rate constant determined for *N*Ac-Met-OMe

1.4 Cell and tissue damage

MPO and the oxidants it produces have been demonstrated to be detrimental to the cellular environment and play a role in the initiation and progression of numerous diseases [2]. This Thesis focuses on damage caused by HOCl and *N*-chloramines, as HOCl-induced damage has been thoroughly characterised and *N*-chloramineshave the capacity to propagate HOCl-induced damage away from inflammation sites. However, the role of other MPO-derived oxidants, particularly HOSCN, should not be discounted in MPO related pathologies, as while the reactivity of this oxidant is less than and more specific compared to HOCl, damage induced by HOSCN may also play a role in disease [193]. The biological effects of HOSCN have been reviewed recently, with particular focus on the differences in reactivity and the extent of damage between HOSCN and HOCl [88, 89].

1.4.1 Beneficial effects

MPO-derived oxidants are generally believed to be important species in neutrophil-mediated bacterial cell killing. MPO knockout mice have been shown to be more susceptible to infections [194, 195], and neutrophils from MPO-deficient people kill some types of bacteria poorly [196]. Furthermore, the introduction of

MPO inhibitors, such as azides, impair the ability of the cells to kill bacteria effectively *in vitro* [197]. This supports MPO-derived oxidants as an important source of antimicrobial activity.

HOCl is proposed to be the major lethal oxidant produced by MPO [198, 199], however roles for the other oxidants, particularly HOSCN cannot be excluded. EPO has been shown to be effective at killing bacteria in the presence of H_2O_2 and Br^- or SCN^- ions [200, 201], indicating that the HOBr and HOSCN produced by this enzyme could play a role in pathogen killing. Secondary oxidants, including *N*-chloramines, may also play significant role as microbicidal agents, with the high flux of HOCl [17], and kinetic predictions that demonstrate the majority of HOCl produced will react with cellular constiuents [198]. TauCl, which is produced at high levels after neutrophil activation, has the capacity to kill numerous bacterial strains and viruses [202-205]. It achieves this by penetrating into the pathogen cytosol and oxidising proteins and thiols [202, 203].

TauCl can prevent host cell damage by multiple pathways, including by the inhibition of $O_2^{\bullet-}$ production by activated neutrophils [206-210]. TauCl can prevent the phosphorylation of $p47^{phox}$ and subsequent translocation to the membrane, preventing the formation of NADPH oxidase machinery and hence $O_2^{\bullet-}$ production [210]. This has been postulated as a mechanism to prevent neutrophils from self-imposed cellular damage due to excessive oxidant production.

1.4.2 Detrimental effects

1.4.2.1 Damage in the cellular environment

HOCl is toxic to cells. Reagent HOCl can kill a number of cell types including red blood cells (from concentrations of 100 nmol HOCl per 10^6 cells) [211-213], endothelial cells (from 25 nmol per 10^6 cells) [214], epithelial cells (from 500 nmol per 10^6 cells) [215, 216], fibroblasts (from 5 μmol per 10^6 cells) [217] and T-cell lines (from 1.5 μmol per 10^6 cells) [218]. Multiple mechanisms have been suggested to be responsible including pore formation due to surface protein crosslinking [219], and inactivation of potassium channels, possibly caused by thiol inactivation [220]. Treatment of cells with lower concentrations induces apoptosis (< 50 nmol per 10^6 cells), though with increasing concentrations of HOCl (> 1 μmol per 10^6

cells), necrosis and cell lysis dominates the cell death pathways [221, 222]. However, in many cases the specific pathways have not been fully defined. *N*-chloramines have also been shown to induce apoptosis via activation of caspases [223] and cause cell death [136, 224].

Treatment of cells with sub-lytic concentrations of HOCl induces the oxidation of thiols and as HOCl reacts very quickly with the thiol components of cells, it is likely that thiols are major targets. Cells exposed to HOCl have decreased levels of GSH and protein thiols [225, 226]. Treatment of human vein endothelial cells (HUVECs) with HOCl showed increases in glutathione sulfonamide, with limited disulfide products being detected [227]. Rapid consumption of GSH has also been observed in human coronary artery endothelial cells (HCAECs) [221] and human monocyte derived macrophages (HMDMs) [228].

Protein oxidation of thiols in cells may lead to enzyme inactivation and have further detrimental consequences for the cell. Cells treated with sub-lethal amounts of HOCl show modifications on a number of proteins including glyceraldehyde-3-phosphate dehydrogenase (GAPDH) and numerous enzymes involved in protein folding [221, 222, 225, 229]. GAPDH has been shown to be preferentially oxidised compared to GSH on exposure of cells to HOCl [225]. The primary function of GAPDH is to catalyse the sixth step of glycolysis, though it is also involved in a number of other cellular processes [230]. For example, GAPDH is involved in apoptosis, and when exposed to oxidants, becomes nitrosylated and binds to DNA and Siah1 leading to apoptosis pathway activation [231, 232]. GAPDH inactivation by HOCl can lead to ATP depletion in cells, though HOCl can affect energy production in multiple ways, including inhibition of mitochondrial respiration or glucose transport [220, 233]. ATP levels are decreased when cells are treated with sub-lethal concentrations of HOCl [215, 220, 225, 234]. HOCl can also react directly with ATP [63].

Peptidylprolyl isomerase A (cyclophilin A) and protein disulfide isomerase are affected by HOCl treatment of endothelial cells [229]. Peptidylprolyl isomerase A and protein disulfide isomerase are enzymes involved in protein folding [235, 236] and inactivation of enzymes related to protein folding could potentially lead to the accumulation of misfolded proteins within cells. This is significant as it may

trigger detrimental signalling cascades, for example, the unfolded protein response, which ultimately leads to apoptosis of the cell [237].

HOCl treatment can also perturb phosphorylation via inactivation of protein tyrosine phosphates (PTPs) [238], and cause disruption of sulfur-metal ion clusters, leading to inactivation or changes in function of enzymes [239-243]. Treatment of enzymes containing thiol-zinc finger motifs causes the release and mobilisation of zinc from these enzymes [239-241]. Exposure of aconitase, an enzyme containing an iron-sulfur cluster, to HOCl induced a release of iron and inhibition of function, from both isolated aconitase and when HCAECs were treated with HOCl [244]. Inducible nitric oxide synthase (iNOS) and endothelial nitric oxide synthase (eNOS), both containing sulfur-metal clusters, when coupled produce $NO^{\bullet}$, but when treated with HOCl, they uncouple resulting in production of $O_2^{\bullet-}$ [242, 243], thereby increasing cellular oxidative stress. Exposure of HCAECs demonstrated an uncoupling of eNOS, with subsequent inhibiton of $NO^{\bullet}$ formation [243].

N-Chloramines have similar potential to oxidise intracellular thiols upon exposure to cells. Exposure of cells to *N*-chloramines causes a consumption of intracellular thiols and GSH [136, 229]. GAPDH, peptidylprolyl isomerase A and protein disulfide isomerase are also targeted by monochloramine (NH_2Cl), GlyCl and HisCl treatment to endothelial cells [229]. While TauCl is a more potent inhibitor of GAPDH and creatine kinase in isolated enzymes studies [245], its inability to cross the cell membrane means that it cannot inactivate intracellular GAPDH [135]. Hence, the ability for *N*-chloramines to oxidise intracellular thiols is dependent upon structure and the potential for these species to cross the cell barrier. However, transchlorination reactions can occur [135, 179], transferring the *N*-chloramine group from amines unable to cross the cell membrane, such as TauCl, to more cell permeable molecules, such as GlyCl, which can then induce oxidative damage in the cytosol [135].

While TauCl is relatively impermeable to the cell membrane, studies have demonstrated the ability to regulate signalling pathways by acting on receptors outside the cell [246]. TauCl can influence the nuclear factor κB (NF-κB) pathways of pro-imflammatory mediators. NF-κB is bound by inhibitor κB (IκB) keeping it in the cytoplasm [247]. When stimulated, IκB becomes phosphorylated by IκB kinase

(IKK) and subsequently ubiquitinated and degraded, releasing NF-κB which translocates to the nucleus and upregulates proinflammatory mediators including iNOS, tissue necrosis factor α (TNF-α) and cyclooxygenase-2 (COX-2) [247]. TauCl inhibits NF-κB translocation to the nucleus, though the exact mechanism in unclear [248, 249]. One study suggests that TauCl inhibits IKK, preventing IκB phosphorylation [250]. Another study demonstrated oxidation of a Met residue on IκB by TauCl, though phosphorylation of serine residues was not inhibited [251]. Others demonstrated a reduced DNA binding affinity of NF-κB suggested to be caused by the inactivation of the extracellular signal-regulated kinase (ERK) pathway [251, 252].

TauCl has been shown to increase nuclear translocation of nuclear response factor 2 (Nrf2). Nrf2 is bound in the cytoplasm by the protein Keap-1, which when oxidised releases Nrf2 for translocation to the nucleus [253], where Nrf2 binds to antioxidant response elements and upregulates genes including heme oxygenase-1 (HO-1), NADPH:quinone oxidoreductase (NQO-1), glutathione peroxidase (GPx), peroxiredoxin (Prx), and Trx [254]. TauCl induced a rapid increase in Nrf2 translocation to the nucleus as well as an increase in cytosolic levels of Nrf2 [255, 256]. Consequently, increases in heme oxygenase 1 (HO-1) protein and activity levels were observed with TauCl treatment of cells [255-257]. Pretreatment of cells with TauCl lead to inhibition of cell death by H_2O_2 [256, 258] and this has been attributed to the effects of TauCl on Nrf-2 activation.

1.4.2.2 MPO in inflammatory pathologies

HOCl-induced damage to tissue can lead to cellular dysfunction, and hence promote disease. MPO and MPO-derived oxidant damage is implicated in numerous inflammatory conditions. For example, elevated levels of MPO are found in disease samples from patients with cystic fibrosis [259-261], Parkinson's disease [262], multiple sclerosis [263], and Alzheimer's disease [264-266]. Increases in MPO levels are accompanied with biomarkers of HOCl-induced damage including elevated levels of 3-Cl-Tyr residues [259] and glutathione sulfonamide [267] in the sputum of cystic fibrosis patients; elevated 3-Cl-Tyr in the brain tissue of patients with Alzheimer's disease [264, 268], Parkinson's disease [269] and multiple sclerosis

[263, 270]. MPO and MPO-oxidant damage is also closely correlated in chronic kidney disease [271] and rheumatoid arthritis [272].

In addition, the role of MPO and HOCl-induced oxidative damage in relation to cardiovascular disease (CVD) and atherosclerosis has been extensively documented. This is of significance as cardiovascular disease is the leading cause of death in Australia being the cause of about 30 % of deaths in Australian population [273]. As MPO plays a significant role in the development of atherosclerosis, which is a major cause of CVD, its contribution to this disease is reviewed in more detail below.

1.4.3 MPO and atherosclerosis

Atherosclerosis is an inflammatory disease characterised by the development of fatty streaks in the arterial wall, caused by the accumulation and deposition of lipid-laden macrophages (or foam cells) [274]. As the lesions develop, more foam cells accumulate leading to plaque formation, characterised by a fibrous cap with a necrotic cell core [274]. MPO has been detected in all stages of atherosclerosis lesion development [275], indicating a significant role for MPO in the progression of the disease. Numerous markers of MPO-induced oxidative damage have been detected in lesions including p-hydroxyphenylacetaldehyde, α-chloro fatty aldehydes, unsaturated lysophosphatidylcholine, 3-Cl-Tyr and 5-chloro-uracil [155, 276, 277]. Binding of antibodies raised against HOCl-damaged proteins (HOP-1) correlate with progression of disease, further implicating MPO as a factor in the progression of the disease [278].

Circulating MPO levels are an independent predictor for presence of coronary artery disease with relative plasma concentrations of MPO correlated with severity of the disease [279, 280]. In healthy subjects, MPO levels increase the risk of cardiovascular disease, though levels could not predict a cardiovascular event [281-284]. However, MPO levels can predict the incidence of cardiovascular events in patients with established coronary artery disease [285-287], and MPO have prognostic value for patients presenting with chest pain, with MPO levels a risk factor for major cardiovascular events in these patients [288]. Higher than median levels of MPO demonstrated a higher all cause mortality in patients who were hospitalised after their first myocardial infarction [289]. It should be noted,

however, that MPO deficient atherosclerotic mice (ApoE or LDL receptor knockout mice) have demonstrated an increase in atherosclerosis [290]. However, in the non-MPO deficient mice, limited levels of MPO derived biomarkers such as 3-Cl-Tyr are observed, suggesting a limited role for MPO in murine atherosclerosis [290]. Mice which express human MPO demonstrate a significant increase in lesion size, suggesting that the species difference in MPO may be a significant factor [291].

Foam cells form when macrophages take up oxidised lipoproteins in an uncontrolled manner via interaction with scavenger receptors [274]. An $MPO/H_2O_2/Cl^-$ system and reagent HOCl have been shown to oxidize LDL [292, 293]. This oxidised LDL is more readily taken up by macrophages [294] and impairs cholesterol efflux [295] leading to lipid accumulation and foam cell formation. As levels of 3Cl-Tyr are elevated in LDL found in the arterial wall compared to that found in circulating LDL, it is suggested that MPO-induced LDL oxidation is occurring within the arterial wall [296].

HOCl is also capable of oxidising high-density lipoprotein (HDL) resulting in impaired cholesterol efflux ability [297-301]. The apolipoprotein A-I (apoA-I) protein residues are the primary target for HOCl, and there is evidence for oxidation of Tyr, Trp and Met residues [124, 298, 302-306]. Loss of Trp residues reduces the efflux capacity of HDL [302], and recent data are consistent with the Trp72 residue being oxidised by HOCl [303]. Oxidised Trp residues are elevated in atherosclerotic lesion, and correlate with increased risk of cardiovascular disease [303]. Selective oxidation of the Tyr192 residue of apoA-I is also correlated with impaired cholesterol efflux capacity [304], and oxidation of Tyr residues can be mediated by a LysCl intermediate [124]. Elevated levels of 3Cl-Tyr and 3-nitro-Tyr are also found on HDL of patients with atherosclerosis, compared to healthy subjects, suggesting that Tyr oxidation may also play a role [124, 298, 305, 307]. In addition to Tyr and Trp, Met residues are oxidised by HOCl, reducing the efflux capacity [306, 307]. Furthermore, HOCl exposure to HDL reduces its anti-inflammatory properties by reducing the ability to inhibit pro-inflammatory pathways [308, 309], and causes the activation NF-κB pathways suggesting HOCl exposure transforms HDL to a more pro-inflammatory mediator [309].

Endothelial dysfunction is also considered to be a contributing factor to the initiation of atherosclerosis and cardiovascular disease, with endothelial function closely related to $NO^{\bullet}$ bioavailability [310]. MPO is capable of binding to endothelial cells through interactions with the negatively charged glycosaminoglycans and is localized to the caveolae [311-313]. The binding of MPO is increased in the presence of albumin [312]. Internalisation of the caveloae allows for transcytosis of MPO, which is dependent on the albumin binding receptor, to the basement membrane where MPO is then localized with fibronectin [311, 312, 314]. The localization of MPO to endothelial thus allows for the modulation of $NO^{\cdot}$ availability and contributes to endothelial dysfunction.

MPO has been suggested to induce endothelial dysfunction by the production of HOCl, which uncouples eNOS and iNOS, hence perturbing $NO^{\bullet}$ production. In both isolated enzymes studies and upon treatment of HCAECs, HOCl is reported to convert these enzymes from the generation of $NO^{\bullet}$ to the production of $O_2^{\bullet-}$ [242, 243]. MPO further reduces $NO^{\bullet}$ availability by consuming it as a substrate [29, 52]. Moreover, HOCl treatment of guinea pig hearts [315] or arterial rings from rats [316] or rabbits [317] inhibits the acetylcholine-dependent relaxation of arterial rings. VPO, a peroxidase which produces HOCl, is elevated in spontaneously hypertensive rats, which exhibit decreased NO availability and lowered response to vasodilators, further implicating HOCl in endothelial dysfunction [318].

Atherosclerotic plaque rupture and the resulting thrombosis is the underlying cause of the majority of heart attacks and stroke [319]. MPO may play a role in plaque rupture as MPO levels predict infarction risk [288, 320]. Similarly, systemic MPO levels are elevated in patients with eroded plaques [321], and monocytes and MPO levels are elevated in patients with ruptured plaques [322]. MPO and HOCl-damaged proteins colocalise in the lesions of patients who have experienced sudden cardiac death [323]. Furthermore, HOCl has been shown to induce apoptosis of endothelial cells leading to destabilised plaques [324]. MPO release is also thought to activate metalloproteins through oxidation of a “cysteine switch” [325], which could further destabilise the plaque [326].

1.5 Prevention of MPO damage

As MPO is a contributing factor to a number of pathologies, particularly atherosclerosis, there is considerable interest in the development of therapeutic strategies to prevent damage caused by the inappropriate production of oxidants.

1.5.1 Inhibition of MPO

A major limiting factor in hypohalous acid production by MPO is the availability of H_2O_2 to form Compound I. The concentration of available H_2O_2 is primarily dependent on the presence of enzymes, such as GPx, catalase and Prxs, which compete with peroxidases for H_2O_2 [2]. Inhibition of NADPH oxidases, which produce $O_2^{\bullet-}$, and hence H_2O_2 by dismutation, can also limit H_2O_2 concentrations [327]. A common inhibitor of NADPH oxidases is diphenylene iodonium chloride, which prevents the production of $O_2^{\bullet-}$ in neutrophils, reducing their effectiveness in bacteria cell killing [328, 329].

Many agents can inhibit MPO, LPO and EPO in a non-specific manner [330]. Heme poisons, such as cyanide and suicide substrates such as hydrazines and hydrazides, can very effectively inhibit peroxidases by heme destruction [330]. However, due to their toxicity and lack of specificity, they are not appropriate for MPO inhibition in a therapeutic setting.

As heme poisons have high toxicity, there has been interest in development of more specific MPO inhibitors. Novel 2-thioxanthine compounds have recently been developed, which have demonstrated ability to inhibit HOCl formation by MPO by initially reacting with Compound I, forming a radical that then covalently binds to the heme group of MPO causing inactivation [331]. Hydrogen sulfide can reversibly bind to the iron in the heme group of MPO at physiological levels, reducing H_2O_2 consumption by MPO [332]. Hydroxymates have been shown to be specific toward MPO in neutrophils, and reversibly bind to the active site cavity of MPO, inhibiting access to the heme moiety inhibiting MPO activity [333]. Ceruloplasmin is capable of binding MPO in serum and reducing it from Compound I to Compound II [334]. The presence of ceruloplasmin has been suggested to inhibit the recovery of the native MPO, keeping as in the Compound II form, inhibiting the production of HOCl [334]. However, another study suggested that the binding of ceruloplasmin may not

be completely inhibiting the halogenation cycle, instead the binding promotes the formation of HOSCN instead of HOCl [335].

Hypohalous acid production by peroxidases can be competitively inhibited by other substrates that react readily with Compounds I and II [336, 337], though this is limited by the necessity for high concentrations of substrate to effectively compete with the halogenation cycle. Acetominophen has been shown to inhibit total oxidant production by MPO, at plasma levels achieved using typical therapeutic doses of the drug [20, 338, 339]. However the initial rate of HOCl production was enhanced, due to the recycling of Compounds II and III [20].

Nitroxides have been shown to prevent oxidative damage by acting as effective radical scavengers [340, 341]. However, they can also act as substrates for MPO, leading to accumulation of Compound II [340]. While Compound II can be recycled by $O_2^{\bullet-}$ nitroxides can act as SOD mimetics diminishing recycling capacity [340]. Nitroxides, particularly 4-amino-2,2,6,6-tetramethylpiperidin-1-yloxyl, are capable of preventing Met oxidation by MPO/H_2O_2/Cl^- systems, using both purified MPO and activated neutrophils [342], however nitroxides can be rapidly reduced by biological reductants [339]. Substitution with longer alkyl chains protect the nitroxide from reduction, allowing more effective inhibition of MPO [339].

Poor peroxidase substrates can inhibit the production of hypohalous acids at low physiological concentrations by trapping the enzyme as Compound II. Trp is one such substrate, which is readily oxidised by Compound I, though reacts very slowly with Compound II [15]. This results in accumulation of Compound II, and hence inhibition of HOCl production [343]. However, in the presence of $O_2^{\bullet-}$, Compound II is recycled quickly, resulting in poor inhibition [43, 336]. Extracellularly, SOD may be able to counter this, but as SOD levels intracellularly are low, SOD may be unable to effectively remove the $O_2^{\bullet-}$ to inhibit MPO turnover [2]. Substrates such as hydroquinone [344] and amascrine [345] can stimulate the production of Compound III, inhibiting the halogenation cycle, but Compound III is also recycled effectively by $O_2^{\bullet-}$ [38].

MPO inhibition may lead to a decrease in oxidation damage, and prevention or inhibition of disease, however, the enzyme is important in the immune system for the role it plays in killing invading pathogens and preventing infection [194, 195].

An alternative method for preventing MPO-related damage may be to remove excess oxidant from the sites of inflammation before the damage can occur.

1.5.2 Endogenous antioxidant enzyme systems

Within cells, there are numerous enzymatic systems that control redox homeostasis, with many containing redox active Cys or Sec sites. A number of these systems scavenge oxidants, including MPO-derived species, before they can cause major detrimental effects on cells. These include GPx, the Trx system and Prxs [98, 101, 346-350]. Other enzymes can reverse oxidative damage caused by cells by reducing the oxidised products. Examples of these are methionine sulfoxide reductase (Msr) [351-355], which reduce MetSO residues, and glutathione reductase (GSR), glutaredoxin and Trx, which are all capable of reducing disulfides [356-360].

1.5.3 SOD and catalase

SOD and catalase are metalloproteins responsible for the removal of $O_2^{\bullet-}$ and H_2O_2 respectively. SODs contain a reactive metal centre, either Cu or Mn, which catalyses the dismutation of $O_2^{\bullet-}$ to form H_2O_2 [361-363]. While H_2O_2 is still an oxidant capable of damaging cellular components, it is significantly less reactive compared to $O_2^{\bullet-}$, and so this is considered to be beneficial. Catalase contains 4 heme centres and removes H_2O_2 via two stages, the first is an initial reaction with one equivalent of H_2O_2 to form an oxyferryl heme, followed by a second reaction with H_2O_2 to produce O_2 and the native catalase [364-367]. Together, they may work to keep the relative level of reactive oxidants in the cell at a manageable level.

1.5.4 Glutathione peroxidase

GPxs were the first identified seleno enzyme, having a selenocysteine at the active site [368]. They play an important regulatory role in the redox state of cells [369]. GPx enzymes are capable of reducing H_2O_2 and other peroxides in a catalytic cycle (Figure 1.5) [346]. The mechanism involves oxidation of the selenol active site to a selenenic acid by peroxides [370], which in turn is reduced by two GSH molecules via a selenosulfide intermediate, with the products being the reduced enzyme and GSSG [346]. The removal of H_2O_2 from the cellular environment by such mechanisms limits the capacity for MPO to produce HOCl and other oxidants.

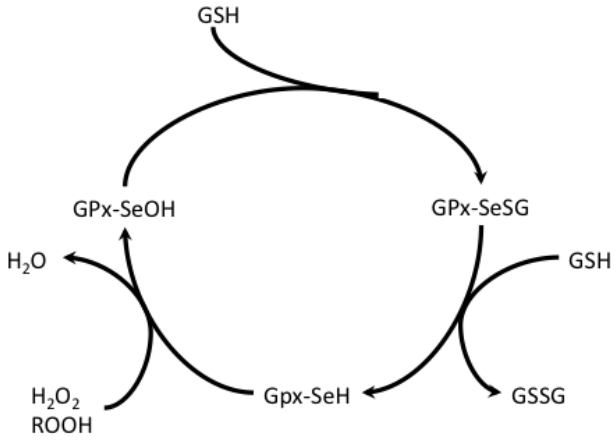

Figure 1.5 - Catalytic cycle of GPx – adapted from [370]

1.5.5 Thioredoxin reductase and thioredoxin

Thioredoxin reductases (TrxR) are dimeric selenoenzymes containing redox active selenocysteines at the active site [371, 372]. TrxRs show direct antioxidant activity through reaction with a wide range of oxidative substrates including H_2O_2, ONOOH and HOSCN, with TrxR being subsequently reduced by NADPH [98, 347, 348]. This system is essential to cells, and lack of it is embryonically lethal [373-375]. The effectiveness of the TrxR system is due to the presence of selenium-containing amino acids at the active site. Loss of the Sec residue reduces the capacity of the enzymes to act as antioxidants [376-379], with substitution of Sec with Cys significantly reducing the catalytic potential of TrxR [379, 380].

Trxs are small proteins that are capable of reducing disulfide bonds in the cell with the activity arising from the presence of redox active Cys residues at the active site (Figure 1.6)[356, 357]. The active site typically consists of a Trp-Cys-Gly-Pro-Cys motif [381]. In its reduced form, the active site consists of two thiols. When in the presence of a protein disulfide, the protein is reduced, and the Cys residues of the Trx active site form a disulfide bond. This occurs through a mixed disulfide intermediate [381, 382].

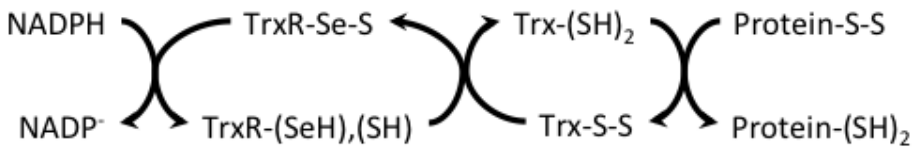

Figure 1.6 - The Trx catalytic system – adapted from [356]

Oxidised Trx is reduced to its active form by TrxR. Mice overexpressing Trx are more resistant to oxidative stress and have a greater life span than wild type mice [383]. Trx is found in higher concentrations in the plasma of people with diseases linked to increased oxidative stress including human immunodeficiency virus, hepatitis C virus and some cancers [384-389]. This enzyme plays essential roles in the reduction of oxidative species, as well as reducing other important enzymes such as the peroxiredoxins, glutathione reductases and methionine reductases (Figure 1.7) [390, 391]. The Trx system is also capable of removing nitrosyl modifications from proteins, though its oxidised form is capable of nitrosylating proteins [392].

Trx play significant roles in signalling pathways involved in the response to a variety of stresses including virus infection, UV-irradiation, H_2O_2 and ischemia-reperfusion injury [393-396]. Reduced Trx inhibits apoptosis through interactions with apoptosis signal-regulating kinase (ASK) [397]. Trx can also promote the DNA binding capabilities of NF-κB via a direct interaction [394]. It enhances DNA binding capabilities of activator protein-1 through interactions with redox factor 1. It also interacts with other cofactors such as hypoxia inducible factor 1 and thioredoxin interacting protein [398]. Hence, Trx plays a role in cell redox status through direct scavenging, reversal of oxidative damage and cell signalling pathways.

1.5.6 Peroxiredoxins

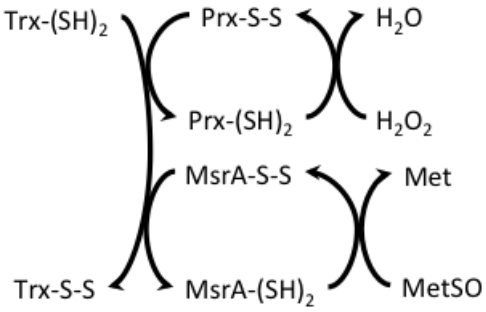

Figure 1.7 – Prx and Msr enzyme systems use the thioredoxin system as electron donors to reduce H_2O_2 and MetSO – adapted from [356]

Prxs are small enzymes that use the Trx system as an electron donor to reduce peroxides [102]. They are capable of detoxifying H_2O_2, ONOOH and other peroxides (Figure 1.7) [101, 349, 350]. The rate constant for the reaction with ONOOH (k = 7 x 10^7 M^{-1} s^{-1}) is 5 times faster than that of GPx [399]. The mechanism of action is

similar to that described for GPx, except that the reactive residue is a Cys, rather than Sec. Prx silencing increases oxidative stress in breast cancer cells [400]. Prx knock out mice develop anemia, have an increased incidence of tumours [401, 402], lower life spans and increased protein oxidation [403]. The loss of Prxs does not appear to be compensated for by increases in other antioxidant enzymes [404]. Thus, Prxs, in conjunction with the Trx system, contribute to antioxidant defense of the cell by maintaining oxidant levels.

Prxs may play a role in H_2O_2 signalling in cells, as H_2O_2 regulates a number of signalling cascades including platelet growth factors and tumor necrosis factors, which can be influenced by Prxs [403, 405-409]. Prxs can be inactivated by hyperoxidation of the active site Cys [103-105], though this only occurs when all factors of the catalytic cycle are present [105]. The inactivation of Prxs is reversible in the presence of sulfiredoxins [105, 410]. The inactivation of Prxs allows for the build-up of H_2O_2 in cell, which can then mediate cell signalling via other pathways [411, 412].

1.5.7 Methionine sulfoxide reductase

Msr are Trx dependent enzymes that repair oxidative damage in cells [413-416]. The Msr family of enzymes reduces methionine sulfoxide back to Met, hence repairing oxidative damage (Figure 1.7). Msrs have either 2 Cys residues or a Sec/Cys pair at the active site and reduce MetSO via a sulfenic acid intermediate, with subsequent formation of an intermolecular disufide bond [351-355]. Msrs is then reduced by the Trx system [417]. However, some isoforms of Msr lack the second resolving Cys and are reduced by a free thiol or seleno group [417-420]. Msrs prefer to reduce oxidised methionine residues on unfolded proteins [413], suggesting a role in reducing the impact of oxidative stress on the protein folding process. Overexpression of Msr reduces oxidative stress levels in cells [414-416]. Msr levels decrease with age [421, 422] and inflammatory diseases such as Alzheimer's disease [423]. Hence, Msrs may play a critical role maintaining cellular function and the redox homeostasis in cells.

1.5.8 Glutathione reductase

GSR is a dimeric flavin-containing enzyme with sub-units of 50 kDa [359, 424, 425]. The primary function of this enzyme is to reduce GSSG to GSH by catalysis of the reaction with NADPH (Figure 1.8) [358-360]. It achieves this by funnelling electrons from NADPH through the FAD domain to the Cys residues present in the GSSG binding site [426]. GSSG is reduced by GSR via disulfide exchange mechanisms with active site Cys residues [427]. This allows for catalytic oxidant scavenging by GSH, where GSH reacts with numerous oxidants to produce GSSG, which can then be reduced by the action of GSR. By maintaining GSH in a reduced state in cells, GSRs play a role in antioxidant defence of cells.

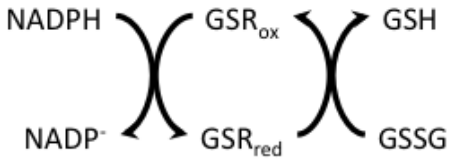

Figure 1.8 – GSR uses NADPH as an electron donor in order to reduce GSSG to GSH – adpated from [427]

1.5.9 Low molecular mass scavengers

In addition to a number of enzymatic oxidant detoxification systems, low molecular mass antioxidants such as ascorbate have been shown to scavenge MPO-derived oxidants and protect cells from oxidative damage [428-430]. Ascorbic acid has been shown to protect Lys and Trp residues of the LDL protein from oxidation by HOCl [429]. Ascorbic acid offers protection of Cys from HOCl and *N*-chloramine oxidation, and displays an ability to reverse *N*-chloramine formation on LDL protein [428, 429]. Ascorbate can also prevent HOCl- and *N*-chloramine induced apoptosis [223, 431, 432], but as thiols are still consumed with ascorbate treatment, this protection may not be due to scavenging of HOCl. However, it has been shown that ascorbate, at levels achieved in plasma in human supplementation studies, is unable to compete kinetically with other targets of HOCl, particularly proteins and amino acids [87].

Low molecular mass thiol compounds are also potent scavengers for MPO-derived oxidants, and are a major target for HOCl and *N*-chloramines in the cellular environment. Cys has been shown to reduce and reverse HOCl oxidative damage to

cells [429] and protect mononuclear leukocytes from inactivation by HOCl [430]. GSH reacts with HOCl and other activated oxygen species to form the oxidised species GSSG or a sulfonamide [433, 434] in a sacrificial manner to protect cell proteins [225]. Differing GSH levels in HMDMs from donors correlate to susceptibility of HOCl-induced toxicity [228]. GSH loss in HOCl-treated red blood cells occurs before loss of protein thiol residues, indicating a protective effect [226] and its presence significantly increases the ability of bacteria to survive treatment with HOCl [435].

Other low molecular mass compounds also demonstrate potential as HOCl scavengers. Bilirubin, a product of heme degradation, inhibited *N*-chloramine formation in plasma after exposure to the MPO/H_2O_2/Cl^- system, and reduced levels of oxidative stress markers [436]. Probucol protects endothelial cells and aortic rings from HOCl-induced inhibition of endothelial relaxation, though as the rate constants for the reaction with HOCl are low ($\sim 10^2$ M^{-1} s^{-1}) it is unlikely to be due to direct scavenging of HOCl [437]. MitoQ, a mitochondrially targeted antioxidant, is able to protect against HOCl-induced mitochondrial dysfunction, and hence cell death [438].

1.6 Selenium compounds as antioxidants

Selenium compounds have gained increasing interest as potential catalytic oxidant scavengers *in vivo* [90, 439-443]. This is primarily due to the rapid reactions with various biological oxidants, which occur at higher rates than the analogous sulfur compounds [90, 98, 439], and subsequent recycling by biological reductants like GSH [444, 445]. The increased reactivity of selenium compounds is primarily attributed to the increased nucleophilicity of selenium compared to sulfur, as well as the lowered pK_a of selenols compared to thiols [446, 447]. As the ability of selenium compounds to act as antioxidants is a focus for this Thesis, the reactions of various selenium compounds with both one- and two-electron oxidants are discussed below.

1.6.1 Ebselen and derivatives

Ebselen is a benzisoselenazolone that has been used to treat inflammatory disorders, due to its capability to act as a GPx mimetic [448]. It has been shown to

have low toxicity as the selenium is not bioavailable. Ebselen has been shown to be capable of scavenging both one-electron oxidants, such as the peroxyl radical $CCl_3OO^{\cdot}$ with a rate constant for the reaction of 2.9 x 10^8 M^{-1} s^{-1} [449], and the two electron oxidants ONOOH [450] and H_2O_2 [451] with second order rate constants of 2.0 x 10^6 M^{-1} s^{-1} and 4.8 M^{-1} s^{-1} respectively [450, 452] (Figure 1.9). The mechanism is thought to involve oxidation to the selenoxide, which is then reduced by two GSH molecules to reform ebselen [450]. In the second mechanism, it is thought that ebselen reacts with two GSH molecules, via a selenosulfide, to produce the selenol, which can then be oxidised to form the selenenic acid. The selenenic acid can eliminate water to reform ebselen, or react directly with GSH to form the selenosulfide [448, 453, 454].

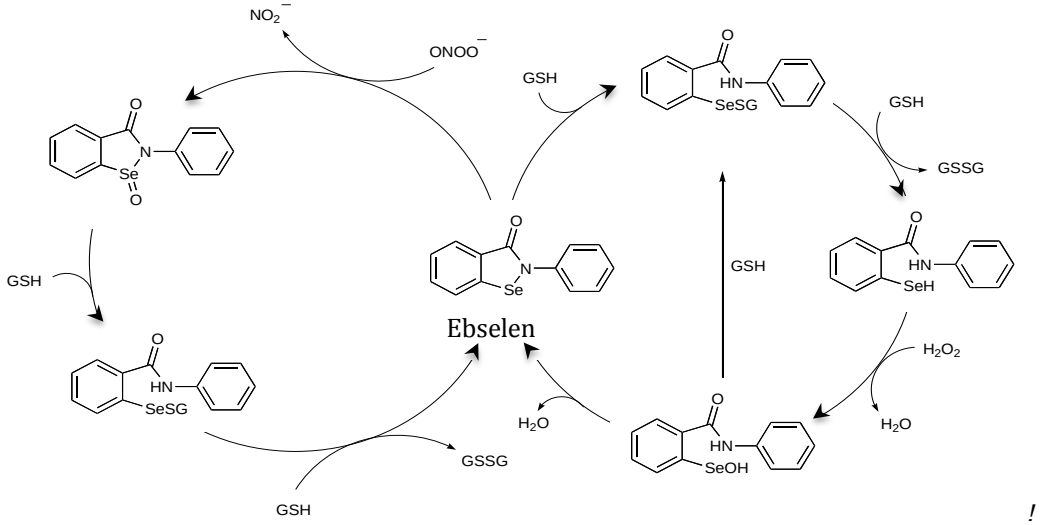

Figure 1.9– Catalytic cycles of ebselen – adapted from [454]

Numerous studies have looked at derivatives of ebselen in order to try to improve the efficacy of the GPx mimetic cycle [440-442]. Substitution of the phenyl group bound to the N demonstrated that for ideal GPx mimetic activity, the group bound needed to have a balance between promoting Se…N interaction to stabilise the selenol, without making the Se-N bond too strong reducing the rate at which oxidants could react with the selenium centre [440, 441]. Addition of amide groups to the benzyl ring in the position next to where Se is bound could increase the GPx mimetic activity via Se...O interactions [442].

Derivatives of ebselen have also been designed as multifunctional drugs [455, 456]. Substitution of methoxy groups to the selenazolone ring, and a benzyl

piperidine structure instead of the phenyl group maintains the GPx mimetic activity of ebselen, though allows for additional cholinesterase inhibition [455]. Similarly, substitution of the phenyl group an alkyl chain linked tacrine demonstrated dual function as a cholinesterase inhibitor and GPx mimetic [456]. This dual function as antioxidant and cholinesterase inhibitor may be beneficial in Alzheimers disease where both oxidative stress and cholinesterase activity can contribute to disease [455, 456].

1.6.2 Selenomethionine

Selenomethione (SeMet) is a selenoether analogous to Met, where a Se atom replaces the sulfur. It is capable of reacting with the MPO-derived oxidants HOCl and HOBr with second order rate constants of 3.2×10^8 and 1.4×10^7 M^{-1} s^{-1} respectively [90]. The rate constants for these reactions are approximately 10 times greater than those reported for Met and similar to those reported for GSH [90]. HOSCN is also capable of reacting with SeMet with a rate constant of 2.8×10^3 M^{-1} s^{-1} [98], whereas it is unreactive towards Met [92].

SeMet has demonstrated rapid reactivity with numerous other one- and two-electron oxidants. SeMet reacts with hydroxyl radicals with a rate constant of 1.4×10^{10} M^{-1} s^{-1} [457], which is comparable to reaction rates of Met [458] and thiols such as Cys [459] and GSH [460], with these sulfur species reacting with rate constants in the range of 1.4×10^{10} – 4×10^{10} M^{-1} s^{-1}. SeMet is capable of reacting with ONOOH, with a rate constants of 2.4×10^3 M^{-1} s^{-1} [461]. The rate constants for reactions of SeMet with oxidants are some of the fastest reported for these oxidants *in vivo* and suggest SeMet would be a competitive target. As such, SeMet is able to protect dihydrorhodamine [462] and super-coiled plasmid DNA [463] from ONOOH mediated oxidation.

SeMet has been shown to form selenomethionine selenoxide (SeMetO) upon reaction with H_2O_2 [464], ONOOH [465, 466] and by the enzymatic action of flavin containing monooxygenases [464]. This is analogous to the formation of MetSO upon oxidation of Met. One-electron oxidation of SeMet (in the presence of O_2) also yields SeMetO via the radical cation $SeMet^{\bullet+}$ [457], however, MetSO is only a minor product under these conditions, with other radicals forming higher abundance products [458, 467-469]. $SeMet^{\bullet+}$, and the analogous species $Met^{\bullet+}$, are stabilised by

a 3-electron bond between the Se or S and the N or O of the amino acid moiety, or interaction with the Se or S of a nearby parent compound [457, 470, 471]. $SeMet^{\bullet+}$ and $Met^{\bullet+}$ can then react with O_2 to form the corresponding SeMetO or MetSO [457, 472]. The higher yield of SeMetO compared to SeMetO is attributed to the increased stability observed for $SeMet^{\bullet+}$, which has a lifetime 300 times greater than that observed for $Met^{\bullet+}$[457, 470, 471]. The increased stability is primarily thought to be due to the presence of Se as opposed to S, though pH dependent effects are also observed [457].

SeMetO can be reduced to reform SeMet in the presence GSH (Figure 1.10) [465, 473]. Cys, ascorbate and methimazole can also achieve the reduction of SeMetO to SeMet [445]. Antioxidant enzymes such as Trx are also capable of reducing SeMetO [474]. It has been shown that the protective effects of SeMet, as well as other selenium-containing antioxidants, can be significantly increased in the presence of GSH [465].

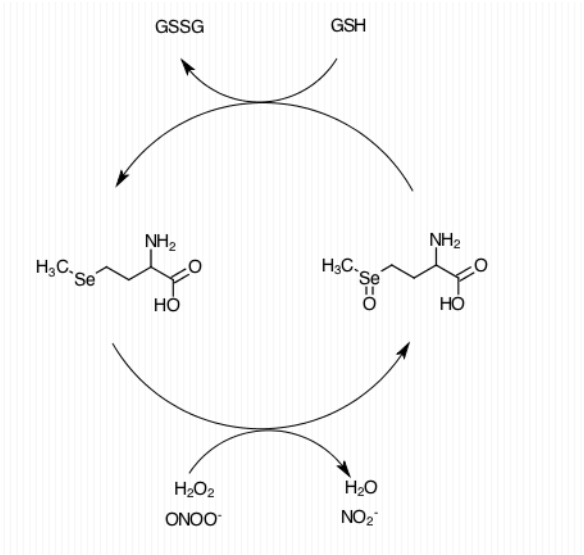

Figure 1.10 – Catalytic cycle of selenomethionine – adapted from [444]

SeMet can be non-selectively incorporated into proteins in place of Met residues [475]. In a cell-free synthesis system in the absence of Met in the cell culture media, 95% of Met residues were replaced with SeMet in the human c-Ha-Ras protein [475]. However, under normal conditions, SeMet incorporation does not occur to this extent. The substitution of Met for SeMet can affect protein structure and function, with SeMet substituted amyloid proteins showing decreased ability to form fibrils and lowered toxicity [476]. However, it is unclear whether this is due to

an antioxidant effect provided by SeMet incorporation or by some other means [476].

1.6.3 Selenols

Selenols are compounds which contain the functional group R-Se-H. The reactions of selenols are difficult to study due to their rapid reaction with atmospheric oxygen and subsequent diselenide formation. As such, most experiments discussed here were performed under N_2 to minimise the contribution of auto-oxidation, even though this does not necessarily reflect *in vivo* conditions. The rates of reaction between selenols and other MPO-derived oxidants have not yet been determined, though it would be expected that they would be faster than for GSH which reacts with HOCl and HOBr with second order rate constants of $\sim 10^8$ and $\sim 10^7$ M^{-1} s^{-1} respectively [90]. Rate constants for the reaction of HOSCN with Sec and derivatives (Sec-methyl ester, selenocystamine and 3-selenopropionic acid) were determined to be in the range of 1.2 – 5.8 x 10^6 M^{-1} s^{-1} [98]. These rate constants are at least 10-fold greater than those reported for the corresponding thiol compounds (k = 7.7 x 10^4 – 1.6 x 10^5 M^{-1} s^{-1}) [92]. Rate constants for the reaction between HOSCN and selenium substituted GSH (GSeH) and the peptide Gly-Sec-Gly were determined to be 1.7 x 10^6 M^{-1} s^{-1}, compared to 2.5 x 10^4 M^{-1} s^{-1} for GSH [98].

GPx contains a Sec residue at the active site, which is capable of reacting with oxidants including H_2O_2 [346], ONOOH [477, 478] and HOSCN [98, 348]. The rate constant for these reactions have been shown to be in the range 10^5 – 10^7 M^{-1} s^{-1} [98, 477]. These values were higher than calculated for free selenocysteine with H_2O_2, with this attributed to hydrogen bonding interactions between the GPx protein structure and H_2O_2 [479].

The reaction of selenols with 2-electron oxidants is proposed to initially result in the formation of a selenenic acid, analogous to thiol oxidation. These selenenic acid intermediates then rapidly react with selenols or thiols to result in diselenide or mixed disulfide-selenide species [480, 481]. Selenenic acid species have not been reported for low molecular mass species in aqueous solution, though they have been described in organic solvents [482]. A selenenic acid intermediate formed at the GPx active site after oxidation has been trapped using dimedone [370]. It has been

proposed that the protein structure stabilises this selenenic acid, which demonstrated stability in the presence of both oxidising and reducing agents [370].

Sec residues also react rapidly with one-electron oxidants. Sec and GSeH react with the phenoxyl radical formed on N-acetyl-Tyr-amide with rate constants of 8 x 10^8 and 5 x 10^8 M^{-1} s^{-1} [483]. The rate constant for this oxidation of Sec is ~3 orders of magnitude greater than that reported for Cys (k = 6 x 10^5 M^{-1} s^{-1}) [483]. Sec and GSeH also reacted with insulin bound Tyr radicals with rate constants of 1.6 x 10^8 and 4 x 10^6 M^{-1} s^{-1} [483]. The lower rate of reaction of GSeH was attributed to steric considerations due to its increased size, though it still reacted significantly faster than GSH (k = 1 x 10^4 M^{-1} s^{-1}) [483].

One-electron oxidation of Sec residues results in the formation of selenyl radicals, analogous to thiyl radicals. However, selenyl radicals have a lower reduction potential than thiyl radicals [484]. Thiyl radicals quickly abstract hydrogen from nearby carbon centres, propagating radical damage [480, 485]. Selenyl radicals are more stable and are less likely to undergo hydrogen abstraction, and primarily undergo radical recombination reactions, preventing the propagation of damage [480]. The increased stability of selenyl radicals is proposed to be protective and may partially explain the use of Sec residues in enzymes such as GPx as opposed to Cys [480].

1.6.4 Other seleno compounds

Novel compounds that incorporate selenium in a cyclic carbohydrate structure also show potential as MPO-derived oxidant scavengers [439]. 1,5-Anhydro-5-seleno-L-gulitol (SeGul) has been shown to have a second order rate constant for reaction with HOCl of ~ 10^7 $M^{-1}s^{-1}$ [439]. A similar compound, 1,4-anhydro-4-seleno-D-talitol (SeTal) also shows promise as an MPO-derived oxidant scavenger, reacting with HOCl, HOBr and HOSCN with rate constants of 1 x 10^8, 1.5 x 10^7 and ~ 1 x 10^2 M^{-1} s^{-1} respectively [486]. Consistent with other selenium species, these selenium species react faster than their sulfur analogues [90, 486]. These cyclic selenides have been shown to protect human serum albumin from oxidative damage induced by HOCl [439, 486]. A related cyclic selenide, *trans*-3,4-dihydroxyselenolane, exhibits GPx like activity, being oxidised by H_2O_2 followed by reduction by thiols groups such as GSH [487].

Selenoethers with the general structure of $Se(CH_2CH_2X)_2$, where X is either OH, CO_2^- or NH_3^+, have GPx mimetic properties, catalysing the reaction between H_2O_2 and GSH [443]. They also react very rapidly with one-electron oxidants such as the model peroxyl radical $CCl_3O_2^\bullet$ (k = 1 x 10^8 – 4.2 x 10^8 M^{-1} s^{-1}) [443]. Pyrazole conjugated selenoethers also demonstrate significant radical scavenging ability, reacting with $HO^\bullet$ and $CCl_3O_2^\bullet$ with rate constants of 1.4 x 10^{10} M^{-1} s^{-1} and 7.8 x 10^8 M^{-1} s^{-1} respectively [488].

Diselenides also react rapidly with radicals, with selenocystamine reacting with $HO^\bullet$ with a rate constant of 8.1 x 10^9 M^{-1} s^{-1} [489] and $(SeCH_2CH_2COOH)_2$ reacting with $CCl_3O_2^\bullet$ with a rate constant of 2.7 x 10^8 M^{-1} s^{-1} [490]. Direct reactions between diselenides and two-electron oxidants have not been studied extensively. However, some have demonstrated GPx activity, with these reacting catalytically with H_2O_2 and ONOOH in the presence of GSH or enzymatic reduction systems [491, 492]. Selenocystine is reduced by GSH or Trx forming the selenol, which then reacts rapidly with oxidants to reform the diselenide, resulting in catalytic scavenging [491, 492]. A novel diselenide nicotinamide derivative, and GSeSeG (selenium substituted GSSG) have also demonstrated this GPx mimetic ability in the presence of GSH [493]. Ebselen is also capable of reacting in this manner, though it is the Se-N bond that is reduced by GSH and Trx, as opposed to a diselenide bond [448].

1.7 Endogenous selenium levels and selenium supplementation

1.7.1 Dietary selenium and the risk of disease

In the light of the above data, there is considerable interest in the biological activity of selenium and optimal dietary selenium levels. Selenium is an essential micronutrient, typically found in human plasma at concentrations of 70 – 140 μg L^{-1} with a recommended daily intake of 55 – 70 μg per day [494]. Deficiency in selenium intake (< 20 μg per day) is known to have detrimental health consequences, with low selenium levels correlating with numerous diseases. Selenium levels have been shown to inversely correlate with instances of cancer, with incidences of prostrate [495, 496], bladder, lung [497] and laryngeal cancers [497] being reduced with higher levels of plasma selenium. Low selenium levels correlate with increased markers of oxidative stress in the plasma of sepsis patients

[498]. Selenium levels in plasma have been shown to correlate inversely with instances of coronary artery disease, myocardial infarction and death from cardiovascular disease [499, 500]. Furthermore, supplementation of selenium in patients with low selenium levels reduced plasma lipid levels [501]. In contrast, where selenium levels were much higher (with a mean of 125.6 ng mL^{-1}), no correlation was observed between selenium levels and cardiovascular disease risk factors [502]. Furthermore, high selenium levels were correlated with elevated lipid levels [503] and hypertension [504], which are both risk factors for cardiovascular disease. These data suggest that selenium supplementation may only be effective in patients where base levels of selenium are low.

The observation that selenium supplementation may only be effective in low-baseline selenium level patients is backed up by observations from the NPC [505] and SELECT [506] trials. Both these trials aimed to reduce incidence of cancer by supplementation of selenium, and in the SELECT trial Vitamin E was also supplemented. The NPC trial demonstrated that patients with lower (though nutritionally sufficient) selenium levels (< 123 ng mL^{-1}) showed a decrease in lung and prostate cancer incidences [496, 507]. This effect was not observed in the SELECT trial, though the mean baseline selenium levels were much higher in this study (135 in SELECT vs 114 in NPC) [505, 506].

1.7.2 Actions of selenium in biological systems

While selenium supplementation may not demonstrate efficacy in preventing incidence of disease states in people with adequate selenium intake, many studies have shown a therapeutic potential of Se compounds in disease models. Selenium has been proposed to exert its effects in 3 ways including induction of reactive oxygen species (ROS) in cancer cells, upregulation of antioxidant enzymes in the selenoproteome and by direct scavenging of oxidants.

Treatment with sodium selenite can induce the formation of ROS in a number of different cell types [508-514]. Selenodiglutathione [514] and selenocystamine [515, 516], which readily react with thiols such as GSH to produce selenolates are also capable of producing ROS [514]. $O_2^{\bullet-}$ production is thought to be the cause of the observed selenium-induced apoptosis, with SOD overexpression inhibiting this apoptosis [517]. Methylated selenium species such as methylselenocysteine

(MeSeCys) and SeMet are much less toxic, though also have demonstrated capacity to induce ROS formation [513, 518, 519], and this is attributed to the formation of methylselenolate after metabolism of MeSeCys and SeMet by methioninases [513]. Cancer cells are believed to be much more susceptible to selenium induced ROS formation than normal cells; this has been demonstrated using selenite and selenocystine in patient matched pairs of cancerous and normal prostate cells [520], fibroblasts [515] and malignant and benign mesothelioma cells [521]. In each case, the cancerous cells were more susceptible to selenium supplementation and this has been attributed to a higher level of oxidative stress already occurring in the cancer cells, which is then exacerbated in the presence of selenium. Furthermore, inhibition of TrxR with auranofin and ethaselen made cancer cells more sensitive to selenium-induced apoptosis [522, 523], further implicating increased levels of ROS as the cause of apoptosis.

Selenium supplementation results in an upregulation of selenium containing enzymes, including GPx, TrxR and other selenoproteins [524-526]. Selenite supplementation enhanced GPx expression in rat cardiomyocytes, human lung cancer cells [527], and HCAECs [528]. SeMet was also capable of increasing GPx expression in the rat cardiomyocytes [529] as well as human trophoblasts [530, 531], but not HCAECs [532]. This increase in GPx activity protected cells from peroxide induced oxidative damage and reduced lipid peroxidation in a hypoxia-reoxygenation model [529]. Upregulation of selenoenymes by supplementation of trophoblasts with SeMet decreased oxidative stress induced by addition of H_2O_2, as well as mitochondrial oxidative stress induced by addition of antimycin [530, 531]. Rats given selenite, selenocystine or SeMet in their diet also demonstrated an increase in GPx activity in blood and tissue samples [524]. Selenite supplementation in rats resulted in a small increase in GPx activity, which improved cardiac outcomes in an ischaemia reperfusion model [525, 526]. Low selenium levels have been shown to correlate with incomplete GPx expression and an increased risk of myocardial infarction [499, 533, 534], and it has been suggested that selenium supplementation could reduce this risk [466]. Patients supplemented with selenite demonstrated an increased GPx expression when their baseline selenium levels were less than 90 ng mL^{-1} [535], which is postulated to be protective in the context of heart disease.

TrxR can also be upregulated by supplementation with selenium compounds. Selenite supplementation increased TrxR expression in HUVECs, and led to increased viability on peroxide exposure [528]. Selenite supplementation in rats also demonstrated an increase in TrxR level at low doses [536]. However, at higher doses, whilst there was an initial increase in TrxR levels, a subsequent decline in levels was observed [525, 526]. MeSeCys and methylselenic acid supplementation demonstrated no effects on TrxR levels in the same study [537].

1.7.3 Selenium supplementation in disease

As discussed above, numerous selenium compounds exhibit GPx mimetic activity, catalysing the reaction of H_2O_2 and other oxidants with GSH. This direct scavenging of oxidants appears to have multiple beneficial effects *in vitro* and *in vivo*, particularly when GPx is absent or downregulated. The presence of (additional) SeMet, MeSeCys and selenocystamine can protect erythrocytes from lipid peroxidation and hemolysis [538]. SeMet also protects J774A.1 murine macrophage cells from peroxide damage [474]. The Trx system can also increase the efficacy of SeMet [474], and has also been shown to enhance the scavenging potential of selenocystamine, ebselen and diselenoglutathione [491, 492].

Selenium containing compounds have demonstrated particular efficacy in models of atherosclerosis. A GPx/ApoE double knock-out mouse model has been developed, and these animals quickly develop atherosclerotic lesions [539, 540]. Supplementation with ebselen decreases lesion size, and decreases inflammation and oxidative stress, and is postulated to achieve this by boosting antioxidant defences [539-541]. Ebselen also prevented diabetes related kidney and retina nephropathy observed in this model [539, 542, 543]. Diphenyldiselenide has been shown to reduce lesion size in an LDL receptor knockout model of atherosclerosis [544]. Selenocystamine-coated stents have also been reported to have improved bio-compatibility compared to bare metal stents, reducing platelet aggregation, smooth muscle proliferation, which is thought to be due to antioxidant activity of the selenocystamine [545].

While selenium supplementation does not appear to reduce the incidence of disease if patients are not selenium deficient, selenium containing compounds have demonstrated efficacy in models of disease where oxidative stress plays a major role

in the pathogenesis, such as atherosclerosis. Furthermore, research has demonstrated that toxicity of selenium is mostly related to selenolate metabolites [519], and toxicity can be reduced by supplementation with different forms of selenium [546]. Therefore, there is potential for the development of selenium containing compounds that may act as antioxidants to reduce or prevent disease.

1.8 Hypothesis and aims

Overall, it is clear from the data above that MPO produces strong oxidants that are designed to kill invading pathogens. However, excessive or misplaced production of these oxidants has been associated with the development of numerous diseases, including atherosclerosis. As sulfur and selenium compounds, and enzymes containing these residues show great potential as catalytic antioxidants due to their fast reaction kinetics it is proposed that they may be able to attenuate damage caused by MPO-derived oxidants, such as HOCl and *N*-chloramines. While the rate constants for the reaction of selenium compounds with HOCl and other hypohalous acids have been determined recently [90, 98], the products of these reactions have not been fully characterised. Furthermore, the rate constants for the reaction with *N*-chloramines are yet to be determined.

The ability for facile recycling of oxidised selenium compounds suggests a potential for a catalytic reduction of MPO-derived oxidants. However, the mechanisms and rate constants for the reduction of selenoxides by thiols have not been determined. Furthermore, antioxidant enzymes with reactive Cys and Sec residues may also be capable of reducing HOCl, *N*-chloramines and selenoxides, though this has yet to be examined.

The hypothesis for this project is therefore that thiol and seleno compounds and related enzymes may modulate oxidative damage induced by myeloperoxidase and related peroxidases during inflammation, by acting as catalytic agents and as such will be able to modulate the development of disease.

The proposed studies will address the following specific aims:

1. Examination of the kinetics and mechanisms of reaction of HOCl and related species with thiol and seleno compounds.

2. Identification of potential repair / recycling mechanism(s) of low-molecular-mass compounds.
3. Determining whether thiol and seleno-dependent enzymes also behave as catalytic protective systems.
4. Examination of the efficacy of these compounds and enzymes in protecting cells from oxidant damage.

2 Materials and Methods

2.1 General Information

This Chapter contains details of the general Materials and Methods used throughout this Thesis.

Nanopure water, referred to as H_2O, is water filtered through a four-stage Milli Q system (Millipore-Water, Lane Cove, NSW, Australia). Solutions were prepared in pH 7.4 0.1 M sodium phosphate buffer (preparation detailed in Section 2.3.1.1) unless otherwise stated. The pH of solutions was determined using a Radiometer Analytical PHM220 pH meter with pHC2401 probe (Radiometer Analytical, Villeurbanne Cedex, France), calibrated with pH 4, 7 and 10 standards (Radiometer Analytical).

All centrifugation was performed on an Eppendorf Refrigerated Micro Centrifuge (Model 5215R, Eppendorf, Hamburg, Germany), unless otherwise stated.

2.2 Materials

Reagent	Supplier
Acetic acid, glacial	Merck Pty Ltd (Vic, Australia)
N-α-acetyl-L-histidine (His)	Sigma-Aldrich (Castle Hill, NSW, Australia)
N-α-acetyl-L-lysine (Lys)	Sigma-Aldrich (Castle Hill, NSW, Australia)
N-acetylselenomethionine (NASM)	Gift from Dr. Lara Malins and Prof. Richard Payne (School of Chemistry, University of Sydney, Sydney)
Acetone	Merck Pty Ltd (Vic, Australia)
Acetonitrile	Merck Pty Ltd (Vic, Australia)
Allophycocyanin-conjugated annexin V	BD Biosciences, Sydney, NSW, Australia
1,4-anhydro-4-seleno-L-talitol (SeTal)	Gift from Prof. Carl Schiesser (School of Chemistry and Bio21 Molecular Science and Biotechnology Institute, University of Melbourne)
Auranofin	Sigma-Aldrich (Castle Hill, NSW, Australia
Bovine serum albumin, essentially fatty acid free (BSA)	Sigma-Aldrich (Castle Hill, NSW, Australia)
Chelex 100 resin	BioRad Laboratories, Inc. (Hercules, CS, USA)
CompleteMini protease inhibitor cocktail tablet	Roche (Mannheim, Germany)
L-Cysteine (Cys)	Sigma-Aldrich (Castle Hill, NSW, Australia)
Deuterium oxide (D_2O)	Sigma-Aldrich (Castle Hill, NSW, Australia)
Dimethylformamide (DMF)	Sigma-Aldrich (Castle Hill, NSW, Australia)
Dimethylsulfone	Sigma-Aldrich (Castle Hill, NSW, Australia)
Dimethylsulfoxide (DMSO)	Sigma-Aldrich (Castle Hill, NSW, Australia)

Reagent	Supplier
Disodium hydrogen orthophosphate dodecahydrate	Ajax FineChem, Ltd. (Sydney, NSW, Australia)
5,5'-dithiobis(2-nitrobenzoic acid) (DTNB)	Sigma-Aldrich (Castle Hill, NSW, Australia)
Dithiothreitol (DTT)	Sigma-Aldrich (Castle Hill, NSW, Australia)
Dulbecco's modified Eagle's medium (DMEM)	Sigma-Aldrich (Castle Hill, NSW, Australia)
Ethidium bromide (EtBr)	Sigma-Aldrich (Castle Hill, NSW, Australia)
Ethylenediaminetetraacetic acid (EDTA)	Sigma-Aldrich (Castle Hill, NSW, Australia
N-ethylmaleimide (NEM)	Sigma Chemical Co. (Castle Hill, NSW, Australia)
Fetal calf serum (FCS)	Invitrogen (Eugene, OR, USA)
Formaldehyde, 37 % Biotechnology Grade	Amresco (Solon, OH, USA)
Formic acid, > 96% ACS reagent	Sigma-Aldrich (Castle Hill, NSW, Australia)
L-Glutamine	Sigma-Aldrich (Castle Hill, NSW, Australia)
Glutathione (GSH)	Sigma-Aldrich (Castle Hill, NSW, Australia)
Glutathione peroxidase, from bovine erythrocytes (GPx)	Sigma-Aldrich (Castle Hill, NSW, Australia)
Glutathione reductase from Baker's yeast (GR)	Sigma-Aldrich (Castle Hill, NSW, Australia)
Glutathione, oxidised approx 98% (GSSG)	Sigma-Aldrich (Castle Hill, NSW, Australia)
Glyceraldehyde 3-phosphate (GAP)	Sigma-Aldrich (Castle Hill, NSW, Australia)
Glycine (Gly)	Sigma-Aldrich (Castle Hill, NSW, Australia)
Hank's balanced buffer solution (HBSS)	Sigma-Aldrich (Castle Hill, NSW, Australia)
Hydrogen peroxide, 30% (w/w) (H_2O_2)	Sigma-Aldrich (Castle Hill, NSW, Australia)
2-[4-(2-hydroxyethyl)piperazin-1-yl]ethanesulfonic acid (HEPES)	Sigma-Aldrich (Castle Hill, NSW, Australia)
5-Iodoacetamidofluorescein (IAF)	Invitrogen (Mount Waverley, VIC, Australia)
2-mercaptoethanol	Sigma-Aldrich (Castle Hill, NSW, Australia
Methane sulfonic acid (MSA), 4 M containing 0.2 % w/v tryptamine	Sigma-Aldrich (Castle Hill, NSW, Australia
Methanol	Merck Pty Ltd (Vic, Australia)
L-Methionine (Met)	Sigma-Aldrich (Castle Hill, NSW, Australia)
Methionine Sulfoxide Reductase A (Human Recombinant) (MSRA)	ProSpec Protein Specialists (East Brunswick, NJ, USA)
Methionine Sulfoxide Reductase B2 (Human Recombinant) (MSRB2)	ProSpec Protein Specialists (East Brunswick, NJ, USA)
Methylselenocysteine hydrochloride (MeSeCys)	Sigma-Aldrich (Castle Hill, NSW, Australia)
Myeloperoxidase (MPO)	Planta Natural Products (Wein, Austria)

Reagent	Supplier
Nicotinamide adenine dinucleotide (NADH)	Roche (Mannheim, Germany)
Nicotinamide adenine dinucleotide (oxidised) (NAD^+)	Roche (Mannheim, Germany)
Nicotinamide adenine dinucleotide phosphate (NADPH)	Roche (Mannheim, Germany)
Nitrogen	Coregas (Yennora, NSW, Australia)
Phorbol 12-myristrate 13-acetate (PMA)	Sigma-Aldrich (Castle Hill, NSW, Australia)
Phthaldialdehyde reagent (Incomplete) (OPA)	Sigma-Aldrich (Castle Hill, NSW, Australia)
PolyMorph Prep	Axis-Shield PoC AS (Oslo, Norway)
Propidium iodide (PI)	BD Biosciences, Sydney, NSW, Australia
Red cell hypotonic lysis buffer	Sigma-Aldrich (Castle Hill, NSW, Australia)
Seleno-bispropionic acid (SeProp)	Gift from Prof. K. Indira Priyadarsini (Radiation and Photochemistry Division, Bhabha Atomic Research Centre, Bombay, India)
Selenocystamine dihydrochloride (SeCysta)	Sigma-Aldrich (Castle Hill, NSW, Australia)
Selenomethionine (SeMet)	Sigma-Aldrich (Castle Hill, NSW, Australia)
Silver nitrate	Sigma-Aldrich (Castle Hill, NSW, Australia)
Sodium acetate trihydrate	Sigma-Aldrich (Castle Hill, NSW, Australia)
Sodium carbonate	Sigma-Aldrich (Castle Hill, NSW, Australia)
Sodium chloride (NaCl)	Sigma-Aldrich (Castle Hill, NSW, Australia)
Sodium deoxycholate	Sigma-Aldrich (Castle Hill, NSW, Australia
Sodium dihydrogen orthophosphate monohydrate	Merck Pty Ltd (Vic, Australia)
Sodium hydroxide (NaOH)	Sigma-Aldrich (Castle Hill, NSW, Australia)
Sodium hypochlorite, 12.5 % w/v (HOCl)	Ajax FineChem, Ltd. (Sydney, NSW, Australia)
Sodium iodide	Sigma-Aldrich (Castle Hill, NSW, Australia)
Sodium pyrophosphate	Sigma-Aldrich (Castle Hill, NSW, Australia)
Sodium pyruvate	Sigma-Aldrich (Castle Hill, NSW, Australia)
Sodium thiosulfate	Sigma-Aldrich (Castle Hill, NSW, Australia)
Taurine (Tau)	Sigma-Aldrich (Castle Hill, NSW, Australia)
3,3',5,5'-tetramethylbenzidine (TMB)	Sigma-Aldrich (Castle Hill, NSW, Australia)
ThioGlo-1 reagent	Berry and Associates (Dexter, MI, USA)
Thioredoxin 1, human (Trx)	IMCO (Stockholm, Sweden)
Thioredoxin reductase, rat (TrxR)	IMCO (Stockholm, Sweden)
Trichloroacetic acid (TCA)	Sigma-Aldrich (Castle Hill, NSW, Australia)
Trifluoroacetic acid (sequencing grade) (TFA)	Sigma-Aldrich (Castle Hill, NSW, Australia)
Triton X-100	Sigma-Aldrich (Castle Hill, NSW, Australia)
Trypan blue	Sigma-Aldrich (Castle Hill, NSW, Australia)

2.3 Methods

2.3.1 Preparation of buffers

2.3.1.1 0.1 M Phosphate buffer pH 7.4

A 0.1 M sodium phosphate pH 7.4 buffer was prepared as previously described [547]. Solutions of 0.1 M monobasic orthophosphate and 0.1 M dibasic orthophosphate were prepared in H_2O. Trace transition metal ions were removed by the addition of washed Chelex resin, followed by stirring for 1 h. The Chelex resin was removed by vacuum filtration. The monobasic solution was then added to the dibasic solution while stirring, until the pH was 7.4.

2.3.2 Preparation of oxidant species

2.3.2.1 Reagent HOCl

HOCl was diluted from a stock solution of sodium hypochlorite (17 % (w/v)) to 10 mM in H_2O, and then further diluted to the desired concentration in phosphate buffer. The concentration of the stock sodium hypochlorite solution was assessed by optical absorbance at 292 nm at pH 11, achieved by dilution into 0.1 M NaOH, using the absorbance co-efficient of OCl^-, $\varepsilon = 350\ M^{-1}cm^{-1}$ [82].

2.3.2.2 Reagent H_2O_2

H_2O_2 was diluted from a stock solution (30 % (w/w)) to 10 mM in water. H_2O_2 stock concentration was determined by optical absorbance at 240 nm of diluted stock samples in water using the absorbance co-efficient of H_2O_2, $\varepsilon = 43.6\ M^{-1}cm^{-1}$ [548].

2.3.2.3 Amino acid *N*-chloramine formation

N-Chloramines were formed on reaction of HOCl with amine groups, including free amino acids, side chains of peptides (e.g. Lys, His) and the N-terminus of proteins [53, 58].

$$RNH_2 + HOCl \rightarrow RNHCl + H_2O \qquad \text{Reaction 2.1}$$

A series of model *N*-chloramines was prepared by reaction of Tau, Gly and *N*-α-acetyllysine (10 mM) by mixing with HOCl (2 mM), which yielded approximately 2 mM

N-chloramine solution. Final *N*-chloramine concentrations were determined using the TNB method (Section 2.3.3.1) prior to use.

2.3.2.4 Protein *N*-chloramine formation

Bovine serum albumin (BSA; 1 mg mL^{-1}, 15 μM) was incubated with equal volumes of HOCl solution (0.5 mM) for 5 min. Protein *N*-chloramine concentrations were determined by the TNB method (Section 2.3.3.1) and the solution diluted to give the desired concentration of *N*-chloramines.

2.3.2.5 Myeloperoxidase system

MPO catalyses the reaction of H_2O_2 and (pseudo)-halides, Cl^-, Br^- and SCN^-, to form the hypohalous acids, HOCl, HOBr and HOSCN respectively (e.g. Reaction 2.2) [24]. MPO (2 μM) was incubated with Cl^- (100 mM) and Tau (10 mM) at 37°C for 10 min before addition of H_2O_2 (50 μM) to initiate HOCl production. Samples were further incubated for 30 min, then the concentration of TauCl (from Reaction 2.3) was determined using TMB (Section 2.3.3.2). Under these conditions approximately 50 μM HOCl, and subsequently TauCl, was formed. Tau was included as it traps HOCl after production as TauCl, a longer-lived oxidant, making it easier to detect [549]. Tau is physiologically relevant as neutrophils contain up 20 - 50 mM Tau [550], which is released upon activation and quickly chlorinated [551, 552].

$$H_2O_2 + Cl^- + H^+ \xrightarrow{MPO} HOCl + H_2O \qquad \text{Reaction 2.2}$$

$$TauNH_2 + HOCl \rightarrow TauNHCl + H_2O \qquad \text{Reaction 2.3}$$

2.3.2.6 Isolation of neutrophils and formation of neutrophil-derived oxidants

Neutrophils were isolated immediately after collection of blood into EDTA-coated tubes (10.0 mL BD Vacutainer, BD biosciences, Sydney, NSW, Australia) from healthy volunteers with informed consent and local ethical approval (Sydney South West Area Health Service, Protocols X09-0013 and X-12-0375) in accordance with the Declaration of Helsinki (2000) of the World Medical Association, as described previously [553]. Neutrophils were isolated using a Polymorphprep density-gradient method. 5 mL of whole blood was layered over 5 mL Polymorphprep and centrifuged at 510 g at 21 °C for 35 min with maximum acceleration and the deceleration set to 0 to ensure slow

braking in an Allegra X-15R Centrifuge (Beckman Coulter). This separated out the plasma, mononuclear cells, neutrophils and the red blood cells (Figure 2.1). The plasma and mononuclear cell layers were removed, and the neutrophils collected and transferred into clean Falcon tubes.

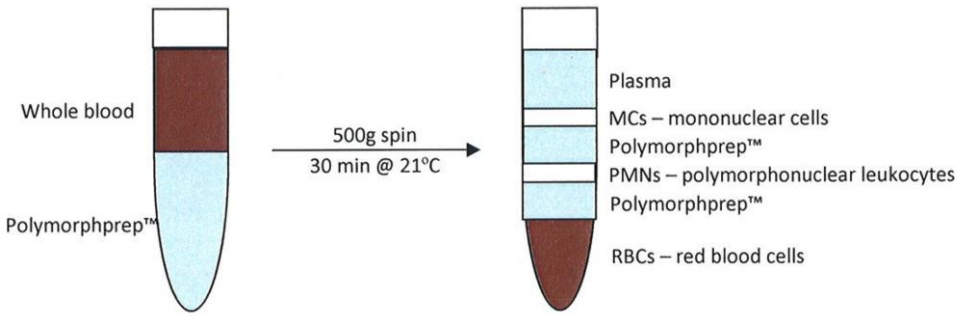

Figure 2.1 – Separation of layers observed after whole blood is layered onto Polymorphprep and centrifuged.

Osmolality was restored by addition of 1.5 mL saline solution (0.45% NaCl). The volume was increased 12 mL with saline solution (0.9% NaCl), and mixed by inversion to wash neutrophils. Neutrophils were pelleted by centrifugation at 400 *g* for 10 min at 21 °C, with maximum acceleration and deceleration. The majority of supernatant was removed, leaving 1 mL in the tube. The pellets were resuspended in 2 mL red cell lysis buffer (Product number: R7757, Sigma-Aldrich, Castle Hill, NSW, Australia) and incubated for 15 min in the dark to remove any residual red blood cell contamination. The volume in tubes was then 12 mL with HBSS, and cells were re-pelleted by centrifugation at 400 *g* for 10 min at 21 °C. If any red cells remained in the pellet, as judged by its colour, the red cell lysis step was repeated. The supernatant was then removed and the neutrophils washed by resuspension in 12 mL HBSS and mixed by inversion. The neutrophils were then pelleted by centrifugation at 400 *g* for 10 min, the supernatant was removed and neutrophils resuspended in 2 mL HBSS for counting.

Cell number and viability was assessed by trypan blue dye exclusion. The neutrophil suspension (10 µL) was mixed with equal volumes of trypan blue dye and mixed by aspiration. 10 µL of mixture was pipetted into a haemocytometer chamber and cells counted under a microscope. Cells that did not take up the dye were counted as viable.

Neutrophils (2 x 10^6 cells mL^{-1}) were incubated at 37 °C for 10 min, before addition of phorbol 12-myristate 13-acetate (PMA; 0.1 µg mL^{-1}) to induce neutrophil activation.

The cells were then incubated for 30 min at 21 °C with gentle agitation to ensure that the cells remained in suspension. Under these conditions, approximately 50 μM of reactive species were produced, as measured by the TMB assay (Section 2.3.3.2).

2.3.3 Assays

2.3.3.1 TNB

5-thio-2-nitrobenozic acid (TNB), a bright yellow thiol species, reacts with *N*-chloramines (and other oxidants), to form the colourless disulfide 5,5'-thiobis(2-nitrobenzoic acid) (DTNB) [554] (Reaction 2.4).

$$2RSH + RNHCl \rightarrow RSSR + RNH_3^+ + Cl^- \qquad \text{Reaction 2.4}$$

The TNB reagent was prepared by alkaline hydrolysis of DTNB (2.5 mg) by NaOH in H_2O (5 mL; 50 mM) and incubated in the dark for 5 min. This stock solution was then diluted 1 : 40 in phosphate buffer (0.1 M, pH 7.4), to give a yellow working solution with an absorbance at 412 nm of between 0.5 – 0.7 absorbance units. The working solution (950 μL) was mixed with oxidant solution (50 μL, 20 - 100 μM) and incubated in the dark for 15 min. The optical absorbance of the solution was measured at 412 nm, and the concentration of remaining TNB was determined using the extinction coefficient ε = 14150 cm^{-1} [555]. The concentration of the oxidant was determined by the difference between TNB concentration in control and oxidant treated samples, based on a 2 : 1 TNB to oxidant stoichiometric ratio.

2.3.3.2 TMB

N-chloramines and HOCl, in the presence of iodide ions (I^-), rapidly react with the colourless 3,3',5,5'-tetramethylbenzidine (TMB) to form a blue oxidised product [549]. I^- catalyses the oxidation of TMB via reaction with *N*-chloramines or HOCl to form hypoiodous acid (HOI), which is then the reactive species that oxidises TMB [549] (Reaction 2.5 – 2.7).

$$RNHCl + H^+ + I^- \rightarrow RNH_2 + ICl \qquad \text{Reaction 2.5}$$

$$ICl + H_2O \rightarrow HOI + HCl \qquad \text{Reaction 2.6}$$

$$HOI + R'H_2 \rightarrow R' + I^- + H^+ + H_2O \qquad \text{Reaction 2.7}$$

The developing reagent was prepared by dissolving 4.8 mg of 3,3',5,5'-tetramethylbenzidine (TMB; 20 mM) in dimethylformamide followed by the addition of sodium acetate buffer (9 mL, 0.44 M, pH 5.4) and sodium iodide solution (50 µL of 2 mM). The developing reagent was prepared immediately prior to addition to the standards and samples to avoid any artifactual autoxidation of TMB.

The TMB assay was used to determine oxidant concentration after sulfur and selenium compounds were used as scavengers of MPO-derived and neutrophil-derived oxidant species produced by systems described above. SeMet, SeTal and Met (0 – 50 µM) were incubated with either the isolated MPO system or neutrophil system (final volume 50 µL). After 30 min, the remaining oxidant was quantified by addition of TMB developing reagent (50 µL) followed by a 5 min incubation period. The absorbance was measured at 645 nm on a Benchmark Plus microplate reader (BioRad). The oxidant concentration was assessed by comparison to a standard curve constructed from standards of TauCl (0 – 100 µM).

2.3.3.3 ThioGlo-1 assay

ThioGlo-1 is a malemide derived florescent dye used to determine thiol levels in biological samples [547]. The ThioGlo-1 reagent specifically reacts with free thiols of Cys residues forming a fluorescent product. ThioGlo reagent (2.6 mM) was dissolved in acetonitrile and stored in the dark at 4 °C before a working solution was prepared by dilution 1 : 100 in phosphate buffer (0.1 M, pH 7.4) immediately prior to use. ThioGlo working solution (50 µL) was added to sample or standard (50 µL; 0 – 5 µM thiol) in a 96-well tissue culture plate and incubated for 10 min in the dark. Fluorescence was then measured at λ_{ex}= 360 nm λ_{em}= 530 nm on an M2e plate reader (Molecular Devices). The thiol concentration was determined by comparison to a standard curve prepared using GSH (0 – 5 µM).

2.3.3.4 Bicinchoninic acid (BCA) protein assay

The BCA assay determines protein levels by measurement of the reduction of Cu^{2+} to Cu^{+} by peptide residues. Cu^{+} is then chelated by the bicinchoninic acid to form a complex that strongly absorbs at 562 nm [556]. Absorbance at 562 nm is proportional to protein content. A working solution was prepared by mixing Pierce BCA Protein Assay Solution A (Thermo Scientific, Rochford, IL, USA) with $CuSO_4$ (4 % (w/v)) in a 50

: 1 ratio. Working solution (200 µL) was then added to protein samples (25 µL) and standards (25 µL; 0.1 – 1 mg mL^{-1}) in a 96-well cell culture plate. Solutions were mixed by gentle shaking, followed by incubation at 60 °C for 10 min. The absorbance at 562 nm was measured on an M2e plate reader (Molecular Devices), and protein concentration determined by comparison to a standard curve prepared using BSA.

2.3.4 Enzymatic reduction assays

2.3.4.1 Glutathione reductase

GSR reduces GSSG to GSH using NADPH as a reducing equivalent [557]. GSSG is formed when GSH is exposed to oxidants including *N*-chloramines and selenoxides [192, 445]. The rate of GSSG removal, by GSR can be determined by monitoring the concentration of NADPH in the presence of GSR and GSH (Reaction 2.8 – 2.9).

$$RNHCl + 2GSH \rightarrow RNH_2 + GSSG + H^+ \qquad \text{Reaction 2.8}$$

$$NADPH + GSSG \xrightarrow{GSR} NADP^+ + 2GSH \qquad \text{Reaction 2.9}$$

Commercially available GSR comes in a solution containing DTT to stabilise the enzyme, which needs to be removed prior to assay as it can interfere by removing oxidants independently of GSR. DTT was removed from the stock solution by passing the GSR through a PD-10 column using phosphate buffer (0.1 M, pH 7.4) to elute the protein. The GSR concentration was then determined using the BCA assay (Section 2.3.3.4).

An Applied Photophysics SX.20MV stopped flow system was used to monitor the loss of NADPH upon addition of oxidants to the GSR system in the presence or absence of SeMet or SeTal. NADPH (500 µM), GSR (25 nM) and GSH (400 µM) was mixed in the stopped flow apparatus with SeMetO, SeTalO or *N*-chloramine (200 µM). *N*-Chloramine reduction experiments were also performed in the presence of SeMet or SeTal (20 or 200 µM). The absorbance at 340 nm, corresponding to loss of NADPH, was monitored over 60 s. A linear slope was fitted to the initial fast decrease in absorbance, from 2 – 12 seconds, where maximum enzymatic activity was observed.

2.3.4.2 Thioredoxin based systems

TrxR is capable of reducing oxidants, including H_2O_2 [528] and HOSCN [348], and disulfides [390] using NADPH as a reducing equivalent. Trx reduces protein disulfides using TrxR and NADPH as the reducing system [390]. In turn Trx can also reduce enzymes including Msrs [417, 420], which reduce MetSO, and GPx [348], which reduces H_2O_2. As NADPH is the reductant used by all of these systems, the rate of enzymatic removal of oxidants can be assessed using the loss of NADPH determined by its optical absorbance at 340 nm.

The ability of TrxR to reduce oxidants was assessed by incubating 700 μM NADPH and 25 nM TrxR before addition of 200 μM selenoxide or *N*-chloramine in the presence or absence of 1.5 μM Trx. *N*-Chloramine reduction experiments were performed in the presence and absence of SeMet or SeTal (20 or 200 μM). This Trx system was also used to assess the ability of MsrA, MsrB2 and GPx to remove oxidants. In this case, MsrA (95 nM), MsrB2 (0.25 μM) or GPx (1.5 μM) were incubated with NADPH (700 μM), TrxR (25 nM) and Trx (1.5 μM) prior to the addition of 200 μM oxidant, with *N*-chloramine experiments also performed in the presence or absence of SeMet or SeTal (20 or 200 μM). The absorbance at 340 nm, reflecting the NADPH concentration, was measured every 30 s for 2 h on M2e plate reader (Molecular Devices). A straight line was fitted to a plot of time vs. [NADPH] to determine rate of NADPH consumption.

2.3.4.3 Reduction of oxidants by cell lysates

The enzymatic removal of oxidants was examined using cell lysates, for a more physiological representation of enzyme ratio and concentrations present *in vivo*. Auranofin, which binds to Sec residues to inhibit selenoproteins [558], was used as an inhibitor of TrxR to enable determination of TrxR's contribution, as well as the contribution of downstream enzymes, on oxidant removal.

J774A.1 cells (10^6 cells) were lysed in 3 mL ice-cold H_2O and incubated on ice for 15 min to maximise lysis. Protein levels in the lysates were determined by BCA assay (Section 2.3.3.4), with this adjusted to 1 mg protein mL^{-1}. Lysate (50 μg protein) was incubated with NADPH (500 μM) in the presence or absence of auranofin (25 nM) for 15 min, and then SeMetO, SeTalO, *N*-chloramine or insulin (200 μM) was then added and absorbance at 340 nm monitored for 2 h. *N*-Chloramine experiments were also

performed in the presence or absence of SeMet or SeTal (20 or 200 µM). The rate of NADPH consumption was determined by fitting a straight line to the resulting NADPH vs time plot.

2.3.5 HPLC methods

Buffers were made as specified in each method, and then vacuum filtered using a hydrophilic polypropylene 0.2 µm membrane filter (Pall, MI, USA) before use. Samples were filtered through 0.2 µm NanoSep centrifugal devices (Pall, MI, USA) before being transfered to HPLC vials with 200 µL glass inserts. Samples were kept in the autosampler at 4 °C until injection onto the column.

2.3.5.1 HPLC instrumentation

A Shimadzu Nexera system, consisting of binary pumps (LC30AD), degasser (DGU-20A5R), autosampler (SIL30AC) and column oven (CTO-20A), was used to perform HPLC experiments. UV-vis detection was performed with a photodiode array (SPD-M20A). Fluorescence measurements were performed with a fluorescence detector (RF-20AXS).

2.3.5.2 SeMet and SeMetO

Separation of SeMet, SeMetO, GSH and GSSG was achieved by injection of 20 µl of each sample onto a Beckman Ultrasphere ODS column (5 µM , 4.6 x 250 mm), at 40 °C as previously described [464]. The mobile phase consisted of acetonitrile (1 % (v/v)) adjusted to pH 2.5 with trifluoroacetic acid (TFA) (TFA < 0.05% (v/v)). An isocratic elution method was employed with a flow rate of 1 ml min^{-1}. SeMetO eluted at 3.2 min and SeMet eluted at 8.6 min, as determined by their UV absorbance. A photodiode array (PDA) detector was used (Shimadzu SPD-M20A) and quantification of peak areas was performed at 220 nm. SeMetO standards were produced as described in Section 2.3.7.1.

2.3.5.3 SeTal and SeTalO

Separation of SeTal and SeTalO was achieved by injecting 20 µL of sample onto a Zorbax carbohydrate column from Agilent, USA (5 µm, 4.6 x 150 mm) at 35 °C with an isocratic elution using a flow rate of 1 mL min^{-1}. SeTal and SeTalO were eluted using acetonitrile (75 % (v/v)) in H_2O with TFA (0.005% (v/v)) for 8 min, followed by a

washing step whereby the H_2O content was increased to 75% over 1 min, held for 3.5 min, before decreasing back to 25% water over 1 min, and re-equilibration for 2.5 min. SeTal and SeTalO eluted at 2.7 min and 4.4 min respectively. SeTal and SeTalO were quantified by their UV absorbance at 220 nm using a PDA detector (Shimadzu SPD-M20A). SeTalO standards were produced as described in Section 2.3.7.1.

2.3.5.4 Selenoxides in the presence of NADPH

The methods described above were unsuitable for separating selenoxides and selenoethers when NADPH was present in the samples, due to coelution of NADPH derived peaks with other peaks of interest. As such, a different HPLC method was developed as described below.

20 µL samples from enzymatic reduction assays (Section 2.3.4) were injected onto an Agilent Zorbax 300SCX column (5 µm, 4.6 x 250 mm) at 30 °C. An isocratic elution was performed using a mobile phase of NaH_2PO_4 (0.01 M, pH 4.8) with a flow rate of 1 mL min^{-1}. SeMet eluted at 3.9 min, SeMetO eluted at 4.4 min, SeTal eluted at 3.4 min and SeTalO eluted at 3.7 min under these conditions. Samples were detected and quantified using their absorbance at 220 nm using a PDA detector (Shimadzu SPD-M20A).

2.3.5.5 Hydrolysis of protein using methane sulfonic acid (MSA)

MSA hydrolysis was employed to digest proteins to their component amino acids, allowing investigation of oxidative changes to these residues [547]. The MSA method was chosen to digest the protein samples, as there is less destruction of MetSO and tryptophan products, unlike other methods such as HCl hydrolysis [547].

Protein samples (200 µL; 1 mg mL^{-1}) contained in glass hydrolysis vials were delipidated then precipitated by addition of TCA (25 µL, 50% (w/v)) and deoxycholate (25 µL 0.3 % (w/v)) and incubated for 5 min on ice. Samples were pelleted by centrifugation at 7500 *g* at 4 °C for 10 min. Samples were washed twice with ice-cold acetone with the protein pelleted by centrifugation (as above) between washes. Acetone was removed and the samples were dried under a gentle stream of nitrogen. Samples were then resuspended in MSA (150 µL, 4 M) containing tryptamine (0.2 % (w/v)), and the hydrolysis vials placed in Pico-tag vessels. The Pico-tag vessels were evacuated using a vacuum pump and flushed with nitrogen three times, before a final

evacuation and incubation overnight in an oven at 110 °C. The samples were then allowed to cool to 21 °C before being neutralised with freshly prepared NaOH (150 µL; 4 M) solution. Samples were filtered using 0.2 µm NanoSep centrifugal devices (Pall, MI, USA), centrifuged for 2 min at 9300 *g*, and 40 µL of each sample was transferred to a HPLC vial with insert for analysis.

Standards were prepared by dilution from stock amino acid standards for protein hydrolysates (Product number A9781, Sigma Aldrich, St Louis, MI, USA) to 0 - 12.5 µM. MetSO (0 – 12.5 µM) was prepared in water and added to the mixed standard. Standards (40 µL) were transferred to HPLC vials and analysed.

Samples were derivatized immediately before injection onto the column in the autosampler by the addition of 20 µL ortho-phthalaldehyde (OPA) (995 µL OPA reagent, 5 µL 2-mercaptoethanol) with 3 mixing cycles and a 1 min incubation, prior to injection of 6 µL of the final mixture onto a Shimadzu ShimPack XR ODS column (2.2 µm, 4.6 x 100 mm) and eluted with a binary gradient method. Buffer A consists of sodium acetate (50 mM; pH 5.3), tetrahydrofuran (THF) (2.5 % (v/v)) and methanol (20 % (v/v)) in H_2O and Buffer B consists of sodium acetate (50 mM; pH 5.3), THF (2.5 % (v/v)) and methanol (80 % (v/v)) in H_2O. The flow rate was set to 1.2 mL min^{-1}, and the initial concentration of buffer B was 0%. The concentration of buffer B was increased to 25 % over 6 min, before 1 min at 25 % buffer B and increasing to 62 % buffer B over 30 sec which was then held for 2.5 min, before increasing to 100 % buffer B over two min and holding for 1 min. The concentration of B was then reduced to 0 % over the next 30 s and held there for 3.5 min to re-equilibrate the column. The detection of derivatised amino acids was achieved by measuring the fluorescence (λ_{ex}= 340 nm, λ_{em}= 440 nm) using a Shimadzu RF-AXS20 fluorescence detector. Figure 2.2 shows a sample chromatogram depicting observed retention time and peak shape for the amino acids standards.

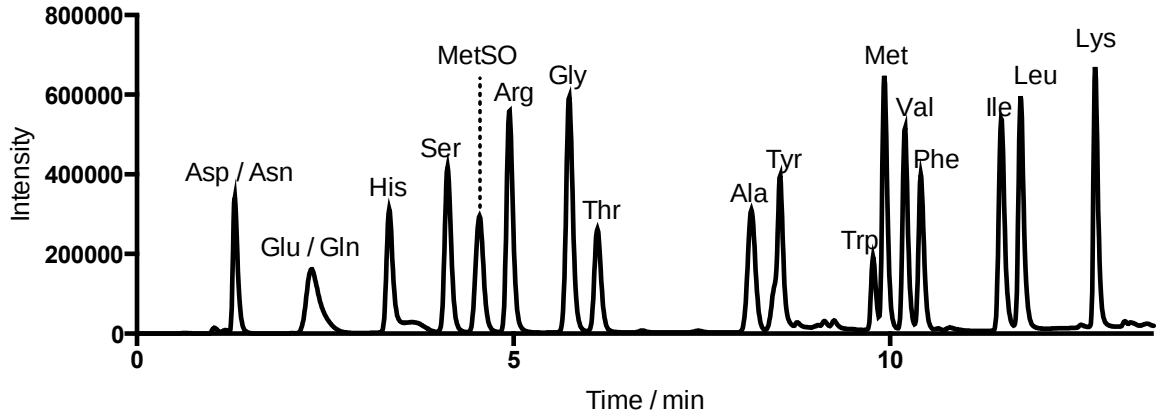

Figure 2.2 – Typical chromatogram observed for amino acid separation using OPA derivatisation. Trace shows a 50 pmol standard.

2.3.6 Mass spectrometry

Samples to be analysed by mass spectrometry were prepared in H_2O before dilution with an equal volume of formic acid (0.2% (v/v)) in methanol. The acidified sample was analysed by direct injection on a Thermo Finnigan LCQ Deca XP Max Plus ion trap mass spectrometer. The analysis was performed in the positive-ion mode, with the electrospray needle held at 4500 V. Nitrogen, the sheath gas, was held at 10 units. The collision gas was helium. The temperature of the heated capillary was 275 °C. For MS/MS studies the normalized collision energy was set at 35%. Mass values were scanned between 100 – 500 *m/z* and spectra were produced by the average of 50 scans.

QualBrowser (Version 1.4, ThermoElectron, Rochford, IL, USA) was used to analyse spectra. Simulations were obtained from QualBrowser with Gaussian outputs, with a 0.4 Da resolution and full width and half maximum (FWHM) valleys.

2.3.7 NMR spectroscopy

Samples to be analysed were dried overnight in a rotational vacuum concentrator (Christ, Osterode am Harz, Germany), before being dissolved in D_2O. A Varian VNMRS 500 MHz instrument (Bruker, MA, USA) was used to collect NMR data. The machine was controlled and analysis performed in VNMR Walkup (Version 6.1, Bruker, MA, USA). Spectra were collected at 25 °C. ^{1}H NMR spectra were recorded with a relaxation delay of 0.01 seconds and a pulse of 60 degrees with an average of 256 scans. ^{13}C experiments were performed with ^{1}H de-coupling with a relaxation delay of 0.01 seconds and a pulse of 45 degrees and spectra produced from the average of 1024

scans. HHCOSY experiments were performed with a relaxation delay of 2.0 scans and spectra produced from the average of 512 scans. HSQCAD experiments were performed with ^{1}H de-coupling with a relaxation delay of 1.5 seconds and spectra produced from the average of 512 scans. Peaks were reported as the ppm shift from the residual H_2O peak set to 4.74 ppm.

2.3.7.1 Preparation and quantification of selenoxides

Selenoxides were formed on selenomethionine, 1,4-anhydro-4-seleno-L-talitol, *N*-acetylselenomethionine, methylselenocysteine and seleno-bispropionic acid. Parent selenoethers (2 mM) were dissolved in water and mixed with either HOCl or H_2O_2 (1 mM in H_2O).

SeMetO and SeTalO concentrations were quantified for use as standards in HPLC experiments. SeMetO and SeTalO were produced as above, and then dried overnight in a rotational vacuum concentrator (Christ, Osterode am Harz, Germany). SeMetO and SeTalO were dissolved in D_2O (500 µL) and the ^{1}H NMR spectrum obtained using a Varian VNMRS 500 MHz instrument. Dimethyl sulfone (100 µL, 5.3 µM) was added as quantification standard, and the ^{1}H NMR spectrum collected again. The concentration of selenoxides was calculated by comparison of peak areas of the dimethyl sulfone (δ = 3.153 ppm, 6H) and product (SeMetO: δ = 2.80 ppm, 3H and δ = 2.71 ppm, 3H; SeTalO: δ = 4.74 ppm, 3H).

2.3.8 Kinetic analysis

Kinetics experiments were carried out using an Applied Photophysics SX.20MV stopped flow system maintained at 22 °C using a thermostatted water bath. The detection system consisted of an ozone-producing Xe light source (150 W; Osram GmbH, Munich, Germany) with wavelength selection achieved using a single monochromator (slit width, 0.5 mm; bandwidth, ±1.2 nm) and photomultiplier detection. The system was controlled by a personal computer running Pro-Data SX (version 2.2.12; Applied Photophysics).

Spectral data from 200 to 310 nm were obtained in a point-by-point manner by acquiring kinetic traces at 10-nm intervals with the photomultiplier over this wavelength region. Second-order rate constants were obtained by global analysis of the kinetic traces using second order models with λ > 240 nm using ProKIV (Applied

Photophysics, Version 1.0.1.4). Rates were confirmed using pseudo-first order analysis at appropriate wavelengths.

2.3.8.1 First and second order reactions

The rates for first and second order rate laws can be expressed as Equation 2.1 for first order reactions, and Equation 2.2 for second order reactions.

$$-\frac{\delta[A]}{\delta t} = k[A]^a \qquad \text{Equation 2.1}$$

$$-\frac{\delta[A]}{\delta t} = k[A]^a[B]^b \qquad \text{Equation 2.2}$$

Integration of these rate laws give rise to Equation 2.3 and Equation 2.4, for first and second order plots respectively, where [A] is the concentration of reactant A at time = t, and $[A]_0$ is the initial concentration of reactant A.

$$\ln[A] = \ln[A]_0 - kt \qquad \text{Equation 2.3}$$

$$\frac{1}{[A]} = \frac{1}{[A]_0} + kt \qquad \text{Equation 2.4}$$

Based on these equations, if a plot of ln[A] vs time graph is linear, the reaction follows first order kinetics. If a plot of $1/[A]$ vs time graph is linear, the reaction follows second order kinetics. As concentration is proportional to absorbance, absorbance data can be used to determine whether the reaction follows first or second order kinetics.

2.3.8.2 Global wavelength analysis

Global wavelength analysis uses mathematical modelling to determine second order rate constants from spectral kinetic data. It monitors the change in absorbance across numerous wavelengths, and can correlate these changes to the contribution of changes in the concentrations of reactants and products simultaneously. Based on this, the model can determine rate constants from each wavelength, and determine an average across the entire range.

This method has significant advantages over pseudo-first order analysis. Under first order conditions, the concentration of [A] is assumed to be constant throughout the reaction but the global analysis is capable of accounting for the changes in [A]. The wavelengths used in pseudo-first order analysis need to be selected so that the

detected absorbance arises primarily from one species, whereas global wavelength analysis can account for a contribution from multiple species at the same wavelength. Global wavelength analysis can also handle more complex models, unlike pseudo-first order analysis which assumes an A + B ➔ C model.

2.3.8.3 Pseudo-first order analysis

Second order bimolecular reactions, characterised by Reaction 2.10, have kinetics that can be described by the rate law in Equation 2.5.

$$A + B \rightarrow Product \qquad \text{Reaction 2.10}$$

$$Rate = k_2[A][B] \qquad \text{Equation 2.5}$$

where [A] and [B] are the concentrations of the reactants and k_2 is the second order rate constant for the reaction. When [A] >> [B], it can be assumed that [A] does not significantly change over the course of the reaction, and hence [A] can be considered constant. The rate can also be expressed as the change in [B] over time. This can be represented by Equation 2.6

$$-\frac{\delta[B]}{\delta t} = k_{obs}[B] \qquad \text{Equation 2.6}$$

where

$$k_{obs} = k_2[A] \qquad \text{Equation 2.7}$$

Integration of Equation 2.7 gives When [B] is kept constant, and initial [A] is varied, this allows the plotting of the observed rate constant against the initial [A], and the second order rate constant can be determined by the gradient of the slope. Single exponential functions were fitted to kinetic traces to give k_{obs} for each concentration of A, using ProData Viewer (Applied Photophysics, Version 4.2.12), which were subsequently used to determine the observed rate constant., and allows the determination of k_{obs} from the absorbance vs. time plots. The absorbance vs time plots are used as the absorbance at a given wavelength is proportional to concentration.

$$[B] = [B]_0 e^{-k_{obs}t} \qquad \text{Equation 2.8}$$

When [B] is kept constant, and initial [A] is varied, this allows the plotting of the observed rate constant against the initial [A], and the second order rate constant can

be determined by the gradient of the slope. Single exponential functions were fitted to kinetic traces to give k_{obs} for each concentration of A, using ProData Viewer (Applied Photophysics, Version 4.2.12), which were subsequently used to determine the observed rate constant.

2.3.9 Cell culture

J774A.1 cells (A.T.C.C. TIB-67) were cultured in Dulbecco's modified Eagle's medium (DMEM) supplemented with fetal calf serum (FCS; 10% (v/v)) and L-glutamine (2 mM), in 175 cm^2 flasks under sterile conditions in an atmosphere of humidified 5% CO_2, at 37 °C. When the cells had reached confluency, they were passaged by first washing twice in warm (37 °C) DMEM, followed by scraping into media (10 mL). 2 mL of cell suspension was added to each new flask and volume made up to 25 mL with DMEM. Cells reached confluency 2-3 days after splitting.

2.3.9.1 Oxidant treatment of cells

Confluent flasks of J774A.1 cells were washed twice with warm (37 °C) DMEM before scraping into media (10 mL). Cell number and viability were assessed by trypan blue dye exclusion. The cell suspension (10 µL) was mixed with equal volumes of trypan blue dye and mixed by aspiration. The resulting mixture (10 µL) was pipetted into haemocytometer chamber and cells counted under a microscope. Cells that did not take up the dye were counted as viable. Cell suspensions were adjusted to 1 x 10^6 cell mL^{-1} and cells plated at a density of 0.5 x 10^6 cells per well in 12-well plates, and allowed to adhere overnight in an atmosphere of humidified 5 % CO_2, at 37 °C. Cells were washed twice with warm (37 °C) HBSS, with various concentrations of SeMet or SeTal (0 – 50 µM) added to the HBSS, prior to addition of HOCl or TauCl (100 or 200 µM) for 20 min or 2 h. Cells were then assessed for changes in viability and function as described in sections below (Section 2.3.10. to 2.3.9.3).

2.3.9.2 GADPH activity

GAPDH is a thiol-dependent cellular enzyme that is critical for glycolysis, and is known to be inactivated when cells are treated with HOCl, HOSCN and *N*-chloramines [229, 245]. GAPDH converts glyceraldehyde 3-phosphate (GAP) to 1,3-bisphosphateglycerate (BPG), reducing NAD^+ to NADH in the process [230] (Reaction 2.11).

$$GAP + NAD^+ \xrightarrow{GAPDH} BPG + NADH$$ Reaction 2.11

J774A.1 cells were prepared and treated as described in Section 2.3.9.1, before washing with warm HBSS and lysis in 600 µL ice cold H_2O, and centrifuged at 5900 g for 5 min at 4 °C to remove any cellular debris. 20 µL of each sample was mixed with 120 µL of pyrophosphate buffer (28.5 mM sodium pyrophosphate, 38 mM sodium phosphate buffer, pH 7.4) and 60 µL of NAD^+/GAP solution (1.2 mM GAP, 2.5 mM NAD^+) in a 96-well plate. The absorbance increase at 340 nm, corresponding to the increase in the concentration of NADH, was measured over 10 min using a M2e plate reader (Molecular Devices). Enzyme activity was determined by the rate of change in absorbance of the resulting time vs absorbance graph.

2.3.9.3 LDH assay

Lactate dehydrogenase (LDH) is a cytosolic enzyme that converts pyruvate to lactate by consuming NADH and forming NAD^+ (Reaction 2.12). LDH activity can be measured by the change in NADH concentration, measured by the change in absorbance at 340 nm. The release of LDH from the cytosol into cell media reflects cell lysis and can be used as a measure of cell viability [559].

$$Pyruvate + NADH \xrightarrow{LDH} Lactate + NAD^+$$ Reaction 2.12

J774A.1 cells were plated at a density of 0.5 x 10^6 cells per well in 12-well plates, and allowed to adhere overnight in an atmosphere of humidified 5 % CO_2, at 37 °C. Cells were washed twice with warm (37 °C) HBSS, then HBSS was added with or without SeMet or SeTal (0 – 50 µM) and incubated for 2 h. The cell media was then collected, and remaining cells washed with warm (37 °C) HBSS, before lysis using 600 µL cold H_2O and incubation on ice for 15 min. The protein content was measured by BCA assay (Section 2.3.3.4). Media or lysate samples (50 µL) were mixed with NADH (375 µM) and sodium pyruvate (2.88 mM) in a total volume of 200 µL, and the absorbance at 340 nm was monitored over 15 min using an M2e plate reader (Molecular Devices). The rate of change in NADH concentration was determined by fitting a linear slope to the Abs vs time plot, which was then normalised to protein concentration. Viability was assessed as LDH activity in the lysate over the total LDH activity in both media and lysate and expressed as a percentage of untreated control.

2.3.9.4 Ethidium bromide release assay

Ethidium bromide (EtBr) interchelates with DNA causing an increase in fluorescence. DNA release from intact cells into the cellular media can be quantified by EtBr fluorescence and used as a measure of cell viability [560].

Neutrophils (2 x 10^6 cells) were incubated in HBSS in the presence of SeMet or SeTal (0, 25 or 50 μM) at 37 °C for 10 min, before centrifugation (13000 *g* for 5 min at 4 °C) to pellet cells. The cell media was removed and cells resuspended in 500 μL H_2O and lysed by addition of Triton-X solution (50 μL, 0.2 % (v/v)). EtBr (25 μM) was added to both the lysate and media samples and incubated for 5 min, before fluorescence was measured (λ_{ex} = 360 nm, λ_{em}= 580 nm) using an M2e plate reader (Molecular Devices). Viability was determined by measuring the fluorescence in the lysate sample as a percentage of total fluorescence (media + lysate).

2.3.9.5 IAF labelling of reversibly oxidised thiols

Oxidation of thiols can result in the formation of various reversible oxidation products including disulfides and sulfenic acids, and also non-reversible products such as sulfonic acids [2]. MPO-derived oxidants are known to deplete cell thiols [225] and cause inactivation of thiol-dependant proteins [245]. If the modifications are reversible, then the cell could potentially recover from the oxidative insult. The effect of SeMet and SeTal on the formation of reversible thiol modification in cells exposed to HOCl or TauCl was assessed using the fluorescent probe 5-iodoacetamide fluorescein (IAF).

J774A.1 cells were prepared and treated as outlined in Section 2.3.9.1, before washing in warm (37 °C) HBSS and lysis in a buffer containing HEPES (35 mM), Triton X (0.1 % (v/v)), Roche complete protease inhibitor (1x) and *N*-ethylmaleimide (NEM; 100 mM). Lysates were centrifuged at 8000 *g* for 5 min, at 4 °C to remove any insoluble cell debris. Excess NEM was removed by filtering the resulting supernatant through a 10 kDa molecular mass cut-off filter (Amicon, 5 min at 9300 *g*) twice with washing using 200 μL phosphate buffer (0.1 M, pH 7.4). Protein concentrations were determined by BCA assay (Section 2.3.3.4) and samples adjusted to 1 mg protein mL^{-1}. DTT (1 M) was added to samples to reduce any reversibly oxidised thiols prior to addition of IAF (100 μM) and incubation for 10 min in the dark. Excess IAF and salts

were removed by addition of 10 % (w/v) TCA to the incubation mixture for 10 min on ice to precipitate the protein, before pelleting the protein by centrifugation at 5900 *g* for 5 min, at 4 °C. The supernatant was then removed and protein pellet washed with ice-cold 80% (v/v) acetone, before centrifugation at 5900 *g* for a further 5 min, at 4 °C. The acetone was then removed and samples air-dried at 22 °C. Samples were then resuspended in 20 µL BioRad NuPage reagent (13 µL H_2O, 5 µL NuPAGE LDS sample buffer (4X), 2 µL Reducing agent (10X)) for electrophoresis.

Samples were loaded onto 4-12% tris-acetate gels, and separated at 200 V for 1 h in the dark. NuPAGE MOPS SDS running buffer was used as the buffer. Gels were then removed and the lower 1 cm of the gel cut off to prevent residual IAF diffusion through the gel. Gels were rinsed in water and scanned for fluoresence using a BioRad FX Plus Pharox Molecular Imager (λ_{ex}= 495 nm, λ_{em}= 520 nm). Gels were stained for total protein levels using either a silver stain [561] or Coomassie blue stain [562].

Gels for silver staining were initially placed in solution containing 50 % (v/v) methanol and 10 % (v/v) acetic acid in H_2O for 30 min to fix the gel, thereby minimising protein diffusion and smearing of the bands. Gels were subsequently washed with 5% (v/v) methanol for 15 min, followed by washing 3 times with H_2O for 5 min. The gels were then soaked in a solution containing sodium thiosulfate (0.02 % (w/v)) in H_2O to sensitise the gel. The gel was then washed with H_2O before soaking in silver nitrate solution (0.2 % (w/v)) in H_2O for 25 min. Excess silver was removed by washing with H_2O for 5 min and the gels were then developed by soaking in a solution containing sodium carbonate (3 % (w/v)), formaldehyde (0.02 % (v/v)) and sodium thiosulfate (0.0004 % (w/v)) in H_2O. The developing solution was removed when a desired level of staining was achieved, and an EDTA solution (1.4 % (w/v)) in H_2O was added to stop further colour development. Gels were imaged using a UMax PowerLook 1120 gel scanner and densitometry using in ImageJ software.

Gels for Coomassie staining were placed in a staining solution containing Coomassie R-250 ((0.1 % (w/v)), ethanol (40 % (v/v)), acetic acid (10% (v/v)) in H_2O and heated in a Panasonic NN-S548WA microwave oven at high power, loosely covered for 1 min, followed by gentle agitation on an orbital shaker for 15 min. The gels were then rinsed with H_2O prior to destaining in a destain solution (ethanol (10 % (v/v)), acetic acid (7.5 % (v/v)) in H_2O and heated in a microwave oven at high power, loosely

covered for 1 min. The gels were then incubated overnight in fresh destain solution prior to imaging using a UMax PowerLook 1120 gel scanner. Densitometry was performed using ImageJ software.

2.3.10 Flow cytometry

Apoptotic and necrotic cell death was determined by dual staining with allophycocyanin-conjugated annexin V (annexin V-APC) and propidium iodide (PI) [563]. Annexin V-APC binds to the phosphatidyl serine that is exposed on the cell surface when cells undergo apoptosis [564]. PI is taken up by necrotic cells and binds to DNA fragments [565].

The J774A.1 cells were plated and treated as described in Section 2.3.9.1 before removal from the 12-well plate and transfer to flow cytometry tubes. Cells were spun down at 2000 *g* for 5 min in an Allegra X-15R Centrifuge (Beckman Coulter) to pellet cells. Cells were then washed twice with warm (37 °C) HBSS, with 5 min spins (as above) to pellet cells between washes. The cells were then resuspended in a master mix of Annexin V-APC and PI stains (100 µL, 5 µg mL^{-1}) in HBSS and incubated in an atmosphere of humidified 5% CO_2, at 37 °C for 15 min. HBSS (400 µL) was added to the samples, before placing on ice until analysis. Flow cytometry was performed on a BD FACSVerse machine (BD Biosciences, Australia) with fluorescence measurement of Annexin V-APC (λ_{ex}= 650 nm, λ_{em}= 661 nm) and PI (λ_{ex}= 493 nm, λ_{em}= 636 nm). Viable cells were determined to be Annexin V and PI negative (Figure 2.3 – lower left quadrant). Annexin-V positive cells were determined to be apoptotic (Figure 2.3 – lower right quadrant), and PI positive cells were determined to be necrotic (Figure 2.3 – upper quadrants).

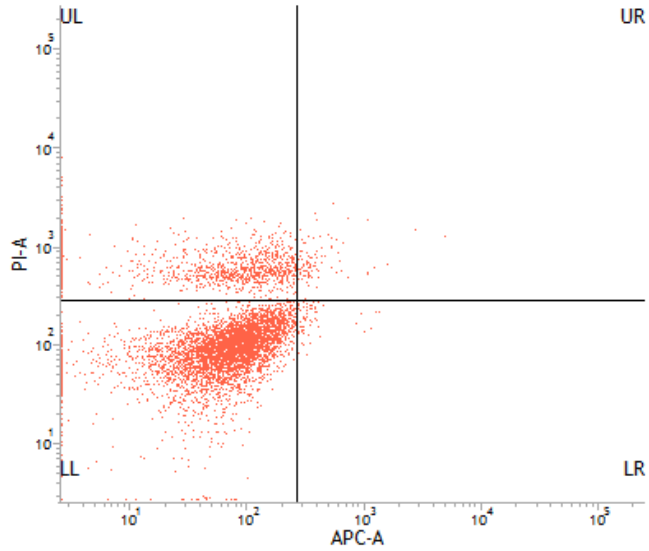

Figure 2.3 – Typical flow cytometry plot obtained for control cells with annexin V-APC and propidium iodide dual staining

2.3.11 Statistical analysis

Data are reported as the mean ± standard deviation from three or more independent experiments, unless otherwise stated. Statistical analyses were performed in GraphPad Prism v6.0 (GraphPad Software, San Diego, USA), with $p < 0.05$ taken as significant. Statistical and post-hoc tests are detailed in relevant Figure legends.

3 Reaction of selenium compounds with MPO-derived oxidants

3.1 Introduction

Neutrophils, via the action of released MPO in the presence of H_2O_2 and Cl^-, produce HOCl together with other strong oxidants in order to destroy invading pathogens as part of the innate immune system. However, when oxidants are produced in excess or inappropriately, they are capable of causing damage to host cells and are believed to play a role in disease initiation and progression [2].

Major targets for the reaction of HOCl in the cellular environment are free thiol groups, such as the Cys residue of GSH, or thioethers such as Met residues [88]. The reaction between HOCl and sulfur residues are some of the fastest reported biological reactions with second order rate constants in the order of 10^7 - 10^8 M^{-1} s^{-1} [86, 90].

HOCl is also known to react with amine groups, such as those on free amino acids, amino acid side chain (e.g. Lys, His) and *N*-terminal amino acids, to form *N*-chloramines, with rate constants ca. 10^5 M^{-1} s^{-1} for alpha amino acids [53, 55, 58, 145, 554]. *N*-Chloramines are also capable of inducing oxidation reactions in a similar manner to HOCl, though they are more specific to sulfur residues [181]. Second order rate constants for the reaction of *N*-chloramines with thiols and thioethers are in the range of 10^2 – 10^3 M^{-1} s^{-1} [136, 192]. *N*-Chloramines have demonstrated potential to inactivate thiol-dependent enzymes, such as GAPDH and creatine kinase (CK) [245]. The higher specificity of *N*-chloramines for thiol sites results in a lower concentration required for GAPDH and CK inactivation compared to HOCl. They also have a demonstrated ability to induce apoptosis and cell death [136, 223, 224]. As *N*-chloramines have higher stability and reduced reactivity compared to HOCl, they are capable of diffusing away from their site of formation and may propagate oxidative damage at remote sites [87, 181, 566]. However, the stability and reactivity of *N*-chloramines is dependent on structure, with primary *N*-chloramines more stable than those formed on other sites such as the imidazole ring of His [134, 136, 179, 181, 192].

Oxidation of Met residues results in the formation of MetSO as a primary product [467]. Dehydromethionine is also formed in a lower yield when Met is oxidised by HOCl and *N*-chloramines [115]. It has been suggested that Met oxidation may play a role in antioxidant defence, as exposed Met residues are preferentially oxidised over other functionally important sites, hence preserving enzymatic function [110, 567, 568].

Oxidation of Met can also lead to inactivation of enzymes, with α_1-antiproteinase activity being inhibited when exposed to HOCl or *N*-chloramines [113, 181].

Organic selenium compounds have been shown to react with peroxides, hypohalous acids and ONOOH [90, 98, 439, 454, 461, 486, 569]. This process is significantly faster for SeMet than Met, with second order rate constants for the reaction with HOCl > 10^8 M^{-1} s^{-1} [90]. Similarly, other selenoethers react with HOCl and HOSCN at a faster rate than the sulfur analogues [90, 98, 439]. These higher rate constants have been attributed to the increased nucleophilicity of selenium compared to sulfur [570]. Analogous to Met oxidation, SeMet is oxidised by ONOOH, H_2O_2 and flavin-containing monooxygenases to form the selenoxide, SeMetO [461, 464, 474, 571].

The increased reactivity of selenium compounds towards MPO-derived oxidants suggests that they may be competitive *in vivo* targets for oxidation. The ability of selenium compounds to react with MPO-derived oxidants before these oxidants can cause damage to cells and cellular components may have therapeutic benefit in inflammatory conditions.

3.2 Aims

The aim of the studies presented in this Chapter was to investigate the reactions between MPO-derived oxidants, specifically *N*-chloramines, with the selenoethers, SeMet and SeTal (structures shown in Figure 3.1). Reaction products were determined by HPLC, mass spectrometry and NMR spectroscopy, and second order rate constants were determined using stopped flow methods.

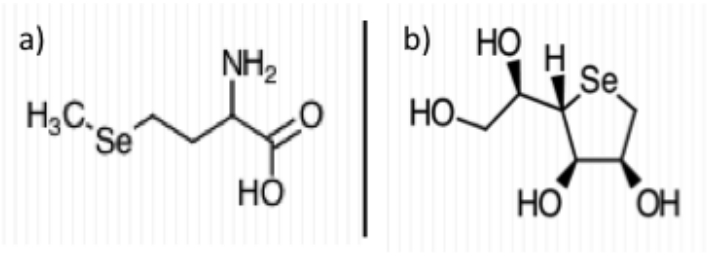

Figure 3.1 - Molecular structures of a) SeMet and b) SeTal

3.3 Results

3.3.1 Sulfur and selenium compounds scavenge MPO-derived oxidants

As previous studies have shown that SeMet, SeTal and Met react with the MPO-derived oxidants HOCl and HOSCN [90, 98, 439], the ability of these compounds to remove oxidants produced enzymatically by the MPO system was investigated. The efficacy of SeMet, SeTal and Met in scavenging oxidants generated by the MPO/H_2O_2/Cl^- system or freshly isolated neutrophils was assessed by the TMB assay in the presence of excess Tau [549]. Tau was present in a large excess (10 mM) to scavenge HOCl, resulting in the formation of the more stable TauCl, which facilitates accurate oxidant measurement [549]. The TMB assay was used as it reacts specifically with HOCl and TauCl, and will not react with the other oxidants present in the system (e.g. H_2O_2) or the selenoxides that may be formed as products.

3.3.1.1 Isolated MPO/H_2O_2/Cl^-

Myeloperoxidase (2 μM) was incubated with Cl^- (100 mM), Tau (10 mM) and SeMet, SeTal or Met (0 – 100 μM) for 10 min at 37 °C. H_2O_2 (50 μM) was added to initiate the production of HOCl by MPO, and allowed to incubate for 30 min at 21 °C. On completion of the incubation period, the concentration of MPO-derived oxidants was assessed using the TMB assay, and quantified by comparison to a standard curve generated using known amounts of TauCl.

The MPO/H_2O_2/Cl^- system produced approximately 50 μM TauCl over 30 min following the addition of H_2O_2, as assessed by the TMB assay, consistent with complete conversion of H_2O_2 to HOCl. Addition of 12.5 μM SeMet to the MPO/H_2O_2/Cl^- system prior to the addition of H_2O_2 caused a 25 % decrease in the presence of TauCl compared to the absence of SeMet (Figure 3.2). Increasing the concentration of SeMet demonstrated a further decrease in remaining oxidant levels. After addition of 50 μM SeMet, essentially no TauCl was observed after the 30 min incubation. Similarly, addition of increasing concentrations of SeTal and Met demonstrated a dose-dependent decrease in the remaining oxidant concentration (Figure 3.2). The decrease in oxidant concentration occurred with a 1 : 1 ratio of scavenger to oxidant removed, with a linear decrease and essentially all oxidant removed at 50 μM of Met and SeTal. IC_{50} values were determined by a non-linear fit (log(inhibitor) vs normalised response

– variable slope) to TMB scavenging data in GraphPad Prism and are reported in Table 3.1. No significant differences were observed in the scavenging ability of the various compounds SeMet, SeTal and Met under these conditions, which may reflect the long (30 min) incubation time employed.

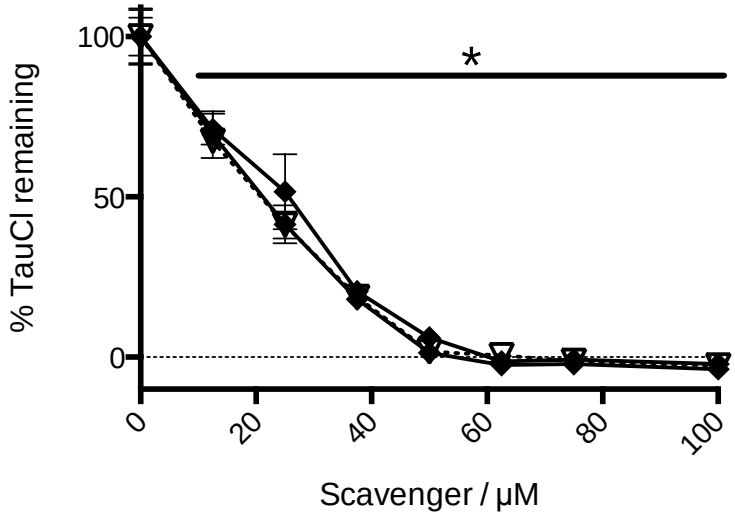

Figure 3.2 – SeMet, SeTal and Met scavenge oxidants produced by the MPO/H_2O_2/Cl^- system

*HOCl and TauCl (ca. 50 µM oxidant over 30 min) were produced by adding H_2O_2 (50 µM) to MPO (2 µM) in the presence of Cl^- (100 mM), Tau (10 mM) and Met ·▽· , SeMet —◆— or SeTal —▼— (0 – 100 µM). The remaining oxidant concentration after 30 min was quantified using the TMB assay. Met, SeMet and SeTal dose dependently decreased the concentration of TauCl present 30 min after addition of H_2O_2. * represents a significant ($p < 0.05$) decrease in remaining TauCl from the 0 µM scavenger control based on one-way ANOVA with Dunnett's post-hoc test.*

Table 3.1 – IC_{50} values (μM) for the scavenging of MPO-derived oxidants by sulfur and selenium compounds.

IC_{50} values were determined by using a non-linear fit (log(inhibitor) vs normalised response – variable slope) to TMB scavenging data using GraphPad Prism 6.0. Values are expressed as IC_{50} ± 95% confidence interval.

Oxidant	Met	SeMet	SeTal
MPO[a]	19 ± 7	22 ± 3	19 ± 2
Neutrophils[b]	23 ± 4	25 ± 4	29 ± 3

[a] MPO system: MPO (2 μM) / H_2O_2 (50 μM) / Cl^- (100 mM)

[b] Neutrophils (2 x 10^6 cells mL^{-1}) stimulated with PMA (0.1 μg mL^{-1}) for 30 min at 21 °C

3.3.1.2 Neutrophil viability

Neutrophils are a potent source of MPO in the circulation, therefore the ability of Met, SeMet and SeTal to scavenge oxidants produced by neutrophils was assessed. Initially, experiments were performed to assess the toxicity of Met, SeMet and SeTal to ensure any reduction in oxidant production was not due to neutrophil death. Neutrophil viability on exposure to Met, SeMet and SeTal was assessed by measuring DNA release using an EtBr assay. Neutrophils (2 x 10^6 cells mL^{-1}) were incubated for 30 min at 37 °C in the presence of Met, SeMet or SeTal (25 or 100 μM), before examining DNA release from the cells as a marker of lysis by measuring changes in EtBr fluorescence. No changes in neutrophil viability were observed with Met, SeMet or SeTal compared to control neutrophils in the absence of these compounds (Figure 3.3).

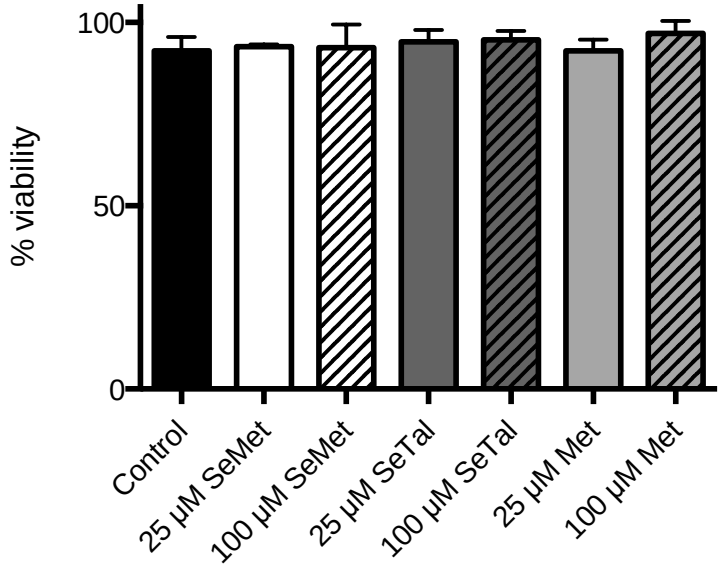

Figure 3.3 – Neutrophil viability is not affected by incubation with Met, SeMet and SeTal.

Neutrophils (2 x 10^6 cell mL^{-1}) were incubated for 30 min at 37 °C in the presence of 0 (black bar), 25 µM (no stripe) or 100 µM (striped) SeMet (white bars), SeTal (dark grey bars) or Met (light grey bars). Neutrophil viability was not affected by presence of these compounds under the conditions employed as measured by DNA release using EtBr. No significant difference was observed relative to control based on one-way ANOVA with Dunnett's post-hoc test. Data are reported as the mean ± SD from 3 independent experiments.

3.3.1.3 Neutrophil derived oxidants

As SeMet, SeTal and Met demonstrated no toxicity for neutrophils under these conditions, the ability of each compound to remove oxidants formed by neutrophils activated by PMA stimulation (0.1 µg mL^{-1}) was assessed using the TMB assay. Freshly isolated neutrophils (2 x 10^6 cell mL^{-1}) were incubated in warm (37 °C) HBSS in the presence of Met, SeMet or SeTal (0 – 100 µM) for 10 min. Neutrophils were stimulated by addition of PMA (0.1 µg mL^{-1}), and incubated for a further 30 min. Under these conditions, approximately 50 µM oxidant was formed as assessed by the TMB assay. The major TMB oxidising species was assumed to be TauCl, as neutrophils release up to 20 mM Tau upon activation, which reacts with HOCl formed by the action of MPO. After 30 min, the remaining oxidant was assessed using the TMB assay, and quantified by comparison to a standard curve prepared using TauCl.

Addition of SeMet, SeTal or Met to the neutrophil suspension prior to activation with PMA resulted in a decrease in the formation of TauCl (Figure 3.4). The

concentration of remaining oxidant decreased in a dose-dependent manner with increasing concentrations of SeMet, SeTal and Met. A significant difference in remaining oxidant relative to the system without added scavenger was achieved with addition of 25 μM scavenger. Essentially no oxidant was detected when 62.5 μM SeMet, SeTal and Met was present in the incubation mixture. This represents a near 1 : 1 stoichiometric scavenging of oxidant produced, similar to that observed in the MPO/H_2O_2/Cl^- system. IC_{50} values were determined by a non-linear fit (log(inhibitor) vs normalised response – variable slope) to TMB scavenging data in GraphPad Prism and are reported in Table 3.1. No significant differences were observed in the scavenging efficacy between the compounds examined under these conditions.

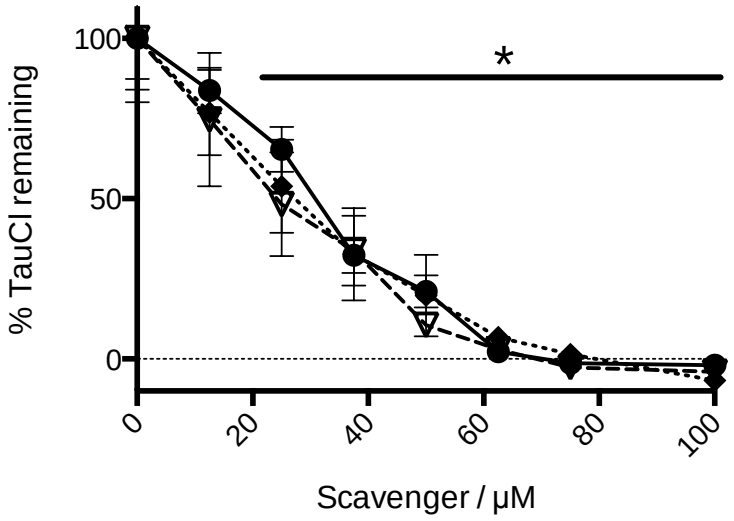

Figure 3.4 - SeMet, SeTal and Met scavenge oxidants produced by activated neutrophils.

*HOCl and subsequently TauCl, (ca. 50 μM oxidant over 30 min) was produced by stimulating neutrophils (2 x 10^6 cells mL^{-1}) with PMA (0.1 μg mL^{-1}) in the presence Met ·▽· , SeMet —◆— or SeTal —▼— (0 – 100 μM). The remaining oxidant concentration after 30 min was quantified by the TMB assay. Met, SeMet and SeTal dose dependently decreased the concentration of TauCl present 30 min after activation of neutrophils. * represents a significant ($p < 0.05$) decrease in remaining TauCl from 0 μM scavenger control based on one-way ANOVA with Dunnett's post-hoc test. Data are reported as the mean ± SD from 3 independent experiments.*

3.3.2 Reaction kinetics of oxidation of SeMet and SeTal by *N*-chloramines

The above data show that Met, SeMet and SeTal can effectively remove *N*-chloramines and MPO-derived oxidants. However, in order to be an effective scavenger

in a more complex system, these compounds would need to have favourable reaction kinetics in order to scavenge oxidants before they react with endogenous species. Second order rate constants for the reaction between *N*-chloramines and Met have previously been reported [192], and were therefore not examined in this study. However, the rate constants for the reaction of a variety of model *N*-chloramines with SeMet and SeTal were determined.

Second order rate constants for the reaction between SeMet, SeTal and model *N*-chloramines, derived from Tau, *N*-α-acetyllysine and glycine were determined using stopped-flow methods. *N*-Chloramines (125 μM) and SeMet or SeTal (0.5 – 2.5 mM) were mixed in the stopped-flow apparatus and kinetic traces recorded for the spectral region between 240 - 310 nm in 10 nm steps.

SeMet and SeTal both absorb in the 200 - 300 nm region and sample spectra are shown in Figure 3.5. *N*-Chloramines are also detectable by UV absorbance and have a maximum absorbance at ca. 250 nm (Figure 3.5c) [554]. Absorbance decreases were observed in the 250 – 290 nm region when each *N*-chloramine was mixed with SeMet or SeTal (Figure 3.6), which is attributed to *N*-chloramine loss. In experiments with SeTal, absorbance decreases were observed between 250 – 300 nm, though at 240 nm an increase in absorbance was observed, possibly due to the formation of a selenoxide (SeTalO).

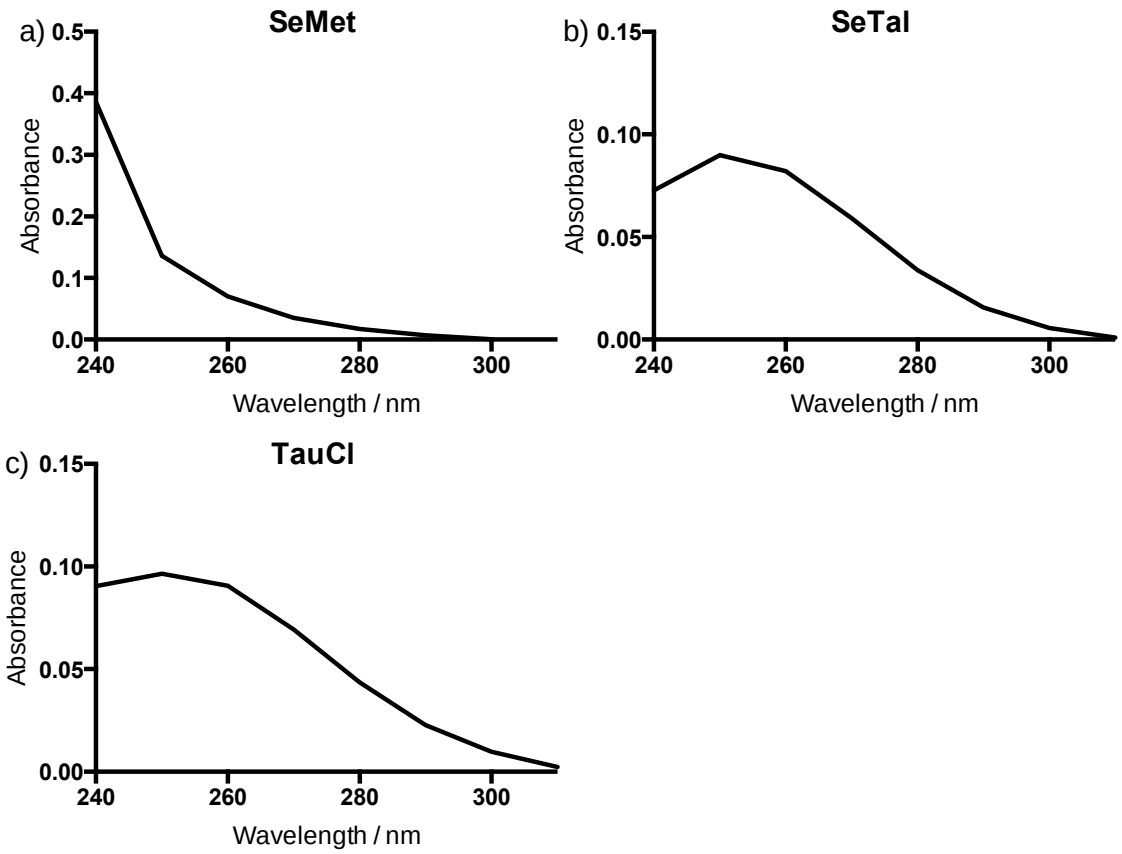

Figure 3.5 – Initial spectra recorded for SeMet, SeTal and TauCl

The UV-vis absorbance spectra were collected at 10 nm steps between 240 – 310 nm for use as fixed spectra in global wavelength analysis. Spectra are a) SeMet (1 mM), b) SeTal (1 mM) and c) TauCl (250 μM) phosphate buffer (in 0.1 M pH 7.4) at 22 °C. Data are representative of three independent experiments.

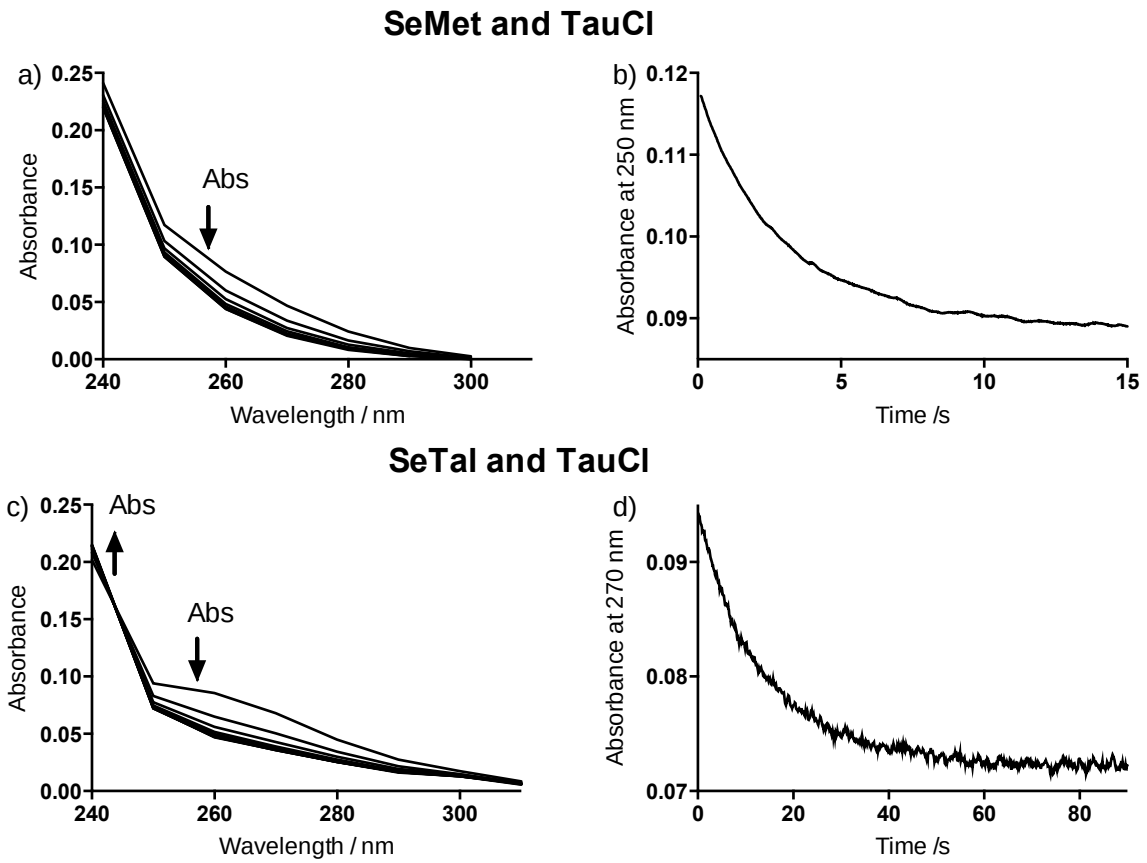

Figure 3.6 – UV absorbance changes over time and at different wavelengths when TauCl (125 µM) was mixed with SeMet (500 µM) or SeTal (500 µM)

Spectral absorbance changes observed over time between 240 – 310 nm recorded at 10 nm intervals for reaction mixtures containing TauCl (125 µM) and a) SeMet (500 µM) or c) SeTal (500 µM) at 22 °C and pH 7.4. For clarity, selected spectra are shown at intervals of 2 s for SeMet and 10 s for SeTal. The direction of absorbance change is indicated by the arrows. b and d) show the typical changes in absorbance over time b) for SeMet at 250 nm and d) SeTal at 270 nm. Data are representative of three independent experiments.

Rate constants were determined by global wavelength analysis in ProKIV (Applied Photophyscis) using a simple "*N*-chloramines + scavenger ➔ Product" second order mechanism and are reported in Table 3.2. Fixed spectra of the reactants (250 µM *N*-chloramine; 1 mM SeMet or SeTal Figure 3.5) were used to aid analysis and allow for the determination of extinction coefficients by the analysis program. Kinetic analysis of data was performed between 240 – 310 nm as below 240 nm limited absorbance changes were observed. This was due to strong absorbance (> 1 Abs unit), which affects the linearity of the response and yields less accurate data. The second order rate constants determined are reported in Table 3.2. The rate constants determined are some of the fastest known for *N*-chloramine reactions, with the rate constants SeMet

being greater than the analogous Met, and the thiol antioxidant GSH [192]. Similarly, the rate constants for SeTal are comparable to those reported for GSH [192].

Table 3.2 – Second order rate constants for the reaction between SeMet and SeTal and model *N*-chloramines

Second order rate constants determined by global wavelength analysis (with 95% confidence limits) at pH 7.4 (0.1 M phosphate buffer) and 22 °C for the reactions of SeMet and SeTal with the N-chloramines formed on Tau, N-α-acetyl-lysine and Gly. Values in brackets are second order rate constants determined by pseudo-first order analysis of the data, and are included as a comparison of the data analysis methods.

N-Chloramine	k_2 (M^{-1} s^{-1})	
	SeMet	SeTal
TauCl	817 ± 20 (890 ± 50)	115 ± 4 (108 ± 3)
LysCl	3430 ± 70 (4600 ± 450)	683 ± 14 (670 ± 60)
GlyCl	2250 ± 40 (2460 ± 170)	430 ± 7 (400 ± 30)

Second order rate constants were confirmed using pseudo-first order analysis at 250 nm for SeMet reactions and 270 nm for SeTal reactions. 250 nm was selected for SeMet, as 250 nm is the maximum for *N*-chloramine absorbance, therefore changes at this wavelength should be primarily due to *N*-chloramine loss. However, absorbance changes at 250 nm for SeTal experiments were complicated by contributions from SeTal, and therefore, absorbance changes at 270 nm were used for pseudo first order analysis. The observed rate constant, k_{obs}, was determined by fitting exponential curves to absorbance vs time plots. Second order rate constants were then derived from the gradient of the line of a [SeMet] or [SeTal] vs k_{obs} plot, and are reported in Table 3.2.

The second order rate constants determined in both analyses agree well with one another (Table 3.2), though the rate constant determined by global analysis is considered to be the more accurate reflection of the rate constant. This is because the global analysis uses data from multiple wavelengths and accounts for the change in concentration of reagents as the reaction progresses, whereas the pseudo first order analysis requires the assumption that scavenger concentration are constant during the

course of the reaction. As a result of these considerations, there should be less error in the global analysis rate constant, compared to the pseudo first order analysis, making the determination more reliable.

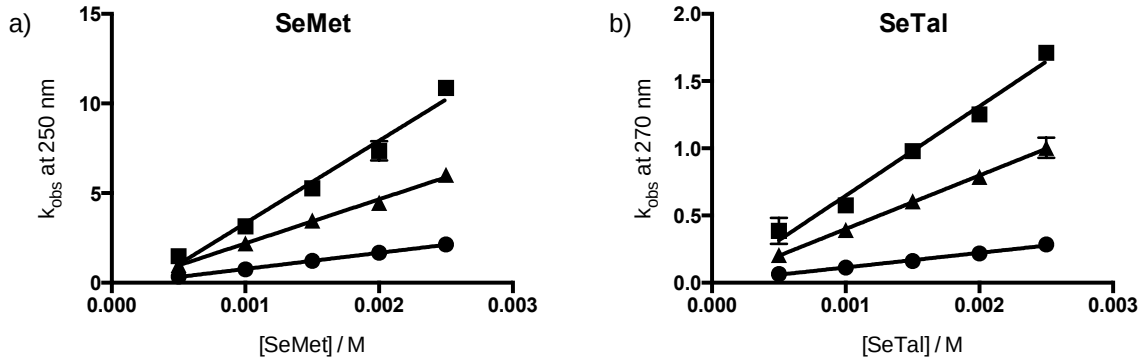

Figure 3.7 – Pseudo first order plots for reaction between SeMet and SeTal and *N*-chloramines

N-chloramine (125 μM) (TauCl (circle), LysCl (triangle) or GlyCl (square)) was mixed with a) SeMet or b) SeTal (0.5 – 2.5 mM) and the absorbance change monitored at 250 nm for SeMet and 270 nm for SeTal. Exponential decay plots were fitted to the resulting kinetic traces to determine the observed rate constant for the reaction, k_{obs}. The gradients of these linear fits provide the rate constant and are reported in the paratheneses in Table 3.2*. Data represent mean ± SD from three independent experiments. Where not visible error bars are hidden by symbol.*

3.3.3 Characterisation of selenomethionine oxidation products

In the previous section, data have been presented which are consistent with SeMet reacting rapidly with MPO-derived oxidants, however, the products of the reaction of SeMet with HOCl and *N*-chloramines have not been characterised. Previous studies have demonstrated that reaction of SeMet with H_2O_2 and ONOOH gives rise to SeMetO, which has been previously characterised [461, 464, 571]. Initial studies focussed on the products formed when HOCl and *N*-chloramines react with SeMet.

3.3.3.1 Mass spectrometry

SeMet (500 μM) in H_2O was mixed with HOCl or H_2O_2 (400 μM) and incubated at 22 °C for 5 min. The resulting solutions were mixed in equal volumes with 0.02% (v/v) formic acid in methanol and analysed by mass spectrometry. H_2O was used for the experiments, rather than the phosphate buffer used in the kinetic studies, to minimise contamination of the mass spectrometer with buffer salts.

Selenium occurs naturally in multiple different isotopes with ^{80}Se being the most abundant (49.6 %), ^{78}Se the second most abundant (23.8 %), followed by ^{76}Se, ^{82}Se, ^{77}Se and ^{74}Se (9.4 %, 8.7 %, 7.6 % and 0.9 % respectively) [572]. This natural abundance gives rise to a characteristic mass spectrum for compounds containing selenium, with peak areas proportional to the abundance of each isotope. This isotope ratio can be observed in the simulated mass spectra for SeMet shown in Figure 3.8b.

The parent SeMet species, $[SeMet+H]^+$, was observed in all samples at *m/z* 198.1 (the ^{80}Se isotope) with the expected pattern for Se from *m/z* 192.4 – 201.2 (Figure 3.8a,c,e). Peaks reported are those for the ^{80}Se isotope, which is the most abundant isotope of selenium. Isotope ratios correspond with the expected patterns, and this was confirmed by computer modelling (Figure 3.8b).

Treatment of the samples with H_2O_2 and HOCl would be expected to yield a selenoxide, on the basis of literature data [571]. However, no peak was detected at *m/z* 214.0, which would be the expected mass of the singly charged selenoxide species $[SeMetO+H]^+$ (Figure 3.8d demonstrates the expected ions for this species based on simulation). This ion may not be seen under the conditions employed due to poor ionisation of the SeMetO species. However, upon treatment of SeMet with HOCl, new peaks were detected at *m/z* 196.3 and 218.2 (^{80}Se peak, with the expected isotope patterns), which corresponds to a loss of 2 mass units or a gain of 20 mass units respectively compared to the parent ion $[SeMet+H]^+$ at *m/z* 198.1. These mass changes are consistent with the loss of H_2 to form dehydroselenomethionine ions as either H^+ or Na^+ adducts, $[DeHSeMet+H]^+$ and $[DeHSeMet+Na]^+$ respectively (supported by computer modelling in Figure 3.8f).

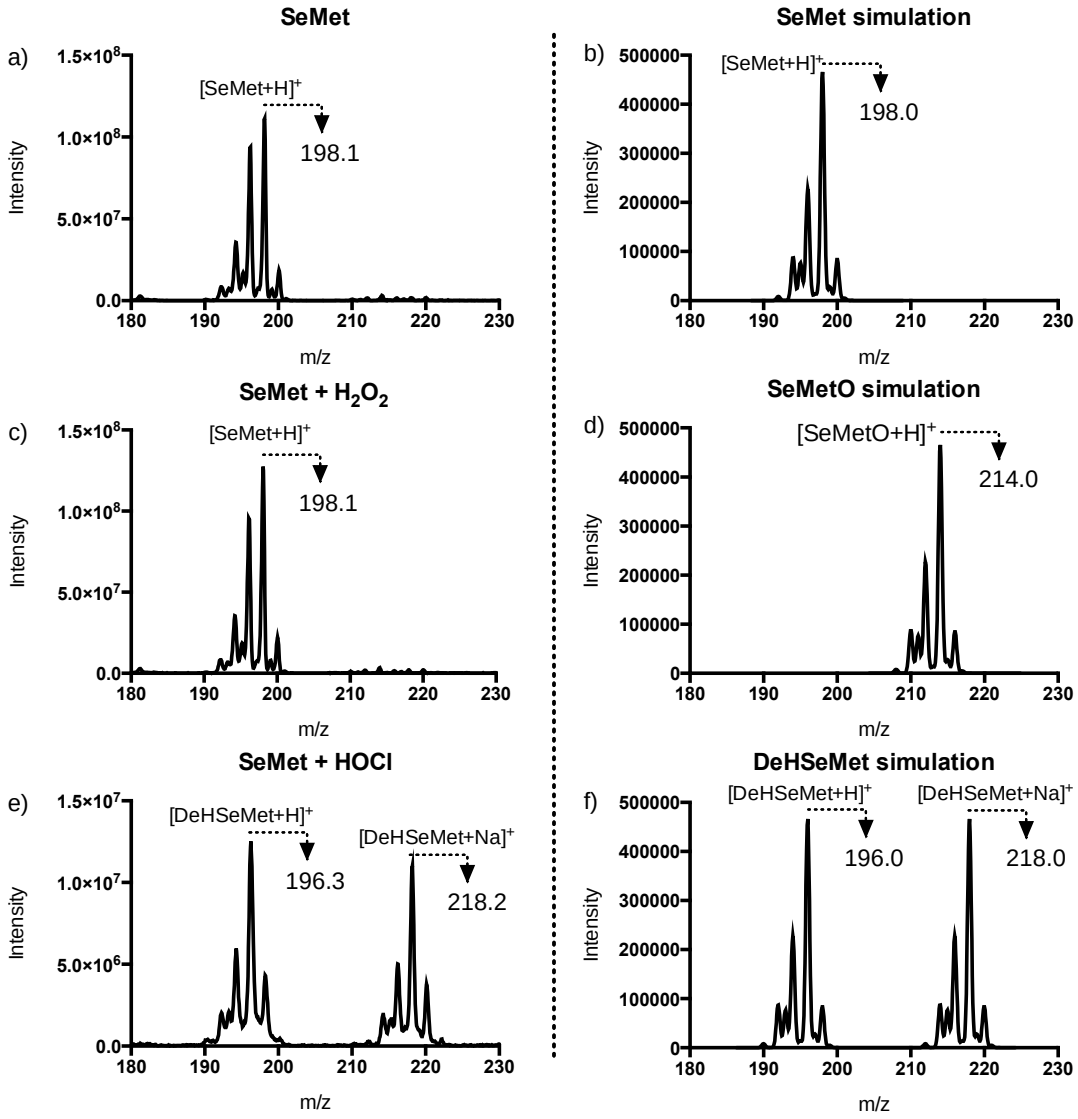

Figure 3.8 – Distribution of ions detected by mass spectrometry when SeMet was treated with HOCl or H_2O_2 with supporting computer simulation.

Species detected by mass spectroscopy on reaction of SeMet (500 µM) with HOCl or H_2O_2 (400 µM). Samples were mixed in a 1 : 1 ratio with 0.02% (v/v) formic acid in methanol before analysis by mass spectrometry. a) Parent SeMet (250 µM). c) SeMet (250 µM) treated with 200 µM H_2O_2. e) SeMet (250 µM) treated with 200 µM HOCl. b, d and f) show computer simulation of b) the parent ion of SeMet, d) the H-adduct of SeMetO and f) the H- and Na-adducts of dehydroselenomethionine. Neither of the experimental spectra show the expected ion pattern for SeMetO at m/z 214.0 for ^{80}Se as seen in the computer simulation d). H_2O_2 only shows ions which correspond to ions from SeMet as seen in the model c). HOCl treatment gives rise to ions that are m/z 2 less than the parent SeMet (m/z 196.3), and are consistent with the dehydroselenomethionine hydrogen adduct, $[DeHSeMet+H]^+$. The peaks centred around m/z 218.2 are consistent with the Na adduct of dehydroselenomethionine, $[DeHSeMet+Na]^+$. f) shows a computer simulation of equal concentrations of $[DeHSeMet+H]^+$ and $[DeHSeMet+Na]^+$. Simulations were produced using QualBrowser by inputting empirical formulae with Gaussian outputs with a 0.4 Da resolution and full width half maximum valleys.

MS/MS fragmentation spectra of the *m/z* 196.3 and 218.2 ions yielded major fragment ions at *m/z* 167.9 and 189.9 (Figure 3.9), corresponding to a loss of 28 mass units. This fragmentation pattern has been previously described for dehydromethionine and is attributed to loss of C_2H_2 [115]. The difference in fragment masses of 22 mass units after fragmentation suggests that the *m/z* 196.3 and 218.2 ions are the same species present as either the H^+ or Na^+ adduct. Thus, the peaks at *m/z* 167.9 and 189.9 are attributed to the ions $[DeHSeMet+H-C_2H_2]^+$ and $[DeHSeMet+Na-C_2H_2]^+$ respectively.

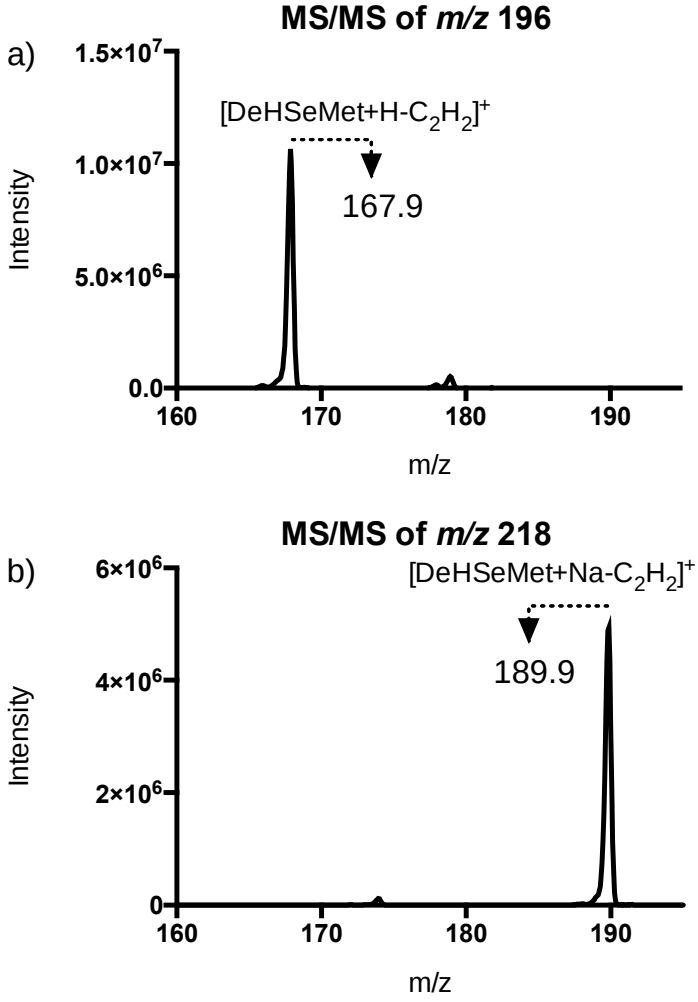

Figure 3.9 – MS/MS fragmentation pattern of *m/z* 196.3 and *m/z* 218.2 peaks for SeMet treated with HOCl.

SeMet (250 µM) treated with HOCl (200 µM) and mixed in a 1 : 1 ratio with 0.02% (v/v) formic acid in methanol before analysis by mass spectrometry. MS/MS analysis was performed on ions at a) m/z 196.3 and b) m/z 218.1. A loss of 28 mass units was observed for both species, and attributed to loss of C_2H_2 giving rise to ions $[DeHSeMet+H-C_2H_2]^+$ and $[DeHSeMet+Na-C_2H_2]^+$ respectively.

3.3.3.2 NMR

Although SeMetO was not observed in the mass spectrometry experiments using the conditions employed in this study, oxidation of SeMet by H_2O_2 has been previously demonstrated to produce SeMetO [464, 571]. Therefore, SeMet was treated with H_2O_2 and the resulting products were analysed by NMR. SeMet (5 mg, 25 μmoles) in H_2O was reacted with equimolar concentrations of H_2O_2 or HOCl for 15 min at 22 °C. The samples were then dried overnight using a rotational vacuum concentrator (Christ, Osterode am Harz, Germany). The resulting white solid was dissolved in 600 μL D_2O and analysed by NMR.

Reaction of SeMet with H_2O_2 resulted in a product consistent with ^1H NMR spectroscopy data previously reported for SeMetO [464]. The spectra demonstrate the formation of two products, which are attributed to SeMetO, and hydrated SeMetO as previously described [464], and chemical shifts and splitting are reported in Table 3.3. Peaks consistent with SeMetO were the only product peaks observed. However, residual signals from the parent SeMet compound were present at 1.893, 2.00-2.16, 2.48-2.56 and 2.73 ppm, as well as overlapping with a SeMetO signal at 3.70 ppm.

Table 3.3 – ^{13}C NMR chemical shifts for selenoxide formed on reaction of SeMet with H_2O_2

	SeMetO			SeMetO.H_2O		
Environment	ppm	Splitting	H	ppm	Splitting	H
A	2.564	s	3	2.654	s	3
B	2.82 - 3.16	Multiplet	2	3.52 - 3.66	Multiplet	2
C	2.20 – 2.26	q	2	2.36 – 2.44	Multiplet	2
D	4.18 - 4.22	t	1	~3.704	obscured	1

SeMet (5 mg, 25 μmol) was also treated an equimolar concentration of HOCl and the product of the reaction analysed by ^1H NMR spectroscopy (Figure 3.11). The most intense signals detected corresponded to SeMetO proton environments with ppm and relative integral areas the same as that observed for H_2O_2 treated SeMet (Figure 3.10). As a result, the primary product of HOCl treatment of SeMet was therefore assigned to the selenoxide, SeMetO. However, HOCl treated SeMet also gave rise to small ^1H NMR

signals at 3.75, 4.11 and 4.42 ppm which could not be attributed to either parent SeMet or SeMetO, and were not observed with H_2O_2 treatment. This suggests the formation of a secondary product, potentially dehydroselenomethionine, though due to low intensity and poor resolution of these peaks, this could not be confirmed from these data. However, this is consistent with the mass spectrometry data that suggest HOCl can lead to formation of dehydroselenomethione, whereas H_2O_2 cannot.

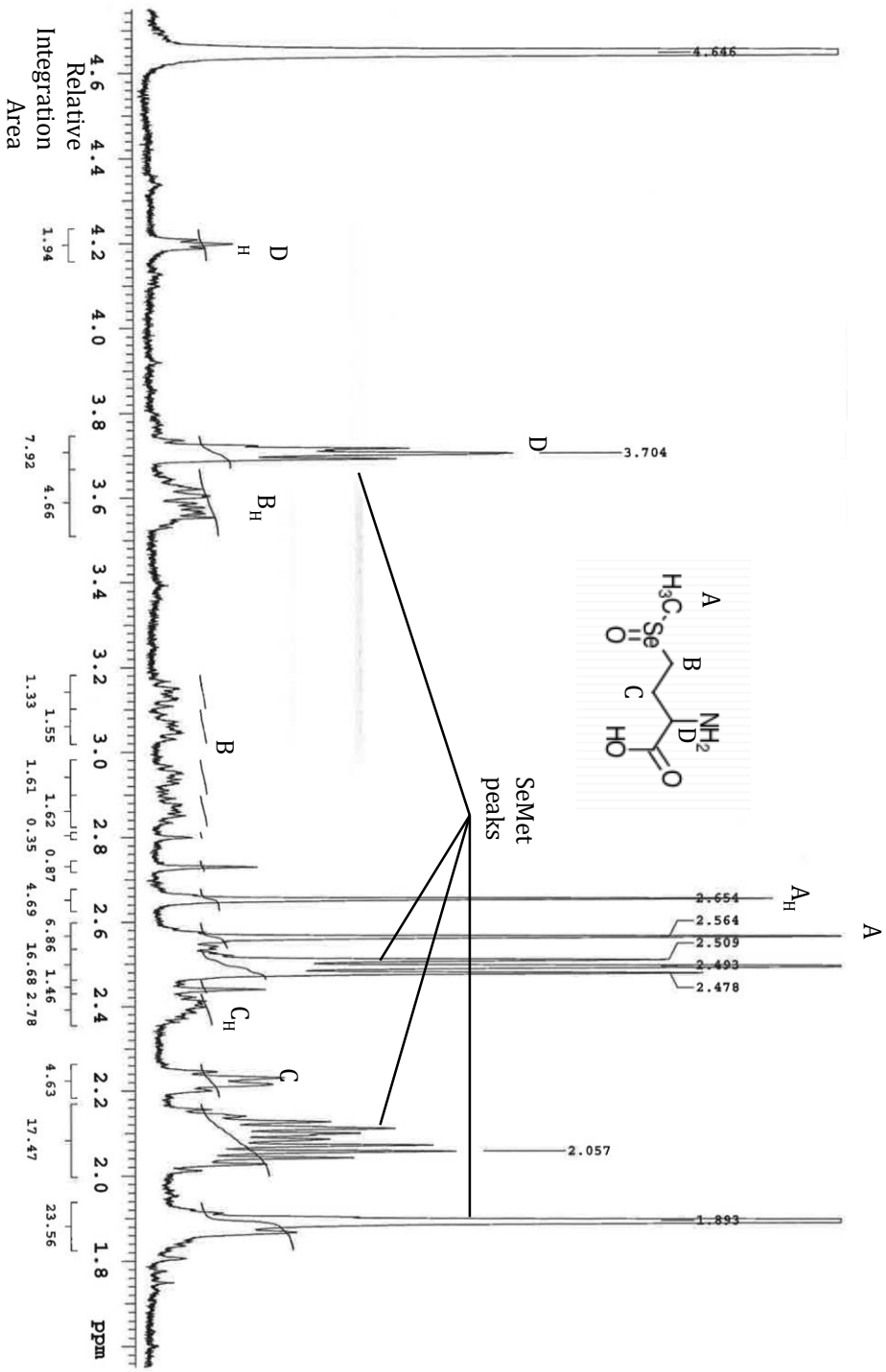

Figure 3.10 – ^{1}H NMR spectra of SeMet treated with H_2O_2

SeMet (5 mg; 25 µmol) dissolved in water was mixed with equimolar H_2O_2, dried overnight and redissolved in D_2O (600 µL) was analysed by ^{1}H NMR spectroscopy. Chemical shifts are reported using the residual H_2O peak as a reference (∂ = 4.64 ppm). Product signals are consistent with those previous reported for SeMetO. The conversion to SeMetO was incomplete with residual parent peaks observed in the spectra.

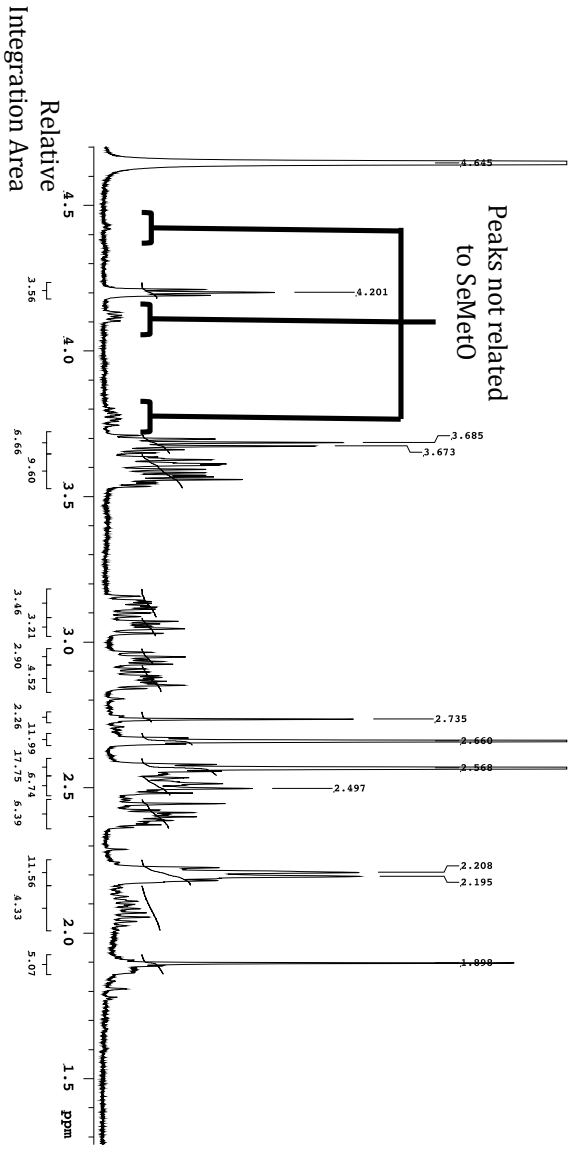

Figure 3.11– ^{1}H NMR spectra of SeMet treated with HOCl

SeMet (5 mg; 25 µmol) dissolved in water was mixed with equimolar HOCl, dried overnight and redissolved in D_2O (600 µL) and analysed by ^{1}H NMR spectroscopy. Chemical shifts are reported relative to the residual H_2O peak set to 4.64 ppm. The largest signals are consistent with the formation of SeMetO. Peaks at 3.75, 4.11 and 4.42 ppm attributed to minor product, possibly dehydroselenomethionine.

3.3.3.3 Standardisation of SeMetO for HPLC

^{1}H NMR spectroscopy was used as a method of quantifying the selenoxide standards for use in HPLC. As the relative peak areas in ^{1}H NMR spectra correlate to the number of protons in the environment, the concentration of products can be determined by comparison to a known concentration of an internal standard.

SeMetO was produced by the reaction of SeMet (25 μmol) with an equimolar concentration of H_2O_2, which was incubated for 15 min, before it was divided into 2 aliquots and dried overnight in a rotational vacuum concentrator (Christ, Osterode am Harz, Germany). One aliquot of the resulting white solid was dissolved in 600 μL D_2O, before addition of the internal standard dimethyl sulfone ($DMSO_2$) (5.3 μM). The ^1H NMR spectra were collected (Varian VNMRS 500 MHz) (Figure 3.10), and the concentration of SeMetO determined by comparison of dimethyl sulfone peaks (∂ = 3.15 ppm, 6H) to SeMetO peaks (∂ = 2.80 ppm, 3H; ∂ = 2.71 ppm, 3H). The calculated concentration for SeMetO was 15 mM, giving a SeMetO recovery of ~85 %. As peaks consistent with unreacted SeMet in the sample were observed, the low recovery may be attributed to unreacted parent SeMet.

3.3.4 Selenoxide formation upon exposure of SeMet to HOCl and *N*-chloramines

The NMR data presented in the previous section suggests that the major oxidation product generated when SeMet reacts with HOCl is SeMetO. An HPLC method was used to enable quantification of SeMetO formation upon exposure of SeMet to HOCl and other MPO-derived species, including *N*-chloramines.

3.3.4.1 HPLC method development

Initial studies employed an HPLC method that has previously been used in the literature [445], which uses a Beckman Ultrasphere ODS column with an isocratic elution using 0.1 % ACN made to pH 2.5 with TFA as a mobile phase. Under these conditions, SeMetO eluted close to the solvent front at 3.2 min. However, a peak was observed in all samples at 3 min that was attributed to the phosphate buffer salts in the samples. Furthermore, a negative peak was observed immediately after the SeMetO peak, which is also believed to buffer-derived. The SeMetO peak eluted between these two features of the chromatogram, and whilst separation was not ideal, the peak was resolved from the buffer peaks. As this made integration of SeMetO difficult, attempts to optimise the separation of SeMetO from SeMet using different HPLC methods and columns were performed.

Numerous buffer compositions and columns were attempted in order to better resolve SeMetO. The columns attempted are detailed in Table 3.4, and were selected based on the varied properties of the stationary phases. The buffer solutions conditions

tested comprised of an isocratic run with a flow rate of 1 mL min^{-1} consisting of varying concentrations of ACN in H_2O made to pH 2.5 with TFA. The concentrations of ACN used were 0, 0.1, 1, 10, 50 or 100 % ACN v/v, to assess whether varying concentrations of organic components in the mobile phase could affect retention times. The range of conditions used has very little difference in SeMetO peak position, which generally eluted either with the solvent front or immediately after the solvent front. As these attempts to increase retention of SeMetO on different columns were unsuccessful, the original HPLC method described in Section 2.3.5.2 was used for further analysis.

Table 3.4 – Columns used in HPLC method development for SeMet oxidation experiments.

Column details
Ultrasphere ODS, 5 µm, 4.6 x 250 mm, Beckman
Hypercarb PGC, 5 µm, 2.1 x 100 mm ThermoScientific
Supelcosil LC-NH2, 5 µm, 4.6 x 250 mm, Supelco
Viva C18, 5 µm, 4.6 x 250 mm, ResTek
Synergi Polar RP 80A, 4 µm, 4.6 x 250 mm, Phenomenex
Zorbax ODS, 5 µm, 4.6 x 250 mm, Agilent
Kinetex C18 100A, 2.6 µm, 100 x 2.1 mm, Phenomenex

3.3.4.2 Quantification of SeMetO formation

Oxidation of SeMet to SeMetO by HOCl, TauCl and BSA-Cl was assessed by HPLC, as described in Section 2.3.5.2. SeMetO standards were prepared by mixing SeMet with H_2O_2 and standardised using NMR with dimethylsulfone as an internal standard as described in Section 3.3.3.3. SeMet (160 µM) was mixed with each oxidant (0 – 320 µM) and allowed to react for 15 min at 22 °C before filtering and analysis by HPLC (Figure 3.12). With HOCl, a decrease in the SeMet peak (8.6 min) was observed when 40 µM oxidant was added to SeMet (160 µM). This corresponded with an increase in the SeMetO peak (3.2 min) area. With increasing oxidant concentrations, further decreases in the SeMet peak area were observed, with corresponding increases in the SeMetO peak (Figure 3.12).

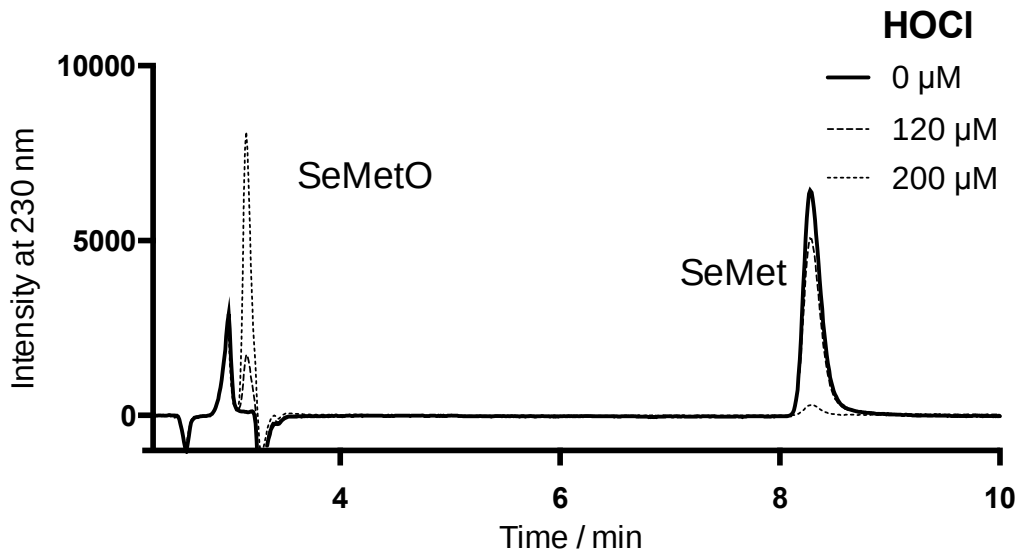

Figure 3.12 – Representative chromatograms of SeMet exposed to 0 - 200 µM HOCl

SeMet (160 µM) was mixed with 0 µM (unbroken line), 120 µM (dashed line) or 200 µM (dotted line) HOCl and subsequently analysed by HPLC. A dose dependent decrease in the parent SeMet peak area (8.6 min) with a concomitant increase in the SeMetO peak area (3.2 min) was observed with increasing oxidant concentration.

Upon quantification, an initial decrease of 36 µM SeMet was observed with the addition of 40 µM HOCl (Figure 3.13a). This corresponded to an increase of 30 µM SeMetO (Figure 3.13b). With each subsequent addition of 40 µM SeMet, a similar ratio of SeMet was consumed with corresponding SeMetO increase. With an excess of HOCl (200 µM) added, essentially all the SeMet was consumed and a maximum SeMetO concentration of 128 µM was detected. When HOCl was in greater excess over SeMet (> 200 µM), decreases in the SeMetO concentration were observed, though these changes were not statistically significant from the concentration observed at 200 µM HOCl. A similar dose-dependent decrease in SeMet concentrations was observed in the corresponding experiments with TauCl where an increase in the formation of SeMetO was also seen (Figure 3.13c,d). In this case, essentially all SeMet was consumed with addition of 200 µM TauCl. A loss of SeMetO was not observed when a molar excess TauCl was added to SeMet, in contrast to experiments with HOCl (Figure 3.13d). A lower conversion of SeMet to SeMetO was seen with BSA-Cl (0 – 320 µM) (Figure 3.13e,f), which was prepared by mixing BSA (1 mg mL^{-1}) with HOCl (0.5 mM) for 5 min and adjusted to 320 µM as assessed by the TNB assay, prior to reaction with SeMet (160 µM). In the case of BSA-Cl (Figure 3.13e,f), approximately 20 µM SeMet was consumed for every 40 µM BSA-Cl added. SeMet was essentially completely consumed upon

addition of 320 μM BSA-Cl, and this corresponded to the maximum amount of SeMetO observed. The percentage conversions of SeMet to SeMetO were calculated by the ratio of the maximum SeMetO observed to the concentration of SeMet consumed, giving values of 80%, 84% and 86% for HOCl, TauCl and BSA-Cl respectively. The highest yields of SeMetO were observed with HOCl and TauCl when the oxidants were in slight excess (200 μM) of SeMet, whereas the maximum conversion of SeMet to SeMetO was observed when BSA-Cl was present with a 2-fold excess of SeMet.

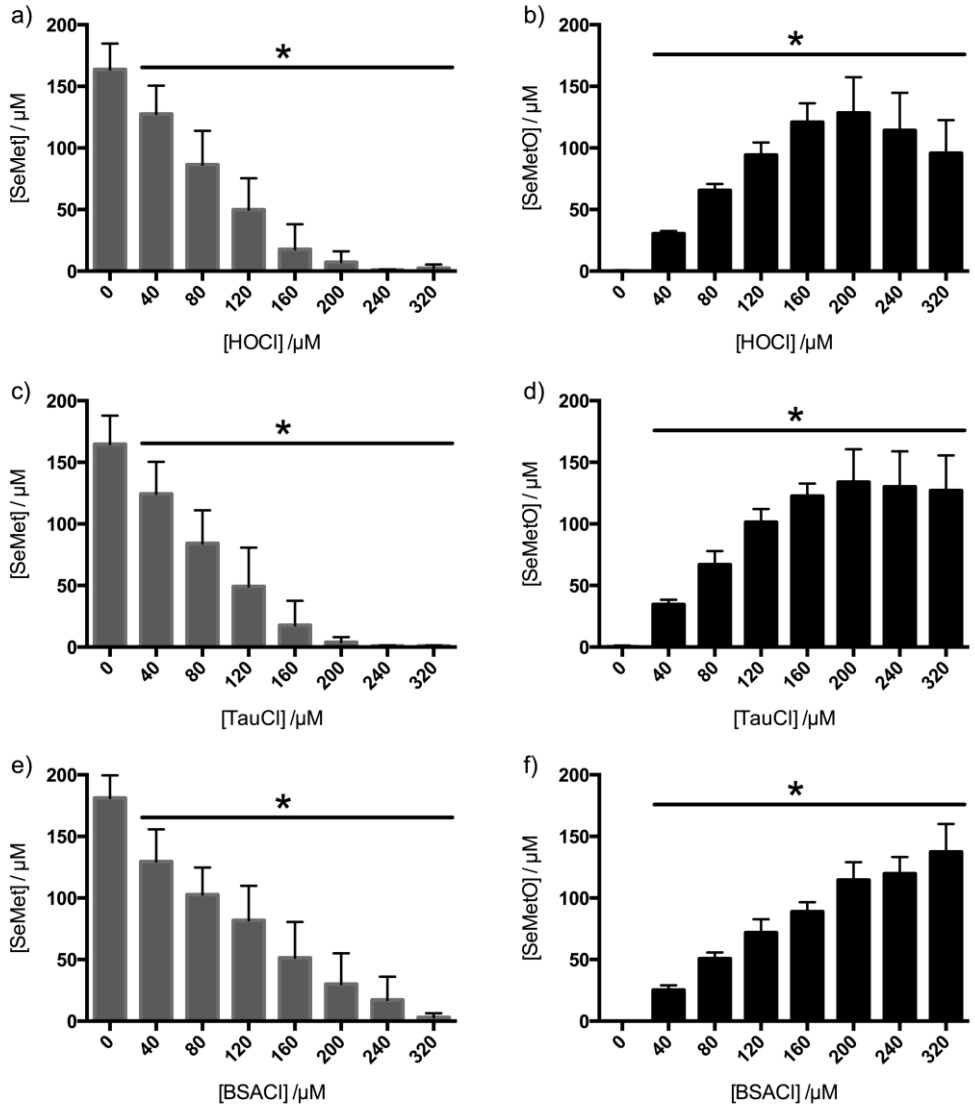

Figure 3.13 – Conversion of SeMet to SeMetO by HOCl, TauCl and BSA-Cl

*SeMet (160 µM) was mixed with a,b) HOCl, c,d) TauCl or e,f) BSA-Cl (0 – 320 µM) and incubated for 15 min at 22 °C before analysis by HPLC. a,c,e) show a dose-dependent decrease in SeMet concentration upon addition of increasing concentrations of each oxidant. b,d,f) show a corresponding increase in the SeMetO concentration. * indicates significant difference from control (0 µM oxidant) based on one-way ANOVA with Dunnett's post-hoc test. Data represent the mean ± SD from 5 independent experiments.*

3.3.5 Characterisation of further oxidation products of SeMetO

As SeMetO formation was decreased with higher excesses of HOCl, preliminary experiments investigating further oxidation products of SeMetO with HOCl were performed. As a similar decrease in SeMetO was not observed with TauCl or BSA-Cl, only higher excesses of HOCl were investigated.

SeMet (200 μM) was incubated with HOCl (0 – 0.8 mM) for 15 min and the resulting products of the reactions were analysed by HPLC using a Beckman Ultrasphere ODS column with a 0.1 % ACN made to pH 2.5 with TFA as the mobile phase. Addition of an increasing concentration of HOCl to SeMet lead to a dose-dependent decrease in the concentration of SeMetO (Figure 3.14). Under these conditions, increases in 2 unidentified peaks were observed (#1 3.1 min, #2 10.2 min). The higher concentrations of HOCl (600 – 800 μM) led to decreases in the size of peak #1, whereas the #2 peak size was more consistent, with a maximum at 1x HOCl, with a subsequent decrease at 2x, with no further changes with increasing concentration.

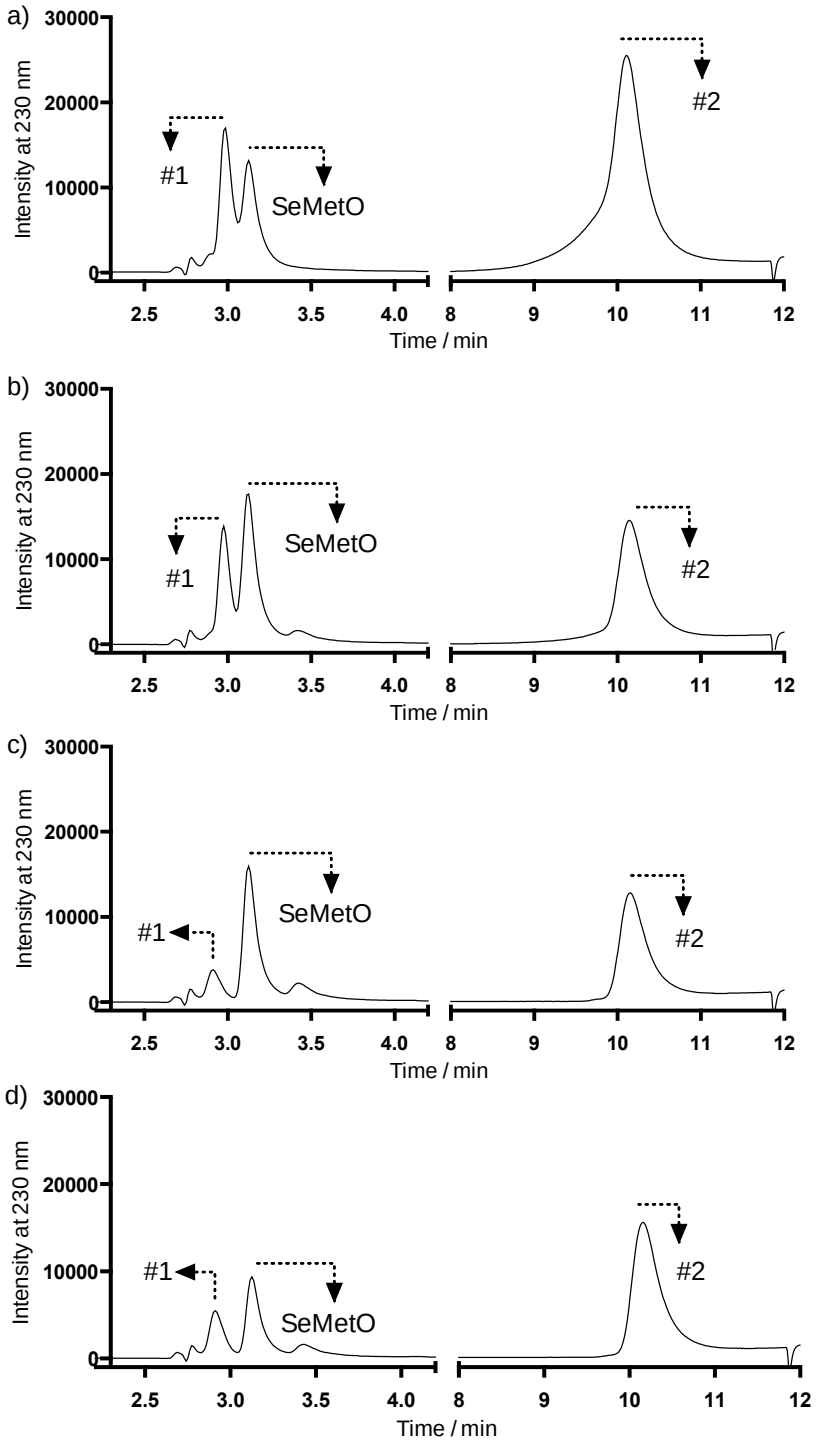

Figure 3.14 – SeMetO reacts with HOCl to form additional products

SeMet (200 µM) was mixed with HOCl (0 – 0.8 mM) and the products analysed by HPLC. Traces show SeMet treated with a) 1 x, b) 2 x, c) 3 x or d) 4 x molar excess of HOCl. 2 unidentified peaks were observed in the HPLC traces at 3.1 min and 10.2 min. A dose-dependent decrease of SeMetO was observed with increasing HOCl. Initially the peak at 3.1 min increased, followed by a decrease with increasing HOCl. The peak at 10.2 min was increased at 1 x excess of HOCl, followed by a decrease at 2 x molar excess and stayi consistent with 3 – 4 x excess.

The differences observed between HOCl and H_2O_2 treated SeMet samples in the mass spectrometry and NMR data, and the unidentified peaks in the HPLC traces after excess HOCl treatment suggested that HOCl could give rise to additional products to H_2O_2, potentially by further reaction with SeMetO. As HOCl is also reactive with the amine group, whereas this is not a favourable site for reaction with H_2O_2, the reaction of SeMetO with HOCl was monitored by UV-vis spectroscopy, to assess potential *N*-chloramine formation and decay. *N*-Chloramines typically absorb at 250 nm [554], therefore changes in absorbance in this region as the reaction progresses may indicate *N*-chloramine formation. SeMetO (500 μM) formed by reaction of SeMet (1 mM) with excess concentrations of H_2O_2 (2.5 mM) was mixed with HOCl (2 mM) using a stopped-flow instrument, and the change in absorbance measured, between 200 and 300 nm with 5 nm steps for 30 s (Figure 3.15). An initial increase in absorbance was observed over the first 6 s in the range between 250 - 280 nm as demonstrated at 260 nm (Figure 3.15 a), before a subsequent decrease in absorbance. This is potentially due to the formation of *N*-chloramines and subsequent rapid decay. Absorbance changes consistent with 2 phases were also observed in the 200 – 235 and 290 – 300 nm ranges, with an initial fast increase in absorbance, followed by a slower further increase in absorbance as demonstrated by absorbance changes at 290 and 225 nm (Figure 3.15 b,c). This is likely due to the formation of the final products that may be further oxidation of the selenium centre forming a selenone analogous to MetSO oxidation [88], or aldehyde formation due to *N*-chloramine decay [86]. As the data is preliminary and the mechanism is not well characterised, kinetic analysis to determine rate constants cannot be performed. However, from these data presented, the observed rate constant was determined to be 0.582 for the intial reaction of SeMetO and HOCl. This gives an estimated rate constant of 5.82×10^5 M^{-1} s^{-1}, which is in the same order of magnitude as the formation of other chloramines [60].

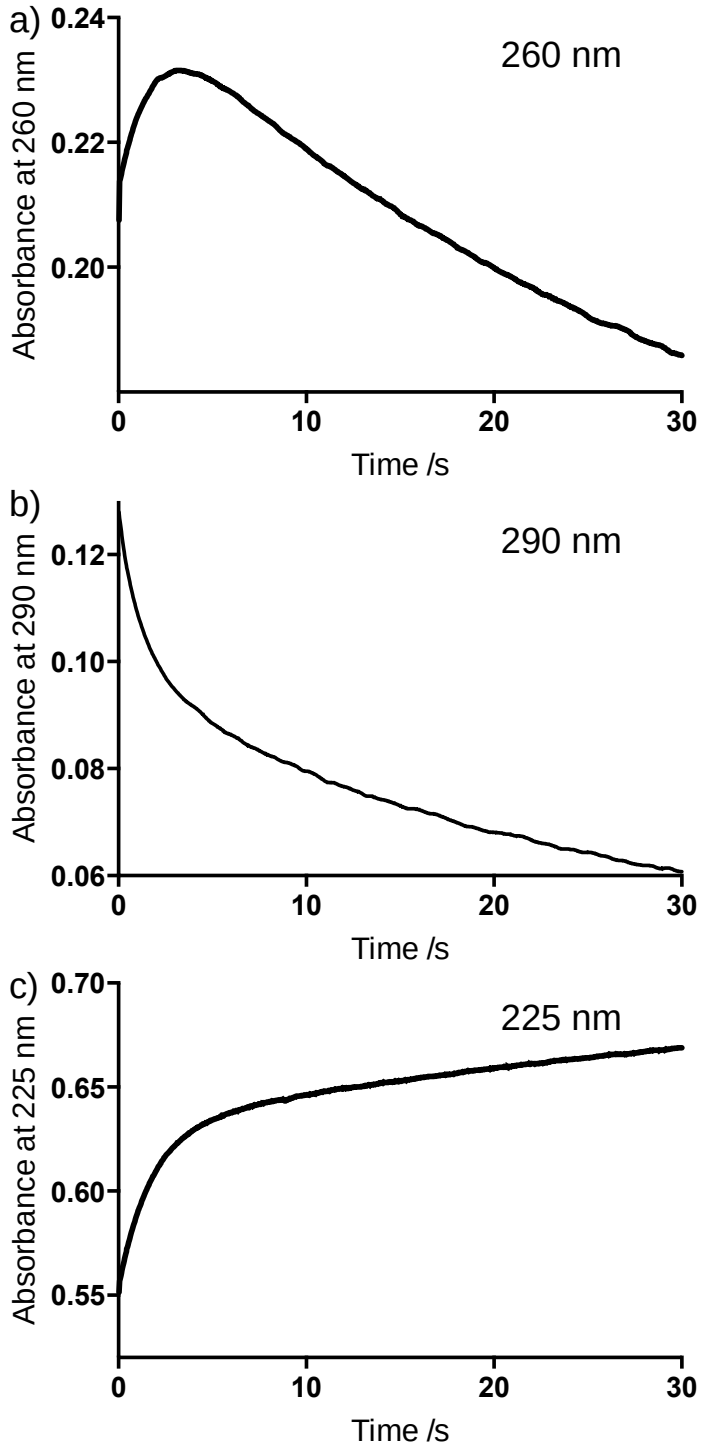

Figure 3.15 – Absorbance vs time traces when pre-formed SeMetO was mixed with HOCl at 260, 290 and 225 nm.

SeMetO (250 μM) and HOCl (500 μM) were mixed in stopped flow apparatus and absorbance changes between 200 and 300 nm were monitored for 30 seconds. Absorbance vs time plots are shown for a) 260 nm, b) 290 nm and c) 225 nm. 2 phase kinetics were observed, at each wavelength with a fast initial phase followed by a slow second phase.

3.3.6 SeTal oxidation products

The data presented in the previous section demonstrate that HOCl and *N*-chloramines react with SeMet to form a selenoxide, though with HOCl there is also evidence for the formation of further oxidation products. As SeTal is a selenoether that is also capable of reacting rapidly with MPO-derived oxidants including HOCl [486], selenoxides are a likely product of this reaction. However, the products of these reactions have not yet been characterised upon exposure of SeTal to HOCl and *N*-chloramines. Experiments were therefore undertaken to characterise potential products, using mass spectrometry and NMR spectroscopy, and to quantify the conversion of SeTal to these products in each case.

3.3.6.1 Mass spectrometry

Initial mass spectrometry studies with SeTal were undertaken with SeTal (250 μM) in a solution containing methanol (50 % (v/v)) and formic acid (0.01 % (v/v)). However, no signal was detected at around *m/z* 229 which is the expected mass for ions of the H-adduct of SeTal, $[SeTal+H]^+$. This is attributed to a low extent of ionisation of SeTal due to the absence of facile protonation sites. Thus, further experiments were undertaken in the presence of NaCl (500 μM) with the expectation that the $[^{80}SeTal+Na]^+$ ion might be detected at *m/z* 251.3, as reported previously [486]. As anticipated, a group of peaks centred at *m/z* 251.3 (Figure 3.16a), attributed to $[^{80}SeTal+Na]^+$, were detected, with the expected isotope ratios for selenium (demonstrated by computer simulation in Figure 3.16b). However, additional peaks were detected at *m/z* 255.0, 257.0 and 259.0. These are attributed to Na adducts of contaminants, as they are also observed with NaCl in the absence of SeTal (Figure 3.16e).

Following detection of the parent $[^{80}SeTal+Na]^+$ ion, HOCl oxidation of SeTal was investigated by taking SeTal in H_2O (500 μM) and mixing with HOCl (400 μM), before incubating at 21 °C for 5 min. The resulting solution was mixed in equal volumes with 0.02% (v/v) formic acid in methanol and analysed by mass spectrometry. NaCl was not added to the samples in this case as the HOCl solution contains high levels of NaCl. The major product peak detected was characterised by an increase of 16 mass units at *m/z* 267.2 (Figure 3.16c) when compared to the parent Na^+ adduct ion, with this attributed to $[^{80}SeTalO+Na]^+$ (demonstrated by a computer model in Figure 3.16d). Weak signals

corresponding to that of the H^+ adduct product $[^{80}SeTalO+H]^+$ were also detected at *m/z* 245.3, but these were partially obscured by residual parent $[SeTal+Na]^+$ peaks.

In order to further characterise the SeTal product and determine the site of oxygen incorporation, MS/MS studies of the $[^{80}SeTalO+Na]^+$ ion were undertaken. This gave rise to numerous fragments (Figure 3.17). The major fragment, *m/z* 248.9, corresponded to a loss of 18 mass units, consistent with loss of water from the $[^{80}SeTalO+Na]^+$ ion. Two subsequent losses of 30 mass units to give ions with *m/z* 218.8 and 188.8, are both consistent subsequent elimination of two CH_2O groups from $[^{80}SeTalO+Na-H_2O]^+$. A final loss of 26 mass units to give the fragment at *m/z* 162.8 is consistent with C_2H_2 loss. The suggested structures of these ions and fragmentation mechanism are presented in Figure 3.18.

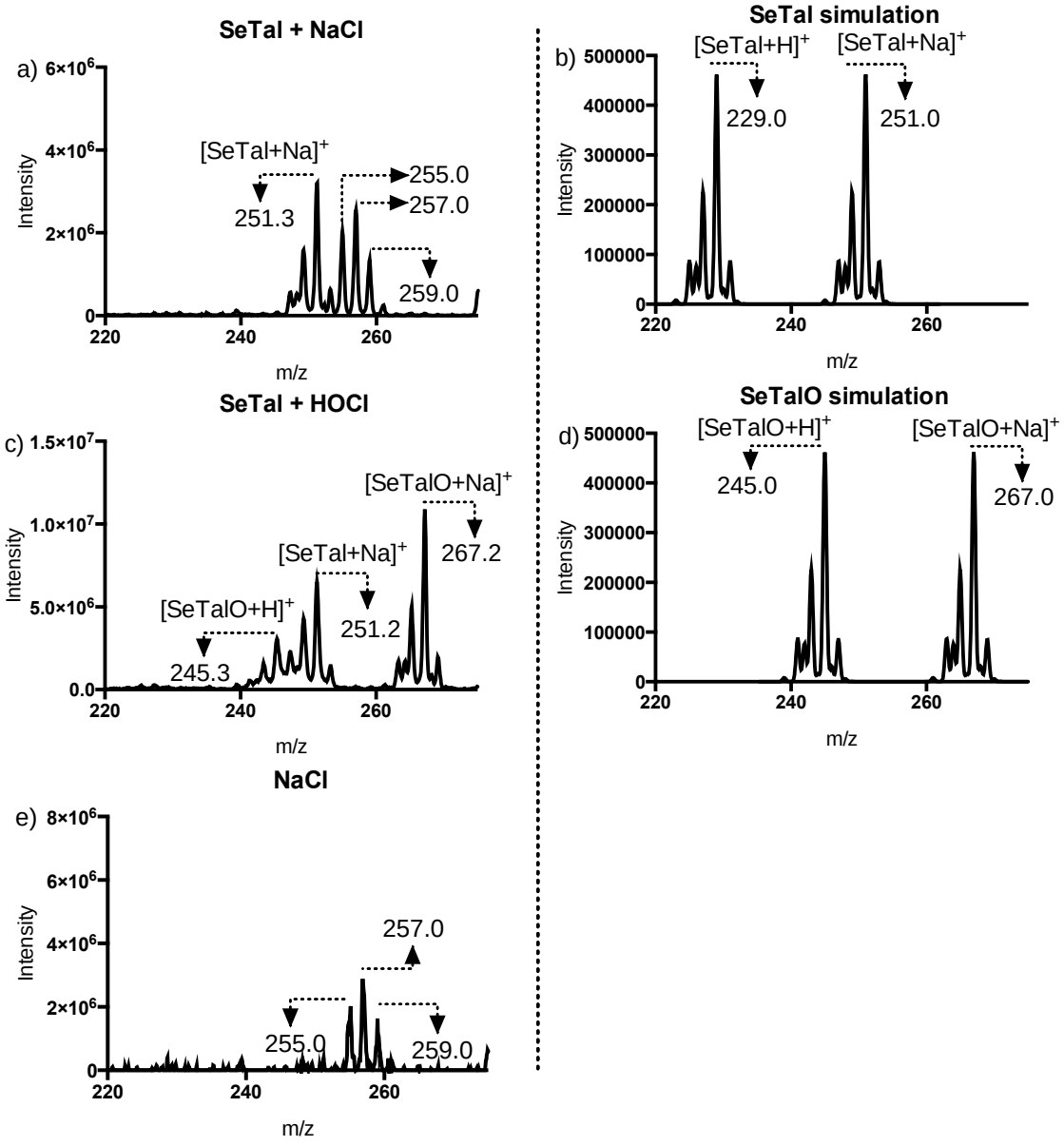

Figure 3.16 – Mass spectra of SeTal and the proposed oxidation product SeTalO

a) SeTal (500 µM) and NaCl (500 µM) were mixed with an equal volume of formic acid (0.02 % (v/v)) in methanol and analysed by mass spectrometry. The peak at m/z 251.3 corresponds to $[^{80}SeTal+Na]^+$ ion as shown by a simulation in b), with the surrounding peaks consistent with the Se isotope pattern. The peaks at m/z 255.0, 257.0 and 259.0 are due to NaCl present in sample, and are observed in e) NaCl (500 µM) control. b) SeTal in H_2O (500 µM) was mixed with HOCl (400 µM) and incubated at 22 °C for 5 min and then mixed in equal volumes with formic acid (0.02 % (v/v)) in methanol and analysed by mass spectrometry. The peak at m/z 267.2 represents a mass increase of 16 mass units from the parent $[^{80}SeTal+Na]^+$ ion consistent with selenoxide formation with the major ion attributed to $[^{80}SeTalO+Na]^+$ as shown by a computer simuution in d). Simulations were produced using QualBrowser by inputting empirical formulae with Gaussian outputs with a 0.4 Da resolution and full width half maximum valleys.

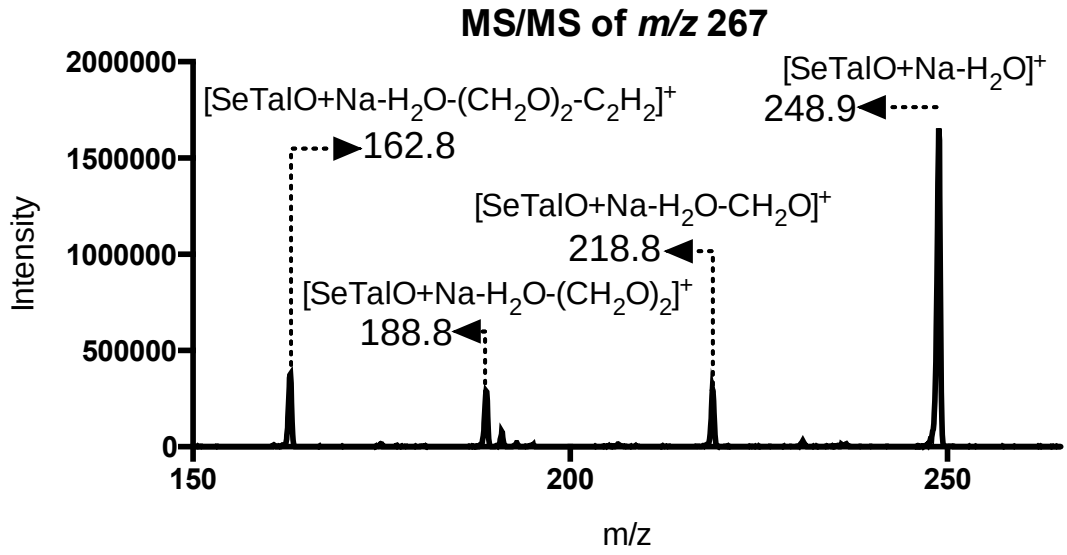

Figure 3.17 – MS/MS fragmentation pattern of the *m/z* 267.2 ion attributed to $[SeTalO+Na]^+$

SeTal in H_2O (500 µM) was mixed with HOCl (400 µM) and incubated at 21 °C for 5 min, prior to mixing with equal volumes of 0.02% (v/v) formic acid in methanol and analysis by mass spectrometry. MS/MS was performed on the ion with m/z 267.2 that is assigned to $[SeTalO+Na]^+$, and gives rise to ions with m/z 247.8, consistent with loss of water $[SeTalO+Na-H_2O]^+$. Peaks at 218.8 and 188.8 correspond to losses of 30 mass units, consistent with 2 subsequent losses of CH_2O, $[SeTalO+Na-H_2O-CH_2O]^+$, and $[SeTalO+Na-H_2O-(CH_2O)_2]^+$ respectively. The peak at m/z 162.8 represents a further loss of 28 mass units consistent with loss of C_2H_2, $[SeTalO+Na-H_2O-(CH_2O)_2-C_2H_2]^+$. Proposed structures are shown in Figure 3.18*.*

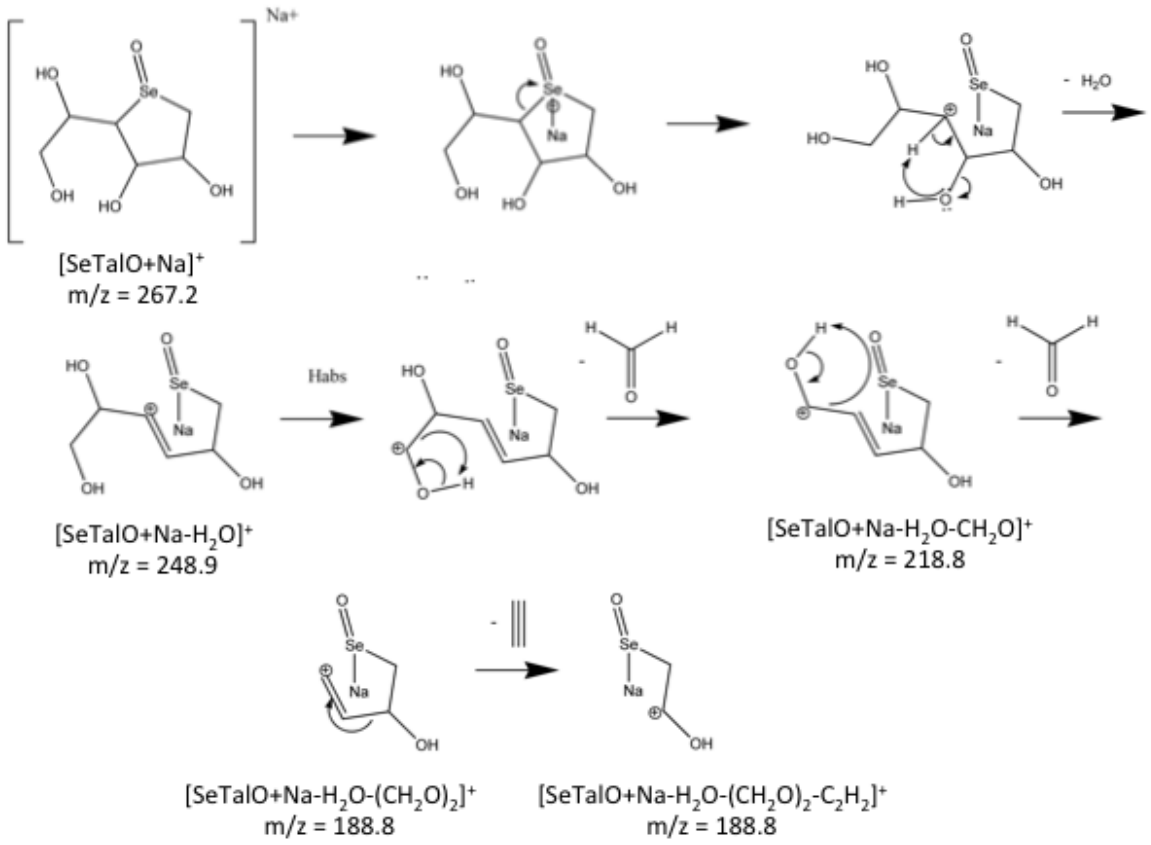

Figure 3.18 – Proposed fragmentation pattern of SeTalO

Figure shows the proposed fragments observed in Figure 3.17 *arising from MS/MS analysis of the peak at 267.2 when SeTal is treated with HOCl.*

3.3.6.2 NMR spectroscopy

The data presented in the previous section are consistent with the addition of an oxygen atom to the SeTal structure. As such, the proposed product was tentatively assigned as a selenoxide (Figure 3.18). NMR spectroscopy studies were performed in order to fully characterise the proposed species. SeTal (5 mg, 22 µmoles) in H_2O was reacted with equimolar concentrations of HOCl for 15 min at 22 °C. Samples were dried overnight using a rotational vacuum concentrator (Christ, Osterodeam Harz, Germany). The resulting white solid was dissolved in 600 µL D_2O and analysed by ^1H NMR spectroscopy, as well as acquisition of the NMR spectra of the parent SeTal compound. The spectra for SeTal agree with previous results, and peaks are assigned in Figure 3.19 and Figure 3.20

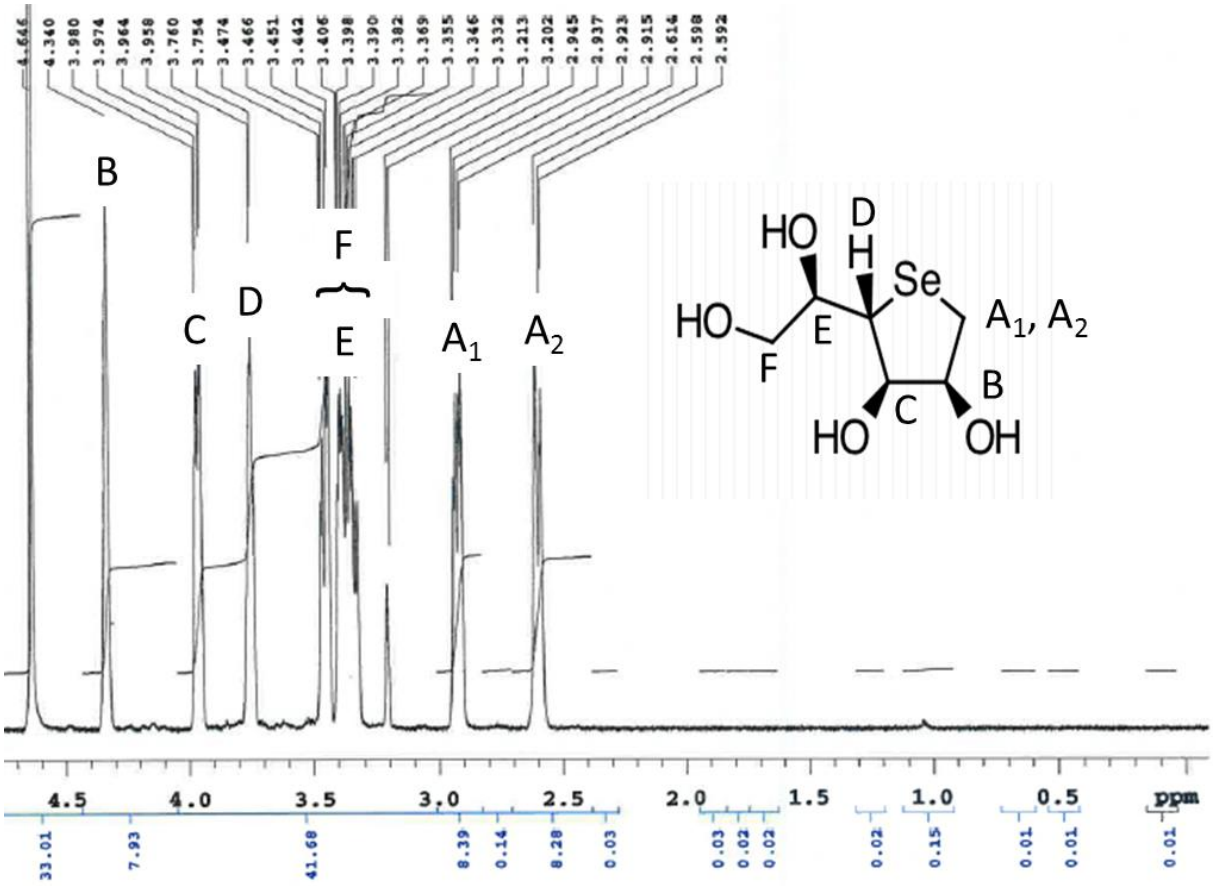

Figure 3.19 – ^{1}H NMR spectrum for SeTal

SeTal (5 mg) was dissolved in 600 µL D_2O and the ^{1}H NMR spectrum collected. Chemicals shifts are reported relative to the residual H_2O peak which was set to 4.64 ppm.

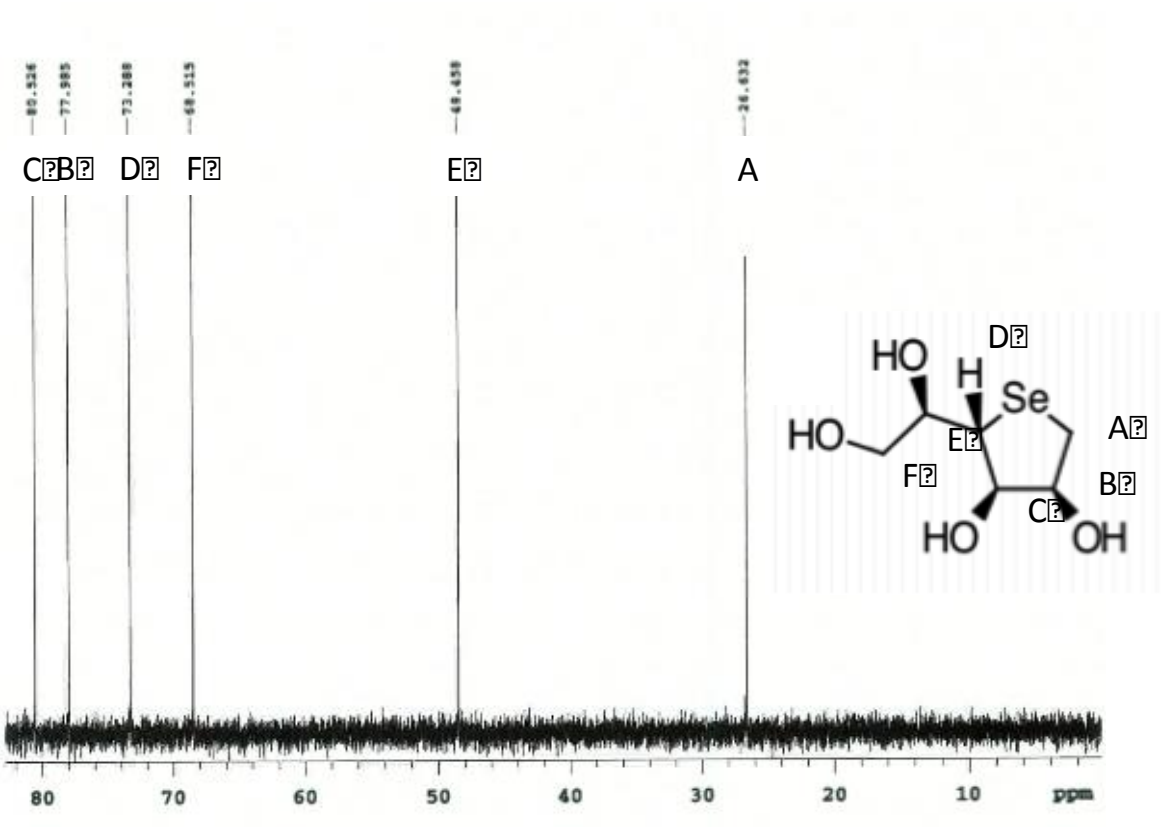

Figure 3.20 – ^{13}C NMR spectrum for SeTal

SeTal (5 mg) was dissolved in 600 µL D_2O and the ^{13}C NMR spectrum collected. Chemical shifts reported as relative ppm.

The ^{13}C NMR spectrum for the oxidised SeTal sample showed a total of 12 product carbon environments for SeTalO, all with similar intensity signals (Figure 3.21). This suggests the formation of two products on exposure of SeTal to HOCl, as SeTal only contains 6 carbons. As addition of an oxygen to the selenium centre can form either R or S isomers of the selenoxide (Figure 3.22), this is consistent with the formation of SeTalO. The ^{13}C peaks were assigned after analysis of the COSY and HSQCAD spectra, though relative ppm is reported here for ease of explanation. All 12 peaks can be attributed to products (Table 3.5), as they are shifted from the parent compound peaks (Figure 3.20), particularly those at lower ppm values, which are closer to the selenium centre. For example, carbon A shifts from 26.6 ppm in the parent SeTal to 55.6 and 51.5 ppm in the R and S isomers respectively. The shift in ppm is consistent with the shielding caused by addition of oxygen to the selenium centre. As the intensities of all peaks are similar, this suggests the products are formed in almost equal ratios.

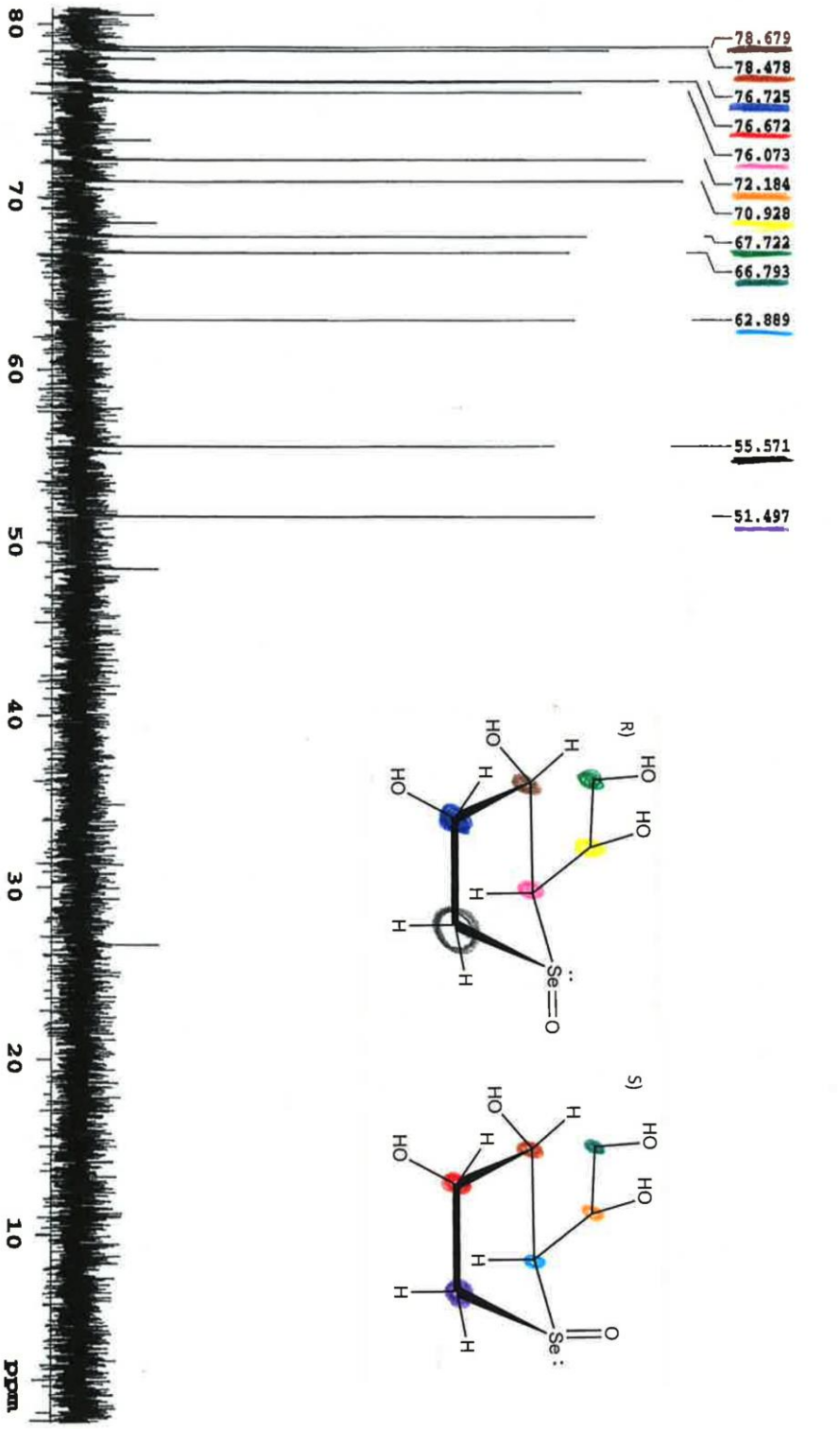

Figure 3.21 – ^{13}C NMR spectra for SeTal treated with HOCl

SeTal (5 mg; 22 µmoles) was dissolved in water, mixed with equimolar HOCl, dried overnight and redissolved in 600 µL D_2O before analysis by ^{13}C NMR spectroscopy. Chemical shifts are reported as relative ppm. Two species with similar concentrations were detected, and determined to be isomers of SeTalO. Peak assignment is given in Table 3.5

Table 3.5 – ^{13}C NMR chemical shifts for selenoxide formed on reaction of SeTal with HOCl.

Environment	R	S
A	55.571	51.497
B	76.725	76.725
C	78.679	78.478
D	76.073	62.889
E	70.928	72.184
F	67.722	66.793

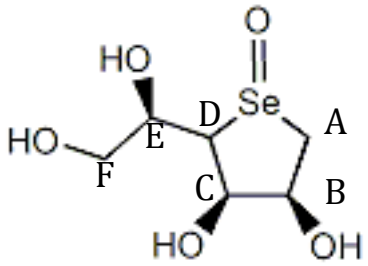

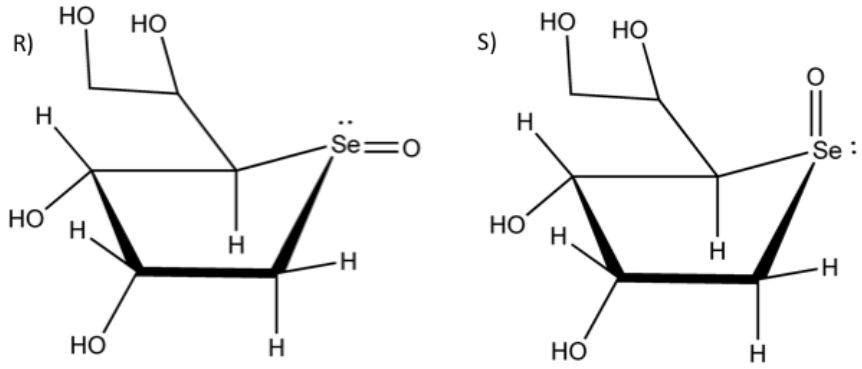

Figure 3.22 – *R* and *S* stereoisomers of SeTalO

The ^{1}H NMR spectrum shows 13 peaks, which corresponds to each isomer containing 7 proton environments, with the peak at a chemical shift of 4.74 being an overlapping signal for a proton environment in both isomers (Figure 3.23). The relative peak integral area supports this, with an integration value consistent with 2 protons being present. The peak identities are reported in Table 3.6, and were assigned using COSY analysis, which are discussed later. The product peaks are shifted downfield from their parent counterparts (Figure 3.19). For example, the protons in environment B in both R and S isomers give rise to a signal at 4.74 ppm, compared to 4.34 in the parent SeTal spectrum. The down field shift is consistent with shielding observed by the addition of an electronegative atom such as oxygen.

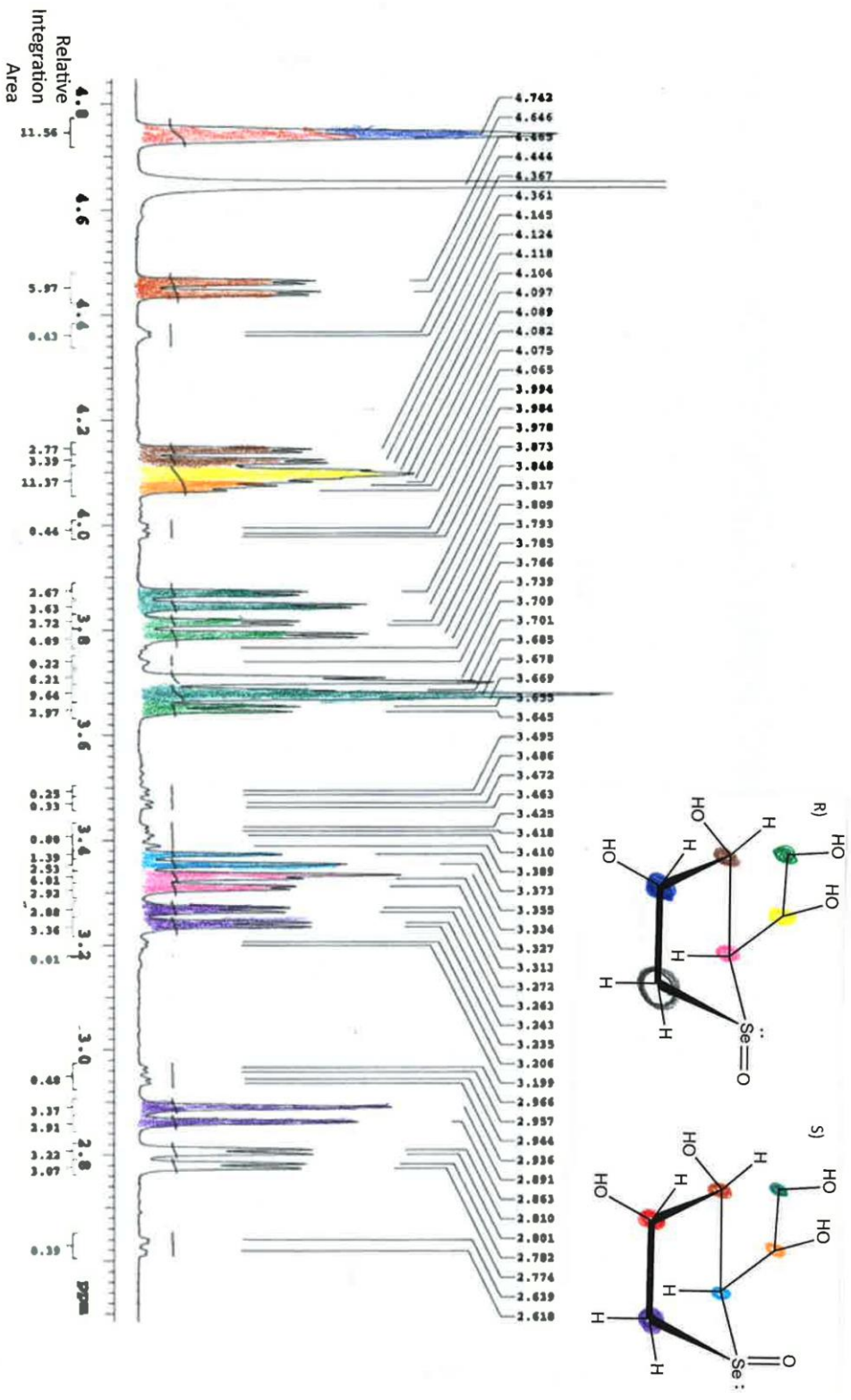

Figure 3.23 – ^{1}H NMR spectrum for SeTal treated with HOCl

SeTal (5 mg; 22 µmoles) dissolved in water, mixed with equimolar HOCl, dried overnight and redissolved in 600 µL D_2O before analysis by ^{1}H NMR spectroscopy. Chemical shifts are reported as ppm relative to the residual H_2O peak set to 4.64 ppm. Two species with similar concentrations were observed, and determined to be isomers of SeTalO. Proton environment and J-coupling constants are assigned in Table 3.6*.*

Table 3.6 - ^{1}H NMR chemical shifts for selenoxide formed on reaction of SeTal with HOCl.

Chirality	R			S		
Environment	ppm	Splitting	H	ppm	Splitting	H
A1	3.71	d; J = 4	1	3.25	d; J = 14	1
A2	2.79	dd; J = 14, 4	1	2.87	dd; J= 14	1
B	4.74	obscured	1	4.74	Obscured	1
C	4.13	dd; J = 12, 4	1	4.45	dd; J = 11, 3	1
D	3.32	dd J = 11, 4	1	3.36	dd; J = 9	1
E	4.10	obscured	1	4.08	obscured	1
F	3.72	dq; J= 70, 12, 4	2	3.76	dq; J = 13, 3	2

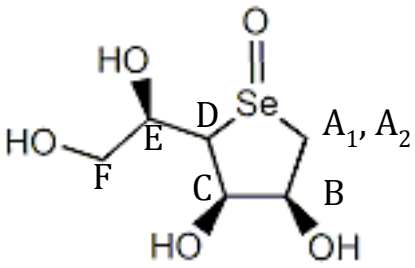

Heteronuclear single quantum coherence experiments (HSQCAD) correlate carbon centres with coupled protons. Signals are observed in the 2D spectrum where the proton signal (across the top) is bound to the carbon (down the left) (Figure 3.24), and allows for the determination of which protons are bound to which carbon centres. The correlation for the proton signals bound to carbon A are outlined as an example. The HSQCAD spectra demonstrated a significant shift in 2 protons bound to the carbon A in the R isomer at chemical shifts of 2.79 and 3.71, and a similar though smaller shift between protons bound to carbon A in the S isomer at 2.87 and 3.25. A large shift in proton environments suggests that one proton from the pair has become significantly shielded compared to the other. This is consistent with the addition of oxygen on an adjacent atom.

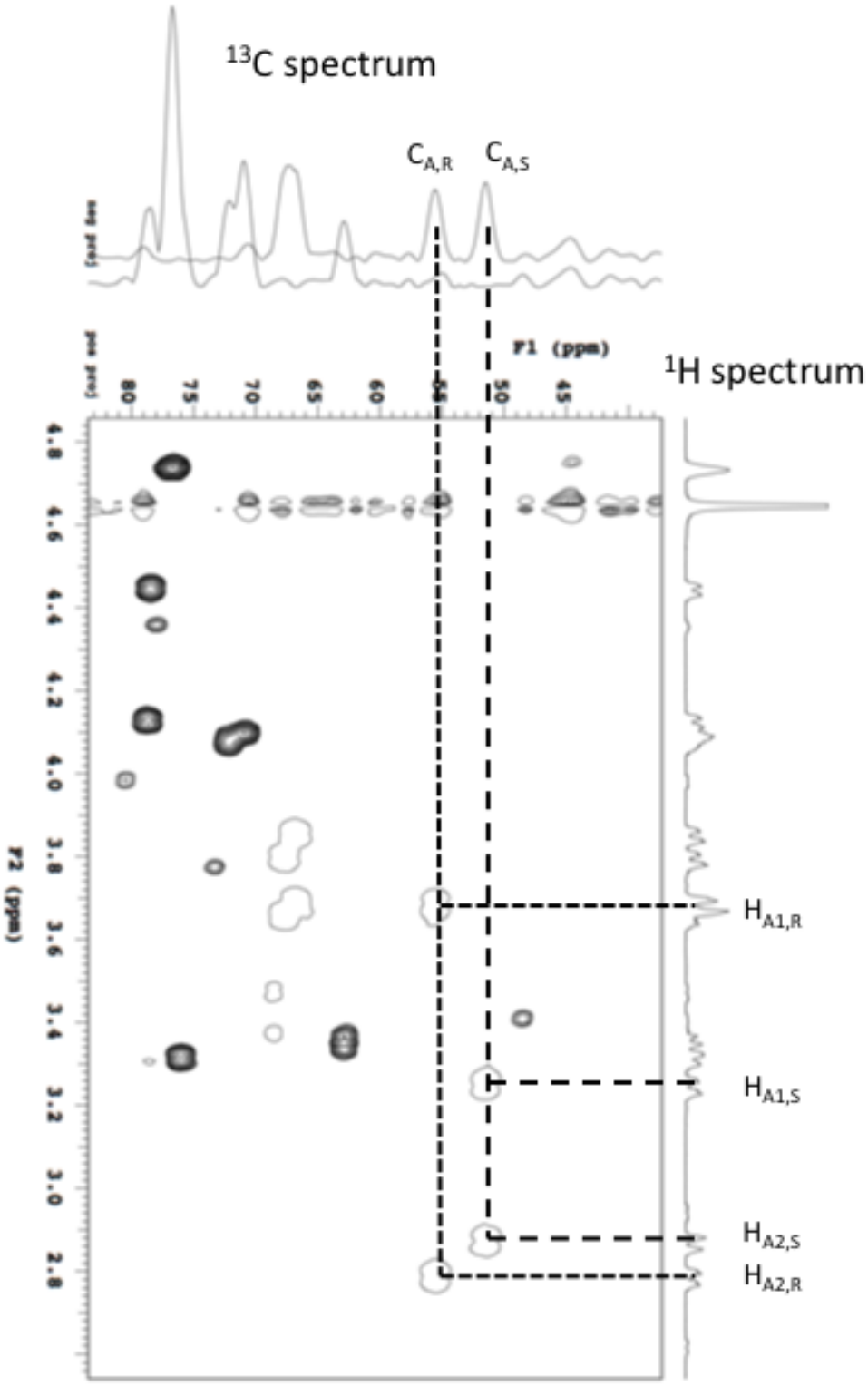

Figure 3.24 – HSQCAD spectra for SeTalO treated with HOCl

SeTal (5 mg; 22 µmoles) dissolved in water was mixed with equimolar HOCl, dried overnight and redissolved in 600 µL D_2O was analysed by HSQCAD NMR. Peaks reported as ppm relative to the residual H_2O peak set to 4.64 ppm.

The formation of a selenoxide would result in the addition of oxygen to the Se atom in SeTal, giving rise to chirality around the Se. As SeTal is cyclic in structure, the formation of R and S isomers of SeTalO (structures in Figure 3.22) would be expected to differentially shield protons above and below the plane of the ring. Assuming that the Se atom is above the plane of the ring structure due to steric considerations, the R isomer, where the oxygen is bound in plane with the ring, would be expected to shield the protons axial to the ring. In the S isomer, where the oxygen is out of plane with the ring, smaller shifts would be expected due to lower shielding. Hence, the protons observed with the more significant shifts are attributed to the R isomer.

Homonuclear correlation spectroscopy (HHCOSY) correlates spin-coupled protons. Signals are observed in the 2D spectrum where 2 proton environments are spin-coupled (Figure 3.25). Therefore signals off the diagonal indicate protons that are on adjacent carbons. This allows for the determination of proton environments that are adjacent to one another, and the assignation of peaks. Protons coupling with the peak at 4.74 is outlined as an example. As this represents an overlapping proton environment from both the R and S isomer, it appears to be coupled to 6 other proton environments. From the HSQCAD spectrum, the signals at 2.79 and 3.71 ppm represent protons bound to carbon A in the R isomer, and signals at 2.87 and 3.25 ppm represent the protons from the S isomer. Therefore the signals at 4.13 and 4.45 ppm must represent the protons from position C. The further down field proton is assigned to the S isomer, due to the greater effect of the oxygen being above the ring. The proton assignation was confirmed using J-coupling values and splitting patterns observed in the ^{1}H spectrum, where these values could be determined. Once the ^{1}H spectrum was assigned, analysis of the HSQCAD spectrum (Figure 3.24) allowed for the carbon centres to be assigned (Table 3.5).

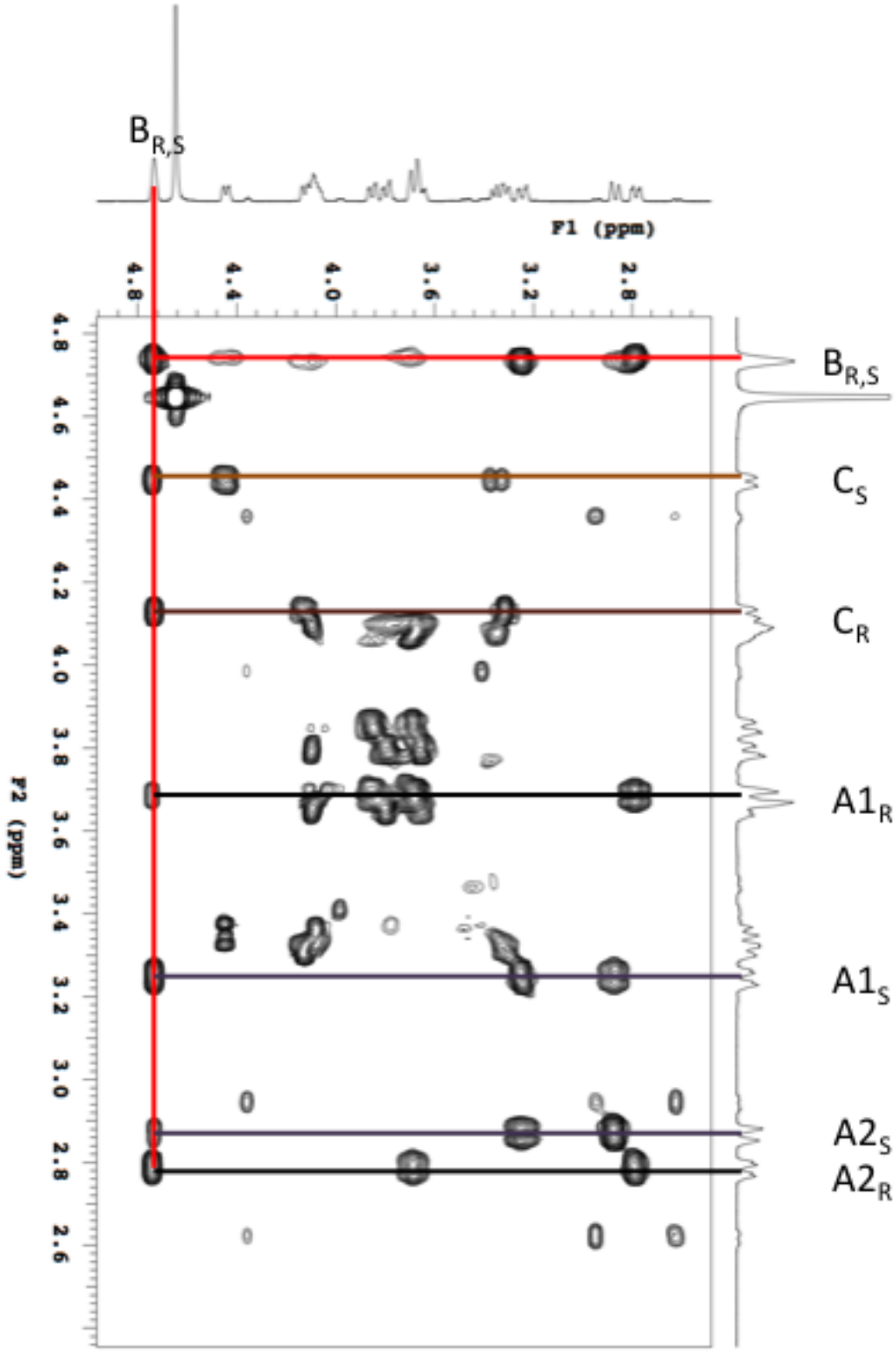

Figure 3.25 – HHCOSY spectra for SeTalO treated with HOCl

SeTal (5 mg; 22 µmoles) dissolved in water was mixed with equimolar HOCl, dried overnight and redissolved in 600 µL D_2O was analysed by HHCOSY NMR. Peaks are reported as ppm relative to the residual H_2O peak set to 4.64 ppm.

3.3.6.3 Standard quantification for HPLC

^{1}H NMR spectroscopy was used a method of quantifying the selenoxide standard for use in HPLC. SeTal was produced by the reaction of SeTal (22 μmol) with equimolar concentration of HOCl for 15 min. The sample was divided into 2 aliquots and dried overnight in a rotational vacuum concentrator (Christ, Osterodeam Harz, Germany). One aliquot of the resulting white solid was dissolved in 600 μL D_2O, before addition of the internal standard dimethyl sulfone ($DMSO_2$) (5.3 μM). The ^{1}H NMR spectra was collected (Varian VNMRS 500 MHz), and the concentration of SeTal determined by comparison of dimethyl sulfone peaks (∂ = 3.15 ppm, 6H) to SeTalO peaks (∂ = 4.74, 2H – 1H from the R and S isomer each). The concentration of SeTalO recovered was determined to be 15 mM, which represents a ~ 96 % recovery of SeTalO.

3.3.7 Selenoxide formation upon exposure of SeTal to HOCl and *N*-chloramines

The mass spectrometry and NMR data demonstrated formation of SeTalO upon addition of HOCl to SeTal, however, the stoichiometry for this reaction could not be determined from these experiments. As such, an HPLC method was developed in order to quantify the conversion of SeTal to SeTalO upon addition of HOCl and model *N*-chloramines.

3.3.7.1 HPLC method development

Initially SeTal oxidation experiments were attempted using the same buffer and column conditions as those reported for SeMet oxidation experiments (Section 3.3.3.1). However, the SeTalO species was not retained by the column very efficiently and eluted immediately after the solvent front. As a result, a carbohydrate specific column was sourced and found to give excellent separation of SeTal and SeTalO. The method is described in Section 2.3.5.3, and example chromatograms can be seen in Figure 3.26.

3.3.7.2 Quantification of SeTalO formation

Oxidation of SeTal to SeTalO by HOCl, TauCl and BSA-Cl was assessed using the HPLC method as optimised above. SeTalO standards were prepared by exposing SeTal to HOCl and were standardised by ^{1}H NMR spectroscopy using an internal standard of dimethylsulfone as described in Section 3.3.7. SeTal (160 μM) was mixed with HOCl, TauCl or BSA-Cl (0 – 320 μM) and allowed to react for 15 min at 22 °C before filtering

and analysis by HPLC (Figure 3.26). Addition of 40 µM of oxidant caused a decrease in area of the SeTal peak. The decrease was concentration dependent with smaller areas observed with higher concentrations of oxidant added. The decreases in SeTal area corresponded with an increase in the area for the SeTalO peak.

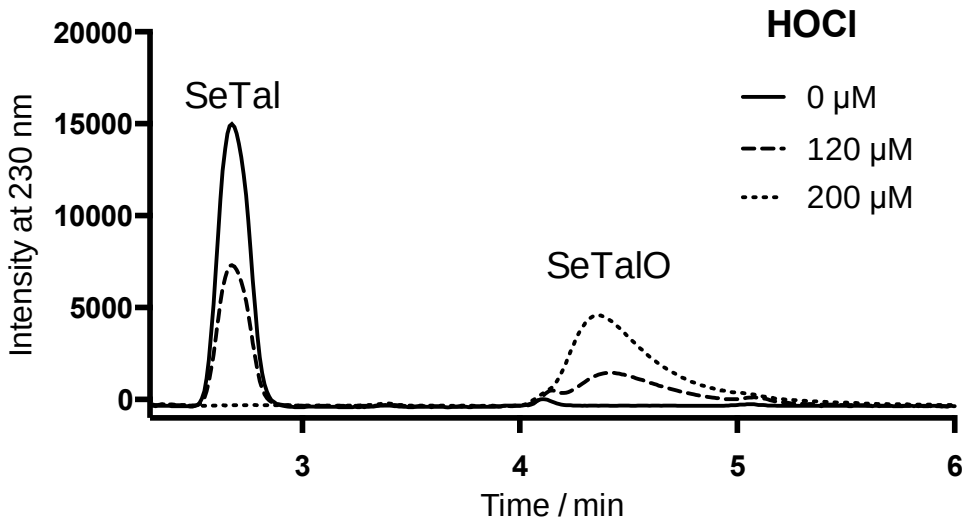

Figure 3.26 – Representative chromatograms of SeTal exposed to 0 - 200 µM HOCl

SeTal (160 µM) was mixed with HOCl (0 µM (unbroken line), 120 µM (dashed line) or 200 µM (dotted line)) and analysed by HPLC. A dose-dependent decrease in the parent SeTal peak area (2.7 min) was observed, with a concomitant increase in the SeTalO peak area (4.4 min).

An initial loss of 40 µM SeTal was observed with addition of 40 µM HOCl to 160 µM SeTal, with a corresponding (40 µM) increase in the SeTalO concentration (Figure 3.27a,b). As the concentration of HOCl increased, further dose-dependent decreases of SeTal were observed until SeTal was completely consumed at a concentration of 200 µM HOCl. This corresponded to increases in SeTalO, which reached a maximum concentration (151 µM) after addition of 200 µM HOCl. TauCl addition resulted in a similar trend with SeTal totally consumed at 200 µM TauCl, which corresponded to a maximum SeTalO yield of 153 µM (Figure 3.27c,d). HOCl and TauCl consumed SeTal in a ratio that was very close to 1 : 1, with concentrations of SeTalO observed very similar to the concentrations of SeTal consumed. Maximum conversion of SeTal to SeTalO was achieved with 200 µM HOCl or TauCl with a 94% and 96% conversion respectively. BSA-Cl addition exhibited a dose-dependent decrease in SeTal concentration with a corresponding SeTalO increase, however, BSA-Cl did not completely consume SeTal

until a 2 : 1 BSA-Cl to SeTal molar ratio was reached, with a maximum conversion to SeTalO of 91% (145 µM) (Figure 3.27e,f).

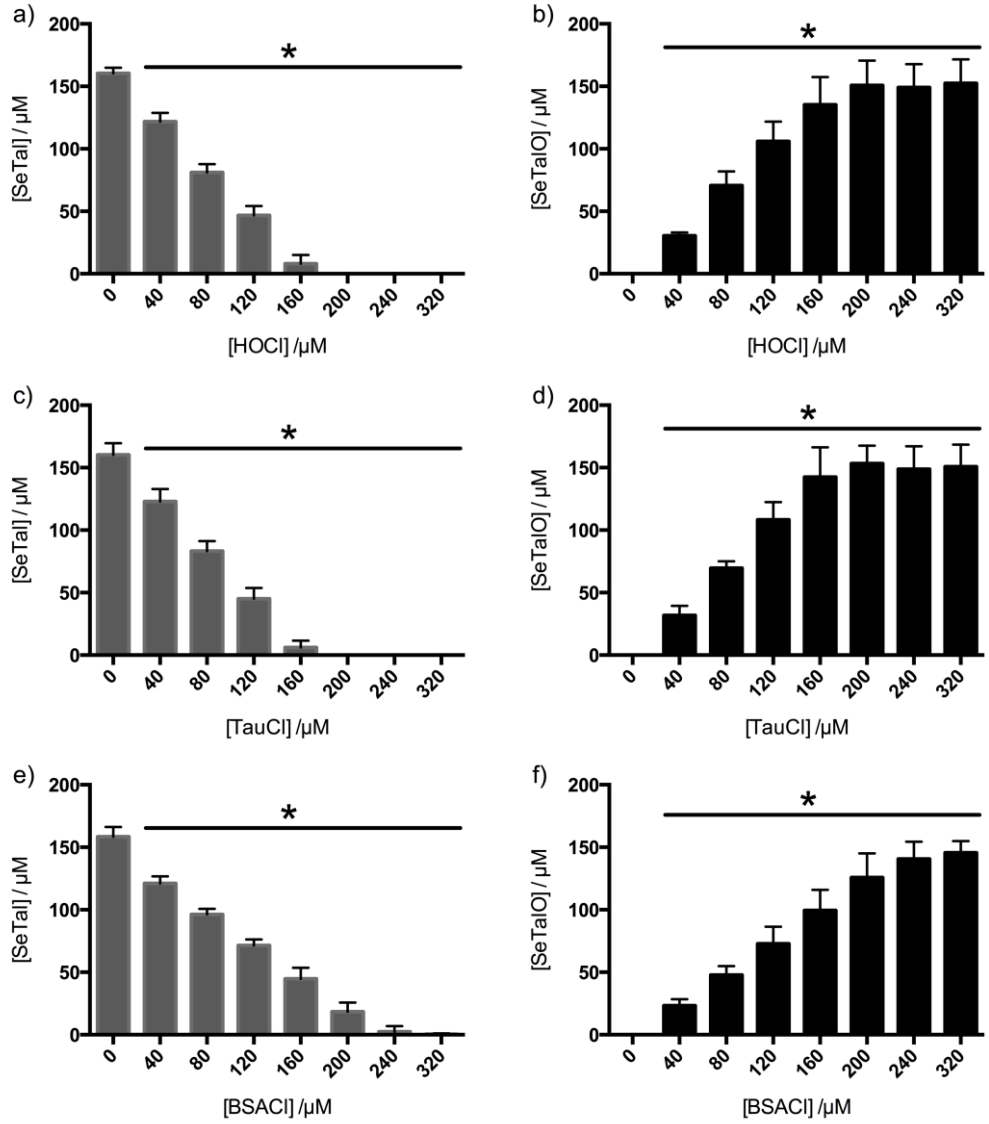

Figure 3.27 – Oxidation of SeTal to SeTalO by HOCl, TauCl and BSA-Cl

*SeTal (160 µM) was mixed a,b) HOCl, c,d) TauCl or e,f) BSA-Cl (with 0 – 320 µM) and incubated for 15 min at 22 °C before analysis by HPLC. a,c,e) show dose-dependent decrease in SeTal upon addition of increasing concentration of each oxidant. b,d,f) show a corresponding increase in SeTalO concentration. * indicates significant difference from control (0 µM oxidant) based on one-way ANOVA with Dunnett's post-hoc test. Data represent the mean ± SD from 3 independent experiments.*

3.4 Discussion

The studies reported in this Chapter examined the reaction between the selenoethers, SeMet and SeTal, and oxidants derived from neutrophils, primarily HOCl

and *N*-chloramines. It has been shown that SeMet and SeTal rapidly scavenge oxidants produced by MPO/H_2O_2/Cl^- and neutrophils, and that the primary oxidation product formed upon reaction with HOCl, TauCl and BSA-Cl was the respective selenoxide.

Met, SeMet and SeTal were capable of reducing concentrations of TauCl present in samples 30 min after initiation of HOCl formation by either an isolated MPO-system or neutrophils. This suggests that SeMet and SeTal may be scavenging HOCl directly before TauCl formation, as the rate constants for this reaction are 10^8 M^{-1} s^{-1} [90] for both species, compared to 10^5 M^{-1} s^{-1} for *N*-chloramine formation [60]. Alternatively, this may be occurring by direct scavenging of H_2O_2 by Met, SeMet and SeTal, reducing the total HOCl and hence TauCl formation, as selenoethers are known to react with H_2O_2 [454, 464, 569, 571]. However the reaction kinetics for the reaction of Met and H_2O_2 are slow (reported as 13.95 M^{-1} h^{-1} (3.9 x 10^{-3} M^{-1} s^{-1}) at pH 4.5) [573], and while rate constants for SeMet and SeTal with H_2O_2 have not been determined, the rate constants for H_2O_2 oxidation of similar selenoethers are in the range of 10 - 10^2 M^{-1} s^{-1} [569]. As MPO has favourable kinetics for the consumption of H_2O_2 [24], it is reasonable to suggest that HOCl is being produced under these conditions. Alternatively, if SeMet and SeTal do not react directly with HOCl, they may be scavenging TauCl after its formation prior to assay with TMB.

SeMet is known to be oxidised to SeMetO by H_2O_2, ONOOH and flavin containing monooxygenases [461, 464, 571]. The primary oxidation product detected in the current study when SeMet and SeTal were oxidised by HOCl, TauCl and BSA-Cl was the respective selenoxide, SeMetO or SeTalO. The stoichiometry of the reaction for SeTal is very close to a 1 : 1 reaction of HOCl and TauCl with SeTal, with SeMet occuring less efficiently with ca. 85 % of SeMet being converted to SeMetO. HOCl oxidation of SeMet also gave rise to a small amount of a second product, which is proposed to be dehydroselenomethionine on the basis of mass spectrometry results. This is analogous to the formation of dehydromethionine upon oxidation of Met by HOCl and *N*-chloramines [115]. In the current study, dehydroselenomethionine was not detected when SeMet was oxidised by H_2O_2. With only 85 % conversion SeMetO upon exposure of SeMet to HOCl or *N*- chloramines, formation of dehydroselenomethionine may account for some of the "missing" SeMet that does not form SeMetO. While the concentrations of dehydroselenomethione formed were not quantified in this study, it

may be possible quantify dehydroselenomethionine concentrations via the use of an iodine assay, as dehydromethionine has been detected via reaction with iodide to form iodine at low pH, or by a HPLC method [115].

Alternatively, the formation of selenones may be occuring, analogous with sulfone formation on Met. Oxidation of MetSO leads to the formation of methionine sulfone, though the reaction occurs slowly [88]. While selenone formation may be possible, direct evidence for the formation of the selenone has not been reported. The data presented in this Chapter do not appear to indicate selenone formation.

Reaction of excess HOCl with SeMet resulted in a loss of SeMetO, suggesting potential further reactions. Initial studies demonstrated that SeMetO treated with HOCl showed a loss of SeMetO that was not observed with H_2O_2. This decrease in SeMetO corresponded to an increase in unidentified peaks detected by HPLC. UV-vis data collected on stopped flow instrumentation demonstrated an initial increase at ca. 250 nm followed by a rapid decrease in intensity. As reactivity was not observed with H_2O_2 and the absorbance changes occur around 250 nm, which is the region where *N*-chloramines absorb, it suggests that the further reactivity of SeMetO with HOCl is mediated through chlorine chemistry at the amine site. Furthermore, SeTalO did not exhibit reactivity with HOCl, further implicating reaction via the amine site.

N-Chloramine formation may be more significant for reaction of SeMetO and HOCl than for SeMet, though chloramine formation on SeMet has not been assessed. Whilst *N*-chloramines are known to be generated on amino acids with rate constants of ca. 10^5 M^{-1} s^{-1} for α-amino acid, and HOCl reacts with SeMet at a rate of 10^8 M^{-1} s^{-1}, indicating that formation of SeMetO is kinetically favourable [60, 90]. Furthermore, *N*-chloramines are capable of oxidising SeMet to SeMetO, so it is conceivable that any *N*-chloramines formed on SeMet would react with a second SeMet to form SeMetO. However, in the case of SeMetO, oxidation of SeMetO to the selenone is likely to be significantly slower than SeMetO formation, if the chemistry is similar to sulfur chemistry. This may mean that the *N*-chloramine formation becomes more favourable once initial oxidation of the selenium centre to the selenoxide has occurred. The decay of the *N*-chloramine, observed at ~ 260 nm, could be due to formation of an aldehyde species, consistent with other *N*-chloramines [86], which may account for the unidentified peaks in the HPLC trace.

The $[SeMetO+H]^+$ formed from SeMetO was not detected by mass spectrometry under the conditions used in this study, though the ^1H NMR data confirm formation of SeMetO. Gamelgaard has previously detected SeMetO at *m/z* 214 for $[^{80}SeMetO+H]^+$, when SeMet was treated with H_2O_2 and then subsequently exposed to microwaves [571]. This is potentially due to microwave induced homolysis of H_2O_2 forming $HO^{\bullet}$ radicals (as previously suggested [574]), which may induce the formation of dehydroselenomethionine. Gamelgaard also detected peaks at *m/z* 196.3 (as observed in the current study), which was attributed to $[SeMetO+H-H_2O]^+$, suggesting a loss of water after ionisation. The ions detected in the current study at *m/z* 196.3 have been attributed to the formation of dehydroselenomethonine, as they were only detected in HOCl treated samples. If the source of the *m/z* 196.3 ion was due to the loss of water from SeMetO, these ions should also be detected in H_2O_2 treated SeMet.

The data obtained in the current study suggest that selenium compounds react more rapidly with *N*-chloramines than the analogous sulfur compounds. The second order rate constants for SeMet determined in this study (k_2 = (0.8 – 3.4) x 10^3 M^{-1} s^{-1}) are at least ten times greater than those previously reported for Met (k_2 = (0.4 – 2.0) x 10^2 M^{-1} s^{-1}) [192]. This is consistent with data for other MPO-derived oxidants, HOCl, HOSCN and HOBr, for both SeMet and SeTal and their respective sulfur analogues [90, 98].

N-chloramines formed in a biological setting are reported to display a selectivity for thiols, which can lead to protein inactivation if the targeted thiol is part of the active site of an enzyme [245]. GSH, a major intracellular thiol antioxidant, would be expected to be a major target of *N*-chloramines *in vivo*, with second order rate constants in the range of (1.1 – 2.6) x 10^2 M^{-1} s^{-1} [192], which are some of the fastest reported for *N*-chloramines. This reactivity is similar to that reported for various peroxides, which have been shown to preferentially oxidise SeMet in the presence of the thiol- and thioether-containing targets GSH and Met [474]. As the reaction of *N*-chloramines and SeTal has similar rate constants to that of GSH, and SeMet rate constants are ca. 10 greater than GSH, it suggests that selenoethers should provide a potential target for *N*-chloramine reactions *in vivo*, providing that they are present in sufficient concentration.

3.5 Conclusions

The data in this Chapter demonstrate that SeMet and SeTal are capable of reacting rapidly with HOCl and model *N*-chloramines (Figure 3.28). The primary products of these reactions are selenoxides, which have been characterised here by mass spectrometry and NMR spectroscopy. The second order rate constants for these reactions determined in these studies suggest that SeMet and SeTal will be competitive *in vivo* targets for the oxidants. The following Chapter investigates potential subsequent reactions that may be mediated by selenoxides.

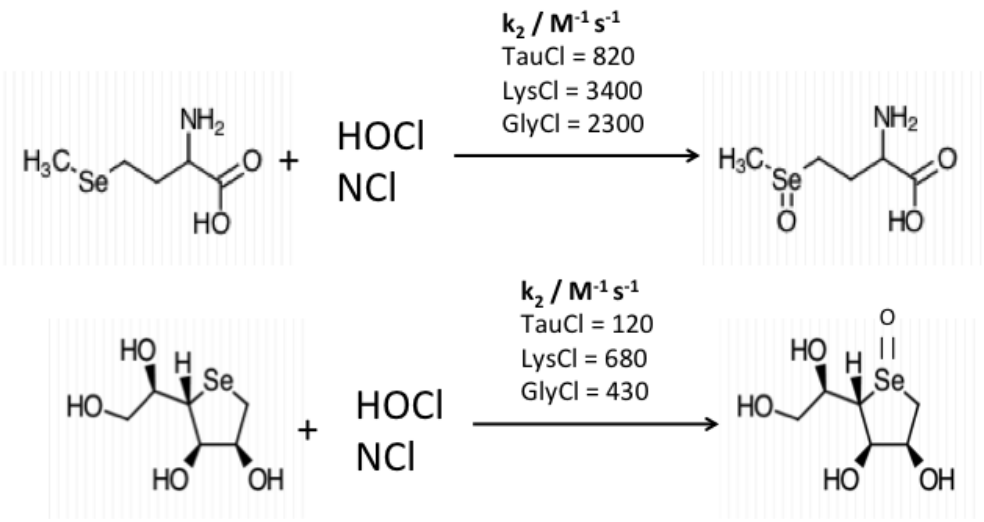

Figure 3.28 – SeMet and SeTal react with MPO-derived chlorinating oxidants to produce selenoxides.

4 Reduction of selenoxides by thiols

4.1 Introduction

Selenoxides are the major product formed when selenoethers are oxidised by peroxides and MPO-derived oxidants [444, 464]. Selenoxides can be subsequently reduced by thiols [444, 445]. Thiol-containing compounds, including GSH, are capable of reducing SeMetO to SeMet, forming a disulfide (Reaction 4.1). Ascorbate is also capable of reducing SeMetO, though this process is significantly slower than for thiols [445].

$$SeMetO + 2RSH \rightarrow SeMet + RSSR + H_2O \qquad \text{Reaction 4.1}$$

One electron reduction of SeMetO has also been demonstrated through pulse radiolysis studies [473]. The reduction is very fast with hydrated electrons, occurring with a rate constant near the diffusion limit ($k = 10^{10}\ M^{-1}s^{-1}$), and with $k = 5.9 \times 10^{8}\ M^{-1}s^{-1}$ and $3.5 \times 10^{7}\ M^{-1}s^{-1}$ for the one electron reductants $CO_2^{\bullet-}$ and $(CH_3)_2C^{\bullet}OH$ respectively [473]. The rate of one electron reduction is enhanced by a nitrogen-selenium non-covalent interaction [473].

The facile reduction of selenoxides has given rise to the hypothesis that selenium compounds may be able to catalytically scavenge oxidants *in vivo*. Numerous selenoethers and other selenocompounds have been described as GPx mimetics, with ebselen being one of the first described [441, 443, 490, 569, 575]. These GPx mimetics catalyse the reaction between GSH and H_2O_2 or other oxidants, which may be lead to a decrease in oxidative damage.

SeMet and SeTal can react rapidly with MPO-derived oxidants to produce the corresponding selenoxides [90, 486]. In order for SeMet and SeTal to act as catalytic oxidant scavengers, the reduction of the selenoxides must also be a favourable and rapid reaction, otherwise a build-up of selenoxide would occur, and inhibit the catalytic cycle. This Chapter explores the reaction rate constants and mechanisms of selenoxide reduction in order to determine the feasibility of the proposed catalytic scavenging cycle in biological systems.

4.2 Aims

The aim of the studies presented in this chapter was to assess and quantify the ability of thiols to reduce selenoxides formed on SeMet (and related selenoethers) and SeTal.

This was achieved by monitoring the concentration of reaction products after thiols were mixed with selenoxides, and by determining the rate constants and mechanisms of these reactions.

4.3 Results

4.3.1 Selenoxides oxidise thiols

Previous studies have demonstrated that SeMetO is reduced by thiols, including GSH, forming SeMet and GSSG [444, 445]. It was therefore hypothesised that GSH should be capable of reducing other selenoxides, including SeTalO and an analogue of SeMetO, methylselenocysteine selenoxide (MSCO). In order to assess this hypothesis, the loss of thiols upon reaction of various selenoxides with GSH was examined using the ThioGlo assay to monitor thiol concentration. SeMetO, SeTalO or MSCO (0 – 1 μM) were added to GSH (4 μM) and incubated for 10 min at 22 °C. Remaining thiol levels were determined by the ThioGlo assay (Figure 4.1).

Initial experiments examined the loss of thiols upon SeMetO addition (Figure 4.1 a). Addition of 0.2 μM SeMetO to 4 μM GSH resulted in a loss of approximately 0.4 μM GSH. Further addition of SeMetO dose-dependently decreased the GSH concentration with the maximum addition of 1 μM SeMetO decreasing the GSH concentration by 2 μM. This represents a 2 : 1 stoichiometry of the reaction of GSH and SeMetO, which is consistent with previous reports [444, 445]. Similar experiments were performed with SeTalO and MSCO. Addition of these selenoxides also resulted in a dose-dependent decrease in GSH concentration. The observed stoichiometry was 2 : 1: for GSH to selenoxide added.

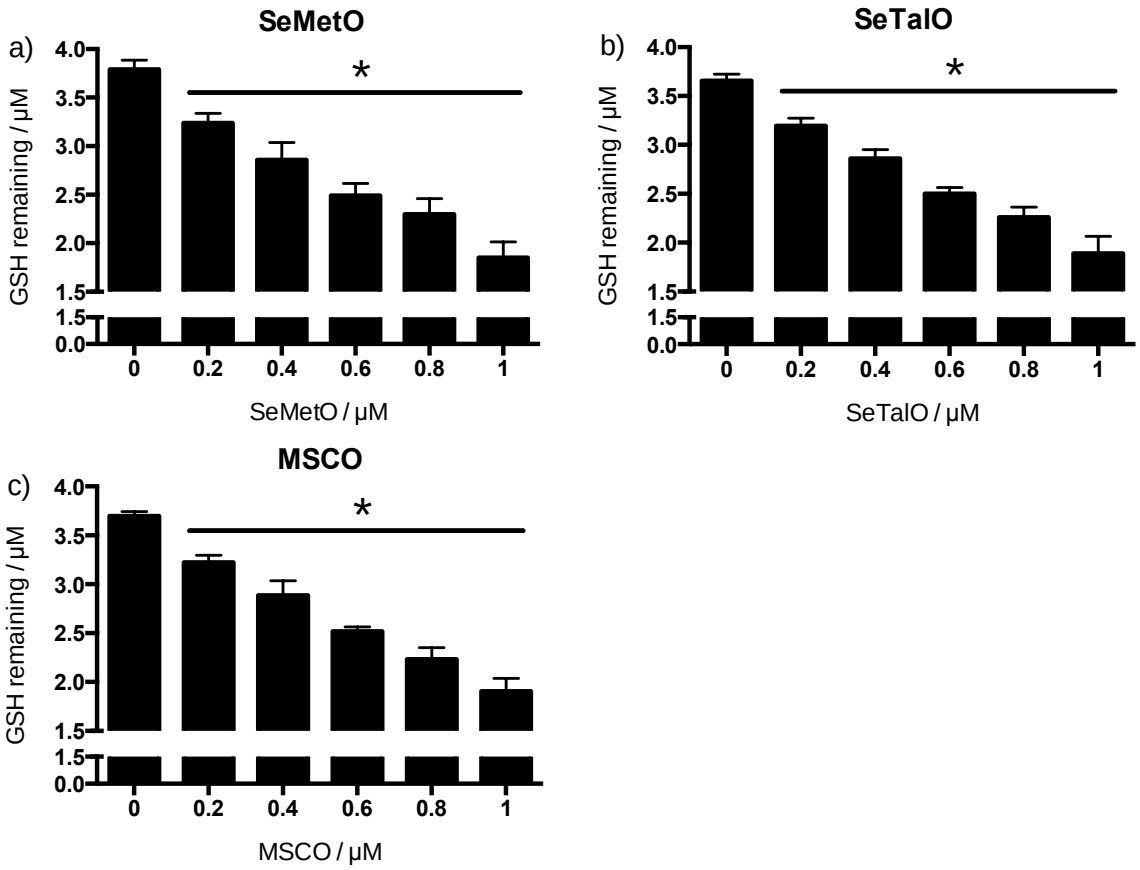

Figure 4.1 – Concentration of GSH remaining after selenoxide addition

*a) SeMetO, b) SeTalO or c) MSCO (0 – 1 µM) was added to GSH (4 µM) and incubated for 10 min at 22 °C. Remaining thiol levels were determined by ThioGlo assay. Thiol levels dose-dependently decreased upon addition of selenoxides in all cases. * represents a significant decrease ($p < 0.05$) in thiol concentration compared to control (0 µM selenoxide) based on one-way ANOVA with a Tukey's post-hoc test. Data represent mean ± SD of three independent experiments.*

4.3.2 GSH reduces selenoxides

The above data indicate that selenoxides are capable of consuming GSH, consistent with previous reports of selenoxide reduction by thiols [444, 445]. As SeTalO also caused a decrease in thiol levels upon addition to GSH, it was anticipated that the reduction of the SeTalO was also occurring. In order to assess these hypotheses, products of the reaction between SeMetO and SeTalO with GSH were assessed by HPLC.

4.3.2.1 Reduction of SeMetO

Initial experiments assessed the ability of GSH to reduce SeMetO, formed by reaction of SeMet (3.2 mM) with HOCl (1.6 mM). An excess of SeMet was used in order to

minimise the formation of products other than SeMetO. Preformed SeMetO (1.6 mM) was mixed with GSH (0 – 3.2 mM) and incubated for 10 min at 22 °C before a 10-fold dilution into H_2O and analysis by HPLC.

Addition of 0.4 mM GSH caused a decrease in the peak area of SeMetO, with a corresponding increase in the SeMet peak area (Figure 4.2). Furthermore a peak for GSSG was observed, and no GSH peak was observed, suggesting complete conversion of GSH to GSSG on reaction with SeMetO. Upon addition of increasing GSH concentrations, further decreases in SeMetO peak size were observed, with increases in the peak area for both SeMet and GSSG.

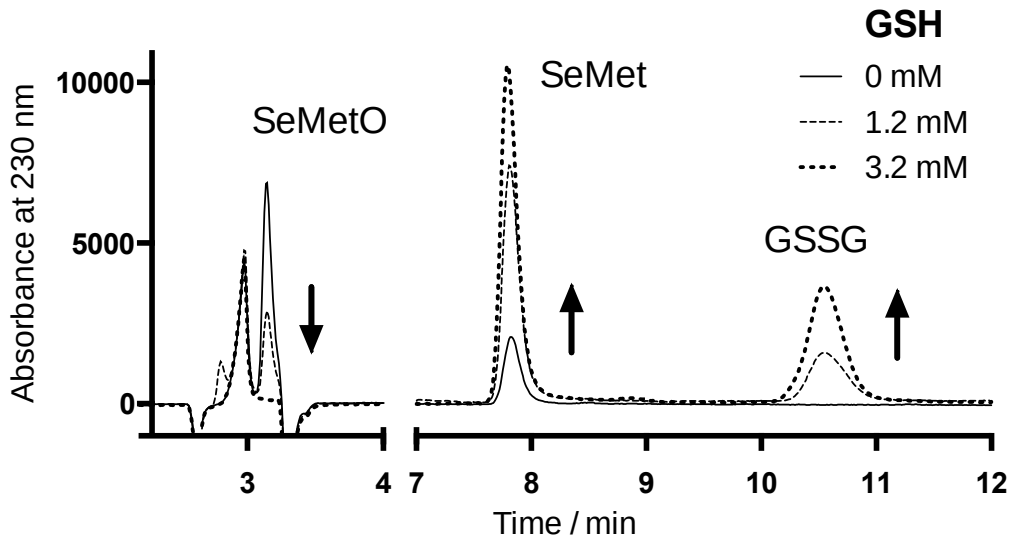

Figure 4.2 – Representative chromatograms of SeMetO (1.6 mM) exposed to GSH (0 – 3.2 mM)

SeMetO (1.6 mM) was mixed with 0 (unbroken line), 1.2 mM (dashed line) or 3.2 mM (dot-dashed line) GSH and incubated for 10 min at 22 °C, prior to 1 in 10 dilution into H_2O and HPLC analysis with UV detection at 230 nm. A dose-dependent decrease of SeMetO was observed with increasing GSH, and this corresponded to an increase in SeMet and GSSG concentrations. Arrows indicate direction of peak change observed with increasing GSH concentration.

Upon quantification (Figure 4.3), a dose-dependent decrease of SeMetO was observed with increasing GSH concentration. Approximately 0.2 mM SeMetO was reduced for every 0.4 mM GSH added to SeMetO. This corresponded with an equal increase in SeMet and GSSG, of about 0.2 mM each for every 0.4 mM GSH added. These data are consistent with the reduction of SeMetO to SeMet by GSH, with the expected stoichiometry observed as described in Reaction 4.2.

$$SeMetO + 2GSH \rightarrow SeMet + GSSG + H_2O \qquad \text{Reaction 4.2}$$

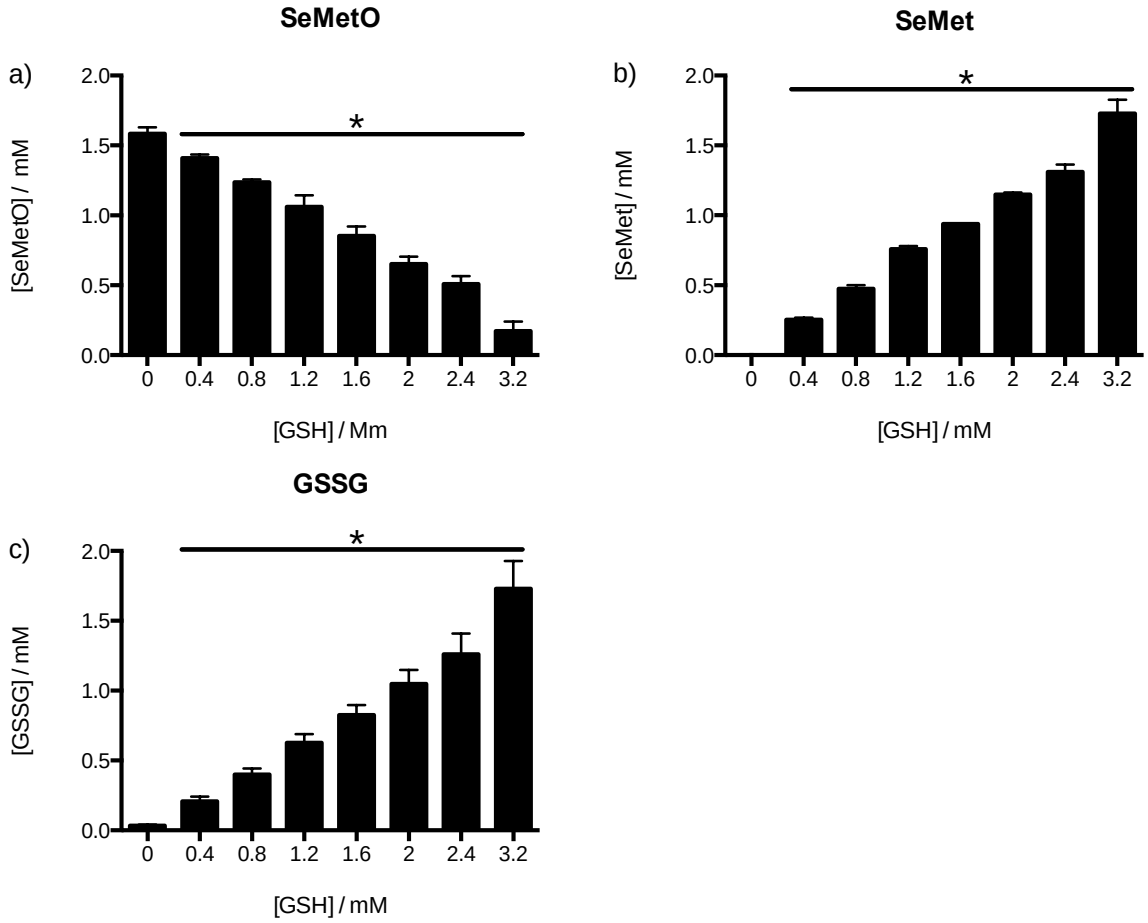

Figure 4.3 – GSH (0 – 3.2 mM) reduces SeMetO (1.6 mM) forming SeMet and GSSG

*SeMetO (1.6 mM), formed by the reaction of SeMet and HOCl, was mixed with GSH (0 – 3.2 mM) and incubated for 10 min before 1 in 10 dilution into H_2O and analysis by HPLC. Species measured were a) SeMetO, b) SeMet and c) GSSG. A dose dependent decrease in SeMetO was observed with increasing GSH concentration, which corresponded with a stoichiometric increase in SeMet and GSSG formation. * represents a significant difference ($p < 0.05$) from control (0 mM GSH) based on one-way ANOVA with a Tukey's post-hoc test. Data represent mean ± SD of three independent experiments.*

4.3.2.2 Reduction of SeTalO

The ability of GSH to reduce SeTalO was also assessed using HPLC analysis. SeTalO (1.6 mM), formed by the reaction of SeTal (3.2 mM) and HOCl (1.6 mM), was mixed with GSH (0 – 3.2 mM) and incubated for 10 min at 22 °C, before a 10-folddilution into H_2O and analysis by HPLC.

Addition of GSH (0 – 3.2 mM) to SeTalO (1.6 mM) resulted in a decrease in peak area for SeTalO, which corresponded to an increase in the peak area for SeTal (Figure 4.4). However, as the HPLC conditions used for the separation of SeTal and SeTalO were different to those employed for the separation of SeMet and SeMetO, no peak corresponding to GSSG or GSH was observed. It is thought that these species were eluting with the solvent front. Higher concentrations of GSH caused a greater decrease in SeTalO peak area, with a corresponding increase in SeTal peak area.

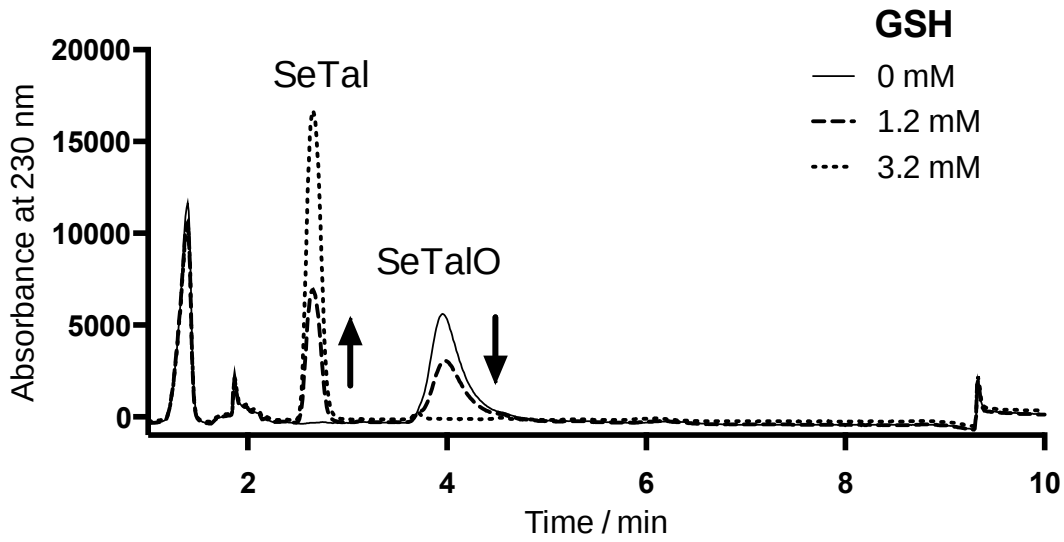

Figure 4.4 – Representative chromatograms of SeTalO (1.6 mM) exposed to GSH (0 – 3.2 mM)

SeTalO (1.6 mM) was mixed with 0 (unbroken line), 1.2 mM (dashed line) or 3.2 mM (dotted line) GSH and incubated for 10 min at 22 °C, prior to 1 in 10 dilution into H_2O and HPLC analysis with UV detection at 230 nm. A dose-dependent decrease of SeTalO was observed with increasing GSH, and this corresponded to an increase in SeTal. Arrows indicate direction of peak change observed with increasing GSH concentration.

Analogous to SeMetO reduction, a dose-dependent decrease in SeTalO concentration was observed with increasing GSH concentrations (Figure 4.5). Addition of 40 μM GSH gave a 20 μM decrease in SeTalO, with a corresponding 20 μM increase in SeTal concentrations. The stoichiometry would be expected to be the same as the reaction of

SeMetO with GSH (Reaction 4.2). However, due to limitations with the HPLC method, GSSG concentrations could not be determined as they eluted with the solvent front.

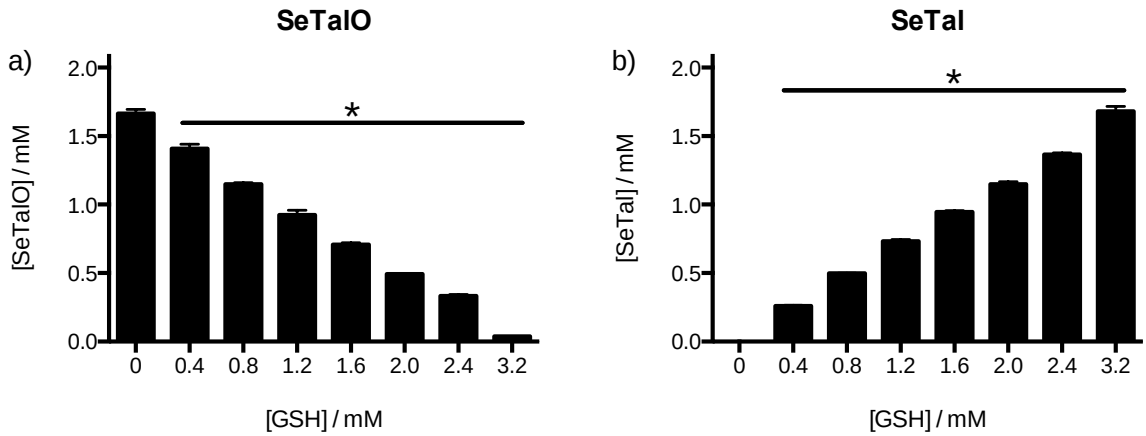

Figure 4.5 – GSH (0 – 3.2 mM) reduces SeTalO (1.6 mM) forming SeTal

*SeTalO (1.6 mM), formed by the reaction of SeTal (3.2 mM) and HOCl (1.6 mM), was mixed with GSH (0 – 3.2 mM) and incubated for 10 min before 1 in 10 dilution into H_2O and analysis by HPLC with UV detection at 230 nm. Species measured were a) SeTalO and b) SeTal. A dose-dependent decrease in SeTalO was observed with increasing GSH concentration, which corresponded to an equal increase in SeTal formation. * represents a significant difference ($p < 0.05$) from control (0 mM GSH) based on one-way ANOVA with a Tukey's post-hoc test. Data represent mean ± SD of three independent experiments.*

4.3.3 Determination of rate constants for selenoxide reduction by thiols

As the above data indicate that GSH is capable of reducing SeMetO and SeTalO to the corresponding selenoethers SeMet and SeTal, in biological systems there is a potential for a catalytic reduction cycle where SeMet and SeTal could consume multiple equivalents of oxidant. However, for this to be biologically relevant, the reduction kinetics would need to be rapid for efficient selenoxide removal. In order to investigate this in more detail, stopped flow kinetic analysis was used to determine the kinetics of the reactions between selenoxides and thiols.

Initially reduction of SeMetO and most biologically relevant thiol, GSH, was attempted. However, the reaction of SeMetO with GSH led to complex kinetics, which were difficult to analyse due to overlap of the selenoxide and thiol absorbance spectra (Section 4.3.3.4). As a result, the aromatic thiol, TNB, which absorbs at 412 nm, was used as a model thiol to investigate the reduction kinetics of selenoxides in an attempt to simplify the observed kinetic data.

4.3.3.1 Reduction of SeMetO and SeTalO by TNB

TNB, which has a yellow colour, can react with oxidants to form the colourless disulfide DTNB [555]. As TNB and DTNB have distinguishable peak absorbance (TNB = 412 nm; DTNB = 324 nm) [555] that do not overlap with the absorbances of selenoxides (200 – 300 nm), TNB presented an ideal model thiol to explore the kinetics and mechanisms of selenoxide reduction.

SeMetO or SeTalO (5 μM) and TNB (25 – 125 μM) were mixed in the stopped flow apparatus and the absorbance monitored at 412 nm (loss of TNB, i.e. thiol consumption) and 324 nm (increase in DTNB product, i.e. disulfide formation). Decreases in absorbance over time were observed at 412 nm, consistent with a consumption of TNB, whilst concomitant increases in absorbance were observed at 324 nm, consistent with DTNB formation.

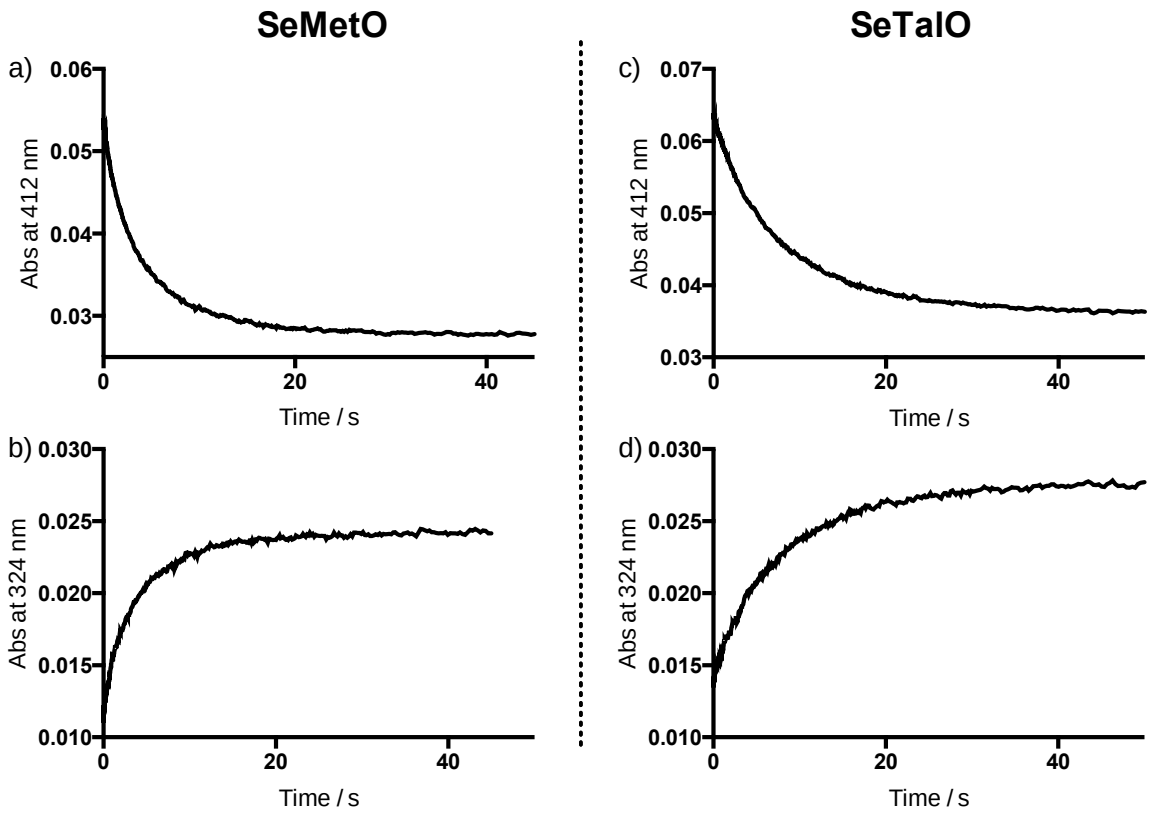

Figure 4.6 – Representative figures demonstrating the change in absorbance at a,c) 412 nm or b,d) 324 nm after a,b) SeMetO (5 μM) or c,d) SeTalO (5 μM) was mixed with TNB (25 μM) monitored by stopped flow apparatus

a,b) SeMetO (5 μM) or c,d) SeTalO (5 μM) was mixed with TNB (25 μM) by stopped flow apparatus in phosphate buffer (pH 7.4, 0.1 M) at 22 °C and the absorbance at a,c) 412 and b,d) 324 nm was monitored over time. In both cases, a loss in absorbance was observed at 412 nm, indicating TNB consumption. Concomitantly, an increase in absorbance was observed at 324 nm, indicating DTNB formation.

First-order (t vs. ln(Abs)) and second-order (t vs. 1/Abs) analysis of the absorbance data at 412 nm obtained when SeMetO or SeTalO were mixed with TNB yielded the graphs in Figure 4.7. For both SeMetO and SeTalO a linear first-order plot was observed, and the second-order plots were non-linear. The linearity of the first-order plots indicates a first order (or, more likely, a pseudo first-order) mechanism is occurring.

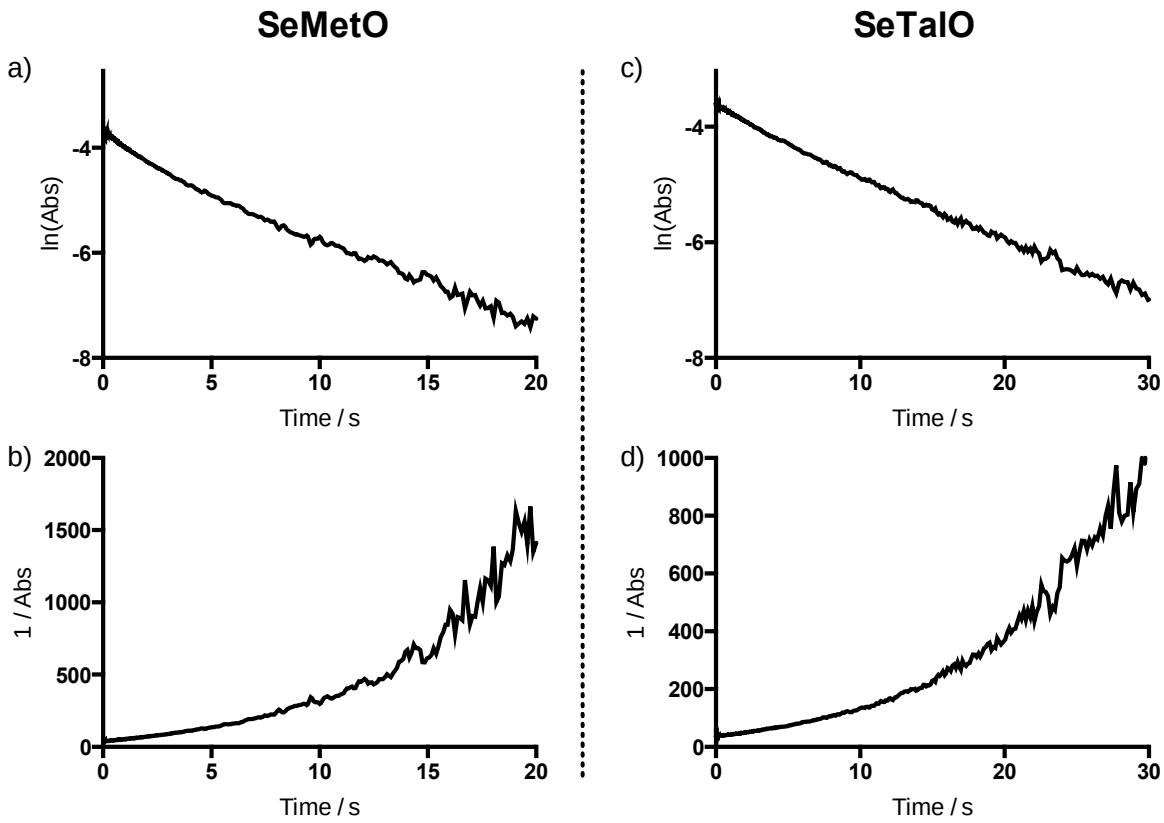

Figure 4.7 – First- and second-order plots for the reaction between a,b) SeMetO (5 μM) or c,d) SeTalO (5 μM) and TNB (25 μM) based on absorbance data obtained at 412 nm

SeMetO (5 μM) or SeTalO (5 μM) was mixed with TNB (25 μM) by stopped flow apparatus in phosphate buffer (pH 7.4, 0.1 M) at 22 °C and the absorbance at 412 nm was monitored over time. The absorbance data obtained was then analysed by either a,c) first-order conditions (ln(Abs) vs time) or b,d) second-order conditions (1/Abs vs time). For both SeMetO and SeTalO, the ln(Abs) vs time plots were observed to be linear, indicating first-order reaction mechanisms are occurring.

The stoichiometry of the reaction of thiols and selenoxides indicate that for every one mole of selenoxide reduced, 2 moles of thiols will be consumed. Based on this, the reaction may be occurring via one of two mechanisms. One potential mechanism is a one-step process where 2 thiol groups meet and react with the selenoxide at the same time. This would result in a kinetic profile demonstrating a second-order reaction with respect to thiols. However, a second-order reaction with respect to thiols was not observed (Figure 4.7).

Alternatively, the reaction may be a two-step process where one thiol group reacts with the selenoxide to form a seleno-sulfide intermediate, with the rate constant for this step designated as k_1. This intermediate could then react with a second thiol group to

produce the disulfide and selenoether, with the rate constant for this step designated as k_2 (Figure 4.8). Kinetic models demonstrate that in such a 2-step system where the $k_1 > k_2$ (for modelling purposes a 10-fold increase of k_1 over k_2 was used), the thiol concentration [RSH] decreases exponentially and the first-order plot is linear (Figure 4.9). k_1 can then be determined from the gradient of the pseudo first-order plot. However, if $k_2 > k_1$, 2-phase kinetics will be observed for [RSH]. This gives a non-linear first-order plot, and a single exponential decay does not fit to the data well.

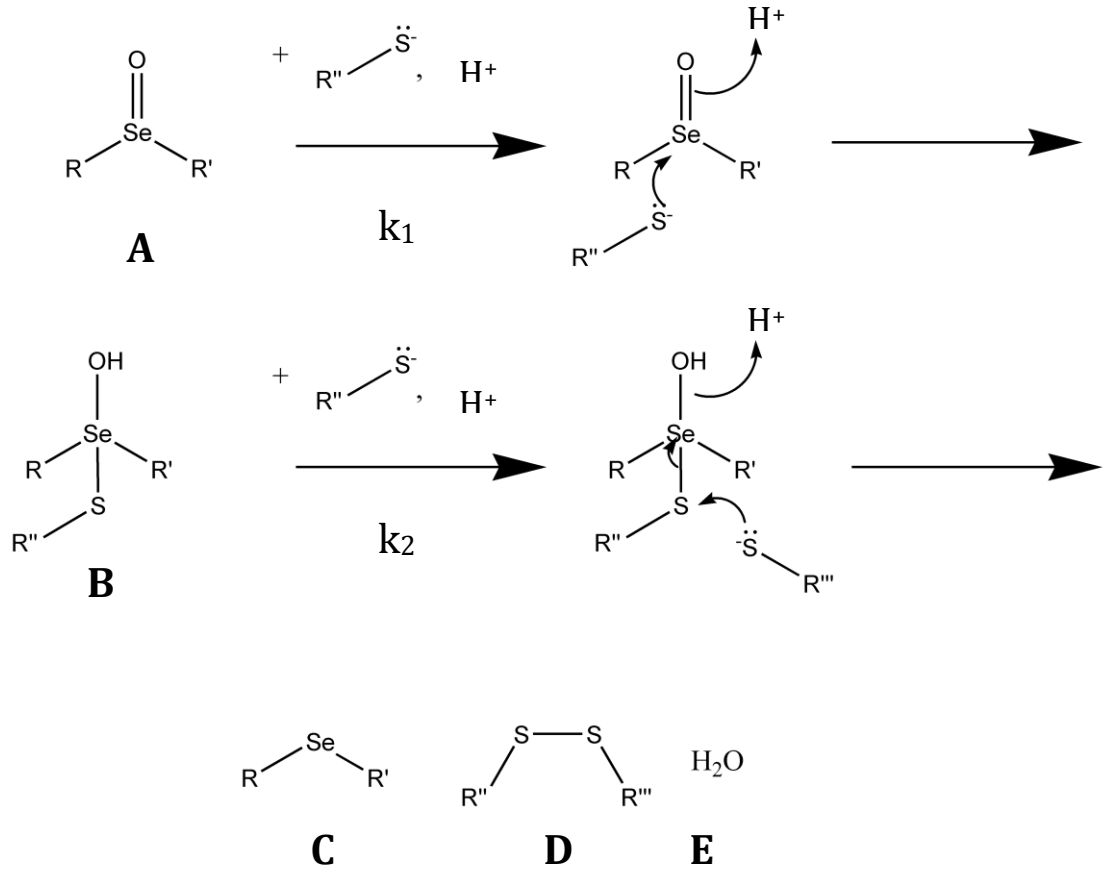

Figure 4.8 – Proposed two-step mechanism of selenoxide reduction by thiols

*Initial reaction of selenoxides (**A**) with thiols is proposed to lead to the formation of a seleno-sulfide intermediate (**B**). The rate constant for the initial reaction is designated as k_1. A second thiol then reacts with the intermediate with a rate constant k_2, producing a selenoether (**C**), disulfide (**D**) and water (**E**) as products.*

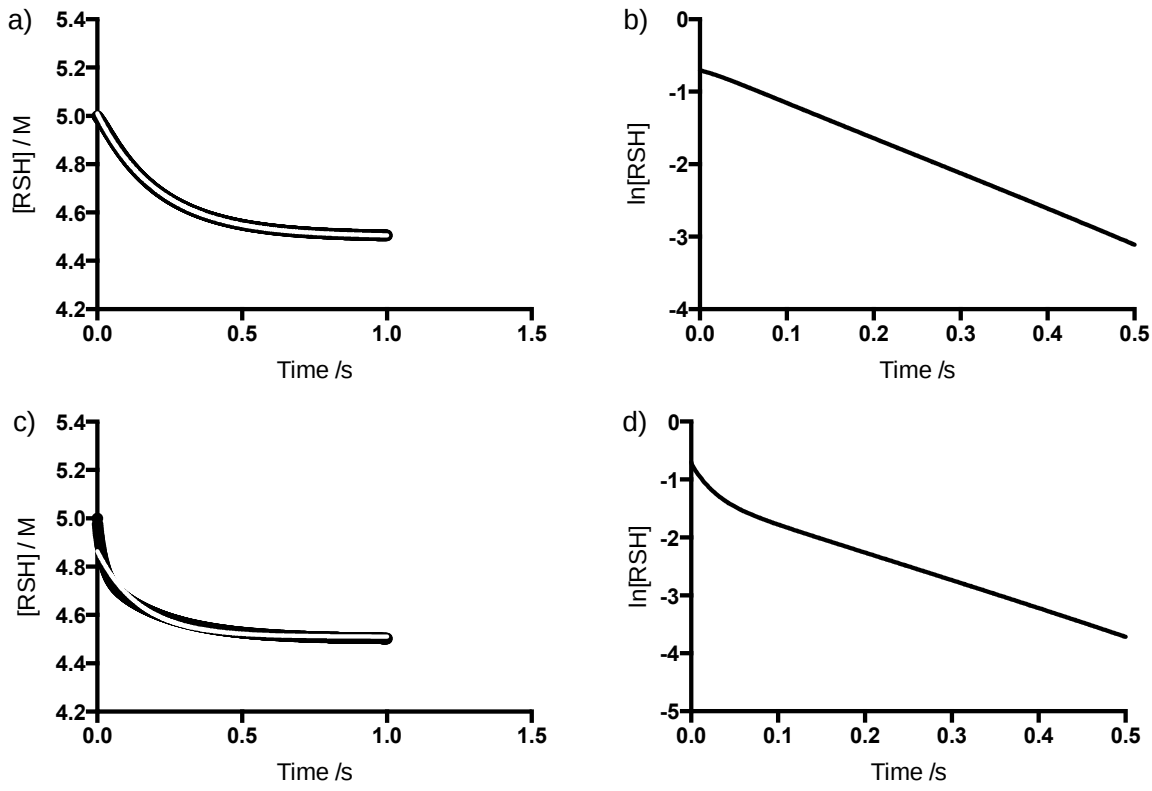

Figure 4.9 – Computational models showing reaction profile for the proposed two-step mechanism

a) shows computational model (black line) of the reaction (A + RSH ➔ C + RSH ➔ D + E + F) where concentration of RSH is set to 5 M, representing a ten-fold excess of the concentration of A, set to 0.5 M. The rate constant for the k_2 was set to 10 and k_1 was set to 1. The simulation was run for 1000 points, with the theoretical concentrations of A and RSH calculated at 0.001 s intervals. An exponential decay function was fitted to the data obtained for concentrations of RSH (white line). c) shows the same model (black line), with k_2 set to 1 and k_1 set to 10, with the exponential fit (white line). The concentration of RSH obtained in a) was plotted as ln[RSH] vs time in b). The concentration of RSH obtained in c) was plotted as ln[RSH] vs time in d). When $k_2 > k_1$ first-order conditions are observed, with concentration data fitting to single exponential curve, and ln[RSH] vs time plots linear. When $k_2 < k_1$, first-order mechanisms are not observed. Computational models were performed in Mechanism-Based Kinetics Simulator available at (http://www.stolaf.edu/depts/chemistry/courses/toolkits/126/js/kinetics/). Exponential fits were performed in Prism v6.

As first-order kinetics were observed when SeMetO and SeTalO were mixed with TNB, based on the linearity of the first-order plots and good fits to single exponential decays, this suggests that the rate limiting step in this reaction is k_1, based on kinetic modelling. The second step, k_2, is not observed, which is consistent with the model. As the kinetics are following a first-order mechanism, the rate constant for the reaction can be determined from the gradient of a plot of the initial concentration of TNB against the

observed rate constant (k_{obs}) for the condition. The k_{obs} values were determined by fitting a single exponential curve to absorbance data in ProData Viewer (Applied Photophysics). The determined second-order rate constants for the reduction of SeMetO and SeTalO by TNB were $k_1 = (3.8 \pm 0.1) \times 10^4$ and $k_1 = (4.9 \pm 0.2) \times 10^3\ M^{-1}\ s^{-1}$ respectively (Figure 4.10).

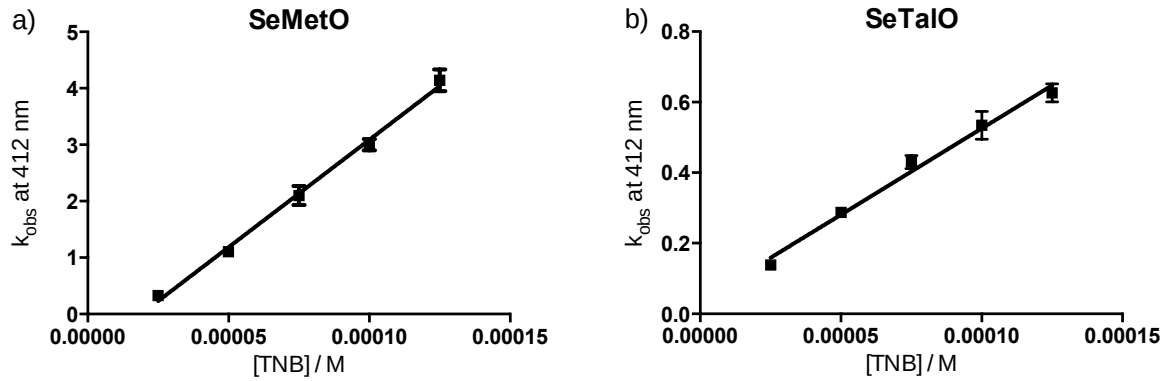

Figure 4.10 – Pseudo-first order plots for the reduction of a) SeMetO and b) SeTalO by TNB

SeMetO (5 µM) or SeTalO (5 µM) was mixed with increasing concentrations of TNB (25 - 125 µM) by stopped flow apparatus in phosphate buffer (pH 7.4, 0.1 M) at 22 °C and the absorbance at 412 nm was monitored over 60 s. The observed rate constant, k_{obs}, for each condition was determined from the absorbance vs time plots using single exponential fitting in ProData Viewer software (Applied Photophysics). k_{obs} was plotted against the initial TNB concentration for a) SeMetO or b) SeTalO, and the second order rate constants determined from the gradients of these plots. Data represent mean ± SD of three independent experiments.

The rate of DTNB production was also measured from the absorbance changes at 324 nm by the same pseudo first-order method. The observed rate constants at 412 nm and 324 nm were very similar, and points overlay one another in the pseudo first-order analysis plots of 412 and 324 nm data. The rate of DTNB production observed was not significantly different to the rate at which TNB was being consumed, with $k_1 = (3.8 \pm 0.1) \times 10^4\ M^{-1}\ s^{-1}$ for SeMetO and $(4.8 \pm 0.2) \times 10^3\ M^{-1}\ s^{-1}$ for SeTalO. This supports the mechanism proposed where a rate-limiting intermediate formation occurs followed by a fast second step where the disulfide is formed.

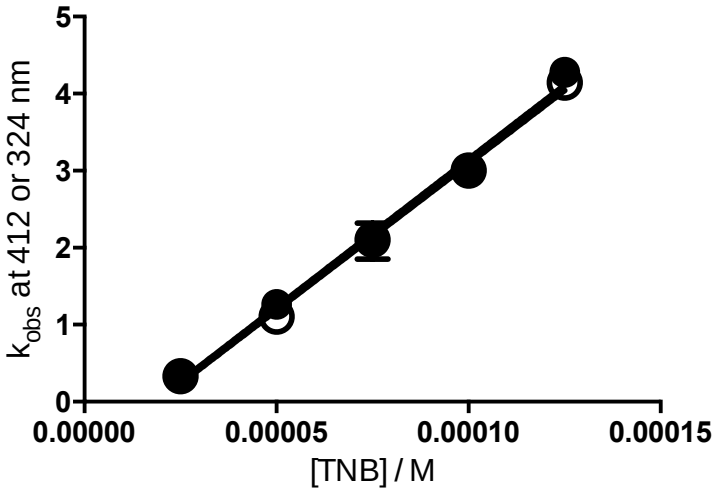

Figure 4.11 – k_{obs} determined from data measured at 324 nm (open circles) and 412 nm (closed circles) when SeMetO (5 μM) was mixed with increasing concentration of TNB (25 – 125 μM)

SeMetO (5 μM) was mixed with increasing concentrations of TNB (25 - 125 μM) by stopped flow apparatus in phosphate buffer (pH 7.4, 0.1 M) at 22 °C and the absorbance at 412 or 324 nm was monitored over 60 s. The observed rate constant, k_{obs}, for the reaction at 412 nm (closed circles) or 324 nm (open circles) was determined from the absorbance vs time plots using single exponential fitting in ProData Viewer software (Applied Photophysics). k_{obs} was plotted against initial TNB concentration for SeMetO, and the second order rate constant determined from the gradients of these plots. Data represent mean ± SD of three independent experiments.

4.3.3.2 Reduction of other selenoxides by TNB

The rate constant determined for the reduction of SeMetO by TNB was an order of magnitude greater than that for SeTalO. It was thought that this may be due to effects of the surrounding molecular environment of the selenoxide moiety, with the amine group of SeMetO potentially interacting with the selenium, and increasing the rate at which the reaction occurs as seen in one-electron reduction of SeMetO [473]. In order to examine this possibility, the rate constants for the reaction of TNB with various selenoxides with structures related to SeMetO were determined.

The selenoxides were chosen based on chemical structures similar to that of SeMetO with the amine group either hindered or absent (Figure 4.12). Se-Methyl selenocysteine selenoxide is also an α-amino acid with one carbon less in the side chain than SeMetO and therefore the nitrogen and selenium atoms should not be able to interact due to steric considerations. *N*-acetylselenomethionine selenoxide has the amine group of

SeMetO blocked by an *N*-acetyl group. SePropO keeps the carboxyl group the same distance from the Se atom, though the amine group is removed.

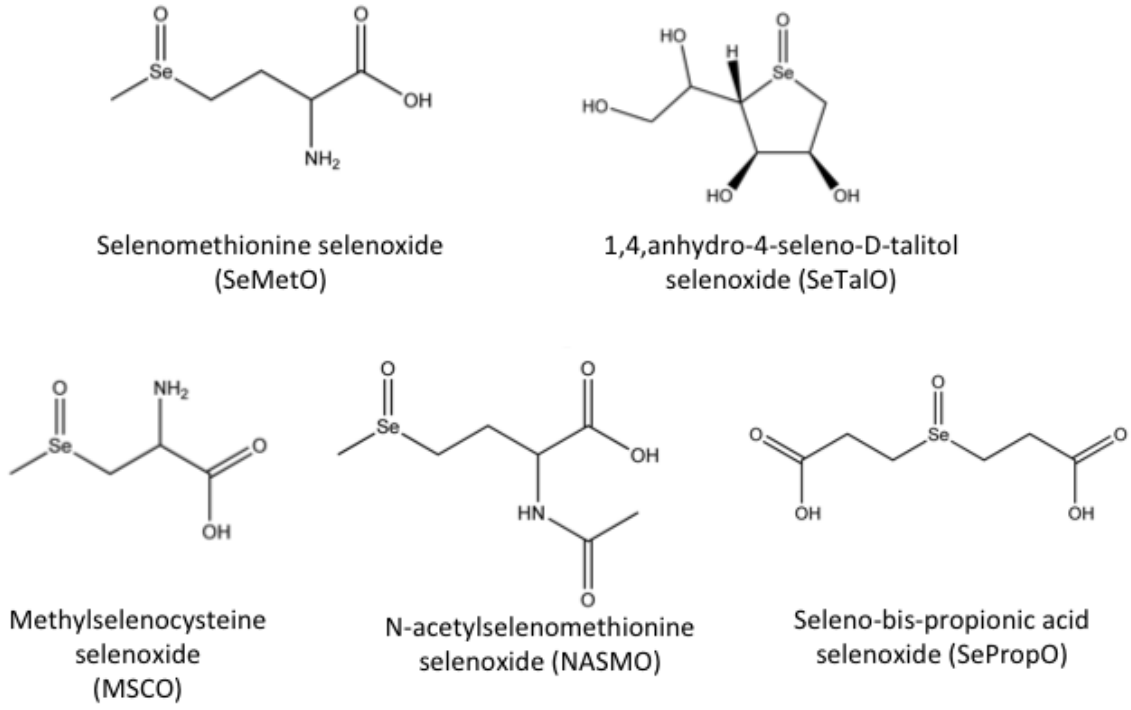

Figure 4.12 – Structures of model selenoxides used in the determination of the mechanisms and kinetics of selenoxide reduction by thiols.

MSCO, NASMO or SePropO (5 μM) were mixed with increasing concentrations of TNB (25 – 125 μM) and absorbance changes monitored at 412 and 324 nm (Figure 4.13). Upon mixing, a time dependent decrease in absorbance was observed at 412 nm, corresponding to consumption of TNB. At the same time, an increase in absorbance at 324 nm was observed, corresponding to formation of DTNB. Absorbance data at 412 nm was used to plot both first- (ln(Abs) vs time) and second-order (1/Abs vs time) plots. The first-order plots for MSCO, NASMO and SePropO were observed to be linear, confirming the mechanism is likely to be the same as that observed in the reduction of SeMetO and SeTalO by TNB.

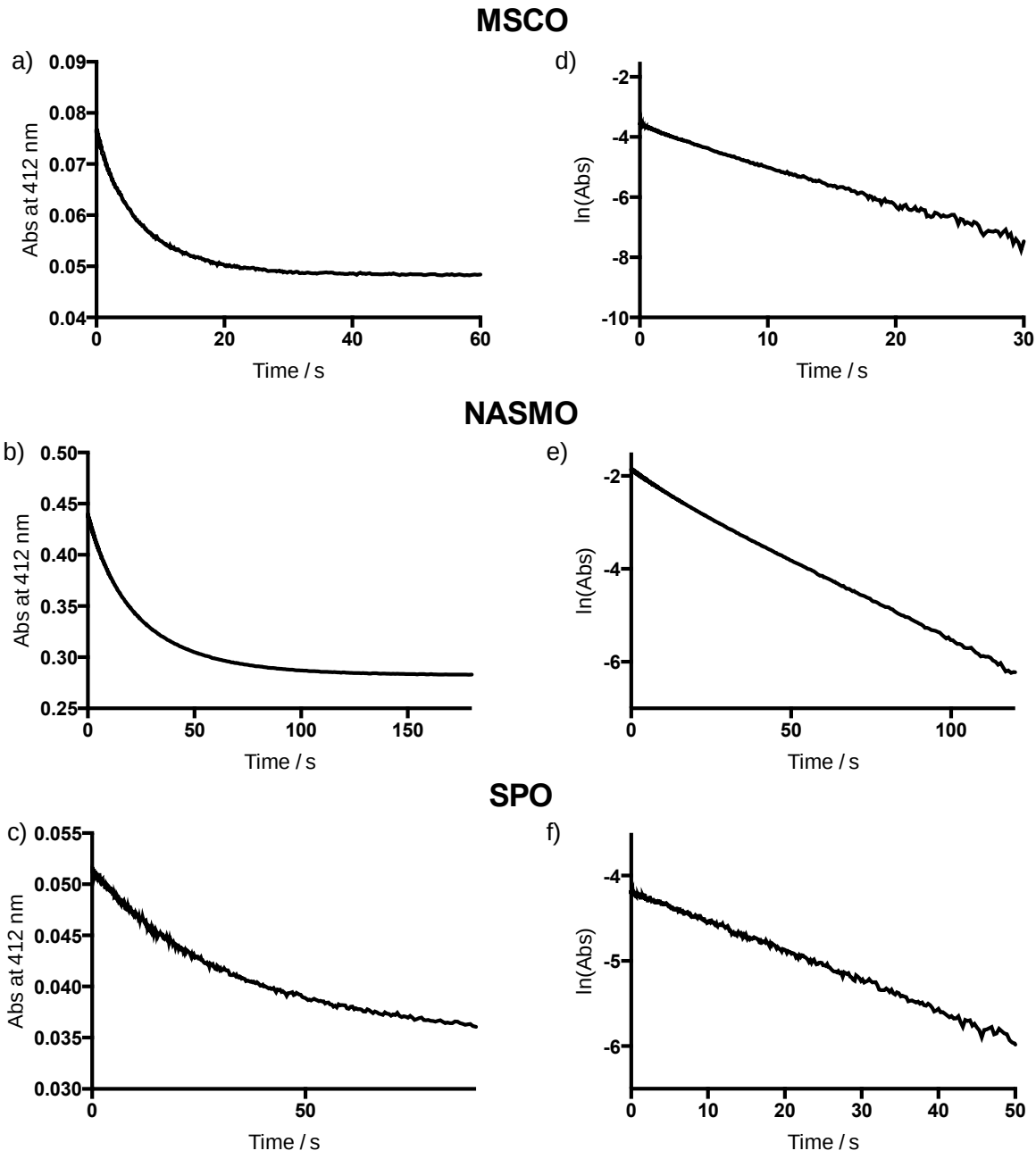

Figure 4.13 – Changes in absorbance at 412 nm over time and the corresponding first-order analysis plots (lnAbs vs time) for the reactions of MSCO, NASMO and SPO with TNB

a) MSCO (5 μM), b) NASMO (5 μM) or c) SePropO (5 μM) were mixed with TNB (25 μM) by stopped flow apparatus in phosphate buffer (pH 7.4, 0.1 M) at 22 °C and the absorbance at 412 nm was monitored over time. Absorbance data were plotted as ln(Abs) vs time for d) MSCO, e) NASMO or f) SePropO in order to determine the order of reaction. The ln(Abs) vs time plots for MSCO, NASMO and SPO were all linear, and therefore the reaction with TNB follows a first-order mechanism.

As a first-order (or pseudo first-order) mechanism was observed, second order rate constants were determined by pseudo first-order analysis. The observed rate constants (k_{obs}) for each condition were determined by fitting exponential curves to the absorbance vs time data for each sample (Figure 4.14). Second-order rate constants for the reaction of MSCO, NASMO and SePropO with TNB were then determined by plotting k_{obs} against initial TNB concentration. The rate constants were determined to be k_1 = (4.4 ± 0.3) x 10^3, k_1 = (1.2 ± 0.04) x 10^3 and k_1 = (1.3 ± 0.03) x 10^3 M^{-1} s^{-1} for MSCO, NASMO and SePropO respectively. The rate constant for the formation of DTNB was also calculated from absorbance data at 324 nm, and the rate constants obtained were not significantly different from those determined at 412 nm (Table 4.1). Interestingly, all these selenoxides gave rate constants about 10-fold lower than those determined for SeMetO, supporting the hypothesis that the presence of an amine group may contribute to the facile reduction of SeMetO.

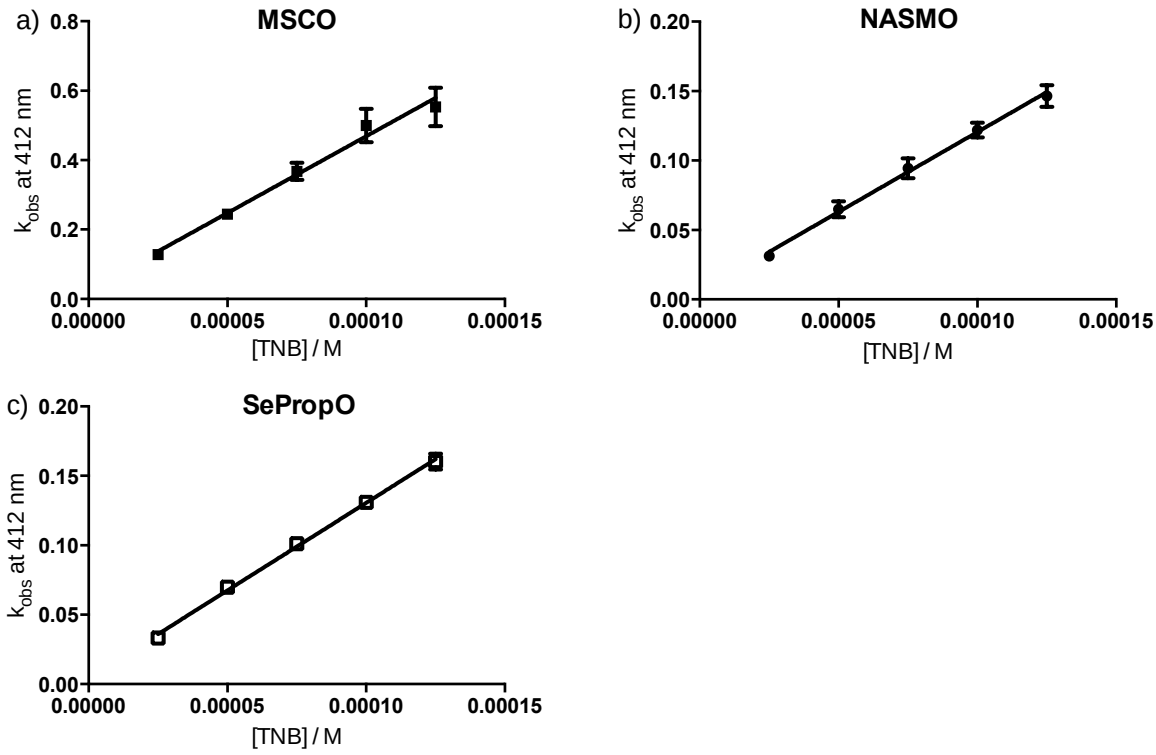

Figure 4.14 – Pseudo first-order plots for the reaction of a) MSCO, b) NASMO and c) SePropO with TNB

MSCO (5 µM), NASMO (5 µM) or SePropO (5 µM) was mixed with increasing concentrations of TNB (25 - 125 µM) by stopped flow apparatus in phosphate buffer (pH 7.4, 0.1 M) at 22 °C and the absorbance at 412 nm was monitored over time. The observed rate constant, k_{obs}, for each condition was determined from the absorbance vs time plots using single exponential fitting in ProData Viewer software (Applied Photophysics). k_{obs} was plotted against initial TNB concentration for a) MSCO, b) NASMO or c) SPO and the second-order rate constants determined from the gradient of these plots. Data represent mean ± SD of three independent experiments.

Table 4.1 – Second-order rate constants for the reduction of selenoxides by TNB

	k_1 / M^{-1} s^{-1}	
Selenoxide	-d[TNB]/dt	+d[DTNB]/dt
SeMetO	(3.8 ± 0.1) x 10^4	(3.8 ± 0.1) x 10^4
SeTalO	(4.9 ± 0.2) x 10^3	(4.8 ± 0.2) x 10^3
MSCO	(4.4 ± 0.3) x 10^3	(4.9 ± 0.6) x 10^3
NASMO	(1.2 ± 0.04) x 10^3	(1.2 ± 0.1) x 10^3
SePropO	(1.3 ± 0.03) x 10^3	(1.3 ± 0.06) x 10^3

4.3.3.3 Contribution of amine group to rate constant

SeMetO has a rate constant for reduction by TNB that is about 10 times higher than the other selenoxides measured (Table 4.1). This is proposed to be due to the amine group present in the structure, as nitrogen and selenium non-bonding interactions have been shown to have effects on redox properties of compounds [473]. Thus, experiments were performed examining the reduction of NASMO and MSCO by TNB in phosphate buffer (pH 7.4, 0.1 M) supplemented with Gly (10 mM) to investigate whether the presence of an extramolecular amine group could effect the rate of reduction.

MSCO, NASMO and TNB were prepared using a phosphate buffer (pH 7.4, 0.1 M) containing Gly (10 mM). The rate of reaction between selenoxides and TNB was assessed by stopped flow as described above. Absorbance changes consistent with the loss of TNB and formation of DTNB were observed. Second-order rate constants were determined from the data by plotting k_{obs} against TNB concentration (Figure 4.15). Linear regression analysis yielded the second-order rate constants shown in Table 4.2. These rate constants were higher than those measured in the absence of Gly, and a statistical comparison of the slope (Prism v6 – unpaired t-test) indicated that there was a significant 2-fold increase in k_1 for NASMO in the presence of Gly. The small increase in k_1 determined for MSCO in the presence of Gly was not significantly different to the k_1 determined in the absence of Gly.

These results initially appear inconsistent. However, the rate constant for the reduction of MSCO by TNB is already elevated compared to NASMO in the absence of Gly. This may arise from the fact that MSCO already contains a free amine group, that though unlikely to interact intramolecularly, may interact intermolecularly with the Se centre. Therefore, the addition of excess in the form of Gly may not have as dramatic an impact compared to the NASMO, which has no free amine. The increased rate constant for NASMO suggests that extramolecular amine groups may interact favourably with selenoxides to facilitate their reduction by thiols, but this effect is not as profound as that of an intramolecular Se…N interaction.

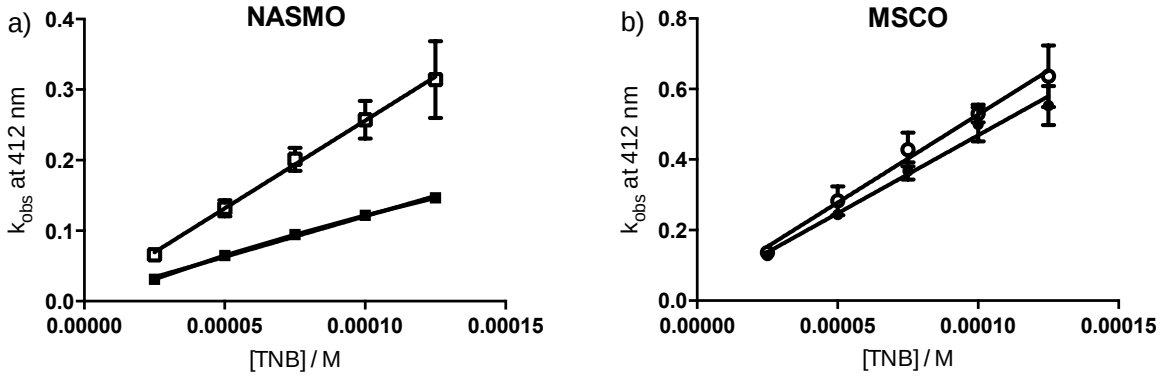

Figure 4.15 – Plots of k_{obs} values measured by stopped flow at 412 nm after a) NASMO (5 µM) or b) MSCO (5 µM) was mixed with increasing TNB (25 – 125 µM) with (open symbol) or without (closed symbol) Gly (10 mM) in buffer

a) NASMO (5 µM) or b) MSCO (5 µM) was mixed with increasing concentrations of TNB (25 - 125 µM) by stopped flow apparatus in phosphate buffer (pH 7.4, 0.1 M) with (closed symbol) or without (open symbol) Gly (10 mM) at 22 °C and the absorbance at 412 nm was monitored over time. The observed rate constant, k_{obs}, for each condition was determined from the absorbance vs time plots using single exponential fitting in ProData Viewer software (Applied Photophysics). k_{obs} was plotted against initial TNB concentration for a) NASMO or b) MSCO and the second order rate constants determined from the gradient of these plots. Data represent mean ± SD of three independent experiments.

Table 4.2 – Comparison of second order rate constants determined for the reaction of NASMO and MSCO in the presence or absence of Gly (10 mM)

Selenoxide	k_1 / $M^{-1} s^{-1}$	k_1 in presence of 10 mM Gly / $M^{-1} s^{-1}$
MSCO	(4.4 ± 0.3) x 10^3	(5.0 ± 0.3) x 10^3
NASMO	(1.2 ± 0.04) x 10^3	(2.5 ± 0.2) x 10^3

4.3.4 Reduction of selenoxides by GSH

In the previous section, TNB was used as a reductant to simplify the kinetics of selenoxide reduction compared to that for GSH. However, TNB is an aromatic thiol that may not be a representative model for reduction of selenoxides by biologically relevant thiols. Thus, the reduction of selenoxides by the endogenous thiol GSH was examined using stopped flow.

SeMetO, SeTalO, NASMO, MSCO or SePropO (125 μM) and GSH (0.5 – 2.5 mM) were mixed in the stopped flow apparatus and absorbance monitored between 200 – 310 nm in 10 nm steps. Upon mixing, increases in absorbance were observed across the spectrum with a maximum increase at around 280 nm (Figure 4.13a). This is likely to correspond to the formation of GSSG, as disulfide bonds are known to exhibit absorbance maxima in the region of 250-300 nm, depending on structure [576, 577].

SeTalO, MSCO, NASMO and SePropO demonstrated pseudo first-order kinetics upon reaction with GSH. This is demonstrated by the linear first-order plots of the absorbance vs time data at 270 nm (Figure 4.16c). The data observed at 270 nm shows a single exponential increase, however due to the small absorbance changes and fluctuations in light source, the data are not completely smooth. As the kinetics demonstrated pseudo first-order kinetics the same mechanism as exhibited for reduction by TNB was used for rate constant determination in ProKIV. The spectra of the reactants were measured at known concentrations and fixed for the analysis procedure in order to simplify the global analysis by decreasing the number of unknown fitting parameters. The second-order rate constants that were determined from these fits and reported in Table 4.3, and were confirmed by pseudo first-order analysis at 270 nm.

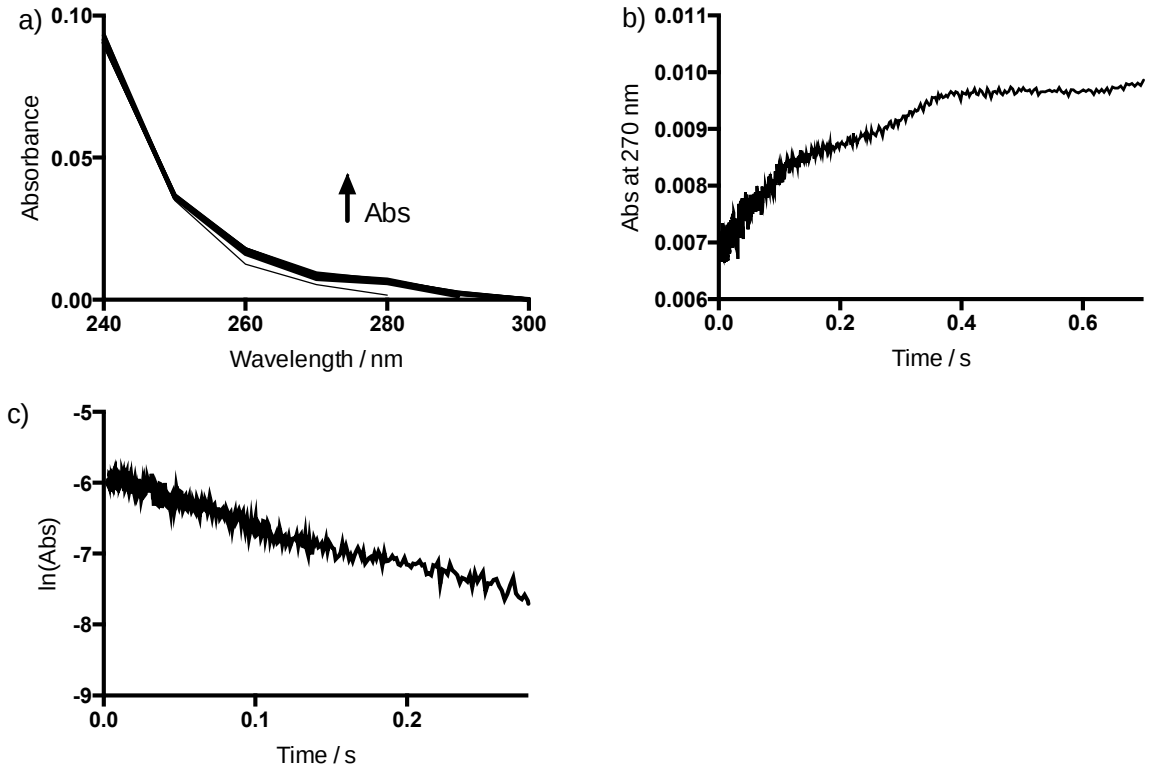

Figure 4.16 – Spectral kinetics, absorbance change at 270 nm and first-order plot for the reaction between SeTalO and GSH

SeTalO (125 μM) was mixed with GSH (0.5 mM) in phosphate buffer (pH 7.4, 0.1 M) at 22 °C by stopped flow apparatus. a) shows the absorbance changes over 0.75 s monitored at wavelengths between 240 - 300 nm at 10 nm steps. b) shows the absorbance change at 270 nm over time after mixing. The absorbance data from b) were analysed for first-order behaviour by plotting as ln(Abs) vs time. As the ln(Abs) vs time is linear, the reaction follows a first-order mechanism.

Table 4.3 - Second order rate constant determined for the reduction of selenoxides with GSH

Selenoxide	**k_1 / $M^{-1} s^{-1}$**
SeTalO	(3.4 ± 0.3) x 10^3
MSCO	(2.5 ± 0.4) x 10^4
NASMO	(1.3 ± 0.2) x 10^3
SePropO	(4.6 ± 0.6) x 10^2

SeMetO showed more complex reaction kinetics with GSH than the other selenoxides. The data obtained for TNB suggest that the mechanism is likely to be occurring via a two-step reduction. The kinetic data for SeMetO reduction by GSH shows two phases, as demonstrated by the change in absorbance over time data at 240 nm (Figure 4.17). The data show an initial fast decrease in absorbance followed by a slower increase in absorbance. This suggests that the initial reaction of the selenoxide, k_1, and the subsequent reaction of the selenosulfide intermediate, k_2, occur on timescales that allow for both to be observed. Thus, it is proposed that the same mechanism is occurring for the TNB reduction, but in the case of SeMetO reduction by GSH, the first step, k_1, is occurring significantly faster than the second step, k_2, and therefore the two phases are observed.

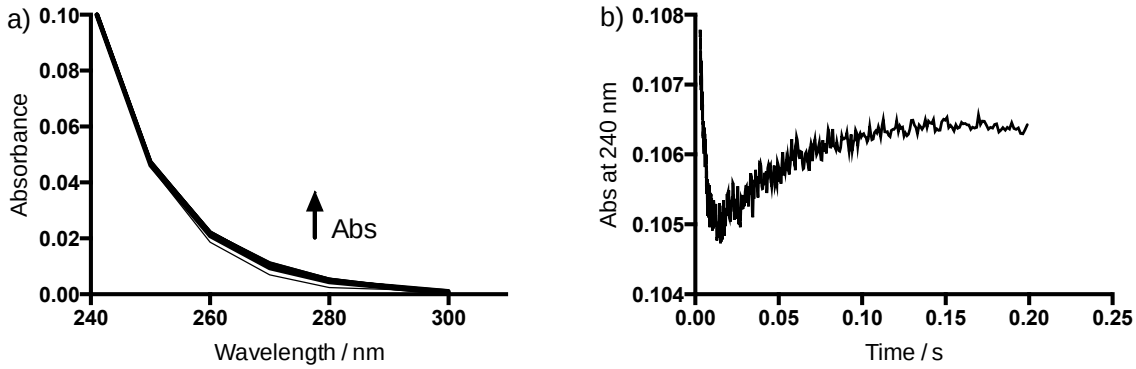

Figure 4.17 - Spectral kinetics and absorbance at 240 nm for the reaction between SeMetO and GSH.

SeMetO (125 µM) was mixed with GSH (0.5 mM) in phosphate buffer (pH 7.4, 0.1 M) at 22 °C by stopped flow apparatus and a) shows the absorbance changes over 0.2 s monitored at wavelengths between 240 – 300 nm at 10 nm steps. b) shows the change in absorbance at 240 nm after mixing SeMetO and GSH. In this plot, two-phase kinetics are observed with an initial rapid drop in absorbance, followed by an increase in absorbance.

Based on these assumptions, a kinetic model based on the mechanism in Figure 4.8 was used for global wavelength analysis. Initial analysis using this model was unable to converge to the data due to too many unknown parameters. In order to assist with the fitting, pseudo first-order analysis of the fast initial decrease, k_1, was performed at 240 nm. This gave a second-order rate constant of 1.2×10^5 $M^{-1} s^{-1}$ (Figure 4.18). The value of k_1 was then fixed in the global analysis fitting using the above model. This resulted in good convergence of the model, and led to the determination of second-order rate

constant for the reaction of the selenosulfide intermediate with GSH, k_2, as 1.5 x 10^4 M^{-1} s^{-1}.

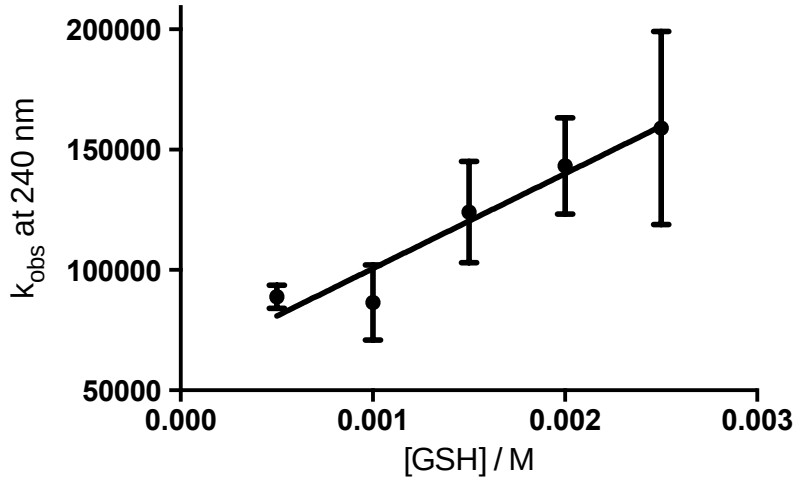

Figure 4.18 - Plots of k_{obs} values for initial absorbance decrease measured by stopped flow at 240 nm SeMetO (125 µM) was mixed with increasing GSH (0.5 – 2.5 mM)

SeMetO (125 µM) was mixed with increasing concentrations of GSH (0.5 – 2.5 mM) by stopped flow apparatus in phosphate buffer (pH 7.4, 0.1 M) at 22 °C and the absorbance at 240 nm was monitored over time. The observed rate constant for the initial decrease in absorbance, k_{obs}, for each condition was determined from the absorbance vs time plots using single exponential fitting in ProData Viewer software (Applied Photophysics). k_{obs} was plotted against initial GSH concentration and the second order rate constants determined from the gradient of this plot. Data represent mean ± SD of three independent experiments.

4.3.5 Reduction of selenoxides by DTT

Reduction of selenoxides by dithiothreitol (DTT) was investigated as it was thought that the presence of a second thiol group could increase the rate of the second step k_2, particularly for SeMetO reduction through intramolecular interactions. It was anticipated that the initial step, k_1, would then become the rate limiting step, thereby resulting in only one phase being detected in the absorbance changes, and hence simplifing the determination of k_1.

SeMetO, SeTalO, NASMO, MSCO or SePropO (125 µM) and DTT (0.5 – 2.5 mM) were mixed in the stopped flow apparatus and the absorbance was monitored between 200 – 310 nm in 10 nm steps. Upon mixing, increases in absorbance were observed with a maximum around 280 nm (Figure 4.15a). This likely corresponds to disulfide formation as these show maxima in this region due to the S-S bond [577]. Decreases in

absorbance were observed at wavelengths < 240 nm, which is potentially due to loss of the selenoxide.

The change in absorbance at 270 nm was plotted in both first- and second-order plots in order to determine the appropriate reaction mechanism. First-order plots for SeTalO, NASMO and SePropO were linear (Figure 4.19), whereas the data for SeMetO and MSCO did not fit to either first- or second-order kinetic analysis (Figure 4.20).

As the first-order plots for SeTalO, NASMO and SePropO were linear, the mechanism was determined to be a pseudo-first order kinetic mechanism. Global wavelength analysis of the data was performed in ProKIV with a a model reflecting the proposed mechanism in Figure 4.8. This mechanism is identical to that for the TNB reduction of selenoxides where only a rate limiting initial reaction, k_1, with one thiol is observed. The spectra of the reactants were measured at known concentrations and fixed for the analysis procedure in order to simplify the global analysis by decreasing the number of unknown fitting parameters. Second order rate constants were confirmed by pseudo-first order analysis of absorbance vs time data at 270 nm. Again, while the single exponential increase is observed at 270 nm (Figure 4.19b), the data are not smooth due to small absorbance changes and fluctuations in the light source.

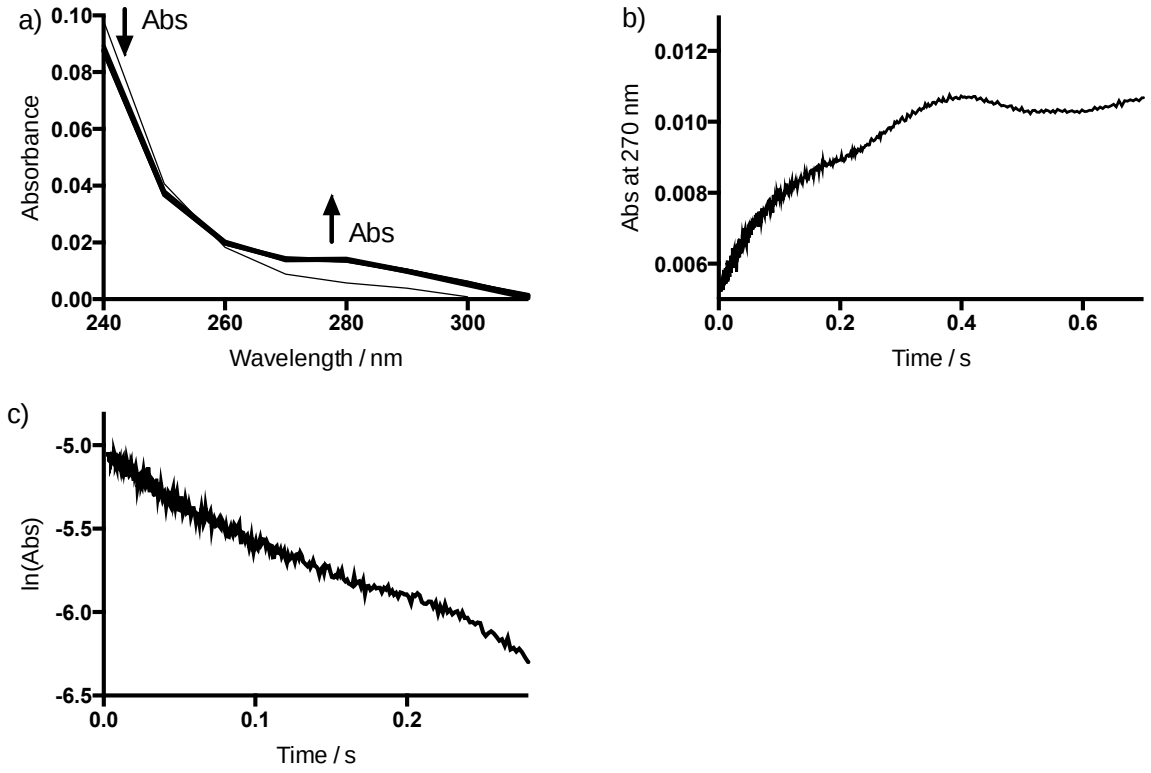

Figure 4.19 – Spectral kinetics, absorbance change at 270 nm and first-order plot for the reaction between SeTalO and DTT

SeTalO (125 μM) was mixed with DTT (0.5 mM) in phosphate buffer (pH 7.4, 0.1 M) at 22 °C by stopped flow apparatus. a) shows the absorbance changes over time monitored at wavelengths between 240 – 300 nm at 10 nm steps. b) shows absorbance change at 270 nm over time after mixing. The absorbance data from b) were analysed for first-order behaviour by plotting as ln(Abs) vs time; as the ln(Abs) vs time is linear, the reaction follows a first-order mechanism.

Table 4.4 – Second order rate constants determined for the reduction of selected selenoxides with DTT

Selenoxide	**k_2 / $M^{-1} s^{-1}$**
SeTalO	(3.0 ± 0.3) x 10^3
NASMO	(2.3 ± 0.3) x 10^4
SePropO	(7.3 ± 1) x 10^2

The absorbance data obtained at 270 nm when SeMetO or MSCO was mixed with DTT were analysed by both first-order (ln(Abs) vs time) or second-order (1/Abs vs time) analysis plots (Figure 4.20c and d respectively), in an attempt to determine the reaction mechanism. However, as neither of these plots were linear, it was concluded that the reduction of SeMetO and MSCO by DTT does not follow either first- or second-order mechanisms.

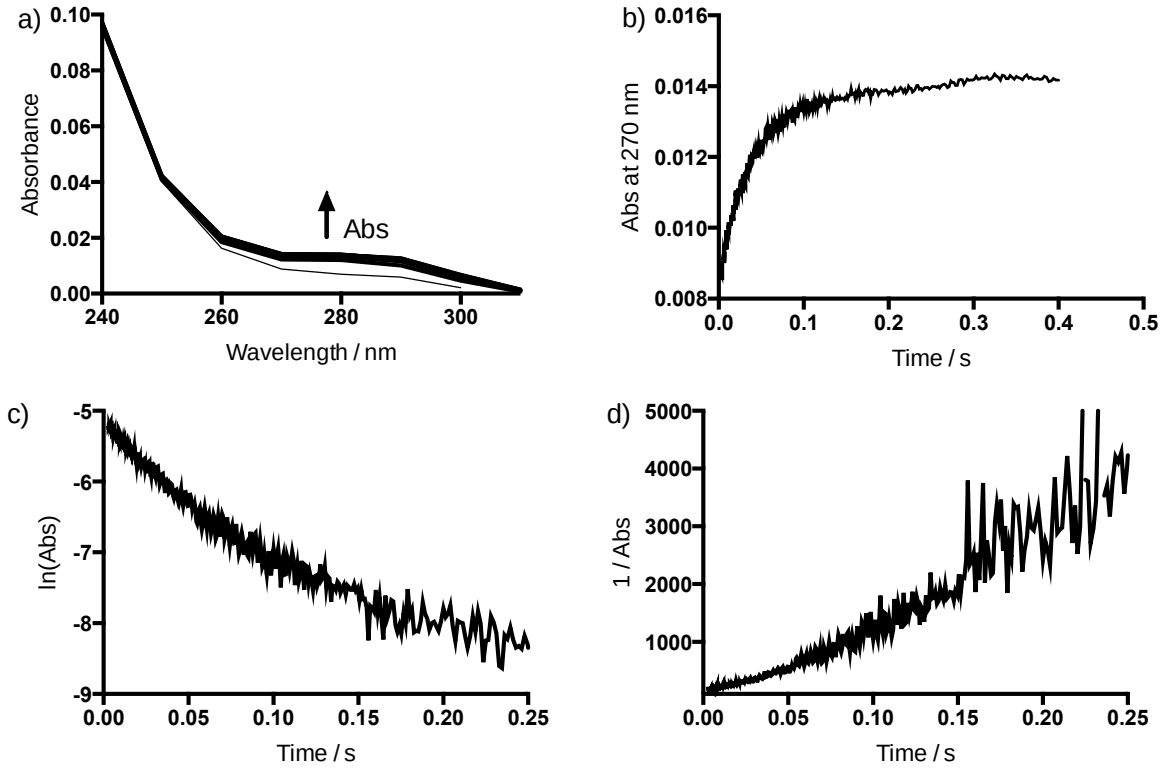

Figure 4.20 - Spectral kinetics, absorbance change at 270 nm and kinetic analysis for the reaction between SeMetO and DTT

SeMetO (125 µM) was mixed with DTT (0.5 mM) in phosphate buffer (pH 7.4, 0.1 M) at 22 °C by stopped flow apparatus and a) shows the absorbance changes over 0.5 s monitored at wavelengths between 240 – 300 nm at 10 nm steps. b) shows absorbance changes measured at 270 nm over time after mixing. The absorbance data from b) were analysed for first-order behaviour by plotting c) ln(Abs) vs time., or second order behaviour by plotting d) 1 / Abs vs time. As neither of these plots are linear, the reaction does not appear to follow either first- or second-order mechanisms.

A number of potential models for the reaction were considered, but none of these yielded satisfactory fits to the data in ProKIV. Models attempted included;

- Se=O + RSH ➔ Intermediate
- Se=O + RSH ➔ Intermediate + RSH ➔ Se + RSSR
- Se=O + RSH ➔ Intermediate ➔ Se + RSSR
- Se=O + RSH ➔ Intermediate A ➔ Intermediate B

The observed complex kinetics are proposed to be due to the initial formation of a seleno-sulfide intermediate as proposed in Figure 4.8 for TNB that can then react via a number of different pathways. Once formed, the intermediate can then react with another DTT thiol, either intramolecularly or extramolecularly. Alternatively, two of the selenosulfide intermediates may react with one another, either at the selenosulfide bond, or at the free thiol on DTT. As the kinetic data were complex, definitive rate constants could not be determined from these data. However, the data suggest that the reduction occurs with a rate constant that is in the same order of magnitude as TNB reduction of selenoxide, due to the similar time frames of the absorbance changes.

4.4 Discussion

The data in this Chapter demonstrate that selenoxides are capable of reacting with thiols, producing disulfides and reforming the parent selenoether compound. The mechanism of these reactions were examined and have been proposed to occur via a selenosulfide intermediate. The rate constants for these reactions have also been defined in this Chapter and are summarised in Table 4.5.

Table 4.5 – Second-order rate constants determined for the reaction between selenoxides and various model low molecular mass thiol compounds

	Second order rate constants determined for the reaction between selenoxides and thiols / $M^{-1} s^{-1}$		
	TNB	**DTT**	**GSH**
SeMetO	3.8×10^4	-	k_1 1.2×10^5 k_2 1.5×10^4
SeTalO	4.9×10^3	3.0×10^3	3.4×10^3
MSCO	4.4×10^3	-	2.5×10^4
NASMO	1.2×10^3	2.3×10^4	1.3×10^3
SePropO	1.3×10^3	7.3×10^2	4.6×10^2

GSH was capable of reducing SeMetO as has been previously described [444, 445]. The products of the reaction between GSH and SeMetO were SeMet and GSSG. The stoichiometry observed was a 2 : 1 ratio of thiol consumed to selenoxide reduced. The reaction between SeTalO and GSH occurred with the same stoichiometry, with 1 mol SeTalO consumed and 1 mole of SeTal recovered for every 2 moles of GSH added. It is reasonable to assume that the reaction would occur via the same mechanism as the reduction of SeMetO, resulting in the formation of GSSG as a product. However, this was unable to be measured due to limitations with the HPLC method employed to separate SeTal and SeTalO. This could be measured with further development of HPLC methods, or using a fluorescent labelling approach to label GSSG, which was though it was considered beyond the scope of this project.

The stopped flow data show that TNB and DTT are also capable of reacting with selenoxides. A decrease in the TNB concentration and concomitant increase in the DTNB concentration was observed by optical absorbance at 412 and 324 nm respectively. With DTT, the likely product will be the disulfide based on the absorbance increases observed around 290 nm, which correspond to the region of disulfide absorbance [576, 577]. The

proposed mechanism is a two-step process, where the initial step is the reaction of the selenoxide and a thiol to form a selenosulfide intermediate. This species could then be reduced by reaction with a second thiol, eliminating water and forming the selenoether and disulfide.

The two-phase reduction mechanism was most clearly observed for the reduction of SeMetO with GSH. At 240 nm, an initial rapid decrease in absorbance is observed, which is proposed to be the initial reaction, followed by a slower increase in absorbance, which is proposed to be due to the second step. The data obtained for the other selenoxide reactions with thiols are also consistent with this mechanism, assuming that the second step has a rate constant (k_2) significantly greater than the rate constant for the first step (k_1). Data obtained for the reduction of SeMetO by GSH suggest that the rate constant for the second thiol reaction (k_2) is in the order of 10^4 M^{-1} s^{-1}. If this rate constant holds for the other selenoxide species and with TNB as the thiol, this value is an order of magnitude greater than that measured for the first thiol reaction. This would give rise to kinetic traces that appear first order, as described in Section 4.3.3.1.

A selenosulfide species has been proposed as the intermediate formed after the reaction with the first thiol. However, studies to characterise this product were not performed, though thermodynamic modelling may provide further evidence to support this as a viable mechanism. A similar selenosulfide has been proposed as an intermediate formed when MsrB reduces MetSO [354, 446, 578]. In the case of the MsrB reaction, the selenol of the active site SeCys attacks the sulfur residue of MetSO, forming a Se-S-OH structure. The resolving Cys residue then reacts with the Se, forming an Se-S bond on MsrB, and Met and H_2O act as leaving groups [354, 446, 578]. This mechanism is similar to the one proposed in this Chapter.

Selenosulfide species are known to react with thiols to produce disulfides and selenol species as products [579]. It is this disulfide exchange mechanism that gives enzymes like TrxR its reducing capability [446]. Previously, the rate constants between low molecular mass thiol and selenosulfide species (DTT and hemi-selenocystine) have been extrapolated from experimental data based on thermodynamic calculations and determined to be ~ 10 M^{-1} s^{-1} [579]. Similar selenosulfide reactions take place during the enzymatic cycles of the Msr family (described above) and TrxR, where disulfide or

selenosulfide exchange reactions occur in order to reduce the oxidised substrates [379, 446, 580, 581]. Analysis of the reaction of the Sec catalytic domain of TrxR with active thioredoxin gives rate constants of up to 10^7 -10^8 M^{-1} min^{-1} [379, 581]. The higher rate constant observed with the enzymatic system likely reflects the positive influence of the surrounding protein structure.

In the current studies, the rate constants determined for further reaction of the selenosulfide intermediate are ~ 10^4 M^{-1} s^{-1}, based on the rate determined for the second step of SeMetO reaction with GSH. This is significantly greater than that calculated for the hemi-selenocysteine and DTT reaction [579], however in this latter case, the selenosulfide intermediate is proposed to still be bound to the –OH group. The presence of the electronegative oxygen atom bound to the Se centre may contribute to the electrophilicity of the Se atom by withdrawing electrons. This would lead to a more rapid nucleophilic reaction of the second thiol.

SeMetO consistently had the highest rate constant for reaction with thiols out of the selenoxides tested, and was about an order of magnitude greater than the other selenoxides examined. This is attributed to a non-bonding interaction between the selenoxide moiety and the free amine, which is present on SeMetO, but not in the other structures excluding MeSeCys. However, as MeSeCys has one carbon less in the side-chain, steric considerations would mean that the amine group is unable to interact strongly with the selenoxide moiety.

In Chapter 3, it was demonstrated that oxidation of SeMet in particular may give rise to other products, with a major secondary product being dehydroselenomethionine (Section 3.3.3). In this Chapter, the ability for thiols to reduce selenoxides was investigated to establish the potential for a catalytic scavenging cycle. If the products of the initial oxidation of SeMet is not SeMetO, there is potential for the proposed cycle to be disrupted. However, if the other products are also capable of being reduced by thiols, the catalytic cycle may still have potential. In the case of dehydroselenomethione, it is likely that a reduction by GSH will occur, as dehydromethionine is reduced by GSH to give methionine [117], and ebselen, a selenocompound containing a Se-N bond like dehydroselenomethionine, also reacts with GSH [454].

As amine interactions appear to have a positive effect on the selenoxide reduction rate constant, experiments were undertaken with Gly supplemented phosphate buffer

(10 mM). An increase in reduction rate was observed with NASMO, though no increase in rate was observed for MSCO. As MSCO already contains an amine group, it is proposed that the increase in extramolecular amine concentration had minimal effect on the rate constant. The increased NASMO reduction rates suggest that amine groups are indeed playing a role in the selenoxide reduction. However, the addition of Gly to the buffer did not increase the rate constant for NASMO reduction to that observed for SeMetO. This is likely due to the fact that interaction with the intramolecular amine group is more favourable for entropic reasons in SeMetO, compared to the extramolecular amine of Gly for NASMO.

Interaction of the amine group with the Se atom of SeMet has been shown to facilitate the one-electron reduction of SeMetO [473]. A three-electron bond between the Se and N atoms forms upon reaction with a hydrated electron, based on transient absorbance changes, and the rate constant determined for this reaction is 1.2×10^{10} M^{-1} s^{-1} [473]. In contrast, the reduction of the sulfur analogue MetSO by the hydrated electron occurs with a significantly lower rate constant of $k = 2 \times 10^{8}$ M^{-1} s^{-1} [582]. It is proposed that the Se-N three-electron bond stabilises the intermediate, allowing for reduction to SeMet, and this stabilisation does not occur with MetSO [473]. Similarly, the same intermediate is proposed to facilitate the one-electron oxidation of SeMet to SeMetO, with stabilisation of the intermediate increasing the rate of one-electron oxidation compared to Met [457, 470, 471].

The rate constants determined for the reduction of selenoxides by GSH are comparable to, or greater than, the rate constants determined in Chapter 3 for the oxidation of SeMet and SeTal by a variety of *N*-chloramines to form the selenoxides. The rapid reduction observed for selenoxides suggests that GSH will be capable of reducing selenoxides *in vivo*, potentially giving rise to a catalytic scavenging cycle of *N*-chloramines. The rate constants suggest that a build-up of selenoxide would not occur, given sufficient thiol concentration, thereby providing rapid turnover of the selenoethers and allowing selenium compounds to further react with oxidants.

The main products of these proposed catalytic reactions appear to be the disulfides, particularly GSSG. Numerous enzymes in the body are capable of reducing disulfides, thus providing a regeneration of the reducing equivalents to keep the catalytic cycle active. Furthermore, many of these enzymes contain either a thiol or selenol at the active

site. The rapid reaction of selenoxides with thiols, and production of disulfide products like GSSG, may lead to the potential of endogenous antioxidant defence systems to interact with selenium compounds in order to reduce oxidative damage. This hypothesis is explored further in Chapter 5.

4.5 Conclusions

SeMetO and SeTalO are readily reduced by GSH and other thiol compounds to reform SeMet and SeTal and disulfide species. The reduction is proposed to happen in a two-step mechanism, via a selenosulfide intermediate. The rate constants for these reactions have been defined and are summarised in Table 4.5. The facile reduction of SeMetO and SeTalO by GSH highlights the potential for a catalytic oxidant scavenging cycle *in vivo*, that may provide therapeutic benefit in inflammatory conditions.

5 Reduction of selenoxides and N-chloramines by redox enzymes

5.1 Introduction

Exposure to MPO-derived oxidants can lead to conformational and functional changes of proteins within the cellular environment [106]. In order to combat oxidative stress the cell uses a variety of redox systems that either detoxify oxidant species, such as GPx [583], or reduce oxidation products, such as TrxR, Trx [357] and Msrs [584].

TrxR is a selenoprotein whose primary function is to reduce protein disulfide bonds, like those formed on oxidised Trx [585]. It achieves this via the formation of intermolecular selenosulfide bonds, which are then reduced by a resolving Cys residue, forming an intramolecular Se-S bond [372]. TrxR uses NADPH as an electron donor to reduce the Se-S formed on oxidised TrxR [372, 585]. TrxR has also demonstrated ability to reduce MPO-derived oxidants, particularly HOSCN (Figure 5.1) [348].

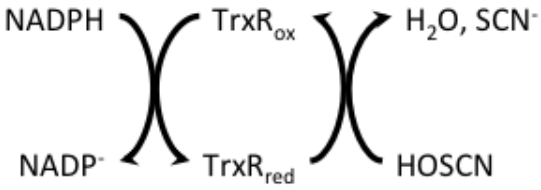

Figure 5.1 – TrxR uses NADPH as a reducing equivalent to detoxify oxidants such as HOSCN

Trx is one of the primary disulfide reductase enzymes present in cells. It reduces disulfides formed on proteins through disulfide exchange processes, forming an intermolecular disulfide bond on Trx [357]. This disulfide can then be reduced by TrxR, regenerating Trx [357]. While TrxR is the primary reductant for Trx, GSH can also perform this role when TrxR is inhibited or down-regulated [586]. Trx participates in antioxidant defence through multiple roles, including reduction of the Prxs, which are redox proteins responsible for detoxification of peroxide species (Figure 5.2) [102].

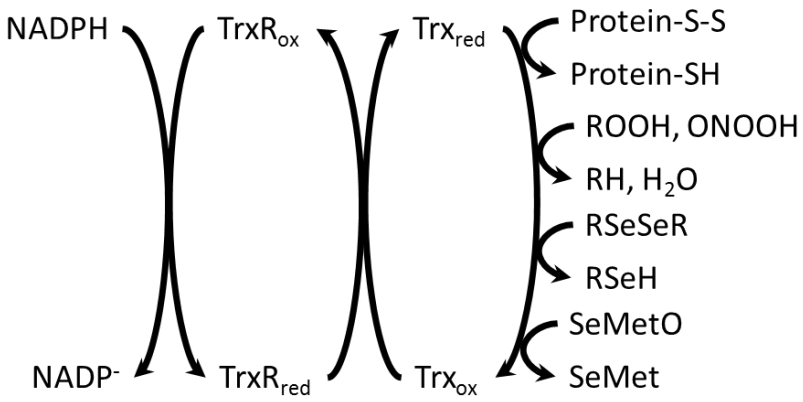

Figure 5.2 – Trx is capable of reducing a wide variety of substrates such as protein disulfides, peroxides, diselenides and SeMetO. Oxidised Trx is then subsequently oxidised by TrxR using NADPH.

The Trx system has been shown to interact with numerous selenium compounds. It is capable of reducing selenite [587], as well as organic selenium species, such as diselenides, selenodiglutathione [588] and selenocystine [492]. The interaction of the Trx system and selenocysteine or ebselen enhances the removal of peroxides [379, 589, 590] and ONOOH [591]. The Trx system has also been shown to reduce SeMetO to SeMet and catalytically remove protein hydroperoxides [474].

Msrs reduce MetSO residues to Met (Figure 5.3) [109, 592]. Msrs are stereospecific with MsrA reducing S stereoisomers of MetSO, and MsrB reducing the R stereoisomer [593, 594]. MsrA is capable of reducing both free and peptide bound MetSO, though it shows a preference for peptide bound residues [109]. MsrB almost exclusively reduces peptide bound MetSO [109], demonstrating a specificity for unfolded protein residues [413]. The presence of Msrs suggests that Met oxidation may play a protective role maintaining protein function under oxidising conditions *in vivo* [110, 567].

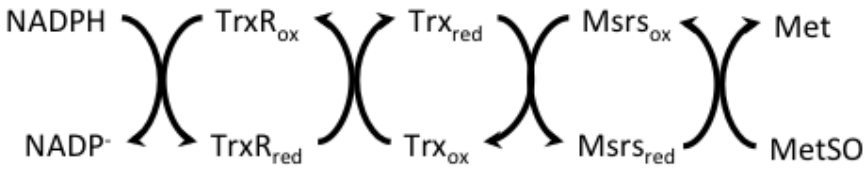

Figure 5.3 – Msrs are capable of reducing MetSO, and are subsequently reduced by the NADPH/TrxR/Trx system

GPx is a selenoprotein that detoxifies H_2O_2 and lipid peroxides (Figure 5.4) [583]. The peroxides oxidise the catalytic Sec residue, forming a seleninic acid (RSeOH) group [370], which is then reduced by 2 equivalents of GSH to reduce the protein and form

GSSG [583]. While GSH is the primary reductant for GPx, the Trx system is also capable of donating electrons to reduce the enzyme [595].

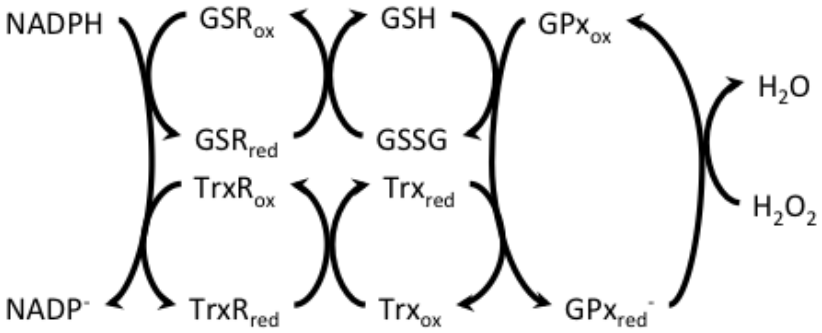

Figure 5.4 – GPx is capable of using either the NADPH/GSR/GSH system or NADPH/TrxR/Trx system to reduce H_2O_2

GSR is a thiol dependent enzyme that is responsible for the reduction of GSSG to GSH (Figure 5.5) [557]. GSH is a key antioxidant in cellular systems and reacts with a variety of oxidants, including *N*-chloramines [192] and selenoxides [444], to form GSSG. GSSG is then recycled back to GSH by the action of GSR [557]. GSR achieves reduction of GSSG by disulfide exchange reactions [427].

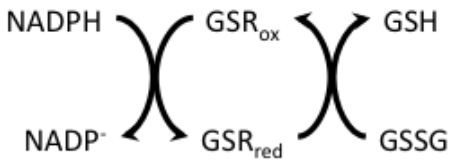

Figure 5.5 – GSR catalyses the reaction between GSSG and NADPH to form GSH

These enzymes use NADPH as a reducing equivalent to reduce their substrates. HOCl and *N*-chloramines can react directly with NADPH, though the reaction of *N*-chloramines is quite slow (~1 M^{-1} s^{-1}) [63, 138, 139]. This reaction forms a chlorohydrin species in a reaction that can not be reversed by the cells enzymatic NADPH recycling enzymes such as GAPDH, and the production of this enzyme is toxic to cells [63, 138, 139].

These enzymatic systems all play a role in the maintenance of redox homeostasis in the cell. The key feature consistent throughout these systems is the presence of a thiol or selenol at the active redox site of the enzyme that takes part in the reaction with oxidants in order to detoxify them. As *N*-chloramines have demonstrated reactivity with thiols [192], it was expected that they should also react with enzymes containing

a Cys active site. HOCl is capable of reacting with selenols, including the Sec active site of GPx, with higher rate constants than analogous thiol compounds [98]. In addition, *N*-chloramines retain the oxidising power of HOCl in relation to thiols, and so *N*-chloramines also have the potential to react with selenols. Furthermore, given that selenoxides also react with thiol groups [444, 445], there may be the potential for these enzymes to reduce selenoxides.

5.2 Aims

Given that many redox enzymes contain either a thiol or selenol at their active site, it was hypothesised that the cellular antioxidant enzymes should be able to react with, and hence reduce, selenoxides and *N*-chloramines. The aim of the studies presented in this Chapter was therefore to determine the ability of redox enzymes to reduce selenoxides and *N*-chloramines.

5.3 Results

5.3.1 Reduction of selenoxides

5.3.1.1 Thioredoxin reductase and thioredoxin

Trx and TrxR are capable of reducing a wide variety of substrates including peroxides [379, 589, 590], disulfides [357] and numerous selenium species [491, 492, 587]. They have previously been shown to reduce SeMetO [474]. Initial experiments aimed to confirm the ability of the Trx system to reduce SeMetO, and assess the ability of this system to reduce SeTalO, as proposed in Figure 5.6.

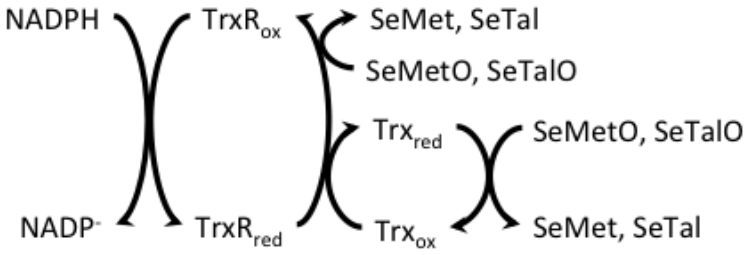

Figure 5.6 – Proposed mechanism for the reduction of SeMetO and SeTalO by NADPH/TrxR/Trx. The selenoxides may be reduced by either the TrxR or Trx in this system.

The ability of TrxR to reduce SeMetO and SeTalO was investigated by both HPLC and the spectrophotometric consumption of NADPH. NADPH (700 μM) and TrxR (25 nM) with or without Trx (1.5 μM) were incubated together for 5 min before addition of SeMetO or SeTalO (200 μM) in phosphate buffer (0.1 M, pH 7.4) at 22 °C. Insulin (200 μM) was also added to the NADPH/TrxR/Trx system as a positive control, as it is a native substrate for Trx. The concentration of NADPH and TrxR were selected based on previously published results [474]. TrxR uses NADPH as a reducing agent, therefore the amount of NADPH consumed should be equal to the amount of substrate reduced. NADPH concentrations were monitored by optical absorbance at 340 nm (Figure 5.8a). The rate of reduction was determined by fitting the initial (25 min) linear section of the [NADPH] vs time graph (Figure 5.8b).

It should be noted that the starting concentration of NADPH in these assays was observed to be about 540 μM, in contrast to the 700 μM NADPH that was added. The reported NADPH concentrations were determined based on the absorbance coefficient at 340 nm (ε = 6300 cm^{-1} M^{-1}). However, based on the UV-vis absorbance spectra obtained for NADPH (50 μM (based on mass)) (Figure 5.7), it is suspected that some impurities were present, as the calculated concentrations of NADPH were 28 and 37 μM based on extinction coefficients at 340 and 260 nm respectively. The increase in apparent concentration using the extinction coefficient at 260 nm is likely to be due to auto-oxidation of NADPH to $NADP^+$, which would also contribute to absorbance at 260 nm. This discrepancy caused an underestimation of the initial starting concentration of NADPH as solutions were prepared assuming the total mass of the sample was NADPH. This may also affect the interpretation of total NADPH consumption, potentially underestimating the concentrations of NADPH consumed, therefore introducing greater error that should be considered when calculating the stoichiometry between NADPH and substrate.

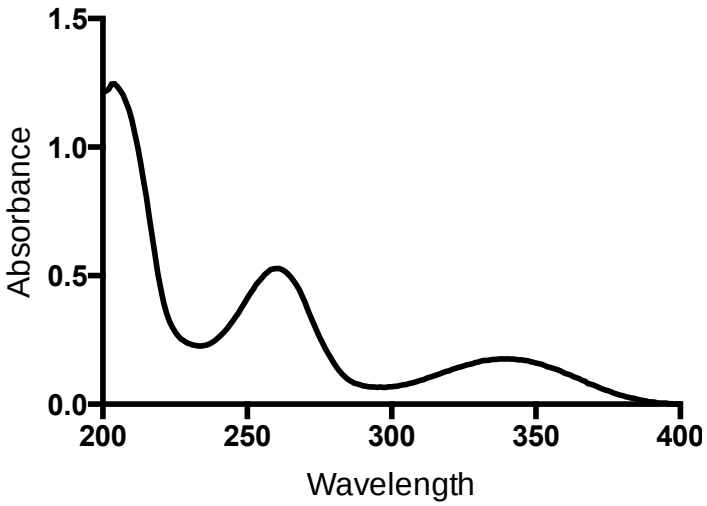

Figure 5.7 – UV-vis spectrum of NADPH

NADPH (50 μM (based on mass)) was prepared in phosphate buffer (0.1 M, pH 7.4) and the UV-vis spectrum between 200 and 400 nm at 22 °C was measured. Absorbance values at 340 nm and 260 nm were 0.177 and 0.528 absorbance units respectively.

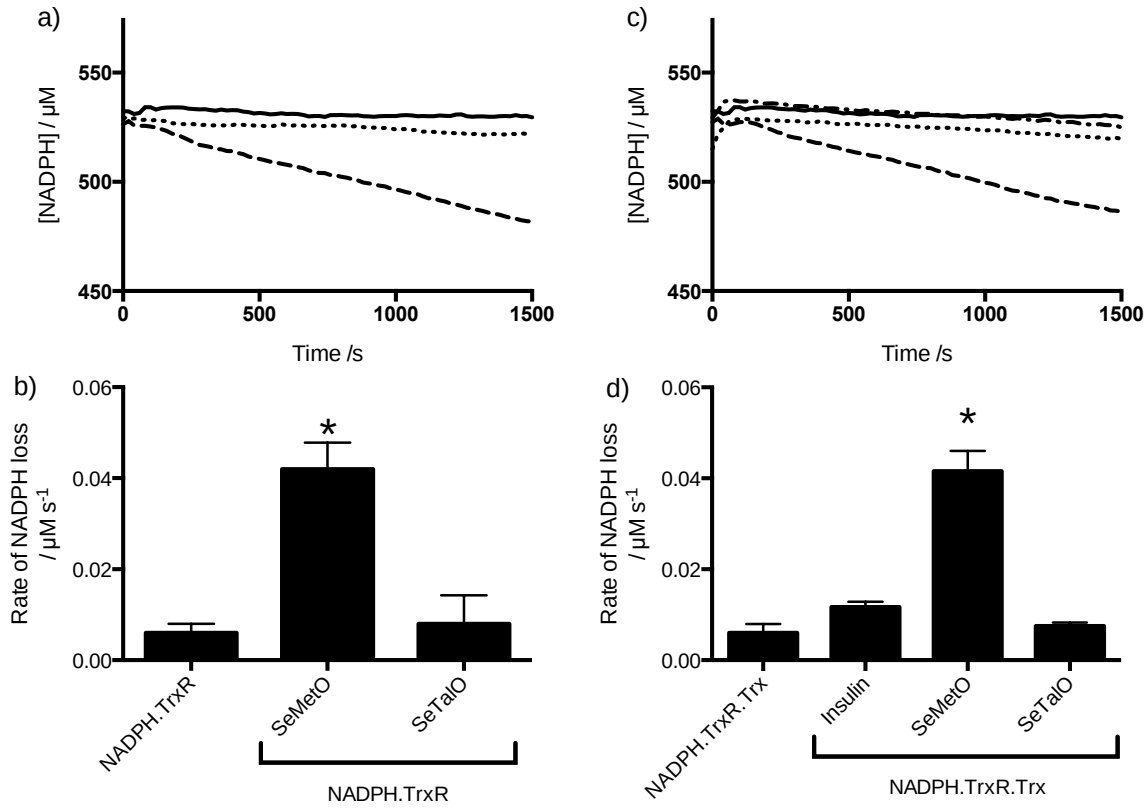

Figure 5.8 – Change in NADPH concentration over 25 min after SeMetO and SeTalO were added to NADPH, TrxR and Trx.

*SeMetO, SeTalO or insulin (200 µM) was added to NADPH (700 µM) and TrxR (25 nM) in the c,d) presence or a,b) absence of Trx (1.5 µM) and the absorbance monitored for 45 min at 340 nm. a, b) show typical [NADPH] vs time plots obtained for the control (solid) or when 200 µM SeMetO (dashed), SeTalO (dotted) and insulin (dot-dashed) were added to a) NADPH/TrxR and c) NADPH/TrxR/Trx. SeMetO increased the rate at which NADPH is consumed compared to the control (NADPH/TrxR) though SeTalO does not. b, d) The rate of NADPH consumption was determined by fitting a straight line to the data represented in a, c). Data in a,c) are representative of 3 independent experiments. Data in b,d) represent mean ± SD from 3 independent experiments. * indicates significant difference ($p < 0.05$) from control based on one-way ANOVA with Tukey's post-hoc test.*

A small time dependent decrease of 6 ± 2 nM s^{-1} in the control sample (700 µM + 25 nM TrxR) was observed and was attributed to the slow auto-oxidation of NADPH. Addition of SeTalO did not produce any further significant increase in the rate of NADPH consumption over the control, with an observed NADPH loss rate of 8 ± 6 nM s^{-1}, suggesting that TrxR is unable to reduce SeTalO. SeMetO increased the rate at which NADPH was consumed to 42 ± 6 nM s^{-1}, which is consistent with a previous report on TrxR reducing SeMetO [474]. Total NADPH consumption reflected the differences in the rate of NADPH consumed by each sample, with SeMetO demonstrating a significant

increase in total NADPH consumed compared to control samples, whereas no significant difference was observed for SeTalO (Figure 5.9).

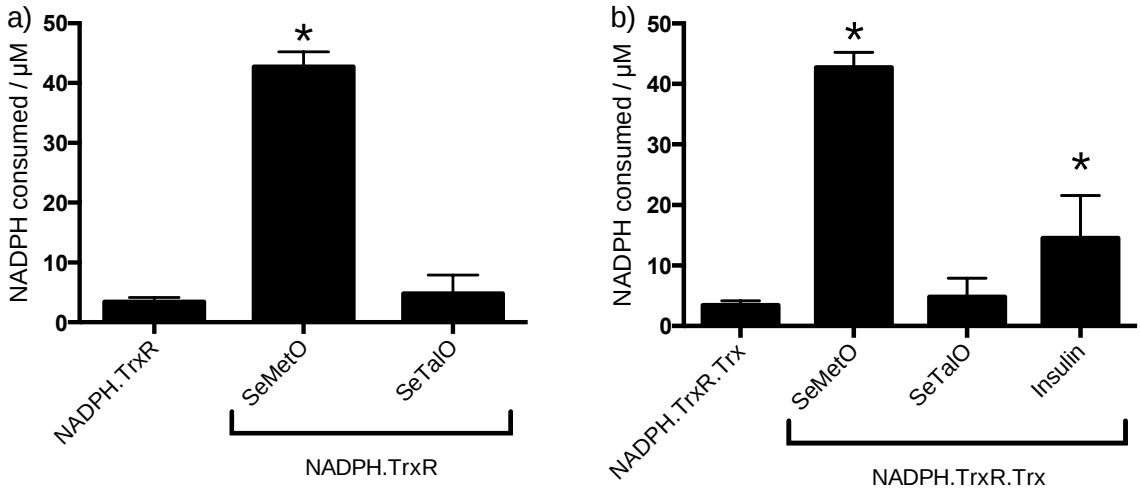

Figure 5.9 – Total NADPH consumed after SeMetO, SeTalO or insulin was added to NADPH and a) TrxR with or without b) Trx

*SeMetO (200 µM), SeTalO (200 µM) or insulin (200 µM) was added to NADPH (700 µM) (control bars) and TrxR (25 nM) and in the b) presence and a) absence Trx (1.5 µM) and the absorbance monitored for 45 min at 340 nm. The difference in NADPH concentration immediately after the addition of SeMetO, SeTalO or insulin and 45 min afterward was determined by absorbance at 340 nm. Addition of SeMetO or insulin caused an increase in NADPH consumption over control, though addition of SeTalO did not. Data represent mean ± SD from 3 independent experiments. * represents a significant difference ($p < 0.05$) from control based on one-way ANOVA with Tukey's post-hoc test..*

The above data indicate that TrxR is capable of reducing SeMetO, and previous studies suggest that the presence of Trx should increase the rate of SeMetO reduction [474]. If Trx is increasing the rate of selenoxide reduction, an increase in rate of NADPH consumption would be expected over that observed for NADPH/TrxR. Similar to the TrxR data, a small time dependent decrease in NADPH was observed in control samples of 6 ± 2 nM s^{-1} (NADPH/TrxR/Trx), and upon addition of SeTalO there was no significant effect on the rate of change of absorbance with a decrease of 8 ± 1 nM s^{-1} observed (Figure 5.8c,d). SeMetO increased the rate of NADPH consumption to 42 ± 4 nM s^{-1}, which is not significantly different to the rate observed with NADPH/TrxR. Again, total NADPH consumption demonstrated the same trend, with SeMetO consuming a significantly greater amount of NADPH than observed in control samples, though SeTalO did not (Figure 5.9b).

As there was no increase in reduction on addition of Trx, insulin was included as a positive control to ensure Trx activity could be observed. An increase in rate of NADPH consumption to 12 ± 1 μM s^{-1} was observed over NADPH/TrxR samples, though this change was not significantly different (Figure 5.8). However, over the course of 45 min, addition of insulin caused a consumption of the NADPH of 14 ± 7 μM compared to the control samples where only of 3 ± 1 μM was consumed (Figure 5.9b).

As NADPH was being consumed by the TrxR and Trx systems after SeMetO addition, HPLC methods were used to determine whether reduction of SeMetO was occurring with a corresponding increase in SeMet (Section 2.3.5.4). Samples were incubated for 2 h before removal of the proteins by centrifugal filtering through 10 kDa molecular mass cut-off filters. The concentrations of selenoxide and parent selenoether were determined by UV-Vis detection of peaks at 220 nm, and the concentrations of SeMet and SeMetO determined by comparison with standard curves generated using authentic materials (Section 2.3.7.1) (Figure 5.10). After 2 h SeMetO (200 μM) had been completely reduced, with a corresponding increase in SeMet concentration. In analogous experiments with SeTalO (200 μM), no change in SeTalO or SeTal concentration was observed after 2 h, consistent with the NADPH data monitored at 340 nm. The levels of SeMet, SeMetO, SeTal and SeTalO were the same whether Trx was present or samples contained TrxR alone, demonstrating that TrxR is capable of reducing SeMetO to SeMet, though is unable to reduce SeTalO. These data suggest that Trx did not contribute any additional reduction potential to the system.

There is a discrepancy between the amount of NADPH consumed by the TrxR and Trx (Figure 5.9) and the concentration of SeMetO reduced (Figure 5.10), though here this is partially explained by the fact that NADPH concentrations were monitored over 45 min, compared to the 2 h when SeMet and SeMetO levels were assessed by HPLC. However, by extrapolating the 45 min data, an underestimation of NADPH consumption compared to the 200 μM expected consumption, based on the amount of SeMetO reduced, still occurs. This is thought to be related to issues that caused an underestimation of the starting concentration of NADPH, discussed earlier in this section.

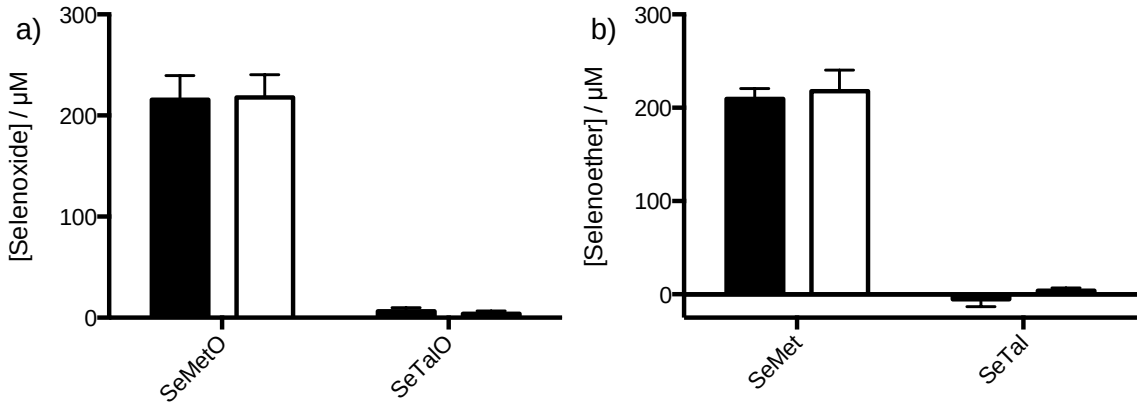

Figure 5.10 – Concentration of selenoxides reduced and selenoether recovered after selenoxides are incubated with NADPH and TrxR with or without Trx.

SeMetO or SeTalO (200 µM) was added to NADPH (700 µM) and TrxR (25 nM) in the presence or absence of Trx (1.5 µM) and incubated for 2 h before analysis by HPLC. a) shows the concentration of selenoxide reduced and b) shows recovery of the respective selenoether. NADPH/TrxR (black) and NADPH/TrxR/Trx (white) were both able to reduce SeMetO (200 µM), with a full recovery of SeMet. No changes were observed for SeTalO. Data represent the mean ± SD from 3 independent experiments.

5.3.1.2 Glutathione peroxidase

GPx, an enzyme with the primary function of removing H_2O_2, contains an active site thiol that may be capable of reducing selenoxides [583]. GPx can use the Trx system, and ultimately NADPH, as a reducing equivalent [595]. The ability of GPx to reduce selenoxides was assessed by UV-vis spectroscopy and HPLC analysis (Figure 5.11).

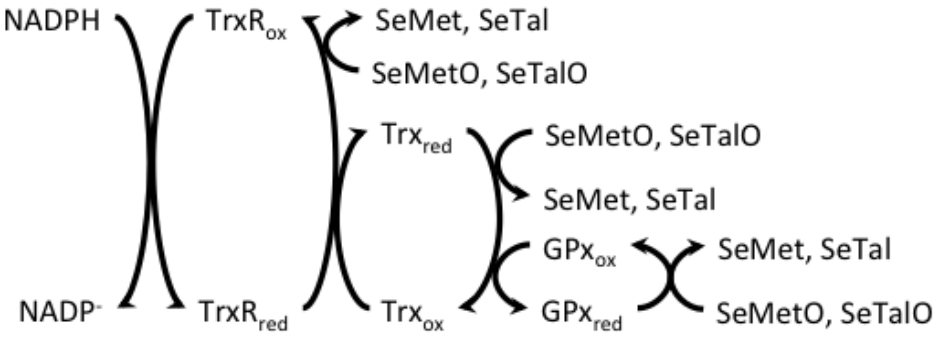

Figure 5.11 – Proposed mechanism for the reduction of SeMetO and SeTalO by NADPH/TrxR/Trx/GPx. The selenoxides may be reduced by the TrxR, Trx or GPx in this system.

The loss of NADPH was monitored after SeMetO, SeTalO or H_2O_2 (200 µM) was added to NADPH (700 µM), TrxR (25 nM), Trx (1.5 µM) and GPx (1.5 µM) (Figure 5.12).

The rate of NADPH loss was determined by fitting the initial (25 min) linear section of the [NADPH] vs time graph (Figure 5.12a). The loss NADPH occurred at 5 ± 0.3 nM s^{-1} in control samples (NADPH + TrxR + Trx + GPx). No change in the rate of NADPH consumption was observed when SeTalO was added to samples with NADPH being consumed at a rate of 3 ± 1 nM s^{-1}. NADPH consumption increased to 32 ± 4 nM s^{-1} upon the addition of SeMetO. This increase was not significantly different to that obtained with NADPH and TrxR alone (Figure 5.8).

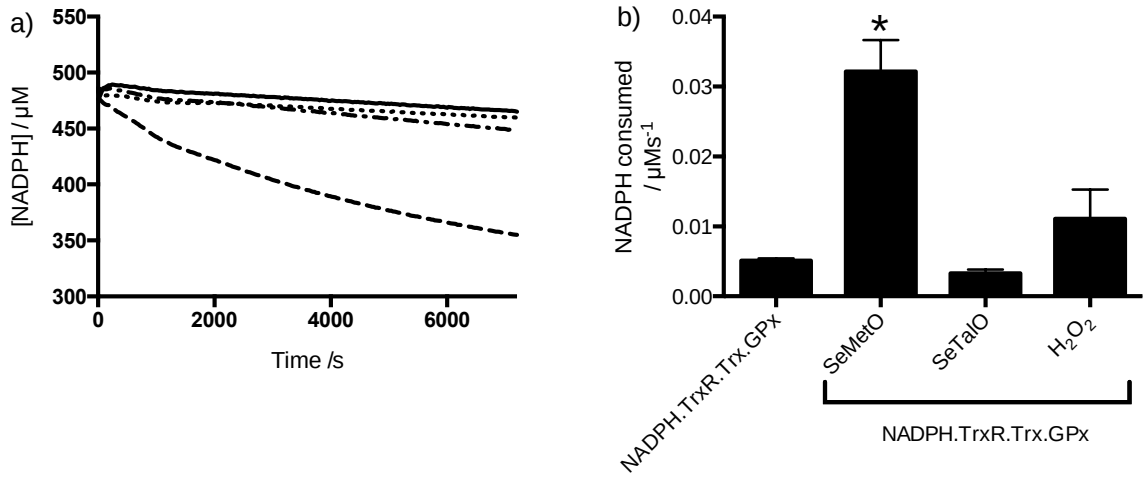

Figure 5.12 – Change in NADPH concentration over time when SeMetO, SeTalO or H_2O_2 were added to the GPx system.

*SeMetO, SeTalO or H_2O_2 (200 µM) was added to NADPH (700 µM) + TrxR (25 nM), Trx (1.5 µM) and GPx (1.5 µM) and the absorbance monitored for 2 h at 340 nm. a) show typical [NADPH] vs time obtained for the control (NADPH/TrxR/Trx/GPx) (solid) or when SeMetO (dashed), SeTalO (dotted) or H_2O_2 (dot-dashed) were added to the NADPH/TrxR/Trx/GPx system. SeMetO increases the rate at which NADPH is consumed compared to the control though SeTalO does not. b) The rate of NADPH consumption was determined by fitting a straight line to the initial 25 min represented in a). Data represent mean ± SD from 3 independent experiments. * indicates significant difference ($p < 0.05$) from control based on one-way ANOVA with Tukey's post-hoc test.*

H_2O_2 is a substrate for GPx and was included as a positive control. An increase to 11 ± 4 nM s^{-1} of NADPH consumption was observed with H_2O_2 addition, though this was not statistically significant compared to NADPH/TrxR/Trx/GPx control samples. However, over the course of 2 h, a significantly higher amount of NADPH was consumed by H_2O_2 samples, with a total of 81 ± 30 µM NADPH consumed, compared to control samples with 37 ± 8 µM NADPH consumed (Figure 5.13). Total NADPH consumption upon addition of SeMetO and SeTalO reflected the trend observed in the

rate of NADPH consumption, with SeMetO consuming a significantly greater amount of NADPH than the NADPH/TrxR/Trx/GPx alone, though SeTalO did not.

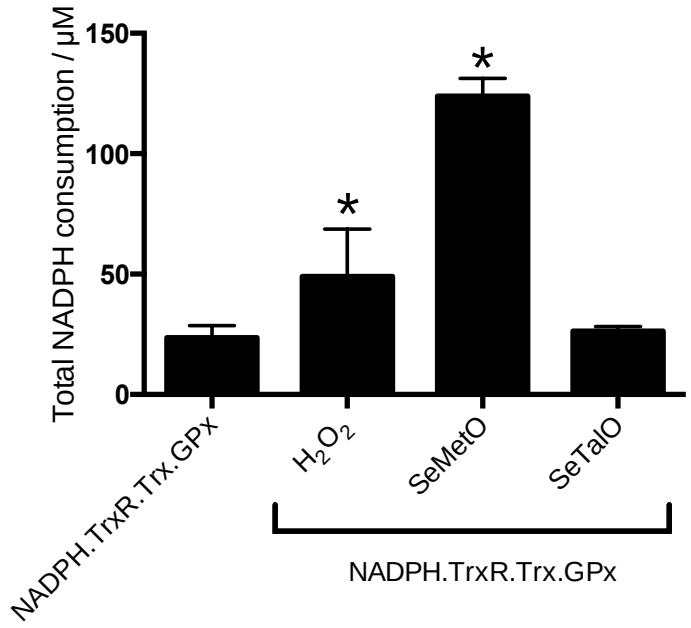

Figure 5.13 - Total NADPH consumed after H_2O_2, SeMetO or SeTalO was added to GPx system

*H_2O_2, SeMetO or SeTalO (200 µM) was added to NADPH (700 µM), TrxR (25 nM), Trx (1.5 µM) and GPx (1.5 µM) and the absorbance monitored for 2 h at 340 nm. The difference in NADPH concentration from addition of H_2O_2 and 2 h post addition was determined by absorbance at 340 nm. H_2O_2 and SeMetO caused an increase in total NADPH consumed over control, whereas SeTalO did not. Data represent mean ± SD from 3 independent experiments. * indicates significant difference ($p < 0.05$) from control based on one-way ANOVA with Dunnett's post-hoc test.*

As NADPH consumption increased with SeMetO addition, this suggested that reduction of SeMetO was occuring. SeMet and SeMetO levels were therefore assessed by HPLC with UV-vis detection at 220 nm to determine whether SeMetO reduction was occuring. Samples were incubated for 2 h before removal of the proteins by filtering through 10 kDa molecular mass cut-off filters and the concentrations of selenoxide and parent selenoether were quantified as described in Section 2.3.5.4. Similar to the Trx system, complete reduction of SeMetO to SeMet was observed after 2 h, but no change was observed for SeTalO (Figure 5.14). There is also a difference between the concentration of NADPH consumed (Figure 5.13) and the amount of SeMetO reduced (Figure 5.14), potentially due to the underestimation of NADPH concentrations based on the extinction co-efficient.

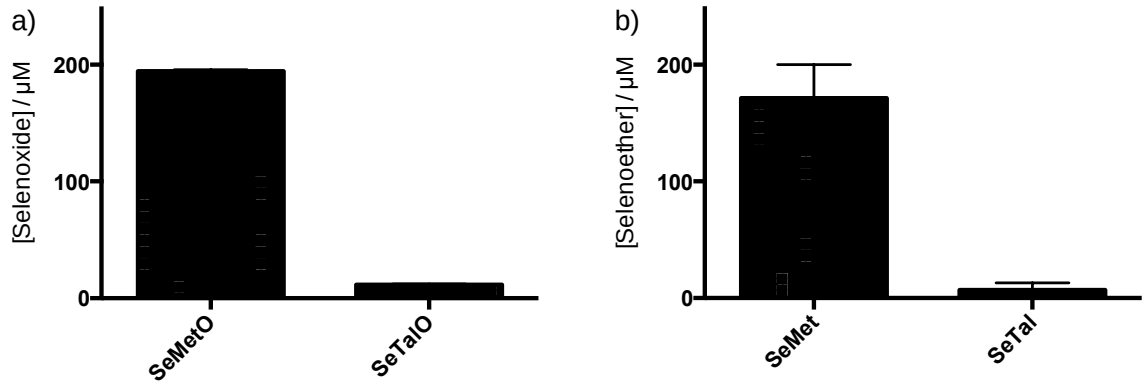

Figure 5.14 – Concentrations of selenoxides and selenoethers following 2 h incubation of SeMetO and SeTalO with the GPx system.

SeMetO or SeTalO (200 µM) was added to NADPH (700 µM), TrxR (25 nM), Trx (1.5 µM) and GPx (1.5 µM) and incubated for 2 h before analysis by HPLC. a) shows concentration of selenoxide reduced and b) shows recovery of the respective selenoether. The GPx system was able to reduce the SeMetO (200 µM), with a full recovery of SeMet. No changes were observed for SeTalO. Data represent mean ± SD from 3 independent experiments. Error bars may not be visible due to small error measured.

In summary, addition of SeMetO to the NADPH/TrxR/Trx/GPx system demonstrated a consumption of NADPH as measured by optical absorbance at 340 nm. This corresponded with a decrease in levels of SeMetO and increase in levels of SeMet 2 hours after SeMetO addition as assessed by HPLC. However, NADPH consumption, or reduction of SeTalO levels were not observed upon addition of SeTalO to the NADPH/TrxR/Trx/GPx system.

5.3.1.3 Methionine sulfoxide reductases

Msrs are enzymes that specifically reduce MetSO residues [109, 592]. As they contain Cys and Sec residues at the active site, there may also be potential for reaction with selenoxides [109, 592]. Furthermore, due to the structural similarity of SeMetO and MetSO, there is potential for Msrs to reduce SeMetO in particular (Figure 5.15).

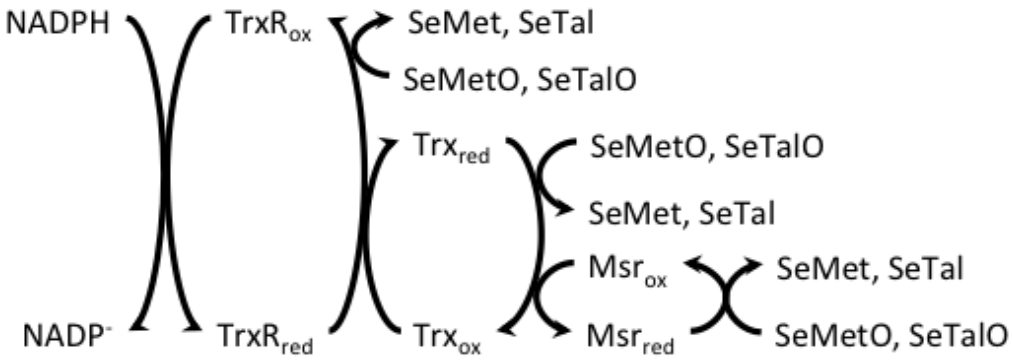

Figure 5.15 – Proposed mechanism for the reduction of SeMetO and SeTalO by NADPH/TrxR/Trx/Msrs. The selenoxides may be reduced by either the TrxR, Trx or Msrs in this system.

The loss of NADPH was monitored after SeMetO, SeTalO or MetSO (200 μM) was added to NADPH (700 μM), TrxR (25 nM), Trx (1.5 μM) and MsrA (95 nM) or MsrB2 (0.25 μM) (Figure 5.16). These concentrations of Msr were chosen as they represent one unit of enzyme activity according to the manufacturer's data sheet. A decrease of 4 ± 1 nM s^{-1} was observed in control samples without addition of selenoxides. Addition of SeMetO (200 μM) increased the rate of NADPH consumption to 51 ± 16 and 51 ± 14 nM s^{-1} for MsrA and MsrB2 respectively. A slight increase in the NADPH consumption rate was observed with MetSO addition to 8 ± 3 nM s^{-1} for MsrA and 10 ± 4 nM s^{-1} for MsrB2, but this was not a significant increase. It is likely that the small observed change with MetSO is because although Msrs are capable of reducing free MetSO, peptide bound MetSO is a more favourable substrate [109]. SeTalO addition did not affect the rate of NADPH consumption with an NADPH consumption rate of 9 ± 5 and 9 ± 8 nM s^{-1} for MsrA and MsrB2 respectively, suggesting no reduction was occurring. As with the other enzyme systems (Figure 5.8 and Figure 5.12), total NADPH consumption reflected the differences in the inital rates of NADPH consumption, with SeMetO causing a significant increase in total NADPH consumed compared to control, where SeTalO does not (Figure 5.17).

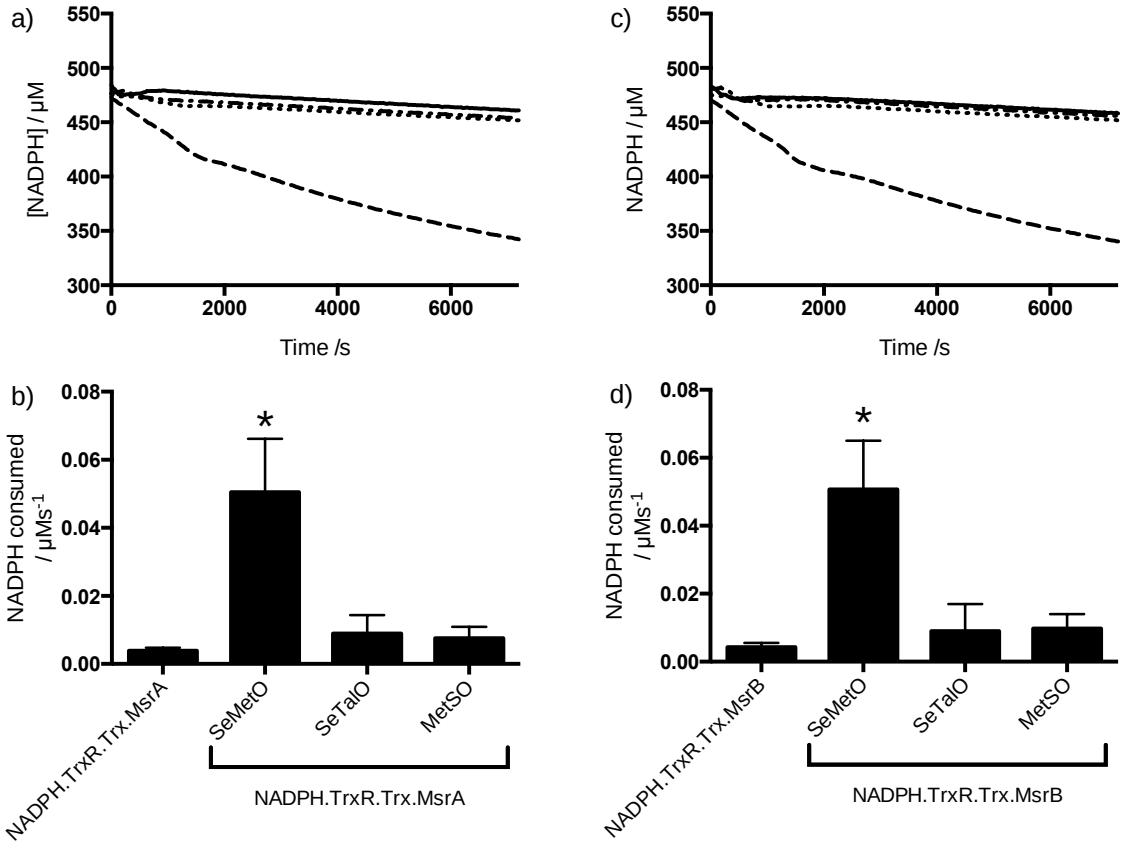

Figure 5.16 – Change in NADPH concentration over time after SeMetO, SeTalO or MetSO were added to Msr systems

*SeMetO, SeTalO or MetSO (200 µM) was added to NADPH (700 µM) + TrxR (25 nM), Trx (1.5 µM) and MsrA (95 nM) or MsrB2 (0.25 µM) and the absorbance monitored for 2 h min at 340 nm. Graphs show typical [NADPH] vs time obtained of the control (solid) or when 200 µM SeMetO (dashed), SeTalO (dotted) and MetSO (dot-dashed) were added to the a) MsrA or c) MsrB2 system. The rate of NADPH consumption was determined by fitting a straight line to the initial 25 min represented in a and c). SeMetO increases the rate at which NADPH is consumed compared to the control though SeTalO does not. b, d) The rate of NADPH consumption was determined by fitting a straight line to the data represented in a, c). Data represent mean ± SD from 3 independent experiments. * indicates significant difference ($p < 0.05$) from control based on one-way ANOVA with Tukey's post-hoc test.*

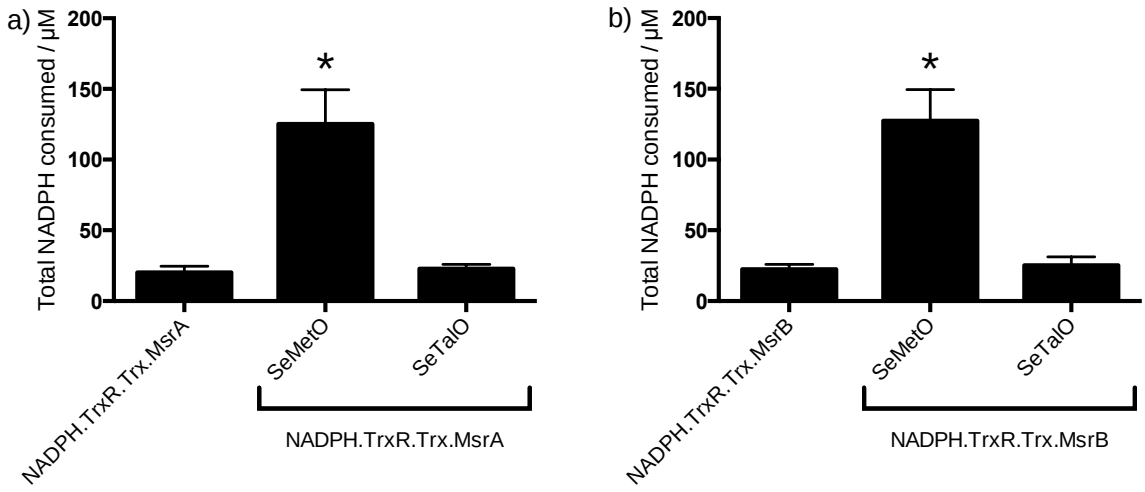

Figure 5.17 – Total NADPH consumed 2 h after SeMetO or SeTalO addition to NADPH, TrxR, Trx and MsrA or MsrB

*SeMetO or SeTalO (200 µM) was added to NADPH (700 µM) + TrxR (25 nM), Trx (1.5 µM) and a) MsrA (95 nM) or b) MsrB2 (0.25 µM) and the absorbance monitored for 2 h at 340 nm. NADPH consumed was determined by the difference in NADPH concentration from the initial reading to 2 h after selenoxide addition. Addition of SeMetO caused a significantly greater consumption of NADPH compared to control, whereas SeTalO addition did not. Data represent mean ± SD from 3 independent experiments. * indicates significant difference ($p < 0.05$) from control based on one-way ANOVA with Tukey's post-hoc test.*

As NADPH consumption was observed with SeMetO addition, it was anticipated that there should be a loss of SeMetO with a corresponding increase in SeMet. SeMet and SeMetO levels were measured after 2 h by HPLC. Samples were incubated for 2 h before removal of enzymes by filtering through a 10 kDa molecular mass cut-off filters and the concentrations of selenoxide and parent selenoether were analysed by HPLC with UV detection, and quantification performed as in Section 2.3.5.4. Similar to the data obtained from the NADPH/TrxR/Trx system (Figure 5.10), after 2 h complete reduction of SeMetO to SeMet was observed, and no change was observed with SeTalO (Figure 5.18). Again, a difference in NADPH consumed and selenoxide reduced is observed, which is believed to be related to the measurement of NADPH concentration discussed in Section 5.3.1.1.

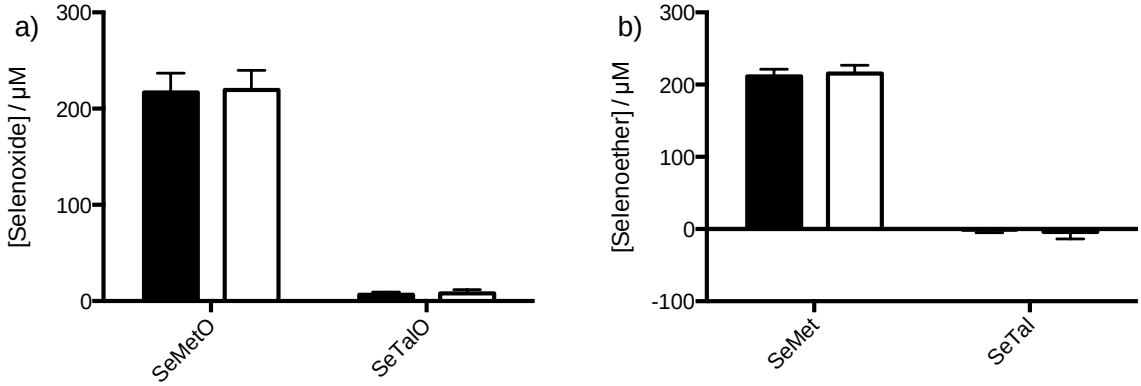

Figure 5.18 – Concentrations of selenoxides and selenoethers following 2 h incubation of SeMetO and SeTalO with the Msr systems

SeMetO or SeTalO (200 µM) was added to NADPH (700 µM), TrxR (25 nM), Trx (5 µM) and MsrA (95 nM) (black bars) or MsrB2 (0.25 µM) (white bars) and incubated for 2 h before analysis by HPLC. a) shows the concentration of selenoxide reduced and b) shows the recovery of corresponding selenoether. The Msr systems were able to reduce the 200 µM SeMetO, with a full recovery of SeMet. No changes were observed for SeTalO. Data represent mean ± SD from 3 independent experiments.

In summary, addition of SeMetO to NADPH/TrxR/Trx/MsrA or MsrB2 resulted in the loss of NADPH as measured by optical absorbance at 340 nm, with a decrease in SeMetO observed with a concomitant increase in SeMet concentrations, as measured by HPLC. SeTalO had no effect when added to these antioxidant enzyme systems.

5.3.1.4 Glutathione reductase

Selenoxides react with GSH to form GSSG as demonstrated in Chapter 4. GSSG should then be reduced by GSR at the expense of NADPH [557]. The ability of the GSR system to reduce SeMetO and SeTalO was monitored by NADPH consumption as assessed by optical absorbance at 340 nm.

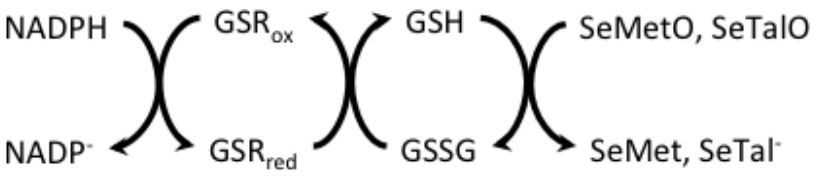

Figure 5.19 – Proposed reaction mechanism for the reduction of selenoxides by the NADPH/GSR.GSH system, with the formation of GSSG by reaction of selenoxides with GSH.

NADPH (500 μM), GSR (25 nM) and GSH (400 μM) was mixed with either SeMetO or SeTalO (200 μM) in phosphate buffer (0.1 M, pH 7.4) at 22 °C by stopped flow apparatus. Consumption of NADPH was monitored by UV-vis absorbance at 340 nm over 1 min (Figure 5.20). It should be noted that the concentration of NADPH was required to be lowered as initial experiments performed with 700 μM NADPH, consistent with other experiments in this Chapter, resulted in the UV-Vis detector attached to the stopped flow apparatus being saturated. Upon addition of selenoxides, an increase in the rate of NADPH consumption was observed over 1 min. The maximum rate of NADPH consumption was determined by fitting a linear slope to the UV-vis data, and this was assumed to correspond to the rate of selenoxide removal from the system. The rate of NADPH consumption was 7.4 ± 1 μM s^{-1} upon mixing the GSR system with SeMetO, and 6.7 ± 0.3 μM s^{-1} with SeTalO addition. Total NADPH consumption upon SeMetO or SeTalO addition is also consistent with the reduction of selenoxides. The loss of NADPH concentration suggests that the NADPH/GSR/GSH system reduced both SeMetO and SeTalO.

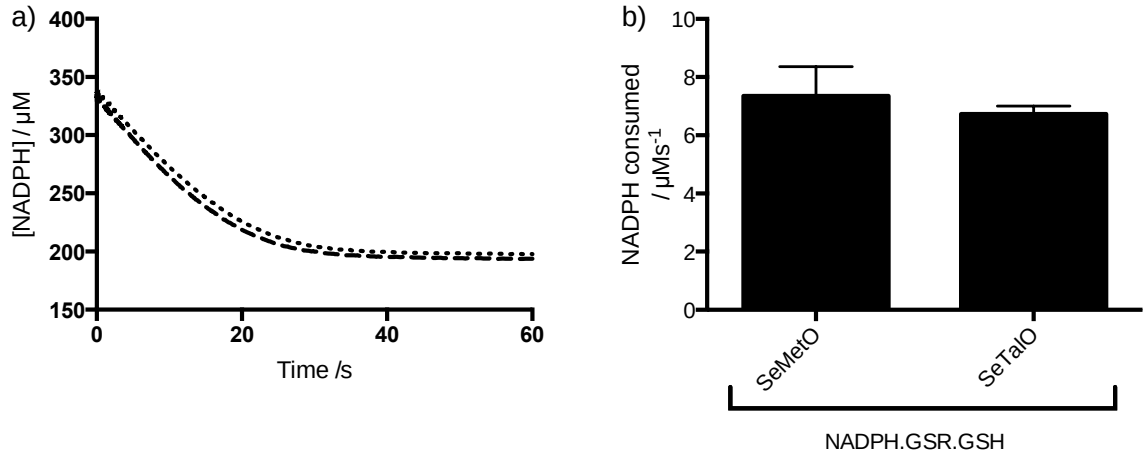

Figure 5.20 - Change in NADPH concentration over time after SeMetO or SeTalO was added to the GSR system.

SeMetO or SeTalO (200 μM) was mixed by stopped flow apparatus with NADPH (500 μM), GSR (25 nM) and GSH (400 μM) and the absorbance monitored for 1 min at 340 nm. a) shows typical [NADPH] vs time data obtained when 200 μM SeMetO (dashed), SeTalO (dotted) were mixed with the GSR system. Both SeMetO and SeTalO induced a steady decrease in NADPH concentration. b) The rate of NADPH consumption was determined by fitting a straight line to the initial 10 s of data represented in a). Data represent mean ± SD from 3 independent experiments.

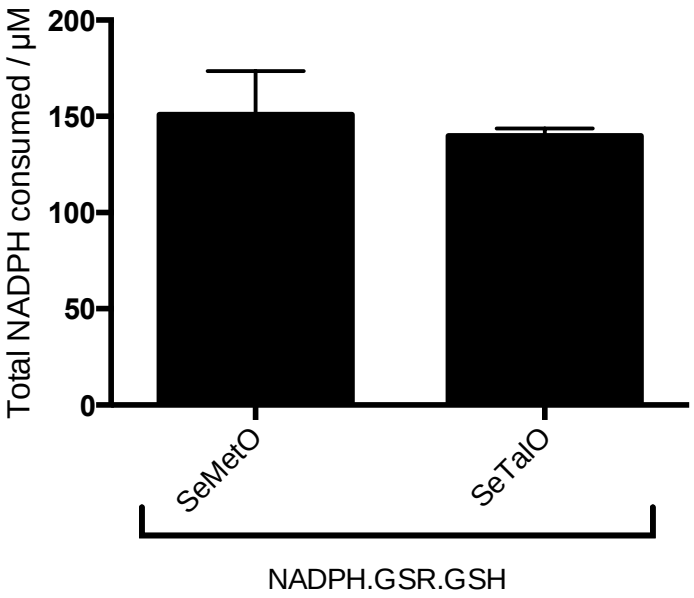

Figure 5.21 – Total NADPH consumed following addition for SeMetO or SeTalO to NADPH, GSH and GSR after 1 min

SeMetO or SeTalO (200 µM) was added to NADPH (500 µM), GSR (25 nM) and GSH (400 µM) and the absorbance monitored for 1 min at 340 nm. NADPH consumed was determined by the difference in NADPH concentration from the initial reading to 1 min after selenoxide addition. Addition of SeMetO and SeTalO both demonstrated an equal consumption of NADPH.

As NADPH consumption was observed that suggested a reduction of selenoxides via GSSG formation, an HPLC method was used to determine the concentrations of selenoethers and selenoxides after incubation of selenoxides with the NADPH/GSR/GSH system (Section 2.3.5.4). After addition of SeMetO to the GSR system, no SeMetO remained in the samples after 10 min, corresponding to a consumption of 200 µM SeMetO. An increase of 200 µM SeMet levels was observed at the same time point, demonstrating that the GSR system was capable of reducing SeMetO to SeMet. A difference between the total NADPH consumed (Figure 5.21) and the concentration of SeMet recovered (Figure 5.22) was observed, with this thought to be due to issues with NADPH concentration determination discussed in Section 5.3.1.1. Unfortunately, due to interference by components of the GSR system, similar experiments to give the concentrations of SeTal and SeTalO could not be determined.

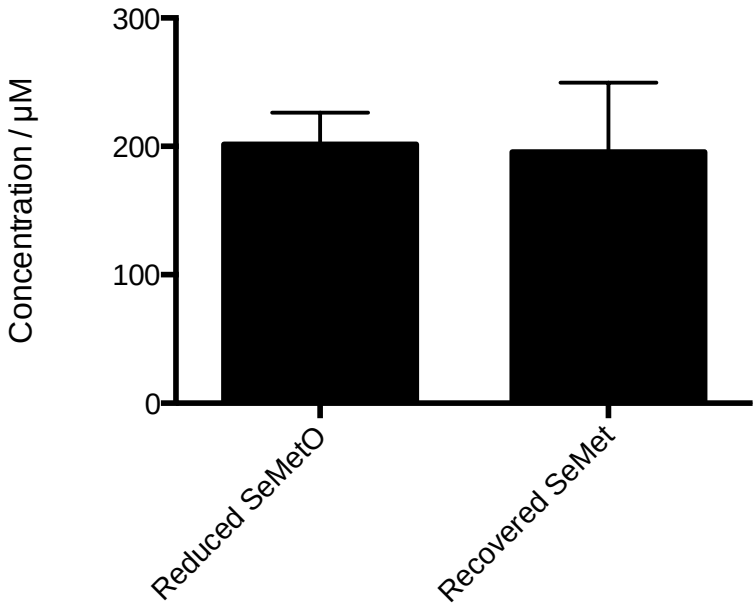

Figure 5.22 – Concentration of SeMetO reduced and SeMet recovered after SeMetO was added to the NADPH/GSR/GSH system

SeMetO (200 µM) was added to NADPH (500 µM), GSR (25 nM) and GSH (400 µM) and incubated for 10 min, before the SeMetO and SeMet concentrations were determined by HPLC. A decrease in SeMetO concentration of 200 µM was observed, which corresponded to an increase in SeMet of 200 µM. Data represent mean ± SD from 3 independent experiments.

In summary, TrxR was capable of reducing SeMetO and the addition of additional enzymes to the TrxR system, i.e. Trx and GPx or Msr, did not result in an increase in the rate of NADPH consumption. The TrxR system was unable to reduce SeTalO, and addition of other enzymes did not allow for reduction to occur. The NADPH/GSR/GSH system however, was capable of reducing both SeMetO and SeTalO, which occurred much more rapidly than the TrxR reduction of SeMetO.

5.3.2 Redox enzymes reducing *N*-chloramines

N-Chloramines have previously been reported to react with thiol groups [192], and selenols are generally more reactive towards oxidants and therefore should be capable of reacting with *N*-chloramines [90, 98]. As redox enzymes often have either a thiol or selenol active site, they should be able to react with *N*-chloramines. This reaction should lead to oxidation of the redox enzyme and reduction of *N*-chloramine. These enzymes therefore may be able to protect cells against oxidative damage via direct antioxidant capacity toward *N*-chloramines. Furthermore, TrxR and GSR have

demonstrated ability to reduce selenoxides, and as selenoethers rapidly scavenge *N*-chloramines, this may lead to enhanced oxidant removal.

5.3.2.1 Thioredoxin reductase

TrxR and Trx can detoxify peroxides, ONOOH and HOSCN, via reaction with active site SeCys and Cys respectively [348, 591]. As they are capable of removing these oxidants, their ability to reduce *N*-chloramines was investigated. In the presence of ebselen and selenocystamine the rate of peroxide removal by the Trx system is enhanced [492], and as TrxR and Trx has demonstrated the ability to reduce SeMetO [474], the presence of selenium compounds may further enhance oxidant removal (Figure 5.23).

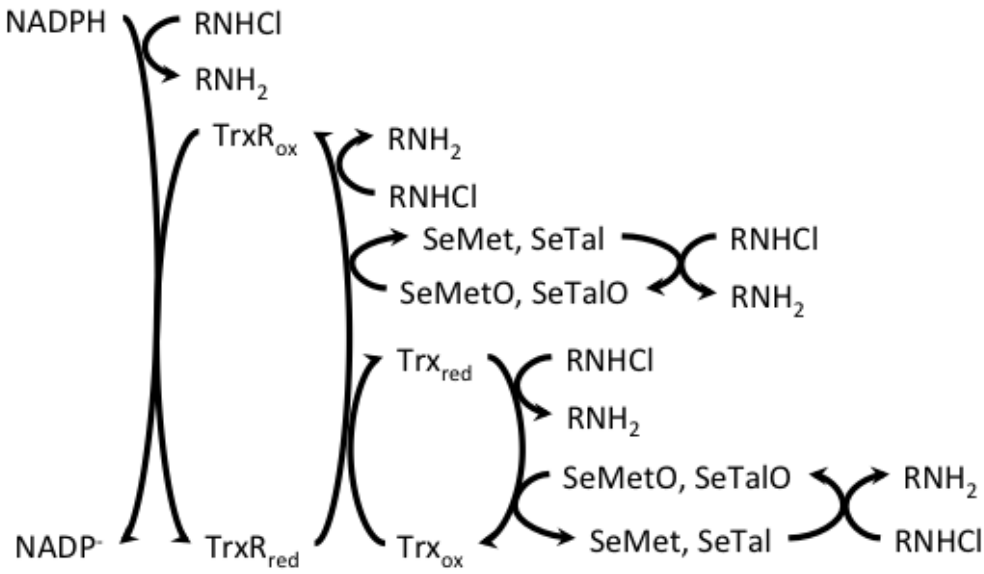

Figure 5.23 – Potential reactions occurring when *N*-chloramines are added to NADPH/TrxR/Trx/SeMet or SeTal. *N*-Chloramines may react directly with NADPH, or with TrxR, or Trx, or with SeMet and SeTal to form selenoxides which are subsequently reduced by TrxR and Trx.

The ability of TrxR to reduce model *N*-chloramines, TauCl, LysCl and GlyCl, was investigated by HPLC and the rate of NADPH consumption. NADPH (700 μM) and TrxR (25 nM) were incubated together for 5 min before addition of *N*-chloramine (200 μM). NADPH concentrations were monitored by optical absorbance at 340 nm (Figure 5.24). Only the UV-vis data for TauCl is shown, as comparable data is obtained with LysCl and GlyCl addition. The rate of NADPH consumption was determined by fitting a line to the initial (25 min) linear section of the [NADPH] vs time graph (Figure 5.25).

A rate of loss of NADPH of 104 ± 2 nM s^{-1} was observed when TauCl was added to NADPH alone. This is attributed to the direct reaction of TauCl with NADPH. The NADPH consumption rate increased to 111 ± 4 nM s^{-1} in the presence of TrxR, however this increase was not statistically significant. The presence of SeMet or SeTal (20 μM) reduced the rate of NADPH consumption to 92 ± 5 and 91 ± 6 nM s^{-1} respectively. Increasing the concentration of SeMet (200 μM) further reduced the rate of NADPH loss to 50 ± 7 nM s^{-1}, whereas with SeTal (200 μM) the NADPH consumption rate was reduced to 18 ± 4 nM s^{-1}. The reduction in the rate of NADPH consumption is attributed to the formation of selenoxides upon *N*-chloramine addition, with higher concentrations of SeMet or SeTal leading to a further reduction in NADPH consumption rate as more selenoxide is formed. As the TrxR system is capable of reducing SeMetO, but not SeTalO (Section 5.3.1.1), the rate of NADPH consumption is further reduced by the formation of SeTalO. The rates of NADPH loss was very similar to that observed in the presence of the selenoxides, consistent with the rapid generation of the selenoxide, which is then reduced by the Trx system (Figure 5.8).

The UV-vis vs time data monitored at 340 nm for LysCl and GlyCl were very similar to that obtained for TauCl (Figure 5.24) and the rate of NADPH consumption was determined by fitting to the NADPH concentration over time data obtained for the 10 min following *N*-chloramine addition (Figure 5.25). The rates of NADPH loss in control samples were higher for LysCl and GlyCl, 211 ± 13 and 184 ± 12 nM s^{-1} respectively, than for TauCl. As with TauCl, no significant difference in the rates of NADPH consumption were seen in the presence of TrxR compared to the control for LysCl or GlyCl, with rates of 203 ± 11 and 179 ± 13 nM s^{-1} respectively. Small decreases in the NADPH consumption rate were observed with SeMet (20 μM) and SeTal (20 μM), though this change was not significant for either LysCl (182 ± 16 and 174 ± 13 nM s^{-1} respectively) or GlyCl (154 ± 12 and 154 ± 9 nM s^{-1} respectively). At higher concentrations, SeMet (200 μM) and SeTal (200 μM) significantly reduced the rate of NADPH consumption to 44 ± 6 and 28 ± 7 nM s^{-1} respectively upon LysCl addition, and 42 ± 4 and 16 ± 9 nM s^{-1} for GlyCl addition. These rates of NADPH consumption are similar to those observed in the reduction experiments with pre-prepared selenoxides (Figure 5.8).

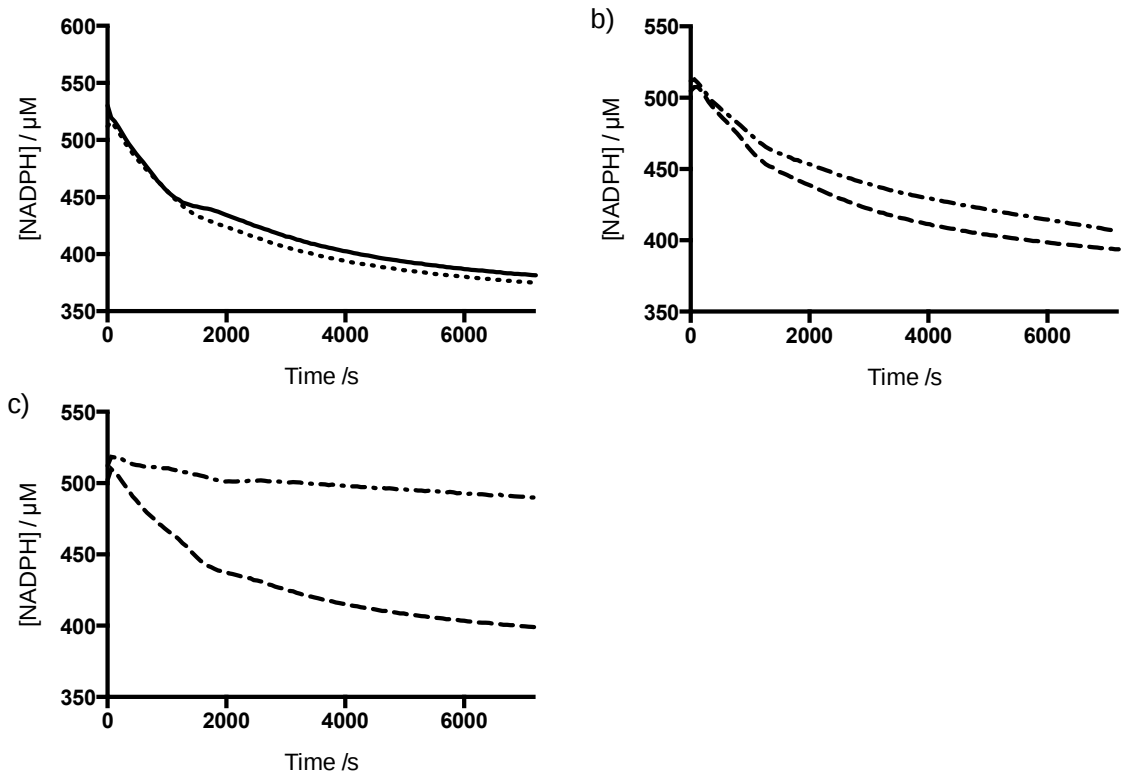

Figure 5.24 – Loss of NADPH over time when TauCl is added to NADPH ± TrxR ± SeMet or SeTal.

UV-vis absorbance at 340 nm was monitored after addition of TauCl to samples containing NADPH, TrxR with or without SeMet and SeTal. a) TauCl (200 µM) was added to NADPH (700 µM) in the a) presence (dotted line) or absence (solid) of TrxR (25 nM). b,c) TauCl (200 µM) was added to NADPH (700 µM) and TrxR (25 nM) in the presence of 20 µM (dashed line) or 200 µM (dot-dashed line) b) SeMet or c) SeTal. Addition of TauCl caused a time dependent decrease in NADPH, which was inhibited by the presence of SeMet and SeTal. Data are representative of 3 independent experiments.

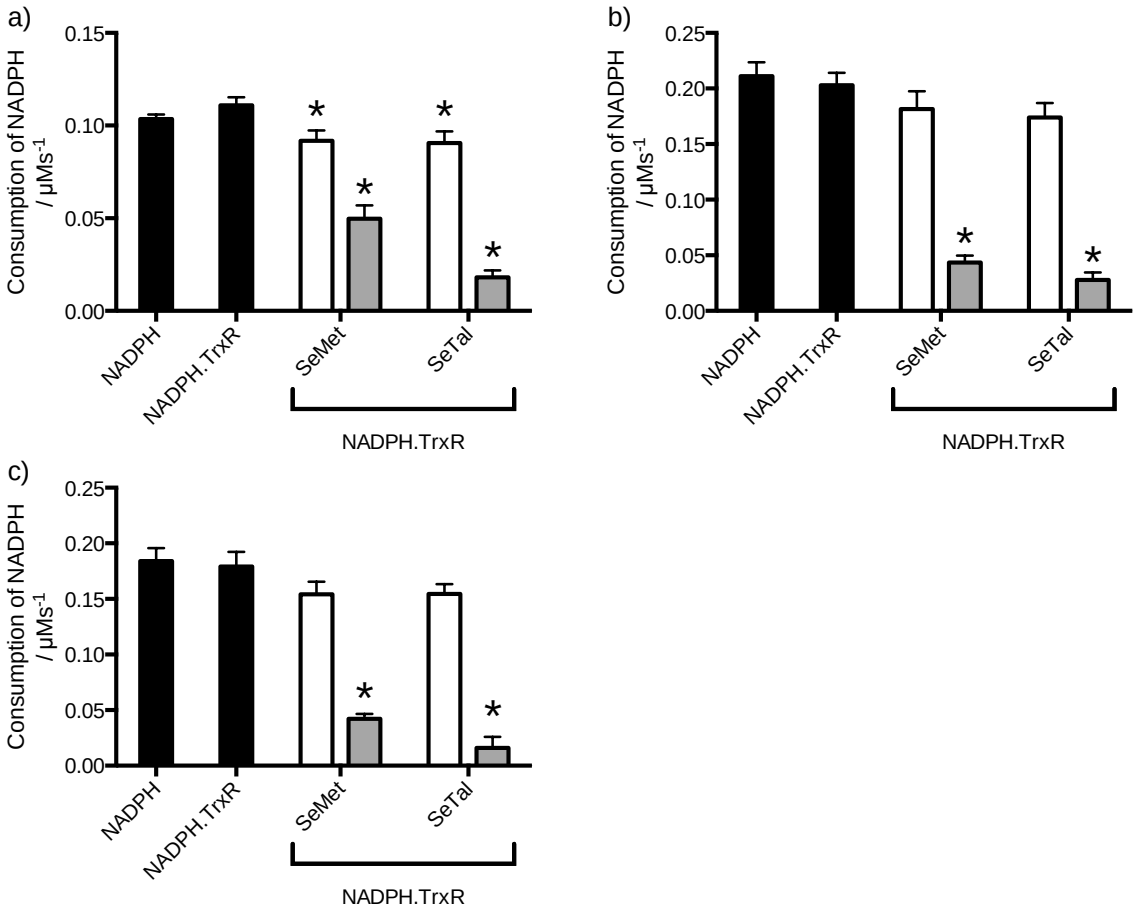

Figure 5.25 - Rate of NADPH consumption when *N*-chloramines were added to NADPH in the presence of TrxR and SeMet or SeTal

*The UV-vis absorbance of NADPH at 340 nm was monitored after a) TauCl (200 µM), b) LysCl (200 µM) or c) GlyCl (200 µM), were added to samples of NADPH (700 µM) ± TrxR (25 nM) (black bars) ± SeMet or SeTal (20 µM (white bars) or 200 µM (grey bars)). The rate of NADPH consumption was determined by fitting a straight line to the data obtained. The presence of N-chloramines caused a high rate of loss of NADPH that was decreased by the presence of SeMet and SeTal in a concentration-dependent manner. Data represent mean ± SD from 3 independent experiments. * indicates significant difference ($p < 0.05$) from control based on one-way ANOVA with Tukey's post-hoc test.*

In addition to examining the initial rate of NADPH loss, the total amount of NADPH consumed 2 h after the addition of *N*-chloramines was assessed (Figure 5.26). A total decrease of 150 ± 5 μM NADPH was observed 2 h after addition of TauCl (200 μM), with 140 ± 6 and 149 ± 4 μM being consumed upon LysCl (200 μM) or GlyCl (200 μM) addition respectively. However, the NADPH consumption may be underestimated due to issues with NADPH concentration measurement, as discussed in Section 5.3.1.1, and it should be noted that these numbers do not account for the loss of NADPH due to autooxidation. The presence of TrxR did not significantly increase the total NADPH consumed upon *N*-chloramine addition, nor did the presence of lower concentration of SeMet or SeTal (20 μM). A slight decrease in the total NADPH consumed was observed in the presence of higher concentrations of SeMet (200 μM) upon TauCl and GlyCl addition, though this was not significant, and probably reflects the ability of NADPH/TrxR to reduce SeMetO though at a lower rate than *N*-chloramines (Figure 5.8). The presence of SeTal (200 μM) significantly reduced the total NADPH consumption upon addition of *N*-chloramines, consistent with the inability of NADPH/TrxR to reduce SeTalO (Figure 5.8).

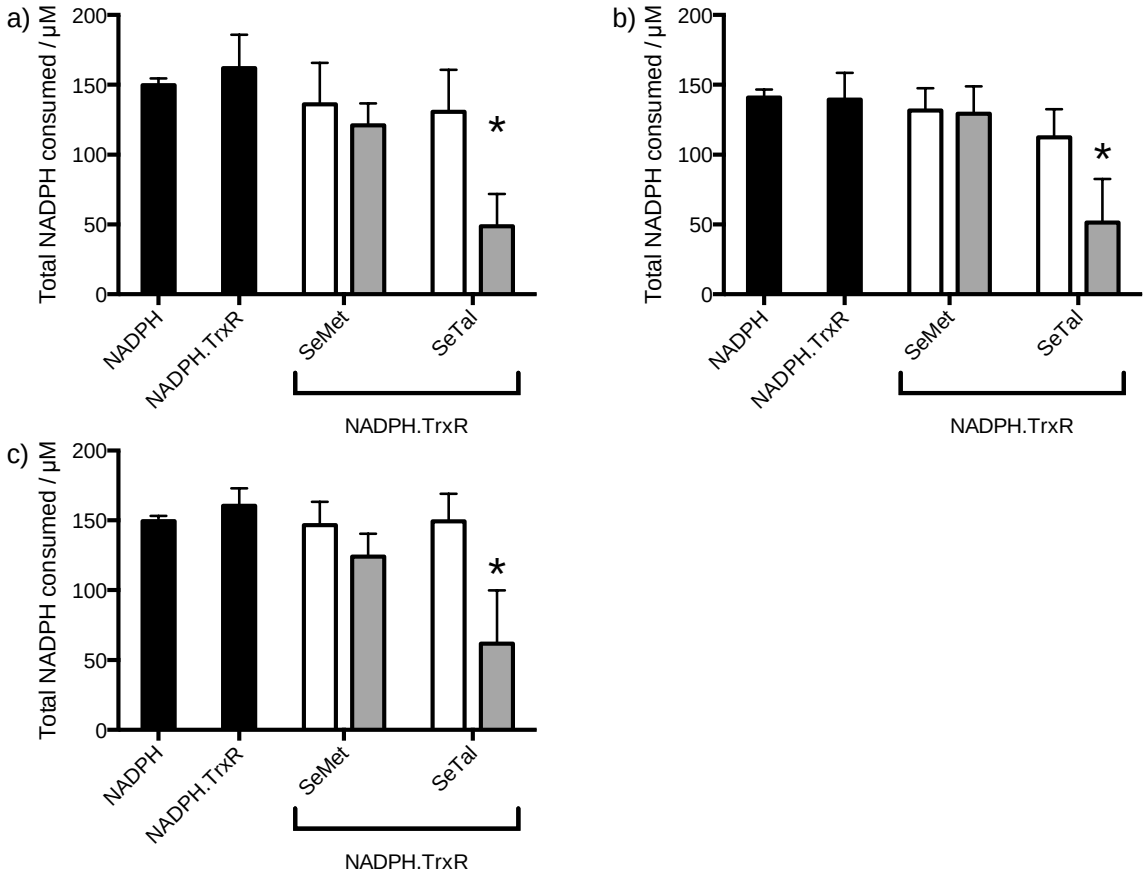

Figure 5.26 - Total NADPH consumed 2 h after *N*-chloramines were added to NADPH in the presence of TrxR and SeMet or SeTal

*The UV-vis absorbance of NADPH at 340 nm was monitored after a) TauCl (200 µM), b) LysC (200 µM)l or c) GlyCl (200 µM), were added to samples of NADPH (700 µM) ± TrxR (25 nM) (black bars) ± SeMet or SeTal (20 µM (white bars) or 200 µM (grey bars)). NADPH consumed was determined by the difference in NADPH concentration from the initial reading to 2 h after N-chloramine addition. The addition of N-chloramines caused consumption of NADPH. There was a slight decrease in NADPH consumption when SeMet (200 µM) was present, though this was not significant. Significantly less NADPH was consumed when SeTal (200 µM) was present for each N-chloramine. Data represent mean ± SD from 3 independent experiments. * indicates significant difference ($p < 0.05$) from control based on one-way ANOVA with Tukey's post-hoc test.*

As the rate consumption of NADPH in the presence of TrxR was significantly decreased in the presence of SeMet (200 µM) or SeTal (200 µM), it was proposed that SeMet and SeTal were scavenging the *N*-chloramines to form the respective selenoxides. The selenoxides are then the species that are reduced by the NADPH/TrxR system rather than the *N*-chloramines themselves. In order to investigate this possible interpretation of the data further, the levels of SeMet, SeTal, SeMetO and SeTalO were

assessed by HPLC with UV detection at 20 min and 2 h after TauCl addition (Figure 5.27).

NADPH (700 μM) and TrxR (25 nM) were incubated with SeMet (200 μM) or SeTal (200 μM) for 5 min before addition of TauCl (200 μM). The proteins were removed by filtering through 10 kDa molecular mass cut-off filters after incubation for 20 min or 2 h after *N*-chloramine addition. The concentration of SeMet and SeTal and the corresponding selenoxides was then determined by HPLC (Section 2.3.5.4).

SeMetO and SeTalO were the primary species present 20 min after TauCl addition to the samples with 164 ± 8 μM SeMetO and 175 ± 6 μM SeTalO present, compared to 56 ± 25 μM SeMet and 19 ± 7 μM SeTal. After 2 h, in SeMet samples, the majority of the SeMetO had been reduced with only 12 ± 13 μM remaining. This corresponded to a recovery of SeMet with a final concentration of 173 ± 10 μM. The concentrations of SeTal and SeTalO remained unchanged between the time points, with 23 ± 16 and 174 ± 10 μM measured at 2 h for SeTal and SeTalO respectively, consistent with the NADPH/TrxR system being unable to reduce SeTalO. These concentrations better reflect the concentration of NADPH consumed in previous experiments (Figure 5.26) compared with the experiments with selenoxide alone, as discussed in Section 5.3.1.1, though it should be noted that total NADPH consumption may be underestimated due to autoxidation of NADPH.

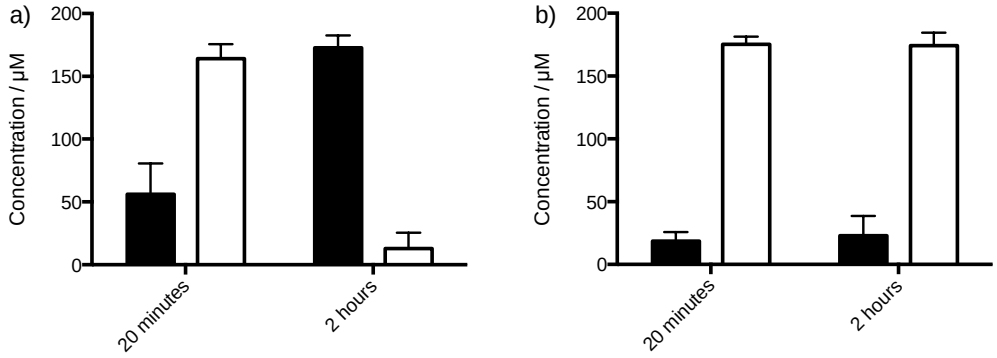

Figure 5.27 – Concentrations of SeMet, SeMetO, SeTal and SeTalO after TauCl was added to NADPH, TrxR and SeMet or SeTal.

NADPH (700 µM) and TrxR (25 nM) were incubated with a) SeMet (200 µM) or b) SeTal (200 µM) for 5 min before addition of TauCl (200 µM). The concentrations of a) SeMet (black bars) and SeMetO (white bars) or b) SeTal (black bars) and SeTalO (white bars) were determined by HPLC at 20 mins or 2 h after addition of TauCl. At 20 min SeMetO and SeTalO were the primary species present. After 2 h SeMetO had been reduced, but no change was observed for SeTalO. Data represent mean ± SD from 3 independent experiments.

In summary, a decrease in the rate of NADPH consumption was observed when *N*-chloramines were added to NADPH in the presence of Trx, however this rate was not significantly different from NADPH alone. The presence of SeMet and SeTal reduced the rate at which NADPH was consumed when *N*-chloramines were added to NADPH/TrxR. This is attributed to the rapid formation of selenoxides, followed by subsequent reduction of SeMetO, though SeTalO could not be reduced by this system (consistent with Section 5.3.1.1). This was confirmed by HPLC studies which showed that high levels of selenoxides were present 20 mins after *N*-chloramine addition for both SeMetO and SeTalO, and SeMetO levels were decreased at 2 hours with a concurrent increase in SeMet, whereas no changes were observed in SeTalO concentrations.

5.3.2.2 Thioredoxin

N-Chloramines, TauCl, LysCl or GlyCl, (200 µM) were added to NADPH (700 µM), TrxR (25 nM) and Trx (1.5 µM) with or without SeMet or SeTal (20 or 200 µM) and the absorbance at 340 nm was monitored for 2 h. The rate of NADPH consumption, and hence *N*-chloramine reduction, was determined by fitting a straight line to the linear portion (10 min) of the NADPH concentration vs. time plots (Figure 5.28).

There was an increase in the rate of NADPH consumption from 104 ± 2 nM s^{-1} in the NADPH controls to 116 ± 6 nM s^{-1} when TauCl (200 μM) was added to NADPH/TrxR/Trx (Figure 5.28a). However, the increase over NADPH/TrxR was not significant. There were no significant increase in NADPH consumption over NADPH alone when LysCl or GlyCl were added to NADPH/TrxR/Trx, with rates of 204 ± 5 and 183 ± 17 nM s^{-1} observed (Figure 5.28b,c).

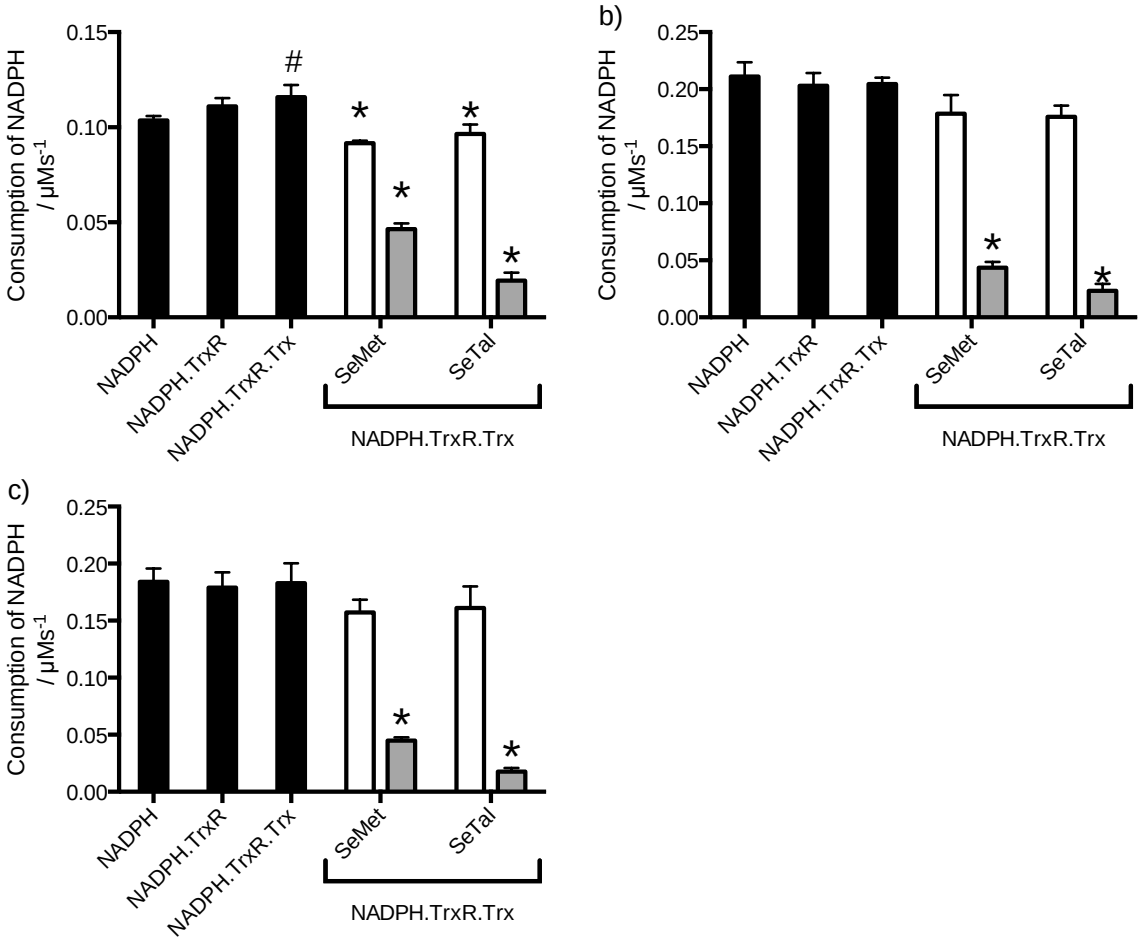

Figure 5.28 – Rate of NADPH consumption when *N*-chloramines were added to the NADPH/TrxR/Trx system with SeMet or SeTal

*The UV-vis absorbance of NADPH at 340 nm was monitored after a) TauCl (200 µM), b) LysCl (200 µM) or c) GlyCl (200 µM), were added to samples of NADPH (700 µM) ± TrxR (25 nM) ± Trx (1.5 µM) (black bars) ± SeMet or SeTal (20 µM (white bars) or 200 µM (grey bars)). The rate of NADPH consumption was determined by fitting a straight line to the data obtained. The presence of both TrxR and Trx increased the rate at which NADPH was consumed when TauCl was added to the system. TrxR and Trx had no effect on NADPH consumption rates when LysCl or GlyCl was added. N-Chloramines caused a rapid rate of consumption of NADPH which could be inhibited by the presence of SeMet and SeTal. Data represent mean ± SD from 3 independent experiments. # indicates significant difference ($p < 0.05$) from NADPH alone, and * indicates significant difference ($p < 0.05$) from NADPH.TrxR.Trx based on one-way ANOVA with Tukey's post-hoc test.*

The presence of SeMet (20 µM) and SeTal (20 µM) significantly decreased the NADPH consumption rate to 92 ± 1 and 96 ± 5 nM s^{-1} respectively when TauCl was added to the Trx system. Small decreases in the NADPH consumption rates were also observed when LysCl and GlyCl were added to the TrxR system in the presence of SeMet or SeTal (20 µM) to 178 ± 16 and 176 ± 10 nM s^{-1} with LysCl (200 µM) addition

and 157 ±11 and 161 ±19 with GlyCl (200 μM) addition (Figure 5.28b,c). As for TauCl, these rates were not significantly different from the rate of NADPH consumption either alone or in the presence of TrxR and Trx. The presence of higher concentrations of SeMet (200 μM) in the NADPH/TrxR/Trx system reduced the NADPH consumption rate further to 46 ± 3, 43 ± 5 and 45 ± 3 nM s^{-1} for TauCl, LysCl and GlyCl respectively. These rates are similar to those observed when 200 μM SeMetO was added to NADPH/TrxR/Trx system (Figure 5.9). The presence of SeTal (200 μM) reduced the NADPH consumption rate to 19 ± 4, 23 ± 6 and 18 ± 3 nM s^{-1} for TauCl, LysCl and GlyCl respectively.

In addition to examining the initial rate of NADPH loss, the total amount of NADPH consumed 2 h after the addition of *N*-chloramines was assessed (Figure 5.29). Total losses of 161 ± 18, 143 ± 22 and 161 ± 18 μM NADPH were observed 2 h after the addition of TauCl, LysCl or GlyCl to NADPH/TrxR/Trx respectively. As for the NADPH/TrxR system (Figure 5.26), this was less than the 1 : 1 ratio as expected. The presence of SeMet (20 μM) or SeTal (20 μM) did not have an affect on total NADPH consumed, but the presence of higher concentrations of SeMet (200 μM) demonstrated a decrease in total NADPH consumed to 117 ± 14, 118 ± 10 and 120 ± 8 μM upon addition of TauCl, LysCl and GlyCl respectively, though this was not significantly different to NADPH/TrxR/Trx alone. The presence of SeTal (200 μM) significantly reduced the total NADPH consumed by the system as seen with the NADPH TrxR system (Figure 5.26), and reflects the inability of NADPH/TrxR/Trx to reduce SeTalO.

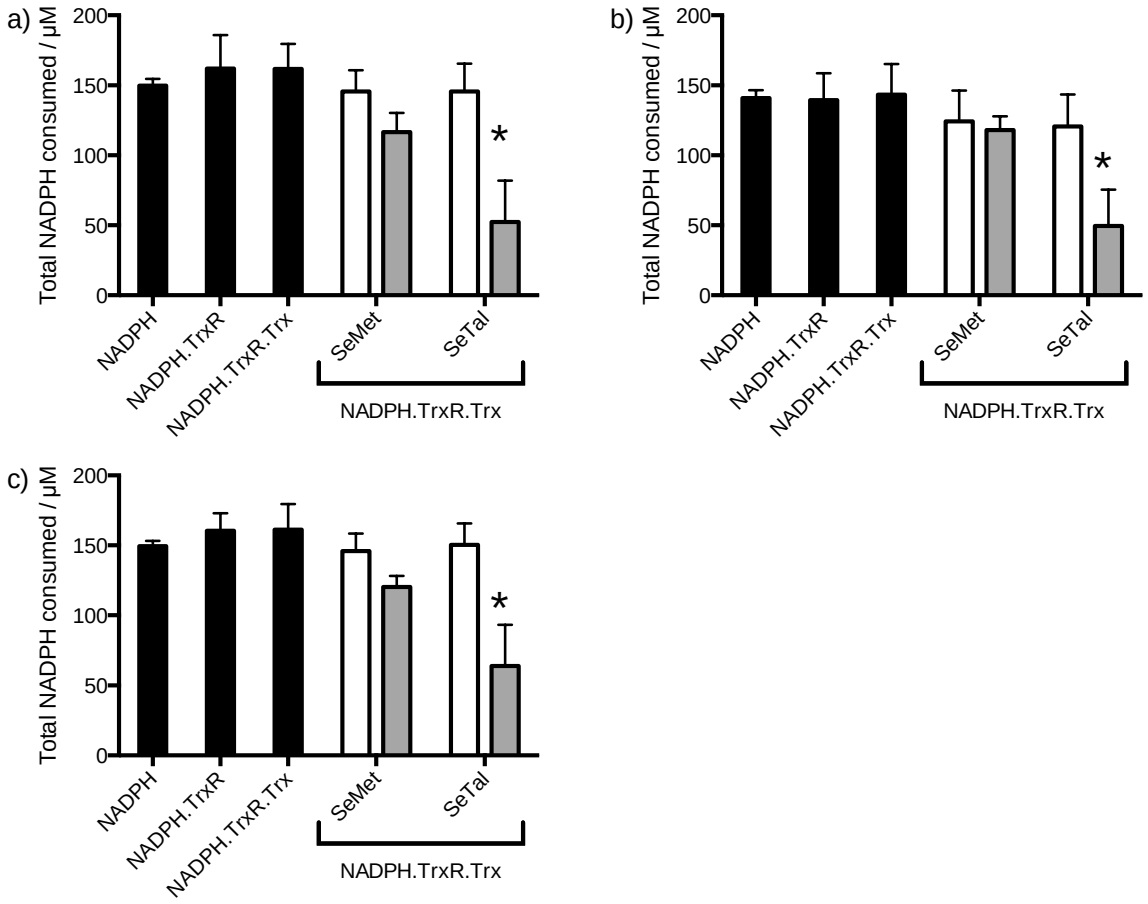

Figure 5.29 - Total NADPH consumed 2 h after *N*-chloramines were added to NADPH in the presence of TrxR, Trx and SeMet or SeTal

*The UV-vis absorbance of NADPH at 340 nm was monitored after a) TauCl (200 µM), b) LysCl (200 µM) or c) GlyCl (200 µM), were added to samples of NADPH (700 µM), TrxR (25 nM) (black bars) and Trx (1.5 µM) ± SeMet or SeTal (20 µM (white bars) or 200 µM (grey bars)). NADPH consumed was determined by the difference in NADPH concentration from the initial reading to 2 h after N-chloramine addition. The addition of N-chloramines caused consumption of NADPH. Less NADPH was consumed when SeMet (200 µM) was present, though this was not significant. Significantly less NADPH was consumed when SeTal (200 µM) was present in each case. Data represent mean ± SD from 3 independent experiments. * indicates significant difference ($p < 0.05$) from control based on one-way ANOVA with Tukey's post-hoc test.*

In light of the above data, it was proposed that *N*-chloramines were reacting with *N*-chloramines to form selenoxides, which are then reduced by the NADPH/TrxR/Trx system. As such, the levels of selenoxides, SeMetO and SeTalO, and parent selenoethers, SeMet and SeTal, were measured by HPLC (Section 2.3.5.4) with UV-vis detection at incubation times of 20 min and 2 h after the addition of TauCl (200 µM) to NADPH (700 µM), TrxR (25 nM) and Trx (1.5 µM) (Figure 5.30). After 20 min, the selenoxides were

the major species present at 165 ± 8 μM and 175 ± 7 μM of SeMetO and SeTalO detected respectively, with the corresponding SeMet and SeTal concentrations being 52 ± 30 and 21 ± 7 μM respectively. After 2 h, the majority of SeMetO had been reduced to SeMet with 12 ± 13 μM SeMetO and 170 ± 10 μM SeMet detected. No significant changes were observed in the concentration of SeTal and SeTalO after 2 h compared to 20 min, with 21 ± 14 and 174 ± 10 μM SeTal and SeTalO measured at 2 h respectively.

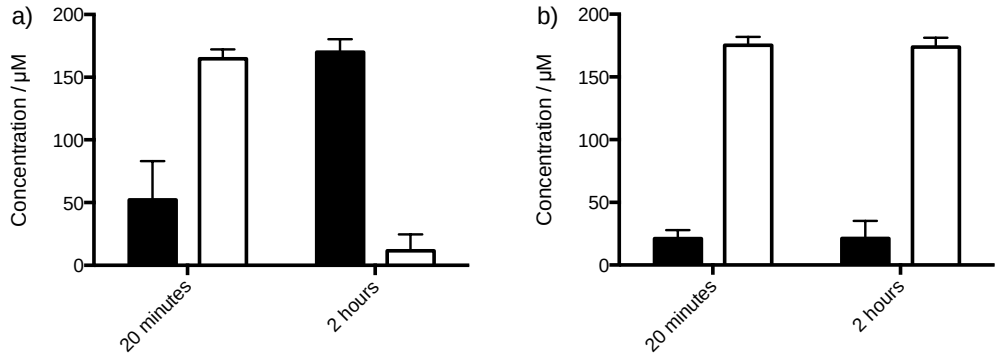

Figure 5.30 – Concentrations of SeMet, SeMetO, SeTal and SeTalO after TauCl was added to NADPH, TrxR, Trx and SeMet or SeTal

NADPH (700 μM) TrxR (25 nM) and Trx (1.5 μM) were incubated with 200 μM a) SeMet or b) SeTal for 5 min before addition of TauCl (200 μM). The concentrations of a) SeMet (black bars) and SeMetO (white bars) or b) SeTal (black bars) and SeTalO (white bars) were determined by HPLC at 20 mins or 2 h after addition of TauCl. After 20 min SeMetO and SeTalO were the primary species present. After 2 h, the concentration of SeMetO had been reduced, whilst no change was observed for SeTalO. Data represent mean ± SD from 3 independent experiments.

A decrease in NADPH was observed when *N*-chloramines were added to NADPH in the presence of TrxR and Trx. The rate of NADPH consumption was only increased when TauCl was added to NADPH/TrxR/Trx. The presence of SeMet and SeTal reduced the rate at which NADPH was consumed when *N*-chloramines was added to NADPH/TrxR/Trx. As with NADPH and TrxR alone, this was attributed to the rapid formation of selenoxides, with reduction of SeMetO levels observed after 2 h.

5.3.2.3 GPx

GPx is capable of reducing peroxides, via reaction of the peroxide with the active site Sec [583]. As HOCl has demonstrated reactivity with SeCys residues [98], *N*-chloramines are also likely to react with this site, thus GPx may be capable of reacting

with and reducing *N*-chloramines. The ability of GPx to reduce *N*-chloramines, and the interactions with SeMet and SeTal were assessed (Figure 5.31).

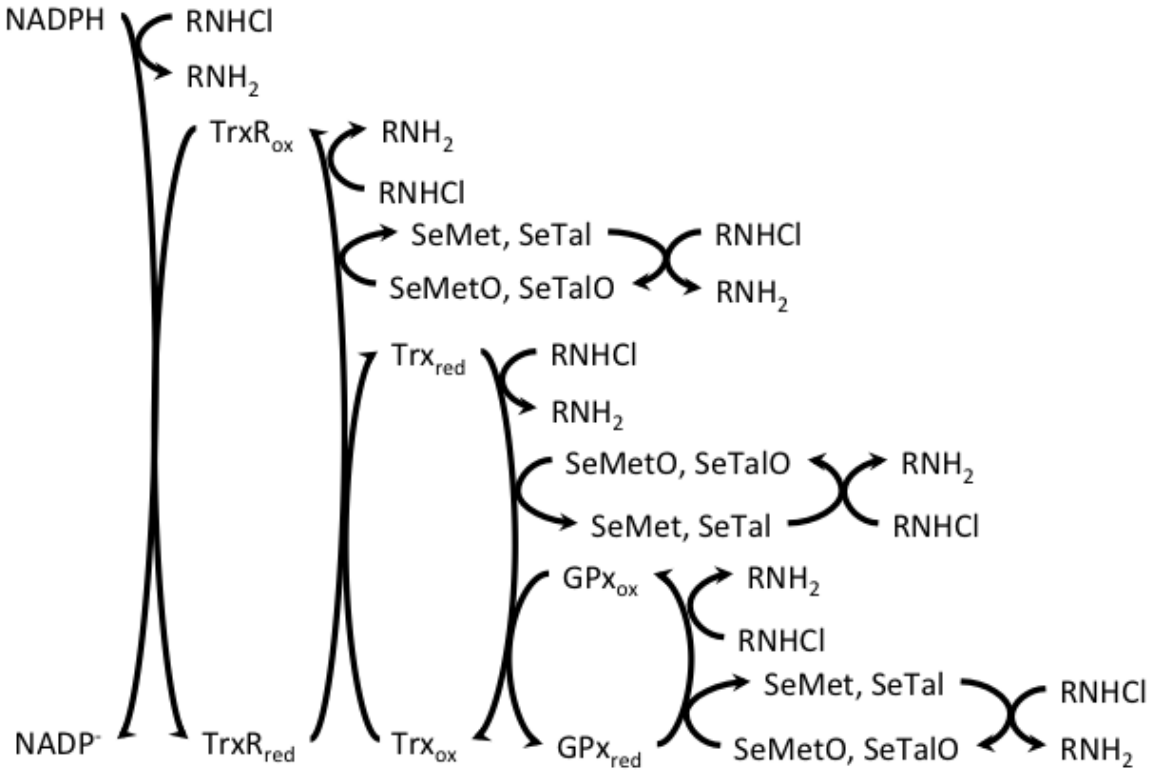

Figure 5.31 – Potential routes of *N*-chloramine consumption when exposed to NADPH/TrxR/Trx/GPx/SeMet or SeTal

The *N*-chloramines, TauCl, LysCl and GlyCl (200 μM), were added to NADPH (700 μM), TrxR (25 nM), Trx (1.5 μM) and GPx (1.5 μM) with or without SeMet or SeTal (20 μM or 200 μM). The changes in absorbance at 340 nm were monitored for 2 h (Figure 5.32), and the rate of NADPH consumption was determined by the fitting of a straight line to the initial 25 min of the resulting NADPH concentration vs time plots (Figure 5.33).

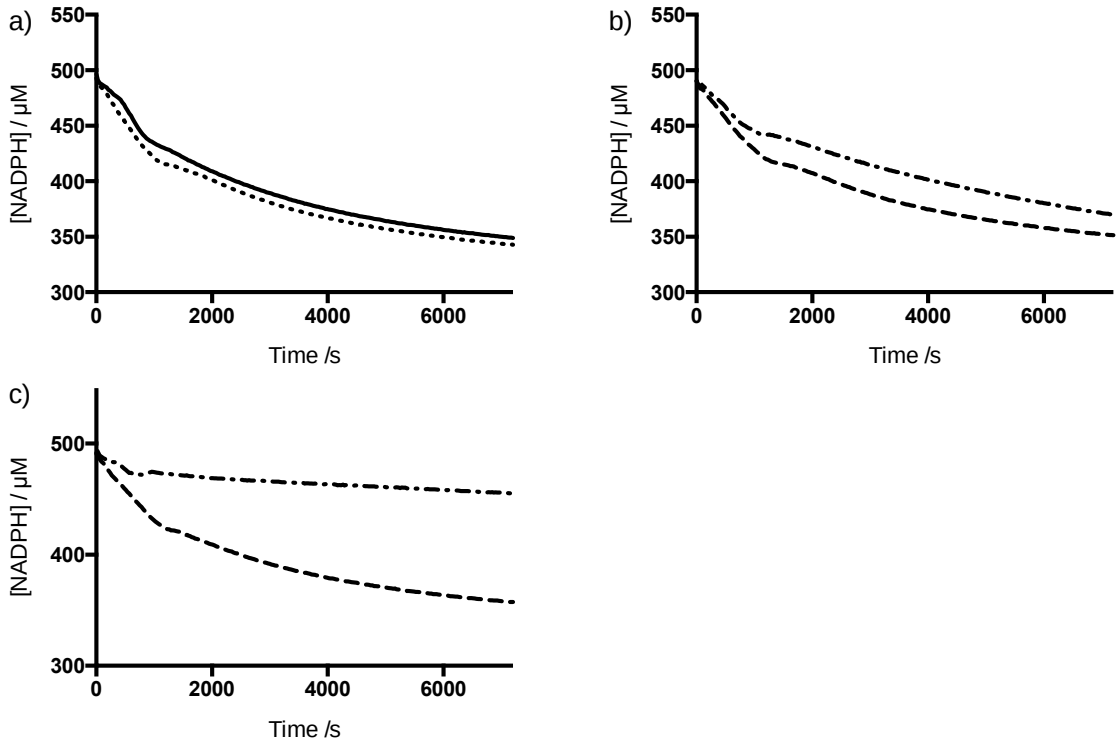

Figure 5.32 – Plots of the NADPH concentration over time after TauCl was added to the GPx system in the presence or absence of SeMet and SeTal.

UV-vis absorbance was monitored at 340 nm after addition of TauCl to samples containing NADPH, TrxR, Trx and GPx with or without SeMet and SeTal. a) TauCl (200 µM) was added to NADPH (700 µM) in the a) presence (dotted line) or absence (solid) of the TrxR (25 nM), Trx (1.5 µM) and GPx (1.5 µM). b,c) TauCl (200 µM) was added to the GPx system in the presence of 20 µM (dashed line) or 200 µM (dot-dashed line) b) SeMet or c) SeTal. Addition of TauCl caused a time dependent decrease in NADPH concentration and the rate of this decreased by presence of SeMet and SeTal. Data are representative of 3 independent experiments.

The addition of *N*-chloramines causes a loss of NADPH in control samples of 106 ± 18, 186 ± 36, and 164 ± 27 nM s^{-1} after addition of TauCl, LysCl and GlyCl respectively (Figure 5.33). The presence of the TrxR/Trx/GPx did not have an effect on the rate of NADPH consumption upon *N*-chloramine addition with rates of NADPH consumption of 112 ± 15, 170 ± 30 and 170 ± 26 nM s^{-1} observed upon addition of TauCl, LysCl and GlyCl to NADPH/TrxR/Trx/GPx respectively. The presence of SeMet (20 µM) lowered the rate of NADPH consumption to 93 ± 19, 126 ± 30 and 137 ± 20 nM s^{-1} for TauCl, LysCl and GlyCl respectively, and 20 µM SeTal lowered the rates to 91 ± 9, 142 ± 35 and 134 ± 11 nM s^{-1}, though none of these changes were not significantly different to NADPH alone and the NADPH/TrxR/Trx system (Figure 5.28). The presence of SeMet

(200 μM) significantly reduced the rate of NADPH consumption for all *N*-chloramines, to 61 ± 20, 56 ± 30 and 69 ± 16 nM s^{-1} for TauCl, LysCl and GlyCl respectively. The presence of SeTal (200 μM) demonstrated a greater reduction in NADPH consumption rate for all *N*-chloramines, to 17 ± 10, 7 ± 9 and 18 ± 9 nM s^{-1} for TauCl, LysCl and GlyCl respectively. The rates of NADPH consumption in the presence of SeMet (200 μM) and SeTal (200 μM) are similar to those observed when SeMetO (200 μM) or SeTalO (200 μM) are added to the GPx system (Figure 5.12).

In addition to examining the initial rate of NADPH loss, the total amount of NADPH consumed 2 h after the addition of *N*-chloramines was assessed (Figure 5.34). Addition of TauCl, GlyCl of LysCl (200 μM) to NADPH/TrxR/Trx/GPx caused a decrease of 145 ± 6, 147 ± 12 and 159 ± 6 μM NADPH respectively. Again, this is less than what might be expected, and could be related to NADPH concentration determination. The presence of SeMet (20 μM) or SeTal (20 μM) did not significantly affect the total NADPH consumed by the system. The presence of 200 μM SeMet and SeTal significantly reduced the total NADPH consumed, reflecting the lower reduction rate of SeMetO and the inability of the system to reduce SeTalO (Section 5.3.1.2).

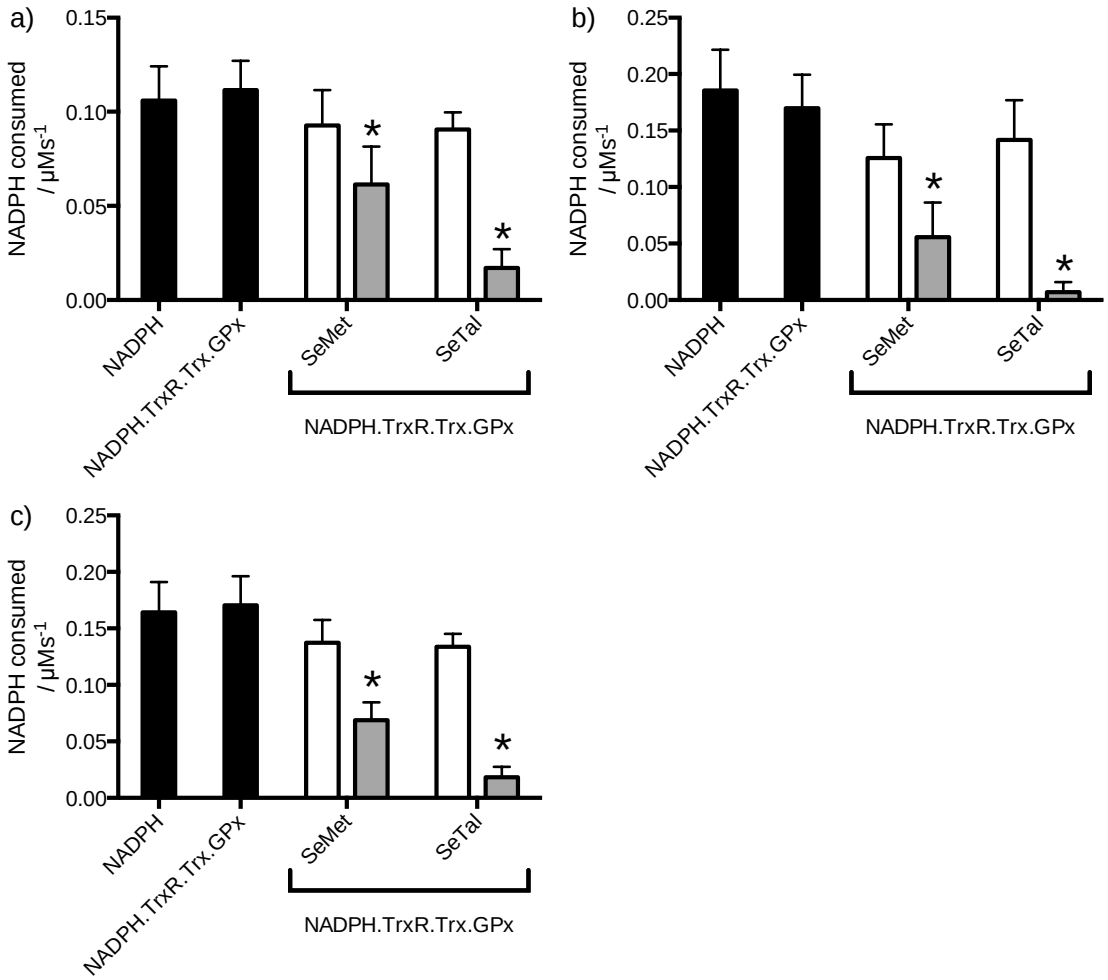

Figure 5.33 – NADPH consumption rates when *N*-chloramines are added to the GPx system in the presence or absence of SeMet and SeTal.

*The UV-vis absorbance of NADPH at 340 nm was monitored after a) TauCl (200 µM), b) LysCl (200 µM) or c) GlyCl (200 µM), were added to samples of NADPH (700 µM) ± TrxR (25 nM) ± Trx (1.5 µM) ± GPx (1.5 µM) ± SeMet or SeTal (20 µM (white bars) or 200 µM (grey bars)). The rate of NADPH consumption was determined by fitting a straight line to the initial 25 min if the data obtained. Addition of TauCl caused a time dependent decrease in NADPH concentration and this rate was decreased by presence of SeMet and SeTal. Data represent mean ± SD from 3 independent experiments. * indicates significant difference ($p < 0.05$) from control based on one-way ANOVA with Tukey's post-hoc test.*

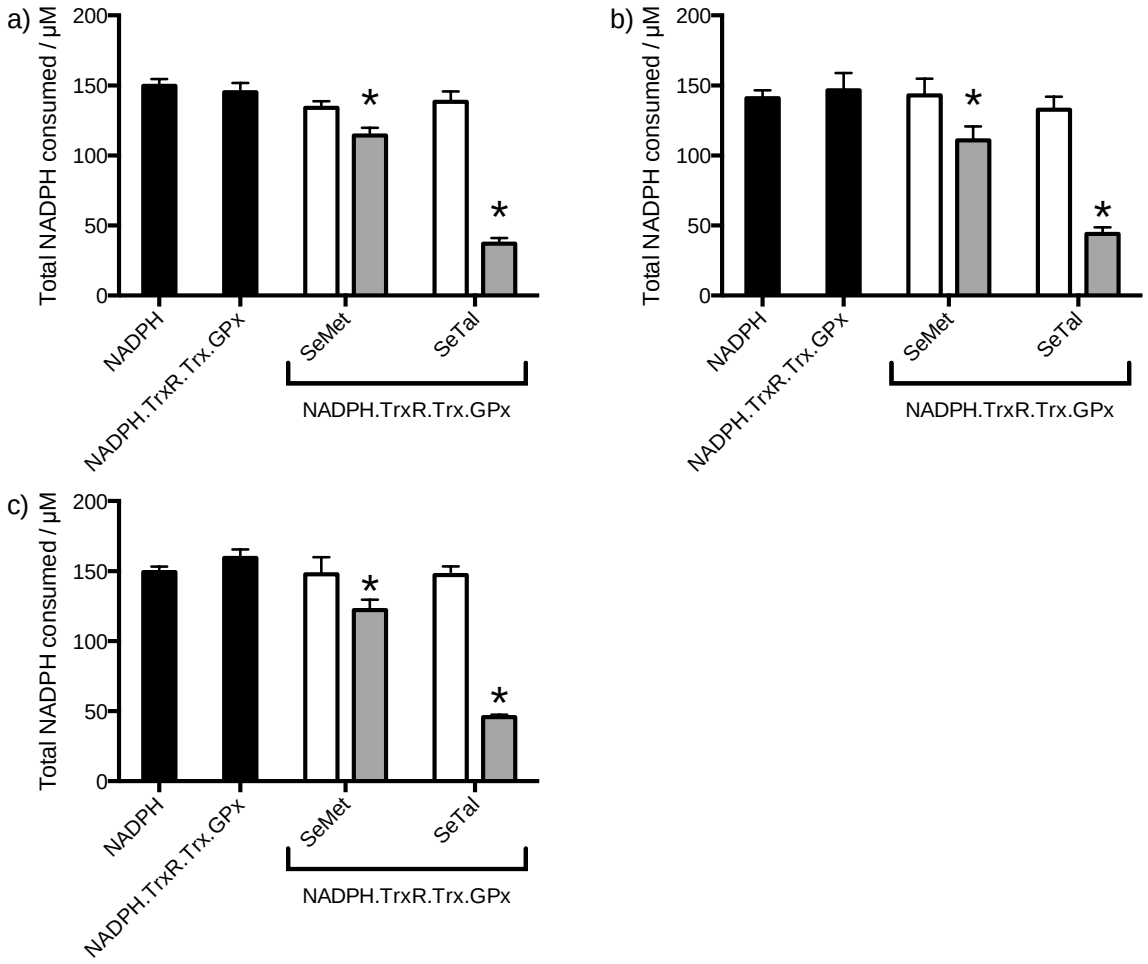

Figure 5.34 - Total NADPH consumed 2 h after *N*-chloramines were added to NADPH in the presence of TrxR, Trx, GPx and SeMet or SeTal

*The UV-vis absorbance of NADPH at 340 nm was monitored after a) TauCl (200 µM), b) LysCl (200 µM) or c) GlyCl (200 µM), were added to samples of NADPH (700 µM) ± TrxR (25 nM) ± Trx (1.5 µM) ± GPx (1.5 µM) ± SeMet or SeTal (20 µM (white bars) or 200 µM (grey bars)). The amount of NADPH consumed was determined by the difference in NADPH concentration from the initial reading to 2 h after N-chloramine addition. The addition of N-chloramines caused consumption of NADPH. Significantly less NADPH was consumed when SeMet (200 µM) or SeTal (200 µM) was present. Data represent mean ± SD from 3 independent experiments. * indicates significant difference ($p < 0.05$) from control based on one-way ANOVA with Tukey's post-hoc test.*

The concentrations of SeMet and SeTal and their respective selenoxides were assessed by HPLC with UV-vis detection after incubation for 2 h of NADPH (700 µM), TrxR (25 nM), Trx (1.5 µM), GPx (1.5 µM) and SeMet (200 µM) or SeTal (200 µM) with TauCl (200 µM) (Figure 5.35). The primary species present after 2 h incubation for the SeMet containing samples was SeMet at a concentration of 160 ± 12 µM, and SeMetO at a concentration of 18 ± 10 µM. At the same time point, the primary species in the SeTal containing samples was SeTalO present at 157 ± 11 µM, with SeTal present at 18 ± 5

μM. This is consistent with results with the TrxR and Trx samples (Section 5.3.2.1 and 5.3.2.2), demonstrating formation of SeMetO and SeTalO, with subsequent enzymatic reduction of SeMetO but not SeTalO.

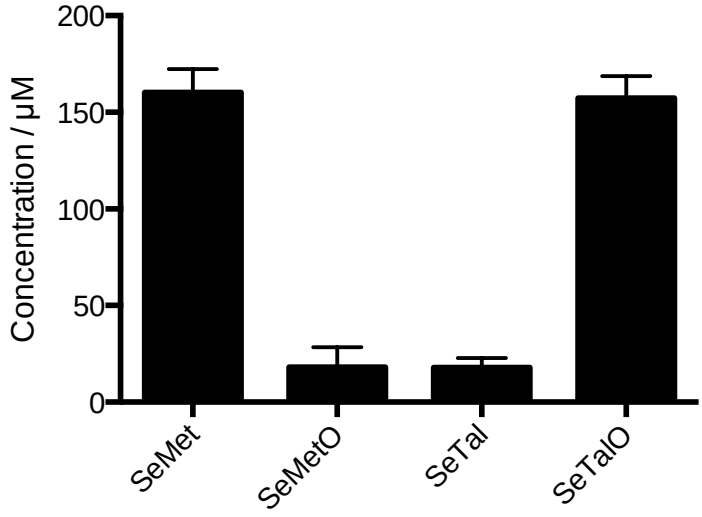

Figure 5.35 – Concentrations of SeMet, SeMetO, SeTal and SeTalO 2 h after TauCl was added to the GPx system in the presence of SeMet or SeTal.

NADPH (700 μM), TrxR (25 nM), Trx (1.5 μM) and GPx (1.5 μM) were incubated with a) SeMet (200 μM) or b) SeTal (200 μM) for 5 min before addition of TauCl (200 μM). After 2 h, SeMet was the major species present in SeMet samples, and SeTalO was the major species present in SeTal samples. Data represent mean ± SD from 3 independent experiments.

A decrease in NADPH was observed when *N*-chloramines were added to NADPH in the presence of TrxR, Trx and GPx, however, no increase in rates were observed compared to NADPH alone. The presence of SeMet and SeTal reduced the rate at which NADPH was consumed when *N*-chloramines were added to NADPH/TrxR/Trx/GPx. This is attributed to the rapid formation of selenoxides upon addition of *N*-chloramines, followed by slower reduction of SeMetO but not SeTalO.

5.3.2.4 Methionine sulfoxide reductases

The active sites of Msrs contain either a Cys, in the case of MsrA, or Sec, in the case of MsrB2 [109, 592]. As many other thiol and seleno enzymes demonstrate ability to reduce oxidants via reaction with active site thiol and selenol active sites, Msrs may also have some reductase ability. NADPH consumption was monitored by UV-vis spectroscopy at 340 nm when TauCl was added to NADPH/TrxR/Trx/MsrA or MsrB2.

TauCl (200 μM) was added to NADPH (700 μM), TrxR (25 nM), Trx (1.5 μM) and MsrA (95 nM) or MsrB (0.25 μM). The change in absorbance at 340 nm was monitored for 2 h. The rate of NADPH consumption was determined by fitting a straight line to the initial 25 min to the NADPH vs time plot. A time dependent decrease in NADPH was observed upon the addition of TauCl to the Msr systems, yielding a decrease of 94 ± 16 and 87 ± 10 nM s^{-1} in NADPH for the MsrA and MsrB2 systems respectively (Figure 5.36). These changes represent a slight decrease in NADPH consumption rate compared to previous systems examined, though this was not statistically significant from NADPH alone (104 ± 2 nM s^{-1}), or the Trx system (116 ± 6 nM s^{-1}) (Section 5.3.2.2). Similarly, no difference was observed in the total NADPH consumed by the system (Figure 5.37), though total NADPH consumption measured was lower than the concentration of TauCl added, which may be due to the underestimation of NADPH concentrations, discussed in Section 5.3.1.1. This may reflect the inability of the Msrs to increase the rate of TauCl removal. Due to limited supply of the Msr enzymes, the analogous experiments were not performed with LysCl and GlyCl, or *N*-chloramines scavenging by these enzyme systems in the presence of SeMet and SeTal. However, it is anticipated based on previous data presented that the same trend of decreased NADPH consumption in the presence of SeMet and SeTal would occur, as the presence of Msr was unable to increase NADPH consumption over that observed for TrxR in the presence of preformed SeMetO or SeTalO.

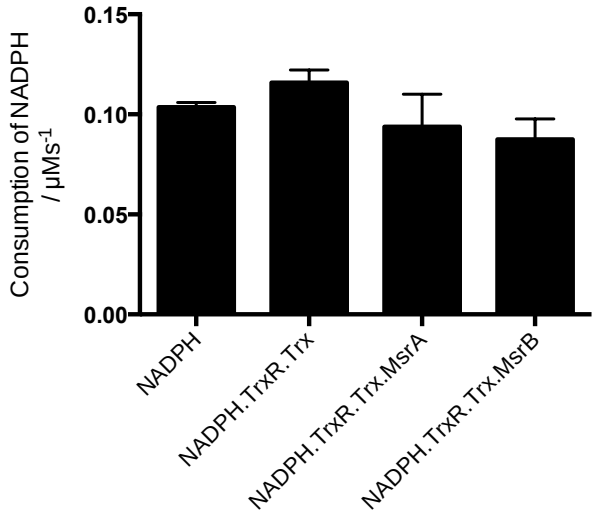

Figure 5.36 - NADPH consumption rates when *N*-chloramines are added to the Msr system.

The UV-vis absorbance of NADPH at 340 nm was monitored after TauCl (200 µM) was added to NADPH (700 µM) ± TrxR (25 nM) ± Trx (1.5 µM) ± MsrA (95 nM) or MsrB2 (0.25 µM). The rate of NADPH consumption was determined by fitting a straight line to the data obtained. N-Chloramine addition caused a loss of NADPH, and no change was observed with the addition of Msrs. Data represent mean ± SD from 3 independent experiments. No significant difference ($p < 0.05$) was observed from control based on one-way ANOVA with Tukey's post-hoc test.

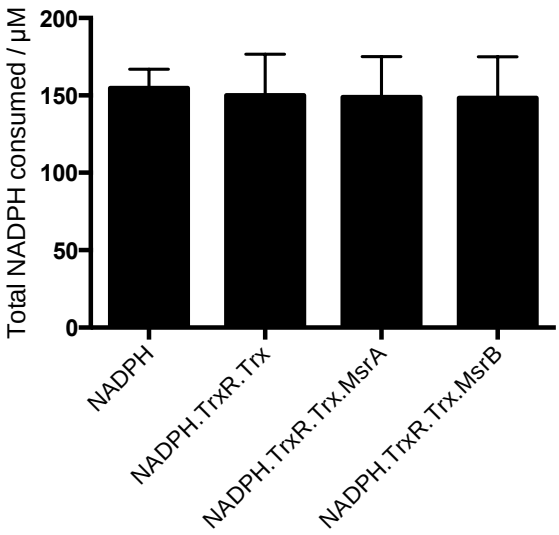

Figure 5.37 – Total NADPH consumed after addition of TauCl to NADPH in the presence or absence of TrxR, Trx and MsrA or MsrB

The UV-vis absorbance of NADPH at 340 nm was monitored after TauCl (200 µM) was added to NADPH (700 µM) ± TrxR (25 nM) ± Trx (1.5 µM) ± MsrA (95 nM) or MsrB2 (0.25 µM). NADPH consumed was determined by the difference in NADPH concentration from the initial reading to 2 h after N-chloramine addition. N-Chloramine addition caused a loss of NADPH, and no change was observed with the addition of Msrs. Data represent mean ± SD from 3 independent experiments. No significant difference ($p < 0.05$) was observed from control based on one-way ANOVA with Tukey's post-hoc test.

5.3.3 Reduction of *N*-chloramines by GSR

N-Chloramines are capable of reacting with GSH to form GSSG [192], which can in turn be reduced by GSR at the expense of NADPH. Therefore, the GSR system should be able to detoxify *N*-chloramines. As SeMet and SeTal react more quickly with *N*-chloramines (Chapter 3), and in turn form selenoxides that react with GSH to form GSSG (Chapter 4), SeMet and SeTal may be able to increase the rate at which the GSR system can detoxify *N*-chloramines. In order to test this hypothesis, NADPH consumption was monsitored by UV-vis absorbance at 340 nm after *N*-chloramines were added to NADPH/GSR/GSH in the presence and absence of SeMet or SeTal.

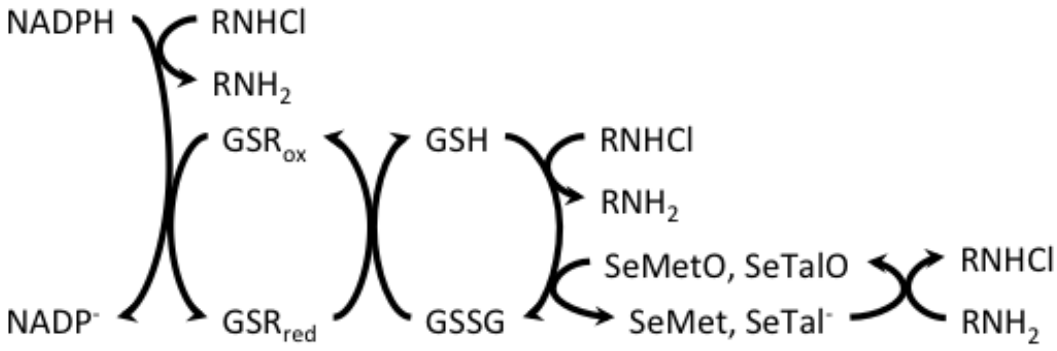

Figure 5.38 – Potential routes of *N*-chloramine consumption upon addition to NADPH/GSR/GSH/SeMet or SeTal

N-Chloramines (200 μM) were mixed with NADPH (500 μM), GSR (25 nM) and GSH (400 μM) in the presence and absence of SeMet or SeTal (20 or 200 μM) using stopped flow apparatus and the absorbance at 340 nm monitored over 1 min (Figure 5.39). A short lag phase in NADPH consumption was observed, which is attributed to the time taken to form GSSG upon addition of oxidant, which is then reduced by GSR. A decrease in NADPH concentration was observed under all conditions. The rate of NADPH consumption was determined by fitting a linear slope to UV-vis data between 2 – 10 s after mixing (Figure 5.40).

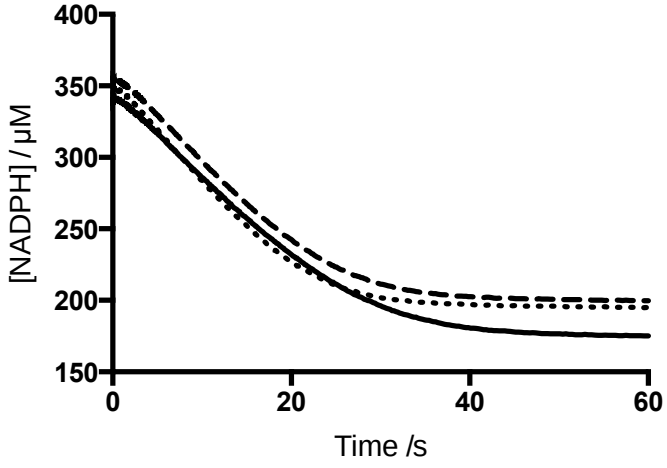

Figure 5.39 – Concentration of NADPH over time after TauCl was added to the GSR system in the presence and absence of SeMet.

TauCl (200 μM) was mixed with NADPH (500 μM), GSR (25 nM) and GSH (400 μM) using stopped flow apparatus in the presence or absence of SeMet (20 or 200 μM). The NADPH concentration, based on absorbance at 340 nm, was monitored for 1 min. The NADPH concentration decreased over time after addition of TauCl consistent with the GSR system detoxifying TauCl.

Addition of TauCl, LysCl and GlyCl (Figure 5.40 a, b and c respectively) showed a decrease in NADPH concentrations at a rate of 6.3 ± 0.2, 7.8 ± 0.2 and 6.9 ± 0.1 μM s^{-1} respectively. Inclusion of lower concentrations of SeMet (20 μM) or SeTal (20 μM) did not significantly effect the rate of NADPH consumption, with NADPH consumption rates of 6.4 ± 0.02, 7.9 ± 0.4 and 7.1 ± 0.1 μM s^{-1} when TauCl, LysCl or GlyCl was added to NADPH/GSR/GSH/SeMet (20 μM) respectively, and 6.0 ± 0.3, 7.4 ± 0.2 and 6.7 ± 0.4 μM s^{-1} when added to NADPH/GSR/GSH/SeTal (20 μM). When higher concentrations of SeMet (200 μM) was present with the GSR system, the rate NADPH consumption was significantly increased to 7.1 ± 0.2 μM s^{-1} upon addition of TauCl. A trend towards an increase in rate was observed with SeTal (200 μM) and TauCl addition though this change was not statistically significant, with an observed NADPH consumption rate of 6.6 ± 0.2 μM s^{-1}. A slight increase in the rate of NADPH consumption was observed in the presence of SeMet (200 μM) or SeTal (200 μM) when GlyCl was added, with rates of 7.5 ± 0.3 and 7.0 ± 0.3 μM s^{-1}, but again this was not statistically significant. The inclusion of SeMet (200 μM) and SeTal (200 μM) did not appear to have any effect on the rate of NADPH consumption when LysCl was added to NAPDH/GSR/GSH in the presence or absence of these compounds, with NADPH consumption rates of 8.1 ± 0.3 and 7.8 ± 0.5 μM s^{-1}. The rate of NADPH consumption by these *N*-chloramines is most likely a reflection of the rate at which these species react with GSH to form GSSG. However, the NADPH consumption rate may also be being limited by the rate at which GSR can reduce GSSG.

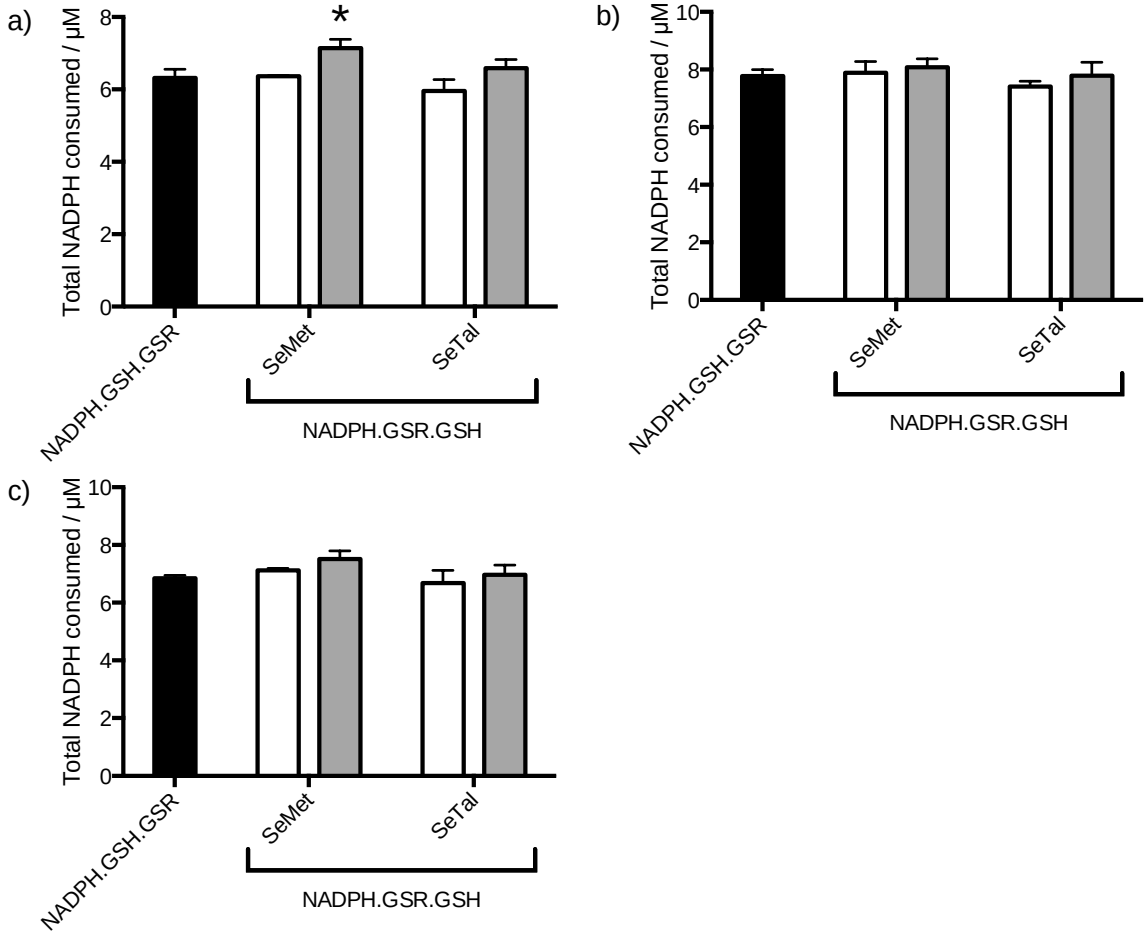

Figure 5.40 – Rate of NADPH consumption after *N*-chloramines were added to the GSR system in the presence and absence of SeMet or SeTal.

*N-Chloramines, a) TauCl, b) LysCl, or c) GlyCl, (200 µM), were mixed with NADPH (500 µM), GSR (25 nM) and GSH (400 µM) by stopped flow apparatus in the presence or absence (black bars) of SeMet or SeTal (20 (white bars) or 200 µM (grey bars)). NADPH concentration, based on absorbance at 340 nm, was monitored for 1 min and the rate of NADPH consumption determined by fitting a linear slope to the slope observed 2 – 10 s after mixing. Addition of N-chloramine caused a decrease in NADPH concentration. 200 µM SeMet increased the rate of TauCl scavenging. No significant difference was observed with any other N-chloramine or SeMet or SeTal concentration. Data represent mean ± SD from 3 independent experiments. * indicates significant difference ($p < 0.05$) from control based on one-way ANOVA with Tukey's post-hoc test.*

In addition to examining the initial rate of NADPH loss, the total amount of NADPH consumed 2 h after the addition of *N*-chloramines was assessed (Figure 5.41). A loss of 172 ± 5, 183 ± 10 and 183 ± 12 µM NADPH was observed 2 h after addition of TauCl, LysCl or GlyCl to NADPH/GSR/GSH, respectively. These values were lower than expected, and attributed to possible impurities in the NADPH, discussed in Section 5.3.1.1. The presence of SeMet (200 µM) demonstrated a very small decrease in total

NADPH consumed compared to the NADPH/GSR/GSH system alone, though this was not statistically significant. The presence of SeTal (20 or 200 μM) reduced the total NADPH consumed upon addition of TauCl (200 μM) compared to the NADPH/GSR/GSH system alone, to 157 ± 2 and 155 ± 4 respectively. The total NADPH consumed upon addition of GlyCl was also reduced by SeTal (200 μM) to 155 ± 9. The total NADPH consumed upon addition of LysCl to the system containing SeTal was also reduced, though this was not significant.

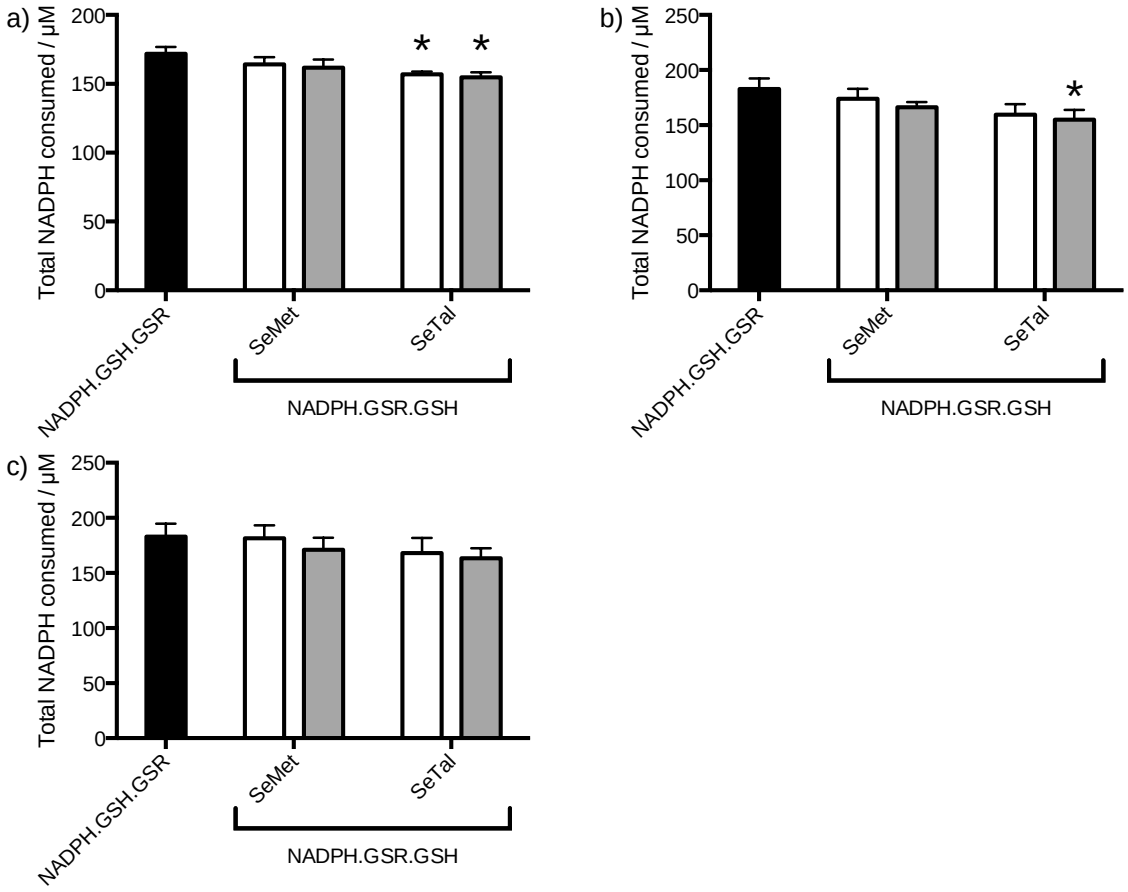

Figure 5.41 – Total NADPH consumption after *N*-chloramines were added to the GSR system in the presence and absence of SeMet or SeTal.

*N-Chloramines, a) TauCl, b) LysCl, or c) GlyCl, (200 μM), were mixed with NADPH (500 μM), GSR (25 nM) and GSH (400 μM) by stopped flow apparatus in the presence or absence (black bars) of SeMet or SeTal (20 (white bars) or 200 μM (grey bars)). NADPH concentration, monitored at 340 nm, was measured for 1 min and the total of NADPH consumption determined by difference of initial and final absorbance observed. The addition of N-chloramine caused a decrease in NADPH concentration. The presence of SeMet did not affect the total NADPH consumed. SeTal reduced total NADPH consumption upon addition of TauCl, and reduced NADPH consumption at 200 μM upon addition of GlyCl. The presence of SeTal did not have an affect with LysCl. Data represent mean ± SD from 3 independent experiments. * indicates significant difference ($p < 0.05$) from control based on one-way ANOVA with Tukey's post-hoc test.*

In parallel with the NADPH consumption experiments, the concentrations of SeMet and SeMetO were assessed by HPLC (Section 2.3.5.4) 10 min after 200 μM TauCl, LysCl and GlyCl were added to NADPH (500 μM), GSR (25 nM), GSH (400 μM) and SeMet (200 μM). For each *N*-chloramine, approximately 200 μM SeMet was observed in the samples (Figure 5.42). No SeMetO was observed in any of the samples after 10 min. This is consistent with the formation of GSSG upon addition of *N*-chloramines, either via selenoxide formation or direct reaction with GSH. The total SeMetO reduced appears to be greater than the amount of NADPH consumed, and this may be due to difficulties with NADPH concentration measurement (see Section 5.3.1.1). Unfortunately, due to interferences in the chromatogram, SeTal and SeTalO levels could not be assessed.

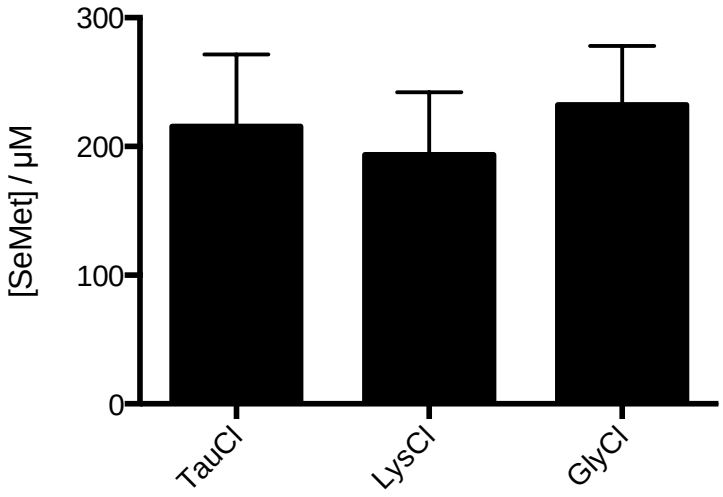

Figure 5.42 – Concentrations of SeMet recovered after *N*-chloramines were added to the GSR system in the presence of SeMet.

TauCl, LysCl and GlyCl (200 μM) were added to NADPH (500 μM), GSR (25 nM), GSH (400 μM) and SeMet (200 μM). The concentration of SeMet was determined after 10 min incubation by HPLC. SeMet (200 μM) was observed in each sample. Data represent mean ± SD from 3 independent experiments.

In summary, the addition of *N*-chloramines to NADPH/GSH/GSR induced a rapid decrease in NADPH concentration. The presence of 200 μM SeMet increased the rate of reduction observed, and a trend to increase was observed when TauCl or GlyCl was added in the presence of SeTal. The proposed mechanism is an initial rapid reaction of *N*-chloramines with SeMet or SeTal to form selenoxides, which then react with GSH to form GSSG and subsequent reduction by GSR. This is in contrast to the TrxR system, with coupled enzymes, where a reduction in the NADPH consumption rate occurs with

the presence of SeMet or SeTal. This is likely due to the reduced rate of selenoxide reduction by the TrxR system compared to the GSR system.

5.3.4 Reduction by J774A.1 cell lysates

As the TrxR and GSR systems demonstrated ability to reduce selenoxides and *N*-chloramines in isolated experiments, their ability to reduce these oxidants in a cell lysate system was investigated. Lysates of J774A.1 cells were prepared by lysing 6 x 10^6 cells in 3 mL ice-cold H_2O and incubating on ice for 15 min. Lysates were centrifuged to remove cellular debris, and the supernatant collected. The protein level was assessed by BCA assay and adjusted to 1 mg protein mL^{-1}.

5.3.4.1 Selenoxides

Lysates (50 μg protein) were incubated with NADPH (500 μM) for 5 min before addition of SeMetO, SeTalO or insulin (200 μM). These experiments were performed in the presence or absence of auranofin (2.5 μM), as auranofin binds to Sec residues inhibiting the function of selenoenzymes, with TrxR being a major target [558]. The addition of auranofin should allow the contribution of the TrxR/Trx system to the overall rate and extent of NADPH loss to be determined. The concentrations of protein in lysates and auranofin used in this study are similar to those used previously [596, 597]. The absorbance of NADPH at 340 nm was monitored for 2 h after the addition of selenoxide or the positive control insulin (Figure 5.43). Rates of NADPH consumption were determined by fitting a straight line to the initial 25 min of the NADPH vs time plot (Figure 5.43).

A decrease of 3 ± 0.4 nM s^{-1} of NADPH concentration was observed in control samples (50 μg lysate and 500 μM NADPH) (Figure 5.43). Addition of SeMetO (200 μM) and SeTalO (200 μM) did not significantly affect the rate of NADPH consumption compared to the control, with NADPH consumption rates of 3 ± 0.5 and 3 ± 0.2 nM s^{-1} respectively. Auranofin had no effect on in the rate of NADPH consumption in either the control (NADPH and lysate alone at 3 ± 0.4 nM s^{-1}) or when SeMetO and SeTalO was added, with rates of 3 ± 0.4 and 3 ± 0.5 nM s^{-1}. Insulin (200 μM) was included as a positive control for TrxR/Trx activity and increased the rate of NADPH consumption over the control to 5 ± 0.4 nM s^{-1}. Treatment of lysates with auranofin slightly decreased the rate of insulin reduction to 4 ± 0.5 nM s^{-1}, though this was not a

significant difference. These data suggest that cell lysates under these conditions are unable to reduce selenoxides, or that the major NADPH consuming reaction are not mediated by the TrxR/Trx system.

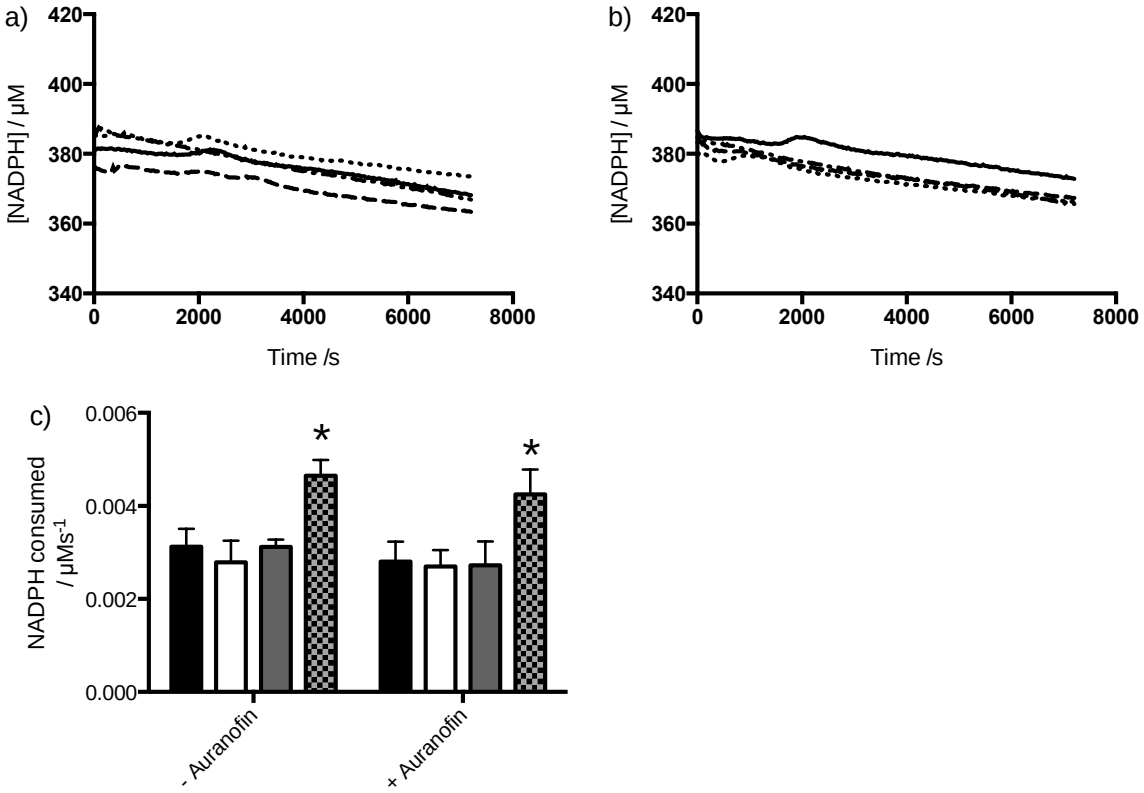

Figure 5.43 – NADPH consumption after selenoxides or insulin were added to cell lysates with or without auranofin.

*NADPH concentration over time when cell lysates (50 µg) with added NADPH (500 µM) (control represented by solid line) were incubated with SeMetO (200 µM) (dashed line), SeTalO (200 µM) (dotted line) or insulin (200 µM) (dot-dashed line) in the a) absence or b) presence of auranofin. Rates of NADPH consumption was determined by fitting a straight line to the data represented in a and b, and represented in c). Control - black bars; SeMetO - white bars; SeTalO - dark grey bars; and insulin - checked bars. Insulin increases the rate of NADPH consumption, however SeMetO and SeTalO did not. Data represent mean ± SD from 3 independent experiments. * indicates significant difference ($p < 0.05$) from control based on one-way ANOVA with Tukey's post-hoc test.*

5.3.4.2 Taurine chloramine

Lysates (50 µg protein) were then incubated with NADPH (500 µM) with and without SeMet or SeTal (20 or 200 µM) for 5 min before addition of TauCl (200 µM). This was carried out in the absence (Figure 5.44a,c) or presence (Figure 5.44b,d) of auranofin (2.5 µM). The absorbance at 340 nm was monitored for 2 h after the addition

of TauCl (Figure 5.44a,b). Rates of NADPH consumption (Figure 5.44c,d) were determined by fitting a straight line to the initial 25 min of the NADPH concentration vs time plot (Figure 5.44a,b).

Addition of TauCl to the cell lysate gave rise to an NADPH consumption rate of 26 ± 0.9 nM s^{-1} (Figure 5.44c). No significant difference in the NADPH consumption rate induced by TauCl was observed when auranofin was pre-incubated with the lysate samples with an NADPH consumption rate of 24 ± 3 nM s^{-1} (Figure 5.44d), which suggests that the NADPH consumption is independent of any selenoenzymes, such as GPx and TrxR as these should be inhibited by auranofin presence. The presence of SeMet (20 μM) or SeTal (20 μM) led to a small decrease in the NADPH consumption to 21 ± 2 and 22 ± 1 nM s^{-1}, though these changes were not statistically significant. The presence of SeMet (200 μM) or SeTal (200 μM) significantly reduced the rate of NADPH consumption to 2 ± 0.6 and 5 ± 5 nM s^{-1}. The addition of auranofin to the lysates again did not demonstrate an effect on the NADPH consumption rate when lysates were exposed to TauCl in the presence of SeMet (200 μM) and SeTal (200 μM). The decrease in rate of NADPH consumption is attributed to the formation of selenoxides, inhibiting direct consumption of NADPH by TauCl.

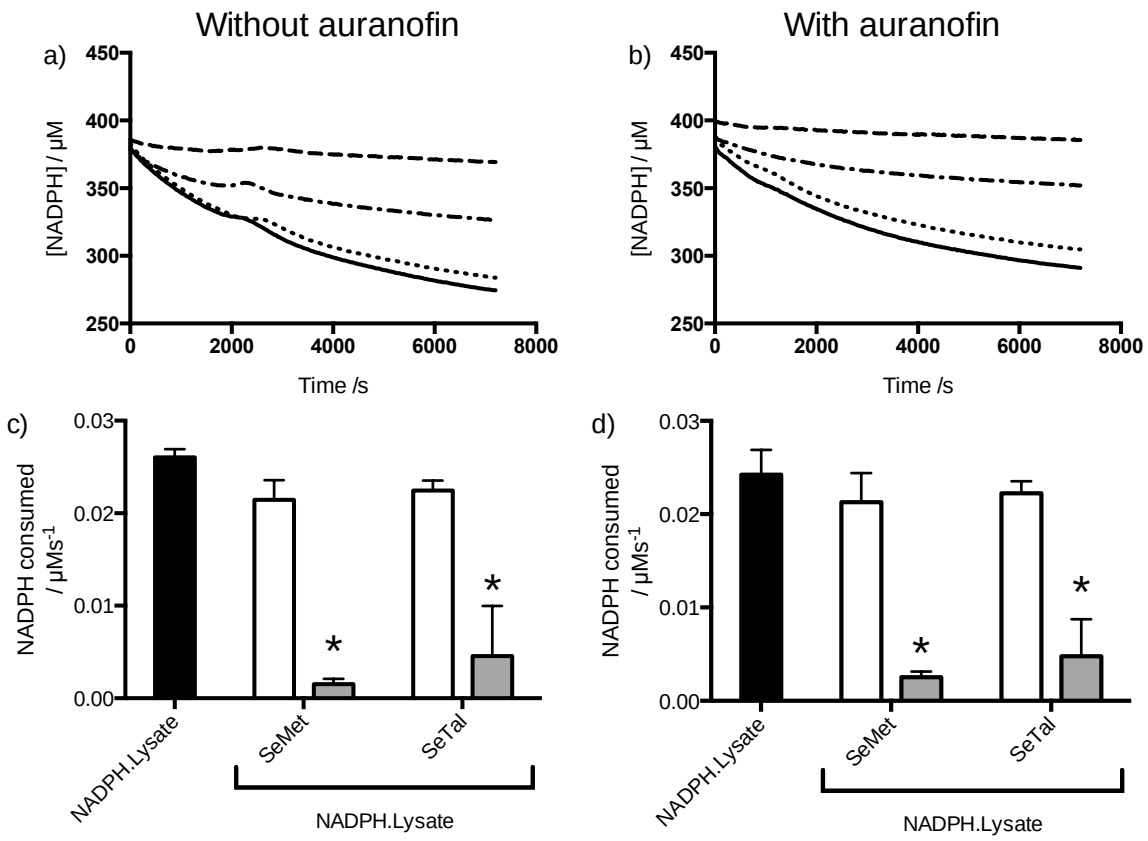

Figure 5.44 – Rate of NADPH consumption after TauCl was added to cell lysates in the presence and absence of SeMet or SeTal

*TauCl (200 µM) was added to cell lysates (50 µg protein) with added NADPH (500 µM) in the presence or absence of SeMet or SeTal (20 or 200 µM). The NADPH concentration, monitored at 340 nm, was measured for 2 h and the rate of NADPH consumption determined by fitting a linear slope to initial 25 min. Addition of TauCl caused a decrease in NADPH concentration. SeMet and SeTal decreased the rate of NADPH consumption, with statistical significance when 200 µM was present. Data represent mean ± SD from 3 independent experiments. * indicates significant difference ($p < 0.05$) from control based on one-way ANOVA with Tukey's post-hoc test.*

5.3.4.3 DTNB

As the cell lysates appeared to be unable to reduce the selenoxides or *N*-chloramines, and auranofin had no effect on insulin reduction, the reduction of DTNB was used as an alternative positive control to ensure activity of the TrxR enzymes in this system. It has been shown previously that the GSR and Trx systems in cell lysates can reduce the colourless DTNB to the yellow TNB, which can be monitored at 412 nm [598, 599]. The contribution of DTNB reduction by the Trx system can be inhibited by the inclusion of auranofin [598, 599].

Cell lysates (50 µg protein) were incubated with NADPH (500 µM) with or without auranofin (2.5 µM) before addition of DTNB (200 µM). The absorbance was monitored at 412 nm for 2 h. The rate of absorbance change was determined by fitting a line to the absorbance vs time plot after the first 15 min, where the rate of absorbance becomes more linear after an initial rapid increase. The change of absorbance occurred at a rate of 0.017 ± 0.001 mAbs units s^{-1} for samples without auranofin. This decreased to a rate of 0.009 ± 0.0003 mAbs units s^{-1} for auranofin treated samples. The ability of the lysates to produce TNB suggests that the lysates used were redox active. Inhibition of TNB production by auranofin demonstrates that selenium enzymes, presumably TrxR, are contributing to TNB formation. However, GPx can also be inhibited by auranofin, which can affect levels of GSH. As GSH can react directly with DTNB, this may also contribute to the TNB formation.

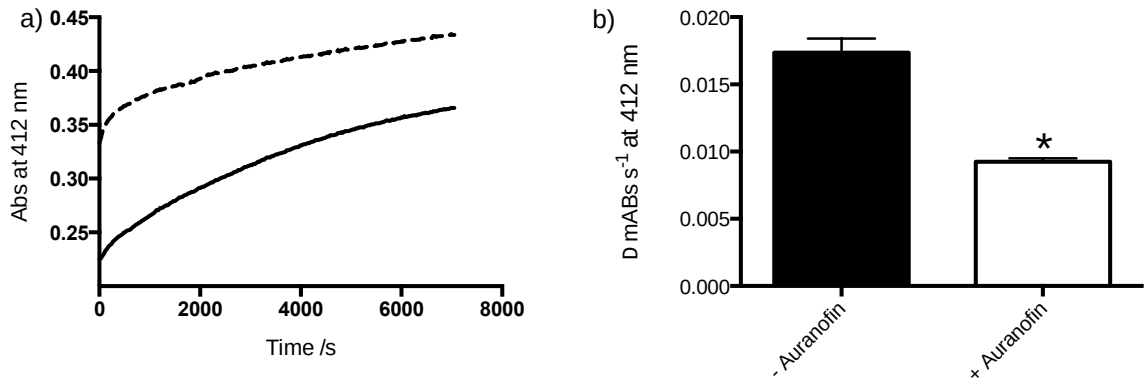

Figure 5.45 – Change in absorbance at 412 nm after DTNB was added to cell lysates with or without auranofin

*DTNB (200 µM) was added to cell lysate (50 µg) with NADPH (500 µM) with or without auranofin (2.5 µM). a) shows absorbance over time after DTNB addition to samples with (dashed line) or without (solid line) auranofin. b) rates of Abs change observed in samples with (black bar) or without (white bar) auranofin. Cell lysates are able to reduce DTNB to TNB, which can be inhibited at least in part by auranofin. Data represent mean ± SD from 3 independent experiments. * indicates significant difference ($p < 0.05$) from control based on unpaired t-test.*

5.4 Discussion

The aims of the experiments performed in this Chapter were to determine whether endogenous antioxidant defence systems could act as a mechanism for the repair of selenoxides, which are the major products formed when SeMet and SeTal react with MPO-derived oxidants. If this repair process is taking place, the interaction between

SeMet and SeTal and these enzymes may represent a potential catalytic scavenging cycle of MPO-derived oxidants *in vivo*. Furthermore, the ability of these enzymes to detoxify *N*-chloramines in the presence and absence of SeMet and SeTal was examined, as thiol and selenium enzymes have demonstrated potential to remove oxidants, including peroxides and HOSCN [98, 347, 348].

The NADPH/TrxR system is capable of reducing SeMetO, but no reduction of SeTalO was observed (Figure 5.10). The inability of TrxR to reduce SeTalO may reflect that SeTalO cannot access the active site of TrxR. However this is unlikely, as the active site of TrxR protrudes from the body of the enzyme on a flexible tail [372], thus accessibility would not be expected to be an issue. It is possible that SeTalO is unable to react with the active site Sec, though as SeTalO is capable of reacting with thiols (see Chapter 4 of this thesis), and selenols are generally considered to have a greater reduction potential than thiols, this explanation also seems unlikely. However, there is no definitive experimental evidence for the reaction of SeTalO with a selenol, though this would be expected to be thermodynamically favourable, as Sec has a higher reduction potential than both GSH and Cys. Thus, it is perhaps more likely that kinetic factors are influencing the reaction and that the rate of reaction is too slow to be relevant under the conditions employed. If the inability of selenoxides to rapidly react with selenols is the cause, it would be anticipated that SeMetO should also be unable to react with the selenol active site. If this is the case, the site of reduction of SeMetO in TrxR may be the N-terminal Cys-X-X-Cys redox centre [372], which SeTalO may not be able to access due to steric considerations.

Trx, in these experiments, was not observed to increase the rate of SeMetO reduction by a NADPH/TrxR/Trx system over that in samples with NADPH/TrxR alone. It has previously been reported that addition of Trx can almost double the rate at which the NADPH absorbance at 340 nm decreased upon addition of SeMetO [474]. However, the previous data were not converted to NADPH consumption rates and cannot therefore be directly compared to the data presented in this Chapter. A key difference that may account for this discrepancy may be that previously 20 μM Trx expressed in E. coli was utilised, compared to 1.5 μM human recombinant Trx used in the current study. 1.5 μM Trx was chosen in these experiments as it best represented the physiological ratio relative to 25 nM TrxR of Trx : TrxR observed in cells [600]. The

increased concentration of Trx used in the studies by Suryo-Rahmanto et al [474] may be sufficient to compete with reduction of SeMetO by TrxR, thereby increasing the rate of reduction compared to the current studies.

Trx, MsrA, MsrB2 and GPx were all unable to increase the rate at which NADPH was consumed upon addition of SeMetO or SeTalO. This may be due to the reduction of TrxR by NADPH being the limiting factor in the reduction cycle, and therefore NADPH consumption is not being increased with the addition of coupled enzymatic systems. Alternatively, the kinetics of the reaction of SeMetO with TrxR may be greater than that observed for the other enzymes, and therefore TrxR preferentially reduces SeMetO directly, and no increase in NADPH consumption is observed. However, it may be a reflection of the inability of SeMetO and SeTalO to oxidise the active site thiols of these other enzymes. This is probably unlikely as the thiols at these sites demonstrate higher reactivity with other oxidants compared to free thiols, which have demonstrated reactivity with selenoxides. Alternatively, it may be a problem of selenoxides accessing the active site, as the active site cysteines are generally buried within protein folds. Again, this is probably unlikely as the selenoxides are comparatively small compared to disulfides formed on protein structures that are the endogenous targets of these enzymes, though other factors such as hydrophilic or hydrophobic interactions, with the protein structure may be affecting the accessibility.

The NADPH/GSR/GSH system was capable of rapidly reducing the SeMetO and SeTalO with 200 μM consumed within 1 min. An initial lag phase was observed, and is attributed to the initial formation of GSSG, by the reaction of the selenoxides with GSH, which is then the species reduced by GSR, which consumes NADPH. A comparison of the observed NADPH consumption rates suggests that selenoxides are more likely to be reduced by the GSR system over the Trx system. As GSH is present in millimolar concentrations in cells [222], compared with much lower levels of enzymes, the GSR route of removal is perhaps the most likely mechanism for selenoxide repair *in vivo*.

The stoichiometry of the reduction of SeMetO and *N*-chloramines does not agree well between UV-vis experiments and HPLC experiments. The HPLC experiments demonstrate near complete reduction of SeMetO, with corresponding recovery of SeMet after 2 h, reflecting a total of 200 μM SeMetO reduced. However, the NADPH consumed as assessed by the extinction coefficient shows less than 200 μM NADPH

consumed, however, the expected ratio would be 1 : 1 for NADPH consumed to SeMetO reduced. It is proposed that the NADPH consumption is being underestimated due to impurities. It was found that the NADPH absorbance at 340 nm was consistently below the expected level based on the mass of NADPH weighed out. This caused an underestimation of NADPH concentration both initially and when the total consumed was calculated. Further experiments would be required, using a more fully characterised NADPH sample, to accurately assess the stoichiometry of the enzymatic reductions observed in this Chapter. Consumption of selenoxides or *N*-chloramines via reaction with amino acid residues may be a possible explanation of the lower than expected NADPH consumption levels, however, this is unlikely. Selenoxides do not appear to react with residues other than Cys based on previous reports [439, 486]. While *N*-chloramines are capable of reacting with other protein residues, a lower than 1 : 1 stoichiometry of NADPH to *N*-chloramine is observed where no protein is present, and therefore reaction with protein residues cannot fully account for the difference. Another possibility is consumption of oxidants by additives in the enzymes solutions, as some of these enzyme solutions contain DTT. When DTT was present, it was removed by solid-phase extraction, though this process may not have been completely efficient. However, this still cannot account for the difference observed when no enzymes were present.

A time-dependent decrease in NADPH concentration was also observed when *N*-chloramines were added to NADPH. Chlorinating oxidants, including HOCl, *N*-chloramides and *N*-chloramines, react with NADPH to form a chlorohydrin product [63, 83, 601-603], though this is a slow process for *N*-chloramines with second order rate constants of about 1 $M^{-1} s^{-1}$ [83]. Previous data have shown that this product cannot be recycled by GAPDH to reform NADPH [603]. The formation of the chlorinated product depletes the NADPH pool making it unavailable for metabolism, thus the formation of the chlorinated nucleoside is considered to be toxic [603].

Selenium and sulfur enzymes have previously demonstrated capability to reduce MPO-derived oxidants [98, 348]. In general, the active site Sec or Cys residue is oxidised, to RSeOH or RSOH respectively, and subsequently reduced via selenosulfide or disulfide exchange mechanisms. As *N*-chloramines have been previously shown to react with thiols [192], it was expected that they would also demonstrate reactivity

with the selenium and sulfur enzymes examined in this study. With the exception of TauCl scavenging by TrxR and Trx, no significant increase in NADPH consumption was observed over control levels when the various enzyme systems were exposed to *N*-chloramines. This may reflect that the rate constants for the reaction of *N*-chloramines with the enzymes are lower than the rate constants for the reaction of the *N*-chloramines with NADPH directly.

There is potential that while no increase in NADPH consumption rates was observed, that the presence of the redox enzymes promoted the formation of $NADP^+$, via the transfer of electrons through the FAD domain of the proteins. $NADP^+$ is a reversible product from which NADPH can be regenerated by the action of enzymes such as GAPDH, as opposed to the chlorohydrin product formed by *N*-chloramine reaction with NADPH, which is irreversible [603]. However, no product studies were performed and the ratios of $NADP^+$ to the chlorohydrin product were not assessed, so further work would be required to demonstrate whether this mechanism is occurring in these systems.

The presence of selenium compounds decreased the rate of NADPH consumption when the NADPH/TrxR system and coupled enzymes were exposed to *N*-chloramines. The rate observed was similar to the rate at which the selenoxides induced NADPH consumption when added directly to the NADPH/TrxR system. Similarly, cell lysates showed a decrease in NADPH consumption in the presence of SeMet and SeTal when exposed to TauCl. This is likely to be due to the rapid formation of selenoxides, as SeMet and SeTal react with *N*-chloramines with rate constants that are 3 orders of magnitude greater than the reaction with NADPH (Chapter 3 of this thesis; [83]). This is supported by the observation of high levels of selenoxides present 20 min after *N*-chloramine addition, which then reduces over the course of 2 h for SeMetO. While the rate of oxidant removal by the Trx system in the presence of SeMet and SeTal was reduced, the reaction product is likely to be $NADP^+$ and not chlorohydrins, due to transfer of electrons through the protein chain, as opposed to chlorination of NADPH by *N*-chloramines. As $NADP^+$ is recyclable through the actions of enzymes such as GAPDH, and the chlorohydrin product is not, this presumably will result in a better outcome in the context of cells. However, studies on NADPH products were not performed, so this proposed switch in mechanism could not be confirmed.

The NADPH/GSR/GSH system demonstrated a more rapid consumption of NADPH upon the addition of LysCl than GlyCl or TauCl. This trend is consistent with the second order rate constants determined for the reaction of GSH with these *N*-chloramines, with LysCl having the highest rate constant, followed by GlyCl and TauCl [192]. SeMetO and SeTalO have rate constants for reaction with GSH significantly higher than those reported for *N*-chloramines (Table 5.1), however, GSR was not able to remove these selenoxides significantly faster than LysCl or GlyCl. Based on the rate constants reported for the reaction of LysCl and GlyCl with GSH, and those reported in Chapter 3 for the reaction with SeMet and SeTal (Table 5.1), it would be expected that in the presence of 200 μM SeMet or SeTal, the majority of *N*-chloramine would be reacting with the selenium compounds as opposed to directly with the GSH. At lower concentrations of SeMet and SeTal, the direct reaction between the *N*-chloramines and GSH would be favoured. The increased rate of GSSG production would be expected to result in an increased rate of NADPH consumption, though this was not observed. This may be because LysCl, GlyCl and the selenoxides produce GSSG at a rate that saturates the GSR activity.

The presence of SeMet when the GSR system was exposed to TauCl increased the rate of NADPH consumption. This is likely due to the rapid reaction of TauCl with SeMet and subsequent reduction, therefore producing GSSG at a faster rate than TauCl alone. A significant increase in NADPH consumption rate was not observed when SeTal was present, and this may reflect the lower rate of reaction of SeTal with TauCl, as well as the slower reduction of SeTalO by GSH.

Table 5.1 – Comparison of second order rate constants for the reaction of *N*-chloramines and selenoxides with GSH, SeMet and SeTal

Oxidant	k_{GSH} / $M^{-1}s^{-1}$	k_{SeMet} / $M^{-1}s^{-1}$	k_{SeTal} / $M^{-1}s^{-1}$
TauCl	115[a]	820 [c]	115 [c]
LysCl	259[a]	3400 [c]	680 [c]
GlyCl	228[a]	2300 [c]	430 [c]
SeMetO	1.5×10^4 [b]	-	-
SeTalO	3.4×10^4 [b]	-	-

[a] Peskin, A et. al. [192]; [b] Chapter 4 of this thesis; [c] Chapter 3 of this thesis

The ability of other selenium compounds, such as ebselen and selenocystamine, to enhance oxidant scavenging has previously been reported, though these function via a different mechanism to that discussed here [492, 589, 590]. It is proposed that the redox enzymes reduce the diselenides or ebselen to a selenol group, which then rapidly reacts with the oxidant to reform the parent compound [492, 589, 590]. Ebselen was more effective at oxidant removal in conjunction with the Trx system compared to the GSR system [589], while the opposite was observed for SeMet and SeTal. This is consistent with the differing mechanism proposed for SeMet and SeTal, where the parent species react directly with the oxidant to form selenoxides, followed by reduction by the enzymes or GSH to reform the parent compound.

Cell lysates did not show an increase in NADPH consumption upon addition of SeMetO or SeTalO. This suggests that enzymatic systems present in these preparations are not recycling the selenoxides efficiently as would be expected by the isolated enzyme results when compared to other NADPH consuming reactions. Enzymes such as TrxR and Trx, while expressed in this cell line [599], may not be expressed at a high enough level to enhance the rate of NADPH consumption when selenoxides are added to the lysates. This may also be the case for insulin reduction, where the increase in the rate of NADPH consumption upon addition of insulin was not significantly inhibited by auranofin as expected. The inability of auranofin to inhibit NADPH consumption in the presence of insulin suggests that NADPH consumption is not due to seleno enzymes as expected. This is in contrast to the DTNB reduction results which demonstrate that

there is some activity of seleno enzymes observed in the lysates as they are capable of reducing DTNB to TNB in a manner that is inhibited by the presence of auranofin. Based on these results, it cannot be discounted that the selenoxides may be reduced by a different mechanism when added to the cell lysates, however, as the concentrations of selenoxides were not measured after exposure to the lysates, so it is unclear whether this could be the case.

5.5 Conclusions

N-Chloramines, MPO-derived oxidants, and selenoxides, the major product formed when selenoethers react with MPO-derived oxidants, can be reduced by the endogenous antioxidant systems NADPH/TrxR and NADPH/GSR/GSH. Furthermore, selenoethers showed the ability to increase NADPH consumption when *N*-chloramines were added to the NADPH/GSR/GSH system, however, SeMet and SeTal reduced the rate at which NADPH was consumed after the addition of *N*-chloramines to the NADPH/TrxR system. Together, the endogenous antioxidant defence systems and the selenoethers, SeMet and SeTal, may be capable of catalytically removing MPO-derived oxidants, preventing oxidative damage and having a therapeutic benefit.

6 Selenium compounds modulating MPO-derived oxidant damage in cells

6.1 Introduction

Macrophages are a key cell type in the initiation and progression of atherosclerosis [274]. They are responsible for the uptake of LDL in the arterial wall with increased uptake occurring after LDL is modified by oxidants [294, 301]. The increased LDL uptake coupled with impaired cholesterol efflux after macrophages are exposed to oxidants induces the formation of foam cells [297, 300]. Accumulation of foam cells is the initial event in the development of fatty streaks in the arterial wall, leading to the development of atherosclerotic plaques [274]. As such, J774A.1 cells, a murine macrophage-like cell line, were chosen for the studies presented in this chapter.

Exposure of cells to high doses of HOCl, including J774A.1 murine macrophages, causes cell death by lysis [221]. The primary cause of lysis is thought to be via modifications to membrane proteins, particularly K^+ pumps [220], which cause cell swelling, or cross linking of membrane proteins causing morphological changes [213, 219]. Lower doses of HOCl can also cause cell death by apoptosis [222]. HOCl treatment has been shown to induce apoptosis in a range of different cell types, with cytochrome *c* release from mitochondria and caspase activation [604-606]. Chloramines are also capable of causing apoptosis through caspase activation leading to cell death [607-609].

HOCl and chloramine treatment causes loss of cellular thiols [162, 221, 222, 225]. HOCl causes a decrease in GSH and total cellular thiols of J774A.1 cells, with a concomitant increase in GSSG [222]. Erythrocytes and endothelial cells treated with HOCl also demonstrate a loss of GSH with a corresponding increase in GSSG [221, 225, 226]. The thiol dependent enzyme glyceraldehyde phosphate dehydrogenase (GAPDH) is a specific target of both HOCl and *N*-chloramines [229]. Exposure of cells to HOCl and model chloramines results in thiol loss and a decrease in GAPDH activity [245], with the extent of thiol loss and GAPDH inactivation induced by *N*-chloramines depending on cell permeability [135]. While TauCl is efficient at inhibiting isolated GAPDH [245], it was unable to affect GAPDH function in HUVECs as it is cell impermeable [135, 246]. However, in the presence of other amines, transchlorination can occur, forming membrane permeable chloramines that can inhibit GAPDH [135]. Numerous other thiol dependent enzymes have been shown to be inhibited on exposure to HOCl and

chloramines including creatine kinase, glutathione *S*-tranferases and membrane ATPases [220, 225, 229, 233].

HOCl and TauCl also react with other protein residues including Met, Tyr and Trp [180]. HOCl and TauCl react with Met residues to form MetSO, which can result in enzyme inhibition [111]. HOCl also reacts with Tyr and Trp residues to form chlorinated products [120, 121, 129, 296]. Chloramines have been shown to mediate Tyr chlorination, though this reaction is slow [121]. These modifications can lead to protein inactivation depending on the site of oxidation, as well as protein cross-linking and aggregation [40, 106]. HOCl is capable of oxidising Met and Trp residues on proteins within cells [220].

Selenium-containing compounds rapidly scavenge HOCl and *N*-chloramines forming selenoxides as the major product (dependent on oxidant concentrations), which can be then recycled by cellular reductants such as GSH [444, 445] (See also Chapters 4 and 5). Thus, antioxidant supplementation with SeMet and SeTal may be an effective strategy in reducing oxidative damage to cells exposed to MPO-derived oxidants. Selenium compounds can react directly with oxidants, and have also demonstrated an ability to upregulate cellular antioxidant enzymes in order to protect against oxidative damage [524-526]. Supplementation of trophoblast cells with SeMet protected against H_2O_2 induced damage [531] or oxidative stress induced by the disruption of mitochondria with antimycin or rotenone [530]. SeMet has also demonstrated efficacy in protecting J774A.1 cells and erythrocytes from H_2O_2 and *t*-butylhydroperoxide induced damage [474, 538]. Isolated protein studies have demonstrated SeMet and SeTal are capable of protecting protein residues from oxidation by HOCl by acting as a direct antioxidant [439, 486]. However, the use of SeMet and SeTal as an antioxidant protecting against MPO-derived oxidants in a cellular context has not yet been explored.

As demonstrated in Chapter 3, SeMet and SeTal react rapidly with HOCl and TauCl and may provide a competitive target for oxidants in a cellular context. The data presented in Chapters 4 and 5 demonstrate the potential for catalytic scavenging cycles, where selenoxides are reduced by endogenous antioxidant systems, leading to an enhanced removal of oxidants. Together, these data suggest that SeMet and SeTal

may be capable of providing cells with protection against cellular damage caused by MPO-derived oxidants.

6.2 Aims

This chapter examines a variety of markers of oxidative consequences arising from the exposure of J774A.1 cells to HOCl and TauCl, including apoptosis and cell death, thiol loss and thiol-dependent enzyme activity, and the oxidation status of amino acid residues in the presence or absence of SeMet and SeTal, to assess the ability of these compounds to modulate cellular damage.

6.3 Results

6.3.1 Cell viability in the presence of SeMet and SeTal

Initial studies were performed to examine the viability of J774A.1 cells when exposed to SeMet and SeTal in the absence of oxidant treatment, as previous studies have shown that SeMet can be toxic under certain conditions [513, 610]. J774A.1 cells were plated at a density of 5 x 10^5 cells mL^{-1} and exposed to increasing concentrations of SeMet or SeTal in HBSS (0 – 200 μM) for 30 min, prior to assessing the viability using the LDH assay (Figure 6.1). No change in viability was observed compared to the control (0 μM SeMet or SeTal) with increasing concentrations of selenium compounds. This suggests that concentrations of up to 200 μM SeMet and SeTal can be tolerated by J774A.1 cells under the conditions employed.

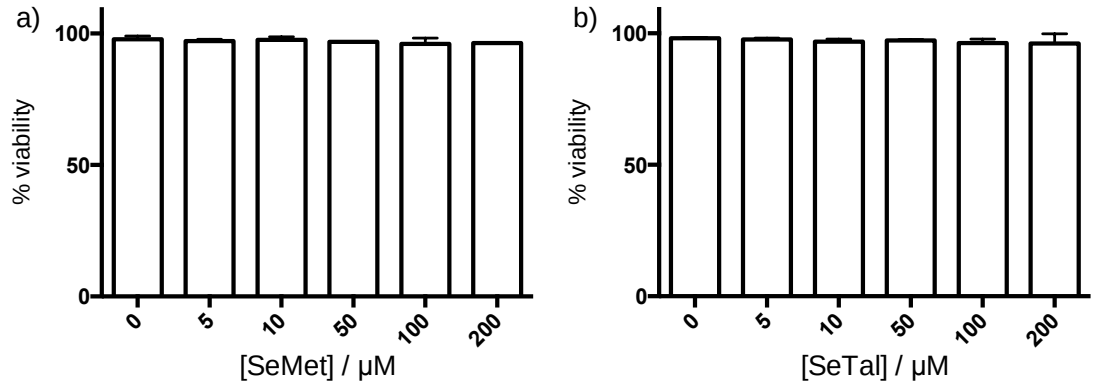

Figure 6.1 – J774A.1 cell viability after supplementation with SeMet or SeTal (0 – 200 µM)

J774A.1 cells were plated at 5 x 10^5 cells mL^{-1} in a 12-well plate and allowed to adhere overnight. Cells were washed with warm HBSS before incubation with SeMet or SeTal (0 – 200 µM) in HBSS for 30 min at 37 °C. Media was collected and cells washed with HBSS before lysis in 600 µL H_2O. LDH activity in media and lysate samples was measured and normalised to protein levels assessed by BCA assay. The viability ratio was determined by LDH activity in the lysate over the total LDH activity. No significant difference from control (0 µM SeMet or SeTal) was observed based on one-way ANOVA with Tukey's post-hoc test. Results are reported as mean ± SD, n = 3.

6.3.2 Cellular thiol levels after oxidant treatment

HOCl and TauCl treatment of cells is known to reduce intracellular thiol levels [162, 221, 222, 225]. As SeMet and SeTal may provide a competitive target for these oxidants in a cellular context, based on results from Chapter 3, supplementation of cells with SeMet and SeTal prior to oxidant treatment may be beneficial. The ability of SeMet and SeTal to modulate cellular thiol loss was assessed using the ThioGlo-1 assay.

6.3.2.1 Intact cells

J774A.1 cells were incubated with SeMet or SeTal (0 - 50 µM) in HBSS for 15 min at 37 °C before addition of HOCl or TauCl (200 µM) and further incubation for 15 min at 37 °C. Cells were lysed in 600 µL H_2O and thiol levels determined by the ThioGlo-1 assay. In each case, thiol levels were normalised to protein concentration as assessed by the BCA assay.

Initial studies were performed to determine the effect of SeMet and SeTal (50 µM) on cellular thiol levels in the absence of oxidant. A trend towards a decrease in thiol levels was observed on incubation of J774A.1 cells with SeMet and SeTal, though this

change was not statistically significant, and is potentially due to increase production of reactive oxygen species by the cell [513]. Next, experiments to measure thiols after cells were exposed to HOCl and TauCl were performed. HOCl treatment of cells reduced the thiol levels to 52% of the non-treated control values (Figure 6.2a,c). TauCl treatment reduced thiol levels to a similar extent (Figure 6.2b,d).

Experiments were then performed to determine whether pre-treatment of cells with SeMet or SeTal could modulate the levels of thiols after oxidant treatment. However, the presence of SeMet (Figure 6.2a) or SeTal (Figure 6.2c) did not significantly reduce thiol loss compared to that observed with HOCl alone. Similarly, no significant difference was seen between the thiol levels in cells exposed to TauCl alone, or TauCl in the presence of SeMet (Figure 6.2b) or SeTal (Figure 6.2d). This may reflect the formation of selenoxides following HOCl and TauCl oxidation of SeMet or SeTal, which can subsequently react with thiols, as demonstrated in previous Chapters.

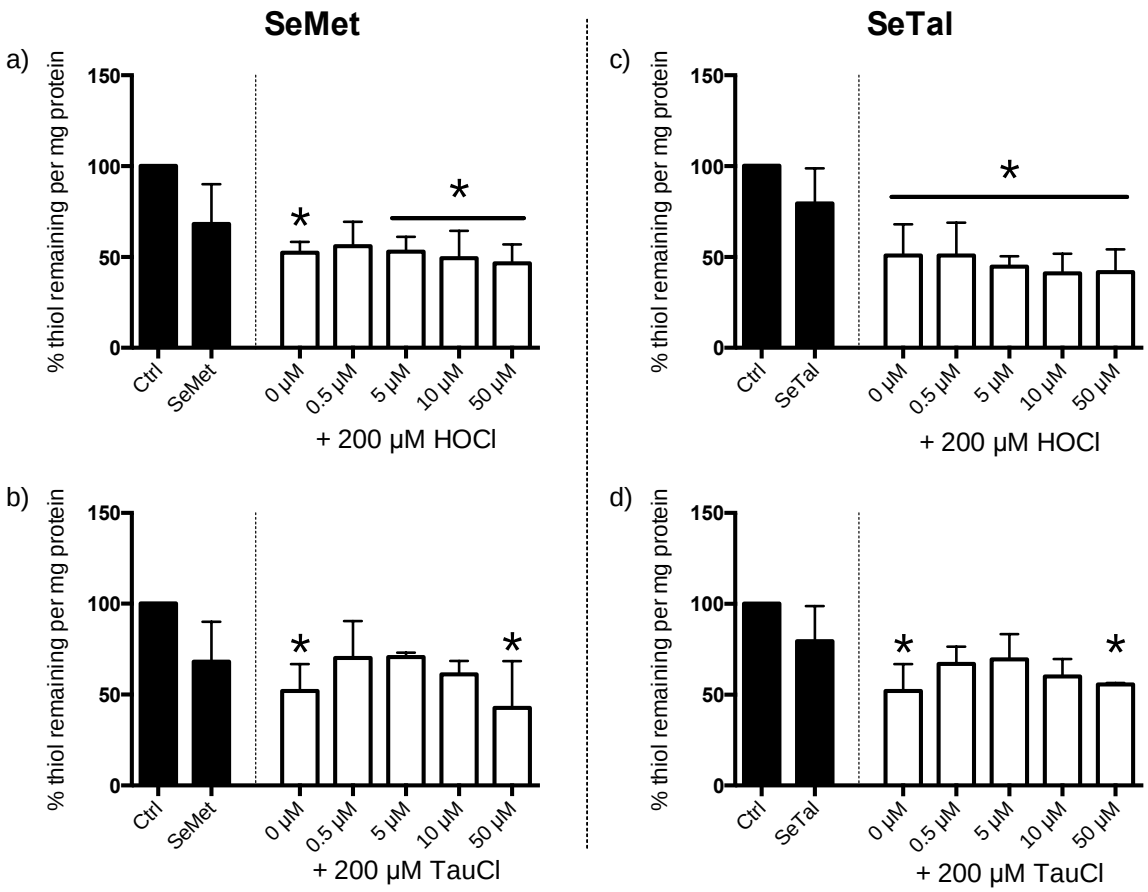

Figure 6.2– Thiol levels after J774A.1 cells treated with HOCl or TauCl in the presence of SeMet or SeTal.

*J774A.1 cells (5 x 10^5 cells per well) were incubated with SeMet (a,b) or SeTal (c,d) (0 - 50 µM) in HBSS for 15 min at 37 °C before addition of HOCl (a,c) or TauCl (b,d) (200 µM) and further incubation for 15 min at 37 °C. Non-treated cells and cells treated with SeMet or SeTal alone (50 µM) were included as control samples (black bars). Cells were lysed in 600 µL H_2O and thiol levels determined by ThioGlo-1 assay, and thiol levels normalised to protein assessed by the BCA assay. A decrease in thiol levels was observed with HOCl and TauCl treatment. No significant difference was observed in thiol levels between cells treated with HOCl or TauCl alone and those treated with HOCl and TauCl in the presence of SeMet or SeTal. * indicates significant difference ($p < 0.05$) from untreated control levels based on one-way ANOVA with Tukey's post-hoc test. Data are reported as mean ± SD from 3 independent experiments.*

6.3.2.2 Cell lysates

SeMet and SeTal did not appear to have an effect on cellular thiol levels when whole cells were exposed to oxidants, however, it was unclear how rapidly and to what extent the SeMet and SeTal were taken up by the cells. As such, lysate experiments were performed in order to determine the effects of oxidants and SeMet and SeTal on thiol levels in the absence of an intact cell membrane.

J774A.1 cells were lysed in H_2O and the lysates adjusted to 1 mg mL^{-1} protein assessed by the BCA assay. The lysates were then supplemented with SeMet or SeTal (0 - 25 μM) before addition of HOCl or TauCl and incubation for 15 min at 22 °C. Thiol levels were assessed by ThioGlo-1 assay. As the thiols in the lysate samples are (presumably) more accessible to oxidants than in intact cells, experiments were performed to optimise the level of oxidant added in each case. Lysates were therefore incubated with increasing HOCl or TauCl (0 – 200 μM) for 15 minutes, before thiol levels were determined by the ThioGlo assay. At 12.5 μM HOCl or TauCl a 92 % loss of thiols compared to the non-treated control was observed (Figure 6.3). Experiments with higher concentrations of HOCl or TauCl resulted in complete thiol consumption. Therefore, 12.5 μM oxidant was used for subsequent experiments.

The addition of SeMet or SeTal (25 μM) to the lysate in the absence of oxidant did not significantly change the thiol levels from that observed in the untreated control lysate samples (Figure 6.3). Addition of HOCl or TauCl (12.5 μM) reduced the thiol concentration by 92 % compared to the non-treated control samples, and a similar extent of thiol loss was seen in the presence of SeTal (Figure 6.3c,d). However, in the presence of SeMet (Figure 6.3a,b) a trend towards a further decrease in thiols compared to HOCl or TauCl alone was observed, though this was not statistically significant. This is attributed to the formation of selenoxides and subsequent reaction with residual cellular thiols. The further decrease observed in the SeMet treated samples may reflect the increased rate of reaction of SeMet with HOCl or chloramines compared to SeTal, resulting in a higher SeMetO yield, causing a greater reduction in thiol levels observed.

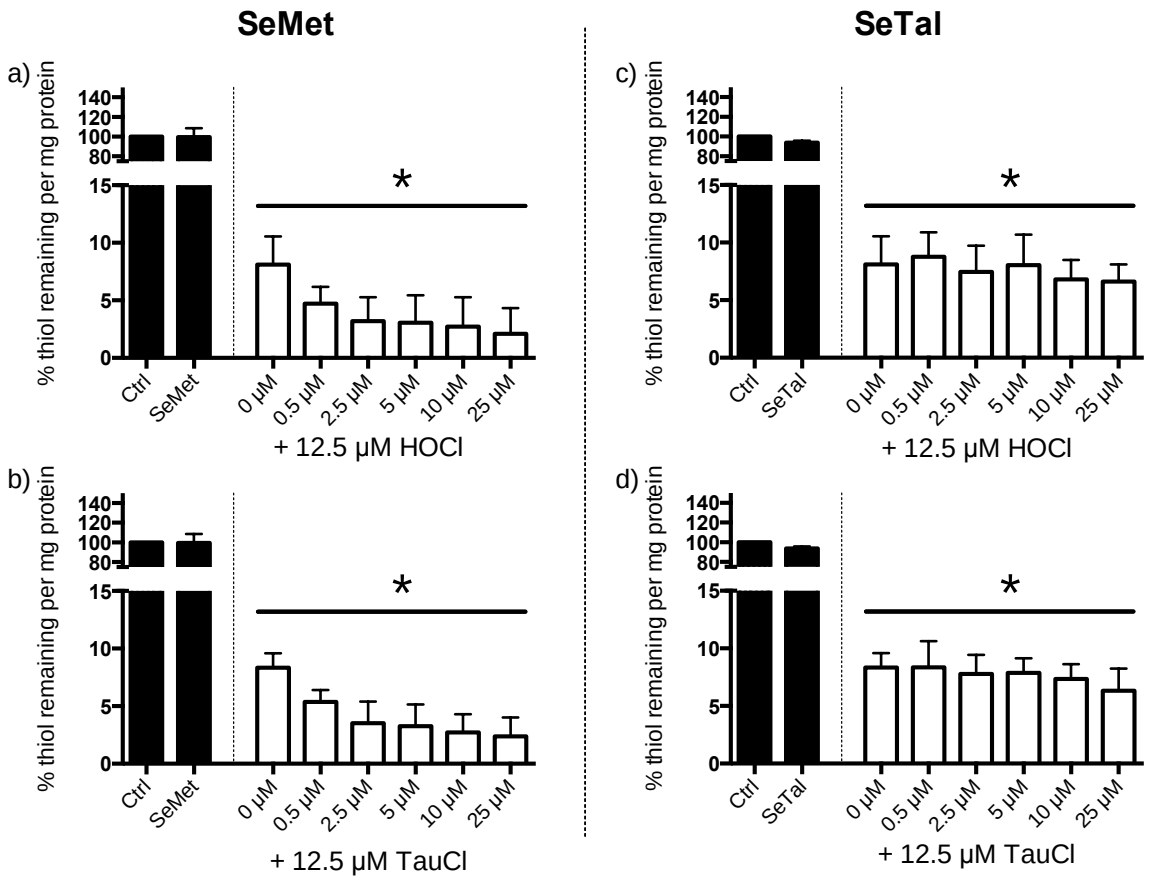

Figure 6.3 - Thiol levels in lysates after HOCl or TauCl treatment in the presence or absence of SeMet or SeTal

*J774A.1 cells were lysed in H_2O and the lysates adjusted to 1 mg mL^{-1} protein assessed by the BCA assay. Lysates were then supplemented with SeMet or SeTal (0 - 25 µM) before addition of HOCl or TauCl (12.5 µM) and incubation for 15 minutes at 22 °C. Non-treated lysates and lysates treated with SeMet or SeTal alone (50 µM) were included as control samples (black bars). Thiol levels were assessed by ThioGlo-1 assay. HOCl and TauCl decreased the thiol concentration by 92 % of that seen in the non-treated control. No significant difference was observed in thiol levels between lysates treated with HOCl or TauCl alone and those treated with HOCl and TauCl in the presence of SeMet or SeTal. Data represent mean ± SD from 3 independent experiments. * indicates significant difference ($p < 0.05$) from untreated control levels based on one-way ANOVA with Tukey's post-hoc test.*

6.3.3 Cellular GAPDH activity after oxidant treatment

As total cellular thiols were reduced by HOCl and TauCl oxidant exposure, the activity of the thiol-dependent enzyme GAPDH was examined. GAPDH is a thiol dependent enzyme that catalyses the conversion of glyceraldehyde-3-phosphate (GAP) to glycerate-1,3-biphosphate (GBP), a step in the glycolysis pathway essential for glucose metabolism and energy production [230]. GAPDH has a thiol at the active site

and is readily inactivated when cells are treated with HOCl and TauCl [245]. The ability of SeMet and SeTal to prevent GAPDH inactivation was therefore assessed.

J774A.1 cells were incubated with SeMet or SeTal (0- 50 μM) in HBSS for 15 min at 37 °C before addition of HOCl or TauCl (200 μM) and further incubation for 15 min at 37 °C. Cells were washed with warm HBSS before lysis in 600 μL H_2O and the measurement of GAPDH activity. GAPDH activity was measured by the increase in NADH concentration after addition of NAD^+ and GAP (as assessed by optical absorbance at 340 nm) with the values normalised to the protein levels (as assessed by BCA assay).

Initial experiments examined the effect of SeMet and SeTal (50 μM) on GAPDH activity in cells (Figure 6.4). A decrease in GAPDH activity was observed in the presence of SeMet alone, though this was not statistically significant. A slight decrease in GAPDH activity in the presence of SeTal was also observed, though this decrease was not as large as that observed with SeMet treatment. This compares well to the extent of loss in total cellular thiols (Figure 6.2).

Treatment of cells with HOCl (200 μM) in the absence of SeMet or SeTal resulted in a significant decrease in GAPDH activity (Figure 6.4a,c) as previously reported [222]. A comparable loss in GAPDH activity was observed on treatment of the cells with TauCl (Figure 6.4b,d), in contrast to previous reports with other cell types [135, 246]. In general, the presence of SeMet and SeTal did not prevent the loss of GAPDH activity. However, a significant increase in GAPDH activity, consistent with prevention of HOCl-induced damage, was seen on pre-treatment of cells with 10 μM SeMet before addition of HOCl (Figure 6.4a).

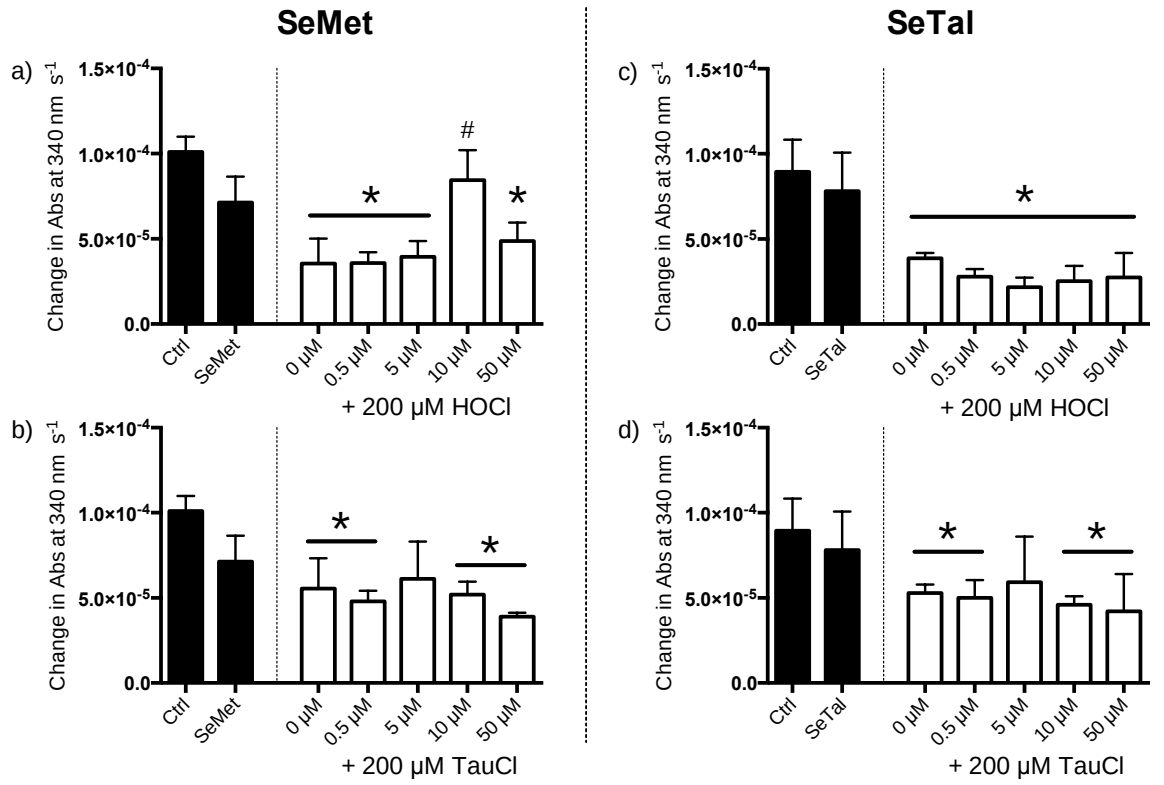

Figure 6.4 – GAPDH activity after J774A.1 cells were treated with HOCl or TauCl in the presence of SeMet or SeTal

*J774A.1 cells (5 x 10^5 cells per well) were incubated with SeMet (a,b) or SeTal (c,d) in HBSS (0- 50 µM) for 15 min at 37 °C before addition of HOCl (a,c) or TauCl (b,d) (200 µM) and further incubation for 15 min at 37 °C. Non-treated cells and cells treated with SeMet or SeTal alone (50 µM) were included as control samples (black bars). Cells were lysed in 600 µL H_2O and GAPDH activity measured by monitoring the increase of NADH at 340 nm after addition of NAD^+ and GAP to the lysates, normalised to protein concentration. Treatment of cells with HOCl or TauCl reduced GAPDH activity levels. Presence of 10 µM SeMet increased GAPDH activity levels back to control, however no effect was seen with TauCl treated cells or any other concentration of SeMet or SeTal. Data represent mean ± SD from 3 independent experiments. * indicates significant difference ($p < 0.05$) from untreated control levels, and # indicates significant difference from HOCl treated cells in the absence of SeMet ($p < 0.05$) based on one-way ANOVA with Tukey's post-hoc test.*

6.3.4 Reversible thiol oxidation

In general, the data presented above are consistent with a lack of protection of thiols by SeMet and SeTal on exposure of macrophages to HOCl or TauCl. However, in the experiments reported above, the nature of the oxidised thiol products was not examined. Oxidation of thiols by HOCl and TauCl can give rise to numerous oxidation products, some of which are irreversible [95]. If HOCl and TauCl react with SeMet or SeTal, it would be expected that selenoxide species would be formed. Selenoxides

should give rise to disulfides as oxidation products upon reaction with thiols [444, 445]. As disulfides are reversible oxidation products, the ability of SeMet and SeTal to promote reversible thiol oxidation was assessed by using the thiol-specific probe IAF after SDS-PAGE to separate cellular proteins.

J774A.1 cells were incubated with SeMet or SeTal (0- 50 μM) in HBSS for 15 min at 37 °C before addition of HOCl or TauCl (200 μM) and further incubation for 15 min at 37 °C. Cells were lysed in the presence of NEM (100 mM) to alkylate any remaining free thiols after oxidant exposure. Reversibly oxidised thiols were reduced by addition of DTT (1 M), before the subsequent addition of IAF to fluorescently label the newly reduced thiol-containing proteins. The IAF labelled proteins were run out on 4-12% Tris-acetate gels and the proteins visualised by fluorescence (λ_{ex} = 495 nm; λ_{em} = 520 nm). Proteins were subsequently stained with Coomassie or silver stain and the fluorescent band density normalised to protein loading based on the total protein staining of 3 separate protein bands (Figure 6.5).

Protein loading ratios were determined by densitometric analysis of 3 bands on the protein stained gels, with the most intense bands selected for protein loading determination. The relative loading of each lane was determined by densitometric analysis of the bands, which were averaged before expressing values as protein loading relative to the non-treated control for the lane. The ratio of bands within the same lane to each other remained consistent across all treatments, suggesting the only difference between lanes should be due to protein loading. However, it is difficult to draw conclusions from these data owing to some discrepancies in the amount of protein loaded that is reflected in the Coomassie stained gels (Figure 6.5a,c). The inconsistent protein loading also made it difficult to attribute differences in IAF fluorescence in samples to changes in reversible thiol levels (Figure 6.5b,d). These difficulties stemmed from redissolving the precipitated protein from the wash steps required for IAF staining. Further method optimisation to ensure equal protein loading before determination of whether SeMet and SeTal can promote irreversible thiol oxidation is needed, but was beyond the scope of this thesis.

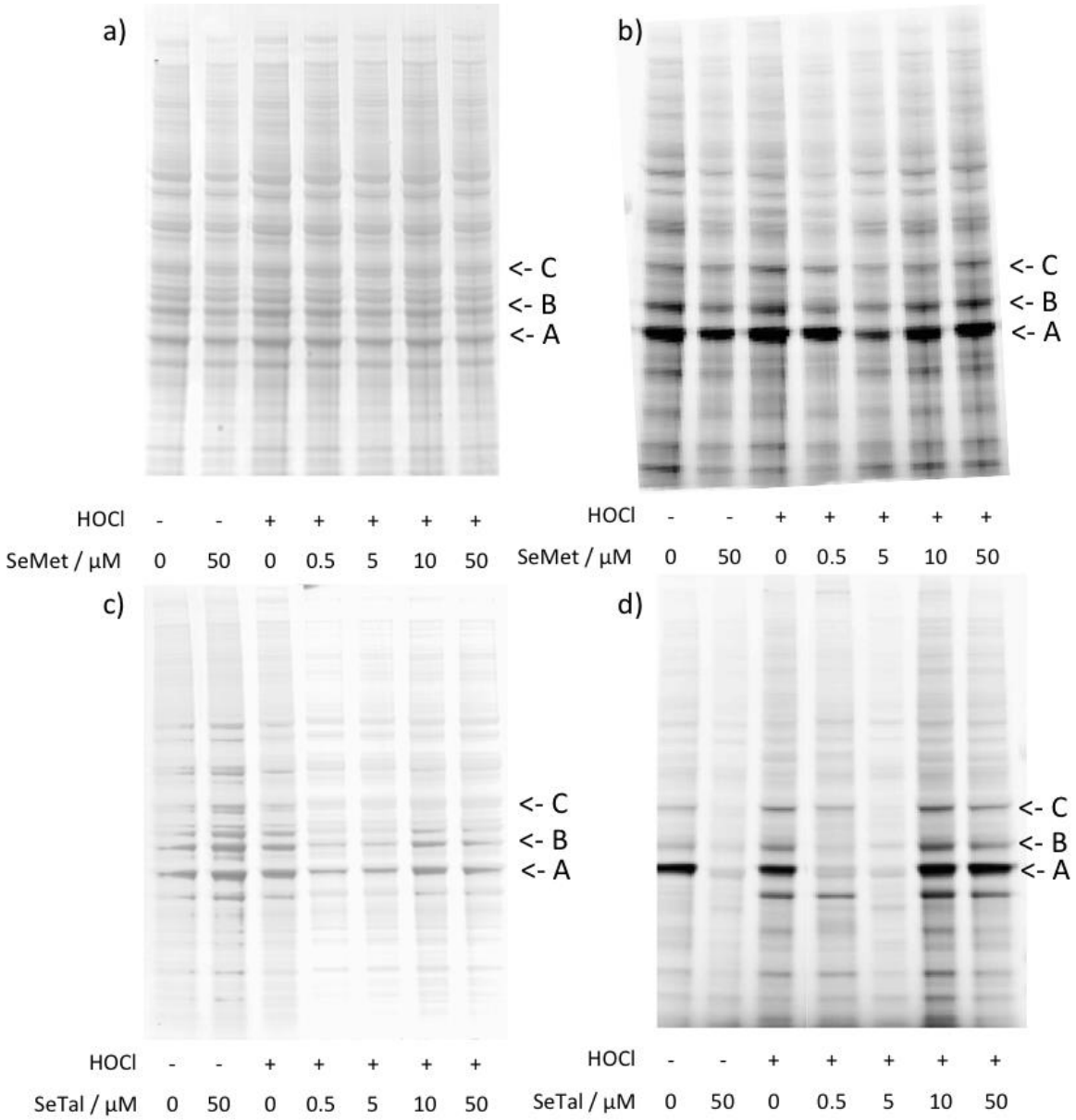

Figure 6.5 – Representative gels showing protein loading and IAF stained reversible thiol products

J774A.1 cells (5 x 10^5 cells per well) were incubated with a,b) SeMet or c,d) SeTal (0 - 50 µM) in HBSS for 15 mins at 37 °C before addition of HOCl (200 µM) and further incubation for 15 min at 37 °C. Non-treated cells and cells treated with SeMet or SeTal alone (50 µM) were included as control samples. Cells were lysed in the presence of NEM and reversible thiols were tagged with IAF after DTT reduction. Proteins were run out on a gel and scanned for IAF fluorescence (λ_{ex} = 495 nm; λ_{em} = 520 nm) (b,d). Gels were stained for protein using Coomassie stain (a,c). A, B and C represent bands chosen for densitometry analysis.

6.3.5 Oxidation of amino acid residues

The above data suggest that SeMet and SeTal are ineffective as protective agents for cellular thiol loss induced by HOCl and TauCl under the conditions employed in this

study. However, Met is another significant target for oxidation by HOCl and TauCl in cells [220], which can influence protein function [111, 112]. SeMet and SeTal can prevent oxidation of Met residues when isolated proteins are exposed to HOCl [439, 486]. Thus, the ability of SeMet and SeTal to protect Met and other amino acid residues from oxidation on exposure of cells to HOCl or TauCl was assessed using an HPLC approach in which the concentration of Met and its oxidation product MetSO were quantified after MSA hydrolysis of cellular proteins.

J774A.1 cells (5×10^5 cells mL^{-1}) were incubated in the presence of SeMet or SeTal in HBSS (0 – 50 μM), before addition of HOCl or TauCl (200 μM) and further incubation for 15 min. Cells were washed with warm HBSS and lysed in 600 μL H_2O, before cellular proteins were isolated by precipitation by TCA (50 % (w/v)) prior to digestion into component amino acids by MSA hydrolysis as described in Section 2.3.5.5. Amino acids were derivatised with OPA and concentrations analysed after separation by HPLC, to assess the concentration of Met and the formation of the oxidation product MetSO. The results are expressed as pmol of Met or MetSO per pmol of Ile, which is generally resistant to oxidation by HOCl and *N*-chloramines [547].

Initially, studies to determine the effect of SeMet or SeTal alone (50 μM) on Met and MetSO levels were performed. No significant differences between the levels of Met and MetSO in the non-treated controls were observed on treating cells with SeMet or SeTal (Figure 6.6). Next, experiments were conducted to determine the effect of HOCl and TauCl on Met and MetSO levels. Surprisingly, no significant loss in Met or formation of MetSO was observed on exposure of the cells to HOCl, even though Met is a known target of HOCl oxidation (Figure 6.6) [86]. Similar results were obtained in the analogous experiments with TauCl (Figure 6.7).

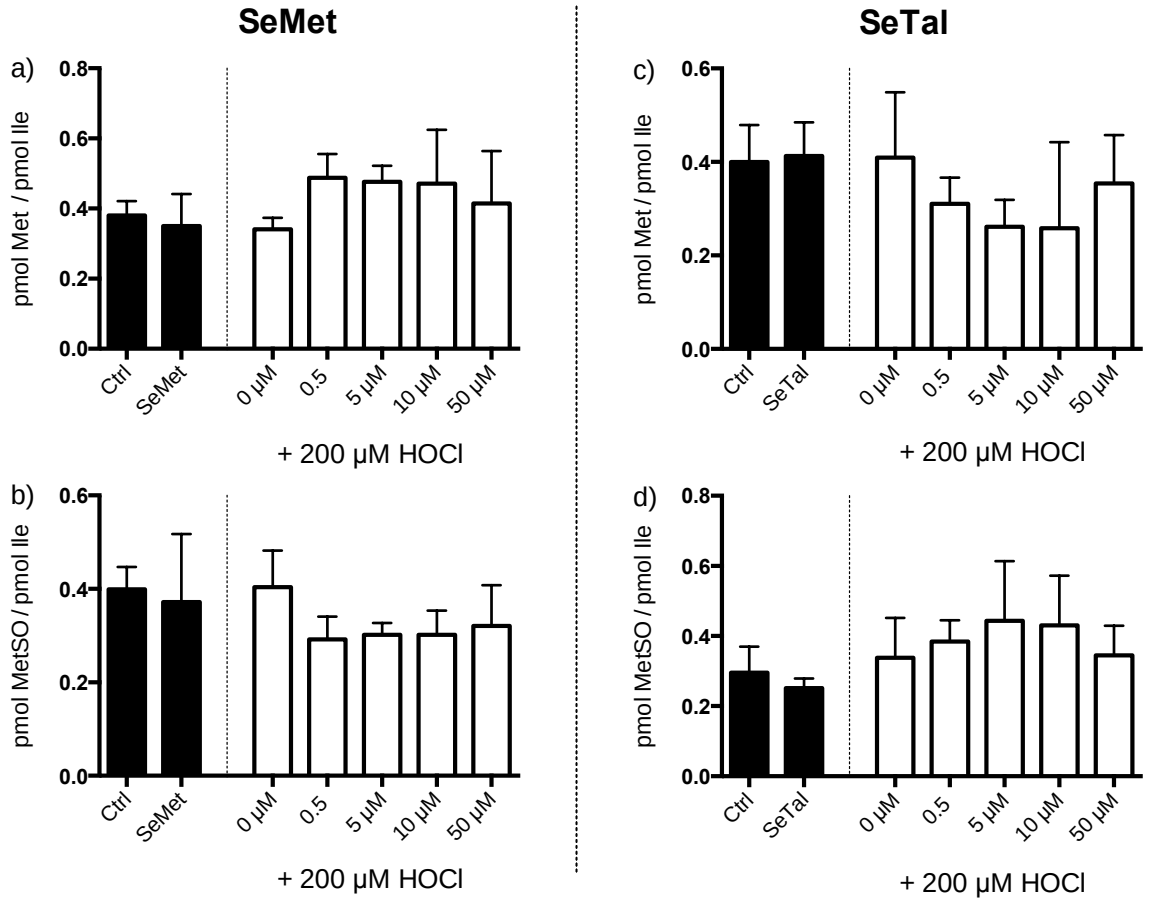

Figure 6.6 – Met and MetSO levels after J774A.1 cells were exposed to HOCl in the presence of SeMet or SeTal

J774A.1 cells (5 x 10^5 cells) were treated with HOCl (200 µM) in the presence or absence of SeMet or SeTal (0 – 50 µM) for 15 min. Non-treated cells and cells treated with SeMet or SeTal alone (50 µM) were included as control samples (black bars). Cells were washed with warm HBSS and lysed in 600 µL H_2O, before protein precipitation and MSA hydrolysis. Amino acids were derivatised with OPA and concentrations analysed by HPLC. Met and MetSO levels are reported relative to Ile. No significant differences were observed between treatments based on one-way ANOVA with Tukey's post-hoc test. Data represent mean ± SD from 3 independent experiments.

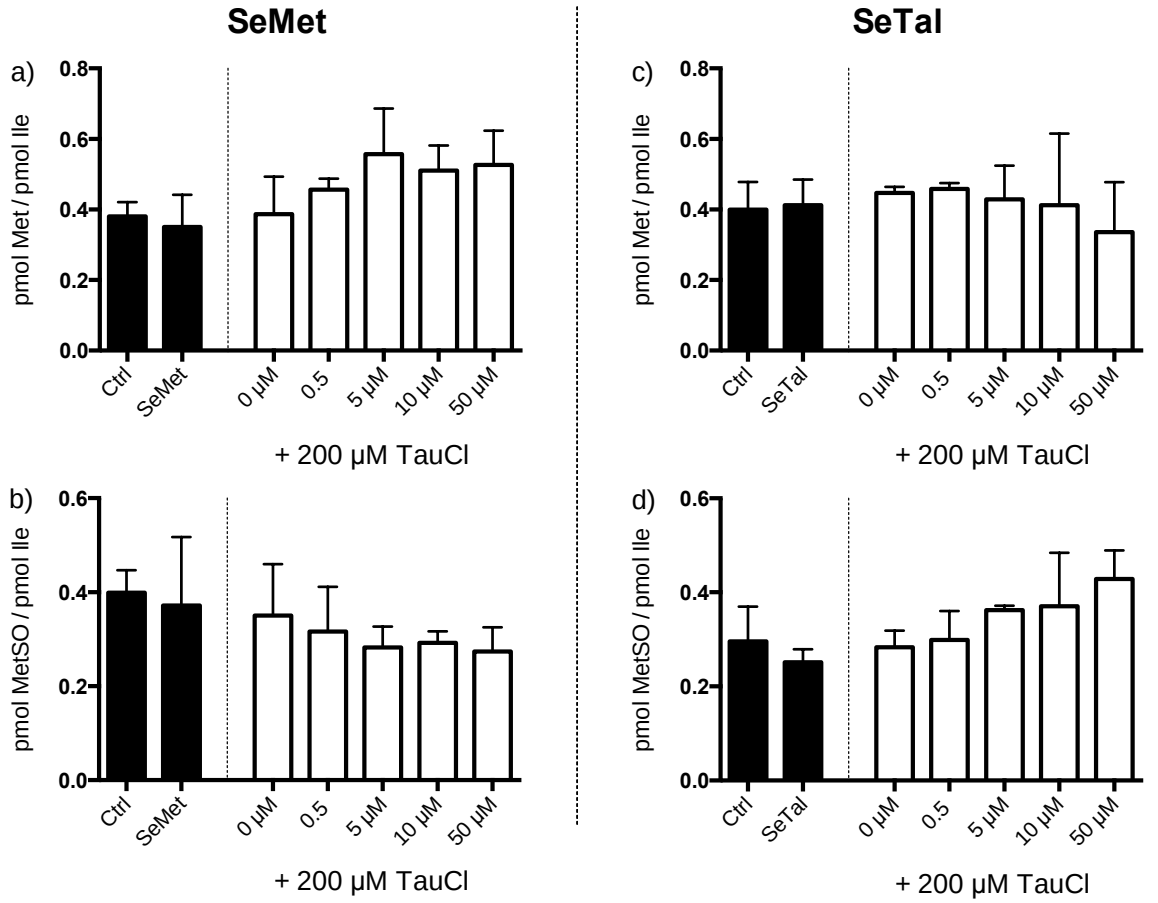

Figure 6.7 – Met and MetSO levels after J774A.1 cells were exposed to TauCl in the presence of SeMet or SeTal

J774A.1 cells (5 x 10^5 cells) were treated with TauCl (200 µM) in the presence or absence of SeMet or SeTal (0 – 50 µM) for 15 min. Non-treated cells and cells treated with SeMet or SeTal alone (50 µM) were included as control samples (black bars). Cells were washed with warm HBSS and lysed in 600 µL H_2O, before protein precipitation and MSA hydrolysis. Amino acids were derivatised with OPA and concentrations analysed by HPLC. Met and MetSO levels are reported relative to Ile. No significant differences were observed between treatments based on one-way ANOVA with Tukey's post-hoc test. Data represent mean ± SD from 3 independent experiments.

Met and MetSO levels did not appear to be effected after treatment of intact cells with HOCl and TauCl, which may reflect protection by the cell membrane, or insufficient concentrations of oxidant. Therefore, as Met are favoured oxidation sites in isolated proteins exposed to HOCl and *N*-chloramines, a lysate model was used to determine whether SeMet and SeTal could afford protection from HOCl and TauCl induced damage. J77A.1 cells were lysed in H_2O and adjusted to 1 mg mL^{-1} protein before incubation with SeMet or SeTal (0 – 50 µM) for 15 min at 22 °C. HOCl or TauCl (200 µM) was then added and samples incubated for a further 15 min, before protein

precipitation and digestion by MSA. Amino acids were derivatised and analysed by HPLC.

SeMet and SeTal alone (50 μM) did not significantly affect Met or MetSO levels in the cell lysate proteins compared to the non-treated control (Figure 6.8). In this case, addition of HOCl (200 μM) significantly decreased Met levels (Figure 6.8a,c), with a corresponding increase in MetSO levels (Figure 6.8b,d). Increasing concentrations of SeMet or SeTal demonstrated a slight trend toward Met protection, with an increase in Met and a decrease in MetSO, though this was not statistically significant.

Addition of TauCl (200 μM) to cell lysates (1 mg protein mL^{-1}) also resulted in a loss of Met residues (Figure 6.9 a,c), with a corresponding increase in MetSO (Figure 6.9 b,d). However, no dose-dependent trend in Met protection was observed in this case. A recovery of Met was seen at the highest levels of SeMet or SeTal, though this difference was not statistically significant from the level detected with TauCl alone (Figure 6.9).

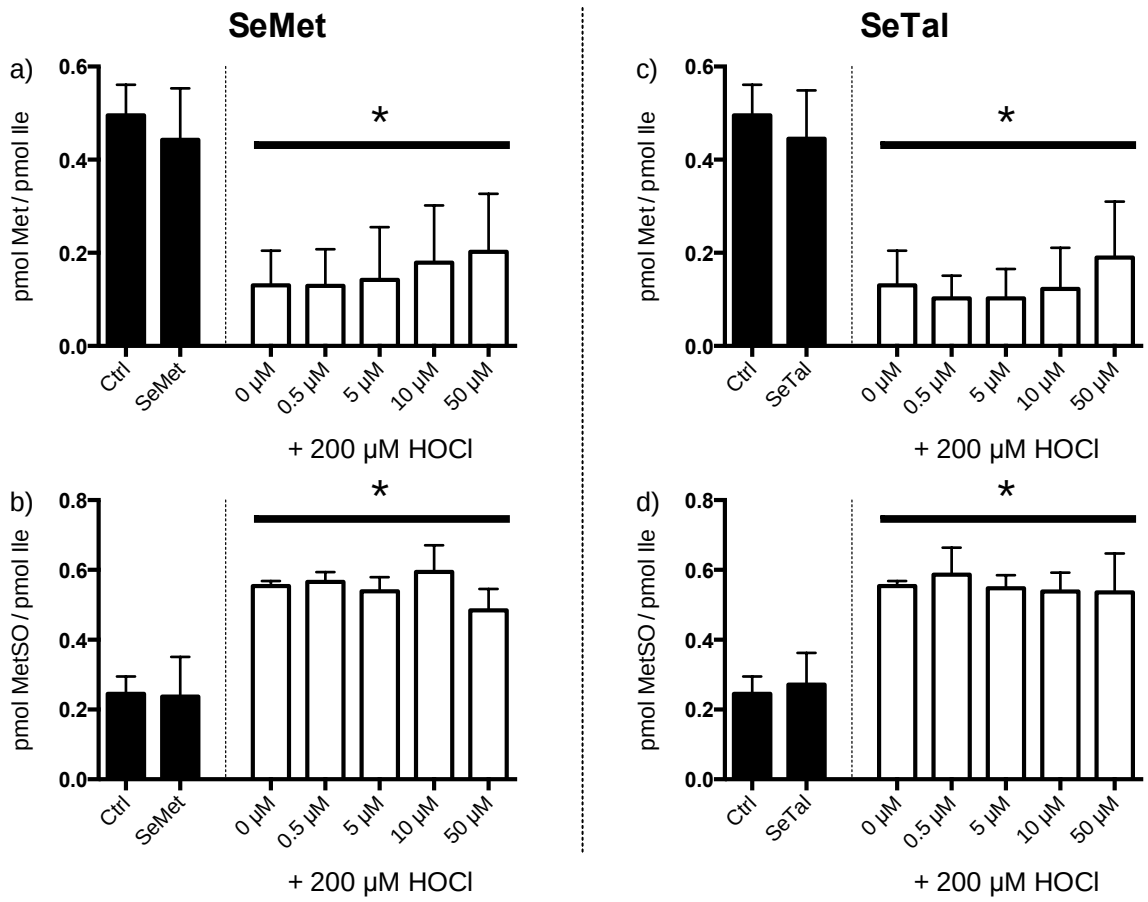

Figure 6.8 - Met and MetSO levels after J774A.1 lysates were exposed to HOCl in the presence of SeMet or SeTal.

*J774A.1 cells were lysed in H_2O and the lysates adjusted to 1 mg mL^{-1} protein assessed by the BCA assay. Lysates were then supplemented with SeMet or SeTal (0 - 50 µM) before addition of HOCl (200 µM) and incubation for 15 min at 22 °C. Non-treated lysates and lysates treated with SeMet or SeTal alone (50 µM) were included as control samples (black bars). Protein was precipitated and digested using MSA hydrolysis and amino acids derivatised with OPA and separated by HPLC. a,c) Met and b,d) MetSO levels are reported relative to Ile concentrations. HOCl treatment decreases levels of Met, with a corresponding increase in MetSO. No significant difference was observed in Met or MetSO levels between cells treated with HOCl or TauCl alone and those treated with HOCl and TauCl in the presence of SeMet or SeTal. Data represent mean ± SD from 3 independent experiments. * indicates significant difference ($p < 0.05$) from untreated control levels based on one-way ANOVA with Tukey's post-hoc test.*

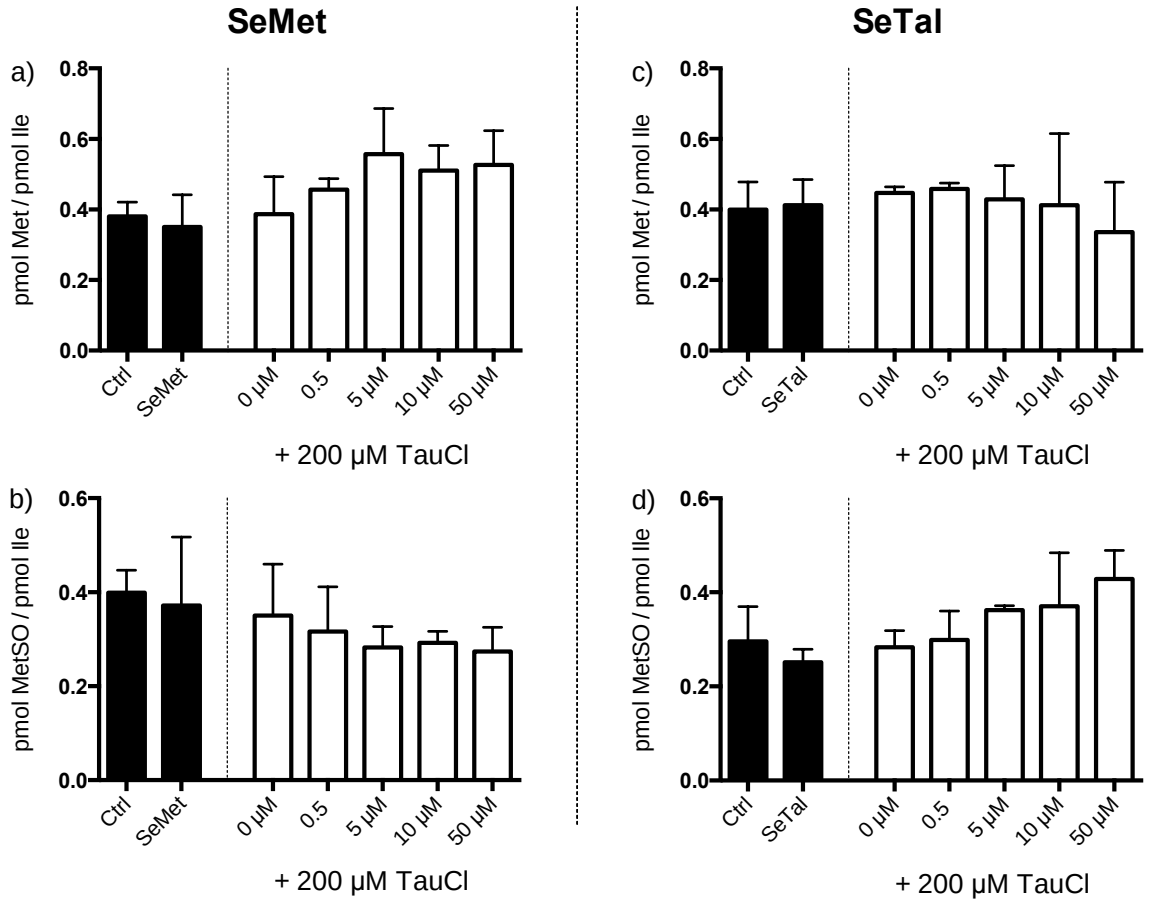

Figure 6.9 - Met and MetSO levels after J774A.1 lysates were exposed to TauCl in the presence of SeMet or SeTal

*J774A.1 cells were lysed in H_2O and the lysates adjusted to 1 mg mL^{-1} protein assessed by the BCA assay. Lysates were then supplemented with SeMet or SeTal (0 - 50 µM) before addition of TauCl (200 µM) and incubation for 15 min at 22 °C. Non-treated lysates and lysates treated with SeMet or SeTal alone (50 µM) were included as control samples (black bars). Protein was precipitated and digested using MSA hydrolysis and amino acids derivatised with OPA and separated by HPLC. a,c) Met and b,d) MetSO levels are reported relative to Ile concentrations TauCl treatment decreases levels of Met, with a corresponding increase in MetSO. No significant difference was observed in Met and MetSO levels between cells treated with HOCl or TauCl alone and those treated with HOCl and TauCl in the presence of SeMet or SeTal. Data represent mean ± SD from 3 independent experiments. * indicates significant difference ($p < 0.05$) from untreated control levels based on one-way ANOVA with Tukey's post-hoc test.*

HOCl and TauCl can also target Tyr, Trp, Lys and His residues, causing an observed decrease in the concentration of these amino acid residues when HOCl or TauCl reacts with them [86]. The levels of these amino acids were also assessed in these experiments, however no changes in their concentrations were observed after oxidant treatment (data not shown).

6.3.6 Cell viability after oxidant treatment

6.3.6.1 Modulation of necrosis observed after 15 min

Although SeMet and SeTal appear to be ineffective or only weakly protective against thiol and Met oxidation on exposure of J774A.1 cells to HOCl and TauCl, it is possible that these compounds may act as protective agents via other pathways. It has been shown previously that HOCl and TauCl can induce cell death via apoptosis and necrosis [219, 222, 606, 607]. It was therefore hypothesised that SeMet and SeTal may modulate the pattern of HOCl and TauCl induced cell damage that cause these pathways to be activated, and hence preserve cell viability after oxidant exposure.

Initially, experiments were performed at 15 min post oxidant exposure to examine changes in viability observed at the same time point as the oxidative changes examined earlier in this Chapter. Cells were preincubated with SeMet or SeTal (0 – 50 μM) for 15 min, prior to the addition of 200 μM HOCl or TauCl, with a further incubation of 15 min. The viability and percentage of necrotic and apoptotic cells were determined by dual staining with propidium iodide (PI) and Annexin-V respectively, with analysis by flow cytometry (Figure 6.10). As 15 min is too short a time period for apoptosis induction, only necrotic cell populations are examined here.

Annexin-V binds to surface exposed phosphatidyl serine residues, which are externalised during the process of cellular apoptosis [564]. Therefore, cells that stain positive for Annexin-V are considered to be apoptotic. PI is taken up by necrotic cells and interchelates with double-stranded DNA [565].

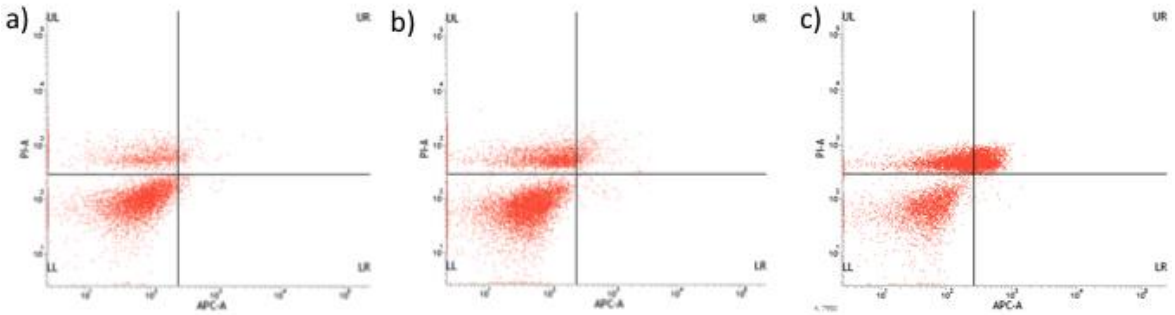

Figure 6.10 – Example flow cytometry plots for control populations and cells treated with HOCl and TauCl

J774A.1 cells (5 x 10^5 cells) were plated overnight before washing and treatment with b) HOCl or c) TauCl (200 µM) in HBSS for 15 min. a) shows HBSS control cells. Cells were scraped and pelleted before washing with HBSS and staining with Annexin-V APC and PI and subsequent analysis by flow cytometry. Cells in the lower left quadrant were considered to be viable, cells in the lower right quadrant were considered apoptotic, and cells in the upper quadrants were considered necrotic. TauCl and HOCl treatment induced necrosis in J774A.1 cells, however, no apoptotic cell population was observed under these conditions.

Initial studies examined the viability of a control population of cells incubated in HBSS in the presence and absence of 50 µM SeMet or SeTal. The J774A.1 control cells were 70% viable after the 30 min incubation in HBSS and removal from the tissue culture plates. In this case, approximately 30% of cells were in the necrotic population (Figure 6.11). The presence of SeMet or SeTal alone (50 µM) did not significantly affect cell viability compared to the non-treated control population, which corresponded with the data observed with the LDH assay (Figure 6.1). Upon addition of HOCl, the viable cell population decreased to 30% of the total cell population (Figure 6.9a,c). There was a corresponding increase in the population of necrotic cells to 70% of the total cell population (Figure 6.9b,d). HOCl treatment is known to cause necrosis at high concentrations due to chemical changes in the cell membrane [222]. Addition of increasing concentrations of SeMet demonstrated a trend toward increasing viability, with a corresponding decrease in necrosis, however, the levels of each population were not significantly different to cells treated with HOCl alone (Figure 6.11a,b). Preincubation with SeTal did not significantly affect the cell viability observed after oxidant treatment (Figure 6.11c,d).

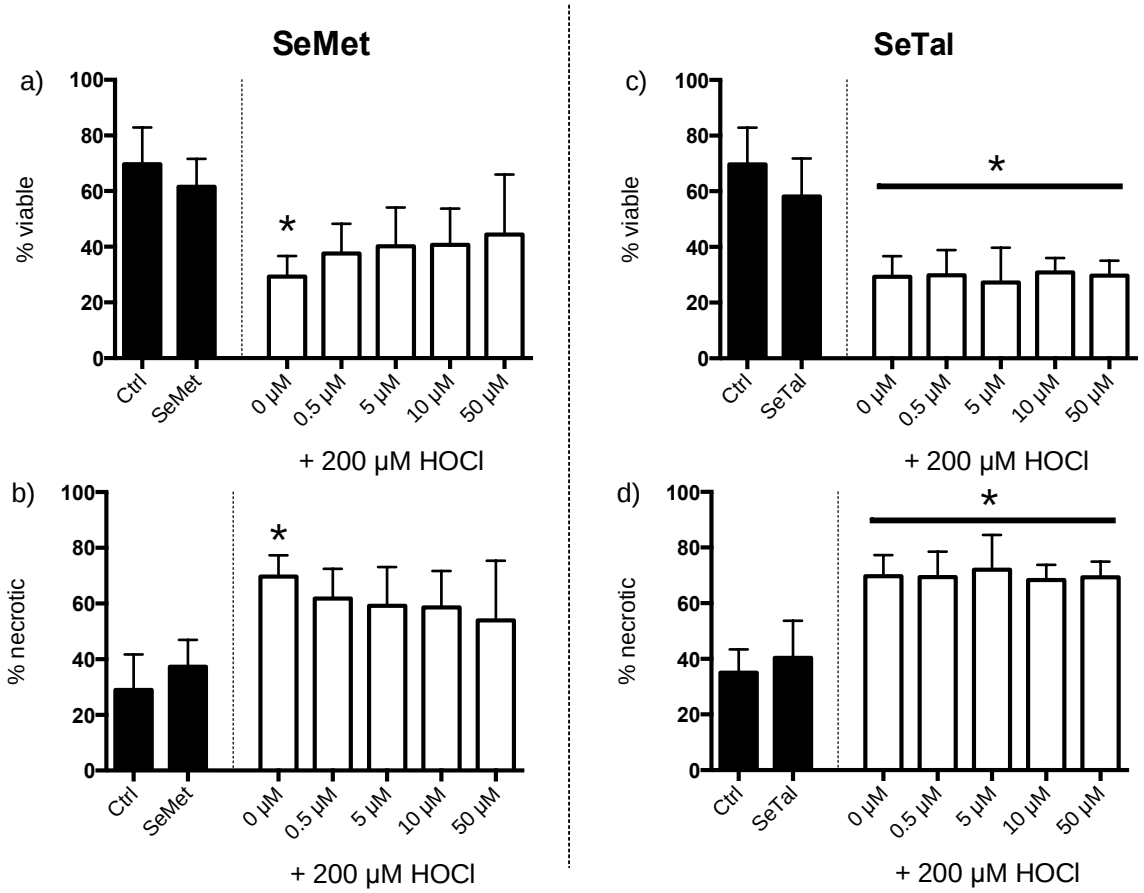

Figure 6.11 – Viable and necrotic cell populations 15 mins after J774A.1 cells were exposed to HOCl in the presence of SeMet or SeTal.

*J774A.1 cells (5 x 10^5 cells) were treated with HOCl (200 µM) in the presence or absence of SeMet or SeTal (0 – 50 µM) for 15 min. Non-treated cells and cells treated with SeMet or SeTal alone (50 µM) were included as control samples (black bars). Cells were pelleted and washed with warm HBSS before addition of Annexin-V APC and PI stains. Cell populations were counted using flow cytometry. A decrease in the viable cell population (a,c) was observed with HOCl treatment, with a corresponding increase in necrosis (b,d). No changes were observed with SeMet (a,b) or SeTal (c,d) treatment. Data represent mean ± SD from 3 independent experiments. * indicates significant difference ($p < 0.05$) from untreated control levels based on one-way ANOVA with Tukey's post-hoc test.*

TauCl treatment also decreased the viability of cells with a corresponding increase in the necrotic cell population, though these differences were not statistically significant after incubation for 15 min (Figure 6.12). Pretreatment of cells with SeMet and SeTal prior to oxidant exposure did not have an effect on the distribution of cell populations (Figure 6.12).

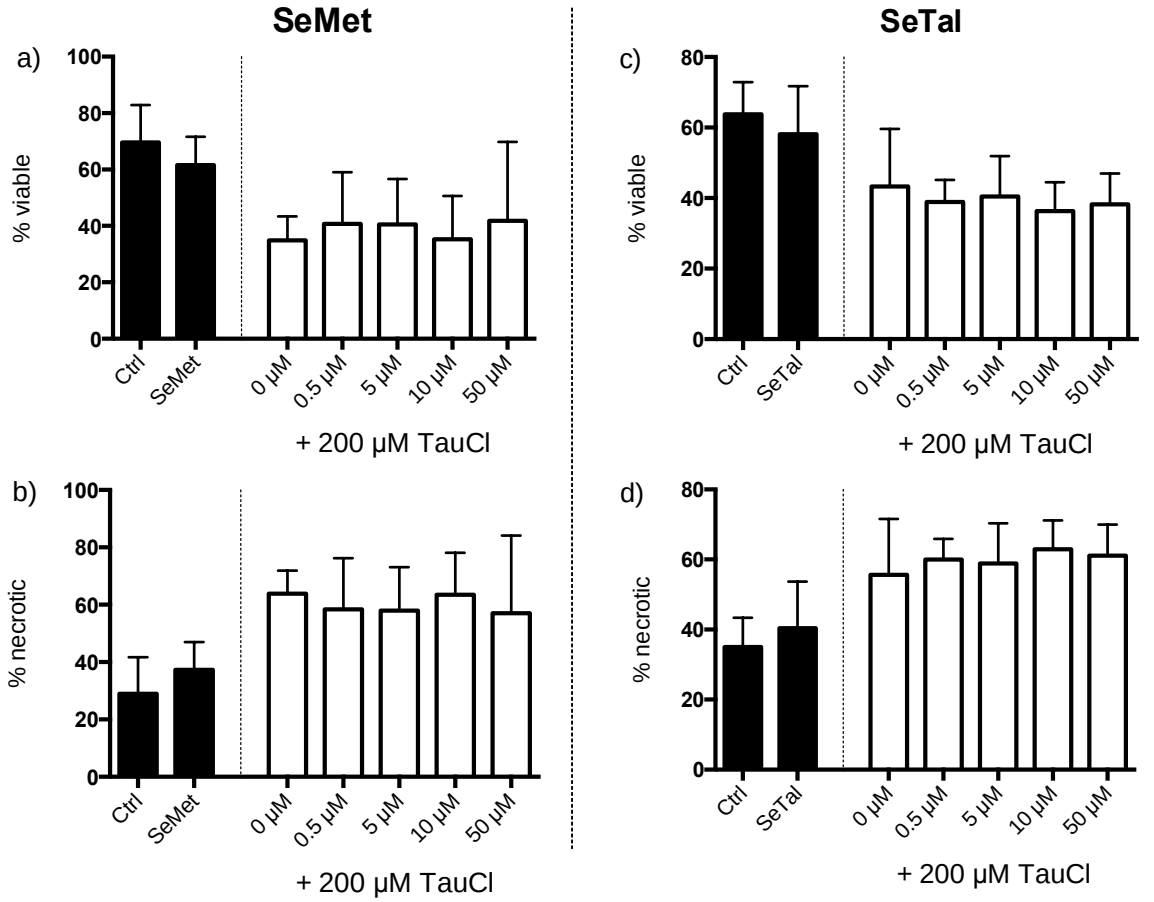

Figure 6.12 - Viable and necrotic cell populations 15 mins after J774A.1 cells were exposed to TauCl in the presence of SeMet or SeTal.

J774A.1 cells (5 x 10^5 cells) were treated with TauCl (200 µM) in the presence or absence of SeMet or SeTal (0 – 50 µM) for 15 min. Non-treated cells and cells treated with SeMet or SeTal alone (50 µM) were included as control samples (black bars). Cells were pelleted and washed with warm HBSS before addition of Annexin-V APC and PI stains. Cell populations were counted using flow cytometry. A decrease in the viable cell population (a,c) was observed with TauCl treatment, with a corresponding increase in necrosis (b,d). No changes were observed with SeMet (a,b) or SeTal (c,d) treatment based on one-way ANOVA with Tukey's post-hoc test. Data represent mean ± SD from 3 independent experiments.

6.3.6.2 Modulation of necrosis observed after 2 h

As 15 min is too short a time to observe apoptosis as it is regulated by signalling pathways, the study was extended to a 2 h incubation before changes in cell viability were assessed. The oxidant concentrations were reduced to 100 µM to minimise the extent of lysis of the cells as previously reported [222].

Initial preliminary experiments were performed to determine the extent of apoptosis observed when the cells were exposed to camptothecin (CPT; 25 µM) or

staurosporin (5 μM) as positive controls [611, 612]. J774A.1 cells were plated at a density of 0.5 x 10^6 cells per well in 12-well plates, and allowed to adhere overnight in an atmosphere of humidified 5 % CO_2, at 37 °C. Cells were washed twice with warm HBSS, before the addition of 25 μM CTP or 5 μM staurosporin in HBSS and further incubation for 2 h. Staurosporin treatment was also performed with a 4 h incubation. Cells were then stained with Anexxin-V APC and PI, and the viable, apoptotic and necrotic cell populations were assessed by flow cytometry (Figure 6.13). Cells treated with these agents demonstrated a decrease in viability with a corresponding increase in necrosis (Figure 6.14). However, again no change in the apoptotic cell populations were observed (Figure 6.14), with less than 1% of the cell population in the lower right quadrant (Figure 6.13). The reason for this discrepancy compared to published data is not certain, but may reflect late stage apoptosis, where PI is also taken up, or that different, early passage cells were used in the current study [222].

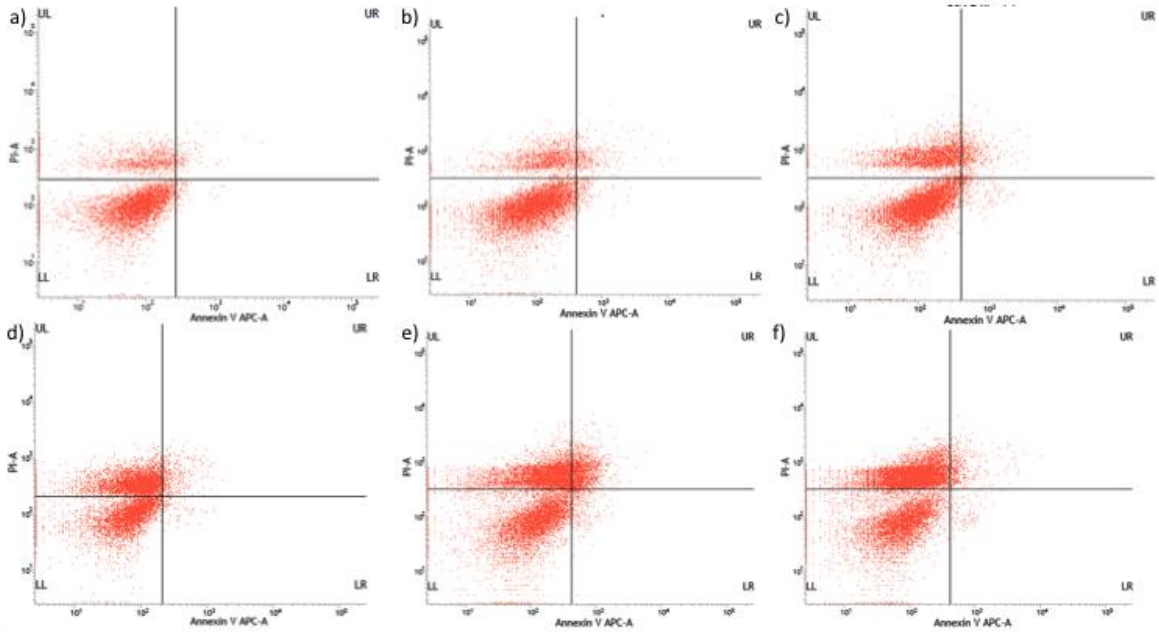

Figure 6.13 – Flow cytometry plots for J774A.1 treated with CPT and staurosporin and stained with Annexin-APC and PI

J774A.1 cells (5 x 10^5 cells) were treated with d) CPT (25 μM) for 2 h, or for staurosporin (5 μM) for e) 2 h or f) 4 h. a, b, c) represent controls for each condition. Cells were scraped and pelleted before being washed with warm HBSS and stained with Annexin-V APC and PI stains. Fluorescence was measured using flow cytometry and cells sorted in quadrants representing: Lower left – Annexin negative, PI negative; Lower right – Annexin positive, PI negative; Upper left – Annexin negative, PI positive; and Upper right – Annexin positive, PI positive.

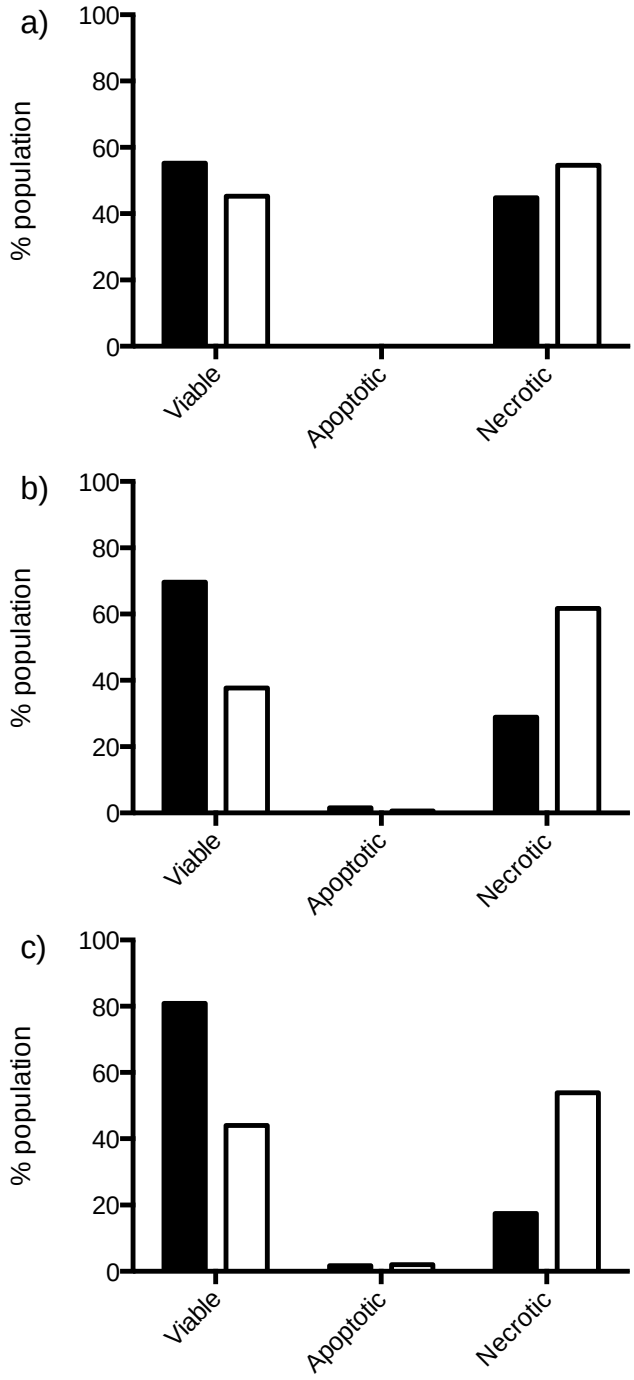

Figure 6.14 - Cell viability for J774A.1 cells treated with CPT and staurosporin

J774A.1 cells (5 x 10^5 cells) were treated with a) CPT (25 μM) for 2 h, or staurosporin (5 μM) for b) 2 h or c) 4 h. Black bars represent incubation with HBSS alone, and white bars represent staurosporin or CPT treatment. Cells were scraped and pelleted before being washed with warm HBSS and stained with Annexin-V APC and PI stains. Cell populations were counted using flow cytometry. All treatments showed a decrease in viability with a corresponding increase in necrosis. No change was observed in apoptotic cell populations. As n =1, no error bars are present.

Experiments to determine the cell viability of a control population of cells in the presence and absence of SeMet and SeTal (50 μM) were performed. However, due to a lack of Annexin V staining in the positive controls, only necrotic cell populations could be assessed. The viability of non-treated control cells was significantly decreased after 2 h in HBSS when compared to that seen at 15 min, with 30 – 40% cells determined as viable (Figure 6.15a,c). The remaining 60-70% of the cell population were found to be necrotic (Figure 6.15b,d). This may be related to an increase in susceptibility of the cells to damage by mechanical scraping required to lift the cells from the plate into suspension for flow cytometry analysis following longer incubation in HBSS. The mechanical scraping could not be avoided as J774A.1 cells are trypsin resistant. The presence of SeMet and SeTal did not affect the cell populations. However, no further loss in cell viability was observed compared to the non-treated control cells on addition of either HOCl (Figure 6.15) or TauCl (Figure 6.16) (100 μM) to the J774A.1 cells. Again, SeMet and SeTal addition did not affect the cell populations observed in cells treated with HOCl (Figure 6.15). This is consistent with the HOCl treated cells, as HOCl did not induce cell death over and above that seen in the non-oxidant treated cells. When cells were treated with TauCl in the presence of SeMet, a trend towards a further decrease in the viable cell population together with an increase in necrotic population was observed, though this was not statistically significant (Figure 6.16a,b). This effect was not observed in the presence of SeTal. However, it should be noted that there was considerable variability in the extent of necrosis seen in the non-oxidant treated cells in these experiments, and repetition would be required to confirm this observation.

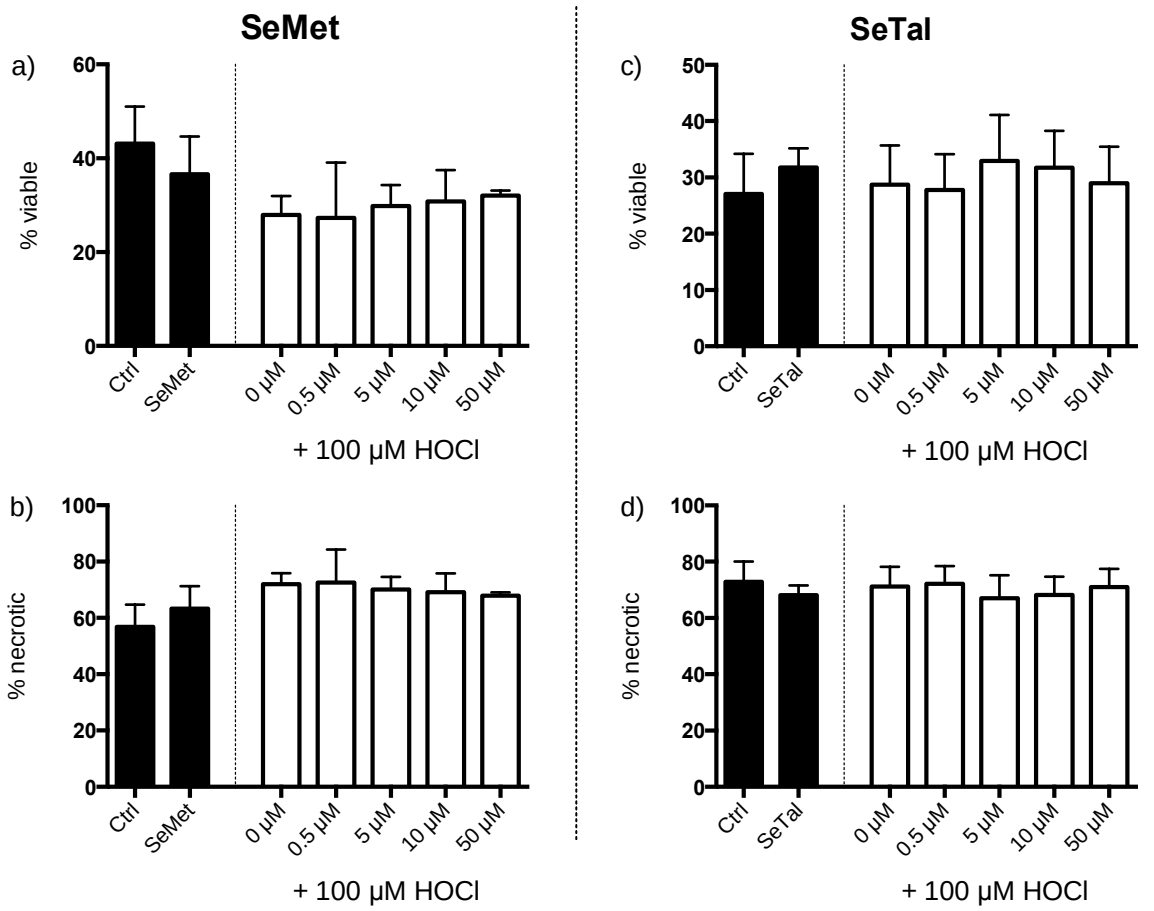

Figure 6.15 - Viable and necrotic cell populations 2 hrs after J774A.1 cells were exposed to HOCl in the presence of SeMet or SeTal.

J774A.1 cells (5 x 10^5 cells) were treated with HOCl (100 µM) in the presence or absence of SeMet or SeTal (0 – 50 µM) for 2 h. Non-treated cells and cells treated with SeMet or SeTal alone (50 µM) were included as control samples (black bars). Cells were pelleted and washed with warm HBSS before addition of Annexin-V APC and PI stains. Cell populations were counted using flow cytometry. No changes were observed in the viable (a,c) or necrotic (b,d) cell populations with HOCl treatment. No significant changes were observed with SeMet (a,b) or SeTal (c,d) treatment compared to HOCl treatment in the absence of SeMet or SeTal based on one-way ANOVA with Tukey's post-hoc test.. Data represent mean ± SD from 3 independent experiments.

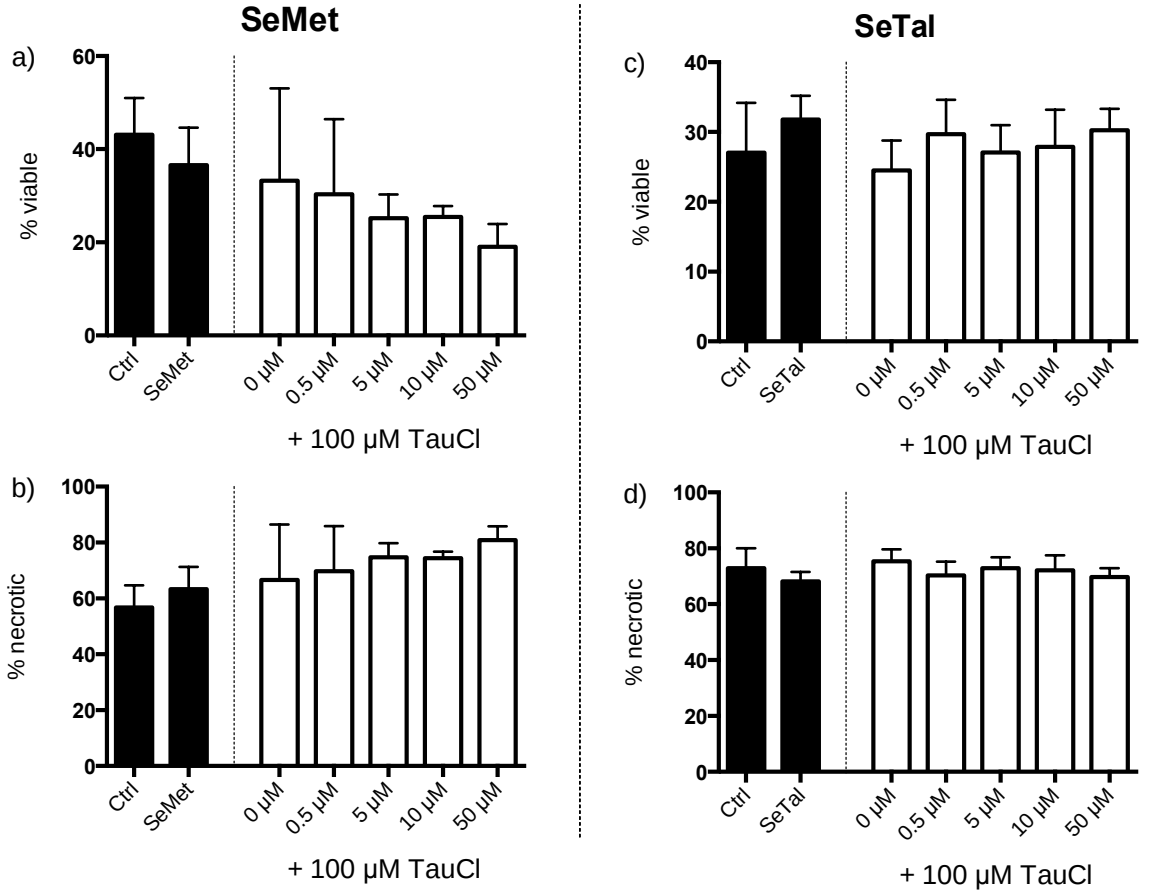

Figure 6.16 – Viable and necrotic cell populations 2 hrs after J774A.1 cells were exposed to TauCl in the presence of SeMet or SeTal.

J774A.1 cells (5 x 10^5 cells) were treated with TauCl (100 µM) in the presence or absence of SeMet or SeTal (0 – 50 µM) for 2 h. Non-treated cells and cells treated with SeMet or SeTal alone (50 µM) were included as control samples (black bars). Cells were pelleted and washed with warm HBSS before addition of Annexin-V APC and PI stains. Cell populations were counted using flow cytometry. No changes were observed in the viable (a,c) or necrotic (b,d) cell populations with TauCl treatment. No significant changes were observed with SeMet (a,b) or SeTal (c,d) treatment compared to TauCl treatment in the absence of SeMet or SeTal based on one-way ANOVA with Tukey's post-hoc test.. Data represent mean ± SD from 3 independent experiments.

6.4 Discussion

Cellular thiols are major targets of HOCl and the levels of protein thiols and GSH are reduced when cells are exposed to this oxidant [221, 222, 229]. As expected HOCl decreased cellular thiols and decreased GAPDH activity, consistent with previous work on murine macrophage-like J774A.1 cells [222]. TauCl, on the other hand, is generally reported to be impermeable to cell membranes [135, 229]. TauCl does not induce oxidation of cellular thiols or cause inactivation of GAPDH when exposed to endothelial

or Jurkat cells, though in the presence of other amines, like Gly or His, transchlorination reactions can occur, forming more cell permeable *N*-chloramines [135, 246]. However, TauCl is taken up by the RAW 264.7 murine macrophage cell line [249] and reversible oxidation of intracellular cofilin by TauCl in a human lymphoma cell line has been reported [609]. Furthermore, TauCl mediated oxidation of Met residues of IκBα resulting in loss of NF-κB activity [251]. In this study, J774A.1 cells treated with TauCl demonstrated a loss of cellular thiols and a decrease in GAPDH activity, which has not been reported with other cell types. This may indicate an increase in permeability of J774A.1 cell membranes compared to other cell types, allowing TauCl access to the cytosol and hence thiol loss. If this is occuring, it could be demonstrated by assessing *N*-chloramine concentration in media after exposure of cells to TauCl, though this experiment was not performed and would not rule out reactivity of TauCl with cell membrane components [246]. It is unlikely that transchlorination reactions would be occurring in the studies performed in this Chapter, as treatments were performed in HBSS, which contains no free amines to undergo these reactions.

Circulating levels of SeMet in patients who have been supplemented with SeMet difficult to demonstrate *in vivo*, due to rapid metabolism and incorporation into protein [613]. SeTal has not previously been used in *in vivo* studies. The concentration of SeMet and SeTal used in this Chapter were selected based on previous supplementation studies [474, 513, 529-531, 538], and at a dose at which no effect on viability was observed.

Incubation of SeMet and SeTal with J774A.1 cells in the absence of oxidant demonstrated a loss of cellular thiols and a decrease in GAPDH activity, though these differences were not statistically significant compared to non-treated control cells. Selenium compounds, including SeMet, have previously been shown to increase ROS production in cells, which is primarily attributed to the formation of selenolates after metabolism of SeMet by methioninases [513]. An increase in ROS due to SeMet and SeTal may be causing the decrease in thiol levels observed. Furthermore, reaction of SeMet and SeTal with basal levels of ROS, forming selenoxides which then react with cellular thiols may also result in a decrease in cellular thiols.

The presence of SeMet and SeTal did not affect the levels of thiols observed in cells after oxidant treatment (Figure 6.2 and Figure 6.3). This is potentially due to the

limited scavenging of oxidant, as in this case, the HOCl or TauCl are in excess of SeMet and SeTal. SeMet and SeTal have higher rate constants for the reaction with the oxidants compared to cellular components, as demonstrated in Chapter 3, so it would be expected that SeMet and SeTal are at least partially consuming the HOCl or TauCl. The primary product produced by the reaction between SeMet or SeTal and HOCl or TauCl would be the respective selenoxides. As demonstrated in Chapter 4, these selenoxides can react with GSH and protein thiols, thus depleting cellular thiols. This may be why no protection from HOCl or TauCl induced damage is observed when cells are supplemented with SeMet and SeTal prior to oxidant addition. Furthermore, the presence of SeMet has a non-statistically significant trend to further reduce the concentration of thiols in cell lysates exposed to HOCl or TauCl (Figure 6.3). This may be reflecting the increased specificity of selenoxides towards thiols compared to HOCl and TauCl, which are capable of reacting with other targets.

In general, the presence of SeMet and SeTal did not modulate GAPDH activity upon oxidant exposure to cells (Figure 6.4). This is potentially due to reaction of the active site of GAPDH with the selenoxides SeMetO and SeTalO formed upon HOCl or TauCl addition, as selenoxides have demonstrated protein thiol reactivity previously [445]. The ability of selenoxides to inactivate GAPDH could be assessed using isolated protein exposed to SeMet and SeTalO and determining activity. Alternatively, as the cells were treated with an excess of HOCl and TauCl over SeMet or SeTal, it may be that the concentration of SeMet and SeTal was not high enough to scavenge sufficient HOCl or TauCl to inhibit the loss of GAPDH activity.

Experiments with cells exposed to HOCl (200 μM) in the presence of 10 μM SeMet consistently demonstrated an increase in GAPDH activity compared to that seen in the absence of SeMet (Figure 6.4a). The protection afforded at 10 μM may be indicative of a "sweet spot" of SeMet supplementation, where the SeMet is scavenging enough HOCl to prevent GAPDH inactivation, but the levels of SeMetO are not high enough for GAPDH to become a target for oxidation by SeMetO. However, more work would be needed in order to fully establish whether this is the case.

HOCl and cell-permeable *N*-chloramines such as those formed on Gly can induce the formation of reversible thiol oxidation products [614]. TauCl is less able to penetrate the cell membrane [135] and therefore a lower of level of intracellular reversible thiol

products may be expected. However, in the data presented here, no increase in reversible thiol products was observed with HOCl or TauCl treatment, which may reflect oxidation of other targets, such as reaction with the cellular membrane. Furthermore, HOCl and TauCl can oxidise thiol residues to sulfinic and sulfonic acids, which are irreversible thiol oxidation products [86]. SeMet and SeTal may react to form selenoxides in cells upon HOCl or TauCl addition, which react with thiols to form disulfides, with no evidence reported for the formation of sulfenic or sulfonic acids [444, 445]. As disulfides are reversible oxidation products, the IAF protocol was attempted to assess levels of reversible thiols (Figure 6.5). However, due to issues with sample preparation, the results for this approach were inconclusive.

The lack of significant changes in reversible oxidation products observed in this study may be due to the large variation between samples. Protein levels of the sample were adjusted prior to reaction of cellular proteins with IAF. However, the pelleting and washing stages that are required after IAF addition may have caused loss of sample. Furthermore, the purified IAF-containing proteins became very insoluble, potentially leading to further variation in protein levels. Thus, in order to obtain more consistent results, protein quantification and subsequent adjustment should be performed prior to protein separation by SDS-PAGE.

HOCl and TauCl oxidise amino acid residues on proteins, particularly Met which is oxidised to MetSO [106]. Oxidation of Met is postulated to play a protective role in cells as they can be repaired by the action of Msrs [351-355]. However, when Met is at the active site of proteins, oxidation of Met residues may inactivate the enzyme [615, 616]. For example, the oxidation of the active site Met of IκBα by TauCl is proposed to result in the inactivation of NF-κB and play a role in the induction of apoptosis [251]. As SeMet and SeTal both have second order rate constants greater than that reported for Met for reaction with both HOCl [90] and TauCl (Chapter 3), this suggests that the SeMet or SeTal should be preferentially oxidised over Met residues, providing their concentration is sufficient and localisation in the cellular environment is appropriate. In the data presented in this Chapter, HOCl and TauCl were both able to decrease the concentration of Met when exposed to cell lysate samples, with a corresponding increase in MetSO observed (Figure 6.8 and Figure 6.9). The addition of SeMet and SeTal to lysate samples showed a trend toward protection of Met residues when the

lysates were exposed to HOCl, though this was not significant. This contrasts with other studies that have reported that the presence of selenium compounds prevents Met residues from oxidation [439, 486], though these studies used isolated proteins, and a higher ratio of selenium compound to oxidant than used in this study. A higher concentration of SeMet and SeTal may therefore increase the potential protective effects of these compounds on HOCl and TauCl induced damage.

HOCl and TauCl treated J774A.1 cells showed no loss of Met or increase in MetSO (Figure 6.6 and Figure 6.7). This may be due to the oxidant reacting with other species, such as thiols, or the lipid bilayer of the cell, with insufficient oxidant remaining to oxidise Met residues. Cells also contain Msrs, which are able to reduce MetSO back to Met [351-355], which could result in repair of Met oxidation prior to its detection by these methods.

While no significant protection of thiol or Met residues was observed with SeMet and SeTal treatment, these residues are not the only targets of HOCl and TauCl in cells. Other chemical markers of oxidation that could be assessed include chlorinated tyrosine and tryptophan products [106]. These products are particularly important in disease settings as they are used as biomarkers of HOCl-mediated damage [119]. However, no change in tyrosine or tryptophan residue concentrations was observed in these experiments, and therefore the presence of these products was not explored further, particularly as they are usually accompanied by significant Met oxidation.

The cellular toxicity of SeMet and SeTal was assessed using the LDH assay as a measure of viability when J774A.1 cells were exposed to SeMet or SeTal (0 – 200 μM) (Figure 6.1). Under these conditions, no changes in viability with a 30 min treatment time were observed. SeMet, is a major form of dietary selenium and is generally well tolerated at low concentrations, although it has been demonstrated to induce apoptosis in cells [513, 610]. This is primarily attributed to the metabolites of SeMet, which cause an increase in ROS production, which subsequently lead to apoptosis and cell death in prostate cancer cell lines [513, 610]. However, at low concentrations of SeMet (3 μM) toxicity required the addition of methioninases to induce the formation of methylselenolates [513]. The studies in prostate cancer cell lines demonstrated apoptosis approximately 48 – 72 hours post SeMet treatment (50 μM) [610], so it is possible that toxicity may only be evident after extended incubation times.

Exposure of J774A.1 cells to HOCl (200 μM) for 15 min demonstrated an increase in necrosis compared to non-treated controls (Figure 6.12). This is consistent with previously reported data where significant cell lysis was observed after J774A.1 cells were exposed to HOCl under the same conditions employed in this study [222], and this has also been demonstrated in other cell types [213, 219, 605]. SeMet and SeTal (0 – 50 μM) were unable to modulate this increase in necrosis (Figure 6.11). After a more prolonged (2 h) exposure to HOCl (100 μM), there was no increase observed in the necrotic population of cells compared to the non-treated control in this study, and the presence of SeMet or SeTal did not have an effect on cell populations (Figure 6.15). The levels of background necrosis observed in non-treated control samples were significantly greater (at ~70 %) in this study than reported previously in J774A.1 cells (~10 %) [222]. This may reflect differences in the cell populations used in each case, with low passage cells used in the current study that may be more susceptible to damage by the mechanical scraping that is required to lift the cells into suspension for analysis by flow cytometry. Due to the high level of necrotic cells in the non-treated controls and large errors, it is difficult to draw conclusions about any changes in cell populations that may be occurring.

No changes in apoptotic cell populations were observed in any of the experiments performed in this study (Figure 6.10 and Figure 6.14). This is in contrast to previous reports that have demonstrated induction of apoptosis after treatment of cells by HOCl, TauCl, CPT and staurosporin [607, 608, 611, 612]. The previous studies used Annexin-V FITC, whereas this current work used Annexin-V APC. Annexin-V APC was used instead of Annexin-V FITC for these studies as the fluorescent profiles of FITC and PI overlap, whereas APC and PI do not. The change should result in less interference between the Annexin-V and PI fluorescence that could confound the results. Furthermore, Annexin-V requires calcium to be present in the buffer in order to bind effectively [617]. Previous work has used binding buffers with increased calcium compared to HBSS [222], which may explain why limited Annexin-V binding was being observed in this study. However, at least some Annexin-V binding was occurring in these experiments (Figure 6.10 and Figure 6.13), but the cell groups that were staining positive for Annexin-V were also PI positive and were therefore considered necrotic. The lack of a positive control makes it difficult to draw any conclusions about any apoptotic cell populations in this study.

In summary, SeMet and SeTal demonstrated limited efficacy in modulating oxidative damage to murine macrophage-like J774A.1 cells that had been exposed to reagent HOCl and TauCl. However, previous studies have demonstrated that SeMet is capable of enhancing peptide-bound hydroperoxide detoxification in J774A.1 cells [474]. Selenium compounds, including SeMet, are also able to reduce hemolysis of erythrocytes and lipid peroxidation induced by H_2O_2 [538]. Thus, SeMet and SeTal may also modulate oxidative damage in ways that have not been assessed in these studies. For example, SeMet has demonstrated efficacy in inducing expression of antioxidant enzymes including GPx and TrxR [529-531]. The increase in GPx expression was able to protect against oxidative damage in a hypoxia-reoxygenation model of damage to rat cardiomyocytes [529]. SeMet was also found to induce the upregulation of selenium enzymes in trophoblast cells and protect them from H_2O_2-mediated damage [531] or oxidative damage induced by mitochondrial dysfunction [530]. While there was no significant cellular protection in J774A.1 cells demonstrated by the assays used in these studies, SeMet and SeTal may be effective in reducing oxidative stress in other contexts, and by other mechanisms.

6.5 Conclusions

SeMet and SeTal showed a limited ability to inhibit the oxidative damage to J774A.1 cells induced by HOCl and TauCl measured in these studies. However, the majority of these changes were assessed only after a very short time frame following oxidative insult, and were only assessed using chemical markers of damage. Over longer time periods, SeMet and SeTal may provide more significant protection to cellular functions such as metabolism, proliferation and differentiation, which were not assessed by the methods used in this study.

7 General discussion and future directions

7.1 General overview

Neutrophils, through the action of MPO, produce the hypohalous acids, HOCl, HOSCN and HOBr in order to destroy invading pathogens [1]. Under physiological conditions, approximately 50 % of the H_2O_2 consumed by MPO goes into the formation of HOCl [24], which can further react with amine groups of various biological molecules to form the secondary oxidants *N*-chloramines [53-58]. HOCl and *N*-chloramines can also cause damage to host tissue if produced inappropriately in excessive quantities [2]. HOCl will react with most components of cellular systems [86], though the fastest reactions reported are those with sulfur residues, particularly thiols, with second-order rate constants of up to 10^8 M^{-1} s^{-1} [90]. *N*-Chloramines retain the oxidising and chlorinating power of HOCl, however, they display a higher specificity for sulfur residues [86, 136, 192]. Thus, the reaction with Met and Cys are some of the fastest reported reactions for *N*-chloramines, with second-order rate constants in the range of 10^2 – 10^3 M^{-1} s^{-1} [86, 136, 192]. Antioxidants may be capable of modulating oxidative damage caused by MPO-derived oxidants by scavenging these oxidants before they are able to react with cellular components causing damage.

Selenium-containing compounds have garnered interest as potential antioxidants to modulate inflammatory damage due to their favourable reaction kinetics [90, 98, 486]. Selenium-containing compounds have consistently demonstrated higher second order rate constants compared to analogous thiol compounds for reactions with biological oxidants including HOCl and HOSCN [90, 98, 486]. The increased reactivity of selenium compounds has been attributed to the increased nucleophilicity of selenium compared to sulfur, and the lowered pK_a of selenols compared to thiols [446, 447]. The increased rate constants suggest that selenium compounds will be competitive *in vivo* targets for oxidants, capable of acting as scavengers to reduce the extent of oxidative damage. Furthermore, selenium compounds have been shown to give rise to products such as selenoxides that can be reduced by thiols, potentially giving rise to catalytic oxidant scavenging cycles [444, 445].

The studies presented in this Thesis were undertaken to examine the potential of the selenoethers SeMet and SeTal to scavenge MPO-derived oxidants, by determining the rate constants and products of these reactions, and characterising potential reduction pathways of the products *in vivo*. The potential of these compounds to

protect cells from damage caused by exposure to MPO-derived oxidants was also assessed.

7.2 Selenium compounds as catalytic oxidant scavengers

A key requirement of antioxidants is their ability to kinetically compete with the typically more abundant biological targets of oxidants, in order to prevent damage to cellular components. In a biological setting, the reaction of the MPO-derived oxidants HOCl and *N*-chloramines with thiols are some of the fastest reported with rate constants of $>10^8$ M^{-1} s^{-1} for the reaction of HOCl with GSH and Cys [90], and 10^2 – 10^3 M^{-1} s^{-1} for the corresponding *N*-chloramine reactions, though these rate constants are dependent on the specific *N*-chloramine [136, 192]. The rate constants for the reaction of SeMet and SeTal with HOCl and the other hypohalous acids produced by MPO, HOBr and HOSCN, have previously been determined [90, 98], and these rate constants are consistently greater than those determined for the analogous sulfur compounds. These rate constants are comparable to those determined for the reactions with thiols and GSH [90, 98], suggesting that SeMet and SeTal would be able to modulate oxidation reactions of HOCl if present at appropriate concentrations. Similarly, the rate constants determined for the reaction of SeMet with biologically relevant *N*-chloramines determined in Chapter 3, demonstrate that in each case, the rate constant is significantly greater than those determined previously for Met [192]. Furthermore, the rate constants for SeMet and SeTal are comparable to those determined for Cys and GSH. Again, this suggests that SeMet and SeTal will be a competitive target for *N*-chloramines *in vivo,* if present at appropriate concentrations and locations.

This study focussed on the use of SeMet and SeTal as scavengers of HOCl and model *N*-chloramines. However, SeMet has demonstrated efficacy as a scavenger of other one- and two-electron oxidants. High rate constants for the reaction between SeMet and HOBr (k = 1.4 x 10^7 M^{-1} s^{-1}) [90], HOSCN (k = 2.8 x 10^3 M^{-1} s^{-1}) [98], ONOOH (k = 2.4 x 10^3 M^{-1} s^{-1}) [461] and $HO^{\bullet}$ (k = 1.4 x 10^{10} M^{-1} s^{-1}) [457] have been reported. SeTal has been less extensively studied, but rate constants have been reported for HOBr (k = 1.5 x 10^7 M^{-1} s^{-1}) and HOSCN (k = ~100 M^{-1} s^{-1}) [90]. The rate constants for SeMet and SeTal reactions with 2-electron oxidants are consistently greater than those reported for Met [90, 92], and comparable to those reported for Cys [90, 92] (Table 7.1). These data

suggest that SeMet and SeTal may be capable of acting as scavengers of multiple species of oxidants *in vivo*, in addition to HOCl and the *N*-chloramines described in this Thesis.

Table 7.1 – Second order rate constants for the reactions of SeMet, SeTal, Met and Cys with biologically relevant oxidant species.

	Second order rate constants / $M^{-1} s^{-1}$				
	HOCl	HOBr	HOSCN	ONOOH	$HO^{\bullet}$
SeMet	3.2×10^{8} [a]	1.4×10^{7} [a]	2.8×10^{3} [b]	2.4×10^{3} [c]	1.4×10^{10} [d]
SeTal	1.0×10^{8} [e]	1.5×10^{7} [e]	~100 [e]	-	-
Met	3.4×10^{7} [a]	3.6×10^{6} [f]	Slow [g]	3.6×10^{3} [h]	2.3×10^{10} [i]
Cys	3.6×10^{8} [a]	1.2×10^{7} [f]	7.8×10^{4} [g]	3.8×10^{3} [h]	4×10^{10} [j]

[a][90]; [b][98]; [c][461]; [d][457]; [e][486]; [f][61] - Met rate constant determined for *N*-Ac-Met-OMe and Cys rate determined for *N*-Ac-Cys; [g][92]; [h][618] – determined at 37 °C; [i][468] ; [j][459]

Thiol and selenol containing antioxidant enzymes have also demonstrated efficacy in detoxifying oxidants. The primary role of the GPx family (a Sec containing enzyme) and the peroxiredoxin family (thiol containing enzymes) is to remove H_2O_2, but they are also capable of removing other oxidants [101, 102, 346, 349, 350, 583]. TrxR is also capable of detoxifying ONOOH, H_2O_2 and the MPO-derived oxidant, HOSCN [98, 347, 348]. In Chapter 5, the ability of selenium and thiol containing enzymes to remove *N*-chloramines was assessed. The NADPH/GSR/GSH system was capable of rapidly removing *N*-chloramines, via the reaction with GSH and formation of GSSG and subsequent reduction by GSR. The system was capable of removing LysCl and GlyCl at a higher rate than TauCl, and this reflects the relative reactivity of the *N*-chloramines [192]. In contrast, the presence of TrxR was not capable of increasing the rate at which NADPH was consumed upon addition of *N*-chloramines, though the presence of both TrxR and Trx increased the rate of NADPH consumption upon TauCl addition. While no increase in NADPH consumption was observed, this does not exclude the possibility that some amount of the *N*-chloramines were reacting with the enzymatic systems. Direct reaction of *N*-chloramines with NADPH leads to the formation of a chlorohydrin, which is damaging to cells as the reaction cannot be reversed to reform NADPH [63, 83]. When NADPH is consumed by the enzymatic systems, $NADP^{+}$ is formed as a

product, which, through the action of enzymes of GAPDH, can be recycled to NADPH [230]. Therefore, the reduction of *N*-chloramines by enzymatic systems may have potential therapeutic benefit by reducing the amount of chlorinated NADPH. Future studies could assess the relative levels of $NADP^+$ to the chlorinated NADPH species formed by the addition of *N*-chloramines to the NADPH/TrxR and related enzyme systems to further characterise the potential for these enzymes to react with *N*-chloramines.

The major products formed when SeMet and SeTal are exposed to HOCl and *N*-chloramines are the respective selenoxides, SeMetO and SeTalO. The selenoxides form in a near 1 : 1 ratio of HOCl or *N*-chloramine scavenged to selenoxide formed, as demonstrated in Chapter 3. As endogenous thiols and redox enzymes can reduce selenoxides, as described in Chapters 4 and 5, this gives potential for a catalytic scavenging cycle *in vivo*. This would allow SeMet and SeTal to remove oxidants with a greater than 1 : 1 ratio, without the destruction of the seleno compounds. These reactions are likely to be of significance as the higher second-order rate constants for SeMet and SeTal suggest that these compounds will remove oxidants more rapidly than endogenous thiols (Table 7.1). This was observed in GSR experiments, where the presence of SeMet increased the rate of NADPH consumption when TauCl was added to the NADPH/GSR/GSH system compared to the NADPH/GSR/GSH system in the absence of SeMet (Chapter 5). The interaction between selenium compounds and the GSR system demonstrated the potential for rapid oxidant detoxification, without complete consumption of thiols by selenoxides. This would allow for the continuation of the catalytic cycle, without a build up of selenoxides occuring.

Conversely, SeMet and SeTal in the presence of the NADPH/TrxR and other enzymes, Trx, Msrs and GPx, reduced the rate at which NADPH was consumed upon addition of *N*-chloramines. This is in contrast to work demonstrating the ability for SeMet to enhance the consumption of peroxides [474]. This may reflect the direct oxidation of NADPH by *N*-chloramines, which does not occur with peroxides [83, 138, 139]. Alternatively, the decrease in NADPH consumption observed may be due to a slower turn over of SeMetO and SeTalO compared to *N*-chloramines, whereas with peroxides this is reversed, with a slow consumption of peroxides and hence an observed increase in NADPH consumption. Rahmanto et al demonstrated that addition

of SeMet led to an increase in peroxide consumption when H_2O_2 or *t*-butylhydroperoxide were exposed to either the NADPH/TrxR/Trx system or J774A.1 cells, which was attributed to the catalytic removal of peroxides by SeMet [474]. The abilities of other selenium compounds to catalytically interact with the NADPH/TrxR/Trx system have been described with diselenides (such as selenocystine and Sec substituted GSSG) and other selenium compounds, such as ebselen, with these species increasing the rate at which H_2O_2 and ONOOH is removed [448, 491, 492]. While reduction of selenoxides mediated by TrxR is significantly slower than by thiols, the TrxR pathway may allow for continued catalytic scavenging of oxidants by SeMet and SeTal after cellular thiols are consumed.

It has been shown that the efficacy of action of selenium compounds as antioxidants may be further increased by optimisation of the surrounding chemical environment. Selenoethers synthesised by Prabhu et al, with the structure $Se(CH_2CH_2CHX)_2$ where X was either -OH, -COOH or NH_3^+ groups demonstrated differing GPx mimetic capabilities [443]. In this case, the –COOH substituted selenoether demonstrated the highest GPx mimetic ability, followed by –OH then $-NH_3^+$ [443]. However, these studies did not determine whether the rate limiting step was the oxidation of the selenoether, or subsequent repair of the oxidised product, and the differences in GPx activity were attributed to the differing stereochemistry between the compounds, with the –COOH substituted compound having the most easily accessible Se atom, and the $-NH_3^+$ substituted compound having the least accessible [443]. Furthermore, it has been proposed that weak interaction between the amino acid residues and the Sec residue of GPx enhance it's nucleophilic reactivity by stabilisation of the selenolate [619]. This reaction cycle however proceeds through a selenenic acid intermediate before GSH reduction, unlike SeMet and SeTal in this study where a selenoxide is formed.

In Chapter 4, it was demonstrated that the availability of amine groups increased the efficiency of selenoxide reduction. Whilst the mechanism was not fully elucidated in these studies, it is proposed that the selenium-amine interaction may facilitate a more efficient catalytic scavenging cycle. This could be further explored through thermodynamic modelling to assess potential interaction between the amine and selenium centre. Thus, strategic substitution of functional amine groups into the structure of new selenium compounds may allow the production of more effective

antioxidant compounds. Furthermore, functionalisation using other moieties may produce more targeted antioxidants, for example, a triphenylphosphine group may make selenium antioxidants more specific for oxidants produced by the mitochondria, due to the attraction of the positive phosphine to the mitochondria. This mitochondrial targeting strategy has been shown to be effective for mitoquinone (MitoQ), which links ubiquinone to a triphenylphosphine group by a long alkyl chain [620]. MitoQ has been shown to protect against hypertension and cardiac hypertrophy, while improving endothelial function in spontaneously hypertensive rats [621]. It has also demonstrated an ability to reduce macrophage numbers in atherosclerotic plaques [622] and prevent HOCl-induced cellular damage [438].

7.3 Potential for selenium compounds to modulate oxidative damage

SeMet and SeTal have demonstrated efficacy in protecting isolated proteins against oxidative damage upon exposure to HOCl [486]. Incubation of BSA and plasma proteins with SeTal and the related selenium-containing carbohydrate, 1,5-anhydro-5-selenogulitol, prior to exposure to HOCl was able to prevent damage to His, Lys, Met, Trp and Tyr residues, and also inhibited 3-Cl-Tyr formation [439, 486].

In Chapter 6, the ability of SeMet and SeTal to modulate oxidative damage to J774A.1 cells upon HOCl or TauCl exposure was assessed using thiol levels and Met oxidation as markers of oxidative damage. Exposure of cells or lysates to HOCl or TauCl caused a loss of thiols and an oxidation of Met residues, but SeMet and SeTal were unable to modulate these changes under the conditions employed. This is in contrast to previous reports where the presence of SeMet or SeTal has been shown to protect Met residues from oxidation when isolated proteins were exposed to HOCl [439, 486]. However, the protection reported by Storkey et al only achieved significance when the ratio of selenium compounds to HOCl was greater than 1 : 4, which was the maximum ratio used in this study [439, 486]. Future studies could potentially use a higher concentration of SeMet and SeTal, which may result in greater protection of protein residues when cells are exposed to HOCl and *N*-chloramines.

A potential limiting factor in the ability of SeMet and SeTal to scavenge hypohalous acids and *N*-chloramines *in vivo* is likely to be achieving a high enough concentration

in order to compete with other reactions. While no protection was observed in experiments measuring the consequences of oxidant exposure to cells in Chapter 6, it is unclear how much of the SeMet or SeTal were taken up by the cells. SeMet is known to be transported into the cell through Met channels [623], but the levels of SeTal taken up by cells have not been measured. This is an important area for further study, and could be done using techniques such ICP-MS [624], or x-ray absorption and fluorescence spectroscopy [625] which have been used to speciate selenium compounds in biological samples, in order to compare levels of selenium in the media to levels in the cytosol after SeMet or SeTal supplementation.

Kinetic modelling of HOCl reactions in plasma suggests that the primary target for HOCl would be protein residues, owing to their abundance, with Met and Cys residues being consumed first, followed by reaction with His and Lys residues [87]. The modelling demonstrates that GSH, which is present at 2 μM in plasma, and has a similarly high rate constant for the reaction with HOCl as SeMet and SeTal, consumes less than 1 % of HOCl [87]. However, the reaction with GSH is likely to be more significant in a cellular context where cytosolic GSH levels are 5-10 mM [626]. Based on these calculations and the rate constants for the reaction of SeMet and SeTal (which are similar to GSH (Table 7.1)), concentrations of SeMet and SeTal would need to reach a concentration of > 2 μM in plasma in order to make a significant contribution by directly scavenging HOCl. These concentrations of SeMet or SeTal may be difficult to achieve in plasma, owing to toxicity and factors such as absorption into the circulation and subsequent metabolism (in the case of SeMet). Possible toxicity and metabolism of SeTal is presently unknown, and should be the focus of future studies.

Scavenging *N*-chloramines may be a more feasible mechanism for SeMet and SeTal. *N*-chloramines are longer-lived oxidants *in vivo* compared to HOCl due to their lower reactivity, and these have a greater specificity for sulfur-containing residues [86, 136, 192]. The increased stability allows for diffusion away from the site of production, potentially inducing oxidative damage at other sites [14, 87, 181]. As the studies in Chapter 3 show that SeMet and SeTal are capable of rapid reaction with *N*-chloramines, they may be able to repair *N*-chloramine formation on proteins and hence reduce the propagation of oxidative damage away from the site of inflammation.

Furthermore, degradation of *N*-chloramines can lead to formation of N-centred radicals [141], which may also propagate HOCl-induced damage, or the formation of reactive aldehydes, which can further react to form advanced glycation end products [188]; these products are thought to be significant in diseases such as diabetes. Carbonyls, as a marker of protein *N*-chloramine or *N*-chloramide degradation after HOCl treatment, could be measured by assay with 2,4-dinitrophenylhydrazine [137, 547]. The ability of SeMet and SeTal to repair *N*-chloramines may lead to a decrease in protein carbonyl formation and therapeutic benefit.

It is also possible that SeMet and SeTal may modulate oxidative damage by other mechanisms, such as the upregulation of antioxidant defences and oxidative repair enzymes of the selenoproteome [529-531]. SeMet has demonstrated an ability to increase the levels of GPx and TrxR *in vivo* [524, 535], however this effect is dependent on baseline selenium levels. In patients with low baseline Se levels, SeMet supplementation increased expression of these selenoproteins [535], but this was not observed in patients with adequate Se levels. In a cellular context, pre-treatment with SeMet in rat cardiomyocytes led to increased viability after ischemia-reperfusion treatment [529]. The effect was attributed to the ability of SeMet to mitigate the increase in oxidative damage seen with ischemia-reperfusion injury. SeMet pre-treatment also prevented oxidative damage to trophoblast cells exposed to H_2O_2 or that induced by mitochondrial dysfunction [530, 531]. While no protection was afforded by SeMet in the current studies, which examine whether SeMet may protect against cell death in J774A.1 cells exposed to HOCl and TauCl, future studies using longer pre-incubation times may demonstrate protection as a result of SeMet-mediated increases in antioxidant defences. The ability of SeTal to upregulate selenoproteins has not yet been examined, and should be the focus of future studies. If, like SeMet, SeTal is capable of upregulating selenoproteins, this may be another pathway that SeTal could be capable of affording protection against oxidant damage.

7.4 Factors that may affect use of selenium compounds as antioxidants *in vivo*

Attempts to measure SeMet in human plasma have concluded that the majority of SeMet is bound to or incorporated into proteins, as free SeMet levels are below the

limits of detection [613]. However, supplementation with SeMet has been shown to increase Se levels in circulation with the increase being proportional to the level of SeMet being administered [505, 506, 627]. However, the speciation of the selenium compounds present in plasma is unclear, with most studies reporting total Se in plasma without identifying the chemical nature. In a study [627] where SeMet was administered at up to 500 μg per day as SeMet, total circulating Se levels were observed to increase with no change of expression of GPx or selenoprotein-P, though it was suggested that SeMet makes up 3% of total plasma Se. However, it should be noted that the reported increases in observed GPx and selenoprotein-P expression when patients are supplemented with SeMet are dependent on the subject's initial baseline selenium levels. Another study [628] showed that less than 0.5% of Se excreted in urine was in the form of SeMet when patients were administered the L-SeMet isomer, though when they were given DL-SeMet the SeMet concentrations in urine increased to 20 % of total Se. This was suggested to be due to the easier metabolism of L-SeMet, as the stereochemistry makes this a preferred substrate [628]. This suggests supplementation with D-SeMet may be a viable option to increase the plasma availability of free SeMet to act as an oxidant scavenger. Similarly to *in vivo* studies, speciation of selenium in cells post-treatment is not performed, though many studies have demonstrated increases in SeMet incorporation into protein, or increases in the selenoproteome, though these generally doesn't account for the total selenium studies [474, 513, 529-531, 538].

The low level of SeMet observed in plasma is likely to be due to either the metabolism of SeMet or due to the incorporation of SeMet into protein. SeMet is the major source of Se in the body [494], and is used by cells to produce Sec for insertion into selenoproteins [623]. SeMet can also be metabolised in the liver producing selenosugars, which are subsequently excreted in urine [623]. Alternatively, SeMet can be non-selectively incorporated into proteins replacing Met residues, as demonstrated by a cell-free synthesis of the human h-Ras protein [475]. When SeMet is incorporated into amyloid proteins, the ability of these proteins to form fibrils is reduced, hence decreasing toxicity [476]. The incorporation of SeMet may protect against oxidative damage, potentially due to the facile reduction of SeMetO, as demonstrated in Chapter 4.

It has been demonstrated that metabolism of SeMet by methioninases increases ROS generation in cells, particularly $O_2^{\bullet-}$, due to formation of selenolates [513]. This is potentially reflected in results from Chapter 6, where a reduction in thiol levels was observed in the presence of SeMet and SeTal, though this decrease was not statistically significant. The increase in ROS is believed to lead to apoptosis by induction of the p53 pathway [513, 518, 519], however, no increase in apoptosis was observed in J774A.1 cells incubated with SeMet in this study. Increases in $O_2^{\bullet-}$ when J774A.1 cells are exposed to SeMet and SeTal could be assessed by electron paramagnetic spectroscopy with spin trapping [629], or by assaying $O_2^{\bullet-}$ production using dihydroethidium and product determination by HPLC coupled with mass spectrometry [630]. Furthermore, induction of p53 may be occurring in J774A.1 cells at a later time point than that assessed in this study (2 h), as apoptosis due to SeMet has been reported after 48 – 72 h in other cells lines [513, 518, 519]. Further work at extended time points may be required in order to more fully elucidate the consequences of SeMet or SeTal incubation with the J774A.1 cells.

SeTal may not face the same limitations as SeMet, which is a primary source of selenium in the diet [494], is readily metabolised, and subsequently causes ROS formation [513] and is incorporated protein [623]. This may make SeTal a better candidate as an antioxidant scavenger by the Se being more available in the circulation, as it may not be metabolised to the same extent as SeMet. SeTal, in the conditions used in this study, was well tolerated by J774A.1 macrophages; however, bioavailability and toxicity have not been extensively examined with SeTal supplementation and should be the subject of future studies.

The studies in Chapter 6 used a macrophage-like murine cell line to assess the potential for SeMet and SeTal to modulate cellular damage due to exposure to HOCl or TauCl. The study could be extended to assess the benefit of SeMet and SeTal supplementation on primary human monocyte-derived macrophages, which would be a more relevant cell model for assessing potential production *in vivo*. Furthermore, future studies could assess the benefit of supplementing endothelial cells with SeMet and SeTal, as endothelial dysfunction induced by oxidant exposure is implicated in the initiation of atherosclerosis [310, 316, 631, 632]. This is significant as HOCl and *N*-chloramines activate independent cellular pathways in different cell types [89].

Supplementation with SeMet and SeTal may also be beneficial in other pathologies. Supplementation with SeMet or the selenium-containing compound ebselen has been reported to protect against alcohol-induced liver injury in rat models [633, 634]. Supplementation with SeMet reduces levels of oxidative stress in brains, which may be beneficial for neurological disorders such as Alzheimer's and Parkinson's disease [476, 635, 636]. *trans*-3,4-dihydroxyselenolane (DHS) is a cyclic selenium compound with similar chemical structure to SeTal and has been demonstrated to reduce indomethacin-induced gastric inflammation [637]. These studies demonstrate that selenium supplementation may be used as a potential therapy in numerous disease states, potentially by reducing of oxidative stress by acting as a catalytic oxidant scavenger as outlined in this thesis.

7.5 Concluding remarks

The studies presented in this Thesis highlight the potential for the use of SeMet and SeTal as catalytic scavengers of MPO-derived oxidants. It has demonstrated that SeMet and SeTal rapidly react with HOCl and *N*-chloramines in order to form selenoxides, which have been chemically characterised. Potential biologically relevant reduction pathways of the selenoxides were identified including rapid reduction by the endogenous thiol GSH, the rate of which has been determined, as well as through direct enzymatic reduction via the activity of TrxR. Taken together, these processes highlight the potential for a catalytic scavenging cycle that may modulate oxidative damage *in vivo.*

However, while SeMet and SeTal demonstrated favourable chemical properties as MPO-derived oxidant scavengers, limited modulation of oxidative damage was observed when cells were exposed to HOCl and TauCl in the presence of the selenium compounds. Given the limitations associated with the treatment conditions and methodology used to assess markers of oxidative damage and the cellular viability assays examined in this thesis, it is clear that more work is required to more fully elucidate how these selenium compounds are metabolised by cells, and whether they can protect cells from damage by MPO-derived oxidants.

The findings in this Thesis contribute significantly to the understanding of the mechanisms through which selenoethers may modulate oxidative damage. This may

provide insight into how better to design protective agents or antioxidants in the future. This has particular relevance for numerous inflammatory pathologies where MPO and oxidative damage induced by HOCl and *N*-chloramines are prevalent, including atherosclerosis, a disease that affects ca. 40 % of the Australian population. The ability of selenoethers to modulate inflammatory damage therefore has important implications for therapeutic application.

References

1. Smith, J.A., *Neutrophils, host-defense, and inflammation - A double-edged sword.* Journal of Leukocyte Biology, 1994. **56**(6): p. 672-686.

2. Davies, M., et al., *Mammalian heme peroxidases: from molecular mechanisms to health implications.* Antioxidants & Redox Signaling, 2008. **10**(7): p. 1199-1234.

3. Borregaard, N. and J.B. Cowland, *Granules of the human neutrophilic polymorphonuclear leukocyte.* Blood, 1997. **89**: p. 3503-3521.

4. Fiedler, T.J., C.A. Davey, and R.E. Fenna, *X-ray crystal structure and characterization of halide-binding sites of human myeloperoxidase at 1.8 Å resolution.* Journal of Biological Chemistry, 2000. **275**(16): p. 11964-11971.

5. Hansson, M., I. Olsson, and W.M. Nauseef, *Biosynthesis, processing, and sorting of human myeloperoxidase.* Archives of Biochemistry and Biophysics, 2006. **445**(2): p. 214-224.

6. Fenna, R., J. Zeng, and C. Davey, *Structure of the green heme in myeloperoxidase.* Archives of Biochemistry and Biophysics, 1995. **316**(1): p. 653-656.

7. Zeng, J. and R. Fenna, *X-ray crystal structure of canine myeloperoxidase at 3 Å resolution* 1.* Journal of Molecular Biology, 1992. **226**(1): p. 185-207.

8. Kooter, I.M., et al., *The sulfonium ion linkage in myeloperoxidase - Direct spectroscopic detection by isotopic labeling and effect of mutation.* Journal of Biological Chemistry, 1999. **274**(38): p. 26794-26802.

9. Furtmuller, P.G., et al., *Active site structure and catalytic mechanisms of human peroxidases.* Archives of Biochemistry and Biophysics, 2006. **445**(2): p. 199-213.

10. Abu-Ghazaleh, R.I., et al., *Eosinophil granule proteins in peripheral blood granulocytes.* Journal of Leukocyte Biology, 1992. **52**: p. 611-18.

11. Cheng, G., et al., *Identification and characterization of VPO1, a new animal heme-containing peroxidase.* Free Radical Biology and Medicine, 2008. **45**(12): p. 1682-1694.

12. Ihalin, R., V. Loimaranta, and J. Tenovuo, *Origin, structure, and biological activities of peroxidases in human saliva.* Archives of Biochemistry and Biophysics, 2006. **445**(2): p. 261-268.

13. O'Brien, P.J., *Peroxidases.* Chemico-Biological Interactions 2000. **129**(1-2): p. 113-139.

14. Kettle, A.J. and C.C. Winterbourn, *Myeloperoxidase: A key regulator of neutrophil oxidant production.* Redox Report, 1997. **3**(1): p. 3-15.

15. Jantschko, W., et al., *Redox intermediates of plant and mammalian peroxidases: A comparative transient-kinetic study of their reactivity toward indole derivatives.* Archives of Biochemistry and Biophysics, 2002. **398**(1): p. 12-22.

16. Furtmuller, P.G., et al., *Spectral and kinetic studies on eosinophil peroxidase compounds I and II and their reaction with ascorbate and tyrosine.* Biochimica Et Biophysica Acta-Protein Structure and Molecular Enzymology, 2001. **1548**(1): p. 121-128.

17. Winterbourn, C.C., et al., *Modeling the reactions of superoxide and myeloperoxidase in the neutrophil phagosome - Implications for microbial killing.* Journal of Biological Chemistry, 2006. **281**(52): p. 39860-39869.

18. Kettle, A.J., et al., *Reactions of superoxide with myeloperoxidase.* Biochemistry, 2007. **46**(16): p. 4888-4897.

19. Marquez, L.A. and H.B. Dunford, *Reaction of compound-III of myleoperoxidase with ascorbic-acid.* Journal of Biological Chemistry, 1990. **265**(11): p. 6074-6078.

20. Marquez, L.A. and H.B. Dunford, *Interaction of acetaminophen with myeloperoxidase intermediates: optimum stimulation of enzyme activity.* Archives of Biochemistry and Biophysics, 1993. **305**: p. 414-420.

21. Arnhold, J., et al., *Redox properties of the couple compound I/native enzyme of myeloperoxidase and eosinophil peroxidase.* European Journal of Biochemistry, 2001. **268**(19): p. 5142-5148.

22. Furtmuller, P.G., G. Regelsberger, and C. Obinger, *Standard reduction potentials of all couples of the peroxidase cycle of lactoperoxidase.* Journal of Inorganic Biochemistry, 2005. **99**: p. 1220-1229.

23. Furtmuller, P.G., et al., *Redox properties of the couples compound I/compound II and compound II/native enzyme of human myeloperoxidase.* Biochemical and Biophysical Research Communnications, 2003. **301**(2): p. 551-557.

24. Van Dalen, C.J., et al., *Thiocyanate and chloride as competing substrates for myeloperoxidase.* Biochemical Journal, 1997. **327**(2): p. 487-492.

25. Van Dalen, C.J. and A.J. Kettle, *Substrates and products of eosinophil peroxidase.* Biochemical Journal, 2001. **358**(1): p. 233-239.

26. Furtmuller, P.G., et al., *Reaction of lactoperoxidase compound I with halides and thiocyanate.* Biochemistry, 2002. **41**(39): p. 11895-11900.

27. Li, H., et al., *Vascular peroxidase 1 catalyzes the formation of hypohalous acids: Characterization of its substrate specificity and enzymatic properties.* Free Radical Biology and Medicine, 2012. **53**(10): p. 1954-1959.

28. Adamson, M. and J. Carlsson, *Lactoperoxidase and thiocyanate protect bacteria from hydrogen peroxide.* Infection and Immunity, 1982. **35**: p. 20-24.

29. Abu-Soud, H.M. and S.L. Hazen, *Nitric oxide is a physiological substrate for mammalian peroxidases.* Journal of Biological Chemistry, 2000. **275**(48): p. 37524-37532.

30. Arnhold, J., et al., *Kinetics and thermodynamics of halide and nitrite oxidation by mammalian heme peroxidases.* European Journal of Inorganic Chemistry, 2006(19): p. 3801-3811.

31. Albert, C.J., et al., *Eosinophil peroxidase-derived reactive brominating species target the vinyl ether bond of plasmalogens generating a novel chemoattractant, α-bromo fatty aldehyde.* Journal of Biological Chemistry, 2003. **278**(11): p. 8942-8950.

32. Albrich, J.M., C.A. McCarthy, and J.K. Hurst, *Biological reactivity of hypochlorous acid: Implications for microbicidal mechanisms of leukocyte myeloperoxidase.*

Proceedings of the National Academy of Sciences of the United States of America, 1981. **78**: p. 210-214.

33. Aldridge, R.E., et al., *Eosinophil peroxidase produces hypobromous acid in the airways of stable asthmatics.* Free Radical Biology and Medicine, 2002. **33**(6): p. 847-856.

34. Senthilmohan, R. and A.J. Kettle, *Bromination and chlorination reactions of myeloperoxidase at physiological concentrations of bromide and chloride.* Archives of Biochemistry and Biophysics, 2006. **445**(2): p. 235-244.

35. Ikeda-Saito, M., *A study of ligand binding to spleen myeloperoxidase.* Biochemistry, 1987. **26**(14): p. 4344-4349.

36. Spalteholz, H., O.M. Panasenko, and J. Arnhold, *Formation of reactive halide species by myeloperoxidase and eosinophil peroxidase.* Archives of Biochemistry and Biophysics, 2006. **445**(2): p. 225-234.

37. Marquez, L.A. and H.B. Dunford, *Kinetics of oxidation of tyrosine and dityrosine by myeloperoxidase compounds I and II - Implications for lipoprotein peroxidation studies.* Journal of Biological Chemistry, 1995. **270**(51): p. 30434-30440.

38. Monzani, E., et al., *Oxidation of phenolic compounds by lactoperoxidase. Evidence for the presence of a low-potential compound II during catalytic turnover.* Biochemistry, 1997. **36**(7): p. 1918-1926.

39. Burner, U., et al., *Mechanism of reaction of myeloperoxidase with nitrite.* Journal of Biological Chemistry, 2000. **275**(27): p. 20597-20601.

40. Heinecke, J.W., et al., *Tyrosyl radical generated by myeloperoxidase catalyzes the oxidative cross-linking of proteins.* Journal of Clinical Investigation, 1993. **91**(6): p. 2866-2872.

41. Savenkova, M.I., D.M. Mueller, and J.W. Heinecke, *Tyrosyl radical generated by myeloperoxidase is a physiological catalyst for the initiation of lipid-peroxidation in low-density-lipoprotein.* Journal of Biological Chemistry, 1994. **269**(32): p. 20394-20400.

42. Ohtaki, S., et al., *Reactions of purified hog thyroid peroxidase with H2O2, tyrosine, and methylmercaptoimidazole (Goitrogen) in comparison with bovine lactoperoxidase.* Journal of Biological Chemistry, 1982. **257**(2): p. 761-766.

43. Kettle, A.J. and L.P. Candaeis, *Oxidation of tryptophan by redox intermediates of myeloperoxidase and inhibition of hypochlorous acid production.* Redox Report, 2000. **5**(4): p. 179-184.

44. Gross, A.J. and I.W. Sizer, *Oxidation of tyramine, tyrosine and related products by peroxidase.* Journal of Biological Chemistry, 1959. **234**(6): p. 1611-1614.

45. Van Dalen, C.J., C.C. Winterbourn, and A.J. Kettle, *Mechanism of nitrite oxidation by eosinophil peroxidase: implications for oxidant production and nitration by eosinophils.* Biochemical Journal, 2006. **394**: p. 707-713.

46. Monzani, E., et al., *Mechanistic insight into the peroxidase catalyzed nitration of tyrosine derivatives by nitrite and hydrogen peroxide.* European Journal of Biochemistry, 2004. **271**(5): p. 895-906.

47. Eiserich, J.P., et al., *Myeloperoxidase, a leukocyte-derived vascular NO oxidase.* Science, 2002. **296**(5577): p. 2391-2394.

48. Baldus, S., et al., *Myeloperoxidase enhances nitric oxide catabolism during myocardial ischemia and reperfusion.* Free Radical Biology and Medicine, 2004. **37**(6): p. 902-911.

49. Abu-Soud, H.M. and S.L. Hazen, *Nitric oxide modulates the catalytic activity of myeloperoxidase.* Journal of Biological Chemistry, 2000. **275**(8): p. 5425-30.

50. Rees, M.D., et al., *Mechanism and regulation of peroxidase-catalyzed nitric oxide consumption in physiological fluids: critical protective actions of ascorbate and thiocyanate.* Free Radical Biology and Medicine, 2014. **72**: p. 91-103.

51. vanderVliet, A., et al., *Formation of reactive nitrogen species during peroxidase-catalyzed oxidation of nitrite - A potential additional, mechanism of nitric oxide-dependent toxicity.* Journal of Biological Chemistry, 1997. **272**(12): p. 7617-7625.

52. Eiserich, J.P., et al., *Formation of nitric oxide derived inflammatory oxidants by myeloperoxidase in neutrophils.* Nature, 1998. **391**(6665): p. 393-397.

53. Armesto, X.L., et al., *Aqueous chemistry of N-halo-compounds.* Chemical Society Reviews, 1998. **27**(6): p. 453-460.

54. Folkes, L.K., L.P. Candeias, and P. Wardman, *Kinetics and mechanisms of hypochlorous acid reactions.* Archives of Biochemistry and Biophysics, 1995. **323**(1): p. 120-126.

55. Hawkins, C.L. and M.J. Davies, *Hypochlorite-induced damage to DNA, RNA, and polynucleotides: Formation of chloramines and nitrogen-centered radicals.* Chemical Research in Toxicology, 2002. **15**(1): p. 83-92.

56. Thomas, E.L., *Myeloperoxidase, hydrogen-peroxide, chloride anti-microbial system - Nitrogen-chlorine derivatives of bacterial components in bactericidal action against escherichia-coli.* Infection and Immunity, 1979. **23**(2): p. 522-531.

57. Winterbourn, C.C., *Comparative reactivites of various biological compounds with myeloperoxidase hydrogen peroxide-chloride, and similarity of the oxidant to hypochlorite.* Biochimica Et Biophysica Acta, 1985. **840**(2): p. 204-210.

58. Armesto, X.L., M. Canle, and J.A. Santaballa, *Alpha-amino-acids chlorination in aqueous-media.* Tetrahedron, 1993. **49**(1): p. 275-284.

59. Schuller-Levis, G.B. and E. Park, *Taurine: new implications for an old amino acid.* FEMS Microbiology Letters, 2003. **226**(2): p. 195-202.

60. Pattison, D.I. and M.J. Davies, *Absolute rate constants for the reaction of hypochlorous acid with protein side chains and peptide bonds.* Chemical Research in Toxicology, 2001. **14**(10): p. 1453-1464.

61. Pattison, D.I. and M.J. Davies, *Kinetic analysis of the reactions of hypobromous acid with protein components: Implications for cellular damage and use of 3-bromotyrosine as a marker of oxidative stress.* Biochemistry, 2004. **43**(16): p. 4799-4809.

62. Pruetz, W.A., *Hypochlorous acid interactions with thiols, nucleotides, DNA and other biological substrates.* Archives of Biochemistry and Biophysics, 1996. **332**(1): p. 110-120.

63. Pruetz, W.A., *Interaction of hypochlorous acid with pyrimidine nucleotides, and secondary reactions of chlorinated pyrimidines with GSH, NADH, and other substrates.* Archives of Biochemistry and Biophysics, 1998. **349**(1): p. 183-191.

64. Hazen, S.L., et al., *Human neutrophils employ chlorine gas as an oxidant during phagocytosis.* Journal of Clinical Investigation, 1996. **98**(6): p. 1283-1289.

65. Henderson, J.P., et al., *Production of brominating intermediates by myeloperoxidase - A transhalogenation pathway for generating mutagenic nucleobases during inflammation.* Journal of Biological Chemistry, 2001. **276**(11): p. 7867-7875.

66. Morgan, P.E., R.T. Dean, and M.J. Davies, *Protective mechanisms against peptide and protein peroxides generated by singlet oxygen.* Free Radical Biology and Medicine, 2004. **36**(4): p. 484-496.

67. Arisawa, F., et al., *MCLA-dependent chemiluminescence suggests that singlet oxygen plays a pivotal role in myeloperoxidase-catalysed bactericidal action in neutrophil phagosomes.* Luminescence, 2003. **18**(4): p. 229-238.

68. Kanofsky, J.R., *Singlet oxygen production by lactoperoxidase. Evidence from 1270 nm chemiluminescence.* Journal of Biological Chemistry, 1983. **258**: p. 5991-5993.

69. Kanofsky, J.R., et al., *Singlet oxygen production by human eosinophils.* Journal of Biological Chemistry, 1988. **263**(20): p. 9692-9696.

70. Kanofsky, J.R., et al., *Biochemical requirements for singlet oxygen production by purified human myeloperoxidase.* Journal of Clinical Investigation, 1984. **74**: p. 1489-1495.

71. Kiryu, C., et al., *Physiological production of singlet molecular oxygen in the myeloperoxidase-H2O2-chloride system.* FEBS Letters, 1999. **443**(2): p. 154-158.

72. Steinbeck, M.J., A.U. Khan, and M.J. Karnovsky, *Intracellular singlet oxygen generation by phagocytosing neutrophils in response to particles coated with a chemical trap.* Journal of Biological Chemistry, 1992. **267**(19): p. 13425-13433.

73. Steinbeck, M.J., A.U. Khan, and M.J. Karnovsky, *Extracellular production of singlet oxygen by stimulated macrophages quantified using 9,10-diphenylanthracene and perylene in a polystyrene film.* Journal of Biological Chemistry, 1993. **268**(21): p. 15649-15654.

74. Tarr, M. and D. Paul Valenzeno, *Singlet oxygen: the relevance of extracellular production mechanisms to oxidative stress in vivo.* Photochemical and Photobiological Sciences, 2003. **2**(4): p. 355-361.

75. Babior, B.M., et al., *Investigating antibody-catalyzed ozone generation by human neutrophils.* Proceedings of the National Academy of Sciences of the United States of America, 2003. **100**(6): p. 3031-3034.

76. Kettle, A.J., B.M. Clark, and C.C. Winterbourn, *Superoxide converts indigo carmine to isatin sulfonic acid - Implications for the hypothesis that neutrophils produce ozone.* Journal of Biological Chemistry, 2004. **279**(18): p. 18521-18525.

77. Klebanoff, S.J., *Myeloperoxidase: friend and foe.* Journal of Leukocyte Biology, 2005. **77**(5): p. 598-625.

78. Pryor, W.A., et al., *Free radical biology and medicine: it's a gas, man!* American Journal of Physiology-Regulatory Integrative and Comparative Physiology, 2006. **291**(3): p. R491-R511.

79. Sies, H., *Ozone in arteriosclerotic plaques: Searching for the "smoking gun".* Angewandte Chemie-International Edition, 2004. **43**(27): p. 3514-3515.

80. Smith, L.L., *Oxygen, oxysterols, ouabain, and ozone: A cautionary tale.* Free Radical Biology and Medicine, 2004. **37**(3): p. 318-324.

81. Wentworth, P., et al., *Evidence for antibody-catalyzed ozone formation in bacterial killing and inflammation.* Science, 2002. **298**(5601): p. 2195-2199.

82. Morris, J.C., *Acid ionization constant of HOCl from 5 to 35 degrees.* Journal of Physical Chemistry, 1966. **70**(12): p. 3798-&.

83. Pruetz, W.A., et al., *On the irreversible destruction of reduced nicotinamide nucleotides by hypohalous acids.* Archives of Biochemistry and Biophysics, 2000. **380**(1): p. 181-191.

84. Ashby, M.T., A.C. Carlson, and M.J. Scott, *Redox buffering of hypochlorous acid by thiocyanate in physiologic fluids.* Journal of the American Chemical Society, 2004. **126**(49): p. 15976-7.

85. Nagy, P., J.L. Beal, and M.T. Ashby, *Thiocyanate is an efficient endogenous scavenger of the phagocytic killing agent hypobromous acid.* Chemical Research in Toxicology, 2006. **19**(4): p. 587-93.

86. Pattison, D.I. and M.J. Davies, *Reactions of myeloperoxidase-derived oxidants with biological substrates: Gaining chemical insight into human inflammatory diseases.* Current Medicinal Chemistry, 2006. **13**(27): p. 3271-3290.

87. Pattison, D.I., C.L. Hawkins, and M.J. Davies, *What are the plasma targets of the oxidant hypochlorous acid? A kinetic modeling approach.* Chemical Research in Toxicology, 2009. **22**(5): p. 807-817.

88. Pattison, D.I., M.J. Davies, and C.L. Hawkins, *Reactions and reactivity of myeloperoxidase-derived oxidants: Differential biological effects of hypochlorous and hypothiocyanous acids.* Free Radical Research, 2012. **46**(8): p. 975-995.

89. Rayner, B.S., D.T. Love, and C.L. Hawkins, *Comparative reactivity of myeloperoxidase-derived oxidants with mammalian cells.* Free Radical Biology and Medicine, 2014. **71**: p. 240-255.

90. Storkey, C., M.J. Davies, and D.I. Pattison, *Reevaluation of the rate constants for the reaction of hypochlorous acid (HOCl) with cysteine, methionine, and peptide derivatives using a new competition kinetic approach.* Free Radical Biology and Medicine, 2014. **73**: p. 60-6.

91. Nagy, P., G.N.L. Jameson, and C.C. Winterbourn, *Kinetics and mechanisms of the reaction of hypothiocyanous acid with 5-Thio-2-nitrobenzoic acid and reduced glutathione.* Chemical Research in Toxicology, 2009. **22**(11): p. 1833-1840.

92. Skaff, O., D.I. Pattison, and M.J. Davies, *Hypothiocyanous acid reactivity with low-molecular-mass and protein thiols: absolute rate constants and assessment of biological relevance.* Biochemical Journal, 2009. **422**: p. 111-117.

93. Armesto, X.L., et al., *First steps in the oxidation of sulfur-containing amino acids by hypohalogenation: Very fast generation of intermediate sulfenyl halides and halosulfonium cations.* Tetrahedron, 2000. **56**(8): p. 1103-1109.

94. Drozdz, R., J.W. Naskalski, and J. Sznajd, *Oxidation of amino-acids and peptides in reaction with myeloperoxidase, chloride and hydrogen-peroxide.* Biochimica Et Biophysica Acta, 1988. **957**(1): p. 47-52.

95. Fu, X.Y., D.M. Mueller, and J.W. Heinecke, *Generation of intramolecular and intermolecular sulfenamides, sulfinamides, and Sulfonamides by hypochlorous acid: A potential pathway for oxidative cross-linking of low-density lipoprotein by myeloperoxidase.* Biochemistry, 2002. **41**(4): p. 1293-1301.

96. Pereira, W.E., et al., *Chlorination studies .2. Reaction of aqueous hypochlorous acid with alpha-amino-acids and dipeptides.* Biochimica Et Biophysica Acta, 1973. **313**(1): p. 170-180.

97. Davies, M.J. and C.L. Hawkins, *Hypochlorite-induced oxidation of thiols: Formation of thiyl radicals and the role of sulfenyl chlorides as intermediates.* Free Radical Research, 2000. **33**(6): p. 719-729.

98. Skaff, O., et al., *Selenium-containing amino acids are targets for myeloperoxidase-derived hypothiocyanous acid: determination of absolute rate constants and implications for biological damage.* Biochemical Journal, 2012. **441**: p. 305-316.

99. Barrett, T.J., et al., *Inactivation of thiol-dependent enzymes by hypothiocyanous acid: role of sulfenyl thiocyanate and sulfenic acid intermediates.* Free Radical Biology and Medicine, 2012. **52**(6): p. 1075-1085.

100. Nagy, P. and M.T. Ashby, *Reactive sulfur species: Kinetics and mechanisms of the oxidation of cysteine by hypohalous acid to give cysteine sulfenic acid.* Journal of the American Chemical Society, 2007. **129**(45): p. 14082-14091.

101. Peshenko, I.V. and H. Shichi, *Oxidation of active center cysteine of bovine 1-Cys peroxiredoxin to the cysteine sulfenic acid form by peroxide and peroxynitrite.* Free Radical Biology and Medicine, 2001. **31**(3): p. 292-303.

102. Chae, H.Z., S.J. Chung, and S.G. Rhee, *Thioredoxin-dependent peroxide reductase from yeast.* Journal of Biological Chemistry, 1994. **269**(44): p. 27670-27678.

103. Woo, H.A., et al., *Reversing the inactivation of peroxiredoxins caused by cysteine sulfinic acid formation.* Science, 2003. **300**(5619): p. 653-656.

104. Rabilloud, T., et al., *Proteomics analysis of cellular response to oxidative stress - Evidence for in vivo overoxidation of peroxiredoxins at their active site.* Journal of Biological Chemistry, 2002. **277**(22): p. 19396-19401.

105. Yang, K.S., et al., *Inactivation of human peroxiredoxin I during catalysis as the result of the oxidation of the catalytic site cysteine to cysteine-sulfinic acid.* Journal of Biological Chemistry, 2002. **277**(41): p. 38029-38036.

106. Hawkins, C.L., D.I. Pattison, and M.J. Davies, *Hypochlorite-induced oxidation of amino acids, peptides and proteins.* Amino Acids, 2003. **25**(3-4): p. 259-274.

107. Harwood, D.T., A.J. Kettle, and C.C. Winterbourn, *Production of glutathione sulfonamide and dehydroglutathione from GSH by myeloperoxidase-derived oxidants and detection using a novel LC-MS/MS method.* Biochemical Journal, 2006. **399**(1): p. 161-8.

108. Raftery, M.J., et al., *Novel intra- and inter-molecular sulfinamide bonds in S100A8 produced by hypochlorite oxidation.* Journal of Biological Chemistry, 2001. **276**(36): p. 33393-33401.

109. Grimaud, R., et al., *Repair of oxidized proteins - Identification of a new methionine sulfoxide reductase.* Journal of Biological Chemistry, 2001. **276**(52): p. 48915-48920.

110. Levine, R.L., et al., *Methionine residues as endogenous antioxidants in proteins.* Proceedings of the National Academy of Sciences of the United States of America, 1996. **93**(26): p. 15036-15040.

111. Matheson, N.R. and J. Travis, *Differential effects of oxidizing agents on human plasma. alpha. 1-proteinase inhibitor and human neutrophil myeloperoxidase.* Biochemistry, 1985. **24**(8): p. 1941-1945.

112. Matheson, N.R. and J. Travis, *Differential-effects of oxidizing-agents on human-plasma alpha-1-proteinase inhibitor and human neutrophil myleoperoxidase.* Biochemistry, 1985. **24**(8): p. 1941-1945.

113. Wasil, M., et al., *The specificity of thiourea, dimethylthiourea and dimethylsulfoxide as scavengers of hydroxyl radicals - Their protection of alpha-1-antiproteinase against inactivation by hypochlorous acid.* Biochemical Journal, 1987. **243**(3): p. 867-870.

114. Halliwell, B., M. Wasil, and M. Grootveld, *Biologically significant scavenging of the myeloperoxidase-derived oxidant hypochlorous acid by ascorbic acid - Implications for antioxidant protection in the inflamed rheumatoid joint.* FEBS Letters, 1987. **213**(1): p. 15-17.

115. Peskin, A.V., et al., *Oxidation of methionine to dehydromethionine by reactive halogen species generated by neutrophils.* Biochemistry, 2009. **48**(42): p. 10175-10182.

116. Beal, J.L., S.B. Foster, and M.T. Ashby, *Hypochlorous acid reacts with the N-terminal methionines of proteins to give dehydromethionine, a potential biomarker for neutrophil-induced oxidative stress.* Biochemistry, 2009. **48**(46): p. 11142-11148.

117. Young, P.R. and A.V. Briedis, *Kinetics and mechanism of the glutathione-dependent reduction of dehydromethionine.* Biochimica Et Biophysica Acta, 1988. **967**(2): p. 318-21.

118. Ronsein, G.E., et al., *Cross-linking methionine and amine residues with reactive halogen species.* Free Radical Biology and Medicine, 2014. **70**: p. 278-287.

119. Winterbourn, C.C. and A.J. Kettle, *Biomarkers of myeloperoxidase-derived hypochlorous acid.* Free Radical Biology and Medicine, 2000. **29**(5): p. 403-409.

120. Kettle, A.J., *Neutrophils convert tyrosyl residues in albumin to chlorotyrosine.* FEBS Letters, 1996. **379**(1): p. 103-106.

121. Domigan, N.M., et al., *Chlorination of tyrosyl residues in peptides by myeloperoxidase and human neutrophils.* Journal of Biological Chemistry, 1995. **270**(28): p. 16542-16548.

122. Drabik, G. and J.W. Naskalski, *Chlorination of N-acetyltyrosine with HOCl, chloramines, and myeloperoxidase-hydrogen peroxide-chloride system.* Acta Biochimica Polonica, 2001. **48**(1): p. 271-5.

123. Chapman, A.L.P., et al., *Comparison of mono- and dichlorinated tyrosines with carbonyls for detection of hypochlorous acid modified proteins.* Archives of Biochemistry and Biophysics, 2000. **377**(1): p. 95-100.

124. Bergt, C., et al., *Lysine residues direct the chlorination of tyrosines in YXXK motifs of apolipoprotein A-I when hypochlorous acid oxidizes high density lipoprotein.* Journal of Biological Chemistry, 2004. **279**(9): p. 7856-7866.

125. Curtis, M.P., A.J. Hicks, and J.W. Neidigh, *Kinetics of 3-chlorotyrosine formation and loss due to hypochlorous acid and chloramines.* Chemical Research in Toxicology, 2011. **24**(3): p. 418-428.

126. Wu, W.J., et al., *Eosinophils generate brominating oxidants in allergen-induced asthma.* Journal of Clinical Investigation, 2000. **105**(10): p. 1455-1463.

127. Aune, T.M., E.L. Thomas, and M. Morrison, *Lactoperoxidase-catalyzed incorporation of thiocyanate ion into a protein substrate.* Biochemistry, 1977. **16**(21): p. 4611-4615.

128. Carvalho, L.C., et al., *A new insight on the hypochlorous acid scavenging mechanism of tryptamine and tryptophan derivatives.* Bioorganic & Medicinal Chemistry Letters, 2010. **20**(22): p. 6475-6478.

129. Estevao, M.S., et al., *Antioxidant activity of unexplored indole derivatives: Synthesis and screening.* European Journal of Medicinal Chemistry, 2010. **45**(11): p. 4869-4878.

130. Fu, X.Y., et al., *Specific sequence motifs direct the oxygenation and chlorination of tryptophan by myeloperoxidase.* Biochemistry, 2006. **45**(12): p. 3961-3971.

131. Aspee, A. and E.A. Lissi, *Chemiluminescence associated with amino acid oxidation mediated by hypochlorous acid.* Luminescence, 2002. **17**(3): p. 158-164.

132. Hawkins, C.L., et al., *Tryptophan residues are targets in hypothiocyanous acid-mediated protein oxidation.* Biochemical Journal, 2008. **416**(3): p. 441-52.

133. Bonifay, V., et al., *Tryptophan oxidation in proteins exposed to thiocyanate-derived oxidants.* Archives of biochemistry and biophysics, 2014. **564**: p. 1-11.

134. Pattison, D.I. and M.J. Davies, *Kinetic analysis of the role of histidine chloramines in hypochlorous acid mediated protein oxidation.* Biochemistry, 2005. **44**(19): p. 7378-7387.

135. Peskin, A.V., et al., *Chlorine transfer between glycine, taurine, and histamine: Reaction rates and impact on cellular reactivity.* Free Radical Biology and Medicine, 2004. **37**(10): p. 1622-1630.

136. Peskin, A.V. and C.C. Winterbourn, *Histamine chloramine reactivity with thiol compounds, ascorbate, and methionine and with intracellular glutathione.* Free Radical Biology and Medicine, 2003. **35**(10): p. 1252-1260.

137. Hawkins, C., D. Pattison, and M. Davies, *Hypochlorite-induced oxidation of amino acids, peptides and proteins.* Amino Acids, 2003. **25**(3): p. 259-274.

138. Prutz, W.A., *Consecutive halogen transfer between various functional groups induced by reaction of hypohalous acids: NADH oxidation by halogenated amide groups.* Archives of Biochemistry and Biophysics, 1999. **371**(1): p. 107-114.

139. Prutz, W.A., R. Kissner, and W.H. Koppenol, *Oxidation of NADH by chloramines and chloramides and its activation by iodide and by tertiary amines.* Archives of Biochemistry and Biophysics, 2001. **393**(2): p. 297-307.

140. Dean, R.T., et al., *Biochemistry and pathology of radical-mediated protein oxidation.* Biochemical Journal, 1997. **324**: p. 1-18.

141. Hawkins, C.L. and M.J. Davies, *Generation and propagation of radical reactions on proteins.* Biochimica Et Biophysica Acta-Bioenergetics, 2001. **1504**(2-3): p. 196-219.

142. Johnson, R.A. and F.D. Greene, *Chlorination with N-chloro amides .1. Intermolecular and intramolecular chlorination.* Journal of Organic Chemistry, 1975. **40**(15): p. 2186-2192.

143. Johnson, R.A. and F.D. Greene, *Chlorination with N-chloro amides .2. Selectivity of hydrogen abstraction by amidyl radicals.* Journal of Organic Chemistry, 1975. **40**(15): p. 2192-2196.

144. Neale, R.S., *Nitrogen radicals as synthesis intermediates - N-Halamide rearrangements and additions to unsaturated hydrocarbons.* International Journal of Methods in Synthetic Organic Chemistry, 1971(1): p. 1-&.

145. Hawkins, C.L. and M.J. Davies, *Hypochlorite-induced damage to proteins: formation of nitrogen-centred radicals from lysine residues and their role in protein fragmentation.* Biochemical Journal, 1998. **332**: p. 617-625.

146. Jerlich, A., et al., *Pathways of phospholipid oxidation by HOCl in human LDL detected by LC-MS.* Free Radical Biology and Medicine, 2000. **28**(5): p. 673-682.

147. Pattison, D.I., C.L. Hawkins, and M.J. Davies, *Hypochlorous acid-mediated oxidation of lipid components and antioxidants present in low-density lipoproteins: Absolute rate constants, product analysis, and computational modeling.* Chemical Research in Toxicology, 2003. **16**(4): p. 439-449.

148. Panasenko, O.M., et al., *Hypochlorite-induced peroxidation of egg yolk phosphatidylcholine is mediated by hydroperoxides.* Free Radical Research, 1997. **27**(1): p. 1-12.

149. Carr, A.C., et al., *Nuclear magnetic resonance characterization of 6 alpha-chloro-5 beta-cholestane-3 beta,5-diol formed from the reaction of hypochlorous acid with cholesterol.* Lipids, 1997. **32**(4): p. 363-367.

150. Heinecke, J.W., et al., *Cholesterol chlorohydrin synthesis by the myeloperoxidase-hydrogen peroxide-chloride system - Potential markers for lipoproteins oxidatively damaged by phagocytes.* Biochemistry, 1994. **33**(33): p. 10127-10136.

151. Skaff, O., D.I. Pattison, and M.J. Davies, *The vinyl ether linkages of plasmalogens are favored targets for myeloperoxidase-derived oxidants: A kinetic study.* Biochemistry, 2008. **47**(31): p. 8237-8245.

152. Lessig, J., et al., *Hypochlorous acid-mediated generation of glycerophosphocholine from unsaturated plasmalogen glycerophosphocholine lipids.* Journal of Lipid Research, 2007. **48**(6): p. 1316-1324.

153. Lessig, J. and B. Fuchs, *HOCl-mediated glycerophosphocholine and glycerophosphoethanolamine generation from plasmalogens in phospholipid mixtures.* Lipids, 2010. **45**(1): p. 37-51.

154. Marsche, G., et al., *2-Chlorohexadecanal derived from hypochlorite-modified high-density lipoprotein–associated plasmalogen as a natural inhibitor of endothelial nitric oxide biosynthesis.* Arteriosclerosis, Thrombosis, and Vascular Biology, 2004. **24**(12): p. 2302-2306.

155. Thukkani, A.K., et al., *Identification of α-chloro fatty aldehydes and unsaturated lysophosphatidylcholine molecular species in human atherosclerotic lesions.* Circulation, 2003. **108**(25): p. 3128-3133.

156. Skaff, O., D.I. Pattison, and M.J. Davies, *Kinetics of hypobromous acid-mediated oxidation of lipid components and antioxidants.* Chemical Research in Toxicology, 2007. **20**(12): p. 1980-8.

157. Exner, M., et al., *Thiocyanate catalyzes myeloperoxidase-initiated lipid oxidation in LDL.* Free Radical Biology and Medicine, 2004. **37**(2): p. 146-55.

158. Ismael, F.O., et al., *Comparative reactivity of the myeloperoxidase-derived oxidants HOCl and HOSCN with low-density lipoprotein (LDL): Implications for foam cell formation in atherosclerosis.* Archives of Biochemistry and Biophysics, 2015. **573**(0): p. 40-51.

159. Dennis, W.H., V.P. Olivieri, and C.W. Kruse, *Reaction of neucleotides with aqueous hypochorous acid.* Water Research, 1979. **13**(4): p. 357-362.

160. Gould, J.P., J.T. Richards, and M.G. Miles, *The kinetics and primary products of uracil chlorination.* Water Research, 1984. **18**(2): p. 205-212.

161. Suzuki, T., et al., *Formation of spiroiminodihydantoin nucleoside by reaction of 8-oxo-7,8-dihydro-2 '-deoxyguanosine with hypochlorous acid or a myeloperoxidase-H2O2-Cl- system.* Chemical Research in Toxicology, 2001. **14**(9): p. 1163-1169.

162. Stanley, N.R., D.I. Pattison, and C.L. Hawkins, *Ability of hypochlorous acid and N-chloramines to chlorinate DNA and its constituents.* Chemical Research in Toxicology, 2010. **23**(7): p. 1293-1302.

163. Henderson, J.P., J. Byun, and J.W. Heinecke, *Chlorination of nucleobases, RNA and DNA by myeloperoxidase: a pathway for cytotoxicity and mutagenesis by activated phagocytes.* Redox Report, 1999. **4**(6): p. 319-320.

164. Masuda, M., et al., *Chlorination of guanosine and other nucleosides by hypochlorous acid and myeloperoxidase of activated human neutrophils - Catalysis by nicotine and trimethylamine.* Journal of Biological Chemistry, 2001. **276**(44): p. 40486-40496.

165. Spencer, J.P.E., et al., *Nitrite-induced deamination and hypochlorite-induced oxidation of DNA in intact human respiratory tract epithelial cells.* Free Radical Biology and Medicine, 2000. **28**(7): p. 1039-1050.

166. Whiteman, M., et al., *Loss of oxidized and chlorinated bases in DNA treated with reactive oxygen species: implications for assessment of oxidative damage in vivo.* Biochemical and Biophysical Research Communications, 2002. **296**(4): p. 883-889.

167. Suzuki, T., A. Nakamura, and M. Inukai, *Reaction of 3',5'-di-O-acetyl-2'-deoxyguansoine with hypobromous acid.* Bioorganic & Medicinal Chemistry, 2013. **21**(13): p. 3674-9.

168. White, W.E., K.M. Pruitt, and B. Mansson-Rahemtulla, *Peroxidase-thiocyanate-peroxide antibacterial system does not damage DNA.* Antimicrobial Agents and Chemotherapy, 1983. **23**(2): p. 267-272.

169. Hawkins, C.L. and M.J. Davies, *Degradation of hyaluronic acid, poly- and monosaccharides and model compounds by hypochlorite: Evidence for radical intermediates and fragmentation.* Free Radical Biology and Medicine, 1998. **24**(9): p. 1396-1410.

170. Rees, M.D. and M.J. Davies, *Heparan sulfate degradation via reductive homolysis of its N-chloro derivatives.* Journal of the American Chemical Society, 2006. **128**(9): p. 3085-3097.

171. Rees, M.D., C.L. Hawkins, and M.J. Davies, *Hypochlorite-mediated fragmentation of hyaluronan, chondroitin sulfates, and related N-acetyl glycosamines: Evidence for chloramide intermediates, free radical transfer reactions, and site-specific fragmentation.* Journal of the American Chemical Society, 2003. **125**(45): p. 13719-13733.

172. Rees, M.D., D.I. Pattison, and M.J. Davies, *Oxidation of heparan sulphate by hypochlorite: role of N-chloro derivatives and dichloramine-dependent fragmentation.* Biochemical Journal, 2005. **391**: p. 125-134.

173. Akeel, A., et al., *Chlorination and oxidation of heparin and hyaluronan by hypochlorous acid and hypochlorite anions: effect of sulfate groups on reaction pathways and kinetics.* Free Radical Biology and Medicine, 2013. **56**: p. 72-88.

174. Sibanda, S., et al., *Efficiencies of fragmentation of glycosaminoglycan chloramides of the extracellular matrix by oxidizing and reducing radicals: potential site-specific targets in inflammation?* Free Radical Biology and Medicine, 2013. **65**: p. 280-290.

175. Rees, M.D., C.L. Hawkins, and M.J. Davies, *Hypochlorite and superoxide radicals can act synergistically to induce fragmentation of hyaluronan and chondroitin sulphates.* Biochemical Journal, 2004. **381**: p. 175-184.

176. Katrantzis, M., et al., *The oxidant hypochlorite (OCl–), a product of the myeloperoxidase system, degrades articular cartilage proteoglycan aggregate.* Free Radical Biology and Medicine, 1991. **10**(2): p. 101-109.

177. Henrotin, Y.E., P. Bruckner, and J.P.L. Pujol, *The role of reactive oxygen species in homeostasis and degradation of cartilage.* Osteoarthritis and Cartilage, 2003. **11**(10): p. 747-755.

178. Kennett, E.C., et al., *Mechanisms and consequences of oxidative damage to extracellular matrix.* Biochemical Society Transactions, 2011. **39**(5): p. 1279.

179. Pattison, D.I. and M.J. Davies, *Evidence for rapid inter- and intramolecular chlorine transfer reactions of histamine and carnosine chloramines: Implications for the prevention of hypochlorous-acid-mediated damage.* Biochemistry, 2006. **45**(26): p. 8152-8162.

180. Pattison, D.I., C.L. Hawkins, and M.J. Davies, *Hypochlorous acid-mediated protein oxidation: How important are chloramine transfer reactions and protein tertiary Structure?* Biochemistry, 2007. **46**(34): p. 9853-9864.

181. Carr, A.C., et al., *Relative reactivities of N-chloramines and hypochlorous acid with human plasma constituents.* Free Radical Biology and Medicine, 2001. **30**(5): p. 526-536.

182. Roemeling, M.D., et al., *Imidazole catalyzes chlorination by unreactive primary chloramines.* Free Radical Biology and Medicine, 2015. **82**(0): p. 167-178.

183. Cunningham, C., K.F. Tipton, and H.B.F. Dixon, *Conversion of taurine into N-chlorotaurine (taurine chloramine) and sulphoacetaldehyde in response to oxidative stress.* Biochemical Journal, 1998. **330**: p. 939-945.

184. Hazen, S.L., et al., *Human neutrophils employ the myeloperoxidase hydrogen peroxide chloride system to oxidize alpha-amino acids to a family of reactive aldehydes - Mechanistic studies identifying labile intermediates along the reaction pathway.* Journal of Biological Chemistry, 1998. **273**(9): p. 4997-5005.

185. Yuan, W., et al., *Hypochlorous acid converts the gamma-glutamyl group of glutathione disulfide to 5-hydroxybutyrolactam, a potential marker for neutrophil activation.* Journal of Biological Chemistry, 2009. **284**(39): p. 26908-26917.

186. Hazell, L.J., J.J.M. Vandenberg, and R. Stocker, *Oxidation of low-denisty-lipoprotein by hypochlorite causes aggregation that is mediated by modification of lysine residues rather than lipid oxidation.* Biochemical Journal, 1994. **302**: p. 297-304.

187. Anderson, M.M., et al., *Human neutrophils employ the myeloperoxidase-hydrogen peroxide-chloride system to convert hydroxy-amino acids into glycolaldehyde, 2-hydroxypropanal, and acrolein - A mechanism for the generation of highly reactive alpha-hydroxy and alpha,beta-unsaturated aldehydes by phagocytes at sites of inflammation.* Journal of Clinical Investigation, 1997. **99**(3): p. 424-432.

188. Basta, G., A.M. Schmidt, and R. De Caterina, *Advanced glycation end products and vascular inflammation: implications for accelerated atherosclerosis in diabetes.* Cardiovascular Research, 2004. **63**(4): p. 582-592.

189. Hawkins, C.L. and M.J. Davies, *Reaction of HOCl with amino acids and peptides: EPR evidence for rapid rearrangement and fragmentation, reactions of nitrogen-*

centred radicals. Journal of the Chemical Society-Perkin Transactions 2, 1998(9): p. 1937-1945.

190. Hawkins, C.L. and M.J. Davies, *Hypochlorite-induced damage to nucleosides: formation of chloramines and nitrogen-centered radicals.* Chemical Research in Toxicology, 2001. **14**(8): p. 1071-81.

191. Pattison, D.I., M.J. Davies, and K.D. Asmus, *Absolute rate constants for the formation of nitrogen-centred radicals from chloramines/amides and their reactions with antioxidants.* Journal of the Chemical Society-Perkin Transactions 2, 2002(8): p. 1461-1467.

192. Peskin, A.V. and C.C. Winterbourn, *Kinetics of the reactions of hypochlorous acid and amino acid chloramines with thiols, methionine, and ascorbate.* Free Radical Biology and Medicine, 2001. **30**(5): p. 572-579.

193. Hawkins, C.L., *The role of hypothiocyanous acid (HOSCN) in biological systems.* Free Radical Research, 2009. **43**(12): p. 1147-58.

194. Aratani, Y., et al., *Severe impairment in early host defense against Candida albicans in mice deficient in myeloperoxidase.* Infection and Immunity, 1999. **67**(4): p. 1828-1836.

195. Hirche, T.O., et al., *Myeloperoxidase plays critical roles in killing Klebsiella pneumoniae and inactivating neutrophil elastase: Effects on host defense.* Journal of Immunology, 2005. **174**(3): p. 1557-1565.

196. Thong, Y.H., *How important is the myeloperoxidase microbicidal system of phagocytic cells?* Medical Hypotheses, 1982. **8**: p. 249-254.

197. Klebanoff, S.J. and R.W. Coombs, *Virucidal effect of stimulated eosinophils on human immunodeficiency virus type 1.* AIDS Research and Human Retroviruses, 1996. **12**(1): p. 25-29.

198. Chapman, A.L.P., et al., *Chlorination of bacterial and neutrophil proteins during phagocytosis and killing of Staphylococcus aureus.* Journal of Biological Chemistry, 2002. **277**(12): p. 9757-9762.

199. Rosen, H., J.R. Crowley, and J.W. Heinecke, *Human neutrophils use the myeloperoxidase-hydrogen peroxide-chloride system to chlorinate but not nitrate bacterial proteins during phagocytosis.* Journal of Biological Chemistry, 2002. **277**(34): p. 30463.

200. Jong, E.C., W.R. Henderson, and S.J. Klebanoff, *Bactericidal activity of eosinophil peroxidase.* Journal of Immunology, 1980. **124**: p. 1378-1382.

201. Jong, E.C., A.A.F. Mahmoud, and S.J. Klebanoff, *Peroxidase-mediated toxicity to schistosomula of Schistosoma mansoni.* Journal of Immunology, 1981. **126**: p. 468-471.

202. Eitzinger, C., et al., *N-Chlorotaurine, a long-lived oxidant produced by human leukocytes, inactivates shiga toxin of enterohemorrhagic Escherichia coli.* Plos One, 2012. **7**(11).

203. Gottardi, W. and M. Nagl, *N-chlorotaurine, a natural antiseptic with outstanding tolerability.* Journal of Antimicrobial Chemotherapy, 2010. **65**(3): p. 399-409.

204. Nagl, M., et al., *Bactericidal activity of micromolar N-chlorotaurine: Evidence for its antimicrobial function in the human defense system.* Antimicrobial Agents and Chemotherapy, 2000. **44**(9): p. 2507-2513.

205. Yazdanbakhsh, M., C.M. Eckmann, and D. Roos, *Killing of Schistosomula by taurine chloramine and taurine bromamine.* American Journal of Tropical Medicine and Hygiene, 1987. **37**(1): p. 106-110.

206. Kim, C., et al., *The production of superoxide anion and nitric oxide by cultured murine leukocytes and the accumulation of TNF-alpha in the conditioned media is inhibited by taurine chloramine.* Immunopharmacology, 1996. **34**(2-3): p. 89-95.

207. Marcinkiewicz, J., et al., *Taurine chloramine down-regulates the generation of murine neutrophil inflammatory mediators.* Immunopharmacology, 1998. **40**(1): p. 27-38.

208. Park, E., et al., *Taurine chloramine inhibits lymphocyte proliferation and decreases cytokine production in activated human leukocytes.* Clinical Immunology, 2002. **102**(2): p. 179-184.

209. Ogino, T., et al., *Monochloramine inhibits phorbol ester-inducible neutrophil respiratory burst activation and T cell interleukin-2 receptor expression by inhibiting inducible protein kinase C activity.* Journal of Biological Chemistry, 1997. **272**(42): p. 26247-26252.

210. Choi, H.S., Y.-N. Cha, and C. Kim, *Taurine chloramine inhibits PMA-stimulated superoxide production in human neutrophils perhaps by inhibiting phosphorylation and translocation of p47(phox).* International Immunopharmacology, 2006. **6**(9): p. 1431-1440.

211. Dallegri, F., et al., *Erythrocyte lysis by PMA-triggered neutrophil polymorphonuclears - Evidence for an hypochlorous acid-dependent process.* Immunology, 1985. **55**(4): p. 639-645.

212. Dallegri, F., et al., *Role of hypochlorous acid and chloramines in the extracellular cytolysis by neutrophil polymorphonuclear leukocytes.* Journal of Clinical & Laboratory Immunology, 1986. **20**(1): p. 37-41.

213. Vissers, M.C.M., et al., *Membrane-changes associated with lysis of red-blood-cells by hypochlorous acid.* Free Radical Biology and Medicine, 1994. **16**(6): p. 703-712.

214. Tatsumi, T. and H. Fliss, *Hypochlorous acid and chloramines increase endothelial permeability: Possible involvement of cellular zinc.* American Journal of Physiology, 1994. **267**(4 PART 2): p. H1597-H1607.

215. Abernathy, F. and E.R. Pacht, *Alteration of adenosine-triphosphate and other nucleotides after sublethal oxidant injury to rat type-II alveolar epithelial cells.* American Journal of the Medical Sciences, 1995. **309**(3): p. 140-145.

216. Grisham, M.B., et al., *Effects of neutrophil-derived oxidants on intestinal permeability, electrolyte transport and epithelial-cell viability.* Inflammation, 1990. **14**(5): p. 531-542.

217. Vile, G.F., L.A. Rothwell, and A.J. Kettle, *Initiation of rapid, p53-dependent growth arrest in cultured human skin fibroblasts by reactive chlorine species.* Archives of Biochemistry and Biophysics, 2000. **377**(1): p. 122-128.

218. Slivka, A., A.F. Lobuglio, and S.J. Weiss, *Potential role for hypochlorous acid in granulocyte-mediated tumor-cell cytotoxicity.* Blood, 1980. **55**(2): p. 347-350.

219. Vissers, M.C.M., A.C. Carr, and A.L.P. Chapman, *Comparison of human red cell lysis by hypochlorous and hypobromous acids: insights into the mechanism of lysis.* Biochemical Journal, 1998. **330**: p. 131-138.

220. Schraufstatter, I.U., et al., *Mechanisms of hypochlorite injury of target-cells.* Journal of Clinical Investigation, 1990. **85**(2): p. 554-562.

221. Lloyd, M.M., et al., *Comparative reactivity of the myeloperoxidase-derived oxidants hypochlorous acid and hypothiocyanous acid with human coronary artery endothelial cells.* Free Radical Biology and Medicine, 2013. **65**: p. 1352-1362.

222. Lloyd, M.M., et al., *Hypothiocyanous acid is a more potent inducer of apoptosis and protein thiol depletion in murine macrophage cells than hypochlorous acid or hypobromous acid.* Biochemical Journal, 2008. **414**: p. 271-280.

223. Vissers, M.C.M., W.G. Lee, and M.B. Hampton, *Regulation of apoptosis by vitamin C: specific protection of the apoptotic machinery against exposure to chlorinated oxidants.* Journal of Biological Chemistry, 2001. **276**(50): p. 46835-46840.

224. Thomas, E.L., M.B. Grisham, and M.M. Jefferson, *Cytotoxicity of chloramines.* Methods in Enzymology, 1986. **132**: p. 585-93.

225. Pullar, J.M., C.C. Winterbourn, and M. Vissers, *Loss of GSH and thiol enzymes in endothelial cells exposed to sublethal concentrations of hypochlorous acid.* American Journal of Physiology-Heart and Circulatory Physiology, 1999. **277**(4): p. H1505-H1512.

226. Vissers, M. and C.C. Winterbourn, *Oxidation of intracellular glutathione after exposure of human red blood cells to hypochlorous acid.* Biochemical Journal, 1995. **307**(1): p. 57-62.

227. Pullar, J.M., M.C.M. Vissers, and C.C. Winterbourn, *Glutathione oxidation by hypochlorous acid in endothelial cells produces glutathione sulfonamide as a major product but not glutathione disulfide.* Journal of Biological Chemistry, 2001. **276**(25): p. 22120-22125.

228. Yang, Y.-t.T., M. Whiteman, and S.P. Gieseg, *HOCl causes necrotic cell death in human monocyte derived macrophages through calcium dependent calpain activation.* Biochimica et Biophysica Acta (BBA) - Molecular Cell Research, 2012. **1823**(2): p. 420-429.

229. Summers, F.A., A.F. Quigley, and C.L. Hawkins, *Identification of proteins susceptible to thiol oxidation in endothelial cells exposed to hypochlorous acid and N-chloramines.* Biochemical and Biophysical Research Communications, 2012. **425**(2): p. 157-161.

230. Tristan, C., et al., *The diverse functions of GAPDH: Views from different subcellular compartments.* Cellular Signalling, 2011. **23**(2): p. 317-323.

231. Hara, M.R., M.B. Cascio, and A. Sawa, *GAPDH as a sensor of NO stress.* Biochimica Et Biophysica Acta-Molecular Basis of Disease, 2006. **1762**(5): p. 502-509.

232. Sen, N., et al., *Nitric oxide-induced nuclear GAPDH activates p300/CBP and mediates apoptosis.* Nature Cell Biology, 2008. **10**(7): p. 866-873.

233. McKenzie, S.M., W.F. Doe, and G.D. Buffinton, *5-Aminosalicylic acid prevents oxidant mediated damage of glyceraldehyde-3-phosphate dehydrogenase in colon epithelial cells.* Gut, 1999. **44**(2): p. 180-185.

234. Dallegri, F., et al., *Neutrophil-induced depletion of adenosine-triphosphate in target cells - Evidence for a hypochlorous acid-mediated process.* Journal of Laboratory and Clinical Medicine, 1988. **112**(6): p. 765-772.

235. Gilbert, H.F., *Protein disulfide isomerases*, in *eLS*. 2001, John Wiley & Sons, Ltd.

236. Gothel, S.F. and M.A. Marahiel, *Peptidyl-prolyl cis-trans isomerases, a superfamily of ubiquitous folding catalysts.* Cellular and Molecular Life Sciences, 1999. **55**(3): p. 423-436.

237. Schroder, M. and R.J. Kaufman, *The mammalian unfolded protein response*, in *Annual Review of Biochemistry*. 2005, Annual Reviews: Palo Alto. p. 739-789.

238. Lane, Amanda E., et al., *The myeloperoxidase-derived oxidant HOSCN inhibits protein tyrosine phosphatases and modulates cell signalling via the mitogen-activated protein kinase (MAPK) pathway in macrophages.* Biochemical Journal, 2010. **430**(Pt 1): p. 161-169.

239. Fliss, H. and M. Menard, *Hypochlorous acid-induced mobilization of zinc from metalloproteins.* Archives of Biochemistry and Biophysics, 1991. **287**(1): p. 175-179.

240. Fliss, H., M. Menard, and M. Desai, *Hypochlorous acid mobilizes cellular zinc.* Canadian Journal of Physiology and Pharmacology, 1991. **69**(11): p. 1686-1691.

241. Tatsumi, T., et al., *Hypochlorous acid mobilizes intracellular zinc in isolated rat heart myocytes.* Japanese Circulation Journal, 1994. **58**(7): p. 449.

242. Xu, J., et al., *Uncoupling of endothelial nitric oxidase synthase by hypochlorous acid - Role of NAD(P)H oxidase-derived superoxide and peroxynitrite.* Arteriosclerosis Thrombosis and Vascular Biology, 2006. **26**(12): p. 2688-2695.

243. Talib, J., et al., *The smoking-associated oxidant hypothiocyanous acid induces endothelial nitric oxide synthase dysfunction.* Biochemical Journal, 2014. **457**(1): p. 89-97.

244. Talib, J., et al., *P20 - Disruption of the iron-sulfur cluster of aconitase by myeloperoxidase-derived oxidants.* Free Radical Biology and Medicine, 2014. **75, Supplement 1**(0): p. S27-S28.

245. Peskin, A.V. and C.C. Winterbourn, *Taurine chloramine is more selective than hypochlorous acid at targeting critical cysteines and inactivating creatine kinase and glyceraldehyde-3-phosphate dehydrogenase.* Free Radical Biology and Medicine, 2006. **40**(1): p. 45-53.

246. Midwinter, R.G., et al., *Extracellular oxidation by taurine chloramine activates ERK via the epidermal growth factor receptor.* Journal of Biological Chemistry, 2004. **279**(31): p. 32205-32211.

247. Bubici, C., et al., *The NF-kB-mediated control of ROS and JNK signaling.* Histology and Histopathology, 2006(21): p. 69-80.

248. Marcinkiewicz, J., et al., *Taurine chloramine, a product of activated neutrophils, inhibits in vitro the generation of nitric oxide and other macrophage inflammatory mediators.* Journal of Leukocyte Biology, 1995. **58**(6): p. 667-674.

249. Park, E., G. Schullerlevis, and M.R. Quinn, *Taurine chloramine inhibits production of nitric-oxide and TNF-alpha in activated RAW-264.7 cell mechanisms that involve transcriptional and translational events.* Journal of Immunology, 1995. **154**(9): p. 4778-4784.

250. Barua, M., Y. Liu, and M.R. Quinn, *Taurine chloramine inhibits inducible nitric oxide synthase and TNF-alpha gene expression in activated alveolar macrophages: Decreased NF-kappa B activation and I kappa B kinase activity.* Journal of Immunology, 2001. **167**(4): p. 2275-2281.

251. Kanayama, A., et al., *Oxidation of I kappa B alpha at methionine 45 is one cause of taurine chloramine-induced inhibition of NF-kappa B activation.* Journal of Biological Chemistry, 2002. **277**(27): p. 24049-24056.

252. Kim, J.W. and C. Kim, *Inhibition of LPS-induced NO production by taurine chloramine in macrophages is mediated though Ras-ERK-NF-kappa B.* Biochemical Pharmacology, 2005. **70**(9): p. 1352-1360.

253. Dinkova-Kostova, A.T., et al., *Direct evidence that sulfhydryl groups of Keap1 are the sensors regulating induction of phase 2 enzymes that protect against carcinogens and oxidants.* Proceedings of the National Academy of Sciences of the United States of America, 2002. **99**(18): p. 11908-11913.

254. Motterlini, R., C.J. Green, and R. Foresti, *Regulation of heme oxygenase-1 by redox signals involving nitric oxide.* Antioxidants & Redox Signaling, 2002. **4**(4): p. 615-624.

255. Kim, C., et al., *Taurine chloramine induces heme oxygenase-1 expression via Nrf2 activation in murine macrophages.* International Immunopharmacology, 2010. **10**(4): p. 440-446.

256. Jang, J.S., et al., *Taurine Chloramine Activates Nrf2, Increases HO-1 Expression and Protects Cells from Death Caused by Hydrogen Peroxide.* Journal of Clinical Biochemistry and Nutrition, 2009. **45**(1): p. 37-43.

257. Olszanecki, R. and J. Marcinkiewicz, *Taurine chloramine and taurine bromamine induce heme oxygenase-1 in resting and LPS-stimulated J774.2 macrophages.* Amino Acids, 2004. **27**(1): p. 29-35.

258. Piao, S., Y.-N. Cha, and C. Kim, *Taurine chloramine protects RAW 264.7 macrophages against hydrogen peroxide-induced apoptosis by increasing antioxidants.* Journal of Clinical Biochemistry and Nutrition, 2011. **49**(1): p. 50-56.

259. Kettle, A.J., et al., *Myeloperoxidase and protein oxidation in the airways of young children with cystic fibrosis.* American Journal of Respiratory and Critical Care Medicine, 2004. **170**(12): p. 1317-1323.

260. van der Vliet, A., et al., *Myeloperoxidase and protein oxidation in cystic fibrosis.* American Journal of Physiology, 2000. **279**(3): p. L537-L546.

261. Regelmann, W.E., et al., *Sputum peroxidase activity correlates with the severity of lung disease in cystic fibrosis.* Pediatric Pulmonology, 1995. **19**: p. 1-9.

262. Chen, H., et al., *Nonsteroidal anti-inflammatory drugs and the risk of Parkinson disease.* Archives of Neurology, 2003. **60**(8): p. 1059-1064.

263. Nagra, R.M., et al., *Immunohistochemical and genetic evidence of myeloperoxidase involvement in multiple sclerosis.* Journal of Neuroimmunology, 1997. **78**(1-2): p. 97-107.

264. Reynolds, W.F., et al., *Myeloperoxidase polymorphism is associated with gender specific risk for Alzheimer's disease.* Experimental Neurology, 1999. **155**(1): p. 31-41.

265. Kruidenier, L., et al., *Imbalanced secondary mucosal antioxidant response in inflammatory bowel disease.* Journal of Pathology, 2003. **201**(1): p. 17-27.

266. Baskol, G., et al., *Investigation of protein oxidation and lipid peroxidation in patients with rheumatoid arthritis.* Cell Biochemistry and Function, 2006. **24**(4): p. 307-311.

267. Kettle, A.J., et al., *Oxidation contributes to low glutathione in the airways of children with cystic fibrosis.* European Respiratory Journal, 2014. **44**(1): p. 122-129.

268. Green, P.S., et al., *Neuronal expression of myeloperoxidase is increased in Alzheimer's disease.* Journal of Neurochemistry, 2004. **90**(3): p. 724-733.

269. Choi, D.K., et al., *Ablation of the inflammatory enzyme myeloperoxidase mitigates features of Parkinson's disease in mice.* Journal of Neuroscience, 2005. **25**(28): p. 6594-6600.

270. Zakrzewska-Pniewska, B., et al., *Association of apolipoprotein E and myeloperoxidase genotypes to clinical course of familial and sporadic multiple sclerosis.* Multiple Sclerosis, 2004. **10**(3): p. 266-271.

271. Madhusudhana Rao, A., U. Anand, and C.V. Anand, *Myeloperoxidase in chronic kidney disease.* Indian Journal of Clinical Biochemistry, 2011. **26**(1): p. 28-31.

272. Stamp, L.K., et al., *Myeloperoxidase and oxidative stress in rheumatoid arthritis.* Rheumatology (Oxford), 2012. **51**(10): p. 1796-803.

273. Statistics, A.B.o., *Causes of death, Australia 2014*. 2014, ABS: Canberra.

274. Linton, M.F. and S. Fazio, *Macrophages, inflammation, and atherosclerosis.* International Journal for Obesity Related Metabolic Disorders, 2003. **27**(S3): p. S35-S40.

275. Daugherty, A., et al., *Myeloperoxidase, a catalyst for lipoprotein oxidation, is expressed in human atherosclerotic lesions.* Journal of Clinical Investigation, 1994. **94**: p. 437-444.

276. Hazen, S.L., et al., *Elevated levels of protein-bound p-hydroxyphenylacetaldehyde, an amino-acid-derived aldehyde generated by myeloperoxidase, are present in human fatty streaks, intermediate lesions and advanced atherosclerotic lesions.* Biochemical Journal, 2000. **352**(3): p. 693-699.

277. Takeshita, J., et al., *Myeloperoxidase generates 5-chlorouracil in human atherosclerotic tissue: a potential pathway for somatic mutagenesis by macrophages.* Journal of Biological Chemistry, 2006. **281**(6): p. 3096-3104.

278. Hazell, L.J., G. Baernthaler, and R. Stocker, *Correlation between intima-to-media ratio, apolipoprotein B-100, myeloperoxidase, and hypochlorite-oxidized proteins in human atherosclerosis.* Free Radical Biology and Medicine, 2001. **31**(10): p. 1254-1262.

279. Zhang, R., et al., *Association between myeloperoxidase levels and risk of coronary artery disease.* Journal of the American Medical Association, 2001. **286**(17): p. 2136-2142.

280. Ndrepepa, G., et al., *Myeloperoxidase level in patients with stable coronary artery disease and acute coronary syndromes.* European Journal of Clinical Investigation, 2008. **38**(2): p. 90-96.

281. Karakas, M., et al., *Myeloperoxidase is associated with incident coronary heart disease independently of traditional risk factors: results from the MONICA/KORA Augsburg study.* Journal of Internal Medicine, 2012. **271**(1): p. 43-50.

282. Tang, W.H.W., et al., *Usefulness of myeloperoxidase levels in healthy elderly subjects to predict risk of developing heart failure.* American Journal of Cardiology, 2009. **103**(9): p. 1269-1274.

283. Meuwese, M.C., et al., *Serum myeloperoxidase levels are associated with the future risk of coronary artery disease in apparently healthy individuals - The EPIC-Norfolk prospective population study.* Journal of the American College of Cardiology, 2007. **50**(2): p. 159-165.

284. Rana, J.S., et al., *Inflammatory biomarkers, physical activity, waist circumference, and risk of future coronary heart disease in healthy men and women.* European Heart Journal, 2011. **32**(3): p. 336-344.

285. Kohli, P., et al., *Myeloperoxidase (MPO) is an independent predictor of adverse cardiovascular outcomes in patients with stable coronary artery disease.* Circulation, 2010. **122**(21).

286. Peacock, W.F., *Myeloperoxidase in the diagnosis of acute coronary syndromes: The importance of spectrum.* American Heart Journal, 2012. **163**(5): p. E41-E41.

287. Apple, F.S., et al., *Myeloperoxidase improves risk stratification in patients with ischemia and normal cardiac troponin I concentrations.* Clinical Chemistry, 2011. **57**(4): p. 603-608.

288. Brennan, M.-L., et al., *Prognostic value of myeloperoxidase in patients with chest pain.* New England Journal of Medicine, 2003. **349**(17): p. 1595-1604.

289. Nedoboy, P.E., et al., *High plasma thiocyanate levels are associated with enhanced myeloperoxidase-induced thiol oxidation and long-term survival in subjects following a first myocardial infarction.* Free Radical Research, 2014. **48**(10): p. 1256-1266.

290. Brennan, M.-L., et al., *Increased atherosclerosis in myeloperoxidase-deficient mice.* The Journal of Clinical Investigation, 2001. **107**(4): p. 419-430.

291. Nauseef, W.M., *The proper study of mankind.* The Journal of Clinical Investigation, 2001. **107**(4): p. 401-403.

292. Heinecke, J.W., *Pathways for oxidation of low density lipoprotein by myeloperoxidase: tyrosyl radical, reactive aldehydes, hypochlorous acid and molecular chlorine.* BioFactors, 1997. **6**(2): p. 145-155.

293. Heinecke, J.W., *Mechanisms of oxidative damage by myeloperoxidase in atherosclerosis and other inflammatory disorders.* Journal of Laboratory and Clinical Medicine, 1999. **133**(4): p. 321-325.

294. Hazell, L.J. and R. Stocker, *Oxidation of low-density lipoprotein with hypochlorite causes transformation of the lipoprotein into a high-uptake form for macrophages.* Biochemical Journal, 1993. **290**: p. 165-172.

295. Dhaliwal, B.S. and U.P. Steinbrecher, *Cholesterol delivered to macrophages by oxidized low density lipoprotein is sequestered in lysosomes and fails to efflux normally.* Journal of Lipid Research, 2000. **41**(10): p. 1658-1665.

296. Hazen, S.L. and J.W. Heinecke, *3-Chlorotyrosine, a specific marker of myeloperoxidase-catalyzed oxidation, is markedly elevated in low density lipoprotein isolated from human atherosclerotic intima.* Journal of Clinical Investigation, 1997. **99**(9): p. 2075-2081.

297. Bergt, C., et al., *Hypochlorite modification of high density lipoprotein: effects on cholesterol efflux from J774 macrophages.* FEBS Letters, 1999. **452**(3): p. 295-300.

298. Zheng, L., et al., *Apolipoprotein A-I is a selective target for myeloperoxidase-catalyzed oxidation and functional impairment in subjects with cardiovascular disease.* Journal of Clinical Investigation, 2004. **114**(4): p. 529-541.

299. Zheng, L., et al., *Localization of nitration and chlorination sites on apolipoprotein A-I catalyzed by myeloperoxidase in human atheroma and associated oxidative impairment in ABCA1-dependent cholesterol efflux from macrophages.* Journal of Biological Chemistry, 2005. **280**(1): p. 38-47.

300. Hadfield, K.A., et al., *Myeloperoxidase-derived oxidants modify apolipoprotein A-I and generate dysfunctional high-density lipoproteins: comparison of hypothiocyanous acid (HOSCN) with hypochlorous acid (HOCl).* Biochemical Journal, 2013. **449**: p. 531-542.

301. Bergt, C., et al., *Human neutrophils employ the myeloperoxidase/hydrogen peroxide/chloride system to oxidatively damage apolipoprotein A-I.* European Journal of Biochemistry, 2001. **268**(12): p. 3523-3531.

302. Peng, D.-Q., et al., *Apolipoprotein A-I tryptophan substitution leads to resistance to myeloperoxidase-mediated loss of function.* Arteriosclerosis, Thrombosis, and Vascular Biology, 2008. **28**(11): p. 2063-2070.

303. Huang, Y., et al., *An abundant dysfunctional apolipoprotein A1 in human atheroma.* Nature Medicine, 2014. **20**(2): p. 193-203.

304. Shao, B., et al., *Tyrosine 192 in apolipoprotein A-I is the major site of nitration and chlorination by myeloperoxidase, but only chlorination markedly impairs ABCA1-dependent cholesterol transport.* Journal of Biological Chemistry, 2005. **280**(7): p. 5983-93.

305. Pennathur, S., et al., *Human atherosclerotic intima and blood of patients with established coronary artery disease contain high density lipoprotein damaged by reactive nitrogen species.* Journal of Biological Chemistry, 2004. **279**(41): p. 42977-42983.

306. Shao, B., et al., *Methionine oxidation impairs reverse cholesterol transport by apolipoprotein A-I.* Proceedings of the National Academy of Sciences, 2008. **105**(34): p. 12224-12229.

307. Shao, B., et al., *Humans With Atherosclerosis Have Impaired ABCA1 Cholesterol Efflux and Enhanced High-Density Lipoprotein Oxidation by Myeloperoxidase.* Circulation Research, 2014. **114**(11): p. 1733-1742.

308. Pirillo, A., P. Uboldi, and A.L. Catapano, *Dual effect of hypochlorite in the modification of high density lipoproteins.* Biochem Biophys Res Commun, 2010. **403**(3-4): p. 447-51.

309. Undurti, A., et al., *Modification of high density lipoprotein by myeloperoxidase generates a pro-inflammatory particle.* Journal of Biological Chemistry, 2009. **284**(45): p. 30825-30835.

310. Shimokawa, H., *Primary endothelial dysfunction: atherosclerosis.* Journal of Molecular and Cellular Cardiology, 1999. **31**(1): p. 23-37.

311. Baldus, S., et al., *Endothelial transcytosis of myeloperoxidase confers specificity to vascular ECM proteins as targets of tyrosine nitration.* Journal of Clinical Investigation, 2001. **108**(12): p. 1759-1770.

312. Tiruppathi, C., et al., *Albumin mediates the transcytosis of myeloperoxidase by means of caveolae in endothelial cells.* Proceedings of the National Academy of Sciences of the United States of America, 2004. **101**(20): p. 7699-7704.

313. Daphna, E.M., et al., *Association of myeloperoxidase with heparin: Oxidative inactivation of proteins on the surface of endothelial cells by the bound enzyme.* Molecular and Cellular Biochemistry, 1998. **183**(1-2): p. 55-61.

314. Baldus, S., et al., *Spatial mapping of pulmonary and vascular nitrotyrosine reveals the pivotal role of myeloperoxidase as a catalyst for tyrosine nitration in inflammatory diseases.* Free Radical Biology and Medicine, 2002. **33**(7): p. 1010-1019.

315. Leipert, B., B.F. Becker, and E. Gerlach, *Different endothelial mechanisms involved in coronary responses to known vasodilators.* American Journal of Physiology, 1992. **262**: p. H1676-H1683.

316. Zhang, C., et al., *Endothelial dysfunction is induced by proinflammatory oxidant hypochlorous acid.* American Journal of Physiology, 2001. **281**(4): p. H1469-H1475.

317. Stocker, R., et al., *Hypochlorous acid impairs endothelium-derived nitric oxide bioactivity through a superoxide-dependent mechanism.* Arteriosclerosis Thrombosis and Vascular Biology, 2004. **24**(11): p. 2028-2033.

318. Yang, L., et al., *Vascular VPO1 expression is related to the endothelial dysfunction in spontaneously hypertensive rats.* Biochemical and Biophysical Research Communications, 2013. **439**(4): p. 511-516.

319. Hazen, S.L., *Myeloperoxidase and plaque vulnerability.* Arteriosclerosis Thrombosis and Vascular Biology, 2004. **24**(7): p. 1143 - 1146.

320. Baldus, S., et al., *Myeloperoxidase serum levels predict risk in patients with acute coronary syndromes.* Circulation, 2003. **108**(12): p. 1440-1445.

321. Ferrante, G., et al., *High levels of systemic myeloperoxidase are associated with coronary plaque erosion in patients with acute coronary syndromes: A clinicopathological study.* Circulation, 2010. **122**(24): p. 2505-2513.

322. Tavora, F., et al., *Monocytes and neutrophils expressing myeloperoxidase occur in fibrous caps and thrombi in unstable coronary plaques.* BMC Cardiovascular Disorders, 2009. **9**(1): p. 27.

323. Sugiyama, S., et al., *Macrophage myeloperoxidase regulation by granulocyte macrophage colony-stimulating factor in human atherosclerosis and implications in acute coronary syndromes.* American Journal of Pathology, 2001. **158**(3): p. 879-891.

324. Sugiyama, S., et al., *Hypochlorous acid, a macrophage product, induces endothelial apoptosis and tissue factor expression.* Arteriosclerosis Thrombosis and Vascular Biology, 2004. **24**(7): p. 1309-1314.

325. Fu, X., et al., *Hypochlorous acid oxygenates the cysteine switch domain of pro-matrilysin (MMP-7): A mechanism for matrix metalloprotein activation and atherosclerotic plaque rupture by myeloperoxidase.* Journal of Biological Chemistry, 2001. **276**(44): p. 41279-41287.

326. Hurst, J.K. and W.C. Barrette, Jr., *Leukocytic oxygen activation and microbicidal oxidative toxins.* Critical Reviews in Biochemistry and Molecular Biology, 1989. **24**: p. 271-328.

327. Babior, B.M., *The respiratory burst oxidase.* Trends in Biochemical Science, 1987. **12**: p. 241-243.

328. Ellis, J.A., S.J. Mayer, and O.T.G. Jones, *The effect of the NADPH oxidase inhibitor diphenyleneiodonium on aerobic and anaerobic microbicidal activities of human neutrophils.* Biochemical Journal, 1988. **251**: p. 887-891.

329. Hampton, M.B. and C.C. Winterbourn, *Modification of neutrophil oxidant production with diphenyleneiodonium and its effect on bacterial killing.* Free Radical Biology and Medicine, 1995. **18**: p. 633-639.

330. Malle, E., et al., *Myeloperoxidase: a target for new drug development?* British Journal of Pharmacology, 2007. **152**(6): p. 838-854.

331. Tiden, A.-K., et al., *2-Thioxanthines are mechanism-based inactivators of myeloperoxidase that block oxidative stress during inflammation.* Journal of Biological Chemistry, 2011. **286**(43): p. 37578-37589.

332. Palinkas, Z., et al., *Interactions of hydrogen sulfide with myeloperoxidase.* British Journal of Pharmacology, 2015. **172**(6): p. 1516-32.

333. Forbes, L.V., et al., *Potent reversible inhibition of myeloperoxidase by aromatic hydroxamates.* Journal of Biological Chemistry, 2013. **288**(51): p. 36636-47.

334. Chapman, A.L.P., et al., *Ceruloplasmin is an endogenous inhibitor of myeloperoxidase.* Journal of Biological Chemistry, 2013. **288**(9): p. 6465-6477.

335. Sokolov, A.V., et al., *Lactoferrin, myeloperoxidase, and ceruloplasmin: complementary gearwheels cranking physiological and pathological processes.* Biometals, 2014. **27**(5): p. 815-828.

336. Kettle, A.J., C.A. Gedye, and C.C. Winterbourn, *Superoxide is an antagonist of anti-inflammatory drugs that inhibit hypochlorous acid production by myeloperoxidase.* Biochemical Pharmacology, 1993. **45**: p. 2003-2010.

337. Jantschko, W., et al., *Exploitation of the unusual thermodynamic properties of human myeloperoxidase in inhibitor design.* Biochemical Pharmacology, 2005. **69**(8): p. 1149-1157.

338. Bessems, J.G.M. and N.P.E. Vermeulen, *Paracetamol (acetaminophen)-induced toxicity: molecular and biochemical mechanisms, analogues and protective approaches.* Critical Reviews in Toxicology, 2001. **31**(1): p. 55-138.

339. Kajer, T.B., et al., *Inhibition of myeloperoxidase- and neutrophil-mediated oxidant production by tetraethyl and tetramethyl nitroxides.* Free Radical Biology and Medicine, 2014. **70**(0): p. 96-105.

340. Soule, B.P., et al., *The chemistry and biology of nitroxide compounds.* Free Radical Biology and Medicine, 2007. **42**(11): p. 1632-1650.

341. Vaz, S.M. and O. Augusto, *Inhibition of myeloperoxidase-mediated protein nitration by tempol: Kinetics, mechanism, and implications.* Proceedings of the National Academy of Sciences, 2008. **105**(24): p. 8191-8196.

342. Rees, M.D., et al., *Inhibition of myeloperoxidase-mediated hypochlorous acid production by nitroxides.* Biochemical Journal, 2009. **421**(1): p. 79-86.

343. Galijasevic, S., I. Abdulhamid, and H.M. Abu-Soud, *Potential role of tryptophan and chloride in the inhibition of human myeloperoxidase.* Free Radical Biology and Medicine, 2008. **44**(8): p. 1570-1577.

344. Kettle, A.J. and C.C. Winterbourn, *Oxidation of hydroquinone by myeloperoxidase. Mechanism of stimulation by benzoquinone.* Journal of Biological Chemistry, 1992. **267**: p. 8319-8324.

345. Kettle, A.J., et al., *Oxidative metabolism of amsacrine by the neutrophil enzyme myeloperoxidase.* Biochemical Pharmacology, 1992. **44**: p. 1731-1738.

346. Stadtman, T., *Biosynthesis and function of selenocysteine-containing enzymes.* Journal of Biological Chemistry, 1991. **266**(25): p. 16257-16260.

347. Pannala, V.R. and R.K. Dash, *Mechanistic characterization of the thioredoxin system in the removal of hydrogen peroxide.* Free Radical Biology and Medicine, 2015. **78**(0): p. 42-55.

348. Chandler, J.D., et al., *Selective metabolism of hypothiocyanous acid by mammalian thioredoxin reductase promotes lung innate immunity and antioxidant defense.* Journal of Biological Chemistry, 2013. **288**(25): p. 18421-18428.

349. Dubuisson, M., et al., *Human peroxiredoxin 5 is a peroxynitrite reductase.* FEBS Letters, 2004. **571**(1-3): p. 161-165.

350. Wong, C.M., et al., *Cooperation of yeast peroxiredoxins Tsa1p and Tsa2p in the cellular defense against oxidative and nitrosative stress.* Journal of Biological Chemistry, 2002. **277**(7): p. 5385-5394.

351. Boschi-Muller, S., et al., *A sulfenic acid enzyme intermediate is involved in the catalytic mechanism of peptide methionine sulfoxide reductase from Escherichia coli.* Journal of Biological Chemistry, 2000. **275**(46): p. 35908-35913.

352. Kumar, R.A., et al., *Reaction mechanism, evolutionary analysis, and role of zinc in Drosophila Methionine-R-sulfoxide reductase.* Journal of Biological Chemistry, 2002. **277**(40): p. 37527-37535.

353. Lowther, W.T., et al., *Thiol-disulfide exchange is involved in the catalytic mechanism of peptide methionine sulfoxide reductase.* Proceedings of the National Academy of Sciences of the United States of America, 2000. **97**(12): p. 6463-6468.

354. Olry, A., et al., *Characterization of the methionine sulfoxide reductase activities of PILB, a probable virulence factor from Neisseria meningitidis.* Journal of Biological Chemistry, 2002. **277**(14): p. 12016-12022.

355. Rouhier, N., et al., *Functional and structural aspects of poplar cytosolic and plastidial type A methionine sulfoxide reductases.* Journal of Biological Chemistry, 2007. **282**(5): p. 3367-3378.

356. Holmgren, A. and J. Lu, *Thioredoxin and thioredoxin reductase: Current research with special reference to human disease.* Biochemical and Biophysical Research Communications, 2010. **396**(1): p. 120-124.

357. Holmgren, A., *Thioredoxin.* Annual Review of Biochemistry, 1985. **54**: p. 237-271.

358. Williams Jr, C.H., *Flavine containing dehydrogenases*. Boyer, Paul D. 1976. 89-173.

359. Worthington, D.J. and M.A. Rosemeyer, *Isolation and properties of glutathione reductase from human erythrocytes.* Biochemical Society Transactions, 1974. **2**(5): p. 927-929.

360. Nakashima, K., S. Miwa, and K. Yamauchi, *Huamn erythrocyte reductase 1. Purification and properties.* Biochimica Et Biophysica Acta, 1976. **445**(2): p. 309-322.

361. Tainer, J.A., et al., *Determination and analysis of the 2 Å structure of copper, zinc superoxide dismutase.* Journal of Molecular Biology, 1982. **160**(2): p. 181-217.

362. Ludwig, M.L., et al., *Manganese superoxide dismutase from Thermus thermophilus: A structural model refined at 1.8 Å resolution.* Journal of Molecular Biology, 1991. **219**(2): p. 335-358.

363. Bowler, C., M.v. Montagu, and D. Inze, *Superoxide dismutase and stress tolerance.* Annual Review of Plant Biology, 1992. **43**(1): p. 83-116.

364. Putnam, C.D., et al., *Active and inhibited human catalase structures: ligand and NADPH binding and catalytic mechanism.* Journal of Molecular Biology, 2000. **296**(1): p. 295-309.

365. Murthy, M.R.N., et al., *The structure of beef liver catalase*, in *The Biological Chemistry of Iron*. 1982, Springer. p. 439-458.

366. Jones, D.P., et al., *Metabolism of hydrogen peroxide in isolated hepatocytes: relative contributions of catalase and glutathione peroxidase in decomposition of*

endogenously generated H 2 O 2. Archives of Biochemistry and Biophysics, 1981. **210**(2): p. 505-516.

367. Fita, I. and M.G. Rossmann, *The active center of catalase.* Journal of Molecular Biology, 1985. **185**(1): p. 21-37.

368. Rotruck, J., et al., *Selenium: biochemical role as a component of glutathione peroxidase.* Science, 1973. **179**: p. 588.

369. Michiels, C., et al., *Importance of Se-glutathione peroxidase, catalase, and Cu/Zn-SOD for cell survival against oxidative stress.* Free Radical Biology and Medicine, 1994. **17**(3): p. 235-248.

370. Li, F., J. Liu, and S. Rozovsky, *Glutathione peroxidase's reaction intermediate selenenic acid is stabilized by the protein microenvironment.* Free Radical Biology and Medicine, 2014. **76**: p. 127-35.

371. Gladyshev, V.N., K.T. Jeang, and T.C. Stadtman, *Selenocysteine, identified as the penultimate C-terminal residue in human T-cell thioredoxin reductase, corresponds to TGA in the human placental gene.* Proceedings of the National Academy of Sciences of the United States of America, 1996. **93**(12): p. 6146-6151.

372. Zhong, L.W., E.S.J. Arner, and A. Holmgren, *Structure and mechanism of mammalian thioredoxin reductase: The active site is a redox-active selenolthiol/selenenylsulfide formed from the conserved cysteine-selenocysteine sequence.* Proceedings of the National Academy of Sciences of the United States of America, 2000. **97**(11): p. 5854-5859.

373. Conrad, M., et al., *Essential role for mitochondrial thioredoxin reductase in hematopoiesis, heart development, and heart function.* Molecular and Cellular Biology, 2004. **24**(21): p. 9414-9423.

374. Jakupoglu, C., et al., *Cytoplasmic thioredoxin reductase is essential for embryogenesis but dispensable for cardiac development.* Molecular and Cellular Biology, 2005. **25**(5): p. 1980-1988.

375. Matsui, M., et al., *Early embryonic lethality caused by targeted disruption of the mouse thioredoxin gene.* Developmental Biology, 1996. **178**(1): p. 179-185.

376. Gorlatov, S.N. and T.C. Stadtman, *Human thioredoxin reductase from HeLa cells: Selective alkylation of selenocysteine in the protein inhibits enzyme activity and reduction with NADPH influences affinity to heparin.* Proceedings of the National Academy of Sciences of the United States of America, 1998. **95**(15): p. 8520-8525.

377. Gorlatov, S.N. and T.C. Stadtman, *Human selenium-dependent thioredoxin reductase from HeLa cells: Properties of forms with differing heparin affinities.* Archives of Biochemistry and Biophysics, 1999. **369**(1): p. 133-142.

378. Gromer, S., et al., *A hypothesis on the catalytic mechanism of the selenoenzyme thioredoxin reductase.* Biochemical Journal, 1998. **332**: p. 591-592.

379. Zhong, L.W. and A. Holmgren, *Essential role of selenium in the catalytic activities of mammalian thioredoxin reductase revealed by characterization of recombinant enzymes with selenocysteine mutations.* Journal of Biological Chemistry, 2000. **275**(24): p. 18121-18128.

380. Gasdaska, J.R., et al., *Regulation of human thioredoxin reductase expression and activity by 3 '-untranslated region selenocysteine insertion sequence and mRNA instability elements.* Journal of Biological Chemistry, 1999. **274**(36): p. 25379-25385.

381. Holmgren, A., *Thioredoxin.6. Amino acid sequence of protein from eschericha Coli B.* European Journal of Biochemistry, 1968. **6**(4): p. 475-&.

382. Weichsel, A., et al., *Crystal structures of reduced, oxidized, and mutated human thioredoxins: Evidence for a regulatory homodimer.* Structure, 1996. **4**(6): p. 735-751.

383. Mitsui, A., et al., *Overexpression of human thioredoxin in transgenic mice controls oxidative stress and life span.* Antioxidants & Redox Signaling, 2002. **4**(4): p. 693-696.

384. Fujii, S., et al., *Coexpression of adult T-cell leukemia-derived factor, a human thioredoxin homolog, and human papillomavirus DNA in neoplastic cervical squamous epithelium.* Cancer, 1991. **68**(7): p. 1583-1591.

385. Kinnula, V.L., P. Paakko, and Y. Soini, *Antioxidant enzymes and redox regulating thiol proteins in malignancies of human lung.* FEBS Letters, 2004. **569**(1-3): p. 1-6.

386. Miyazaki, K., et al., *Elevated serum level of thioredoxin in patients with hepatocellular carcinoma.* Biotherapy, 1998. **11**(4): p. 277-288.

387. Nakamura, H., et al., *Expression of thioredoxin and glutaredoxin, redox-regulating proteins, in pancreatic cancer.* Cancer Detection and Prevention, 2000. **24**(1): p. 53-60.

388. Nakamura, H., et al., *Chronic elevation of plasma thioredoxin: Inhibition of chemotaxis and curtailment of life expectancy in AIDS.* Proceedings of the National Academy of Sciences of the United States of America, 2001. **98**(5): p. 2688-2693.

389. Sumida, Y., et al., *Serum thioredoxin levels as an indicator of oxidative stress in patients with hepatitis C virus infection.* Journal of Hepatology, 2000. **33**(4): p. 616-622.

390. Lillig, C.H. and A. Holmgren, *Thioredoxin and related molecules - From biology to health and disease.* Antioxidants & Redox Signaling, 2007. **9**(1): p. 25-47.

391. Martin, J.L., *Thioredoxin - A fold for all reasons.* Structure, 1995. **3**(3): p. 245-250.

392. Sengupta, R. and A. Holmgren, *The role of thioredoxin in the regulation of cellular processes by S-nitrosylation.* Biochimica Et Biophysica Acta-General Subjects, 2012. **1820**(6): p. 689-700.

393. Masutani, H., S. Ueda, and J. Yodoi, *The thioredoxin system in retroviral infection and apoptosis.* Cell Death and Differentiation, 2005. **12**: p. 991-998.

394. Hirota, K., et al., *Distinct roles of thioredoxin in the cytoplasm and in the nucleus - A two-step mechanism of redox regulation of transcription factor NF-kappa B.* Journal of Biological Chemistry, 1999. **274**(39): p. 27891-27897.

395. Nakamura, H., K. Nakamura, and J. Yodoi, *Redox regulation of cellular activation.* Annual Review of Immunology, 1997. **15**: p. 351-369.

396. Nakamura, H., H. Masutani, and J. Yodoi, *Extracellular thioredoxin and thioredoxin-binding protein 2 in control of cancer.* Seminars in Cancer Biology, 2006. **16**(6): p. 444-451.

397. Saitoh, M., et al., *Mammalian thioredoxin is a direct inhibitor of apoptosis signal-regulating kinase (ASK) 1.* EMBO Journal, 1998. **17**(9): p. 2596-2606.

398. Yoshihara, E., et al., *Thiol redox transitions by thioredoxin and thioredoxin-binding protein-2 in cell signalling*, in *Methods in Enzymology, Vol 474: Thiol Redox Transitions in Cell Signaling, Pt B: Cellular Localization and Signaling*, E. Cadenas and L. Packer, Editors. 2010, Elsevier Academic Press Inc: San Diego. p. 67-82.

399. Trujillo, M., G. Ferrer-Sueta, and R. Radi, *Kinetic studies on peroxynitrite reduction by peroxiredoxins.* Methods in Enzymology, 2008. **441**: p. 173-96.

400. Stresing, V., et al., *Peroxiredoxin 2 specifically regulates the oxidative and metabolic stress response of human metastatic breast cancer cells in lungs.* Oncogene, 2013. **32**(6): p. 724-35.

401. Lee, T.H., et al., *Peroxiredoxin II is essential for sustaining life span of erythrocytes in mice.* Blood, 2003. **101**(12): p. 5033-5038.

402. Neumann, C.A., et al., *Essential role for the peroxiredoxin Prdx1 in erythrocyte antioxidant defence and tumour suppression.* Nature, 2003. **424**(6948): p. 561-565.

403. Wang, X.S., et al., *Mice with targeted mutation of peroxiredoxin 6 develop normally but are susceptible to oxidative stress.* Journal of Biological Chemistry, 2003. **278**(27): p. 25179-25190.

404. Smith-Pearson, P.S., et al., *Decreasing peroxiredoxin II expression decreases glutathione, alters cell cycle distribution, and sensitizes glioma cells to ionizing radiation and H(2)O(2).* Free Radical Biology and Medicine, 2008. **45**(8): p. 1178-1189.

405. Jin, D.Y., et al., *Regulatory role for a novel human thioredoxin peroxidase in NF-kappa B activation.* Journal of Biological Chemistry, 1997. **272**(49): p. 30952-30961.

406. Kang, S.W., et al., *Mammalian peroxiredoxin isoforms can reduce hydrogen peroxide generated in response to growth factors and tumor necrosis factor-alpha.* Journal of Biological Chemistry, 1998. **273**(11): p. 6297-6302.

407. Kang, S.W., et al., *Cytosolic peroxiredoxin attenuates the activation of JNK and p38 but potentiates that of ERK in HeLa cells stimulated with tumor necrosis factor-alpha.* Journal of Biological Chemistry, 2004. **279**(4): p. 2535-2543.

408. Veal, E.A., et al., *A 2-Cys peroxiredoxin regulates peroxide-induced oxidation and activation of a stress-activated MAP kinase.* Molecular Cell, 2004. **15**(1): p. 129-139.

409. Zhang, P., et al., *Thioredoxin peroxidase is a novel inhibitor of apoptosis with a mechanism distinct from that of Bcl-2.* Journal of Biological Chemistry, 1997. **272**(49): p. 30615-30618.

410. Biteau, B., J. Labarre, and M.B. Toledano, *ATP-dependent reduction of cysteine-sulphinic acid by S-cerevisiae sulphiredoxin.* Nature, 2003. **425**(6961): p. 980-984.

411. Rhee, S.G., et al., *Intracellular messenger function of hydrogen peroxide and its regulation by peroxiredoxins.* Current Opinion in Cell Biology, 2005. **17**(2): p. 183-189.

412. Kang, S.W., et al., *2-Cys peroxiredoxin function in intracellular signal transduction: therapeutic implications.* Trends in Molecular Medicine, 2005. **11**(12): p. 571-578.

413. Tarrago, L., et al., *Methionine sulfoxide reductases preferentially reduce unfolded oxidized proteins and protect cells from oxidative protein unfolding.* Journal of Biological Chemistry, 2012. **287**(29): p. 24448-24459.

414. Cabreiro, F., et al., *Overexpression of mitochondrial methionine sulfoxide reductase B2 protects leukemia cells from oxidative stress-induced cell death and protein damage.* Journal of Biological Chemistry, 2008. **283**(24): p. 16673-16681.

415. Moskovitz, J., et al., *Overexpression of peptide-methionine sulfoxide reductase in Saccharomyces cerevisiae and human T cells provides them with high resistance to oxidative stress.* Proceedings of the National Academy of Sciences of the United States of America, 1998. **95**(24): p. 14071-14075.

416. Ruan, H., et al., *High-quality life extension by the enzyme peptide methionine sulfoxide reductase.* Proceedings of the National Academy of Sciences of the United States of America, 2002. **99**(5): p. 2748-2753.

417. Kim, H.Y. and J.R. Kim, *Thioredoxin as a reducing agent for mammalian methionine sulfoxide reductases B lacking resolving cysteine.* Biochemical and Biophysical Research Communications, 2008. **371**(3): p. 490-494.

418. Sagher, D., et al., *Selenocompounds can serve as oxidoreductants with the methionine sulfoxide reductase enzymes.* Journal of Biological Chemistry, 2006. **281**(42): p. 31184-31187.

419. Saghert, D., et al., *Thionein can serve as a reducing agent for the methionine sulfoxide reductases.* Proceedings of the National Academy of Sciences of the United States of America, 2006. **103**(23): p. 8656-8661.

420. Vieira Dos Santos, C., et al., *Specificity of thioredoxins and glutaredoxins as electron donors to two distinct classes of Arabidopsis plastidial methionine sulfoxide reductases B.* FEBS Letters, 2007. **581**(23): p. 4371-6.

421. Petropoulos, I., et al., *Rat peptide methionine sulphoxide reductase: cloning of the cDNA, and down-regulation of gene expression and enzyme activity during aging.* Biochemical Journal, 2001. **355**: p. 819-825.

422. Picot, C.R., et al., *The peptide methionine sulfoxide reductases, MsrA and MsrB (hCBS-1), are downregulated during replicative senescence of human WI-38 fibroblasts.* FEBS Letters, 2004. **558**(1-3): p. 74-78.

423. Gabbita, S.P., et al., *Decrease in peptide methionine sulfoxide reductase in Alzheimer's disease brain.* Journal of Neurochemistry, 1999. **73**(4): p. 1660-1666.

424. Schulz, G.E., et al., *Crystals of human erythrocyte glutathione reductase.* FEBS Letters, 1975. **54**(1): p. 86-88.

425. Worthing.Dj and Rosemeye.Ma, *Human glutathione reductase - Purification of crystalline enzyme from erythrocytes.* European Journal of Biochemistry, 1974. **48**(1): p. 167-177.

426. Zappe, H.A., G. Krohneehrich, and G.E. Schulz, *Low resolution structure of human erythrocyte glutathione reductase.* Journal of Molecular Biology, 1977. **113**(1): p. 141-152.

427. Pai, E.F. and G.E. Schulz, *The catalytic mechanism of glutathione-reductase as derived from x-ray-diffraction analyses of reaction intermediates.* Journal of Biological Chemistry, 1983. **258**(3): p. 1752-1757.

428. Carr, A., T. Tijerina, and B. Frei, *Vitamin C protects against and reverses specific hypochlorous acid-and chloramine-dependent modifications of low-density lipoprotein.* Biochemical Journal, 2000. **346**(Pt 2): p. 491.

429. Smit, M. and R. Anderson, *Inhibition of mitogen-activated proliferation of human lymphocytes by hypochlorous acidin vitro: Protection and reversal by ascorbate and cysteine.* Inflammation Research, 1990. **30**(3): p. 338-343.

430. Smit, M. and R. Anderson, *Biochemical mechanisms of hydrogen peroxide-and hypochlorous acid-mediated inhibition of human mononuclear leukocyte functionsin vitro: Protection and reversal by anti-oxidants.* Inflammation Research, 1992. **36**(1): p. 58-65.

431. Jenner, A.M., et al., *Vitamin C Protects Against Hypochlorous Acid–Induced Glutathione Depletion and DNA Base and Protein Damage in Human Vascular Smooth Muscle Cells.* Arteriosclerosis, Thrombosis, and Vascular Biology, 2002. **22**(4): p. 574-580.

432. Melinda, C.M. and C.C. Anitra, *Myeloperoxidase-dependent caspase-3 activation and apoptosis in HL-60 cells: protection by the antioxidants ascorbate and (dihydro)lipoic acid.* Redox Report, 2002. **7**(1): p. 47-53.

433. Bilzer, M. and B. Lauterburg, *Glutathione metabolism in activated human neutrophils: stimulation of glutathione synthesis and consumption of glutathione by reactive oxygen species.* European Journal of Clinical Investigation, 1991. **21**(3): p. 316-322.

434. Winterbourn, C.C. and S.O. Brennan, *Characterization of the oxidation products of the reaction between reduced glutathione and hypochlorous acid.* Biochemical Journal, 1997. **326**: p. 87-92.

435. Chesney, J.A., J.W. Eaton, and J.R. Mahoney Jr, *Bacterial glutathione: a sacrificial defense against chlorine compounds.* Journal of Bacteriology, 1996. **178**(7): p. 2131-2135.

436. Boon, A.C., et al., *Bilirubin scavenges chloramines and inhibits myeloperoxidase induced protein/lipid oxidation in physiologically relevant hyperbilirubinaemic serum.* Free Radical Biology and Medicine, 2015.

437. Witting, P.K., et al., *Probucol protects against hypochlorite-induced endothelial dysfunction: identification of a novel pathway of probucol oxidation to a*

biologically active intermediate. Journal of Biological Chemistry, 2005. **280**(16): p. 15612-8.

438. Whiteman, M., et al., *Do mitochondriotropic antioxidants prevent chlorinative stress-induced mitochondrial and cellular injury?* Antioxidants & Redox Signaling, 2008. **10**(3): p. 641-650.

439. Storkey, C., et al., *Synthesis and antioxidant capacity of 5-selenopyranose derivatives.* Chemical Communications, 2011. **47**: p. 9693-9695.

440. Satheeshkumar, K. and G. Mugesh, *Synthesis and antioxidant activity of peptide-based ebselen analogues.* Chemistry, 2011. **17**(17): p. 4849-57.

441. Bhabak, K.P. and G. Mugesh, *Synthesis, characterization, and antioxidant activity of some ebselen analogues.* Chemistry-a European Journal, 2007. **13**(16): p. 4594-4601.

442. Zade, S.S., et al., *Convenient synthesis, characterization and GPx-like catalytic activity of novel ebselen derivatives.* European Journal of Organic Chemistry, 2004(18): p. 3857-3864.

443. Prabhu, P., et al., *Effect of functional groups on antioxidant properties of substituted selenoethers.* Free Radical Research, 2011. **45**(4): p. 461-468.

444. Assmann, A., K. Briviba, and H. Sies, *Reduction of methionine selenoxide to selenomethionine by glutathione.* Archives of Biochemistry and Biophysics, 1998. **349**(1): p. 201-203.

445. Krause, R.J. and A.A. Elfarra, *Reduction of L-methionine selenoxide to seleno-L-methionine by endogenous thiols, ascorbic acid, or methimazole.* Biochemical Pharmacology, 2009. **77**(1): p. 134-140.

446. Hondal, R.J., S.M. Marino, and V.N. Gladyshev, *Selenocysteine in thiol/disulfide-like exchange reactions.* Antioxidants & Redox Signaling, 2013. **18**(13): p. 1675-1689.

447. Jacob, C., et al., *Sulfur and selenium: The role of oxidation state in protein structure and function.* Angewandte Chemie-International Edition, 2003. **42**(39): p. 4742-4758.

448. Müller, A., et al., *A novel biologically active seleno-organic compound--1:: Glutathione peroxidase-like activity in vitro and antioxidant capacity of PZ 51 (Ebselen).* Biochemical Pharmacology, 1984. **33**(20): p. 3235-3239.

449. Schoneich, C., et al., *Reactivity of ebselen and related selenoorganic compounds with 1,2-dichloroethane radical cations and halogenated peroxyl radicals.* Archives of Biochemistry and Biophysics, 1990. **282**(1): p. 18-25.

450. Masumoto, H., et al., *Kinetic study of the reaction of ebselen with peroxynitrite.* FEBS Letters, 1996. **398**(2-3): p. 179-182.

451. Fischer, H. and N. Dereu, *Mechanism of the catalytic reduction of hydroperoxides by ebselen: A selenium 77 NMR study.* Bulletin des Societes Chimiques Belges, 1987. **96**(10): p. 757-768.

452. Morgenstern, R., I.A. Cotgreave, and L. Engman, *Determination of the relative contributions of the diselenide and selenol forms of ebselen in the mechanism of*

its glutathione peroxidase-like activity. Chem Biol Interact, 1992. **84**(1): p. 77-84.

453. Maiorino, M., et al., *Kinetic mechanism and substrate specificity of glutathione peroxidase activity of ebselen (PZ51).* Biochemical Pharmacology, 1988. **37**(11): p. 2267-2271.

454. Sies, H., *Ebselen, a selenoorganic compound as glutathione peroxidase mimic.* Free Radical Biology and Medicine, 1993. **14**(3): p. 313-323.

455. Luo, Z., et al., *Synthesis and biological evaluation of a new series of ebselen derivatives as glutathione peroxidase (GPx) mimics and cholinesterase inhibitors against Alzheimer's disease.* Bioorganic & Medicinal Chemistry, 2014. **22**(4): p. 1355-1361.

456. Mao, F., et al., *Novel tacrine–ebselen hybrids with improved cholinesterase inhibitory, hydrogen peroxide and peroxynitrite scavenging activity.* Bioorganic & Medicinal Chemistry Letters, 2013. **23**(24): p. 6737-6742.

457. Mishra, B., et al., *Novel reactions of one-electron oxidized radicals of selenomethionine in comparison with methionine.* Journal of Physical Chemistry B, 2009. **113**(21): p. 7709-7715.

458. Hiller, K.O. and K.D. Asmus, *Formation and reduction reaction of alpha-amino radicals derived from methionine and its derivatives in aqueous-solutions.* Journal of Physical Chemistry, 1983. **87**(19): p. 3682-3688.

459. Nucifora, G., et al., *Transient radicals of DNA bases by pulse radiolysis - Effects of cysteine and cysteamine as radioprotectors.* Radiation Research, 1972. **49**(1): p. 96-&.

460. Eriksen, T.E. and G. Fransson, *Formation fo reducing radicals on radiolysis of glutathione and some related-compounds in aqueous-solution.* Journal of the Chemical Society-Perkin Transactions 2, 1988(7): p. 1117-1122.

461. Padmaja, S., et al., *Rapid oxidation of DL-selenomethionine by peroxynitrite.* Free Radical Biology and Medicine, 1996. **21**(3): p. 317-322.

462. Briviba, K., et al., *Attenuation of oxidation and nitration reactions of peroxynitrite by selenomethionine, selenocystine and ebselen.* Biochemical Journal, 1996. **319**: p. 13-15.

463. Roussyn, I., et al., *Selenium-containing compounds protect DNA from single-strand breaks caused by peroxynitrite.* Archives of Biochemistry and Biophysics, 1996. **330**(1): p. 216-218.

464. Krause, R.J., et al., *Oxidative metabolism of seleno-L-methionine to L-methionine selenoxide by flavin-containing monooxygenases.* Chemical Research in Toxicology, 2006. **19**(12): p. 1643-1649.

465. Sies, H., et al., *Protection against peroxynitrite by selenoproteins.* Zeitschrift für Naturforschung. C, Journal of Biosciences, 1998. **53**(3-4): p. 228-232.

466. Steinbrenner, H. and H. Sies, *Protection against reactive oxygen species by selenoproteins.* Biochimica et Biophysica Acta (BBA)-General Subjects, 2009. **1790**(11): p. 1478-1485.

467. Schoneich, C., *Methionine oxidation by reactive oxygen species: reaction mechanisms and relevance to Alzheimer's disease.* Biochimica Et Biophysica Acta-Proteins and Proteomics, 2005. **1703**(2): p. 111-119.

468. Hiller, K.O., et al., *Mechanism of the OH. radical induced oxidation of methionine in aqueous-solution.* Journal of the American Chemical Society, 1981. **103**(10): p. 2734-2743.

469. Schoneich, C., et al., *Free radical reactions of methionine in peptides: Mechanisms relevant to beta-amyloid oxidation and Alzheimer's disease.* Journal of the American Chemical Society, 2003. **125**(45): p. 13700-13713.

470. Priyadarsini, K.I. and B. Mishra, *Radical cations of some water-soluble organoselenium compounds: Insights from pulse radiolysis studies.* Radiation Physics and Chemistry, 2008. **77**(10-12): p. 1294-1299.

471. Priyadarsini, K.I. and B. Mishra, *A brief account on radiation chemical studies of antioxidants : Examples from natural phenols, sulfur and selenium compounds.* Journal of the Indian Chemical Society, 2010. **87**(2): p. 147-157.

472. Huang, M.L. and A. Rauk, *Reactions of one-electron-oxidized methionine with oxygen: An ab initio study.* Journal of Physical Chemistry A, 2004. **108**(29): p. 6222-6230.

473. Assmann, A., et al., *One-electron reduction of selenomethionine oxide.* Free Radical Research, 2000. **32**(4): p. 371-376.

474. Rahmanto, A.S. and M.J. Davies, *Catalytic activity of selenomethionine in removing amino acid, peptide, and protein hydroperoxides.* Free Radical Biology and Medicine, 2011. **51**(12): p. 2288-2299.

475. Kigawa, T., et al., *Selenomethionine incorporation into a protein by cell-free synthesis.* Journal of Structural and Functional Genomics, 2002. **2**(1): p. 29-35.

476. Martinez, J., et al., *Selenomethionine incorporation into amyloid sequences regulates fibrillogenesis and toxicity.* Plos One, 2011. **6**(11).

477. Briviba, K., et al., *Kinetic study of the reaction of glutathione peroxidase with peroxynitrite.* Chemical Research in Toxicology, 1998. **11**(12): p. 1398-1401.

478. Padmaja, S., G.L. Squadrito, and W.A. Pryor, *Inactivation of glutathione peroxidase by peroxynitrite.* Archives of Biochemistry and Biophysics, 1998. **349**(1): p. 1-6.

479. Cardey, B. and M. Enescu, *Selenocysteine versus cysteine reactivity: A theoretical study of their oxidation by hydrogen peroxide.* Journal of Physical Chemistry A, 2007. **111**(4): p. 673-678.

480. Hondal, R.J. and E.L. Ruggles, *Differing views of the role of selenium in thioredoxin reductase.* Amino Acids, 2011. **41**(1): p. 73-89.

481. Cho, C.-S., et al., *Irreversible inactivation of glutathione peroxidase 1 and reversible inactivation of peroxiredoxin II by H2O2 in red blood cells.* Antioxidants & Redox Signaling, 2010. **12**(11): p. 1235-1246.

482. Zielinski, Z., et al., *Redox chemistry of selenenic acids and the insight it brings on transition state geometry in the reactions of peroxyl radicals.* Journal of the American Chemical Society, 2014. **136**(4): p. 1570-1578.

483. Steinmann, D., et al., *Kinetics of tyrosyl radical reduction by selenocysteine.* Biochemistry, 2008. **47**(36): p. 9602-9607.

484. Nauser, T., D. Steinmann, and W.H. Koppenol, *Why do proteins use selenocysteine instead of cysteine?* Amino Acids, 2012. **42**(1): p. 39-44.

485. Mozziconacci, O., T.D. Williams, and C. Schoeneich, *Intramolecular hydrogen transfer reactions of thiyl radicals from glutathione: Formation of carbon-centered radical at Glu, Cys, and Gly.* Chemical Research in Toxicology, 2012. **25**(9): p. 1842-1861.

486. Storkey, C., et al., *Preventing protein oxidation with sugars: Scavenging of hypohalous acids by 5-selenopyranose and 4-selenofuranose derivatives.* Chemical Research in Toxicology, 2012. **25**(11): p. 2589-2599.

487. Fumio Kumakura, B.M., K. Indira Priyadarsini and Michio Iwaoka, *A water-soluble cyclic selenide with enhanced glutathione peroxidase-like catalytic activities.* European Journal of Organic Chemistry, 2010. **2010**: p. 440-445.

488. Barik, A., et al., *Pulse radiolysis studies of 3,5-dimethyl pyrazole derivatives of selenoethers.* Journal of Physical Chemistry A, 2014. **118**(44): p. 10179-10187.

489. Mishra, B., K.I. Priyadarsini, and H. Mohan, *Effect of pH on one-electron oxidation chemistry of organoselenium compounds in aqueous solutions.* Journal of Physical Chemistry A, 2006. **110**(5): p. 1894-1900.

490. Kunwar, A., et al., *3,3'-diselenodipropionic acid, an efficient peroxyl radical scavenger and a GPx mimic, protects erythrocytes (RBCs) from AAPH-induced hemolysis.* Chemical Research in Toxicology, 2007. **20**(10): p. 1482-1487.

491. Bjornstedt, M., et al., *Human thioredoxin reductase directly reduces lipid hydroperoxides by NADPH and selenocystine strongly stimulates the reaction via catalytically generated selenols.* Journal of Biological Chemistry, 1995. **270**(20): p. 11761-4.

492. Bjornstedt, M., S. Kumar, and A. Holmgren, *Selenodiglutathione is a highly efficient oxidant of reduced thioredoxin and a substrate for mammalian thioredoxin reductase.* Journal of Biological Chemistry, 1992. **267**(12): p. 8030-8034.

493. Prabhu, P., et al., *Stable selones in glutathione-peroxidase-like catalytic cycle of selenonicotinamide derivative.* Organic & Biomolecular Chemistry, 2014. **12**(15): p. 2404-2412.

494. Rayman, M.P., *Selenium and human health.* Lancet, 2012. **379**(9822): p. 1256-1268.

495. Geybels, M.S., et al., *Advanced prostate cancer risk in relation to toenail selenium levels.* Journal of the National Cancer Institute, 2013. **105**(18): p. 1394-1401.

496. Hurst, R., et al., *Selenium and prostate cancer: systematic review and meta-analysis.* American Journal of Clinical Nutrition, 2012. **96**(1): p. 111-122.

497. Jaworska, K., et al., *A low selenium level is associated with lung and laryngeal cancers.* Plos One, 2013. **8**(3).

498. Mertens, K., et al., *Low zinc and selenium concentrations in sepsis are associated with oxidative damage and inflammation.* British Journal of Anaesthesia, 2015: p. aev073.

499. Salonen, J.T., et al., *Association between cardiovascular death and myocardial infarction and serum selenium in a matched-pair longitudinal study.* Lancet, 1982. **320**(8291): p. 175-179.

500. Navarro-Alarcon, M., et al., *Serum and urine selenium concentrations in patients with cardiovascular diseases and relationship to other nutritional indexes.* Annals of Nutrition and Metabolism, 1999. **43**(1): p. 30-36.

501. Rayman, M.P., et al., *Effect of supplementation with high-selenium yeast on plasma lipids: A randomized trial.* Annals of Internal Medicine, 2011. **154**(10): p. 656-W240.

502. Bleys, J., A. Navas-Acien, and E. Guallar, *Serum selenium levels and all-cause, cancer, and cardiovascular mortality among US adults.* Archives of Internal Medicine, 2008. **168**(4): p. 404-410.

503. Laclaustra, M., et al., *Serum selenium and serum lipids in US adults: National Health and Nutrition Examination Survey (NHANES) 2003-2004.* Atherosclerosis, 2010. **210**(2): p. 643-648.

504. Laclaustra, M., et al., *Serum selenium concentrations and hypertension in the US population.* Circulation-Cardiovascular Quality and Outcomes, 2009. **2**(4): p. 369-376.

505. Clark, L.C., et al., *Effects of selenium supplementation for cancer prevention in patients with carcinoma of the skin a randomized controlled trial - A randomized controlled trial.* Journal of the American Medical Association, 1996. **276**(24): p. 1957-1963.

506. Lippman, S.M., et al., *Effect of selenium and vitamin E on risk of prostate cancer and other cancers: The selenium and vitamin E cancer prevention trial (SELECT).* Journal of Urology, 2009. **181**(4): p. 1686-1687.

507. Duffield-Lillico, A.J., et al., *Baseline characteristics and the effect of selenium supplementation on cancer incidence in a randomized clinical trial: A summary report of the Nutritional Prevention of Cancer Trial.* Cancer Epidemiology Biomarkers & Prevention, 2002. **11**(7): p. 630-639.

508. Shen, H.M., C.F. Yang, and C.N. Ong, *Sodium selenite-induced oxidative stress and apoptosis in human hepatoma HepG(2) cells.* International Journal of Cancer, 1999. **81**(5): p. 820-828.

509. Kim, E.H., et al., *Sodium selenite induces superoxide-mediated mitochondrial damage and subsequent autophagic cell death in malignant glioma cells.* Cancer Research, 2007. **67**(13): p. 6314-6324.

510. Park, S.-H., et al., *Induction of apoptosis and autophagy by sodium selenite in A549 human lung carcinoma cells through generation of reactive oxygen species.* Toxicology Letters, 2012. **212**(3): p. 252-261.

511. Peyroche, G., et al., *Sodium selenide toxicity Is mediated by O-2-dependent DNA breaks.* Plos One, 2012. **7**(5).

512. Li, J., et al., *Induction of apoptosis by sodium selenite in human acute promyelocytic leukemia NB4 cells: involvement of oxidative stress and mitochondria.* Journal of Trace Elements in Medicine and Biology, 2003. **17**(1): p. 19-26.

513. Zhao, R., F.E. Domann, and W. Zhong, *Apoptosis induced by selenomethionine and methioninase is superoxide mediated and p53 dependent in human prostate cancer cells.* Molecular Cancer Therapeutics, 2006. **5**(12): p. 3275-3284.

514. Wallenberg, M., et al., *Selenium compounds are substrates for glutaredoxins: a novel pathway for selenium metabolism and a potential mechanism for selenium-mediated cytotoxicity.* Biochemical Journal, 2010. **429**: p. 85-93.

515. Chen, T. and Y.-S. Wong, *Selenocystine induces reactive oxygen species-mediated apoptosis in human cancer cells.* Biomedicine & Pharmacotherapy, 2009. **63**(2): p. 105-113.

516. Liu, C., et al., *Intracellular glutathione content influences the sensitivity of lung cancer cell lines to methylseleninic acid.* Molecular Carcinogenesis, 2012. **51**(4): p. 303-314.

517. Xiang, N., R. Zhao, and W. Zhong, *Sodium selenite induces apoptosis by generation of superoxide via the mitochondrial-dependent pathway in human prostate cancer cells.* Cancer Chemotherapy and Pharmacology, 2009. **63**(2): p. 351-362.

518. Jung, U., et al., *Se-methylselenocysteine induces apoptosis mediated by reactive oxygen species in HL-60 cells.* Free Radical Biology and Medicine, 2001. **31**(4): p. 479-489.

519. Suzuki, M., et al., *Rapamycin suppresses ROS-dependent apoptosis caused by selenomethionine in A549 lung carcinoma cells.* Cancer Chemotherapy and Pharmacology, 2011. **67**(5): p. 1129-1136.

520. Husbeck, B., et al., *Tumor-selective killing by selenite in patient-matched pairs of normal and malignant prostate cells.* Prostate, 2006. **66**(2): p. 218-225.

521. Nilsonne, G., et al., *Selenite induces apoptosis in sarcomatoid malignant mesothelioma cells through oxidative stress.* Free Radical Biology and Medicine, 2006. **41**(6): p. 874-885.

522. Selenius, M., et al., *Treatment of lung cancer cells with cytotoxic levels of sodium selenite: Effects on the thioredoxin system.* Biochemical Pharmacology, 2008. **75**(11): p. 2092-2099.

523. Rigobello, M.P., et al., *Interaction of selenite and tellurite with thiol-dependent redox enzymes: Kinetics and mitochondrial implications.* Free Radical Biology and Medicine, 2011. **50**(11): p. 1620-1629.

524. Deagen, J.T., et al., *Effects of dietary selenite, selenocysteine and selenomethionine on selenocysteine lyase and glutathione-peroxidase activites and on selenium levels in rat-tissues.* Journal of Nutrition, 1987. **117**(1): p. 91-98.

525. Berggren, M.M., et al., *Effect of selenium on rat thioredoxin reductase activity - Increase by supranutritional selenium and decrease by selenium deficiency.* Biochemical Pharmacology, 1999. **57**(2): p. 187-193.

526. Erkhembayar, S., et al., *Selenium homeostasis and induction of thioredoxin reductase during long term selenite supplementation in the rat.* Journal of Trace Elements in Medicine and Biology, 2011. **25**(4): p. 254-259.

527. Romanowska, M., et al., *Effects of selenium supplementation on expression of glutathione peroxidase isoforms in cultured human lung adenocarcinoma cell lines.* Lung Cancer, 2007. **55**(1): p. 35-42.

528. Miller, S., et al., *Selenite protects human endothelial cells from oxidative damage and induces thioredoxin reductase.* Clinical Science, 2001. **100**(5): p. 543-550.

529. Bordoni, A., et al., *Selenium supplementation can protect cultured rat cardiomyocytes from hypoxia/reoxygenation damage.* Journal of Agricultural and Food Chemistry, 2003. **51**(6): p. 1736-1740.

530. Khera, A., J.J. Vanderlelie, and A.V. Perkins, *Selenium supplementation protects trophoblast cells from mitochondrial oxidative stress.* Placenta, 2013. **34**(7): p. 594-598.

531. Watson, M., et al., *Selenium supplementation protects trophoblast cells from oxidative stress.* Placenta, 2012. **33**(12): p. 1012-1019.

532. Schnabel, R., et al., *Selenium supplementation improves antioxidant capacity in vitro and in vivo in patients with coronary artery disease: The SElenium Therapy in Coronary Artery disease Patients (SETCAP) Study.* American Heart Journal, 2008. **156**(6): p. 1201-1201.

533. Rayman, M.P., *Food-chain selenium and human health: emphasis on intake.* British Journal of Nutrition, 2008. **100**(2): p. 254-268.

534. Suadicani, P., H. Hein, and F. Gyntelberg, *Serum selenium concentration and risk of ischaemic heart disease in a prospective cohort study of 3000 males.* Atherosclerosis, 1992. **96**(1): p. 33-42.

535. Brigelius-Flohe, R. and A. Kipp, *Glutathione peroxidases in different stages of carcinogenesis.* Biochimica Et Biophysica Acta-General Subjects, 2009. **1790**(11): p. 1555-1568.

536. Baker, A., et al., *Thioredoxin, a gene found overexpressed in human cancer, inhibits apoptosis in vitro and in vivo.* Cancer Research, 1997. **57**(22): p. 5162-5167.

537. Ganther, H.E. and C. Ip, *Thioredoxin reductase activity in rat liver is not affected by supranutritional levels of monomethylated selenium in vivo and is inhibited only by high levels of selenium in vitro.* Journal of Nutrition, 2001. **131**(2): p. 301-304.

538. Kumar, B.S., et al., *Anti-hemolytic and peroxyl radical scavenging activity of organoselenium compounds: An in vitro study.* Biological Trace Element Research, 2011. **140**(2): p. 127-138.

539. Chew, P., et al., *Antiatherosclerotic and renoprotective effects of ebselen in the diabetic apolipoprotein E/GPx1-double knockout mouse.* Diabetes, 2010. **59**(12): p. 3198-3207.

540. Tan, S.M., et al., *The modified selenenyl amide, M-hydroxy ebselen, attenuates diabetic nephropathy and diabetes-associated atherosclerosis in ApoE/GPx1 double knockout mice.* Plos One, 2013. **8**(7).

541. Chew, P., et al., *Site-specific antiatherogenic effect of the antioxidant ebselen in the diabetic apolipoprotein E-deficient mouse.* Arteriosclerosis Thrombosis and Vascular Biology, 2009. **29**(6): p. 823-U131.

542. Chew, P., et al., *Lack of the antioxidant glutathione peroxidase-1 (GPx1) accelerates nephropathy in the diabetic apoE(-/-)GPx1(-/-) mouse, and this effect is ameliorated by the GPx-mimetic ebselen.* Nephrology, 2009. **14**: p. A37-A37.

543. Tan, S.M., et al., *Late-intervention study with ebselen in an experimental model of type 1 diabetic nephropathy.* Free Radical Research, 2015. **49**(3): p. 219-227.

544. Hort, M.A., et al., *Diphenyl diselenide effectively reduces atherosclerotic lesions in LDLr -/- mice by attenuation of oxidative stress and inflammation.* Journal of Cardiovascular Pharmacology, 2011. **58**(1): p. 91-101.

545. Weng, Y., et al., *Immobilization of selenocystamine on TiO2 surfaces for in situ catalytic generation of nitric oxide and potential application in intravascular stents.* Biomaterials, 2011. **32**(5): p. 1253-1263.

546. Weekley, C.M. and H.H. Harris, *Which form is that? The importance of selenium speciation and metabolism in the prevention and treatment of disease.* Chemical Society Reviews, 2013. **42**(23): p. 8870-8894.

547. Hawkins, C.L., P.E. Morgan, and M.J. Davies, *Quantification of protein modification by oxidants.* Free Radical Biology and Medicine, 2009. **46**(8): p. 965-988.

548. Noble, R.W. and Q.H. Gibson, *Reaction of ferrous horseradish peroxidase with hydrogen peroxide.* Journal of Biological Chemistry, 1970. **245**(9): p. 2409-&.

549. Dypbukt, J.M., et al., *A sensitive and selective assay for chloramine production by myeloperoxidase.* Free Radical Biology and Medicine, 2005. **39**(11): p. 1468-1477.

550. Fukuda, K., et al., *Free amino-acid content of lymphocytes and granulocytes compared.* Clinical Chemistry, 1982. **28**(8): p. 1758-1761.

551. Weiss, S.J. and A. Slivka, *Monocyte and granulocyte-mediated tumor-cell destruction - A role for the hydrogen peroxide-myeloperoxidase-chloride system.* Journal of Clinical Investigation, 1982. **69**(2): p. 255-262.

552. Grisham, M.B., et al., *Chlorination of endogenous amines by isolated neutrophils - ammonia-dependent bactericidal, cytotoxic and cytolytic activities of the chloramines.* Journal of Biological Chemistry, 1984. **259**(16): p. 404-413.

553. Ferrante, A. and Y.H. Thong, *Optimal conditions for simultaneous purification of mononuclear and polymorphonuclear leucocytes from human blood by the hypaque-ficoll method.* Journal of Immunological Methods, 1980. **36**(2): p. 109-117.

554. Thomas, E.L., M.B. Grisham, and M.M. Jefferson, *Preparation and characterization of chloramines.* Methods in Enzymology, 1986. **132**: p. 569-85.

555. Eyer, P., et al., *Molar absorption coefficients for the reduced Ellman reagent: reassessment.* Analytical Biochemistry, 2003. **312**(2): p. 224-227.

556. Smith, P.K., et al., *Measurement of protein using bicinchoninic acid.* Analytical Biochemistry, 1985. **150**(1): p. 76-85.

557. Carlberg, I. and B. Mannervik, *Glutathione-Reductase.* Methods in Enzymology, 1985. **113**: p. 484-490.

558. Gromer, S., et al., *Human placenta thioredoxin reductase - Isolation of the selenoenzyme, steady state kinetics, and inhibition by therapeutic gold compounds.* Journal of Biological Chemistry, 1998. **273**(32): p. 20096-20101.

559. Fotakis, G. and J.A. Timbrell, *In vitro cytotoxicity assays: Comparison of LDH, neutral red, MTT and protein assay in hepatoma cell lines following exposure to cadmium chloride.* Toxicology Letters, 2006. **160**(2): p. 171-177.

560. Krieg, K., *Viability assay on animal cells with ethidium bromide by fluorescence microscopy.* Zentralblatt fuer Allgemeine Pathologie und Pathologische Anatomie, 1978. **122**(1-2): p. 17-19.

561. Shevchenko, A., et al., *Mass spectrometric sequencing of proteins from silver stained polyacrylamide gels.* Analytical Chemistry, 1996. **68**(5): p. 850-858.

562. Candiano, G., et al., *Blue silver: A very sensitive colloidal Coomassie G-250 staining for proteome analysis.* Electrophoresis, 2004. **25**(9): p. 1327-1333.

563. Martin, D. and M. Lenardo, *Morphological, biochemical, and flow cytometric assays of apoptosis.* Current protocols in molecular biology / edited by Frederick M. Ausubel ... [et al.], 2001. **Chapter 14**: p. Unit 14.13-Unit 14.13.

564. Zhang, G.H., et al., *Early detection of apoptosis using a fluorescent conjugate of annexin V.* Biotechniques, 1997. **23**(3): p. 525-&.

565. Boehme, S.A. and M.J. Lenardo, *Ligand-induced apoptosis of mature T-lymphocytes (propriocidal regulation) occurs at distinct stages of the cell-cycle.* Leukemia, 1993. **7**: p. S45-S49.

566. Winterbourn, C.C. and M.B. Hampton, *Thiol chemistry and specificity in redox signaling.* Free Radical Biology and Medicine, 2008. **45**(5): p. 549-561.

567. Luo, S. and R.L. Levine, *Methionine in proteins defends against oxidative stress.* FASEB Journal, 2009. **23**(2): p. 464-472.

568. Levine, R.L., et al., *Methionine residues may protect proteins from critical oxidative damage.* Mechanisms of Ageing and Development, 1999. **107**(3): p. 323-332.

569. Kumakura, F., et al., *A Water-Soluble Cyclic Selenide with Enhanced Glutathione Peroxidase-Like Catalytic Activities.* European Journal of Organic Chemistry, 2010(3): p. 440-445.

570. Huber, R.E. and R.S. Criddle, *Comparison of chemical properties of selenocysteine and selenocystine with their sulfur analogs.* Archives of Biochemistry and Biophysics, 1967. **122**(1): p. 164-&.

571. Gammelgaard, B., et al., *Combination of LC-ICP-MS, LC-MS and NMR for investigation of the oxidative degradation of selenomethionine.* Talanta, 2003. **59**(6): p. 1165-1171.

572. Rosman, K.J.R. and P.D.P. Taylor, *Isotopic compositions of the elements 1997 (Technical Report).* Pure and Applied Chemistry, 1998. **70**(1): p. 217-235.

573. Yin, J., et al., *Effects of antioxidants on the hydrogen peroxide-mediated oxidation of methionine residues in granulocyte colony-stimulating factor and human parathyroid hormone fragment 13-34.* Pharmaceutical Research, 2004. **21**(12): p. 2377-2383.

574. Sanz, J., et al., *Microwave and Fenton's reagent oxidation of wastewater.* Environmental Chemistry Letters, 2003. **1**(1): p. 45-50.

575. Takei, T., et al., *Model Study Using Designed Selenopeptides on the Importance of the Catalytic Triad for the Antioxidative Functions of Glutathione Peroxidase.* Journal of Physical Chemistry B, 2014. **118**(2): p. 492-500.

576. Avi-Dor, Y. and R. Lipkin, *A spectrophotometric method for the determination of reduced glutathione.* Journal of Biological Chemistry, 1958. **233**(1): p. 69-72.

577. Cleland, W.W., *Dithiothreitol: New protective reagent for SH groups.* Biochemistry, 1964. **3**(4): p. 480-&.

578. Boschi-Muller, S., et al., *The enzymology and biochemistry of methionine sulfoxide reductases.* Biochimica et Biophysica Acta (BBA) - Proteins and Proteomics, 2005. **1703**(2): p. 231-238.

579. Steinmann, D., T. Nauser, and W.H. Koppenol, *Selenium and Sulfur in Exchange Reactions: A Comparative Study.* Journal of Organic Chemistry, 2010. **75**(19): p. 6696-6699.

580. Lacey, B.M., et al., *Selenium in Thioredoxin Reductase: A Mechanistic Perspective.* Biochemistry, 2008. **47**(48): p. 12810-12821.

581. Eckenroth, B.E., et al., *Investigation of the C-terminal redox center of High-M-r thioredoxin reductase by protein engineering and semisynthesis.* Biochemistry, 2007. **46**(33): p. 9472-9483.

582. Buxton, G.V., et al., *Critical-review of rate constants for reactions of hydrated electrons, hydrogen-atoms and hydroxyl radicals in aqueous-solution.* Journal of Physical and Chemical Reference Data, 1988. **17**(2): p. 513-886.

583. Arthur, J.R., *The glutathione peroxidases.* Cellular and Molecular Life Sciences, 2000. **57**(13-14): p. 1825-1835.

584. Lee, B.C., et al., *Functions and evolution of selenoprotein methionine sulfoxide reductases.* Biochimica Et Biophysica Acta-General Subjects, 2009. **1790**(11): p. 1471-1477.

585. Tamura, T. and T.C. Stadtman, *A new selenoprotein from human lung adenocarcinoma cells: Purification, properties, and thioredoxin reductase activity.* Proceedings of the National Academy of Sciences of the United States of America, 1996. **93**(3): p. 1006-1011.

586. Du, Y.T., et al., *Glutathione and glutaredoxin act as a backup of human thioredoxin reductase 1 to reduce thioredoxin 1 preventing cell death by aurothioglucose.* Journal of Biological Chemistry, 2012. **287**(45): p. 10.

587. Kumar, S., M. Bjornstedt, and A. Holmgren, *Selenite is a substrate for calf thymus thioredoxin reductase and thioredoxin and elicits a large nonstoichiometric oxidation of NADPH in the presence of oxygen.* European Journal of Biochemistry, 1992. **207**(2): p. 435-439.

588. Bjornstedt, M., et al., *Selenium and the thioredoxin and glutaredoxin systems.* Biomedical and Environmental Sciences, 1997. **10**(2-3): p. 271-279.

589. Zhao, R., H. Masayasu, and A. Holmgren, *Ebselen: A substrate for human thioredoxin reductase strongly stimulating its hydroperoxide reductase activity and a superfast thioredoxin oxidant.* Proceedings of the National Academy of Sciences of the United States of America, 2002. **99**(13): p. 8579-8584.

590. Zhao, R. and A. Holmgren, *A novel antioxidant mechanism of ebselen involving ebselen diselenide, a substrate of mammalian thioredoxin and thioredoxin reductase.* Journal of Biological Chemistry, 2002. **277**(42): p. 39456-39462.

591. Arteel, G.E., K. Briviba, and H. Sies, *Function of thioredoxin reductase as a peroxynitrite reductase using selenocystine or ebselen.* Chemical Research in Toxicology, 1999. **12**(3): p. 264-269.

592. Brot, N., et al., *Enzymatic reduction fo protein-bound methionine sulfoxide.* Proceedings of the National Academy of Sciences of the United States of America-Biological Sciences, 1981. **78**(4): p. 2155-2158.

593. Moskovitz, J., et al., *Identification and characterization of a putative active site for peptide methionine sulfoxide reductase (MsrA) and its substrate stereospecificity.* Journal of Biological Chemistry, 2000. **275**(19): p. 14167-14172.

594. Sharov, V.S., et al., *Diastereoselective reduction of protein-bound methionine sulfoxide by methionine sulfoxide reductase.* FEBS Letters, 1999. **455**(3): p. 247-250.

595. Bjornstedt, M., et al., *The thioredoxin and glutaredoxin systems are efficient electron donors to human plasma glutathione peroxidase.* Journal of Biological Chemistry, 1994. **269**(47): p. 29382-4.

596. Marzano, C., et al., *Inhibition of thioredoxin reductase by auranofin induces apoptosis in cisplatin-resistant human ovarian cancer cells.* Free Radical Biology and Medicine, 2007. **42**(6): p. 872-881.

597. Cox, A.G., et al., *The thioredoxin reductase inhibitor auranofin triggers apoptosis through a Bax/Bak-dependent process that involves peroxiredoxin 3 oxidation.* Biochemical Pharmacology, 2008. **76**(9): p. 1097-1109.

598. Rahmanto, A.S., et al., *Cellular effects of photogenerated oxidants and long-lived, reactive, hydroperoxide photoproducts.* Free Radical Biology and Medicine, 2010. **49**(10): p. 1505-1515.

599. Rahmanto, A.S., D.I. Pattison, and M.J. Davies, *Photo-oxidation-induced inactivation of the selenium-containing protective enzymes thioredoxin reductase and glutathione peroxidase.* Free Radical Biology and Medicine, 2012. **53**(6): p. 1308-1316.

600. Wang, M., et al., *PaxDb, a database of protein abundance averages across all three domains of life.* Molecular & Cellular Proteomics, 2012. **11**(8): p. 492-500.

601. Auchere, F., et al., *Purification and structure of the major product obtained by reaction of NADPH and NMNH with the myeloperoxidase/hydrogen peroxide/chloride system.* European Journal of Biochemistry, 2001. **268**(10): p. 2889-2895.

602. Auchere, F. and C. Capeillere-Blandin, *NADPH as a co-substrate for studies of the chlorinating activity of myeloperoxidase.* Biochemical Journal, 1999. **343**: p. 603-613.

603. Griffin, B.W. and R. Haddox, *Chlorination of NADH - Similarites of the HOCl-supported and chloroperoxidase-catalysed reactions.* Archives of Biochemistry and Biophysics, 1985. **239**(1): p. 305-309.

604. Whiteman, M., et al., *Hypochlorous acid-mediated mitochondrial dysfunction and apoptosis in human hepatoma HepG2 and human fetal liver cells: Role of mitochondrial permeability transition.* Free Radical Biology and Medicine, 2005. **38**(12): p. 1571-1584.

605. Pullar, J.M., M.C.M. Vissers, and C.C. Winterbourn, *Living with a killer: The effects of hypochlorous acid on mammalian cells.* IUBMB Life, 2000. **50**(4-5): p. 259-266.

606. Vissers, M.C.M., W.G. Lee, and M.B. Hampton, *Regulation of apoptosis by vitamin C - Specific protection of the apoptotic machinery against exposure to chlorinated oxidants.* Journal of Biological Chemistry, 2001. **276**(50): p. 46835-46840.

607. Englert, R.P. and E. Shacter, *Distinct modes of cell death induced by different reactive oxygen species - Amino acyl chloramines mediate hypochlorous acid-induced apoptosis.* Journal of Biological Chemistry, 2002. **277**(23): p. 20518-20526.

608. Klamt, F. and E. Shacter, *Taurine chloramine, an oxidant derived from neutrophils, induces apoptosis in human B lymphoma cells through mitochondrial damage.* Journal of Biological Chemistry, 2005. **280**(22): p. 21346-21352.

609. Klamt, F., et al., *Oxidant-induced apoptosis is mediated by oxidation of the actin-regulatory protein cofilin.* Nature Cell Biology, 2009. **11**(10): p. 1241-1246.

610. Goel, A., et al., *Selenomethionine induces p53 mediated cell cycle arrest and apoptosis in human colon cancer cells.* Cancer Biology & Therapy, 2006. **5**(5): p. 529-535.

611. Ruckdeschel, K., et al., *Interaction of Yersinia enterocolitica with macrophages leads to macrophage cell death through apoptosis.* Infection and Immunity, 1997. **65**(11): p. 4813-4821.

612. Fan, X.X., et al., *Macrophage surface expression of annexins I and II in the phagocytosis of apoptotic lymphocytes.* Molecular Biology of the Cell, 2004. **15**(6): p. 2863-2872.

613. Encinar, J.R., et al., *Determination of selenomethionine and selenocysteine in human serum using speciated isotope dilution-capillary HPLC-inductively coupled plasma collision cell mass spectrometry.* Analytical Chemistry, 2004. **76**(22): p. 6635-6642.

614. Stacey, M.M., et al., *Protein thiol oxidation and formation of S-glutathionylated cyclophilin A in cells exposed to chloramines and hypochlorous acid.* Archives of Biochemistry and Biophysics, 2012. **527**(1): p. 45-54.

615. Maier, K.L., et al., *Different selectivities of oxidants during oxidation of methionine residues in the α-1-proteinase inhibitor.* FEBS Letters, 1989. **250**(2): p. 221-226.

616. Ossanna, P.J., et al., *Oxidative regulation of neutrophil elastase-α-1-proteinase inhibitor interactions.* Journal of Clinical Investigation, 1986. **77**(6): p. 1939-1951.

617. Tait, J.F. and D. Gibson, *Phospholipid binding of annexin V: effects of calcium and membrane phosphatidylserine content.* Archives of Biochemistry and Biophysics, 1992. **298**(1): p. 187-91.

618. Alvarez, B., et al., *Kinetics of peroxynitrite reaction with amino acids and human serum albumin.* Journal of Biological Chemistry, 1999. **274**(2): p. 842-848.

619. Epp, O., R. Ladenstein, and A. Wendel, *The refined structure of the selenoenzyme glutathione peroxidase at 0.2-nm resolution.* European Journal of Biochemistry, 1983. **133**(1): p. 51-69.

620. James, A.M., et al., *Interactions of mitochondria-targeted and untargeted ubiquinones with the mitochondrial respiratory chain and reactive oxygen species - Implications for the use of exogenous ubiquinones as therapies and experimental tools.* Journal of Biological Chemistry, 2005. **280**(22): p. 21295-21312.

621. Graham, D., et al., *Mitochondria-targeted antioxidant MitoQ(10) improves endothelial function and attenuates cardiac hypertrophy.* Hypertension, 2009. **54**(2): p. 322-U233.

622. Mercer, J.R., et al., *The mitochondria-targeted antioxidant MitoQ decreases features of the metabolic syndrome in ATM(+/-)/ApoE(-/-) mice.* Free Radical Biology and Medicine, 2012. **52**(5): p. 841-849.

623. Roman, M., P. Jitaru, and C. Barbante, *Selenium biochemistry and its role for human health.* Metallomics, 2014. **6**(1): p. 25-54.

624. Gammelgaard, B., O. Jons, and L. Bendahl, *Selenium speciation in pretreated human urine by ion-exchange chromatography and ICP-MS detection.* Journal of Analytical Atomic Spectrometry, 2001. **16**(4): p. 339-344.

625. Weekley, C.M., et al., *Metabolism of selenite in human lung cancer cells: X-ray absorption and fluorescence studies.* Journal of the American Chemical Society, 2011. **133**(45): p. 18272-18279.

626. Hwang, C., A.J. Sinskey, and H.F. Lodish, *Oxidized redox state of glutathione in the endoplasmic reticulum.* Science, 1992. **257**(5076): p. 1496-502.

627. Burk, R.F., et al., *Effects of chemical form of selenium on plasma biomarkers in a high-dose human supplementation trial.* Cancer Epidemiology Biomarkers & Prevention, 2006. **15**(4): p. 804-810.

628. Kuehnelt, D., et al., *Selenium metabolites in human urine after ingestion of selenite, L-selenomethionine, or DL-selenomethionine: a quantitative case study by HPLC/ICPMS.* Analytical and Bioanalytical Chemistry, 2005. **383**(2): p. 235-246.

629. Rosen, G.M. and B.A. Freeman, *Detection of superoxide generated by endothelial cells.* Proceedings of the National Academy of Sciences, 1984. **81**(23): p. 7269-7273.

630. Zhao, H., et al., *Detection and characterization of the product of hydroethidine and intracellular superoxide by HPLC and limitations of fluorescence.* Proceedings of

the National Academy of Sciences of the United States of America, 2005. **102**(16): p. 5727-5732.

631. Bonetti, P.O., L.O. Lerman, and A. Lerman, *Endothelial dysfunction a marker of atherosclerotic risk.* Arteriosclerosis, thrombosis, and vascular biology, 2003. **23**(2): p. 168-175.

632. Davignon, J. and P. Ganz, *Role of endothelial dysfunction in atherosclerosis.* Circulation, 2004. **109**(23 suppl 1): p. III-27-III-32.

633. González-Reimers, E., et al., *Relative and combined effects of selenium, protein deficiency and ethanol on hepatocyte ballooning and liver steatosis.* Biological Trace Element Research, 2013. **154**(2): p. 281-287.

634. Kono, H., et al., *Ebselen prevents early alcohol-induced liver injury in rats.* Free Radical Biology and Medicine, 2001. **30**(4): p. 403-411.

635. Kumar, B., et al., *Selenomethionine prevents degeneration induced by overexpression of wild-type human alpha-synuclein during differentiation of neuroblastoma cells.* Journal of the American College of Nutrition, 2005. **24**(6): p. 516-523.

636. Di Domenico, F., et al., *Strategy to reduce free radical species in Alzheimer's disease: an update of selected antioxidants.* Expert Review of Neurotherapeutics, 2015. **15**(1): p. 19-40.

637. Chakraborty, S., et al., *DL-trans-3,4-Dihydroxy-1-selenolane (DHSred) accelerates healing of indomethacin-induced stomach ulceration in mice.* Free Radical Research, 2012. **46**(11): p. 1378-1386.